A STUDY OF TRANSPORT OF MICELLAR FLUIDS IN POROUS MEDIA

BY

MOJDEH DELSHAD, B.S., M.S.

DISSERTATION

Presented to the Faculty of the Graduate School of

The University of Texas at Austin

in Partial Fulfillment

of the Requirements

for the Degree of

DOCTOR OF PHILOSOPHY

THE UNIVERSITY OF TEXAS AT AUSTIN

May 1986

A STUDY OF TRANSPORT OF MICELLAR FLUIDS

IN POROUS MEDIA

APPROVED BY SUPERVISORY COMMITTEE:

Gary A. Pope

Larry W. Lake

Mark A. Miller

Bruce A. Rouse

G. B. Thurston

TO THE MEMORY OF

MY FATHER

HASSAN DELSHAD

A STUDY OF TRANSPORT OF MICELLAR FLUIDS IN POROUS MEDIA

BY

MOJDEH DELSHAD, B.S., M.S.

DISSERTATION

Presented to the Faculty of the Graduate School of

The University of Texas at Austin

in Partial Fulfillment

of the Requirements

for the Degree of

DOCTOR OF PHILOSOPHY

THE UNIVERSITY OF TEXAS AT AUSTIN

May 1986

ACKNOWLEDGMENTS

Many individuals have contributed greatly to the completion of this investigation. Special recognition must go to the followings,

- Jamal Hakim for his assistance in collecting the data and also his aid and patience in history matching the numerous tracer data.

- Dennis Wagoner for his sincere assistance in the great number of analyses which had to be performed.

For technical advice and effort in reviewing this manuscript, I would like to express my appreciation to professors Mark Miller and George Thurston.

I have to express my special gratitude to Dr. Bruce Rouse for his boundless assistance with equipment design and maintenance as well as technical advice and effort in reviewing this manuscript.

A great deal of credit must go to professor Larry Lake for serving as advisor and providing guidance during the course of this work.

I am deeply indebted to professor Gary Pope, my advisor, for infinite guidance and technical suggestion

through the duration of this research project.

I also acknowledge support by U.S. Department of Energy and the following companies: Amoco, Arco, Adref, British Petroleum, CDC, Chevron, Cities Service, Conoco, Core Data, Cray Research, Eta Systems, Exxon, Halliburton, Imperical Chemical Industries, Intevep, Japex, Mobil, Norsk Hydro, Phillips, Schlumberger, Shell, Sohio, Sun, Tenneco, Texaco, Union Oil of California.

I am thankful to Texas Mining and Mineral Resources for a two-year fellowship awarded to me. I am grateful to professor van Rensberg for nominating me for this fellowship. I also appreciate the three-year fellowship awarded to me by Atlantic Richfield Company.

I would like to thank Silvia B. Craveiro de Sa, who with patience and dedication typed this dissertation.

Special appreciation is expressed to my mother for her love and inspiration.

Lastly, I would like to express my love and undying thanks to my husband, Kamy, for his unending patience and encouragement; without him, I would surely have "given up" long ago.

A STUDY OF TRANSPORT OF MICELLAR

FLUIDS IN POROUS MEDIA

Publication No._____

Mojdeh Delshad, Ph.D.
The University of Texas at Austin, 1985

Supervising Professors: Gary A. Pope and
Larry W. Lake

Two- and three-phase relative permeabilities have been measured for a low interfacial tension brine-oil-surfactant-alcohol mixture in a Berea sandstone core. The measurements were done at steady-state with a constant nominal capillary number of 10^{-2}.

Residual phase saturation (capillary desaturation curve) and endpoint relative permeability have also been measured for three-phase micellar fluids as a function of capillary number in a Berea core.

Continuous and slug displacements of both partitioning and non-partitioning radioactive tracers were run for each steady-state experiment. The experimental effluent tracer data from these experiments were analyzed by a capacitance model. The phase

dispersivities and dispersion coefficients estimated from the capacitance analysis as a function of phase saturation and velocity are illustrated.

Both excess phases (oil and brine) flowing with the microemulsion showed significant capacitance effects, but the microemulsion did not. The absence of capacitance and higher residual saturation than those of excess phases at the same capillary number indicate that the microemulsion was probably the wetting phase in these low interfacial tension flows, even more wetting than the excess brine phase.

The relative permeability of each phase is a function only of its own saturation during three-phase flow. Based on this observation and the trend of experimental data, an exponential function is recommended to model three-phase relative permeability at high capillary number.

TABLE OF CONTENTS

LIST OF TABLES

LIST OF FIGURES

CHAPTER 1

INTRODUCTION

The use of surfactant to displace crude oil is the least proven of all enhanced oil recovery processes. The field results to date, in contrast with results obtained in laboratory on the use of surfactants for enhanced recovery have not been encouraging. This discrepancy may be resolved by better and more adequate understanding of the mechanisms of interaction between the injected fluid and resident fluids which control the mobilization and displacement of the oil from a reservoir. Limited research has been directed toward understanding what effects the injected chemicals would have on the fluid distribution and flow behavior other than mobilizing the residual oil.

To resolve some of the aformentioned problems, the goal of this research was to experimentally investigate transport properties --- phase trapping,

relative permeability, dispersivities, and capacitance parameters --- in two- and three-phase flow.

Capillary desaturation (the relation between residual phase saturation and the capillary number) is one of the most important physical relations of the micellar process. The main reason for this is that the microscopic trapping of the phases by capillary forces determines the reduction in residual oil saturation and the amount of tertiary fluid required for complete mobilization.

Despite this importance, a complete set of experimental capillary desaturation curves for micellar fluids does not appear to have been reported in the literature. Therefore, the first objective of this study was to obtain these data for three-phase micellar fluids as a function of capillary number ($N_c = \frac{k\Delta\phi}{L\sigma}$) in a Berea sandstone core. These results may also have a pronounced effect on the outcome of a micellar-polymer simulation.

The effect of ultra-low interfacial tension (IFT) on relative permeability curves has received limited treatment in the petroleum literature. Two-phase relative permeability measurements using low IFT fluids have been reported by several investigators [A.2,B.4,D.10,F.4,H.1,T.7]. What sets the current work

apart is:

(1) I measured relative permeabilities in three-phase flow at ultra-low IFT ($\sigma \approx 7 \times 10^{-4}$ dyne/cm) and constant capillary number.

(2) I estimated phase saturations using both material balance and tracer breakthrough data. Salter and Mohanty [M.2,S.3] used non-partitioning tracers for both oil and brine phases during two-phase flow. Here I present the results of tracer displacements for two- and three-phase flows with partitioning tracers. To my knowledge, no other three-phase flow tracer data has been reported.

(3) I used tracer slugs in some cases. Although the study of miscible slug displacements goes back to 1965 by Raimondi and Torcaso [R.1], this is the first time that slugs have been used for multiphase flow or low IFT surfactant fluid experiments.

Deans [D.3], and Coats and Smith [C.5] were among the first to develop a model (capacitance) of single phase flow which divided the pore space into flowing and dead-end fractions. Stalkup [S.13] and Baker [B.1] extended the capacitance model to two-phase, steady-state miscible displacements. Salter and Mohanty [S.3] modified this

model for tracer displacements under steady-state, two-phase flow.

Salter and Mohanty assumed that each phase has flowing, dendritic, and isolated fractions. Only the flowing and dendritic fractions can be produced. Their model did not include mass transfer between phases. The resulting capacitance-dispersion equation was solved by Laplace Transform [B.1].

Here, we take an approach similar to that of Salter and Mohanty to model the breakthrough curves for low IFT fluids. The major differences over the Salter and Mohanty approach are:

- The model divides each phase into two parts, flowing and dendritic, rather than three. Since the experiments are performed at a very low IFT and the possibility of having an isolated portion is small.

- The model allows mass transfer between phases.

- The model can be used for both two- and three-phase flow, and

- The capacitance-dispersion equations are solved by finite differences.

Presented in Chapter 2 are reviews of the literature on the following subjects

1- Capillary desaturation curves.

2- The effect of IFT on two-phase relative permeabilities.

3- Three-phase relative permeability curves.

4- Dispersion and capacitance in single-phase and multiphase displacements.

A description of mathematical models is in Chapter 3. The convection-diffusion and capacitance-dispersion equations for multiphase flow of partitioning tracers are presented in this chapter.

The experimental apparatus is divided into three categories, (1) flow apparatus, (2) analytical equipment, and (3) physical property apparatus. A description of these is in Chapter 4. The preparation of the porous media, fluids and the flow procedures are discussed in Chapter 5.

The results of capillary desaturation, two- and three-phase relative permeability and capacitance-dispersion measurements are summarized in Chapter 6. Also presented in this chapter is a comparison of my results with those found in the literature.

Several relative permeability models have been tested using my two- and three-phase data. Significant changes in previous models had to be made to even approximately fit these data. A new model is presented

which quantitatively represents all of these data. In Chapter 7 are the details of this model. Also shown are comparisons of the model with experimental data.

Chapter 8 deals with equilibrium in miscible flow studied by Raimondi and Torcaso [R.1]. A detailed analysis of Raimondi and Torcaso results using the capacitance-dispersion model is in this chapter.

Chapter 9 presents the important conclusions drawn from this program and recommendations for further research.

CHAPTER 2

LITERATURE SURVEY

2.1 Relative Permeability Curves

This section is a survey on relative permeability curves for:

- Two-phase flow at low interfacial tension
- Three-phase flow of oil-water-gas
- Three-phase flow at low interfacial tension

2.1.1 Two-Phase Flow at Low Tension

A summary of relevant experimental two-phase relative permeability data reported in literature is shown in Table 2.1.

Leverett [L.5] reported in 1938 the effect of viscosity, interfacial tension (IFT), and sand structure on relative permeabilities. Unconsolidated sandpacks with three different size assortments were used. The interfacial tension was lowered by the addition of amyl alcohol. The results showed that

- The relative permeabilities were independent of liquid viscosity,

- The relative permeabilities were considerably affected by sand type, and

- There was a 20-30 percent increase in oil and water relative permeabilities with a decrease in IFT from 24 to 5 mN/m.

Talash [T.3] in 1976 presented relative permeability curves for a low tension sulfonate system. These were two-phase flow experiments in Berea rock and were among the first reported using sulfonate to lower the IFT. The lengths of the cores were 0.305 m and 0.076 m. Two Mobil surfactants and a Witco surfactant were used at concentrations between 0.004 and 0.5 weight percent. No indication was given as to the IFT values and flow rates employed. The result for the low IFT system showed a reduction in the residual oil saturation but no change in the residual water saturation. The relative permeabilities to both oil and water increased as IFT decreased.

Bardon et al. [B.2] in 1978 reported gas-oil relative permeability experiments at high pressure (up to 400 psi) and temperature (up to 120°C) in a Fontainbleau sandstone (38.2 cm long and 5 cm in diameter) over a

wide range of IFTs. The core was vertically oriented and the fluids were injected from the top. The fluids used were a binary mixture of pure hydrocarbons. His results showed that residual oil saturation and relative permeabilities are strongly affected by IFT, especially when lower than 10^{-2} mN/m. The relative permeabilities to both oil and gas increased as IFT decreased.

Batycky et al. [B.4] in 1978 reported the results of a series of displacement tests with oil and water for IFTs ranging from 50 to 0.02 mN/m. The interfacial tension was lowered by the addition of 0.2 wt% TRS 10-80. Steady-state relative permeability and dynamic displacement measurements were performed on two unconsolidated sandpacks at 40 cm^3/hr. The results showed that a decrease in IFT caused the relative permeability curves to become less curved. No reduction in residual water saturation was observed, but a decrease in residual oil saturation was noted. All relative permeabilities increased as IFT decreased.

Klaus [K.1] in 1979 reported a series of displacement tests for IFTs from 39.8 to 0.0149 mN/m in Berea sandstone. The fluids used were isopropyl alcohol (IPA), 2% calcium chloride ($CaCl_2$) brine, and Soltrol 170. Alcohol was used because of surfactant adsorption

in a sandstone core. The core was 122 cm long and the frontal velocity was 6.1 m/day. The flow rate, pressure drop, and volumes were measured and the methods of Welge [W.1] and Johnson et al. [J.1] (unsteady-state) were applied to determine two-phase relative permeability. His conclusions based on the experimental results were

(1) Little or no effect on oil relative permeability was seen at IFT values higher than 1.63 mN/m but oil relative permeability increased as interfacial tension decreased below 1.63 mN/m,

(2) Water relative permeability for both imbibition and drainage increased with decreasing IFT over the whole range,

(3) Oil and water hystereses were slightly influenced by IFT,

(4) Residual oil saturation decreased sharply below 1.63 mN/m while residual water saturation showed a minor decrease between 5.9 to 0.0149 mN/m.

Amaefule and Handy [A.2] in 1981 reported the effect of IFT on relative permeability. Both steady-state and unsteady-state displacement methods were used to generate relative permeability curves. The different combinations of oil (octane, dodecane, kerosene, mineral oil), surfactant (TRS 10-80), alcohol (sec-butanol), and

brine used gave a range of IFT from 34 to 0.07 mN/m. All the experiments were conducted in fired Berea sandstone (9.6-15.2 cm long) at 25°C. They concluded that (1) oil and water relative permeabilities increased with decreasing IFT, and (2) the residual oil saturation and the residual water saturation decreased while the total relative mobility increased with decreasing IFT.

Amaefule and Handy also used an empirical relative permeability relationship to fit the experimental data. The expression used was an extension of Coats empirical relationships for gas-oil systems and the parametric expressions of Thomas et al. [T.5] for water-oil systems. The water-oil relative permeability data were correlated with the capillary number as follows.

$$k_{rw}(S_w,\sigma) = b\ S_{wr}\left[\frac{S_w-S_{wr}}{1-S_{wr}}\right]^n + [1-b\ S_{wr}]\left[\frac{S_w-S_{wr}}{1-S_{wr}}\right] \tag{2.1}$$

$$k_{ro}(S_w,\sigma) = a\ S_{or}\left[\frac{1-S_{or}-S_w}{1-S_{or}-S_{wr}}\right]^p + [1-a\ S_{wr}]\left[\frac{1-S_{or}-S_w}{1-S_{or}-S_{wr}}\right] \tag{2.2}$$

where the residual saturations (S_{wr} and S_{or}) are correlated with the capillary number ($N_c = \frac{u\mu}{\sigma}$).

The experimental data were matched using the above expression and the empirical constants found to be a = 5, b = 2.5, n = 3 and P = 2.

Delshad [D.8] in 1981 carried out steady-state measurements of two-phase relative permeability in a two-foot Berea sandstone core. The measurements were performed at 30°C. The fluids used were the three equilibrated phases of a mixture of TRS 10-410 / n-decane/ Isobutyl alcohol / brine. The IFT between middle-phase microemulsion and excess phases was about 10^{-3} mN/m. The frontal velocity was kept constant at 3.70 m/day during the experiments.

Experiments were run vertically, with injection at the top, to prevent phase segregation. The fluid saturations were measured using both material balance and tracer breakthrough curves. Both microemulsion-excess oil and microemulsion-excess brine two-phase relative permeability curves were measured. The results showed that:

- The relative permeabilities increased significantly compared to high tension values.
- The relative permeability curves were not straight lines and showed significant curvature.
- The irreducible oil and water saturations were

lower than those at high tension.

- A significant amount of residual microemulsion existed at the low IFT of 10^{-3} mN/m.

MacAllister [M.1] in 1982 reported the results of steady-state measurements of two-phase relative permeability in a sandpack. He conducted steady-state tests at 30°C. Ottawa Sand was packed in a two-foot stainless steel pressure vessel with pressure taps at 1/4 of the total distance from each end. The intermediate pressure drop across the center was used to avoid end effects. The fluids used were the three equilibrated phases of a mixture of brine/oil/surfactant/alcohol. The surfactant used was Witco TRS 10-410 (1.5 v% active), the alcohol was isobutanol (1.5 v%), the oil was n-decane (50 v%), and the brine consisted of water, sodium chloride (1.1 wt%). The IFT was on the order of 10^{-3} mN/m. The fluid velocity was kept constant at 3.72 m/day during the tests. The fluid saturations were measured using both material balance and tracer breakthrough curves. Two-phase relative permeability curves were measured for both microemulsion - excess brine and microemulsion - excess oil phases. The results showed that:

- There was a significant increase in relative permeability compared to high tension values, but there

was significant curvature in two-phase relative permeability curves.

- Residual phases were zero except for residual microemulsion to excess brine phase.

Fulcher [F.3,F.4] in 1983 reported the results of measurements of two-phase relative permeabilities in Berea rock samples. He conducted steady-state tests at 25°C to examine the effect of parameters such as velocity, interfacial tension, and wetting phase viscosity on two-phase relative permeabilities. The tests were carried out in 60.96 cm long, 5.08 cm diameter fired Berea sandstone cores. In order to reduce differences in porosity, permeability, and lithology, cores were reused for several tests. The fluids used were mixture of Soltrol 170 oil, 2% calcium chloride brine, isopropyl alcohol (IPA), and glycerin. The alcohol was used as a tension reducer, while glycerin acted as a viscosifying agent to increase the aqueous phase viscosity. Fluid saturations were determined by material balance. A 3.4 atm pressure differential across the core was maintained in order to avoid capillary end effects. The total flow rate was varied from 80 cm^3/hr to 400 cm^3/hr. There were no significant changes observed in the relative permeability curves with flow

rate. The range of oleic-aqueous interfacial tension was from 37.9 mN/m to 0.0389 mN/m. The relative permeability curves were measured for the above mentioned IFT range while the total flow velocity ($q/A\phi$) was maintained at 12.2 m/day and the fluid viscosities were kept at approximately 2.0 mPa/sec. The relative permeability curves exhibited less curvature as IFT was lowered. The relative permeabilities were also increased by lowering IFT. The effect of aqueous phase viscosity on relative permeabilities was also tested. The aqueous phase viscosity range was from that of $CaCl_2$ brine (0.947 mPa/sec) to that of glycerin (954.0 mPa/sec). The fluid velocity was 12.2 m/day and IFT was kept at 30 mN/m. The results showed that the aqueous phase relative permeabilities were increased while the oleic phase relative permeabilities were decreased in approximately the same order of magnitude as viscosity was increased. The curvature in the aqueous phase relative permeability curves was also reduced by increasing aqueous phase viscosity.

The effect of combining interfacial tension reductions and aqueous viscosity increases (capillary number effect) was also measured. The capillary number ($N_c = \frac{u\mu_w}{\sigma\phi}$) ranged from 5.5×10^{-5} to 4.37×10^{-3}. The

residual oil saturation was decreased by increasing the capillary number, but there was no significant change in residual aqueous phase saturation. The relative permeability curves showed less curvature at higher capillary number.

Fulcher also developed a relative permeability model based on his experimental results. A regression analysis was utilized in order to determine the best coefficients. The following functional forms were found for imbibition oil and aqueous relative permeabilities

$$k_{ro} = A\ \bar{S}_o^{[B+C\ \ln\sigma\ +\ D\ \ln(\mu_w/\mu_o)]} \tag{2.3}$$

$$k_{rw} = A\ \bar{S}_w^{[B+D\ \ln\ (\mu_w/\mu_o/\sigma)]} \tag{2.4}$$

where

$$\bar{S}_o = \frac{S_o - S_{or}}{1 - S_{or}} \tag{2.5}$$

$$\bar{S}_w = \frac{S_w - S_{wr}}{1 - S_{wr}} \tag{2.6}$$

Similar functions were also suggested for

drainage relative permeabilities.

The regression constants A, B, C, and D were found to be

oleic phase: A=1.568, B=1.338, C=0.092, D=0.0853

aqueous phase: A=0.611, B=1.258, C=0.0, D=-0.0708

Harbert [H.1] in 1983 reported the results of low tension two-phase relative permeability measurements in reservoir rocks. The rock samples were 3.2 cm diameter by 7.5 cm long. The reservoir rock samples were cleaned with alcohol (IPA), pentane and dried with nitrogen prior to testing. The fluids used were a mixture of tertiary butyl alcohol (TBA), brine, and Soltrol 130. The IFTs ranged from 0.14 to 2.26 mN/m. No indication was given as to the flow rates employed. The experiments were arranged to illustrate the effect of (1) base permeability, (2) IFT, (3) capillary number ($N_c = \frac{u(\mu_w+\mu_o)}{2\sigma}$), and (4) saturation history on low IFT relative permeability curves. The results showed that:

- At constant capillary number and interfacial tension, the less permeable core had a higher final residual saturation value at the same capillary number, and thus lower water relative permeability.

_ At constant capillary number, the oil relative permeability increases as IFT decreased. The water

relative permeability increased at low water saturation and then decreased at water saturation higher than 0.75 by increasing IFT from 0.14 to 1.54 mN/m. The effect of lowering IFT on both oil and water relative permeabilities was small and was mostly due to the difference in final residual saturations.

- At a constant IFT, the water relative permeability did not change while increasing the capillary number from 6×10^{-5} to 6×10^{-4}. On the other hand, the oil relative permeability curve shifted to the right by increasing the capillary number. The residual oil saturation was reduced from 30 to 12 percent by increasing the capillary number by a factor of ten, but there was no change observed in the residual water saturation.

- Oil relative permeability showed hysteresis while water relative permeability was not affected by the saturation path.

Torabzadeh and Handy [T.7] in 1984 conducted experiments to measure the effect of high temperature and low IFT on two-phase relative permeability curves. Experiments were performed on fired Berea sandstone cores (2.54 cm in diameter and 21.60 cm long). Fluids used for their study were n-dodecane as the oil phase, and a

surfactant solution containing 0.2 wt% Petrostep 465 and 2 wt% NaCl as the aqueous phase. The total flow rate varied from 30 to 180 cm^3/hr. The fluid saturations were measured volumetrically. Both steady-state imbibition and drainage relative permeabilities were obtained at temperatures from 22°C to 175°C.

The results of the relative permeability for low tension at different temperatures showed that:

- At temperatures below 100°C, relative permeability to both phases increased with increasing temperature. Interfacial tension ranged from 0.015 to 0.187 mN/m in these experiments.

- Above 100°C, relative pemeability to water decreased while the oil relative permeability increased.

- As the interfacial tension decreased, relative permeability to both oil and water increased.

- Hysteresis decreased with increasing temperature and decreasing IFT. Hysteresis disappeared at 175°C and IFT of 0.015 mN/m.

2.1.2 Three Phase Flow

There are several situations in the exploitation of petroleum reservoirs which involve simultaneous flow of water-oil-gas mixtures. A few examples are

- waterflooding with free gas present
- gas cap expansion drive
- alternate water/gas drive

The enhanced oil recovery techniques such as thermal recovery, carbon dioxide immiscible displacement and surfactant flooding also generate simultaneous flow of three phases within the oil reservoir. An important parameter that characterizes the flow behavior of these multiphases in porous media is the relative permeability of each phase.

Despite the importance of three-phase relative permeabilities, only a few experimental studies have been reported using gas, oil and water. The experimental results for flow of three liquid phases at low interfacial tension (or high capillary number) are rare. In the following subsections, a literature survey on water/gas/oil and water/microemulsion/oil relative permeability experiments and mathematical models is presented.

2.1.2.1 Three Phase Flow of Water-Oil-Gas

Most of the experiments reported to date are summarized in Table 2.2. The ternary graphs of the reported relative permeabilities (isoperms) to gas, water, and oil are shown in Figures 2.1 - 2.3.

Leverett and Lewis [L.6] made the first measurements of three-phase water-gas-oil relative permeabilities in 1941. The steady-state measurements were performed in a sandpack. The conditions for equilibrium were (1) the flow rates of the three fluids were constant, (2) static and differential pressures were constant, and (3) resistance was uniform over six sections of the cell. The relative permeabilities to gas and to oil were found to be dependent on the saturations of the remaining two-phases. The relative permeabilities to water during three-phase flow were close to a smooth curve which closely approximated values found for the water-gas and oil-water systems. Leverett and Lewis suspected two sources of errors in their measurements as follows:

1) Dead space in the cell

2) Failure to reach equilibrium

The first error was inherent in the design of apparatus and introduced errors as high as 6 percent in the computed oil and gas saturations. The second was thought to introduce errors of about 2 percent in the computed relative permeability to oil.

Caudle, Slobod, and Brownscombe [C.2] in 1951 reported the results of three-phase relative permeability

measurements in consolidated sandstone cores. An unsteady-state method was used and the saturations were determined by means of distillation and weighing. The relative permeabilities to water, gas, and oil were found to depend on the saturations of the remaining two-phases. Hysteresis was also observed when the oil saturation was increased after originally being reduced to connate water and residual oil with a gas drive.

Corey et al. [C.6] reported in 1956 results of three-phase oil and gas relative permeabilities in Berea sandstone cores. The water was rendered immobile by placing the cores between capillary barriers so that water relative permeability could not be measured. However, water isoperms were calculated by making the assumptions of: (1) water permeability is dependent on water saturation only and (2) water permeability in a water-wet medium is the same as the oil permeability in an oil-wet (oil-gas) medium. Nine different core samples were used at different water saturations (17 to 71 percent). Two of the nine cores had gas relative permeability curves which were very different from those of the other cores, particularly in the high liquid saturation region. But, Corey et al. used the results obtained from the remaining seven cores in constructing

the gas isoperms. They considered that gas relative permeability was a function of gas saturation alone. They also compared their data with those obtained by Leverett and Lewis [L.6] on unconsolidated sandpacks. The agreement was surprisingly good.

Snell [S.11] (1962) reported measurements of three-phase relative permeabilities in a sandpack. Snell improved the accuracy of the three-phase saturation determination by using a complex combination of radio frequency circuitry and neutron diffraction to obtain the water and gas saturations. Using the material balance, oil saturation was obtained. Gas and oil isoperms were convex toward 100% gas and 100% water saturation respectively.

Sarem [S.7] (1966) used an extension of Welge's two-phase unsteady-state method to obtain three-phase relative permeabilities. In order to analyze the experiments, he assumed that the fractional flow and relative permeability of each phase are functions of the saturation of that phase only. These assumptions may introduce a significant error in calculated oil and gas relative permeabilities since other investigators observed the dependency of gas and oil relative permeabilities on two saturations. He also neglected end

effects and saturation hysteresis effects caused by differences in the saturation history of the core between tests. The assumptions of insolubility of gas in liquids and incompressibility of gas as well as neglecting the effects due to gravity and capillary pressure were also made during the derivation of fractional flow equations. Relative permeability measurements were done on one Berea core and one reservoir core. The results showed that three-phase relative permeabilities are influenced by initial saturation conditions.

Saraf and Fatt [S.5] (1967) reported measurements of two and three-phase relative permeabilities in Boise sandstone. The end effect due to capillary forces was avoided by taking pressure measurements over the central region of the cores. They assumed that three-phase water relative permeability depends only on water saturation and based on this assumption they estimated the water saturation from the water flow rate. The oil saturation was measured by a nuclear magnetic resonance technique. Three-phase oil permeability was found to depend on both oil and water saturations. They also concluded for the first time that gas relative permeability is a function of gas saturation only, even though there was considerable experimental

scatter due to low gas relative permeabilities (≈0.04).

Land [L.2] (1968) reported a method for estimating the relative permeability functions for two and three-phase flow with the saturation changes in the imbibition direction. Two and three-phase imbibition relative permeability of water-wet rocks can be obtained using his method after selecting two rock properties: the residual non-wetting phase saturation and the capillary pressure curve. The relations developed by Land for two and three-phase imbibition relative permeability were derived from theory of the dependence of relative permeability on pore size distribution. Land could not evaluate the accuracy of the equations due to the lack of complete two and three-phase relative permeability data.

Schneider and Owens [S.9] reported in 1970 steady-state and unsteady-state measurements of three-phase relative permeabilities in a variety of sandstone and carbonate core samples having different wetting properties. The relative permeability tests were performed both with two flowing phases and a third nonflowing phase and with three flowing phases. The gas saturation was measured using an x-ray absorption technique while water saturation was determined using a four-electrode resistivity method. Schneider and Owens

measured the effect of trapped gas saturation on the relative permeability to oil and water. Their results showed that for oil-wet cores the presence of trapped gas reduces only the water relative permeability while it affects both oil and water relative permeabilities in water-wet cores. Three-phase flow experiments were performed in two water-wet core samples (Torpedo and Nellie Bly sandstones). Each of the three-phase tests were performed using a constant water-oil ratio, but with an increasing gas-liquid ratio. The water-oil ratios used were 0.1, 0.25, 1, 4 and 10. The results of water relative permeability in the presence of trapped oil, or under conditions of simultaneous flow of three-phases, supported the hypothesis that water relative permeability is a function of water saturation alone. However, the water relative permeability during two-phase flow of water and oil with the presence of trapped gas showed variations of ±0.04 for which an adequate explanation was not given. The gas relative permeability showed dependence both on the direction of changes in the gas saturation and the amount of oil trapped. But, the hypothesis that the gas relative permeability is a function of its own saturation can be applied as long as the residual oil saturation is constant.

In 1970, Stone [S.14] developed a probability model which uses the two sets of two-phase data to predict the three-phase relative permeability. His model is such that it will yield the correct two-phase data when only two-phases are flowing, and will provide interpolated data for three-phase flow. The data required for the calculation of three-phase relative permeability are water-oil and gas-oil data sets.

Based on the channel flow theory which says that in any flow channel there is only one mobile fluid, Stone states that at equal water saturations, the microscopic fluid distributions at the water-oil interface will be identical in a water-oil flow and in a water-oil-gas system, as long as the direction of change of water saturation is the same in both. A similar theory can be applied to the gas relative permeability. These assumptions have been supported by many investigators [C.6,S.5,S.7].

The relative permeability to oil during three-phase flow of oil-water-gas can be predicted from the following equations (Model I):

$$k_{ro} = \bar{S}_o \, \beta_w \beta_g \qquad (2.7)$$

where

β_w and β_g are functions of water and gas saturations respectively and can be obtained from two-phase data as follows

$$\beta_w = \frac{k_{row}}{1-\bar{S}_w} \tag{2.8}$$

and

$$\beta_g = \frac{k_{rog}}{1-\bar{S}_g} \tag{2.9}$$

where the normalized saturations are defined as

$$\bar{S}_o = \frac{S_o - S_{om}}{1 - S_{wc} - S_{om}} \tag{2.10}$$

$$\bar{S}_w = \frac{S_w - S_{wc}}{1 - S_{wc} - S_{om}} \tag{2.11}$$

$$\bar{S}_g = \frac{S_g}{1 - S_{wc} - S_{om}} \tag{2.12}$$

S_{om} is a minimum residual oil and was treated as a constant in his paper even though the possibility of

its dependence on fluid saturation was anticipated. Stone also compared his method against three sets of experimental results (Corey [C.6], Dalton [D.2], Saraf [S.5]). The agreement between predicted and experimental values was reasonably good for all three cases.

Stone [S.15] (1973) revised his probability model (Model I) to yield improved estimates of three-phase relative permeabilities. The new model used two sets of two-phase data of water-oil and gas-oil for estimating three-phase data. This new model gives better results especially in the region of low oil saturations. This new approach is also capable of providing estimates of residual oil data in the three-phase region.

For given values of water saturation (S_w) and gas saturation (S_g) in a three-phase system, S_w is used to obtain k_{rw} and k_{row} from the water-oil data; and S_g is used to obtain k_{rg} and k_{rog} from the gas-oil data. The gas and water relative permeabilities, k_{rg} and k_{rw}, apply directly to the three-phase system. The three-phase oil relative permeability k_{ro} is then calculated using the following equation (Model II):

$$k_{ro} = (k_{rw}+k_{row})(k_{rg}+k_{rog})-(k_{rw}+k_{rg}) \qquad (2.13)$$

Estimates obtained from the new model were compared to three-phase relative permeability data of Corey [C.6], Dalton [D.2] and Saraf [S.5]. The comparisons showed that three-phase relative permeability can be predicted with good accuracy from two sets of two-phase data. However, these comparisons were least favorable in the region of high water and low gas saturations. He stated that the quality of the predictions in this region can be improved by using the residual oil data in three-phase region.

Dietrich and Bondor [D.11] (1976) described two variations of an indirect technique for predicting three-phase oil relative permeabilities. The first model was developed by Hirasaki which was a modification of Stone's model proposed in 1970. The second model was presented by Stone in 1973, as a revision of his first technique.

The expression for three-phase oil relative permeability derived by Hirasaki (Model I) is as follows Model I:

$$k_{ro} = (k_{row}+k_{rog}-k^{\circ}_{ro})+(S_w+S_o)\,(k^{\circ}_{ro}-k_{row})\,(k^{\circ}_{ro}-k_{rog})/k^{\circ}_{ro} \qquad (2.14)$$

where k°_{ro} is the oil relative permeability at connate water saturation.

While Stone's Model II is of the form of

$$k_{ro} = (k_{row}+k_{rw})(k_{rog}+k_{rg})-(k_{rw}+k_{rg}) \qquad (2.15)$$

which was corrected by Dietrich and Bondor for the case of a non-unit k°_{ro} as follows

Model II:

$$k_{ro} = (k_{row}+k_{rw})(k_{rog}+k_{rg})/k^{\circ}_{ro}-(k_{rw}+k_{rg}) \qquad (2.16)$$

Five sets of three-phase relative permeability data of Saraf [S.5], Donaldson and Dean [D.13], Holmgren and Morse [H.5], Leverett and Lewis [L.6] and Snell [S.11] were used to evaluate oil relative permeability (k_{ro}) values predicted by Models I and II.

These comparisons showed that

- The oil isoperms generated by Models I and II are convex toward 100 percent oil saturation which is consistent with the work of Snell and Saraf.

- Model I provides the best match for a case where the oil relative permeability at connate water and zero gas saturation is extremely low. ($k^{\circ}_{ro} < 0.1$)

- Model II gives better results in all applications with $k^{\circ}_{ro} > 0.3$.

Saraf and Co-workers [S.4] (1982) reported steady-state and unsteady-state measurements of three-phase relative permeability in fired Berea sandstone. The same core was used for both steady-state and unsteady-state tests. No cleaning procedure was used, but before the start of each run, the core was evacuated for several hours. Saturations were measured by material balance. The unsteady-state three-phase relative permeabilities were calculated using Sarem's procedure [S.7] (an extension of Welge's method). In the case of steady-state, all three phases were allowed to flow simultaneously. Capillary end effects were minimized by measuring pressure drops 2.5 cm from each end of the core.

Based on the steady-state measurements, the authors concluded that water relative permeability was a function of water saturation only and it did not depend on saturation history. Steady-state gas relative permeabilities were also found to be dependent on gas saturation alone. The gas relative permeabilities for steady-state flow were much lower than the unsteady-state results. The observed hysteresis effects were small for steady-state measurements.

Oil relative permeabilities were found to

depend on saturations of all the phases present and were not influenced by saturation histories.

The three-phase relative permeabilities were calculated using Stone's Models I and II with two sets of two-phase relative permeabilities. The comparision of these predictions with experimental results showed that predicted values of relative permeabilities were lower, especially in the region of low oil saturation, with the Model II predictions being the worst of the two.

Van Spronsen [V.1] (1982) reported measurements of three-phase relative permeabilities using the centrifuge technique on Weeks Island and Berea sandstone samples. The three-phase oil isoperms in Weeks Island samples were found to be concave toward the oil apex for the low value of permeabilities. This finding is contrary to the calculations using Stone's Model. There was a lot of scatter in the water relative permeabilities, but Van Spronsen claimed that the three-phase water relative permeability is not just a function of the water saturation. The results in the Berea sandstone samples showed that the oil and water isoperms are concave towards their respective apexes. Based on the shape of the isoperms on the ternary diagram, the author claimed that the three phase relative permeability

to oil or water was relatively insensitive to the presence of other phases.

O'Meara and Lease [O.2] (1983) reported measured relative permeabilities for oil, water and gas in Berea sandstone samples using an improved automated centrifuge. The automated centrifuge uses a linear photodiode array in conjunction with a microcomputer to image and identify recovered fluids from centrifuge rock samples. This method was used to measure both relative permeability and capillary pressure. The end-effect was overcome during the relative permeability experiment by using high centrifuge speed. Only few (about 10 points) three-phase relative permeability points were measured in Berea sandstone cores. No conclusion was given on the dependency of the three-phases on the saturations.

Summarizing the experimental evidence it can be found that the majority of experimentalists claim that water relative permeability is a function of water saturation alone. For the gas relative permeability the majority of experimentalists claim that it is a function of gas saturation alone.

More detailed review of three-phase gas/water/oil relative permeability have been done by Fayers and Matthews [F.1], Donaldson and Kayser [D.14],

and Saraf and McCaffery [S.6].

2.1.2.2 Three-Phase Flow of Water-Oil-Microemulsion

Hirasaki et al. [H.4] in 1980, developed a three-phase relative permeability model for surfactant flooding which was a modification of Stone's model. They stated that the three-phase relative permeability for surfactant flooding differs from three-phase water-oil-gas flow in the following respects:

- Endpoint saturations are variable.

- Saturations can become less than residual saturations due to the phase behavior.

- The curvatures of the relative permeability curves are variable.

- The microemulsion is the wetting phase at low salinities and the non-wetting phase at high salinities.

Another mathematical model developed for the three-phase flow at high capillary number is by Lake [L.1]. The model was developed with the basic philosophy which says that in the absence of original wetting phase, the intermediate wetting phase becomes the wetting phase (and vice versa). In his model the relative permeability functions are in the same form as in Hirasaki's model.

A full description of these two models will be presented in the following Chapters.

In 1982, MacAllister [M.1] reported the results of three-phase flow of microemulsion-oil-brine in a sandpack. He only performed three two-phase endpoints and three three-phase points. The microemulsion phase relative permeabilities were essentially unchanged since the microemulsion fractional flow was kept constant. Aqueous and oleic phase relative permeabilities seemed to be approximately equal and dependent on their individual saturations.

TABLE 2.1.1

Summary of Two-Phase Relative Permeability Results

Authors	Date	Porous Medium	Experimental Technique	IFT mN/m	Effect of lowering IFT on k_{ro}	k_{rw}	S_{or}	S_{wr}
Leverett [L.5]	1938	sandpack	steady-state	5-24	increases	increases	-	-
Talash [T.3]	1976	Berea	steady-state	-	increased	increased	decreased	unchanged
Batycky [B.4]	1978	sandpack	steady-state and unsteady-state	0.02-50	increased	increased	decreased	unchanged
Klaus [K.1]	1979	Berea	unsteady-state	0.015-39.8	increased	increased	decreased	minor reduction
Amaefule and Handy [A.2]	1981	Berea	steady-state and unsteady-state	0.07-34	increased	increased	decreased	decreased
Delshad [D.8]	1981	Berea	steady-state	0.001	increased	increased	decreased	decreased
McAllister [M.1]	1982	sandpack	steady-state	0.001	increased	increased	decreased	decreased
Fulcher [F.3]	1983	Berea	steady-state	0.039-37.9	increased	increased	decreased	decreased
Harbert [H.1]	1983	reservoir rocks	steady-state	0.14-2.26	decreased	increased	decreased	decreased
Torabzadeh and Handy [T.7]	1984	Berea	steady-state	0.015-0.187	increased	increased	decreased	decreased

TABLE 2.2

Summary of Three-Phase Relative Permeability Experimental Results

Authors	Date	Porous Medium	Experimental Technique	Saturation Measurement	End Effect	RELATIVE PERMEABILITY IS A FUNCTION OF k_{rw}	k_{ro}	k_{rg}
Leverett & Lewis [L.6]	1941	unconsolidated sand	steady-state	water by electrical resistivity & gas by P.V. rel.	neglected	S_w	S_o, S_w, S_g	S_g, S_o, S_w
Caudle [C.2]	1951	consolidated sandstone	steady-state	weighing & vacuum distillation	neglected	S_w, S_o, S_g	S_o, S_w, S_g	S_g, S_o, S_w
Corey [C.6]	1956	Berea sandstone	Hassler capillary method	gravimetric	minimized	S_w	S_o, S_w, S_g	S_g
Snell [S.11]	1961	unconsolidated sand	Hassler capillary method	water by RCL circuit & gas by neutron diffraction	eliminated	S_w, S_o, S_g	S_o, S_w, S_g	S_g, S_o, S_w
Sarem [S.7]	1966	Berea sandstone	unsteady-state	-	neglected	S_w	S_o	S_g
Donaldson & Dean [D.13]	1966	Berea sandstone & Arbucle limestone	unsteady-state	-	minimized	S_w, S_o, S_g	S_o, S_w, S_g	S_g, S_o, S_w
Saraf & Fatt [S.5]	1967	Boise sandstone	unsteady-state	NMR	eliminated	S_w	S_o, S_w, S_g	S_g
Schneider & Owens [S.9]	1970	Torpedo sandstone	unsteady-state	gas by x-ray, water by elec. resistivity	not discussed	S_w	S_o, S_w, S_g	S_g, S_o, S_w
Saraf [S.4]	1982	fired Berea sandstone	steady-state and unsteady-state	material balance	minimized	S_w	S_o, S_w, S_g	S_g
Van Spronsen [V.1]	1982	Berea sandstone	centrifuge method	volumetric balance	minimized	S_w	S_o	-
O'Meara & Lease [O.2]	1983	Berea sandstone	automated centrifuge	volumetric balance	minimized	-	-	-

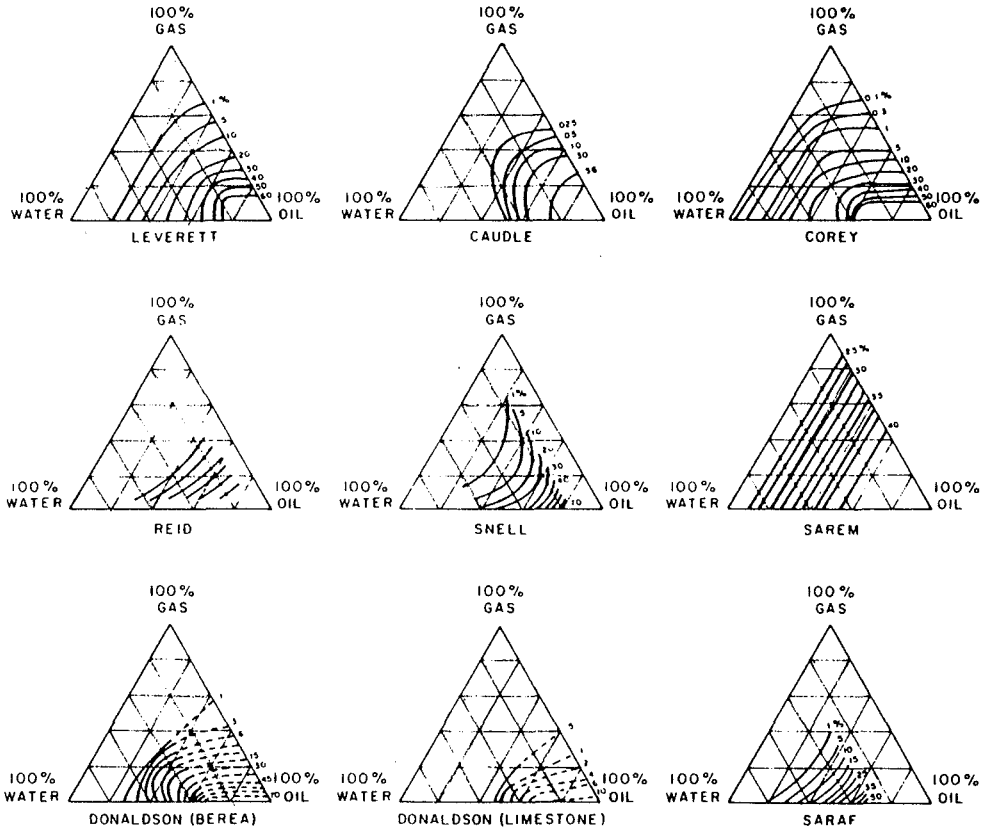

Figure 2.1 Published Three-Phase Oil Relative Permeability Isoperms (after Donaldson et al [D.14])

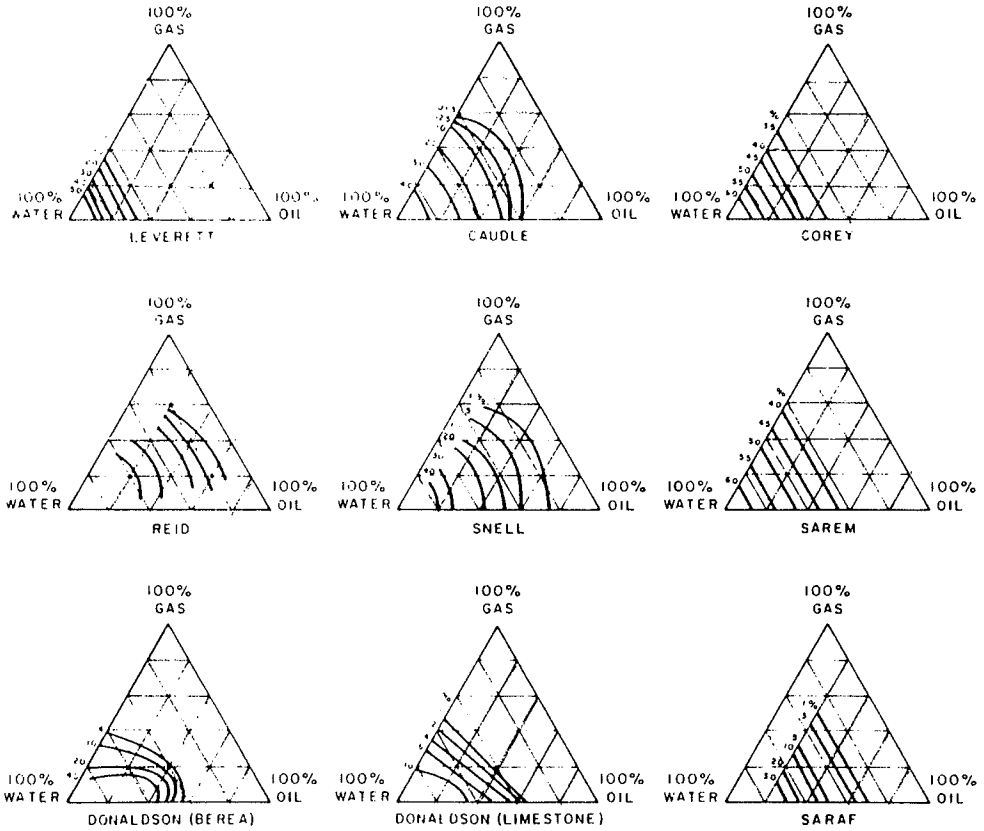

Figure 2.2 Published Three-Phase Water Relative Permeability Isoperms (after Donaldson et al [D.14])

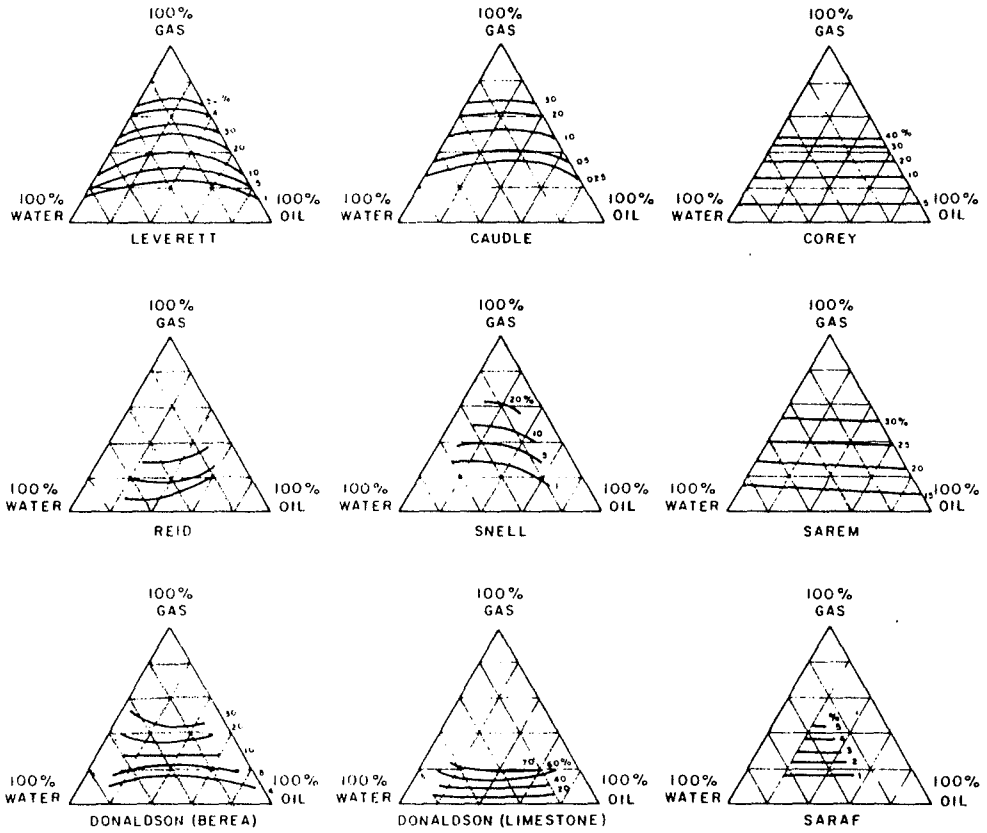

Figure 2.3 Published Three-Phase Gas Relative Permeability Isoperms (after Donaldson et al [D.14])

2.2 Capillary Desaturation Curve (CDC)

The flow of a pair of fluid phases through porous media is partly controlled by capillary forces. The inefficiency of any immiscible displacement process in a porous medium is partly due to capillary forces. The efficiency of the displacement can be increased by either increasing the viscous forces or reducing capillary forces by lowering the interfacial tension.

The degree of recovery of a residual phase by reduction of capillary forces depends upon their magnitude relative to the viscous forces. The ratio of these two forces is the capillary number. Various experimenters have proposed a number of different, although more or less equivalent, definitions of the capillary number.

Because of its significance to oil recovery from water wet reservoirs, most of the reported work has been carried out in strongly water wet porous materials with results determined only for displacement of the nonwetting phase by the wetting phase. The data on the desaturation of the wetting phase is rather sparse.

What follows is a review of reported experimental work correlating the capillary number to the residual saturations. Another recent review of the

literature on this subject has been done by Bhuyan [B.5] and an earlier review was done by Larson [L.3].

Figures 2.4 through 2.6 show capillary number correlations found by several experimenters for a variety of porous materials and a broad range of conditions.

In 1947, Brownell and Katz [B.9] reported capillary number correlations for consolidated sand and a variety of unconsolidated sandpacks. They applied the principle of dimensional analysis to find the dimensionless correlating factor as $N_c = \frac{k\Delta P}{Lg_c\sigma\cos\theta}$. The log-log plot of residual water saturation as a function of capillary number was a straight line and was formulated as

$$S_{wr} = \frac{1}{86.3}\left(\frac{k\Delta P}{g_c L\sigma\cos\theta}\right)^{-0.264} \qquad (2.17)$$

Ojeda, Preston, and Calhoun [O.1] (1953) carried out displacement tests in acid treated Berea cores. Fluids used were n-octane as the nonwetting phase and water with and without surfactant additive as the wetting phase. The log-log plot of residual oil saturation versus capillary number ($N_c = \frac{k\Delta P}{L\sigma}$) showed a linear correlation.

Dombrowski and Brownell [D.12] in 1954, reported measured capillary desaturation data using different types of fluids in unconsolidated sandpacks and also packs of a variety of particles such as glass spheres, quartz and others. The fluids used were mineral oil, kerosene, distilled water, acetic acid and calcium chloride solution. These fluids (wetting phase) were displaced by air using gravitational and centrifugal forces as driving forces. The definition of capillary number used included the effects of these forces as follows

$$N_c = (\frac{k}{g})(\frac{\rho + \rho a + \Delta P/L}{\sigma \cos\theta}) \qquad (2.18)$$

which includes permeability (k); fluid density (ρ); surface tension (σ); contact angle (θ); centrifugal force, a, and pressure gradient ($\Delta P/L$). Their results showed that the residual saturation was less than 0.10 for the capillary numbers ranging from 10^{-6} to 10^{-2} and was zero at capillary number of around 2.0.

Moore and Slobod [M.3] (1956) studied the displacement of oil by water in several sandstone samples. They carried out the tests in both short (2.54

cm plug) and long (up to 3 m) cores. The fluids used for the aqueous phase were water, ethylene glycol, glycerine or mixtures of them. The oil phase was either pentane, triisobutylene, or mineral oil. Low IFT fluids were prepared by blending water, naphtha and tertiary butyl alcohol. The oil saturations at the time of water breakthrough were plotted against the capillary number for Torpedo, Elgin, and Bandera outcrop sandstone samples. Their results indicated that oil saturation remained constant up to a capillary number of 10^{-5}.

Taber [T.1] in 1968, reported the results of a large number of oil displacements in several Berea cores. The fluids used were Soltrol C, a C_{10} to C_{12} aliphatic hydrocarbon as the oil phase and 2.5 percent brine or equilibrated surfactant solution as the aqueous phase. It was shown that there was no removal of residual oil until a specific critical value of $\frac{\Delta P}{L\sigma}$ was exceeded. This value was found to be in the range of 2 to 6 (psi/ft)/(dyne/cm). The effect of individual variables in the correlating group on the residual oil saturation was studied.

Lefebvre du Prey [L.4] (1970) reported the measurement of CDC using three different artificial sintered media, namely, sintered Teflon, stainless steel

and alumina. The three media used correspond to three possible cases of wettability. The contact angle measurements showed that Teflon is strongly oil-wet, alumina is strongly water-wet and stainless steel has intermediate wettability. Different pairs of fluid were used with interfacial tension varying from 0.25 to 35 dyne/cm, and viscosity from 0.9 to 60 mPa.s. The residual wetting and nonwetting phase saturations were obtained as a function of the correlating group $\pi = \frac{\sigma}{\mu v}$ which is the inverse of capillary number. His results indicated that for all the three types of media used, the residual wetting saturations were higher than the nonwetting phase residuals at a comparable π number.

Foster [F.2] in 1973 carried out nonwetting phase displacement experiments in fired Berea sandstone cores. There was no mention in his paper on how the high capillary number ($N_c = \frac{\mu_w u_w}{\sigma \phi}$) values were achieved. The results showed that the plateau residual nonwetting phase saturations were in the range of 40% to 50% while at the capillary number of around 10^{-2} the residual saturation was zero.

Ehrlich, Hasiba, and Raimondi [E.1] (1974) reported oil displacement results in Berea and Jelm sandstone cores. They indicated that the correlating

group $\frac{k\Delta P}{L\sigma\phi}$ was constant for both types of rocks. The residual oil saturations were plotted against $\Delta P/\Delta P_{critical}$. The residual oil saturation was 61% of the waterflood residual at $\Delta P/\Delta P_c$ of 10 and was around 2% at $\Delta P/\Delta P_c$ of 1.

Abrams [A.1] in 1975, reported the results of displacement tests in six different sandstone cores and one limestone core to show the effect of viscosity, interfacial tension and velocity on residual oil saturation. Abrams could correlate the residual oil saturations to the dimensionless group defined as $F = (\frac{u\mu_w}{\sigma})(\frac{\mu_w}{\mu_o})^{0.40}$ for strongly water-wet media. Displacement tests were performed using cores with high initial oil saturation at the beginning of each flood. At this saturation, the nonwetting phase is connected from one end of the core to the other. Therefore, the correlations found were for displacement of continuous oil only. The plateau residual nonwetting phase saturations were ranged from 30 to 38 percent (at $F = 10^{-7}$ to 10^{-6}) for all the core samples and the complete desaturation occurred at F values around 10^{-2} to 10^{-1}.

Gupta and Trushenski [G.3] in 1978, reported the measured capillary desaturation curves for both

wetting and nonwetting phases in fired and acidized Berea sandstone cores. The fluids used were equilibrated n-decane and aqueous micellar solution as the nonwetting and wetting phases respectively. Three different (30.5 cm long and 5.08 cm in diameter) Berea cores were used for the experiments.

Their results indicated a plateau residual oil saturation of 25 percent for all the three cores. They carried out the displacement up to a capillary number ($N_c = \frac{u\mu}{\sigma}$) of 10^{-2} where the residual oil saturation was approximately 2.5 percent. Their results also showed that a capillary number 10 times higher is required to displace the wetting phase. The plateau residual water saturation was 45 percent and at the capillary number of 10^{-2} the residual water saturation was around 7 percent.

Batycky and McCaffery [B.4] reported in 1978, the results of nonwetting displacements in two unconsolidated sandpacks. Displacement measurements were conducted for three interfacial tension levels, nominally 50, 0.2 and 0.02 mN/m. The fluids used were equilibrated n-decane or n-octane as the oil phase and microemulsion as the aqueous phase. The capillary number defined as $N_c = \frac{u\mu}{\sigma\phi}$ was varied by changing IFT and flow rate. The plateau residual oil saturation was around 7 percent and

the complete displacement occurred at the capillary number of 2×10^{-3}.

Bardon and Longeron [B.2] in 1980 conducted experiments to measure capillary desaturation curves for Fontainebleau sandstone cores. Most of the displacement tests were performed using equilibrated n-heptane and methane at 71°C. The liquid saturations displaced by the vapor phase were plotted as a function of capillary number ($N_c = \frac{u\mu_w}{\sigma}$). Their results indicated that the liquid saturation was constant up to a capillary number of around 10^{-6} and decreased significantly with increasing N_c, and approached zero at capillary number of 6.5×10^{-4}.

Chatzis and Morrow [C.4] (1981) presented capillary number relationships for displacement of residual oil from sandstone samples. The core samples were fired to about 800°C for one hour and cleaned with IPA between runs. The fluids used were mineral oil and brine. Normal waterfood residual oil saturations varied between 22 to 43 percent for the 16 sandstone samples. For the various Berea sandstone samples used, the residual oil saturations varied between 30 and 43 percent. The displacement tests were conducted for both continuous and discontinuous (mobilization) oil phase.

Their results indicate that complete recovery of oil corresponded to values of $N_c = \frac{k\Delta P}{L\sigma}$ of about 1.5×10^{-3} as compared with about 2×10^{-5} for onset of mobilization. The results also showed that after displacing 50% of the plateau residual oil saturations, capillary desaturation curves for the two types of displacement were indistinguishable.

Amaefule and Handy [A.2] in 1981, reported capillary desaturation curves for both wetting and nonwetting phases in fired Berea sandstone cores. Equilibrated phases of a surfactant solution were used for the displacement tests. Normalized residual oil and water saturations were presented as a function of capillary number ($N_c = \frac{u\mu}{\sigma}$). The plateau residual saturations were 0.2 and 0.4 for oil and water phases respectively. At a capillary number of 6.5×10^{-3}, the residual water saturation was 0.20 while oil saturation was only 0.02. Log-log plots of residual oil and water saturations against capillary number fell on a straight line.

Mohanty and Salter [M.2] (1983) reported experimental results on the residual nonwetting phase in a completely and strongly nonwetting medium, a completely and strongly wetting medium, and a mixed-wet medium. The

three media used in their work were fired, acidized Berea sandstone, silanized Berea sandstone, and silanized and caustic treated Berea sandstone as strongly water-wet, strongly oil-wet, and mixed-wet media, respectively. The cores were 5.08 cm in diameter and 5.08 cm long. Oil phase fluids used were mineral oil and iso-octane. The capillary number ($N_c = \frac{k\Delta P}{L\sigma}$) was varied by changing the flow rate only. The results showed that the plateau residual oil saturation in strongly water-wet media was 0.35 and it decreased sharply by increasing the capillary number and was zero at N_c of around 10^{-3}. The residual oil saturation in oil-wet cores was higher (around 0.48) than in the water-wet medium and it changed more steadily. The residual oil saturation of 0.28 was observed at a capillary number of 10^{-3} in oil-wet cores. Residual saturations measured in the mixed wet core were similar in shape to those found in strongly oil-wet cores. Depending on the viscosity of oil used, the magnitude of the end-point oil saturation was changed. The lowest plateau residual oil saturation observed was for iso-octane (low viscosity) in the mixed wet core.

Fulcher, Eterkin, and Stahl [F.3,F.4] (1983) conducted displacement tests in fired Berea sandstone cores using alcohol as the interfacial tension reducer

and glycerin as the wetting phase viscosifier. The capillary number defined as $\frac{u\mu_w}{\sigma\phi}$ was changed by varying flow rate, IFT, and viscosity values. The tests were carried out in 60.96 cm long, 5.08 cm in diameter cores fired at 1000°C. Their results indicated a large reduction in residual oil saturation from 0.4 to 0.0, corresponding to a capillary number increase from 10^{-6} to 10^{-2} respectively. There was much scatter in the aqueous phase residual saturation data and no correlation with capillary number was found.

Recently (1985), Bhuyan [B.5] measured the capillary desaturation curves for both aqueous and oleic phases using a 10 cm long and 2.5 cm diameter Berea sandstone core under three different wetting conditions. The fluid pair used was the equilibrated phases of a brine-isooctane-isopropanol mixture. He obtained these three wettability conditions as follows

1- Using the core as received (untreated core)

2- Drying the core after cleaning with isopropanol and then saturating and flushing with 0.25 Dri-Film 104 Solution in toluene and then drying with vacuum (0.25% D-F treated core).

3- Drying the Berea core after cleaning with isopropanol and then saturating and flushing with 2.5

Dri-Film 104 Solution in toluene and drying it with vacuum (2.5% D-F treated core).

Both Amott and USBM methods were used to determine the wettability of the core. Amott's wettability index, ratio of the spontaneously imbibed volume to the total volume of the phase imbibed under a centrifuge force, showed that

- The untreated core is moderately strongly aqueous-phase-wet,

- The 0.25% D-F treated core is moderately strongly oleic-phase-wet, and

- The 2.5% D-F treated core is somewhat stronger oleic-phase-wet.

Bhuyan, however, obtained completely opposite wettabilities in all three cases when using the USBM wettability index values.

His results based on the capillary desaturation measurements are summarized as follows

- The critical capillary number ($N_c = \frac{k\Delta\Phi}{L\sigma}$) for oil phase in untreated core found to be 1.5×10^{-5} with the complete desaturation at a capillary number of 5.2×10^{-4} which were in agreement with the results obtained by Chatzis and Morrow [C.4]. For the aqueous-phase desaturation process, the critical capillary number was

about 3 x 10^{-5} which also agrees well with Gupta and Trushenski's [G.3] wetting phase data.

- In the 0.25% D-F treated core, the critical capillary numbers for oil and aqueous phases were around 8 x 10^{-6} and 8 x 10^{-4} respectively.

- The critical capillary number for oleic phase in a 2.5% D-F treated core was not established since the oleic phase was the strongly wetting phase in this case. For the aqueous phase, the critical capillary number was about 6 x 10^{-6} and the CDC showed a significant change in slope when the residual saturation was about 50% of initial plateau value.

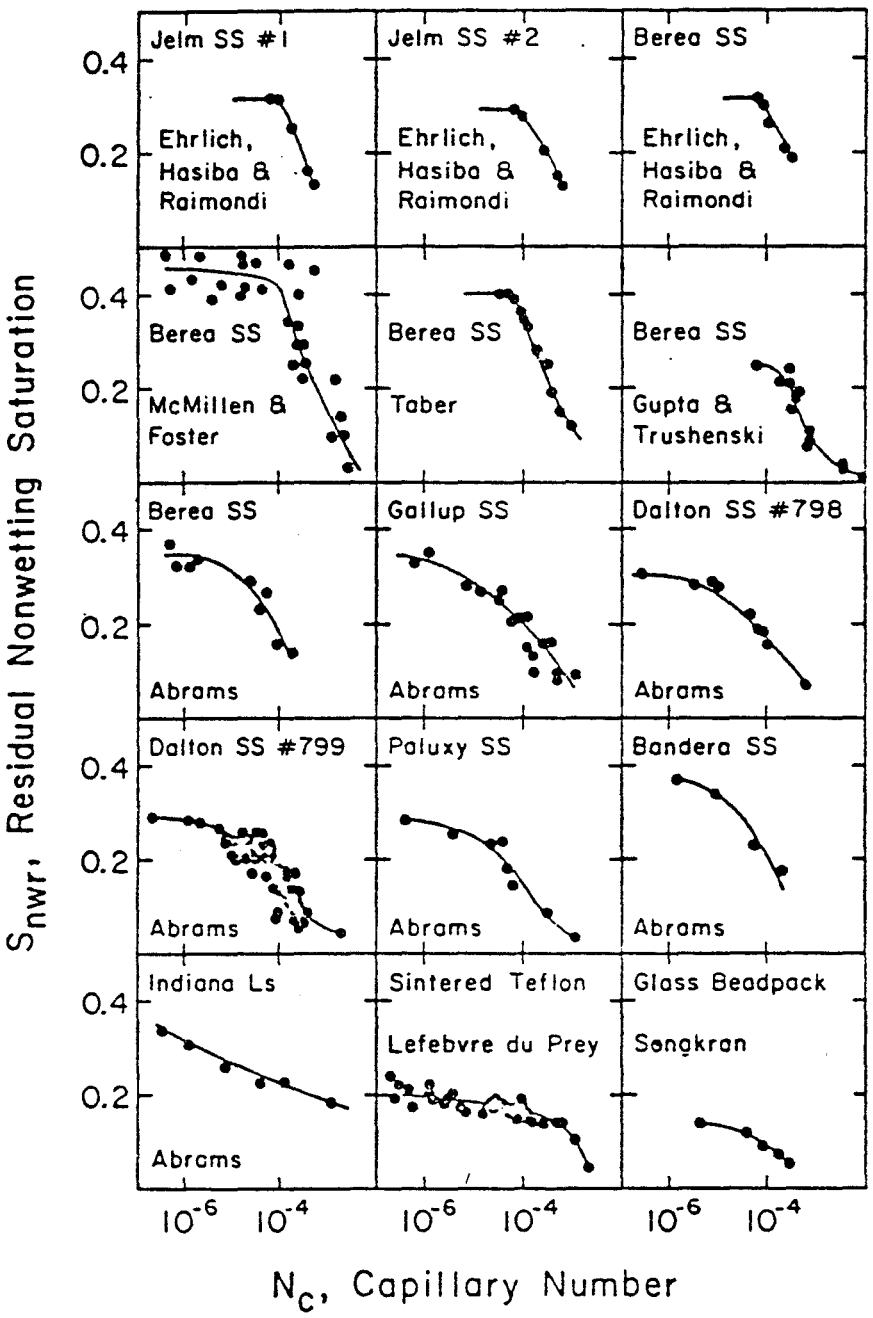

Figure 2.4 Capillary Number Correlation for a Variety of Porous Materials (after Larson et al [L.3])

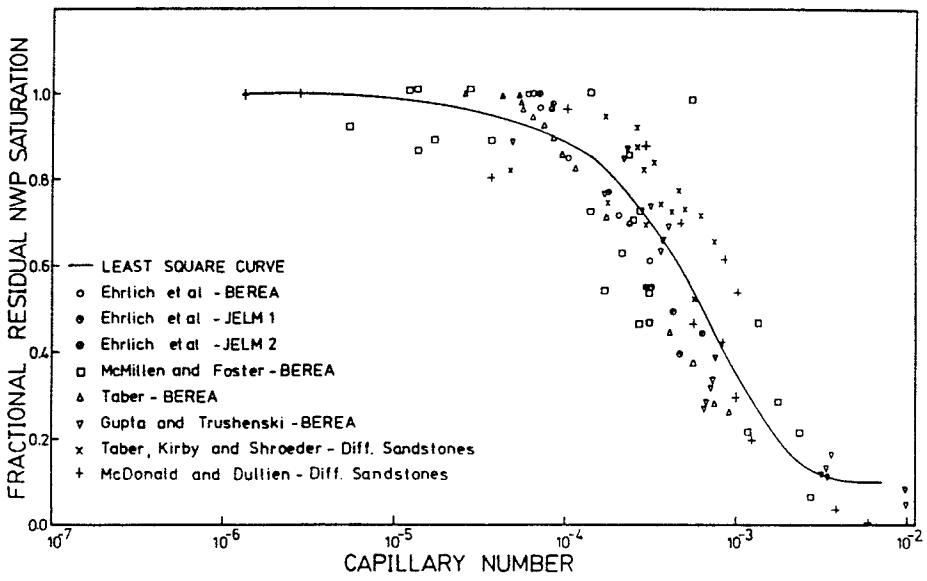

Figure 2.5 Fractional Non-Wetting Phase Saturation for Displacement (after Ramakrishnan et al [R.3])

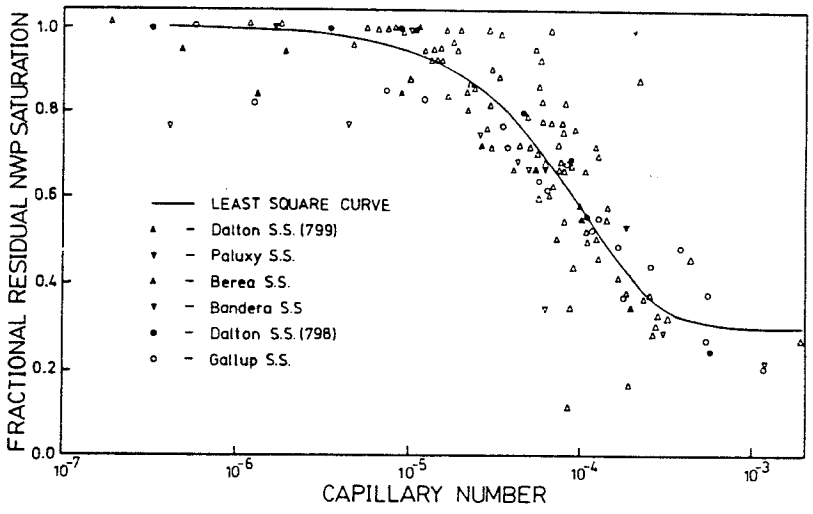

Figure 2.6 Fractional Non-Wetting Phase Residual for Mobilization (after Ramakrishnan et al [R.3])

2.3 Dispersion - Capacitance

When a fluid containing a chemical or radioactive tracer in solution is displaced from a porous medium by the same fluid without a tracer, this miscible displacement results in a tracer concentration distribution which depends on microscopic flow velocity, tracer diffusion rates and other chemical and physical processes. The concentration of tracer gradually increases going upstream from its initial value, usually zero, to its full concentration as injected for the case of a large slug or continuous injection; otherwise a pulse is formed with a bell-like shape for the small slug case. This spreading of the tracer is usually called dispersion in the permeable medium. Dispersion is one of the important phenomena known to depend fundamentally on flow conditions as well as on fluid and medium properties.

Most of the work reported to date has been on single phase flow. One of the earliest studies was reported by Brigham et al. [B.8] in 1961. Blackwell [B.6], Brigham et al. [B.8], and Shuler [S.10] have shown that for a miscible and uniform flow (uniform in both rock and fluid properties) in a saturated medium, the flow can be described by the convection-dispersion

equation. In this equation, the flow can be characterized by a single-parameter, the Peclet number (N_{pe}).

Raimondi et al. [R.2], Thomas et al. [T.5], Stalkup [S.13] and Shuler [S.10] have shown that in actual miscible displacements in an unsaturated medium, the effluent composition curves are not symmetric and have long tails and cannot be predicted by the convection-dispersion equation.

Deans [D.3] and Coats and Smith [C.5] in 1963 proposed models to account for the asymmetry. Both models (capacitance) divide each phase into two fractions flowing and deadend. The matching parameters of the capacitance models are as follows

- Flowing fraction
- Peclet number
- Mass transfer coefficient

Only a few attempts have been made to measure the dispersion in multiphase flow.

What follows is the literature review on both experimental and theoretical works reported during single and multiphase flow in porous media.

2.3.1 Single Phase Displacements

Brigham, Reed and Dew [B.8], in 1961, were

among the first who studied the mixing during miscible displacements in both glass bead packs and natural cores (Berea and Torpedo sandstones). The effect of velocity, travel length, beadsize, diameter of beadpack, and viscosity ratio on the amount of mixing was investigated. They concluded that

(1) dispersion is proportional to the rate to the 1.2 power for natural cores at reservoir rates, but not for the glass beadpacks,

(2) at very low rates, the dispersion is proportional to the Fick's diffusion coefficient,

(3) the dispersion depends on the viscosity ratio. An unfavorable viscosity ratio caused elongated and asymmetric breakthrough curves.

The results of the work done by Taylor [T.4]; Perkins and Johnston [P.1]; Blackwell [B.6]; Shuler [S.10] and others can be summarized as follows

- The dispersion is the sum of a diffusion term and a mechanical, microscopic, mixing term which depends on the frontal velocity ($v = \frac{q}{A\phi}$) to a power β as follows

$$K_\ell = \frac{D}{F\phi} + \alpha_\ell \, v^{\beta\ell} \qquad (2.19)$$

$$K_t = \frac{D}{F\phi} + \alpha_t \, v^{\beta t} \qquad (2.20)$$

- The dispersivities are different for longitudinal and transverse directions and depend on the porous material.

- The ratio α_ℓ/α_t is on the order of 30.

- The power exponent is usually about 1.2, but varies between at least 1.0 and 1.4.

The theoretical treatments on dispersion show that the flow in a porous rock can be described by a convection-dispersion equation of the form,

$$\phi \frac{\partial C}{\partial t} + \nabla\cdot(uC) - \phi\nabla\cdot K\nabla C = 0 \qquad (2.21)$$

And in one-dimensional corefloods with uniform velocity, we have

$$\frac{\partial C_D}{\partial t_D} + \frac{\partial C_D}{\partial x_D} = \frac{1}{N_{pe}} \frac{\partial^2 C_D}{\partial x_D^2} \qquad (2.22)$$

where u is the Darcy velocity, $x_D = x/L$, $t_D = \frac{ut}{\phi L}$ and $\frac{1}{N_{pe}} = \frac{\phi K}{uL}$, the Peclet number. Therefore, in this case, the flow is characterized by a single parameter, the Peclet number.

The solution to Eq. (2.22) is given by several authors for different sets of boundary conditions. For

one set of boundary condition (infinite medium), the solution is given by Aronofsky and Heller [A.3] as follows

$$\frac{C}{C_o} = \frac{1}{2}\,\mathrm{erfc}\left(\frac{x - ut}{2\sqrt{Kt}}\right) \qquad 0 < x < \ell \tag{2.23}$$

The dispersion coefficient can be determined from effluent composition data.

A plot of effluent compositions against pore volumes injected will be slightly asymmetric due to the fact that the transition zone continues to grow during the time period during which it is produced. In actual displacements, however, history plots are often very asymmetric and cannot be fit with a simple convective-dispersion model. Deans [D.3] in 1963 was among the earliest who developed a three-parameter model to explain deviations in observed effluent concentration from that predicted by the convective-dispersion model.

Deans [D.3] in 1963 developed a three-parameter mathematical model for one dimensional flow in porous media. He assumed that some portion of the fluid in the porous medium might be stagnant, so that bypassed fluid (in deadend pores) would be recovered only by mass

transfer into the flowing stream. Deans included only the diffusion term in his model, but used a numerical dispersion in the solution of the diffusion equation.

Coats and Smith [C.5] (1964) proposed a three parameter model to account for the asymmetry observed in effluent concentration curves. This model acounted for both longitudinal dispersion and mass transfer from dead-end pores. Similar to the model proposed by Deans, this model defines a stagnant fraction (1-F) of the fluid volume containing an average concentration $(\overset{+}{C})$. If a first-order rate expression is used for the mass transfer between the stagnant volume and the main flow channels, the resulting equations are

$$F \frac{\partial C}{\partial t_D} + (1-f) \frac{\partial \overset{+}{C}}{\partial t_D} + \frac{\partial C}{\partial x_D} - \frac{1}{N_{pe}} \frac{\partial^2 C}{\partial x_D^2} = 0 \qquad (2.24)$$

$$(1-F) \frac{\partial \overset{+}{C}}{\partial t_D} = M_D (C - \overset{+}{C}) \qquad (2.25)$$

where C is the concentration in the flowing stream, F the flowing fraction, $\overset{+}{C}$ is the concentration in the deadend volumes, $M_D = \frac{\phi LM}{u}$, and M is the mass transfer coefficient. Therefore, besides the dispersion

coefficient, the flowing fraction and the mass transfer coefficient are introduced as new parameters. Coats and Smith conducted experiments in Ottawa sand, Torpedo sandstone and Alundum using five percent calcium chloride as the injection fluid. The cores were initially saturated with 5 percent sodium chloride. For those consolidated cores which exhibited asymmetry and early breakthrough of 50 percent of the injected concentration, Coats and Smith obtained a much improved fit with the data using the capacitance model. The flowing fraction values ranged from 0.9 to 0.976. In these cases it was found that forcing a poor fit of the diffusion-type model would result in prediction of too large of a dispersion coefficient. The capacitance and the convection-dispersion (C-D) models gave about the same value for the dispersion coefficient for the cases that data were matched well by the C-D equation.

Brigham [B.7] in 1974 reported laboratory displacement results in Zama Lake core that exhibited some deadend pore volume. The deadend model of Coats and Smith was used to fit the data. The matching parameters were found to be F = 0.92, M_D = 0.15, and N_{pe} = 11.45. He also showed that the convective-dispersion equation can describe the flowing or in-situ concentration,

depending on the boundary conditions chosen for the solution.

In 1977, Baker [B.1] reported the results of extensive miscible displacements in carbonate cores. He examined the velocity dependence of the capacitance parameters. The capacitance equations were solved in the complex frequency domain by taking the Laplace transforms of the equations and combining the resulting ordinary differential equations. The data then were transformed into the frequency domain and an algebraic curve-fitting procedure was used. The displacement tests were run using benzene and meta-xylene using both Berea sandstone and limestone cores. The capacitance model was used to match the composition data. For the Berea core, the data were fit using a dispersion model. But, the dispersion model was not appropriate for the limestone sample due to its pronounced heterogeneity. The flowing fraction for the data obtained in limestone core was found to be independent of velocity with an average value of $F = 0.64$. For the limestone core, Baker found the dispersion coefficient increased to the 1.0 power of velocity, and the mass transfer coefficient to the 0.84 power.

Spence and Watkins [S.12] (1980) reported

miscible displacement data for carbonate, Boise and Berea cores. The displacements consisted of stabilized tertiary CO_2-flood displacements of live reservoir fluid and stabilized CO_2 floods of cores containing no water saturation. The core flood results were matched using the capacitance model of Coats and Smith. For the data in sandstone cores, an excellent fit was found with little capacitance (F = 0.957) and a small amount of dispersion. The fit was insensitive to the mass transfer coefficient. On the contrary, the data obtained in carbonate cores showed substantial capacitance (F = 0.828) and dispersion. The dependence of matching parameters on velocity was examined. They observed that for the Berea sandstone only, the dimensionless mass transfer coefficient (M_D) was independent of velocity. Flowing fraction declined with increasing velocity, and the dispersion coefficient varied to the 1.26 power of velocity. For the carbonate cores, the parameter M_D and Peclet number (N_{pe}) were insensitive to the velocity. The flowing fraction increased slowly with decreasing velocity. These results implied that both the dispersion and mass transfer coefficients were linearly dependent on velocity.

Batycky, Maini, and Fisher [B.3] (1982)

reported the results of miscible gas displacements in one Berea sandstone and several carbonate cores. They examined the dependencies of the capacitance parameters as functions of the velocity and water saturation. Dispersion coefficients were determined using the Coats-Smith model. The effluent concentration profiles were obtained by finite difference solution to capacitance equations. Dispersion coefficients were not affected by the presence of residual water saturation for either the carbonates or the sandstone. The dispersion coefficients obtained in the carbonate cores showed a strong dependency on the flow velocity. The values for flowing fraction of gas in the presence of water saturation ranged from 0.524 to 0.978. The flowing fraction was found to be above 0.9 for the Berea core and to be decreasing by increasing the flow velocity in the carbonate cores. The dependency of flowing fraction on water saturation was also examined. They found that the flowing fraction was insensitive to the water saturation in Berea core but it decreased as water saturation increased in the carbonate cores.

2.3.2 Multiphase Displacements

Raimondi, Torcaso and Henderson [R.2] appear to be among the first who studied the effect of varying

wetting phase saturation on miscible displacements. The displacements were carried out at water saturations ranging from zero to 0.866 using a 1.83 m long, 5.08 cm diameter Berea sandstone core. The miscible displacement was carried out in the oil phase only at water saturations up to 0.42. At water saturations above 0.42 miscible displacement was carried out simultaneously in both phases. The water phase was a brine solution. The displaced oil was commercial heptane and the displacing phase was ethyl benzene. Their results indicated that the displacement of the wetting phase was not pronouncedly affected by the presence of the non-wetting phase. But, the displacement of oil was strongly dependent on the initial oil and water saturations. The mixing coefficient of the wetting phase was found to lie between 0.16 and 3.4 cm for a wide range of saturation conditions. They also observed that all of the non-wetting phase was recoverable by miscible displacement even at low saturations.

Thomas, Countryman, and Fatt [T.5] in 1963 studied dispersion for two-phase immiscible flow in Boise sandstone. The cores were 1.52 m long and 5.08 square in cross section. The fluids used were commercial mixed hexane as the oil phase and a solution of sucrose and

methanol in water as the labelled water phase. The sucrose-methanol solution acted as double tagged water in which the methanol was a fast diffusing tracer to indicate both mixing and molecular diffusion while the slow diffusing sucrose showed only the effect of mixing. The displacement efficiency in the oil phase was also measured using liquid paraffin. The core was saturated with liquid paraffin, and then air was injected to establish a non-wetting saturation. Their results indicated that the breakthrough curve, when there was no paraffin, was symmetric and passed through the 50% concentration point at one pore volume throughput. When paraffin (wetting phase) was added, the displacement of water (non-wetting phase) by an aqueous solution gave very asymmetric breakthrough curves which showed early breakthrough. They concluded that some of the non-wetting phase was located in dead-end or dendritic pores and such flows could not be described by a convection-dispersion model.

Stalkup [S.13] (1970) reported dispersion for a nonwetting phase using consolidated sandstone cores (Berea, Boise, Torpedo). The displacements were conducted at high water saturations in 2.43-10.97 m long cores where oils were displaced by propane. His results

also supported the hypothesis that much of the bypassed oil is in communication with the flowing solvent by diffusion. The breakthrough curves of nonane (C_9) displacing undecane (C_{11}) at varying water saturation were matched using the Coats-Smith model. However, the displacement of C_9 by propane could not be successfully predicted by the Coats-Smith model. Stalkup argued that the diffusion of solvent into bypassed oil and of bypassed oil into flowing solvent might be characterized by a spectrum of mass transfer coefficients. A model was proposed in which two separate stagnant fractions were allowed to have different mass transfer coefficients. The model would be represented as follows

$$\frac{1}{N_{pe}} \frac{\partial^2 C}{\partial x_D^2} - \frac{\partial C}{\partial x_D} = f\frac{\partial C}{\partial t_D} + F_1\frac{\partial \overset{+}{C}_1}{\partial t_D} + F_2\frac{\partial \overset{+}{C}_2}{\partial t_D} \qquad (2.26)$$

$$F_1 \frac{\partial \overset{+}{C}_1}{\partial t_D} = M_{D_1}(C - \overset{+}{C}_1) \qquad (2.27)$$

$$F_2 \frac{\partial \overset{+}{C}_2}{\partial t_D} = M_{D_2}(C - \overset{+}{C}_2) \qquad (2.28)$$

The two-stagnant-volume model did improve the

match to experimental results, but the agreement was still not as good as for the stable miscible displacements.

Shuler [S.10,R.4] in 1978, reported the results of miscible displacements in saturated and also partially saturated porous media. The sucrose displacements were conducted in an approximately 26.7 cm long and 3.81 cm diameter fired Berea cores. The breakthrough curves for the saturated core (S_w = 1.0) were symmetric with 50% concentration point at about one pore volume of fluid injected. The data were matched using both convective-dispersion and capacitance models. The dispersion coefficients obtained from both models were essentially the same and were increasing with the slope of 1.35 with the velocity. The breakthrough curves of the partially saturated core (S_w = 0.68, S_{or} = 0.32) were matched using the capacitance model. The flowing fraction ranged from 0.87 to 0.98 and showed a slight decrease with an increase in velocity. Shuler also injected both oil and water at a fixed volumetric ratio (f_w =0.5) varying the velocity. The tracer (sucrose) effluent concentration curves were modelled using the capacitance model. The dispersion coefficient were again increasing with velocity with about the same slope as in the saturated

cores. His conclusions were that

- The dispersion coefficient at a given velocity was higher at lower water saturations.

- The flowing fraction was in the order of 0.95 and velocity independent at low water saturation.

- The mass transfer coefficient increases with velocity at all saturations with a slope of about 1.20.

- Use of a three-parameter model to match the tracer data indicated that little capacitance mixing occurred for a single-phase, but became more important as the medium was desaturated. The dispersion model seemed adequate for non-partitioning tracer in a single-phase flow and at residual oil saturation in laboratory cores.

Salter and Mohanty [S.3] in 1982 reported extensive two-phase steady-state corefloods in an acidized and fired Berea core. The displacement tests were performed using tracers in both the wetting and non-wetting phases. The experiments were conducted in the primary drainage, imbibition, and secondary drainage directions over a wide range of fractional flows. The Berea core used was 121.5 cm long and 5.08 cm diameter. The injection fluids were sodium chloride solution at different salinity and various pure hydrocarbons. The miscible displacements in each phase were performed with

matched viscosity fluids to eliminate the complications of flow instabilities. The capacitance model used was based on the Coats-Smith model with the modification of dividing each phase into three fractions: flowing, dendritic, and isolated. The effluent tracer concentration curves in both phases were matched using the model. Their results indicated that

- The recovery of tracer in the wetting phase was 100% in every case, while the recovery of tracer in the non-wetting phase was in the range of 37 to 99 percent.

- The dispersion coefficients, during the two-phase flow, of both the wetting and non-wetting phases were higher than the single-phase dispersion coefficient.

- The flowing fraction for brine phase was decreasing at low saturation ($S_o < 0.5$) and increasing at higher values of oil saturation. The flowing fraction of oil phase during drainage, imbibition, and secondary drainage cycles increased as the oil saturation increased.

All of the results mentioned are for high tension fluids with no mass transfer between the phases. The work done at the University of Texas by Delshad [D.8,D.9], McAllister [M.1], and Delshad [D.6] is believed to be original in the sense that they studied

for the first time the effect of low interfacial tension and interphase mass transfer on dispersion during single, two, and three-phase flows in both Berea sandstone cores and a sandpack.

CHAPTER 3

THEORETICAL MODELS

In this chapter, the description of the equations used in the determination of phase saturation, dispersion coefficient, dispersivity, mass transfer coefficient, flowing and dendritic fractions and other related quantities are introduced.

Delshad and Co-workers [D.10] in 1981 gave the derivation and solution of the convection-diffusion equation for the multiphase flow of low interfacial tension fluids with partitioning tracers. The capacitance-dispersion model developed here is based on Salter and Mohanty's [S.3] approach but with a different method of solution.

The later section in this chapter gives equations for estimating phase saturation during steady-state multiphase flow using both material balance and tracer breakthrough data.

The equations used in determination of permeability, relative permeability, relative mobility and capillary number are found in Appendix A.

3.1 Convection-Diffusion Model

The material balance equation for an ideal, noninteractive tracer i, which partitions at the most between two phases (1 and 3) during multiphase flow through a homogeneous, linear porous media is described by convection-diffusion equation as follows:

$$\phi A \frac{\partial}{\partial t}(S_1 C_{i1} + S_3 C_{i3}) + q \frac{\partial}{\partial x}(f_1 C_{i1} + f_3 C_{i3}) = \phi A \frac{\partial}{\partial x}(S_1 K_{i1} \frac{\partial C_{i1}}{\partial x} + S_3 K_{i3} \frac{\partial C_{i3}}{\partial x}) \quad (3.1)$$

Arbitrary choose phases 1 and 3 for the phases between which tracer i partitions. The phase saturations and fractional flow rates are considered constant since dispersion experiments are performed at steady-state. The partition coefficient for tracer i $(K_{31}^{(i)} = \frac{C_{i3}}{C_{i1}})$, and longitudinal dispersion coefficients (K_{i1}, K_{i3}) are also constant for a given experiment. Then the equation 3.1 becomes

$$(S_1 + S_3 K_{31}^{(i)}) \frac{\partial C_{i1}}{\partial t} + \frac{q}{A\phi}(f_1 + f_3 K_{31}^{(i)}) \frac{\partial C_{i1}}{\partial x} = (S_1 K_{i1} + S_3 K_{i3} K_{31}^{(i)}) \frac{\partial^2 C_{i1}}{\partial x^2} \quad (3.2)$$

Define dimensionless variables as follows

$$C_D = \frac{C_{i1}}{C^{\circ}_{i1}},\ x_D = \frac{X}{L},\ t_D = \frac{qt}{A\phi L} \cdot \frac{(f_1 + f_3 K^{(i)}_{31})}{(S_1 + S_3 K^{(i)}_{31})} \equiv \frac{v_T \cdot t}{L} \tag{3.3}$$

where

$$t^{BT}_{Di} = \frac{S_1 + S_3 K^{(i)}_{31}}{f_1 + f_3 K^{(i)}_{31}} \tag{3.4}$$

and also define the weighted average of dispersion coefficients ($\bar{K}_i$) as

$$\bar{K}_i = \frac{S_1 K_{i1} + S_3 K_{i3} K^{(i)}_{31}}{S_1 + S_3 K^{(i)}_{31}} \tag{3.5}$$

Equation 3.2 becomes

$$\frac{\partial C_D}{\partial t_D} + \frac{\partial C_D}{\partial x_D} = \frac{\bar{K}_i}{L v_T} \frac{\partial^2 C_D}{\partial x_D^2} \tag{3.6}$$

and let

$$N^{-1}_{pe} \equiv \frac{\bar{K}_i}{L v_T} \tag{3.7}$$

$$\bar{\alpha} \equiv \bar{K}_i / v_T \tag{3.8}$$

The well-known error function solutions to equation 3.6 for the following cases are

Case a: A continuous injection, infinite porous medium, and $N_{pe} > 14$ [B.7]

$$C_D = 0 \qquad X_D \to \pm \infty \tag{3.9}$$

$$C_D = 0 \qquad t_D = 0, \ -\infty \leq X_D \leq +\infty \tag{3.10a}$$

$$C_D = 1 \qquad t_D > 0, \ X_D = 0 \tag{3.10b}$$

$$C_D = \frac{1}{2}\left[1 - \operatorname{erf}\left(\frac{1 - t_D}{\sqrt{4\ N_{pe}^{-1}\ t_D}}\right)\right] \tag{3.11}$$

Case b: A continuous slug flow through a semi-infinite medium

$$C_D = 0 \qquad t_D = 0, \ X_D \geq 0 \tag{3.12}$$

$$C_D = 0 \qquad X_D \to +\infty, \ t_D \geq 0 \tag{3.13}$$

$$C_D = 1.0 \qquad X_D = 0, \ t_D > 0 \tag{3.14}$$

$$C_D = \frac{1}{2}\operatorname{erfc}\left(\frac{1 - t_D}{\sqrt{4N_{pe}^{-1}\ t_D}}\right) + \frac{e^{N_{pe}}}{2}\operatorname{erfc}\left(\frac{1 + t_D}{\sqrt{4N_{pe}^{-1}\ t_D}}\right) \tag{3.15}$$

This solution has been derived by Naiki [N.1] using Laplace Transforms.

Case c: A finite slug (of size t_{DS}) flows through a semi-finite

medium

$$C_D = 0 \qquad t_D = 0,\ X_D > 0 \tag{3.16}$$

$$C_D = 1 \qquad X_D = 0,\ 0 < t_D < t_{DS} \tag{3.17}$$

$$C_D = 0 \qquad t_D > t_{DS},\ X_D > 0 \tag{3.18}$$

$$C_D = 0 \qquad X_D \to +\infty \tag{3.19}$$

Using the principle of superposition, the solution is

$$C_D = \frac{1}{2}\left[\operatorname{erfc}\left(\frac{1 - t_D}{\sqrt{4N_{pe}^{-1}t_D}}\right) + e^{N_{pe}} \operatorname{erfc}\left(\frac{1 + t_D}{\sqrt{4N_{pe}^{-1}t_D}}\right)\right] -$$

$$\frac{1}{2}\left[\operatorname{erfc}\left(\frac{1 - (t_D - t_{DS})}{\sqrt{4(t_D - t_{DS})N_{pe}^{-1}}}\right) + e^{N_{pe}} \operatorname{erfc}\left(\frac{1 + (t_D - t_{DS})}{\sqrt{4(t_D - t_{DS})N_{pe}^{-1}}}\right)\right] \tag{3.20}$$

where t_{DS} is defined as

$$t_{DS} = \frac{\text{slug size in pore volume}}{t_{D_i}^{BT}} \tag{3.21}$$

The convection-diffusion equation (Equation 3.6) was solved also using an explicit finite difference formulation with the following boundary conditions.

$$C_D = 1.0 \qquad X_D = 0,\ t_D > 0 \quad \text{(for continuous slug)} \tag{3.22}$$

$$\frac{\partial C_D}{\partial X_D} = 0.0 \qquad X_D = 1,\ t_D > 0 \tag{3.23}$$

3.2 Capacitance-Dispersion Model

Several investigators [D.1,D.3,C.5,S.3,S.10] have shown that the simple convection-diffusion equation does not always fit the tracer breakthrough profiles precisely. In a miscible displacement experiment or displacements in the presence of a second fluid phase, the effluent composition curves can be asymmetric, and show long tails. Deans [D.3], Coats and Smith [C.5], Salter and Mohanty [S.3], and Dai and Orr [D.1] proposed models to account for this behavior. These models hypothesize that a fraction of the porous medium is stagnant, so the fluids in these fractions can be recovered only by diffusion into the flowing fraction. The models proposed by Coats and Smith, Salter and Mohanty, and Dai and Orr accounted for both longitudinal dispersion and convection in the flowing fraction of the phase. But, Deans used a numerical dispersion in the solution of the diffusion equation.

An approach similar to that of Salter and Mohanty was taken here to model dispersion during multiphase flow of low interfacial tension fluids and allowing for interphase mass transfer. The model presented here differs from Salter and Mohanty by the following:

- The model is appropriate for both two and three-phase flow.

- The tracer can partition between at most two phases.

- Each phase is divided into two fractions: flowing ($S_j^f = S_j F_j$) and dendritic ($S_j - S_j^f$).

- The model is applied to the flow of low interfacial fluids.

- A finite difference solution rather than an analytical solution is chosen to solve the equations.

- The boundary conditions are appropriate for a finite core. Salter and Mohanty solved the equations for a semi-finite core.

The following equations describe the capacitance-dispersion model for the case of three-phase flow.

- The material balance equation for tracer 1 which partitions into phases 1 and 3 (see Figure 3.1) is

$$(S_1F_1+S_3F_3K_{31}^{(1)})\frac{\partial C_{11}}{\partial t} + \frac{q}{A\phi}(f_1+f_3K_{31}^{(1)})\frac{\partial C_{11}}{\partial x} + (1-F_1)S_1\frac{\partial C_{11}^+}{\partial t} + (1-F_3)S_3\frac{\partial C_{13}^+}{\partial t} = (S_1F_1K_{11} + S_3F_3K_{13}K_{31}^{(1)})\frac{\partial^2 C_{11}}{\partial x^2} \qquad (3.24)$$

- The material balance equation for tracer 2 which partitions into phases 2 and 3 is

$$(S_2F_2+S_3F_3K_{32}^{(2)})\frac{\partial C_{22}}{\partial t} + \frac{q}{A\phi}(f_2+f_3K_{32}^{(2)})\frac{\partial C_{22}}{\partial x} + (1-F_2)S_2\frac{\partial C_{22}^+}{\partial t}$$

$$+ (1-F_3)S_3\frac{\partial C_{23}^+}{\partial t} = (S_2F_2K_{22} + S_3F_3K_{23}K_{32}^{(2)})\frac{\partial^2 C_{22}}{\partial x^2} \qquad (3.25)$$

- Balances for dendritic fractions yield

$$S_1(1 - F_1)\frac{\partial C_{11}^+}{\partial t} = M_{11}(C_{11} - C_{11}^+) \qquad (3.26)$$

$$S_3(1 - F_3)\frac{\partial C_{13}^+}{\partial t} = M_{13}(C_{13} - C_{13}^+) \qquad (3.27)$$

$$S_2(1 - F_2)\frac{\partial C_{22}^+}{\partial t} = M_{22}(C_{22} - C_{22}^+) \qquad (3.28)$$

$$S_3(1 - F_3)\frac{\partial C_{23}^+}{\partial t} = M_{23}(C_{23} - C_{23}^+) \qquad (3.29)$$

The phase saturations, fractional flows, partition coefficients and dispersion coefficients are

constant due to the reasons mentioned in Section 3.1. Phase flowing fractions (F_j) and mass transfer coefficients (M_{ij}) are also assumed to be constant. In the above equations C's are the concentrations of tracer in the flowing fraction of that particular phase while C^+'s are the concentrations in the dendritic fraction. Flowing fraction is defined as

$$F_j = \frac{S_j^f}{S_j} \qquad j=1,2,3 \qquad (3.30)$$

Equations 3.24 through 3.29 were solved numerically with an explicit, backward in space, forward in time finite difference representation.

Dimensionless forms and finite difference forms of equations 3.24, 3.26 and 3.27 are described as below. A similar treatment can be applied to the material balance equation for tracer 2.

First define the dimensionless parameters as follows:

$$X_D = X/L \qquad (3.31)$$

$$t_D = \frac{\int_0^t qt}{A\phi L} = \frac{vt}{L} \qquad (3.32)$$

$$C_{D_{ij}} = \frac{C_{ij}}{C^{\circ}_{11}} \qquad i = 1 \text{ and } j = 1 \text{ and } 3 \qquad (3.33)$$

and Damkholer number ($M_{D_{ij}}$) as

$$M_{D_{ij}} = \frac{M_{ij}L}{v} \qquad i = 1 \text{ and } j = 1 \text{ and } 3 \qquad (3.34)$$

Further introduce

$$\alpha_{ij} = \frac{K_{ij}}{v_j} \qquad \left(v_j = \frac{qf_j}{A\phi S_j}\right) \qquad \begin{matrix} i = 1 \text{ and} \\ j = 1 \text{ and } 3 \end{matrix} \qquad (3.35)$$

Also, define the following expressions:

$$\alpha_{D_{ij}} = \frac{\alpha_{ij}F_j}{L} \qquad i = 1 \text{ and } j = 1 \text{ and } 3 \qquad (3.36)$$

$$\bar{S} = S_1F_1 + S_3F_3K_{31}^{(1)} \qquad (3.37)$$

$$\bar{f} = f_1 + f_3K_{31}^{(1)} \qquad (3.38)$$

$$\bar{\alpha}_D = f_1\alpha_{D_{11}} + f_3\alpha_{D_{13}}K_{31}^{(1)} \qquad (3.39)$$

Therefore, the dimensionless forms of equations 3.24, 3.26 and 3.27 are

$$\bar{s}\frac{\partial C_{D_{11}}}{\partial t_D} + \bar{f}\frac{\partial C_{D_{11}}}{\partial X_D} + S_1(1-F_1)\frac{\partial C^+_{D_{11}}}{\partial t_D} + S_3(1-F_3)\frac{\partial C^+_{D_{13}}}{\partial t_D}$$

$$= \bar{\alpha}_D \frac{\partial^2 C_{D_{11}}}{\partial X_D^2} \qquad (3.40)$$

$$S_1(1-F_1)\frac{\partial C^+_{D_{11}}}{\partial t_D} = M_{D_{11}}(C_{D_{11}} - C^+_{D_{11}}) \qquad (3.41)$$

$$S_3(1-F_3)\frac{\partial C^+_{D_{13}}}{\partial t_D} = M_{D_{13}}(C_{D_{13}} - C^+_{D_{13}}) \qquad (3.42)$$

3.2.1 Finite Difference

Now, substitute equations 3.41 and 3.42 into equation 3.40 and write them in the finite difference form, dropping the subscript D, gives

$$\bar{s}\left(\frac{C^{K+1}_{11,i} - C^K_{11,i}}{\Delta t}\right) + \bar{f}\left(\frac{C^K_{11,i} - C^K_{11,i+1}}{\Delta X}\right) + M_{11}(C^K_{11,i} - C^{+K}_{11,i}) +$$

$$+ M_{13}(C^K_{13,i} - C^{+K}_{13,i}) = \bar{\alpha}\left(\frac{C^K_{11,i+1} - 2C^K_{11,i} + C^K_{11,i-1}}{(\Delta X)^2}\right) \qquad (3.43)$$

$$S_1(1-F_1)\frac{C^{+K+1}_{11,i} - C^{+K}_{11,i}}{\Delta t} = M_{11}(C^K_{11,i} - C^{+K}_{11,i}) \qquad (3.44)$$

$$S_3(1-F_3)\frac{C_{13,i}^{+K+1}-C_{13,i}^{+K}}{\Delta t} = M_{13}(C_{13,i}^{K}-C_{13,i}^{+K}) \qquad (3.45)$$

Equations 3.43 through 3.45 were solved (for example for the case of a continuous injection) using the following boundary and initial conditions:

$$(C_{11,i} = C_{11,i}^{+} = C_{13,i} = C_{13,i}^{+})^{K} = 0 \quad 1 < i < N_B \text{ and } K = 0 \qquad (3.46)$$

where N_B is number of the blocks.

$$C_{11,i}^{K} = 1.0 \quad i = 1 \quad , \quad K > 0 \qquad (3.47)$$

$$C_{13,i}^{K} = K_{31}^{(1)} \quad i = 1 \quad , \quad K > 0 \qquad (3.48)$$

$$\left(\frac{C_{11,i}-C_{11,i+1}}{\Delta X}\right)^{K} = \left(\frac{C_{13,i}-C_{13,i+1}}{\Delta X}\right)^{K} = 0 \quad i = N_B,\ K > 0 \qquad (3.49)$$

The equations were solved numerically for C_{11}, C_{13}, C_{11}^{+} and C_{13}^{+} using appropriate sets of the parameters F_1, F_3, M_{11}, M_{13}, S_1, S_3, K_{11}, K_{13}, $K_{31}^{(1)}$. The first eight are matching parameters; the last one is measured.

The computed curves $(C_{ij}|X=L)$ were visually matched with the experimental breakthrough curves to estimate the set of parameters which gave the best

agreement.

3.2.2 Algorithm used to solve the Capacitance-Dispersion equations

a- Calculate convection and dispersion terms for the previous time step (old)

$$CONVT = \bar{f}\left(\frac{C_{11,i}-C_{11,i+1}}{\Delta X}\right)^{old}$$

$$DISPT = \bar{\alpha}\left[\frac{C_{11,i+1}-2C_{11,i}-C_{11,i-1}}{(\Delta X)^2}\right]^{old}$$

b- Calculate the capacitance term at old time step

$$CAPT = M_{11}(C_{11,i}-C^{+}_{11,i})^{old} + M_{13}(C_{13,i}-C^{+}_{13,i})^{old}$$

c- Calculate new dendritic concentrations

$$C^{+new}_{11,i} = C^{+old}_{11,i} + \frac{M_{11}}{S_1(1-F_1)}\,(C^{old}_{11,i}-C^{+old}_{11,i})\,\Delta t$$

$$C^{+new}_{13,i} = C^{+old}_{13,i} + \frac{M_{13}}{S_3(1-F_3)}\,(C^{old}_{13,i}-C^{+old}_{13,i})\,\Delta t$$

If $F_1 = 1$ or $F_3 = 1$, then $C^{+new}_{11,i} = C^{+new}_{13,i} = 0$

d- Calculate new flowing concentrations

$$C_{11,i}^{new} = C_{11,i}^{old} + \frac{\Delta t}{\bar{S}} \text{ (DISPT - CONVT - CAPT)}$$

$$C_{13,i}^{new} = C_{11,i}^{new} \times K_{31}^{(1)}$$

e- Rename new to old and return to a

3.2.3 Numerical Dispersion

Numerical dispersion arises from truncation error in the numerical representation of the first derivative terms in the equations. The solution to the capacitance-dispersion equations using the finite difference formulation is affected by numerical dispersion. The actual dimensionless dispersivity ($\alpha_{D_{ij}}$) for a numerical solution is the sum of the input value and a numerical contribution,

$$\alpha_{D_{ij}}^{t} = \alpha_{D_{ij}}^{I} + \alpha_{D_{ij}}^{N} \qquad \begin{matrix} i=1, \\ j=1 \text{ and } 3 \end{matrix} \qquad (3.50)$$

where $\alpha_{D_{ij}}^{t}$ is the total dimensionless dispersivity, $\alpha_{D_{ij}}^{I}$ is the value used in the equations, and $\alpha_{D_{ij}}^{N}$ is the numerical contribution.

The numerical dispersion (α_D^N) is defined as

follows

$$\alpha_D^N = \frac{\Delta X_D - \Delta t_D}{2} \quad , \quad \Delta t_D = \frac{\text{Pore volumes injected}}{N_p}$$

$$\text{or} \quad \alpha_D^N = \frac{1 - \Delta t_D/\Delta X_D}{2\ N_B} \approx \frac{1}{2\ N_B} \quad , \quad \Delta X_D = 1/N_B$$

Here, N_B (the number of blocks) and N_p (the number of time steps) are input variables in the simulator. In the above expression, $\Delta t_D/\Delta X_D$ is ignored since $\Delta t_D/\Delta X_D$ is usually very small. The input values used for N_B and N_p were as follows

- When the total dispersivity is $\alpha_{ij}^t < 0.60$ cm, then $N_B = 100$, $N_p = 7000$.

- When the total dispersivity is $\alpha_{ij}^t > 0.60$ cm, then $N_B = 50$, and $N_p = 5000$ were adequate to produce stable numerical solutions.

3.3 Phase Saturation

The material balance equation and also the steady-state tracer breakthrough curves are means for estimating the phase saturation for a steady-state experiment.

3.3.1 Material Balance Method

Phase saturations were estimated by material

balances on each phase of the effluent samples. The phase (j) balance assuming no partitioning, no adsorption, and incompressible fluids of constant composition gives

$$\text{IN} - \text{OUT} = \text{accumulation}$$

$$\sum_{i=1}^{N} (V_i f_j^{ss} - V_i f_{ji}) = V_p S_j^{ss} - V_p S_j^{I} \qquad (3.51)$$

Solving for S_j^{ss} yields

$$S_j^{ss} = \frac{\sum_{i=1}^{N} (V_i f_j^{ss} - V_i f_{ji}) + V_p S_j^{I}}{V_p} \qquad (3.52)$$

where i is the subscript for sample number, and V_i is the total volume of sample number i.

3.3.2 Calculation of Saturation using Tracer History Plot

Tracer history is the plot of normalized tracer concentration versus cumulative pore volume. The cumulative pore volume produced up to and including the i^{th} sample is calculated from

$$t_{D_i} = \frac{\sum_{i=1}^{N} V_i - V_E}{V_p} \qquad (3.53)$$

where V_E is the volume of fluid in the tube extended from the outlet of core to the sample collector.

However, tracer concentration data should be plotted at the midpoint of the i^{th} sample pore volume which is

$$t_{D_i}^{mid} = t_{D_{i-1}} + 1/2\ (t_{D_i} - t_{D_{i-1}}) \qquad (3.54)$$

This value is labelled "pore volume" on the figures.

- Convection-diffusion equation

Estimate the saturations using Equation (3.4) and the breakthrough time at 50 percent effluent tracer concentration. This approximation is an excellent one when the Peclet number is greater than 14. If the Peclet number is less than 14, then the computed curves are generated using the analytical solution (Eq. 3.15) for different values of N_{pe} and t_D. The saturation and dispersivity which give the best agreement between computed and experimental results are used.

- Capacitance-dispersion model

The phase saturations are also estimated using the capacitance-dispersion equations. A detailed procedure for estimating saturation during two- and three-phase

flow using the capacitance-dispersion model is given in Appendix B.

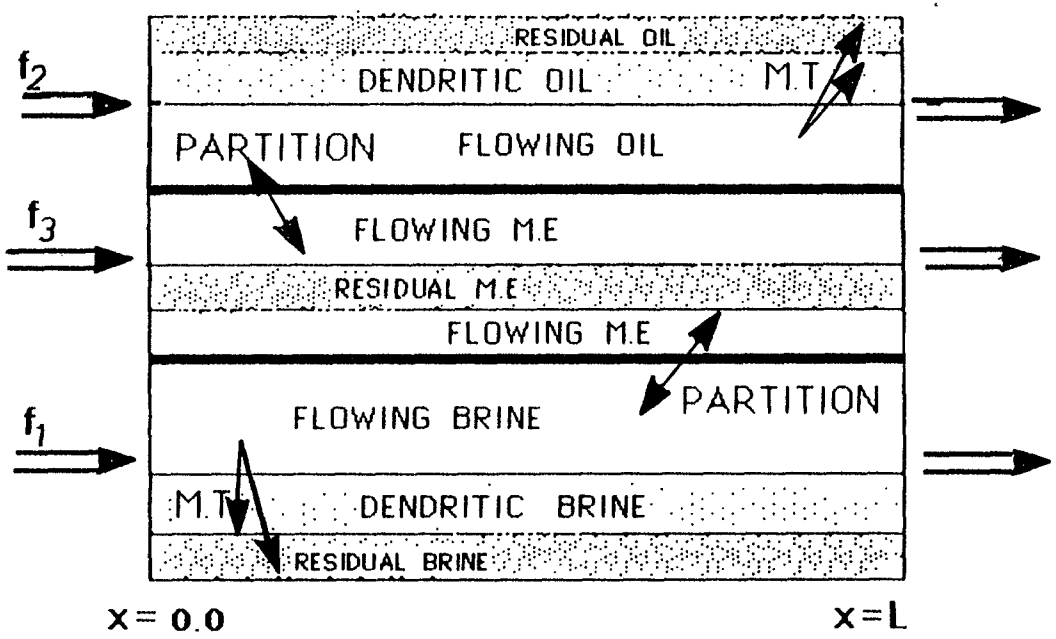

Figure 3.1 Schematic Diagram for the Capacitance-Dispersion Model

CHAPTER 4

DESCRIPTION AND OPERATION OF EXPERIMENTAL APPARATUS

The equipment used in this study is identical to that of Reference D.8 except for the Liquid Scintillation Counting (L.S.C.) and Sulfur Analyzer. The equipment is divided into three categories:

1- Flow apparatus: Pumps, flow oven, pressure transducers, demodulator, sample fraction collector, and solution reservoirs.

2- Analytical equipment: Gas chromatography, atomic absorption, liquid scintillation counting, and sulfur analyzer used for analysis of the sample composition.

3- Physical property equipment: Spinning drop tensiometer, Couette viscometer, and densiometer used to measure interfacial tension, viscosity and density of samples respectively.

The list of equipment and manufacturers is given in Table 4.1.

4.1 Flow Apparatus

4.1.1 Pumps

Two different types of pumps were used during this study: (a) Zenith pump, and (b) Cheminert pump.

The flow rate settings on these pumps used only for nominal adjustment of the flow rate at the start of each experiment, since actual effluent volumes were measured for calculations.

(a) The Zenith Metering Unit

This unit consists of a motor driven assembly (Model QM) containing the pumps (type BPB) and a digital motor speed control power package. The Zenith pump is a rotary gear metering pump of high precision. The small size pump (type BPB) with an output of 0.160 cm^3/revolution was used. The speed range is from 3 to 180 revolutions per minute. Thus, flow rates from 0.48 to 28.8 cm^3/min can be achieved. The type BPB is suitable to operate at pressures up to 3000 psig.

(b) Cheminert Metering Pump (type CMP-3)

The type CMP "Cheminert" metering pump utilizes two independent pump chambers each consisting of a Kel-F cylinder, borosilicate glass piston, and Teflon piston seal. The two pistons are driven by two rotary cams 180° out of phase. The shape of the cam is such that one

piston pumps at a constant rate while the other piston goes through the three phases of its filling operation as follows:

(a) switch pump chamber from outlet to inlet

(b) fill chamber

(c) switch chamber from inlet to outlet

The maximum discharge pressure of the pump is 500 psig. The flow rate is adjustable from 0.24 to 120 cm^3/hour. The values of 0.24 to 120 cm^3/hour are nominal values and are not calibrated. During the experiments the actual output in the effluent samples was used as the flow rate.

One problem can arise when introducing organic solvents into the pump. This is associated with the fact that some solvents cause the Kel-F cylinders to swell, resulting in failure of the pistons to withdraw for filling of the cylinder. Therefore, only brine was used with this pump.

4.1.2 Pressure Measuring/Recording Apparatus

Pressure transducers were utilized in the flow experiments to measure the pressure drop across the porous medium. Validyne model DP15 Variable Reluctance Differential Pressure transducers were chosen because this model is designed for low and medium pressure

measurements.

The MCI module case is multi-channel, housing up to 20 plug-in units and providing the necessary carrier and DC operating voltages for a broad line of plug-in units and associated transducers. CD19 Carrier Demodulator was selected as a plug-in unit. The gain switch has five positions from 1 mv/v to 50 mv/v for 10 volts output. The electrical output is connected to a chart recorder. A Potentiometric Strip Chart recorder manufactured by Texas Instruments Inc., was used. It is a multipoint, self balancing recorder for accurate recording of multiple DC signals.

A more detailed description of the pressure transducer, carrier demodulator, chart recorder, and calibration procedure is given by Yuan [Y.1].

4.1.3 Sample Collector

A fraction collector was used for collecting the effluent samples. Depending on the setting on this model (328) of collector, the size of fractions can be controlled by time, volume, drops, external control signals, or manually. The unit has the capacity to hold 200 rack-mounted tubes. Easy exchangeability of individual racks of tubes enables continuous sample collection. In all experiments, fractions were

controlled by time. The actual flow rate can be calculated by recording the volume (s) in the graduated test tubes, which had a capacity of 15 cm^3 with 0.1 cm^3 divisions.

4.1.4 Solution Reservoir

A Glenco chromatographic glass column was used as a solution reservoir. This column has 2 inches inside diameter and is 24 inches long. Glenco Series 3400 columns are constructed of borosilicate glass with polypropylene collars and endpieces. The 3500 Series are identical except that they have Teflon end plates for complete chemical resistance to organic solvents. Each column of this series is constructed with non-clogging bed supports which consist of a thin 10 micron membrane suspended over a woven grid. Upper end plates have a side vent port which can be used to bleed air.

The pistons that were used in solution reservoir were constructed by The University of Texas at Austin, Petroleum Engineering Department. The pistons used to prevent contact of driving fluids (mineral oil, water) and injected fluids (brine, microemulsion, oil) are made of Teflon with two Viton "O" rings. The piston is one solid piece of Teflon with the diameter of 4.921 cm and a height of 2.54 cm. Two "O" ring grooves

were cut and fitted with Parker 125 O-rings to provide both a double seal and add stability, preventing torsion of the piston within the column.

4.1.5 Temperature Controlled Air Bath

All of the micellar flow experiments were conducted at 30°C in an enclosed, heated fiberglass hood with outside dimensions of 182.88 cm long by 152.4 cm high by 91.44 cm deep.

The hood was constructed of fiberglass reinforced plastic, with 1.27 cm urethane sandwiched between two fiberglass sheets each 0.3175 cm thick. The glass door is 152.4 cm long and 76.2 cm high, and slides vertically. The hood has two electric heaters, thermostatically controlled. One blower on each heater is connected so that the blower can run continually, but the heaters will not operate without the blowers running. All the flow equipment except the pumps were set up in the oven.

The temperature range of the temperature controller (Athena Model 74-6) is -17.78 to 148.9°C. The temperature was measured every day by a mercury thermometer that was placed in the oven and the recorded data showed a consistent temperature (±0.5°C).

4.2 Analytical Equipment

4.2.1 Gas Chromatography (GC)

Analysis of volatile compounds (water, alcohol, and oils) in individual samples for determination of chemical composition was done using a Tracor Model 560 gas chromatograph equipped with a model 770 Auto sampler. The two detectors used were placed in series with the column effluent passing first through a thermal conductivity (T.C.) detector for water analysis before passing through a flame ionization detector (F.I.D.). Since the thermal conductivity analysis is non-destructive, this arrangement allowed for a single sample injection to be analyzed simultaneously for both water content (T.C.) and volatile organics (F.I.D.).

Conditions for operation of the materials on a 91.44 cm by 0.3175 cm stainless steel column packed with 80/100 porapak Q were as shown in Table 4.2.1.

Prepared standards of each of the materials of interest were analyzed concurrently with the experimental samples. A calibration curve for each material was constructed and used for quantification of the unknowns.

In some instances, changes in gas flow occur during extended runs. The errors for this include changes in flow pressure, column plugging, and plugging

of the F.I.D. assembly. This can result in a high degree of error in the analysis. In the absence of such difficulties the error is estimated to be in the range of ±3%.

4.2.2 Liquid Scintillation Counting (LSC)

The experiments which were conducted utilized both material (or phase) balance calculation and dispersion data for determination of saturations. The dispersion data were obtained through the use of four radioactive tracers; tritiated sulfonate (TS) for the microemulsiton phase, Carbon-14 (^{14}C) labelled n-decane for the oleic phase and chloride-36 (^{36}Cl) labelled sodium chloride or tritiated water (T_2O) for the aqueous phase.

After measuring the volume of the phase (s) present in the effluent samples a 0.10-0.25 cm^3 sample of each labelled phase present was added to 10 cm^3 (or 5 cm^3 for minivials) of liquid scintillation cocktail (Beckman, Ready-Solv HP) suitable for counting either organic or aqueous samples. The prepared samples were counted using a Beckman Model LS 9800 liquid scintillation counter.

The Beckman counter has a capacity of 300 samples. Model LS 9800 is equipped with control keyboard, printer, three count channels, ten user count

programs, CRT display, H# (instrumental quench-monitoring value), quench compensation factor, two phase monitor, single, dual, and triple label disintegration per minute (DPM) programs. The floppy disc DPM programs utilizes the quench correction for single-labelled, dual-labelled and triple-labelled samples. Standards with known DPM are quenched and are counted on a LSC to obtain counts per minute (CPM). The counting efficiency of these standards is calculated using the following equation,

$$\text{Counting efficiency} = \frac{\text{CPM}}{\text{DPM}} \qquad (4.1)$$

The quench curve is then formed by plotting this counting efficiency as a function of some instrumental quench-monitoring value (such as H# or sample channel ratio). When an unknown sample is counted, its quench monitor is also obtained. The counting efficiency is then estimated from quench curve, then using the following equation DPM's are calculated.

$$\text{DPM} = \frac{\text{CPM}}{\text{counting efficiency}} \qquad (4.2)$$

For multi-label calculations, the quench monitor is always H#.

The complications of multi-label corrections arise due to the presence of multi-beta radionuclides with different energies. Therefore, dual-labelled samples must be counted in two channels and triple-labelled in three channels. Generally, the lower energy isotope is counted in channel 1, and the highest energy isotope in channel 3. The energy and half-life values for the isotopes used in this study are as follows:

Isotope	Energy (MEV)	Half-Life (Years)
Chloride-36	0.714	3×10^5
Carbon-14	0.156	5500
Tritium	0.018	12

The experimental samples were counted for two minutes. Values of DPM of each isotope were printed for each sample.

4.2.3 Atomic Absorption

Calcium and magnesium concentrations were determined by Atomic Absorption spectrophotometry using a standard addition technique. The spectrophotometer used was a Perkin-Elmer Model 360 using Perkin-Elmer multi-

element lamps for Ca^{++}, Mg^{++}, and Al^{+++} as light sources.

Brine samples required no pre-treatment prior to the preparation of appropriate dilutions. Middle phase microemulsions were broken by the addition of 95% ethanol at a volume equal to 10% of the microemulsion volume. Following gentle heating and centrifugation, the oleic phase was measured and discarded. The resultant brine phase was then ready for dilution and analysis. Two aliquots of 1.5 cm^3 were taken from each brine sample. One was diluted without further treatment to 25 cm^3. The second aliquot had calcium and magnesium added to give 2 ppm calcium and 0.2 ppm magnesium when diluted to 25 cm^3.

Diluted samples were run using standard operating conditions and standardization techniques. Appropriate calculations were used to determine the concentration of the ions in the original solutions. In the case of the microemulsion, corrections also had to be made for the added alcohol and, if the results were to be expressed in terms of total microemulsion, or the percentage of water in the microemulsion.

4.2.4 Sulfur Analyzer

The concentration of sulfur in the experimental samples were measured using a Fisher Model 475 Sulfur

Analyzer equipped with a high temperature tube furnace to form a complete system for the fast and accurate measurement of sulfur in fossil fuels. The sulfur analyzer utilizes a titration technique to measure SO_2 in the effluent produced during combustion of sulfur-bearing materials. There is also an integral microprocessor combined with the titration which is programmed to convert titrant volume consumed to either percent or parts per-million sulfur content in the sample. This model is capable of measuring sulfur concentrations in the range of 0.005 to 100% with an accuracy of 3%.

4.3 Physical Property Equipment

4.3.1 Spinning Drop Tensiometer

Interfacial tension measurements were made using a spinning drop technique [C.3]. The technique depends upon centrifugal force as generated within a rapidly spinning tube containing two immiscible fluids. The forces produced cause separation of the fluids and, if the lower density fluid volume is small, a drop is formed at the center of rotation. The ratio of the length of the drop to its diameter is a function of the interfacial tension, rate of rotation, and density difference between the fluids.

Density measurements were made using a

Mettler/paar digital densiometer model DMA46. The spinning drop machines with associated period indicator and measurement optics were manufactured at The University of Texas at Austin.

Samples were subjected to continuous spin for a minimum of 8 hours, with observations taken at 1, 2, and 8 hours. If no change in the measurement occurred between 2 and 8 hours, these values were taken. If there were changes in the measurement values between 2 and 8 hours, measurements were continued for 24 hours. Interfacial tension values were calculated from these equilibrium measurements.

4.3.2 Contraves Low-Shear Viscometer (LS-30)

The viscosity of each fluid (microemulsion, oil, brine, etc.) was measured using a Contraves Low-Shear Viscometer, LS-30. The LS-30 is a rotational viscometer based on a Couette principle which measures the stresses between two concentric cylinders with one rotating (cup) and the second being fixed (bob). There are 30 fixed angular speeds which, for the bob and cup used, give a range of shear rates from 0.0174 to 128.5 sec^{-1}. Torque values are read from a digital display, with 5 ranges of sensitivity, and converted to viscosity by multiplying by the appropriate conversion

factor for the specific range and speed. Temperature control was maintained by a constant temperature water bath which circulates water through the cup. Temperature was checked by placing a mercury thermometer in the cup.

The operating procedure used is as follows:

1. Turn on the main power, the motor, and the water circulator. Wait for 15 minutes until the temperature stabilizes at the desired value .

2. Put 1 cm^3 of the sample in the cup. Insert the spindle into the sample (in the middle of the cup) being sure to avoid the formation of bubbles (if there is an air bubble formed it must be removed).

3. Adjust the zero point using the zero adjustment, with the speed at zero, and the range set at 1.

4. Take readings for every other speed from lowest to highest. As soon as the reading goes over scale (199), switch to the next higher range.

5. Using the appropriate conversion factor, the viscosity is the product of the reading and the factor.

TABLE 4.1

Equipment List and Type

EQUIPMENT	MODEL	MANUFACTURER
Zenith Pump	QM/BPB	The Zenith Corporation, 432 Cherry Street, West Newton, Massachusetts 02165
Cheminert Pump	CMP-3	Laboratory Data Control, P.O.Box 10235 Interstate Industrial Park, Riverea Beach, Florida 33404
Pressure Transducer	DP15	Validyne Engineering Corporation, 19414 Londelius Street, Northridge, California 91324
Demodulator	CD-19	Validyne Engineering Corporation, 19414 Londelius Street, Northridge, California 91324
Sample Collector	Isco Model 328	Instrumentation Specialities Company, P.O.Box 5347, Lincoln, Nebraska 68505
Solution Reservoir (packed column)	Glenco 3400, 3500	Glenco Scientific Inc., 2802 White Oak Drive, Houston, Texas 77007
Pressure Recorder	FMWSE6C	Texas Instruments Inc., Recorder Department, 12203 Southwest Freeway, Stafford, Texas 77477
Air Bath	-	Contemporary Products, Inc., P.O. Box 6249, 2204 East 6th Street, Austin, Texas 78762
Temperature Controller	Athena 74-6	Athena Controls Inc.,W.Conshohocken, Pennsylvania 19476
Scintillation Counter	3400 Beckman LS 9800	Beckman Instruments, Inc., Fullerton, California 92634
Gas Chromatograph	Tracor Model 560	Tracor, Inc., 6500 Tracor Lane Austin, Texas 78721

TABLE 4.1 (continued)

Digital Densiometer	Mettler/Paar DMA46	Mettler/Paar
Contraves Low-Shear Viscometer	LS-30	Contraves A.G., Zurich, Schaffhauser Strasse 580, P.O.Box CH-8052, Zurich Switzerland
Sulfur Analyzer	Fisher Model 475	Fisher Scientific Company, 711 Forbes Ave. Pittsburgh, Pennsylvania 15219
Atomic Absorption Spectrophotometer	Perkin-Elmer Model 360	Perkin-Elmer Corporation Norwalk, Connecticut
Spinning Drop Tensiometer	-	The University of Texas at Austin Austin, Texas 78712

TABLE 4.2.1

Operating Conditions for
Gas Chromatographic Analysis

Carrier Gas Flow (Helium)	30 cm^3/min
Thermal Conductivity Reference Flow (Helium)	30 cm^3/min
Flame Ionization Detector (F.I.D.) Gas Flow (Hydrogen)	30 cm^3/min
Flame Ionization Support Gas Flow (Compressed Air)	470 cm^3/min
Injection Port Temperature	250°C
Thermal Conductivity Detector Temperature	250°C
Flame Ionization Detector Temperature	250°C
Initial Oven Temperature	110°C
Final Oven Temperature	225°C
Program Temperature Change Rate	20°C/min
Initial Hold	5 min
Final Hold	20 min
F.I.D. Electrometer	
Input Range	X 1000
Output Attenuator	16
Output Connection	10
Recorder Attenuator	1 mv/volt
Thermal Conductivity Detector	
Sensitivity	low
Filament Current	110 mA
Output Attenuation	8

CHAPTER 5

EXPERIMENTAL PROCEDURES

In this chapter, the preparation of the porous media and fluids of interest are discussed.

5.1 Porous Media

5.1.1 Preparation of Berea Sandstone Core

The data presented in this study were obtained from a Berea sandstone core. The Berea sandstone was first cut to desired dimensions of 5.08 cm by 5.08 cm square and 60.96 cm long. This will hereafter be referred to as the core.

Three thin coats of epoxy were used to cover the core (one each day). The preparation of epoxy is as follows:

(1) Weigh 70 grams of R-828 resin

(2) Weigh 30 grams of versamid 125 polyamide

(3) Mix these two solutions by hand for 5 minutes and let set one to three hours to allow the bubbles to

come out and to let it thicken. While the first coat was being brushed on: Square (5.08 cm by 5.08 cm) plexiglass endpieces were fitted at each end. Nylon screening material of 500 micron opening size was placed between the endpieces and the core face to provide a good initial fluid contact area. Endpieces were drilled and tapped to allow for a 0.3175 cm (1/8 inch) NPT Nylon Swagelok fitting. The same fitting as above (0.3175 cm) were positioned on the top of the uncoated core, 15.24 cm from each end, providing two pressure taps 30.48 cm apart.

After the core had dried (after three coats) it was pressure tested to 1.36 atm (20 psig).

5.1.2 Saturation, Porosity, and Reference Permeability Measurements

The following procedure was used in determination of the porosity and reference (100 percent brine) permeability of the core.

(1) Connect one end of the core to a vacuum pump. Close valves at the other end and at intermediate pressure taps. Evacuate the core for 30 minutes, close the valve, and then disconnect from the vacuum pump.

(2) Fill a burette with brine solution of the desired salinity (preferably, the same as the salinity of

micellar solution).

(3) Purge out the bubbles by filling the line from burette to the core. Connect one side of the core to the burette.

(4) Open the valve to the burette (while the other valve is closed). The hydraulic head and the pressure differential in the burette will pull the brine in and saturate the core.

(5) The volume decreases in the burette less the volume of brine in the lines from the core to the valves (can be calculated by knowing the diameter and length of tubes) is the pore volume of the core (V_p). The bulk volume of the core can be calculated by knowing the length and cross-sectional area. The porosity (ϕ) is the ratio of the pore volume to the bulk volume.

The reference permeability was determined by flooding the core with a brine solution at a selected flow rate until the pressure drop was constant. At steady state the values of pressure drop across the entire length, pressure drop between the intermediate pressure taps, and the volume of brine in effluent samples were recorded. In all the core flood experiments the intermediate pressure drop was used for calculation to avoid end-effects. By knowing the steady-state pressure

drop, actual flow rate in the effluent samples at steady state (the effluent volume divided by the time interval on sample collector), and brine viscosity (measured by LS 30), the reference permeability was calculated using Darcy's law.

5.1.3 Pressure Transducer Arrangement and Potential Drop Measurements in Vertical Flow

There are a total of five transducers in the system (Figure 5.1.1). Two measure the intermediate pressure drop (across the center one-foot section), one measures the overall pressure drop across the full 2 foot core, and the other two measure the pressure drop across the 1/4 of the total distance from each end of the core. The lines to and from the transducers were filled with excess oil to prevent corrosion of transducers and because of the possibility of contact of microemulsion and oil in the lines. The two way valves were used in the bypass lines to zero the transducers. The measured pressure across the transducer (ΔP_T) shown in Figure 5.1.1 is as follows

$$\Delta P_T = (P_{in} + \rho_x g X) - (P_{out} - \rho_x g(h-X)] \qquad (5.1)$$

or

$$\Delta P_T = (P_{in} - P_{out}) + \rho_x gh = \Delta P + \rho_x gh \qquad (5.2)$$

where ρ_x is the density of the fluid in lines to the transducer.

Now, the potential drop for any phase flowing through the core with the density of ρ_j is

$$\Delta\phi_j = \Delta P + \rho_j gh \qquad (5.3)$$

Substituting the pressure drop across the core (ΔP) from equation 5.2 in equation 5.3, we have

$$\Delta\phi_j = \Delta P_T + (\rho_j - \rho_x)gh \qquad (5.4)$$

If the fluids are injected from the bottom, then

$$\Delta\phi_j = \Delta P_T - (\rho_j - \rho_x)gh \qquad (5.5)$$

This equation implies that by adding or subtracting the net hydrostatic head of each flowing fluid to the transducers signal, the potential drop for that phase can be calculated.

5.1.3.1 Test on Accuracy of Transducer

The following procedure is used to test the

accuracy of any of the pressure transducers used in the flow experiment.

- Inject single phase at different flow rates until steady-state is attained.

- Record the steady-state pressure drop at each flow rate.

The pressure drop versus flow rate should be a straight line passing through the origin when there is no correction necessary on the data. When the intercept of the y-axis (pressure drop) is positive or negative, the same value should be subtracted or added to the data to get corrected pressure drop.

5.1.4 Relative Permeability Measurement

- Apparatus

Shown in Figure 5.1.1 is a schematic diagram of the relative permeability determination apparatus. It consists essentially of fluid reservoirs with pistons, constant-rate cheminert pumps, pressure transducers, automatic sample collector, and an air bath. Pistons were used in reservoir columns to separate the displacing water from the fluid being injected. Apparatus except for the pumps was placed in the temperature-controlled air bath at 30°C.

- Sample Preparation and Steady-State Tests

After determining the reference permeability and porosity, the brine was displaced by oil to its irreducible value (S_{wr}). The oil relative permeability, k_{ro}, at the residual water saturation was subsequently determined. Then, the oil was displaced by water to residual oil saturation (S_{or}) to calculate the brine relative permeability at S_{or}.

The steady-state was the method used for evaluation of the relative permeability of fluids. The fluids, were injected at a specific fractional flow (cut) until a steady-state was reached. Steady-state criteria were

- constant pressure drop across all the sections
- the fractional flow of phases in produced samples is the same as the injected cut
- the phase compositions in the effluent samples are the same as the injected one
- constant total flow rate

Each cut at steady-state conditions, gives one point on the relative permeability curve. Saturation of phase at each cut can be estimated from the material balance equation (Eq. 3.52) or from the tracer breakthrough curve using the dispersion-capacitance model.

5.1.5 Capillary Desaturation Measurement

The relationship between the residual phase saturation and the capillary number which is commonly called the capillary desaturation curve (CDC) was measured using a three-phase micellar formulation in a Berea sandstone core. The procedure for determining, for example, the residual microemulsion to brine as a function of capillary number involved the following sequence of floods:

1- Flood the core with microemulsion until steady-state is attained. Estimate the saturation using the material balance equation. Record the steady-state pressure for capillary number and relative permeability calculations.

2- Inject the same microemulsion containing radioactive tracers. Analyze the tracer breakthrough histories to estimate the phase saturation.

3- Flood the core with the excess brine phase at a low flow rate until steady-state is attained. Record the pressure drop at steady-state and estimate the saturations from material balance.

4- Inject the excess brine phase containing a radioactive tracer at the same flow rate. Estimate the saturations from the tracer breakthrough curve.

5- Increase the capillary number step-wise by repeating steps 3 and 4 at increasing flow rates.

The core was horizontal during the capillary desaturation measurements since problem of gravity segregation during these displacements did not arise. This was confirmed by visual observation through plexiglass endpieces on the core.

The same procedure as mentioned was followed to measure the following:

- Residual excess brine saturation to microemulsion
- Residual microemulsion to excess oil
- Residual excess oil to microemulsion

5.2 Fluids

The following subsection describes the preparation of fluids for both the flow and static test tube experiments. The fluids used were,

(1) 95 percent pure n-decane ($n\text{-}C_{10}$)

(2) Brine at various salinities of NaCl and $CaCl_2$

(3) Micellar solution (Isobutanol (IBA), n-decane, TRS 10-410, brine).

Brine solutions were mixed on a weight percentage of salt in de-ionized water basis as described in following subsection. Oil and alcohol were used as is.

Two batches of surfactants were used in preparation of micellar solutions. They both were petroleum sulfonates TRS 10-410 manufactured by Witco. Chemical composition of these batches given by the manufacturer is in Table 5.2.1.

All of the fluids used for flow purposes were filtered through 0.45 micron Millipore type AA filter paper with a diameter of 9 cm. The filter machine was a Fann pressure unit operated at 40 psi pressure drop.

Refer to Table 5.2.2 for chemicals and the suppliers.

5.2.1 Preparation of Micellar Solution

The procedure for preparation of micellar solution for the static experiments is somewhat different from that of the flow experiments since

- The samples for static experiments are made up in 25 cm^3 vials while a 15 liter glass bottle is used for mixing the micellar solution for flow experiment.

- The fluids (surfactant, alcohol, n-decane, brine) for flow experiments were measured by weight rather than volume for more accuracy.

- For the flow experiments, n-decane, brine, and surfactant are filtered while this is not necessary for phase behavior samples.

- The micellar solution made up for flow experiment is at a fixed salinity while the salinity varies in the phase behavior samples.

- Static Experiments

The formulation used for static physical property experiments consisted of TRS 10-410, n-decane, iso-butanol, and brine. The overall composition was chosen so that most of the composition points would fall into the multiphase region (when the sulfonate concentration is low). The brine was treated as a pseudo component; thus, the total volume of brine was held constant while the salt concentration varied. Based on the activity of Witco sulfonate in the batch received, the concentration of sulfonate was corrected for this activity and reported on an active basis. The temperature was chosen as 30°C for both static and flow experiments.

Consider the following notes and steps in preparing of a micellar solution:

(1) The sulfonate batch was heated in a 50°C water bath for 1 1/2 hours and then mixed by hand. This step was necessary in order to obtain a repeatable sample from the sulfonate batch.

(2) The impurities (oil, water, salt) in the Witco

TRS 10-410 were about 38 percent. The amount of TRS 10-410 was multiplied by the activity percent (about 0.62) to convert to an active basis.

(3) The order of mixing of the fluids (TRS 10-410/n-decane/IBA/brine) was important in order to obtain fast equilibration of the resulting phases. The order of mixing that gave the shortest equilibration time was (1) brine, (2) Surfactant and alcohol (Stock A), (3) de-ionized water, and (4) oil (see 5.2.5).

(4) The salinity reported was on a water basis. For example, if the only electrolyte present is sodium chloride (NaCl), then a salinity in weight percent means the weight of NaCl times 100 divided by the weight of the water plus NaCl. This brine is then treated as a pseudo component. The concentration of the other components (TRS 10-410, alcohol, oil) based on the overall fluid volumes.

(5) The prepared samples were tightly sealed to prevent evaporation of the components (e.g. alcohol).

- Flow Experiments

The selection of the formulation was the most important choice of experimental conditions. TRS 10-410 was used as the surfactant in all the core floods of this study. TRS 10-410 has the advantage that a great deal of

data has been published for it [H.3,G.1,M.1,D.6,D.8]. The alcohol should be a good co-solvent and it is desirable that its partition coefficient be about the same as the sulfonate. The standard alcohol chosen to be IBA.

The criteria used to select the oil were that it be a pure or nearly pure hydrocarbon with an EACN (Equivalent Alkyl Carbon Number) in the range considered typical of crude oils (5 to 15), and be available at low cost. N-decane (with 95 percent purity) was the oil selected for this study.

Sodium chloride brine was used for simplicity. Calcium chloride was also added, since about 15 ppm Ca^{++} continued to be produced from Berea core at 30°C. The calcium chloride was added in the amount such that approximately 15 ppm Ca^{++} is concentrated in the microemulsion phase. Thus, the solution is saturated with respect to clay and calcite.

The formulation TRS 10-410/n-decane/IBA and 1.1% NaCl and 13.7 ppm Ca^{++} brine was used for batch numbers 1 and 3, while 1.2% NaCl and 13.7 ppm Ca^{++} brine was used for batch numbers 4-14 in the flow experiments. The primary reasons for choosing the 1.1% NaCl salinity were:

(1) From the IFT measurements, the two IFT curves cross at a salinity of 1.1 wt% (this is one definition used for optimal salinity).

(2) The volume fraction diagram shows that at about 1.1 wt% NaCl the volume of upper phase oil and lower phase brine are almost equal (another indication of being near optimal salinity is equal solubilization of oil and water).

(3) The volume percentage of the resulting three phases is reasonable (enough volume of each phase is in a 15-liter bottle for flow experiments to be conducted).

(4) The viscosity of the middle phase microemulsion was about 5 cp which is not too low nor too high to make viscosity and pressure drop measurements. Also, the value was constant with shear rate over the range used (see Jones [J.2] for a more complete analysis of the rheology of this microemulsion).

(5) The phases equilibrated fast at this salinity. This fits the general trends observed by Graciaa et al. [G.2], who reported that equilibration is faster near optimal salinity.

The same reasoning applied to the stock with salinity of 1.2 wt% NaCl, except that the optimal salinity shifted to approximately 1.2% due to the use of

a new batch of surfactant with a slightly different composition.

The microemulsion composition of the micellar solution that was used in all the flow experiments was as follows:

1.5 vol% TRS 10-410 (active basis)	Total fluid volume basis
1.5 vol% IBA	
50 vol% n-decane	
47 vol% brine (1.1 or 1.2 wt% NaCl and 13.7 ppm Ca^{++})	

The fluids were mixed in the same order as discussed before in an inverted 15 liter glass bottle which had a two-hole rubber stopper. Two glass tubes fit the holes in the rubber. One glass tube was long enough to be above the fluid level (used for pulling a vacuum and drawing the fluids into the bottle) while the other one extended only to the top of the stopper. The bottle was partially evacuated, and held on a fixed frame placed in the oven (30°C). The minimum required time for equilibration was one month (see 5.2.1.3). The resulting equilibrated phases, upper phase oil, middle phase microemulsion, and lower phase brine were gravity separated. By introducing air to the bottle through the same tube extending above the fluid surface before

opening drain tube, the desired phases could then be poured into the solution reservoirs to be used in the flow experiments.

Appendix C gives a numerical example for mixing the phase behavior samples and the micellar solution for the flow experiment.

5.2.1.1 Volume Fraction Diagram

The phase volume fractions versus salinity is called a volume fraction diagram. A series of samples were mixed for physical property information. Micellar solutions containing surfactant, alcohol, oil, and brine were prepared at various NaCl concentrations. The samples mixed in 25 cm^3 vials having a constant internal diameter were equilibrated at 30°C. The volume of the resulting phases are proportional to the height of the phases in the vial (the height was measured with a ruler). The height of the specific phase divided by the total height of solution is the volume fraction of that phase.

5.2.1.2 Optimal Salinity

Reed and Healy [R.5,H.2] gave three definitions for optimal salinity as follows

1- Interfacial tension optimal salinity

The salinity at which minimum interfacial

tension between the middle and excess oil phases (σ_{mo}) and the middle and exceses brine phases (σ_{mw}) occurs.

2- Phase behavior optimal salinity

The salinity at which equal volumes of oil and brine are solubilized into the middle microemulsion phase (intersection of V_o/V_s with V_w/V_s). Solubilization parameters, V_o/V_s and V_w/V_s as the volume of oil and brine solubilized in a microemulsion phase by surfactant, are measures of interfacial activity too. As salinity increases, σ_{mo} decreases and σ_{mw} increases. As either tension decreases, the appropriate solubilization parameter increases (Refer to Figures 6.1.4 and 6.1.5).

3- Optimal salinity for miscibility

The salinity that minimizes height of the multiphase region at 50/50 water-oil ratio (WOR).

At a constant WOR and surfactant concentration, the optimal salinities from the above definitions are about the same. In this study, the first two definitions were used to identify the optimal salinity for the formulation used.

5.2.1.3 Equilibration Times

Factors that seemed to be important in the equilibrium phase behavior of the micellar solution were time and the order of mixing of the constituents (oil,

alcohol, brine, surfactant).

For the flow samples, the heights of the two interfaces (microemulsion/oil and microemulsion/brine) were recorded every day. The phases were considered to be at equilibrium when the level of interfaces became constant. A period of 30 to 45 days was adequate for equilibration of the three-phase micellar solution at a salinity close to the optimal salinity (Figures 5.2.1 - 5.2.3).

During the course of mixing the phase behavior samples, it was noted that the order of mixing oil, brine, surfactant, and alcohol has an effect on the time required for separation and equilibration of the resulting phases. The daily record of phase volumes of duplicate samples, only with a different order of mixing, showed that samples with the order of mixing of 1) brine, 2) surfactant and alcohol, 3) water, and 4) oil gave the shortest equilibration time.

5.2.2 Counting Procedure for Radioactive Samples

The four types of radioactive tracers used in this study are as follows:

1- Tritium for brine and microemulsion phases.

2- Carbon-14 labelled n-decane for oil and microemulsion phases.

3- Tritium labelled sulfonate for the microemulsion phase.

4- Chloride-36 labelled sodium chloride for brine and microemulsion phases. Tritium was replaced by chloride-36 when sulfonate was labelled.

Add the tracer to the desired phase (S) and pour in the solution reservoir while wearing triflex vinyl gloves for safety on radioactive contamination.

At the begining of the dispersion experiments, if the line extended from the outlet of the core to the sample collector (V_E) was flushed out, there was no correction needed in Equation 3.53. Otherwise, this volume should be taken into account. At the start of each dispersion run, the concentration of radioactive tracer in the core from the previous run should be counted to make sure all tracers have been flushed out during the previous steady-state experiment. For the case of a continuous dispersion experiment, inject the radioactive material until the concentration in effluent samples is the same as in the injected fluid (check this by counting the effluent samples by Liquid Scintillation Counter (LSC).

The collected volume in effluent samples was usually 11-14.5 cm^3. The preparation of samples for

counting by LSC was as follows:

(1) Depending on the size of vials, put 10 or 5 cm^3 of the liquid scintillation cocktail in 20 or 6 cm^3 polyethylene liquid scintillation vials. The small vials (6 cm^3) are placed in a special adapter in order to fit in the slots of the LSC.

(2) Add 0.1-0.25 cm^3 of the labelled phase (remove this with a pipet without disturbing the other phases) and shake the vial well.

(3) Place the sample in LSC and count the samples using the appropriate program setting on the counter.

5.2.3 Procedure for Calcium and Magnesium Measurement

The concentration of calcium and magnesium of the stock solution and effluent core flood samples was measured using Atomic Absorption Spectrophotometer (AA) with the standard addition method. The phase of interest was mainly microemulsion phase due to sensitivity of phase behavior to the divalent concentration. The following preparation was done on microemulsion phase of stock or effluent sample:

(1) Remove as much as possible of the microemulsion (m.e.) phase using Pasteur pipets and place in another tube. At least 5-6 cm^3 of m.e. is needed (may have to combine adjacent tubes).

(2) Record the amount of m.e. phase in the tube, then add a volume of 95 percent pure ethanol equal to 10 percent of m.e. volume.

(3) Seal with Silicon stoppers, shake gently.

(4) Loosen stopper, place in 80°C oven for about 15-20 minutes.

(5) Centrifuge 15-20 minutes at about 500 rpm.

(6) At this point the m.e. should be broken into two transparent phases, an upper oil and a lower aqueous phase. Record both of these volumes. If two transparent phases do not form, add more ethanol (5 percent total initial m.e. volume).

(7) Remove the upper phase using a suction apparatus.

(8) Using an automatic pipet, put 1.5 cm^3 aqueous phase in 25 cm^3 volumetric flasks, labelled 1a and 1b.

(9) Add 5 cm^3 of 10 ppm calcium solution and 5 cm^3 of 1 ppm magnesium solution to flask 1b.

(10) Add de-ionized water to 25 cm^3 in both flasks, and shake gently.

Then, take the following steps using AA:

- Set up the AA for Calcium

(1) run a 2 ppm calcium standard and adjust the scale to read 20.

(2) Run sample 1a (let run for 5 seconds), push the "Read" switch on AA, let red light go out, remove sample, record reading. Repeat three times. Reading should be in the medium range of AA scale (5-75). If greater than 75, dilute 1a with de-ionized water to make new 1a and 1b.

(3) Run sample 1b. Reading should be 15-25 units higher than 1a.

(4) Take the arithmetic average of the three readings on samples 1a and 1b and represent them as $\overline{1a}$ and $\overline{1b}$.

(5) Calculate the difference between $\overline{1b}$ and $\overline{1a}$ to get ($\overline{1b}$ - $\overline{1a}$).

The difference between $\overline{1b}$ and $\overline{1a}$ represents the number of divisions on the scale equal to 2 ppm calcium for that particular sample. The difference should be 15-25 divisions, since we set 20 divisions equal to 2 ppm calcium with the calcium standard.

(6) Find the calcium concentration in the microemulsion as follows:

$[Ca]_{m.e.}$ = (Calcium reading in $\overline{1a}$) x (standard addition factor) x (dilution factor) x (correction for m.e. basis)

$$\text{Standard addition factor} = \frac{2 \text{ ppm Ca}}{\bar{1}b - \bar{1}a}$$

$$\text{Dilution factor} = \frac{25}{1.5}$$

$$\text{Correction for m.e. basis} = \frac{\text{cm}^3 \text{ aqueous in step 6}}{\text{cm}^3 \text{ aqueous in step 2}}$$

- Set up the AA for magnesium

(1) Run the 0.2 ppm magnesium standard and adjust the scale to read 20.

(2) Run 1a and 1b for three times.

(3) Take the average of the three magnesium readings on samples 1a and 1b and represent them by $\bar{1}a$ and $\bar{1}b$.

(4) Calculate the difference between $\bar{1}b$ and $\bar{1}a$ to get $(\bar{1}b - \bar{1}a)$.

(5) Find the magnesium concentration in the microemulsion as follow:

$[Mg]_{m.e.}$ = (Magnesium reading in $\bar{1}a$) x (standard addition factor) x (dilution factor) x (correction for m.e. basis)

where

$$\text{Standard addition factor} = \frac{0.2 \text{ ppm Mg}}{(\bar{1}b - \bar{1}a)}$$

and the dilution factor and correction for m.e. basis are the same as before.

TABLE 5.2.1

Composition of Witco Petroleum Sulfonate

(Weight Percent)

Batch Number	TRS 10-410	Oil	Water	Salt
1	62.1	32.2	4.6	0.1
2	61.4	33.7	4.8	0.1

TABLE 5.2.2

Names of Chemicals and Companies

CHEMICAL	TRADE NAME OR ABBREVIATION	COMPANY NAME AND ADDRESS	PURPOSE
Resin	Shell R-828	The Ring Chemical Company, 1112 Rosine Street, Houston, TX 77109	Epoxy
Versamid 125 Polyamide	Versamid 125	The Ring Chemical Company	Epoxy
Carbon-14		ICN Chemical and Radioactive Div. 207 Campus Drive, Irvine, California 92715	Tracer
Chloride-36		ICN Chemical and Radioactive Div.	Tracer
Tritium		New England Nuclear	Tracer
Tritiated Sulfonate	TRS 10-410	Ashland Oil Company	Tracer
Petroleum Sulfonate		Witco Chemical Corporation, 3230 Brookfield, Houston, TX 77045	Micellar Solution
n-Decane	$n\text{-}C_{10}$	Chem Samp Co., P.O.Box 20305, Columbus, Ohio 43220	Micellar Solution
Iso-butyl Alcohol	IBA	Mallinckrodt, Inc., St. Louis, Missouri 63147	Micellar Solution
-	Beckman Ready Solv	Beckman Instruments, Inc. Fullerton, California 92634	Cocktail for LSC

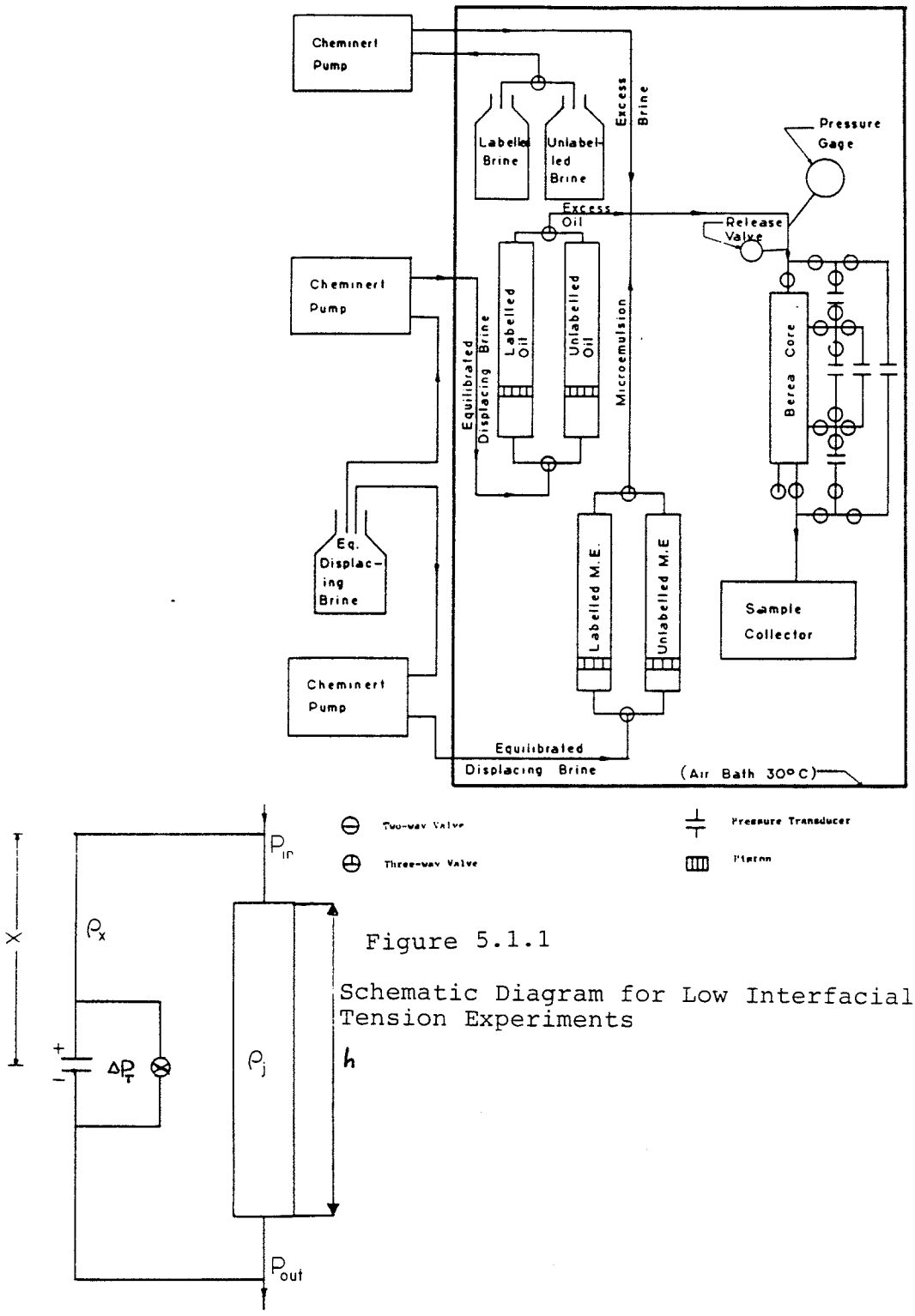

Figure 5.1.1

Schematic Diagram for Low Interfacial Tension Experiments

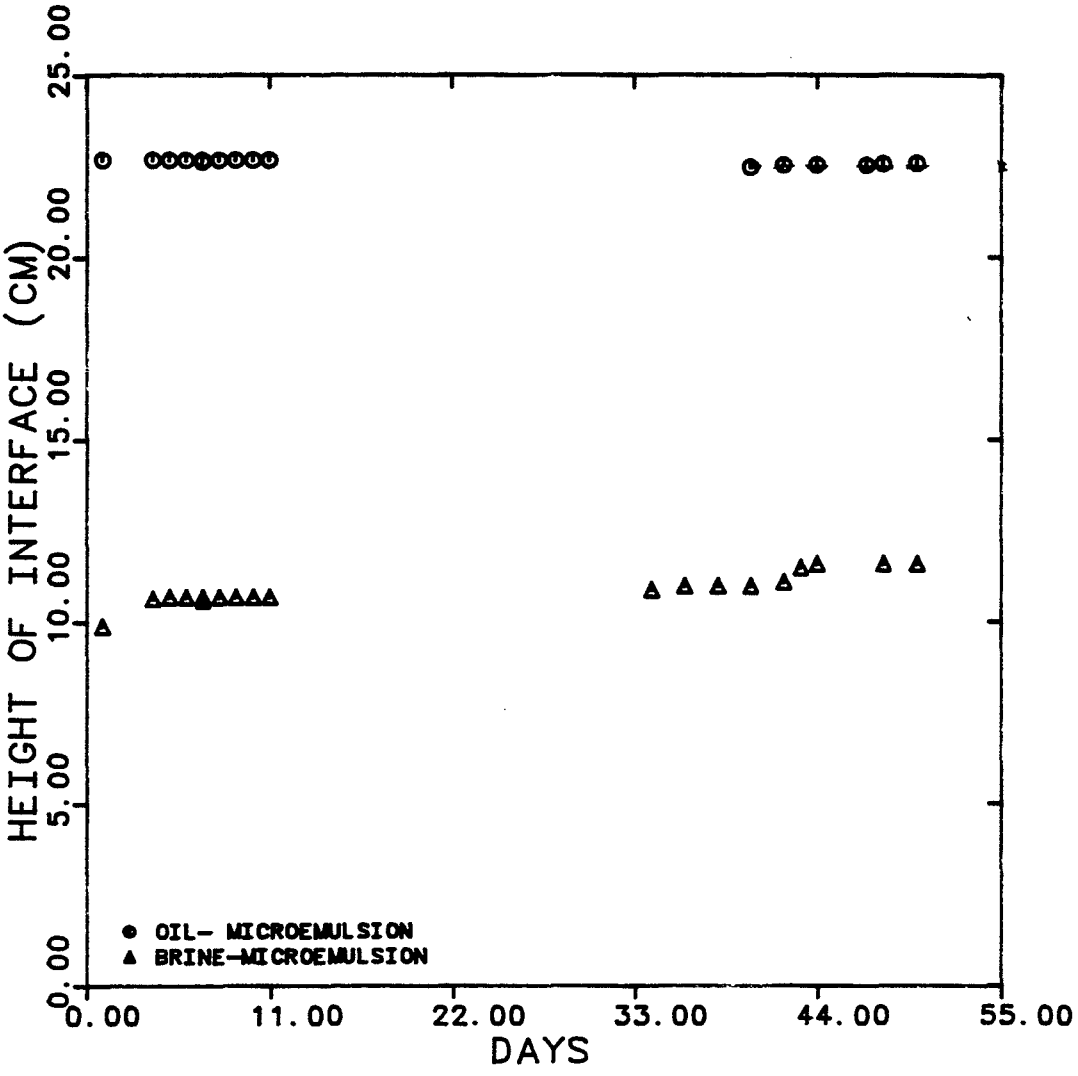

Figure 5.2.1 Equilibration Time for Stock 11

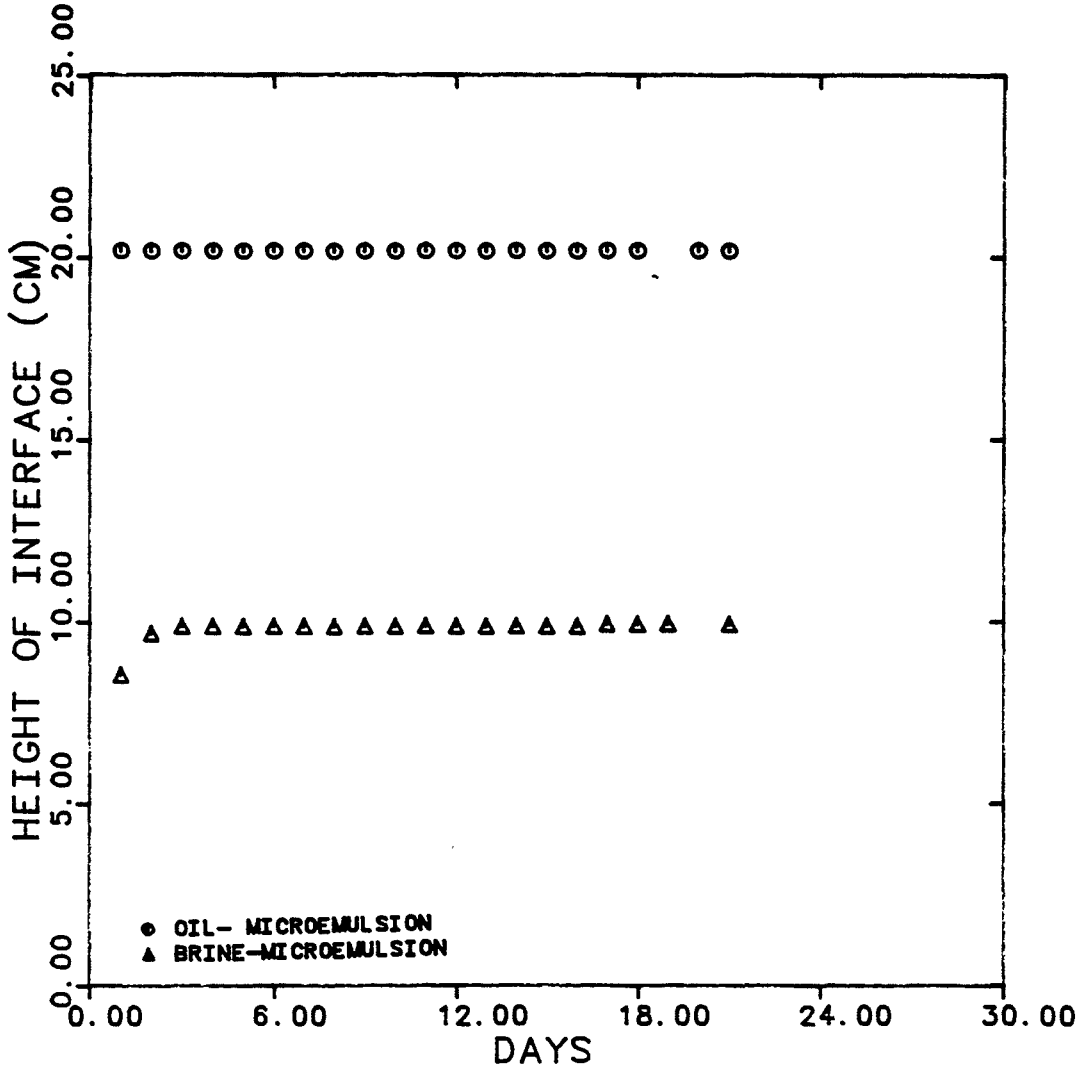

Figure 5.2.2 Equilibration Time for Stock 13

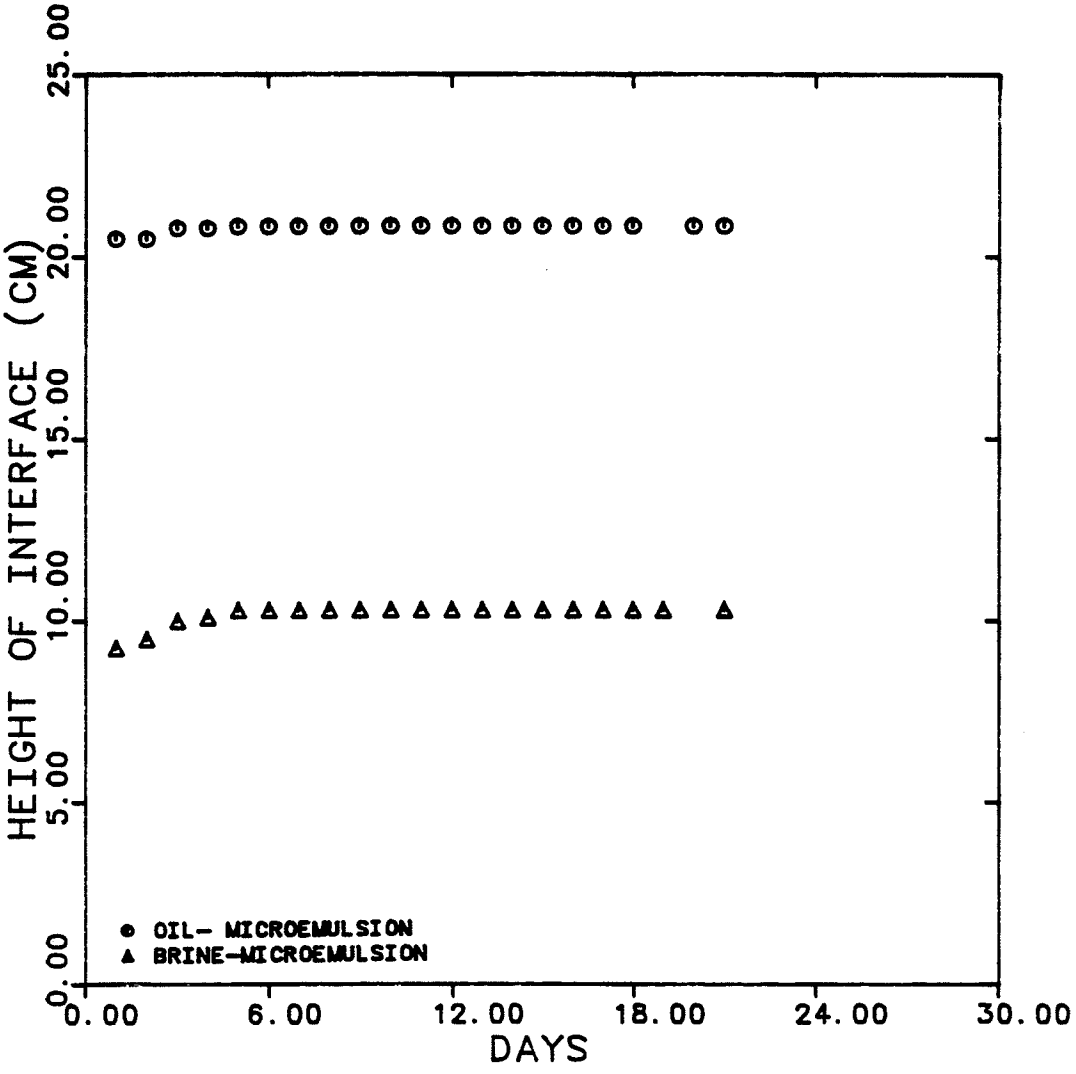

Figure 5.2.3 Equilibration Time for Stock 14

CHAPTER 6

RESULTS AND DISCUSSIONS

6.1 Physical Property Experiments

In order to have a better understanding of the behavior of micellar solutions in core floods, several static physical property experiments were conducted. These experiments included phase behavior (volume fraction), viscosity and interfacial tension measurements. The physical properties of the fluids must be known in order to evaluate the flow experiments. For example, fluid viscosities are used in determining the reference and relative permeabilities. The physical property experiments also were needed to select and characterize the micellar formulation. The specific micellar composition selected was as follows

1.5% Witco TRS 10-410 (active basis)

1.5% IBA

50% n-decane

47% Brine

The salinity of the brine varied. This is given on a water basis by weight percent (i.e. grams of NaCl per 100 grams of brine).

6.1.1 Micellar Behavior Dependence on Salinity

Exp. No. 410-5D-S (TRS 10-410, n-decane, sodium chloride)

When a series of micellar formulations containing varying amounts of sodium chloride are equilibrated with a comparable volume of an oil, multiphase microemulsion systems are formed and the well-documented transition from a lower to middle to upper phase microemulsion is observed as a function of increasing salinity [D.8,J.2,M.1,S.1,S.2,R.5]. Table 5.2.1 lists the composition of Witco TRS 10-410 for Batch #1 used in this experiment. No calcium was added to the samples. Figure 6.1.1 shows the relative volume fraction versus salinity. Figure 6.1.1 shows classical phase behavior with the mid-point of the three phase region at about 1.1 wt% NaCl.

The viscosity of the microemulsion phase of each of these same sample compositions was measured using the LS-30 over a shear rate range of 0.018 to 128.5 sec^{-1}. Figure 6.1.2 shows viscosity of the microemulsion phase as a function of shear rate for the samples with

the salinity of 0.9, 1.0, and 1.1 wt% NaCl. This figure indicates Newtonian behavior for the microemulsion phase with the exception of the microemulsion at 0.9% salinity. The onset of shear rate dependence is at about 40 sec^{-1} and is consistent with Delshad [D.8] and MacAllister [M.1] results. Figure 6.1.3 shows the measured viscosity at constant shear rates of 0.512 and 69.5 sec^{-1} as a function of salinity. The viscosities were measured taking one cm^3 of microemulsion phase with a pipet from the sample without disturbing or mixing the phases.

The interfacial tension of the equilibrated phases was measured using the spinning drop tensiometer. These data were plotted two ways. Figure 6.1.4 shows the result of IFT measurements as a function of salinity. These data show the typical characteristic behavior for such fluids. By one of the several definitions in common use, the optimal salinity is where these curves cross. The interfacial tension at this optimal salinity (1.1 wt%) is about 8.5×10^{-4} dyne/cm. One of the reasons for measuring these data was to locate this point. The second means of analysis of the IFT data is shown in Figure 6.1.5 which the IFT is plotted as a function of the solubilization ratio of either water or oil to active surfactant.

Exp. No. 410-5D-D (TRS 10-410, n-decane, divalent)

A phase behavior experiment similar to that of the previous one was performed using sulfonate Batch #1. In this experiment, an amount of calcium chloride was added to the composition sufficient to produce a calcium concentration in the m.e. of 15 ppm, based on the assumption that all the calcium will partition into the microemulsion phase. The selection of 15 ppm Ca^{++} corresponds to an amount of Ca^{++} produced at steady-state flow of microemulsion without calcium.

Figure 6.1.6 shows the volume fraction for this formulation. Comparisons with previous data (Exp. No. 410-5D-S) do not show any significant difference in the upper part of the curve (type II (-)), but shows a slight shift to the left in the lower portion of the volume fraction diagram. This shift corresponds to a mid-point salinity of the three phase region of about 1.0% as compared to that of 1.1% in Figure 6.1.1.

The viscosity of the microemulsion phase at salinities of 0.9, 1.0, and 1.1 wt% NaCl is plotted as a function of shear rate in Figure 6.1.7. The microemulsion viscosities (at 1 and 1.1 percent NaCl) seem Newtonian and show an increasing trend by the addition of 15 ppm Ca^{++} to the m.e. Consistent with

results in Figure 6.1.2, the onset of shear rate dependence for the viscosity of microemulsion at 0.9% salinity is about 40 sec^{-1}. Figure 6.1.8 shows the measured microemulsion viscosity versus salinity at constant shear rates of 0.0512 and 69.5 sec^{-1}. The appearance of high viscosity microemulsion at the transition from type II (-) to type III behavior is consistent with previous results obtained by Delshad [D.8]; Jones [J.2] and McAllister [M.1]. These results show a slight increase in viscosity when compared with the viscosity of microemulsion without calcium (Figure 6.1.3).

The interfacial tension of the equilibrated phases was also measured and are plotted in Figure 6.1.4 and 6.1.5. Figure 6.1.4 indicates that the interfacial tension curves for the fluids with calcium are shifted to the left with lower IFT values for microemulsion-oil and higher values for microemulsion-brine fluid pairs. The cross-over points also shifted to the left indicating a lower optimal salinity of about 1.0 wt% NaCl. Figure 6.1.5 also includes the data of Exp. No. 410-5D-S and the data published by Glinsmann [G.1,H.3] for the same composition.

Exp. No. 410-5D-D2 (TRS-10-410, n-decane - divalent)

Due to the differences in composition of the batches of sulfonate received from the manufacturer, a preliminary phase behavior study was done to specifically locate the optimal salinity for this new batch of surfactant. Table 5.1 lists the composition of sulfonate Batch #2. Shown in Figure 6.1.9 is the volume fraction diagram which once again demonstrates the typical transition from type II (-), through III to type II(+) behavior with increasing salinity. Figure 6.1.9 shows a significant change in the lower part of volume fraction diagram and also indicates a higher value for the mid-point salinity of the three phase region when compared with Figure 6.1.6. Figure 6.1.10 shows the solubilization ratio of either oil or brine to active surfactant (V_o/V_s, V_w/V_s) as a function of salinity. The curves cross at 1.2 wt% NaCl, taken to be the optimal salinity of this batch of surfactant.

TOTAL FLUID COMPOSITION	
TRS 10-410	1.5 VOL.%
IBA	1.5 VOL.%
N-DECANE	50 VOL.%
BRINE	47 VOL.%

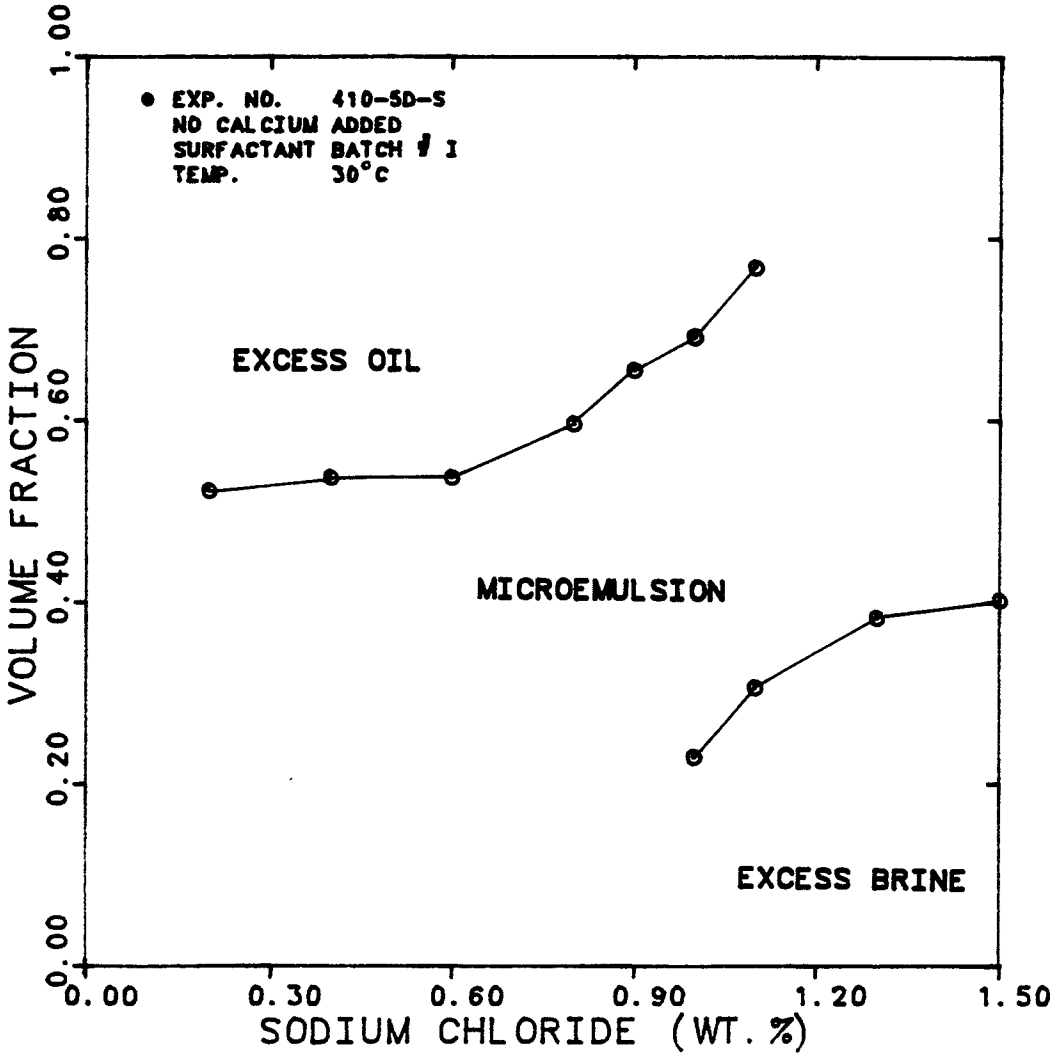

Figure 6.1.1 Volume Fraction Diagram for Surfactant Batch Number 1 (without Calcium)

TOTAL FLUID COMPOSITION	
TRS 10-410	1.5 VOL.%
IBA	1.5 VOL.%
N-DECANE	50 VOL.%
BRINE	47 VOL.%

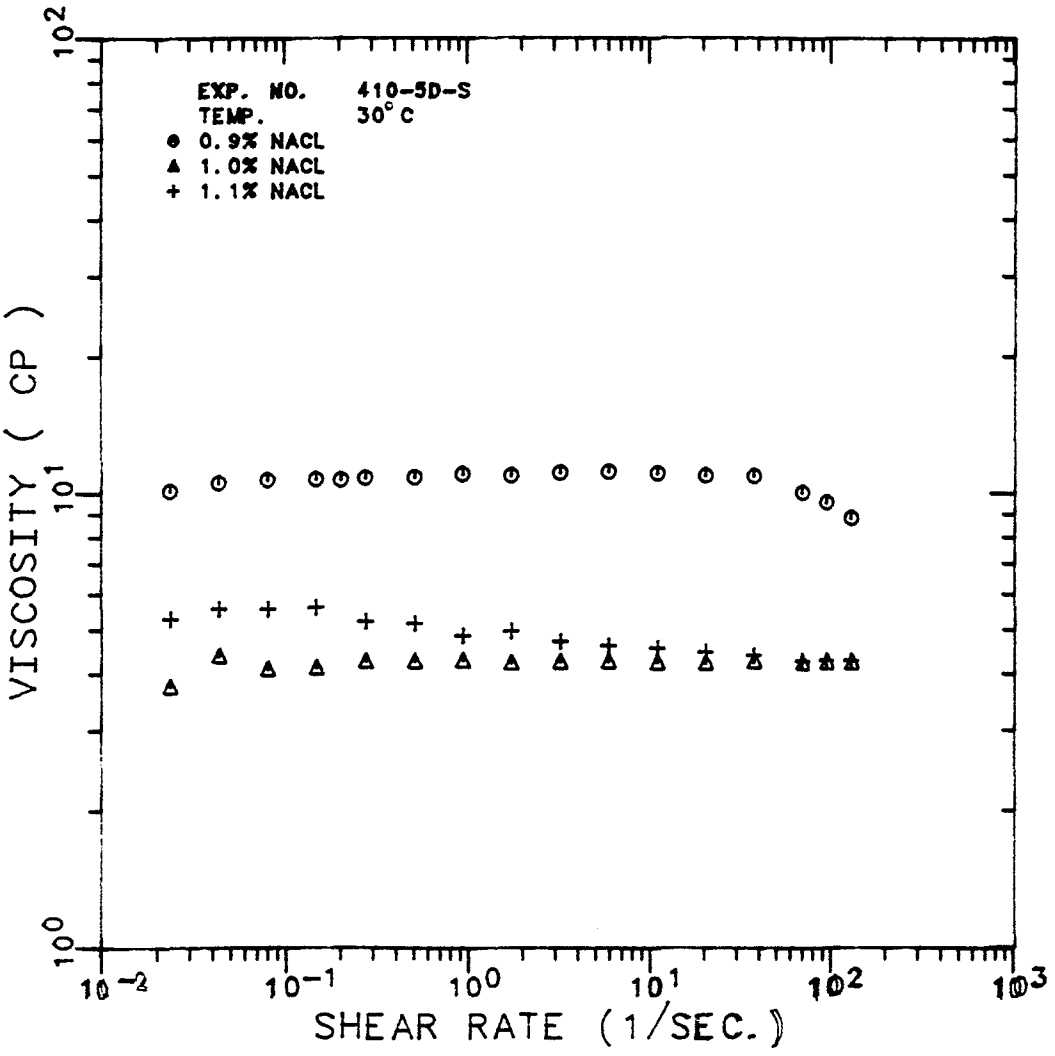

Figure 6.1.2 Viscosity of Microemulsion as a Function of Shear Rate at Salinities of 0.9, 1.0, and 1.1 percent

TOTAL FLUID COMPOSITION	
TRS 10-410	1.5 VOL.%
IBA	1.5 VOL.%
N-DECANE	50 VOL.%
BRINE	47 VOL.%

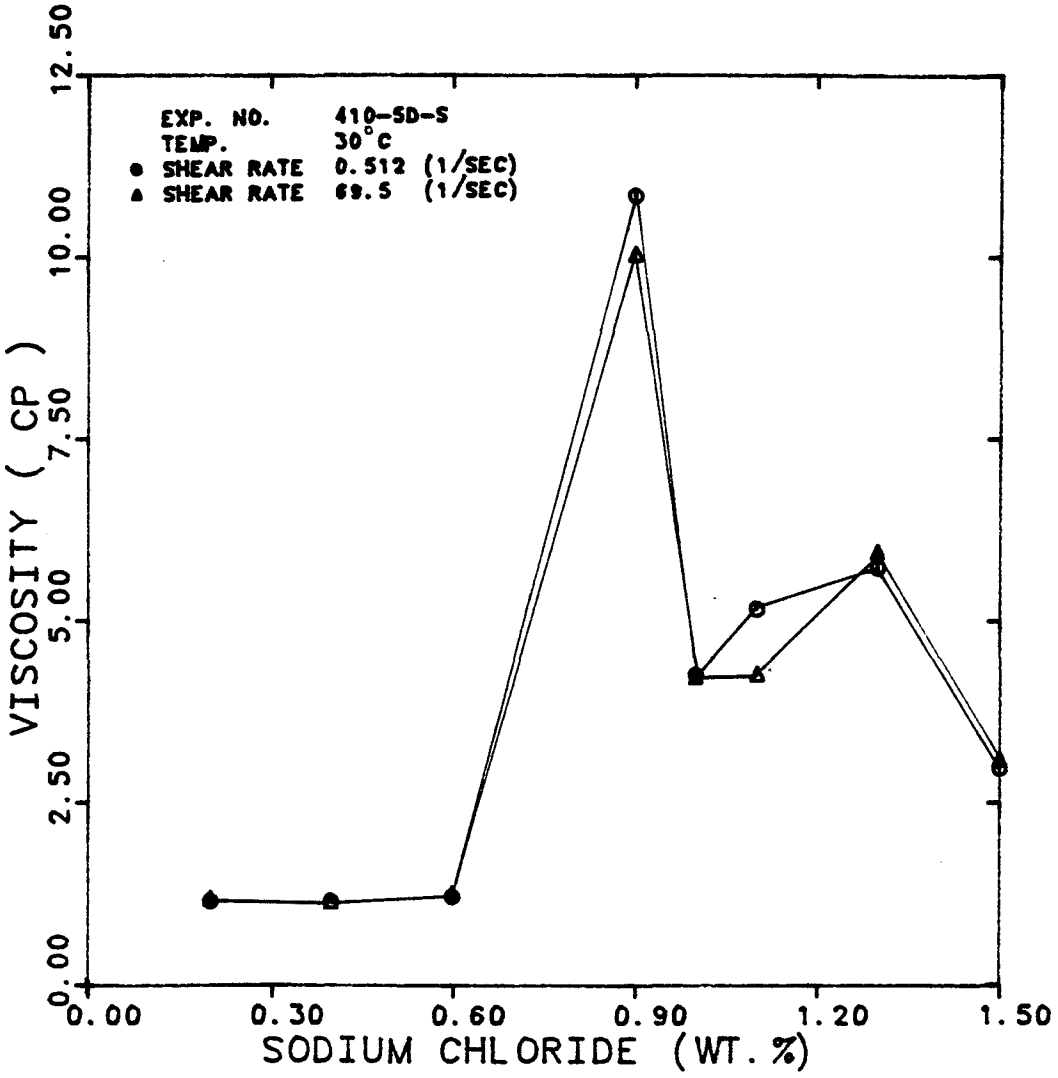

Figure 6.1.3 Viscosity of Microemulsion as a Function of Salinity at Shear Rate of 0.512 and 69.5 1/sec

TOTAL FLUID COMPOSITION	
TRS 10-410	1.5 VOL.%
IBA	1.5 VOL.%
N-DECANE	50. VOL.%
BRINE	47. VOL.%

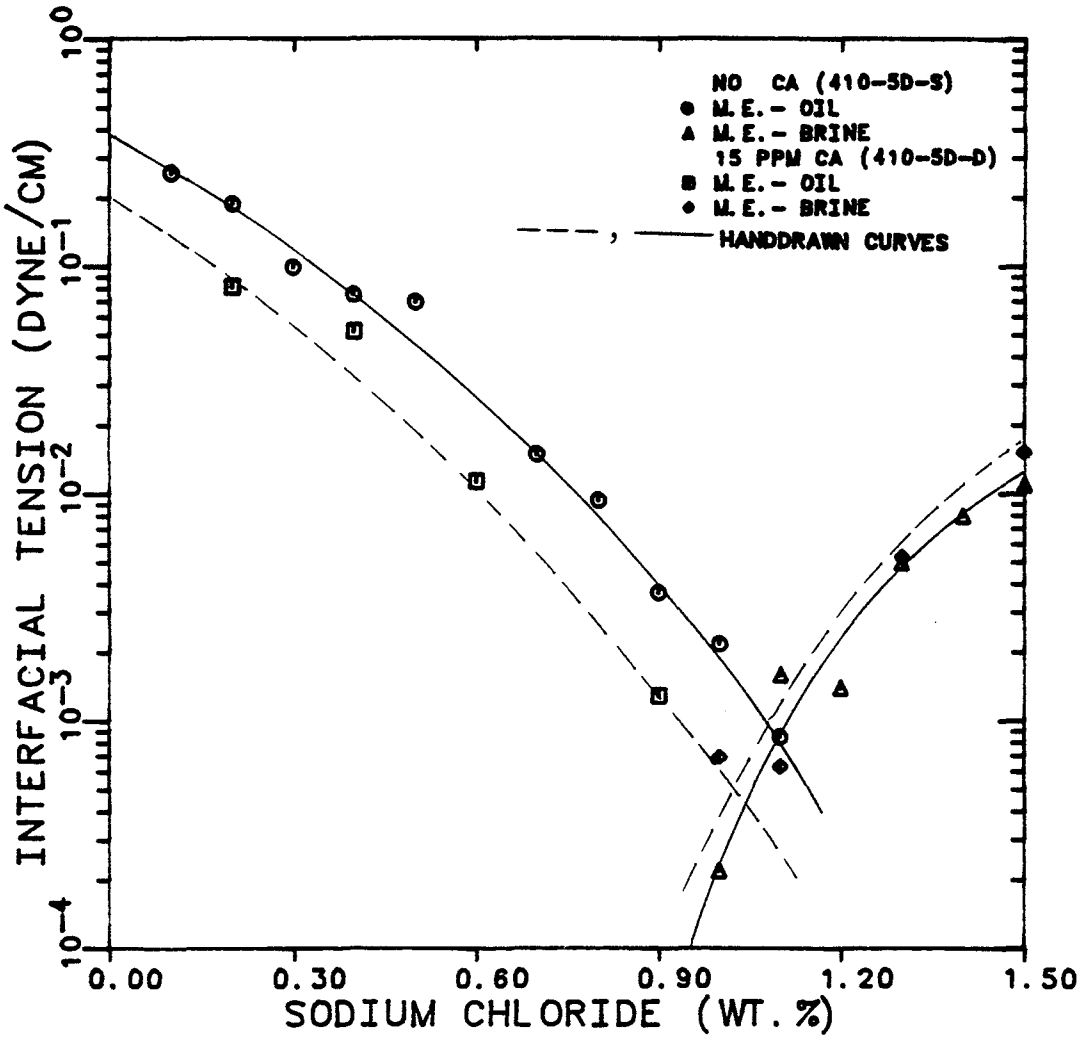

Figure 6.1.4 Interfacial Tension as a Function of Salinity With and Without Calcium

TOTAL FLUID COMPOSITION	
TRS 10-410	1.5 VOL.%
IBA	1.5 VOL.%
N-DECANE	50. VOL.%
BRINE	47. VOL.%

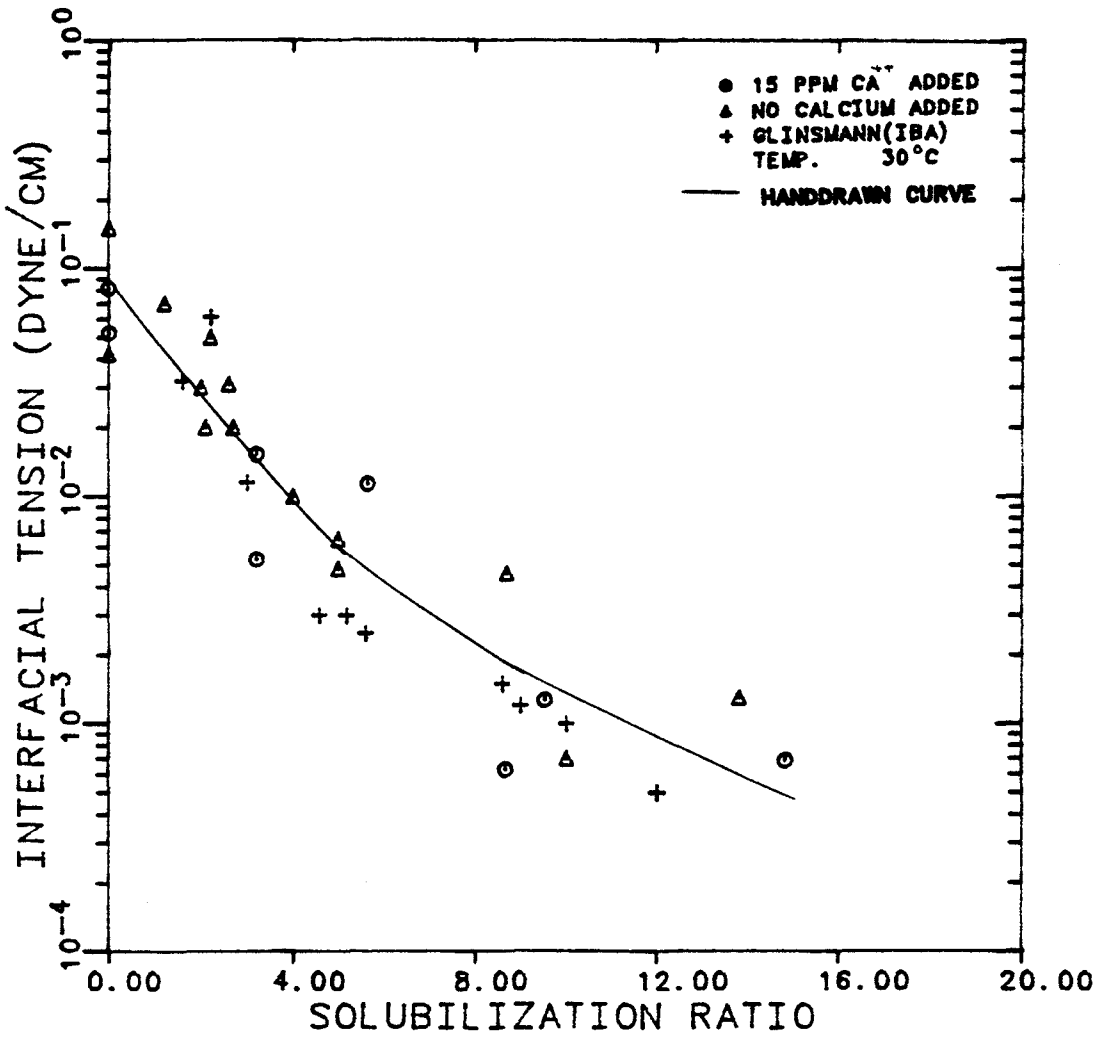

Figure 6.1.5 Interfacial Tension as a Function of Solubilization Ratio

TOTAL FLUID COMPOSITION	
TRS 10-410	1.5 VOL.%
IBA	1.5 VOL.%
N-DECANE	50 VOL.%
BRINE	47 VOL.%

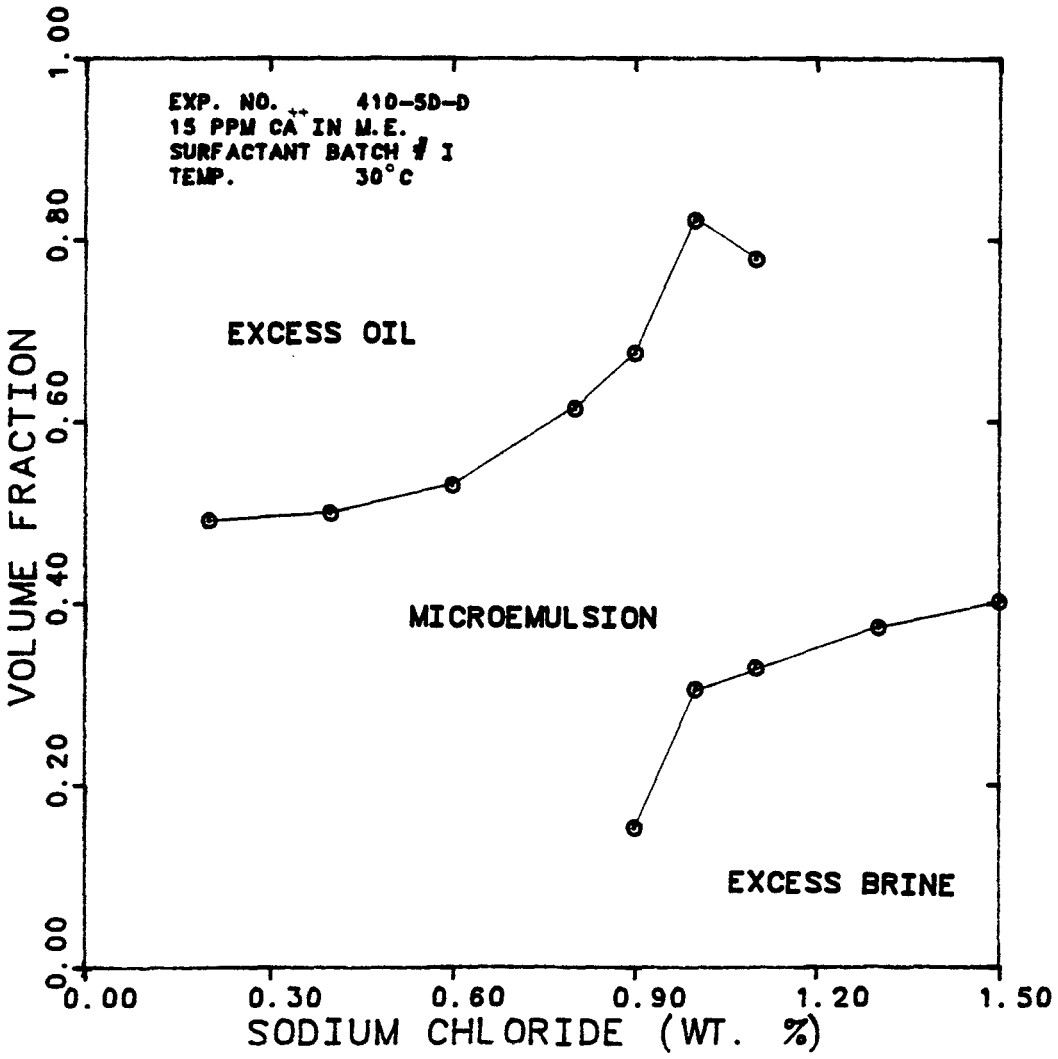

Figure 6.1.6 Volume Fraction Diagram for Surfactant Batch Number 1 (with Calcium)

TOTAL FLUID COMPOSITION	
TRS 10-410	1.5 VOL.%
IBA	1.5 VOL.%
N-DECANE	50 VOL.%
BRINE	47 VOL.%

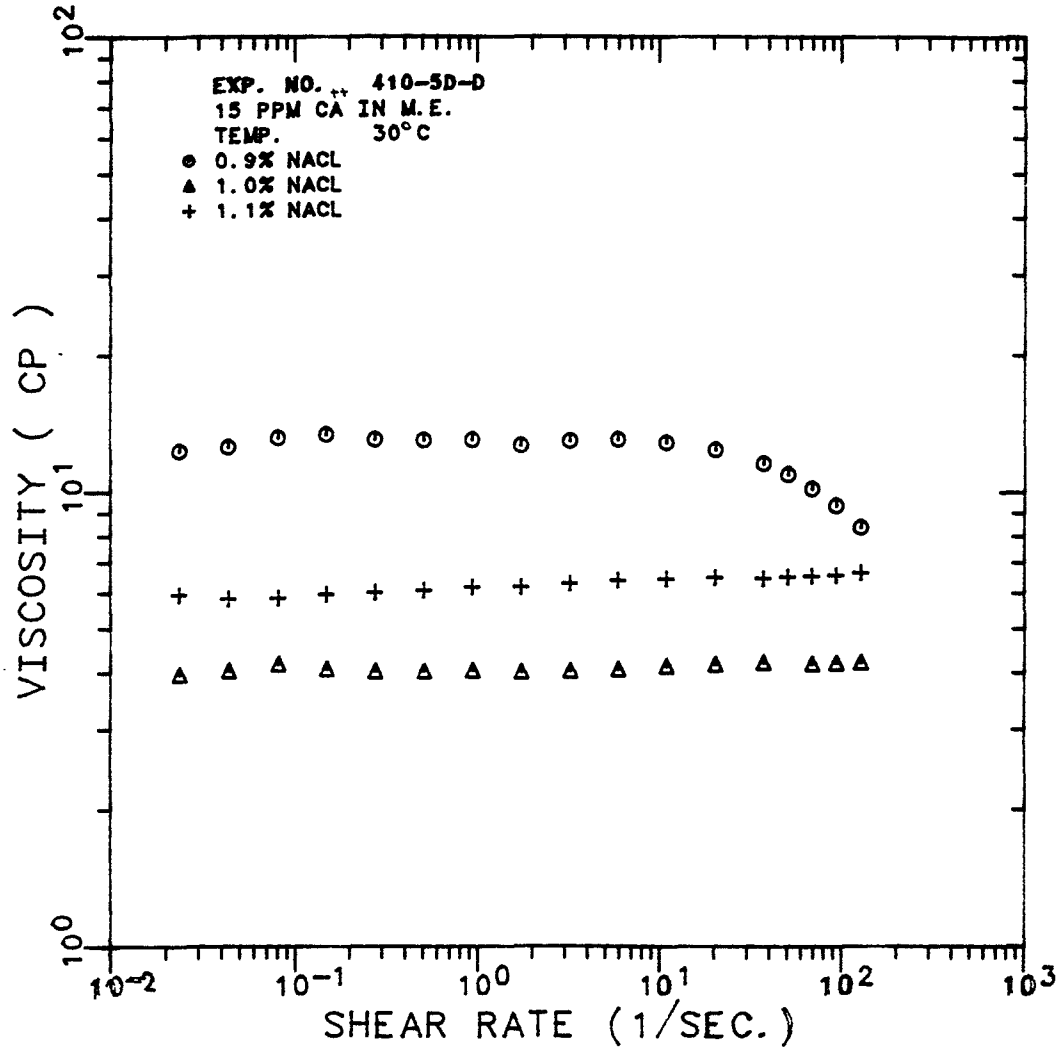

Figure 6.1.7 Viscosity of Microemulsion as a Function of Shear Rate and at Salinities of 0.9, 1.0, and 1.1 percent

TOTAL FLUID COMPOSITION	
TRS 10-410	1.5 VOL.%
IBA	1.5 VOL.%
N-DECANE	50 VOL.%
BRINE	47 VOL.%

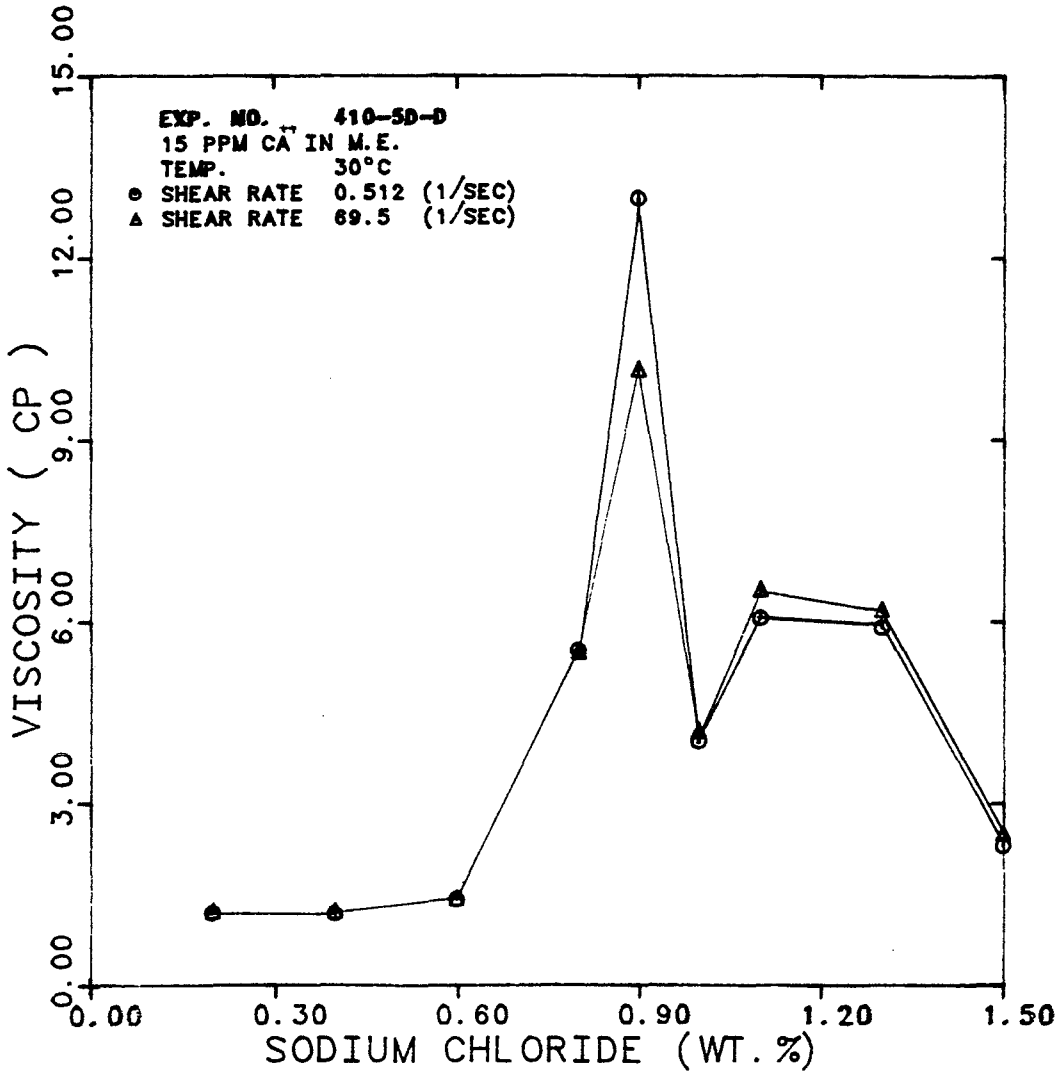

Figure 6.1.8 Viscosity of Microemulsion (with Calcium) as a Function of Salinity at Shear Rates of 0.512 and 69.5 1/sec

TOTAL FLUID COMPOSITION	
TRS 10–410	1.5 VOL.%
IBA	1.5 VOL.%
N-DECANE	50 VOL.%
BRINE	47 VOL.%

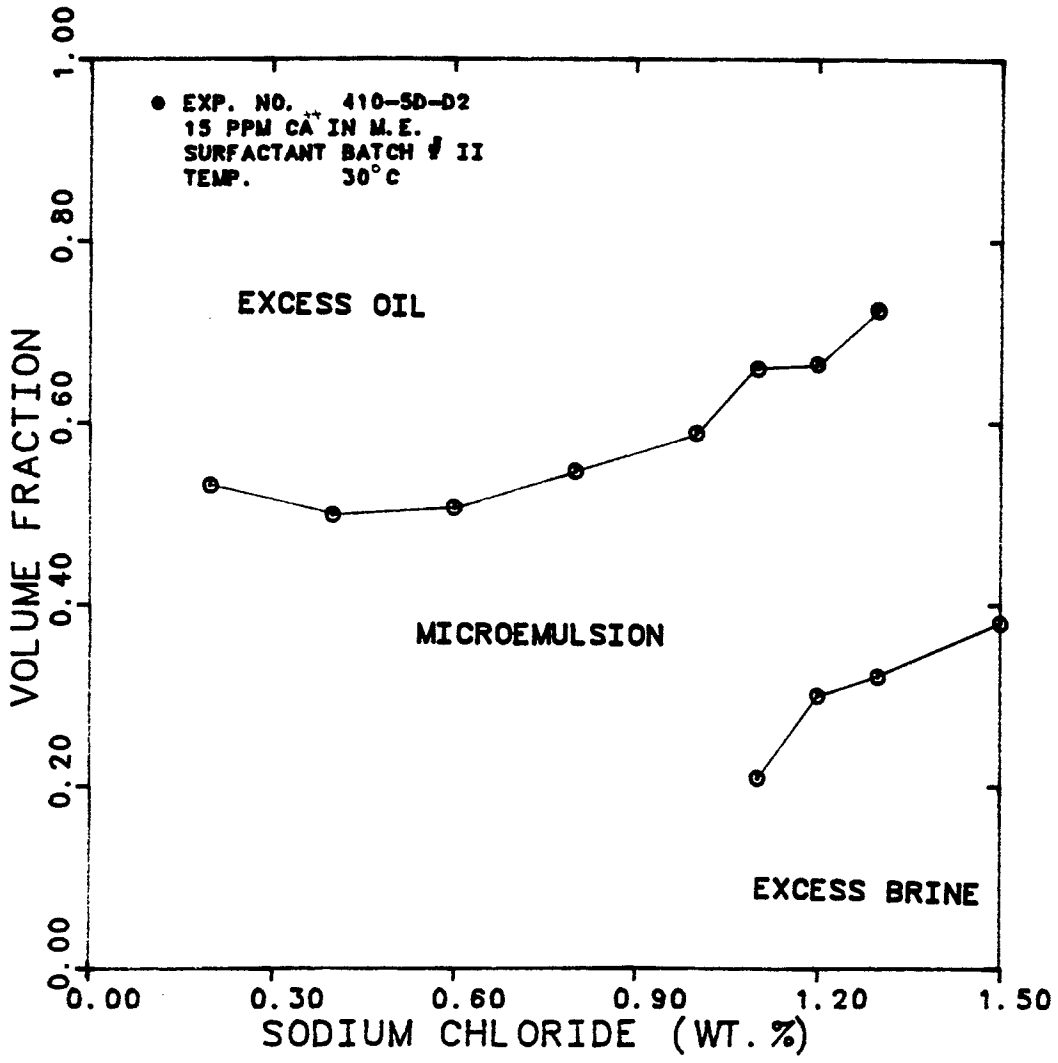

Figure 6.1.9 Volume Fraction Diagram for Surfactant Batch Number 2 (with Calcium)

TOTAL FLUID COMPOSITION	
TRS 10-410	1.5 VOL.%
IBA	1.5 VOL.%
N-DECANE	50. VOL.%
BRINE	47. VOL.%

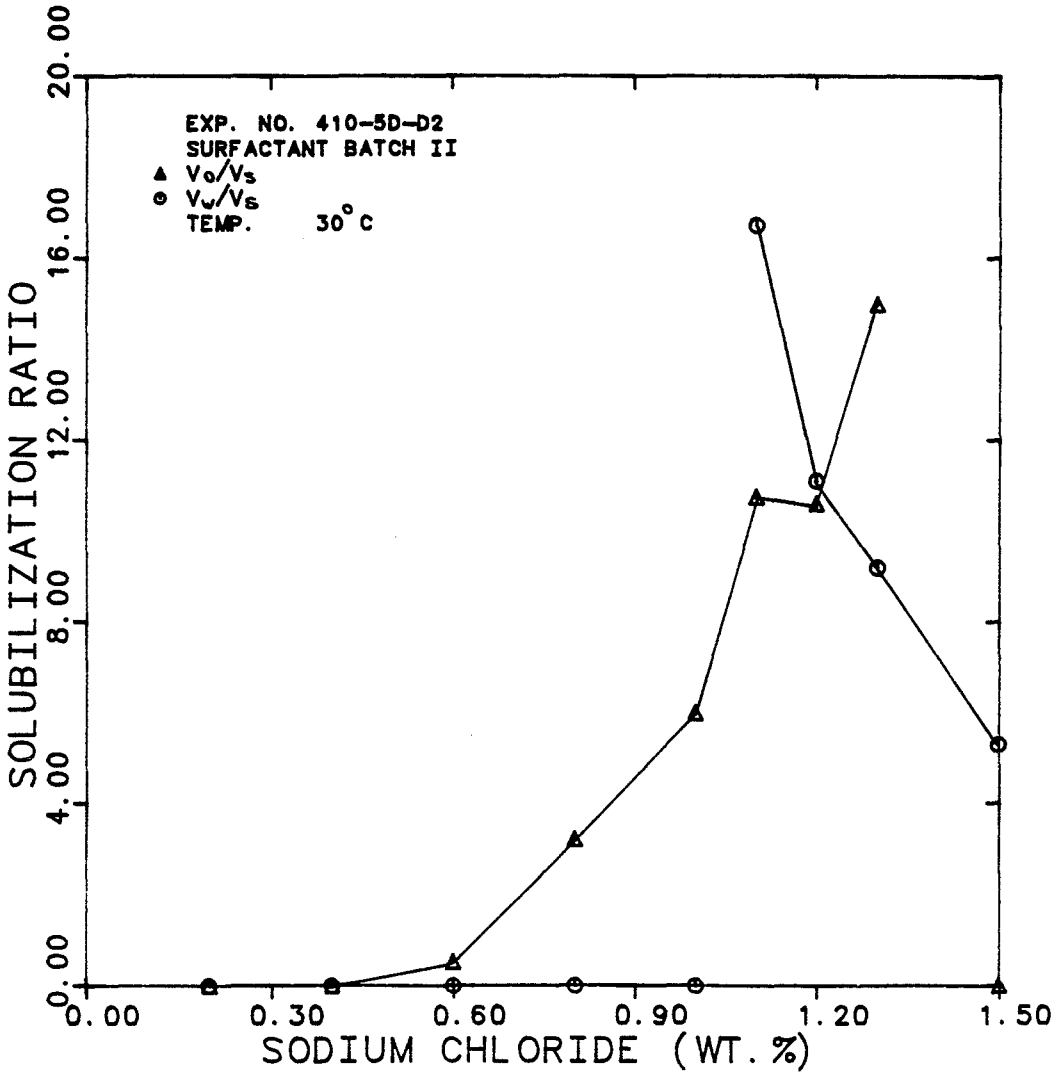

Figure 6.1.10 Solubilization Ratio as a Function of Salinity

6.1.2 Physical Property Measurements of Micellar Solution Used in the Flow Experiments

A three-phase micellar solution with a salinity close to the optimal salinity was chosen for all the flow experiments performed in this study. Large batches, with total composition of 1.5 v% active Witco TRS 10-410, 1.5 v% isobutanol, 50 v% n-decane, and 47 v% brine containing water, sodium chloride and calcium chloride, were made up in 15 liter glass bottles. The fluids were prepared with the procedure discussed in Section 5.2 and allowed to equilibrate at 30°C for a period of 30-45 days. Two batches were made at the same time, one containing no tracer (cold) and the other with radioactive tracers (hot). Equilibrated phases were separated and analyzed for density, viscosity, interfacial tension, tracer concentration, and composition. The results of these measurements are shown in Table 6.1.1.

Interfacial tensions were estimated from the solubilization ratio curve (Figure 6.1.5) if measurements were not available. The solubilization ratio of water and oil are defined as the ratio of the volume of water and oil present in the microemulsion phase to the active surfactant as

$$R_{sw} = \frac{V_w}{V_s} \quad , \quad R_{so} = \frac{V_o}{V_s} \qquad (6.1)$$

The partition coefficient of each tracer was estimated using the measured concentration of tracer in equilibrated phases of the hot batch of micellar solution. The calculation for the partition coefficient of each tracer, $k_{ij}^{(i)}$ was as follows

- Tritiated water, T_2O or chloride-36, ^{36}Cl (i=1)

These are partitioning tracers for the excess brine and the microemulsion phases.

$$K_{31}^{(1)} = \frac{C_{13}}{C_{11}} \qquad (6.2)$$

- Carbon-14 labelled decane, ^{14}C (i=2)

This is a partitioning tracer for the excess oil and the microemulsion phases

$$K_{32}^{(2)} = \frac{C_{23}}{C_{22}} \qquad (6.3)$$

- Tritium labelled sulfonate, T.S. (i=3)

Due to the low concentration of surfactant in the excess brine and excess oil phases (Table 6.1.1), this tracer is a non-partitioning tracer for the microemulsion phase.

$$K_{13}^{(3)} = \frac{C_{31}}{C_{33}} \qquad (6.4)$$

The partition coefficient is another way of representing the concentration of water and oil in the microemulsion phases since T_2O or ^{36}Cl and ^{14}C dissolve in water and oil portions of microemulsion, respectively.

Table 6.1.1 also presents the composition of all the three equilibrated phases. The concentration of oil and water in the microemulsion phase is from the tracer concentration analysis. Alcohol (IBA) concentration in each phase is measured by gas chromatography. The surfactant concentration in each phase is also from the tracer concentration analysis. The values obtained are in a very good agreement with the ones measured using the sulfur analyzer. The concentration of water and oil in the excess brine and oil are then estimated from the material balance calculation.

TABLE 6.1.1
The Analytical Results of Micellar Solution

Batch #	Sodium Chloride Salinity (%)	Phase Volume Fraction			Total Volume (cm^3)	Density (g/cm^3)			Viscosity (cp)			Partition Coefficient			
		Brine	Oil	M.E.		Brine	Oil	M.E.	Brine	Oil	M.E.	^{36}Cl	^{14}C	T.S.	T_2O
1) cold	1.1	0.279	0.268	0.453	14920	1.0008	0.7275	0.8508	0.84	0.78	4.0	-	-	-	-
1) hot	1.1	0.268	0.260	0.472	14840	0.999	0.7373	0.8484	0.84	0.78	4.0	-	0.495	-	0.423
2) cold	1.1	0.277	0.240	0.483	15002	1.0018	0.7247	0.8637	0.897	0.824	4.50	-	-	-	-
2) hot	1.1	0.280	0.260	0.460	15148	1.0016	0.7257	0.8562	0.890	0.867	4.58	-	0.555	-	0.407
4) cold	1.2	0.286	0.244	0.470	15095	1.0012	0.7291	0.8383	0.906	0.840	4.55	-	-	-	-
4) hot	1.2	0.292	0.233	0.475	14896	1.0012	0.7266	0.8343	0.897	0.844	4.47	-	0.590	-	0.336
6) cold	1.2	0.280	0.359	0.361	15454	1.0017	0.726	0.8827	0.99	0.92	4.81	-	-	-	-
6) hot	1.2	0.267	0.330	0.403	1990	1.005	0.725	0.879	0.988	0.870	5.0	0.496	0.465	0.05	-
7) cold	1.2	0.276	0.324	0.400	15315	1.0017	0.725	0.8641	0.986	0.94	4.9	-	-	-	-
7) hot	1.2	0.287	0.341	0.372	15181	1.0018	0.725	0.874	0.991	0.912	5.0	0.462	0.492	0.04	-
9) cold	1.2	0.279	0.319	0.402	15186	1.0018	0.725	0.868	0.983	0.91	4.57	-	-	-	-
9) hot	1.2	0.275	0.324	0.401	15275	1.0018	0.725	0.869	0.980	0.93	4.55	0.407	0.499	0.042	-
13) cold	1.2	0.287	0.341	0.372	15144	1.0017	0.725	0.873	0.950	0.89	4.75	-	-	-	-
13) hot	1.2	0.282	0.343	0.375	15106	1.0016	0.725	0.875	0.950	0.89	4.50	0.481	0.484	0.045	-
14) cold	1.2	0.282	0.348	0.370	15236	1.0018	0.725	0.8793	0.950	0.89	4.70	-	-	-	-
14) hot	1.2	0.280	0.348	0.372	15113	1.0018	0.725	0.879	0.950	0.89	4.80	0.426	0.428	0.05	-
Average	-	0.2798	0.305	0.415	15127.6	1.0016	0.726	0.864	0.936	0.873	4.60	0.454	0.501	0.0	0.388

TABLE 6.1.1 (continued)

	Composition																Solubilization Ratio		Interfacial Tension (Dyne/cm)		
	Brine (%)			Decane (%)			Surfactant (%)			IBA (%)			Ca^{++} (ppm)		Mg^{++} (ppm)						Surfactant
Batch #	Brine	Oil	M.E.	Brine	Oil	M.E.	Brine	Oil	M.E.	Brine	Oil	M.E.	Brine	M.E.	Brine	M.E.	V_w/V_s	V_o/V_s	σ_{mw}	σ_{mo}	Batch #
1	97.3	0.0	42.3	0.0	99.65	49.5	0.21	0.050	3.10	2.50	0.30	1.60	0.89	21.0	-	-	12.0	15.33	7.6×10^{-4}	4×10^{-4}	1
2	97.70	0.0	40.7	0.0	99.65	55.5	0.21	0.053	3.20	2.10	0.30	1.81	2.10	10.0	0.45	5.0	12.22	17.72	7.4×10^{-4}	3×10^{-4}	1
4	97.75	0.0	33.6	0.0	99.55	59.0	0.25	0.055	3.10	2.0	0.40	1.73	3.0	17.0	0.15	0.63	11.93	11.49	8.6×10^{-4}	3×10^{-4}	2
6	97.83	0.0	49.6	0.0	99.66	46.5	0.27	0.040	3.60	1.9	0.30	2.20	2.5	15.3	0.95	0.50	13.74	12.05	5.4×10^{-4}	8.8×10^{-4}	2
7	97.3	0.0	46.2	0.0	99.56	49.2	0.20	0.04	3.24	2.50	0.40	1.36	2.60	16.5	0.16	0.50	12.10	12.5	7.7×10^{-4}	7.7×10^{-4}	2
9	98.10	0.0	40.7	0.0	99.60	49.9	0.22	0.060	3.60	1.70	0.35	2.20	1.8	16.0	-	-	12.2	12.5	7.3×10^{-4}	6.9×10^{-4}	2
13	97.87	0.0	48.1	0.0	99.66	48.4	0.23	0.040	3.8	1.9	0.30	2.20	2.0	17.0	-	-	11.82	11.09	8×10^{-4}	9.4×10^{-4}	2
14	97.74	0.0	42.6	0.0	99.67	42.8	0.26	0.033	3.85	2.0	0.30	2.24	-	-	-	-	12.04	10.60	7.6×10^{-4}	10^{-3}	2

TABLE 6.2.1

Characteristics of Berea Core

Length	60.96	cm
Cross-Section area	25.5	cm^2
Bulk volume	1554.5	cm^3
Pore volume	330.0	cm^3
Porosity	0.212	
100% brine permeability	0.739	Darcy
Residual brine saturation (S_{wr})	0.35	
Residual oil saturation (S_{or})	0.30	
Dispersivity at S_w=1.0	0.30	cm

6.2 Capillary Desaturation Curves (Exp. No. CDC3)

The relationship between residual phase saturation and the capillary number, commonly called the capillary desaturation curve, is one of the most important physical relations of the micellar process. Despite its importance, a complete set of experimental capillary desaturation curves for micellar fluids has never been performed. Therefore, the main purpose of experiment CDC3 was to obtain these data for a three-phase micellar fluids in a Berea sandstone core.

There are six possible CDC curves for three-phase as follows

1- The residual excess brine to microemulsion

2- The residual microemulsion to excess brine

3- The residual excess oil to microemulsion

4- The residual microemulsion to excess oil

5- The residual excess oil to excess brine

6- The residual excess brine to excess oil

The first four curves were measured in this study. The reason for not considering the last two curves was the formation of a third macroemulsion (nonequilibrated microemulsion) phase upon mixing of the excess brine and excess oil phases in a test tube.

Experiments were performed on a two-foot long

by two-inch square epoxy-coated Berea sandstone core at 30°C. Porosity was determined by saturating the core with 1.1 wt% NaCl brine. The core was then flushed with the same brine to measure the reference permeability. The core was used in a horizontal configuration with the characteristics listed in Table 6.2.1. The core flood setup (Figure 6.2) consisted of three different range pressure transducers (5, 20, 50 psi) between the intermediate pressure taps; two for each six-inch section (1 and 20 psi); and two for the whole length (5 and 100 psi), one Cheminert pump, one Zenith pump, solution reservoirs, and the sample collector. The whole apparatus except for the pump was in the flow oven at 30°C. A single phase dispersion run was also performed in order to measure the dispersivity and examine the homogeneity of the core. The breakthrough curve of tritium in brine is shown in Figure 6.2.1. This figure shows also the matching parameters which are:

1- Flowing fraction of phase 1 (F_1)

2- Saturation of Phase 1 (S_1)

3- Dispersivity of tritium in Phase 1 (α_{11})

4- Mass transfer coefficient of tritium in Phase 1 (M_{11})

The flowing fraction of $F_1 = 1.0$ and mass transfer

coefficient of M_{11} = 0.0 imply that the convection-diffusion equation (Eq. 3.2) adequately matches the data, with the dispersivity of 0.30 cm. The curve is almost symmetric with C/C_o = 0.50 at 1.013 P.V.. The next step was to measure the residual brine and oil saturations (Table 6.2.1) as follows:

- saturate the core with n-decane at high flow rate (32 psi pressure drop over 2 ft) to get the true residual water saturation. Saturations were calculated by means of material balance (Eq. 3.52).

- Inject n-decane containing carbon-14 labelled decane at a flow rate of 4.0 cm^3/min to measure the dispersion and also estimate the saturations. The latter was done by matching the experimental breakthrough curve against the capacitance model (Figure 6.2.2). The results showed that the convection-diffusion (C-D) equation was adequate to match the data (since the values of flowing fraction and mass transfer coefficient were 1.0 and 0.0, respectively).

- The core was then flooded with 1.1 wt% NaCl brine to irreducible oil saturation. At steady-state brine containing tritium was injected. The breakthrough curve is shown in Figure 6.2.3 where the solid curve is the calculated curve using the C-D equation.

The core was flushed with several pore volumes of 1.1% NaCl brine at 4 cm^3/min to reduce the calcium concentration. The calcium concentration in the effluent samples was measured by atomic adsorption. After about 15 pore volume throughput, the Ca^{++} and Mg^{++} concentrations were about 19 and 2 ppm, respectively. Calcium was added to the micellar solutions so that the injected and produced values would be about the same.

Two 15 liter batches (hot and cold) of micellar fluids (stock 1) with the total composition of 1.5 v% TRS 10-410, 1.5 v% IBA, 50 v% n-decane, and 47 v% water were made up at 1.1 wt% NaCl and 13.7 ppm Ca^{++} and allowed to equilibrate. The composition of microemulsion phase was determined to be 42.3 v% brine, 49.5 v% n-decane, 1.60 v% IBA, and 3.10 v% TRS 10-410. The physical properties of all the three phases are tabulated in Table 6.1.1. The tracers added to the hot batch were carbon-14 labelled n-decane and tritium.

Equilibrated lower phase brine was used to drive the middle phase microemulsion and excess oil phase from the solution reservoir into the core. The lower phase brine was injected through a Cheminert pump to drive the reservoir solution.

The experiment involved the following sequence

of floods, starting with a core containing a known residual oil (S_{2r} = 0.30) from the waterflood.

1- The core was flooded with microemulsion to steady-state at a flow rate of 1.97 cm^3/min and material balance calculations done to determine the saturation state of the core. The core was then flooded with the same microemulsion containing both carbon-14 and tritium as tracers. The latter step is used to evaluate the saturations by tracer breakthrough data to compare with material balance calculations and to determine the dispersivity and dispersion coefficients. The residual saturations based on the tracer data were brine S_{1r} = 0.065 and excess oil S_{2r} = 0.0 (Figures 6.2.4 and 6.2.5).

2- The next step of the experiment was to measure the residual microemulsion saturation to excess brine at various capillary numbers (Exp. Nos. CDC3-12 through CDC-18). To accomplish this objective, the core was flooded with the excess brine phase at a low flow rate (low capillary number) until steady-state conditions were achieved. Brine containing tritium was then injected at the same flow rate. Effluent samples were analyzed and dispersion curves and saturations were determined.

3- The capillary number was increased step-wise by

repeating step 2 at increasing flow rates for the injection of brine.

The tritium breakthrough curves are shown in Figures 6.2.6 through 6.2.9. The solid curves shown in the figures are the calculated curves. The analysis showed that adequate fits were obtained using the convection-diffusion equation. Figure 6.2.9 is the tritium breakthrough curve at the highest capillary number obtained of 0.433 (q = 51 cm^3/min) where it shows the typical s-shaped trend.

The same protocol as above was followed for measuring the following data:

- Residual excess brine to microemulsion (CDC3-20 through CDC3-26)
- Residual microemulsion to excess oil (CDC3-28 through CDC3-32)
- Residual excess oil to microemulsion (CDC3-34 through CDC3-38)

Figures 6.2.10 through 6.2.26 are the tracer breakthrough curves for the above floods. These breakthrough curves were all matched reasonably well with the convection-diffusion equation. The experimental results are presented in Tables 6.2.2 through 6.2.4.

The capillary desaturation data for residual

microemulsion to brine, residual brine to microemulsion, residual microemulsion to oil, and residual oil to microemulsion are plotted as a function of capillary number (Eq. A.7) in Figures 6.2.27 through 6.2.30 consecutively. The residual brine saturation at the highest capillary number of 0.433 was about 7 percent, the residual microemulsion saturation to both oil and brine was zero at this capillary number, while the residual oil saturation even at the lowest capillary number of 0.0037 was zero. These values were based on the dispersion results.

Two sets of data are shown in Figures 6.2.27 through 6.2.3. One is based on dispersion data and the other based on material balance. The saturation values from material balance are higher than those obtained using the tracer breakthrough curves. These differences could be partly due to the errors in saturation estimated by both methods. The sources of error in dispersion calculations are 1) counting procedure, 2) measurement of partition coefficient, and 3) the accuracy of the matching procedure.

In phase balance rather than material balance calculations the two sources of errors are 1) an error in reading the volumes in produced samples which is

cumulative and 2) an error due to a possible phase behavior change during the transient period before the steady-state is reached. To investigate the latter, the composition of effluent samples of microemulsion was analyzed using GC and compared to that of the injected microemulsion. Figures 6.2.31 and 6.2.32 show the composition of effluent microemulsion as a function of pore volumes injected for cut numbers CDC3-21 and CDC3-25, respectively. At the start of cut CDC3-21, the core is saturated with excess brine at residual microemulsion saturation. Both figures indicate that at each capillary number before reaching steady-state, the concentration of oil is lower and brine is higher than those of the injected values. In other words, part of the brine phase has been solubilized in the microemulsion and has been produced with the microemulsion. As a result, the volume balance obtained on the produced (visible) brine phase is lower than the actual value. This explains the high values of residual brine saturation estimated from the material balance compared to those obtained from dispersion (Fig. 6.2.28). The problem of phase behavior change does not arise in dispersion experiments since they are done at steady-state and also the components (oil and water) are tracked rather the phases.

Hereafter, the material balance means the phase balance on effluent samples.

As previously mentioned, the residual oil saturation to microemulsion at the lowest capillary number was zero. After a sequence of two- and three-phase flow experiments (will be discussed later), the following experiment was done to obtain a point with a non-zero residual oil saturation.

- Inject excess oil (Stock 9) from the top at the rate of 2.08 cm^3/min (note that core is in a vertical configuration at the time of this experiment). This was followed by injection of oil containing tracer at 1 cm^3/min. Figure 6.2.33 shows the carbon-14 breakthrough curve along with the computed curve using the convection-diffusion equation. The saturations obtained were $S_{1r} = 0.16$, $S_{2r} = 0.84$ and $S_{3r} = 0.0$.

- Inject microemulsion (Stock 9) at 0.0095 cm^3/min. Due to this low flow rate and in consequence the low pressure drop, the microemulsion was injected from the bottom to attain a higher output signal on the transducers. This way we take advantage of the gravitational head of the microemulsion (Eq. 5.5).

The transducers used were: two 0.2 psi for the middle section, 1 psi for inlet and outlet sections, and

1,2 psi for the overall section.

Steady-state conditions were fulfilled after injection of about 1.64 P.V. of microemulsion phase. Then, the triple-labelled microemulsion (Stock 9) was injected at the same flow rate. The breakthrough curves of tritium labelled sulfonate, choride-36, and carbon-14 are shown in Figures 6.2.34 through 6.2.36, consecutively. The saturations obtained from the analysis of these curves were $S_{1r} = 0.314$, $S_{2r} = 0.033$, and $S_3 = 0.65$. The residual oil saturation obtained at this capillary number of 0.00088 is also shown in Figure 6.2.30.

Figure 6.2.37 shows all of the phase saturations calculated from the dispersion measurements as a function of capillary number. The most significant feature of these capillary desaturation curves is that the residual saturation of microemulsion to brine does not go to zero until a capillary number of approximated 0.4 is reached. At this capillary number a residual saturation of brine ($S_{1r} = 0.07$) to microemulsion remains. The 7% residual brine saturation might be due to a film of brine left in the core. The residual oil to microemulsion is zero at a capillary number of 0.0037, while residual microemulsion to oil is about 10% at about

the same capillary number.

The endpoint effective permeabilities at each capillary number were calculated using the measured pressure drop and Darcy's equation (Eq. A.2). These permeabilities were then normalized by the 100% brine permeability to obtain relative permeabilities. Figure 6.2.38 shows the endpoint relative permeabilities for the injected fluids as a function of capillary number. The endpoint relative permeability for oil and microemulsion is already at a plateau value at a capillary number of 0.001, while the relative permeability to brine does not approach a plateau until the capillary number exceeds 0.10.

The single-phase longitudinal dispersion coefficients for tritium in brine, carbon-14 in oil, and all four tracers used in the microemulsion are plotted as a function of phase frontal velocity ($q_j/A\phi S_j$) in Figures 6.2.39 through 6.2.41. All curves show an increase in dispersion coefficient with increasing velocity similar to that observed by many others for single-phase flow. A straight line on a log-log scale is obtained for these data for each phase with a reasonable value for the slope. The slope corresponds to the exponent in the following equation:

$$K_{ij} = \frac{D_{ij}}{F\phi} + \alpha_{ij}\, v_j^{\beta} \qquad (6.4)$$

The slope is about 1.08 for the oil phase, 1.09 for the microemulsion phase, and 1.11 for the brine phase. These values are typical for single-phase flow reported by other investigators [R.4,S.3,S.10]. No values for microemulsion have been previously reported.

The single-phase longitudinal dispersivity for tracers in each phase is plotted as a function of phase saturation in Figure 6.2.42. This figure indicates that the majority of the dispersivities lie between 0.1-0.4 cm for the range of saturation of 0.6-0.8.

Discussions

The breakthrough curves of tracers in microemulsion during single-phase microemulsion flow of cut numbers CDC3-26 (Figs. 6.2.16 and 6.2.17), CDC3-34 (Figs. 6.2.21 and 6.2.22), and CDC3-38 (Figs. 6.2.25 and 6.2.26) were not successfully matched against the C-D equation. The breakthrough times of both carbon-14 and tritium are greater than what they should be from the solution to the C-D equation. This delay in breakthrough time is opposite of the capacitance behavior. Therefore, the possibility of matching these data against the capacitance model is ruled out.

Figures 6.2.37 and 6.2.38 indicate the obvious need for more data on the residual excess oil to microemulsion at capillary number of less than 10^{-3}. The performance of experiment to obtain these data is not feasible using the present fluid composition. This is because of the ultra-low interfacial tension ($\sigma \approx 10^{-3}$ dyne/cm) at our optimal fluid composition. Therefore, in order to obtain capillary numbers of at least an order of magnitude lower than 10^{-3}, the pressure drop would be unreasonably low. One alternative is to consider a fluid composition in type II(-) environment with higher interfacial tension. Such experiments are underway by Mohammad Delshad [D.7].

TABLE 6.2.2
Material Balance (Steady-State) Results of Capillary Desaturation Experiments
(Exp. CDC3)

Experiment Number	Phase Fractional Flow			Total Flow Rate (cm^3/min)	Phase Saturation			Phase Relative Permeability (1)			Relative Mobility (cp^{-1})			Total Pore Volumes Inj. (P.V.)	Capillary Number $N_{cj}=\frac{k\Delta\Phi_j}{L\sigma}$
	Brine	Oil	M.E.		Brine	Oil	M.E.	Brine	Oil	M.E.	Brine	Oil	M.E.		
CDC3-2	1.0	-	-	3.925	1.0	-	-	1.0	-	-	1.117	-	-	6.0	-
CDC3-4	-	1.0	-	28.0(4.0)	0.358	0.642	-	-	0.918	-	-	1.055	-	10.1	0.0000052
CDC3-8	1.0	-	-	3.97	0.70	0.30	-	0.0933	-	-	0.104	-	-	8.92	0.0000050
CDC3-10	-	-	1.0	1.97	0.065	0.0	0.935	-	-	0.976	-	-	0.244	3.67	0.069
CDC3-12	1.0	-	-	0.134	0.69	0.0	0.310	0.470	-	-	0.525	-	-	3.0	0.00206
CDC3-14	1.0	-	-	2.86	0.768	0.0	0.232	0.793	-	-	0.886	-	-	3.13	0.0260
CDC3-16	1.0	-	-	51	0.871	0.0	0.129	0.849	-	-	0.948	-	-	2.67	0.433
CDC3-18	1.0	-	-	2.06	0.871	0.0	0.129	0.918	-	-	1.026	-	-	1.24	0.0156
CDC3-20	-	-	1.0	0.031	0.277	0.0	0.723	-	-	0.90	-	-	0.225	1.33	0.00119
CDC3-22	-	-	1.0	0.260	0.235	0.0	0.765	-	-	0.969	-	-	0.242	2.13	0.0092
CDC3-24	-	-	1.0	2.86	0.235	0.0	0.765	-	-	0.949	-	-	0.237	2.25	0.104
CDC3-26	-	-	1.0	11.70	0.208	0.0	0.792	-	-	0.927	-	-	0.232	1.97	0.433
CDC3-28	-	1.0	-	0.195	0.07	0.818	0.112	-	1.05	-	-	1.346	-	2.65	0.00236
CDC3-30	-	1.0	-	0.875	0.07	0.818	0.112	-	0.916	-	-	1.17	-	1.545	0.012
CDC3-32	-	1.0	-	47.5	0.07	0.818	0.112	-	0.938	-	-	1.20	-	2.10	0.644
CDC3-34	-	-	1.0	0.056	0.07	0.110	0.82	-	-	0.986	-	-	0.246	1.74	0.0037
CDC3-36	-	-	1.0	0.940	0.07	0.110	0.82	-	-	0.931	-	-	0.232	1.75	0.066
CDC3-38	-	-	1.0	12.81	0.07	0.110	0.82	-	-	0.923	-	-	0.231	1.76	0.906
CDC3-50	-	1.0	-	2.08	0.16	0.84	0.0	-	0.971	-	-	1.067	-	8.45	0.014
CDC3-54	-	-	1.0	0.0095	0.160	0.05	0.79	-	-	0.317	-	-	0.0694	1.63	0.00088

(1) Permeabilities are normalized by permeability at 100% Brine saturation (k = 0.739 D)

TABLE 6.2.3
Pressure Drop Results of Capillary Desaturation Experiment
(Experiment CDC3)

Experiment Number	Phase Potential Drop (1) (psi/ft)			Phase Potential Drop (2) (psi/ft)			Phase Potential Drop (3) (psi/ft)			Position of the core
	Brine	Oil	M.E.	Brine	Oil	M.E.	Brine	Oil	M.E.	
CDC3-2	1.40	-	-	1.72	-	-	1.40	-	-	Horizontal (H)
CDC3-4	-	16.0	-	-	*	-	-	*	-	H
CDC3-8	15.2	-	-	20.20	-	-				H
CDC3-10	-	-	3.20	-	-	3.30	-	-	3.60	H
CDC3-12	0.095	-	-	0.140	-	-	0.09	-	-	H
CDC3-14	1.20	-	-	1.78	-	-	1.20	-	-	H
CDC3-16	20	-	-	22.4	-	-	22.0	-	-	H
CDC3-18	0.725	-	-	0.415	-	-	0.72	-	-	H
CDC3-20	-	-	0.055	-	-	0.070	-	-	0.062	H
CDC3-22	-	-	0.425	-	-	0.480	-	-	0.45	H
CDC3-24	-	-	4.8	-	-	5.4	-	-	5.0	H
CDC3-26	-	-	20.0	-	-	19.8	-	-	20.80	H
CDC3-28	-	0.0575	-	-	0.06	-	-	0.07	-	H
CDC3-30	-	0.295	-	-	0.30	-	-	0.28	-	H
CDC3-32	-	15.65	-	-	15.60	-	-	16.2	-	H
CDC3-34	-	-	0.09	-	-	0.114	-	-	0.10	H
CDC3-36	-	-	1.60	-	-	1.58	-	-	1.64	H
CDC3-38	-	-	22.0	-	-	23.2	-	-	24.0	H
CDC3-50	-	0.545	-	-	0.76	-	-	0.70	-	Vertical
CDC3-54	-	-	0.075	-	-	*	-	-	*	Vertical

(1) Pressure drop measured across the center section of the core (1.0 foot)
(2) Pressure drop measured across the inlet section (0.5 foot)
(3) Pressure drop measured across the outlet section (0.5 foot)

TABLE 6.2.4
Dispersion Results of Capillary Desaturation Experiments
(Exp. CDC3)

Experiment Number	Phase Saturation			Dispersivity (cm)				Dispersion Coefficient (cm^2/sec)				Phase Velocity (cm/sec) $V_j = \frac{qf_j}{A\phi S_j}$			Total Pore Volumes Inj. (P.V.)	Tracer Recovery (%)		
	Brine	Oil	M.E.	T_2O in Brine	^{14}C in Oil	T_2O in M.E.	^{14}C in M.E.	T_2O in Brine	^{14}C in Oil	T_2O in M.E.	^{14}C in M.E.	Brine	Oil	M.E.		T_2O	^{14}C	T.S.
CDC3-2	1.0	-	-	0.30	-	-	-	0.0036	-	-	-	0.012	-	-	2.10	97.0	-	-
CDC3-4	0.35	0.65	-	-	0.16	-	-	-	0.003	-	-	-	0.0189	-	2.90	-	100.0	-
CDC3-8	0.70	0.30	-	0.22	-	-	-	0.0038	-	-	-	0.0176	-	-	2.48	99.4	-	-
CDC3-10	0.065	0.0	0.935	-	-	0.42	0.261	-	-	0.0027	0.0017	-	-	-	1.96	92	98.4	-
CDC3-12	0.774	0.0	0.226	0.12	-	-	-	0.000064	-	-	-	0.00053	-	-	2.19	99.1	-	-
CDC3-14	0.931	0.0	0.069	0.18	-	-	-	0.0017	-	-	-	0.0095	-	-	2.38	99.3	-	-
CDC3-16	1.0	0.0	0.0	0.30	-	-	-	0.00471	-	-	-	0.157	-	-	1.99	97.0	-	-
CDC3-18	1.0	0.0	0.0	0.10	-	-	-	0.00064	-	-	-	0.0064	-	-	1.82	98.2	-	-
CDC3-20	0.171	0.0	0.829	-	-	0.24	0.18	-	-	0.000026	0.000020	-	-	0.00011	1.98	96.3	97.1	-
CDC3-22	0.076	0.0	0.924	-	-	0.16	0.20	-	-	0.00014	0.00017	-	-	0.00087	2.24	96.4	95.0	-
CDC3-24	0.070	0.0	0.930	-	-	0.13	0.15	-	-	0.00012	0.00014	-	-	0.00095	1.94	97.2	97.8	-
CDC3-26	0.070	0.0	0.930	-	-	0.206	0.23	-	-	0.0080	0.0089	-	-	0.0388	2.0	96.0	97.0	-
CDC3-28	0.070	0.811	0.119	-	0.14	-	-	-	0.0001	-	-	-	0.00074	-	2.0	-	99.6	-
CDC3-30	0.070	0.930	0.0	-	0.12	-	-	-	0.00035	-	-	-	0.0029	-	1.78	-	100	-
CDC3-32	0.070	0.930	0.0	-	0.25	-	-	-	0.0392	-	-	-	0.157	-	2.0	-	99.0	-
CDC3-34	0.070	0.0	0.93	-	-	0.15	0.10	-	-	0.000027	0.000018	-	-	0.00018	1.70	94.0	100	-
CDC3-36	0.070	0.0	0.93	-	-	0.14	0.10	-	-	0.00043	0.00031	-	-	0.0031	2.0	96.0	97.8	-
CDC3-38	0.070	0.0	0.93	-	-	0.30	0.18	-	-	0.0126	0.0076	-	-	0.042	1.54	96.0	97.3	-
CDC3-50	0.16	0.84	0.0	-	0.271	-	-	-	-	-	-	-	0.0076	-	2.10		98.5	-
CDC3-54	0.314	0.033	0.653	-	-	0.88*	7.2	-	-	0.000040*	0.00032	-	-	0.000045	2.45	100 (^{36}Cl)	100	98.7

*^{36}Cl in M.E.; dispersivity of T.S. in M.E. = 1.20 cm
*^{36}Cl in M.E.; dispersion coeff. of T.S. in M.E. = 0.000054 cm^2/sec

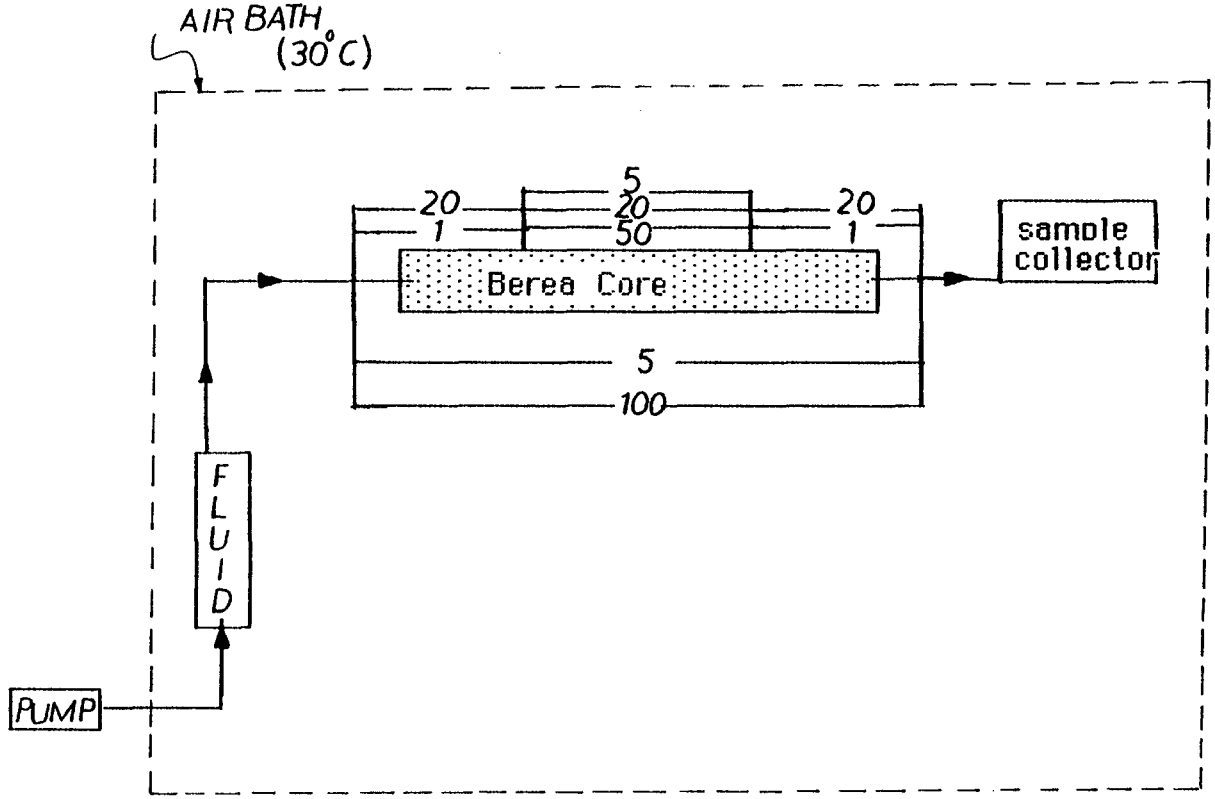

Figure 6.2 Schematic Diagram for Capillary Desaturation Experiment

EXPERIMENT NUMBER		CDC3-2	
TRACER & PHASE		TRITIUM	BRINE
FRACTIONAL FLOW		1:1.0	
MAX. & INJ. CONC.	(DPM/CC)	81200	81200
FLOW RATE		3.925	CC/MIN.

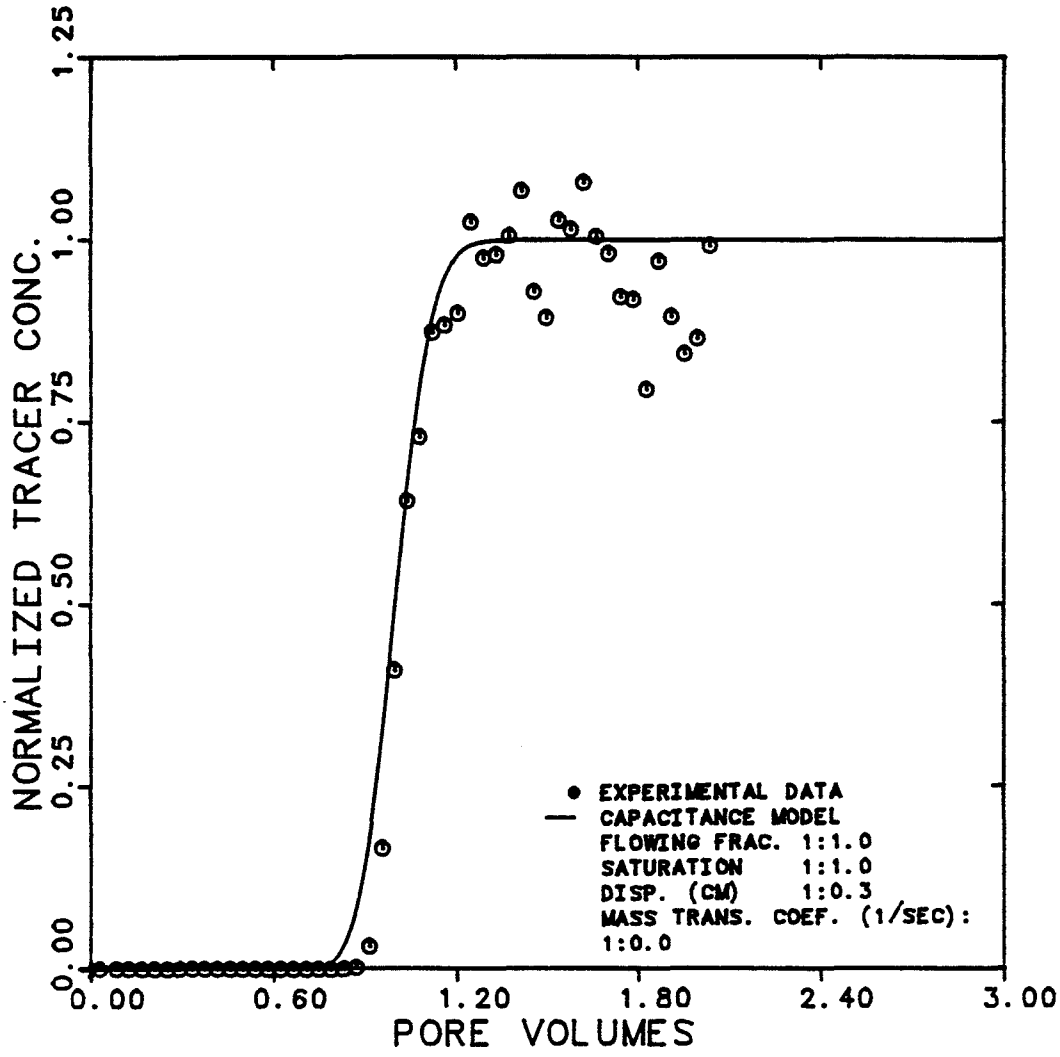

Figure 6.2.1 Effluent History for Tritiated Water in Brine for Single-Phase Brine Flow

EXPERIMENT NUMBER		CDC3-4
TRACER & PHASE		CARBON-14 OIL
FRACTIONAL FLOW		2:1.0
MAX. & INJ. CONC.	(DPM/CC)	8200 8200
FLOW RATE		4.0 CC/MIN.

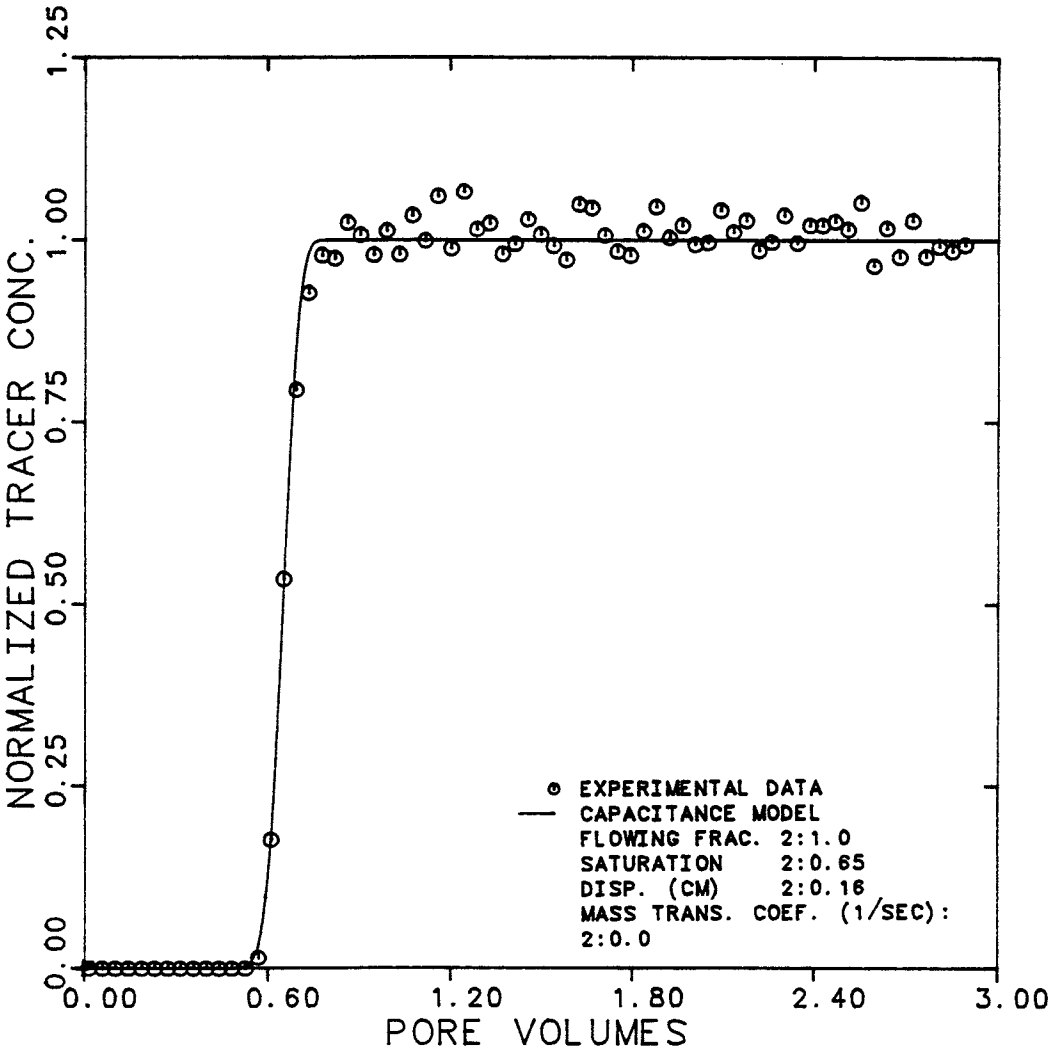

Figure 6.2.2 Effluent History for Carbon-14 in Oil for Single-Phase Oil Flow at Residual Brine Saturation

EXPERIMENT NUMBER		CDC3-8
TRACER & PHASE		TRITIUM BRINE
FRACTIONAL FLOW		1:1.0
MAX. & INJ. CONC.	(DPM/CC)	152000 152000
FLOW RATE		4.00 CC/MIN.

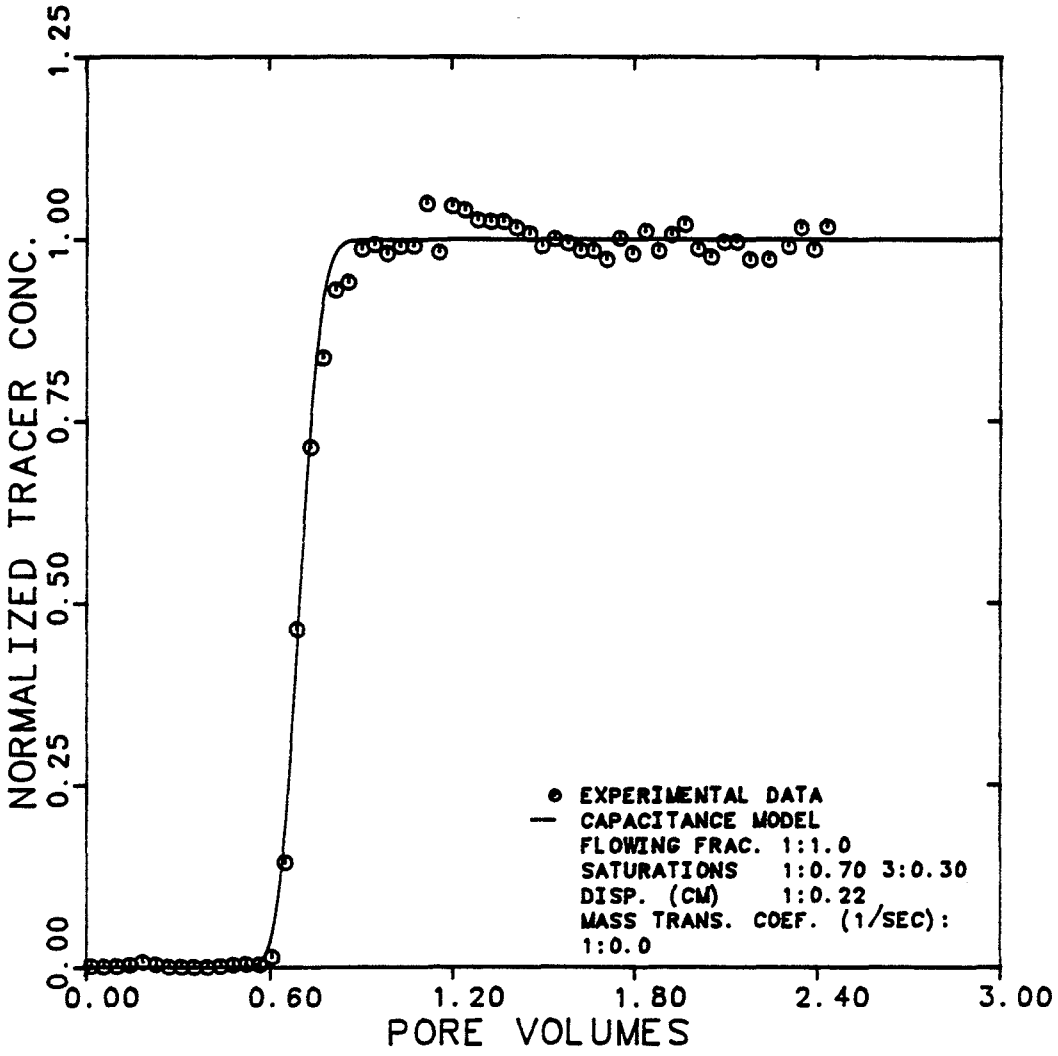

Figure 6.2.3 Effluent History for Tritiated Water in Brine for Single-Phase Brine Flow at Residual Oil Saturation

EXPERIMENT NUMBER	CDC3-10
TRACER & PHASE	CARBON-14 M.E.
FRACTIONAL FLOW	3: 1.0
MAX. & INJ. CONC.	5112 5112 DPM/CC
FLOW RATE	1.92 CC/MIN.

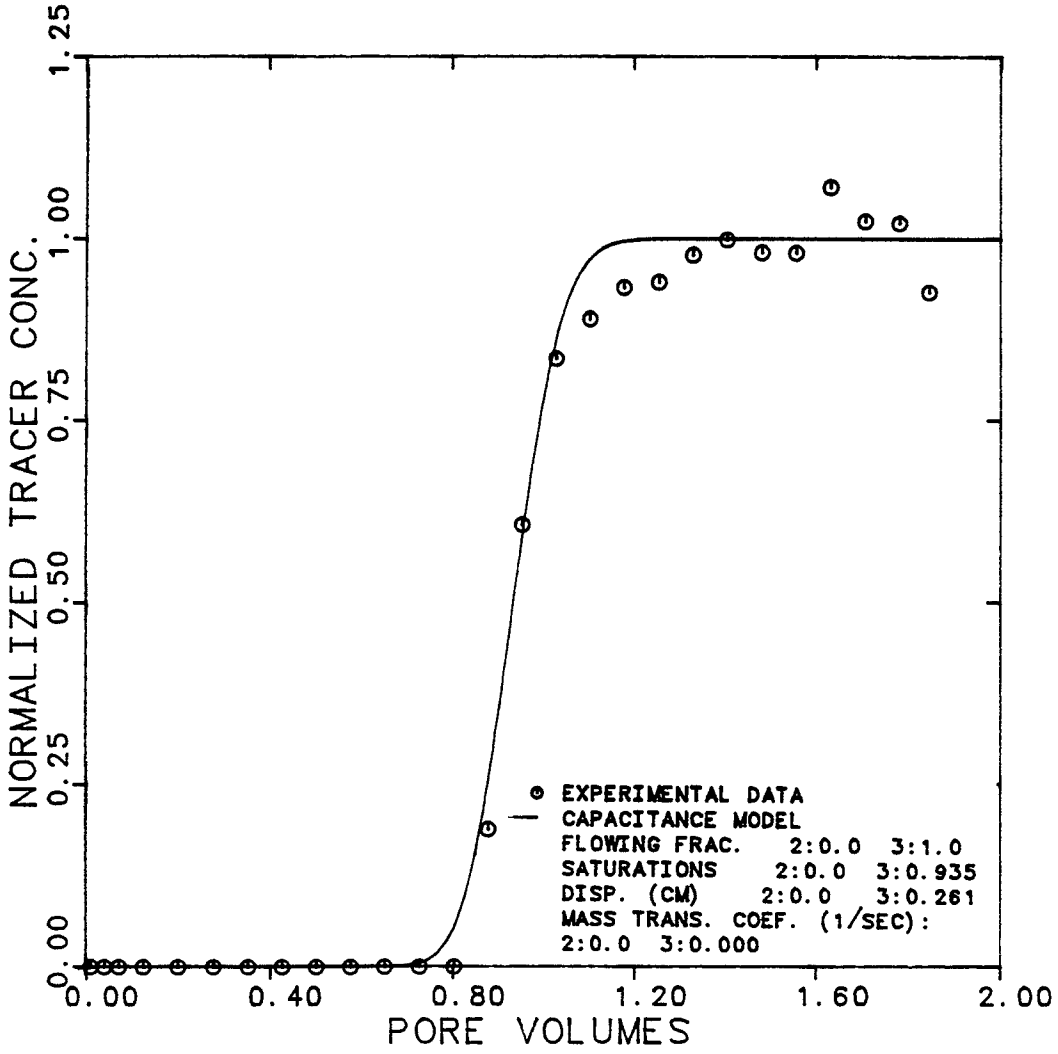

Figure 6.2.4 Effluent History for Carbon-14 in M.E. for Single-Phase M.E. Flow

EXPERIMENT NUMBER	CDC3-10	
TRACER & PHASE	TRITIUM	M.E.
FRACTIONAL FLOW	3: 1.0	
MAX. & INJ. CONC.	25384 25384	DPM/CC
FLOW RATE	1.92	CC/MIN.

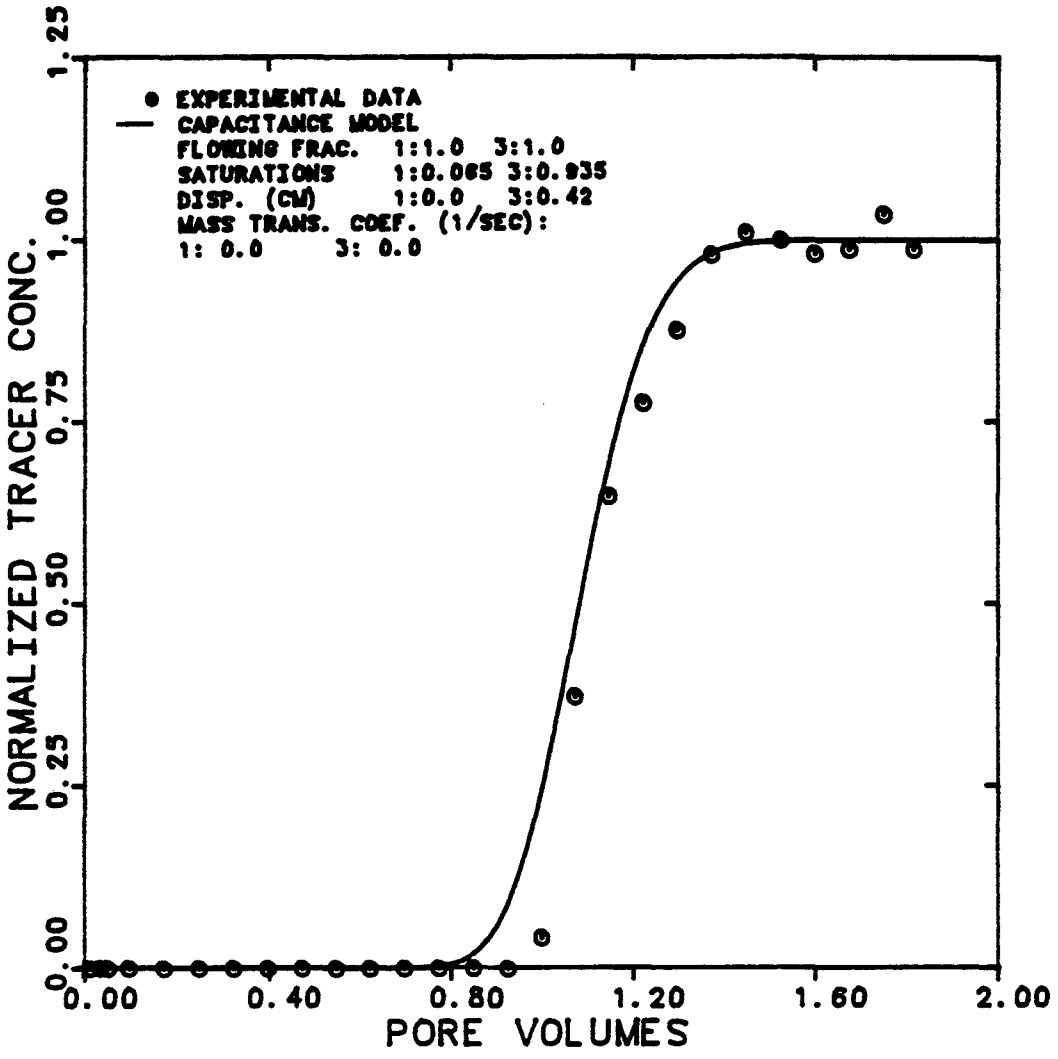

Figure 6.2.5 Effluent History for Tritiated Water in M.E. for Single-Phase M.E. Flow

EXPERIMENT NUMBER		CDC3-12
TRACER & PHASE		TRITIUM BRINE
FRACTIONAL FLOW		1:1.0
MAX. & INJ. CONC.	(DPM/CC)	54800 54800
FLOW RATE		0.134 CC/MIN.

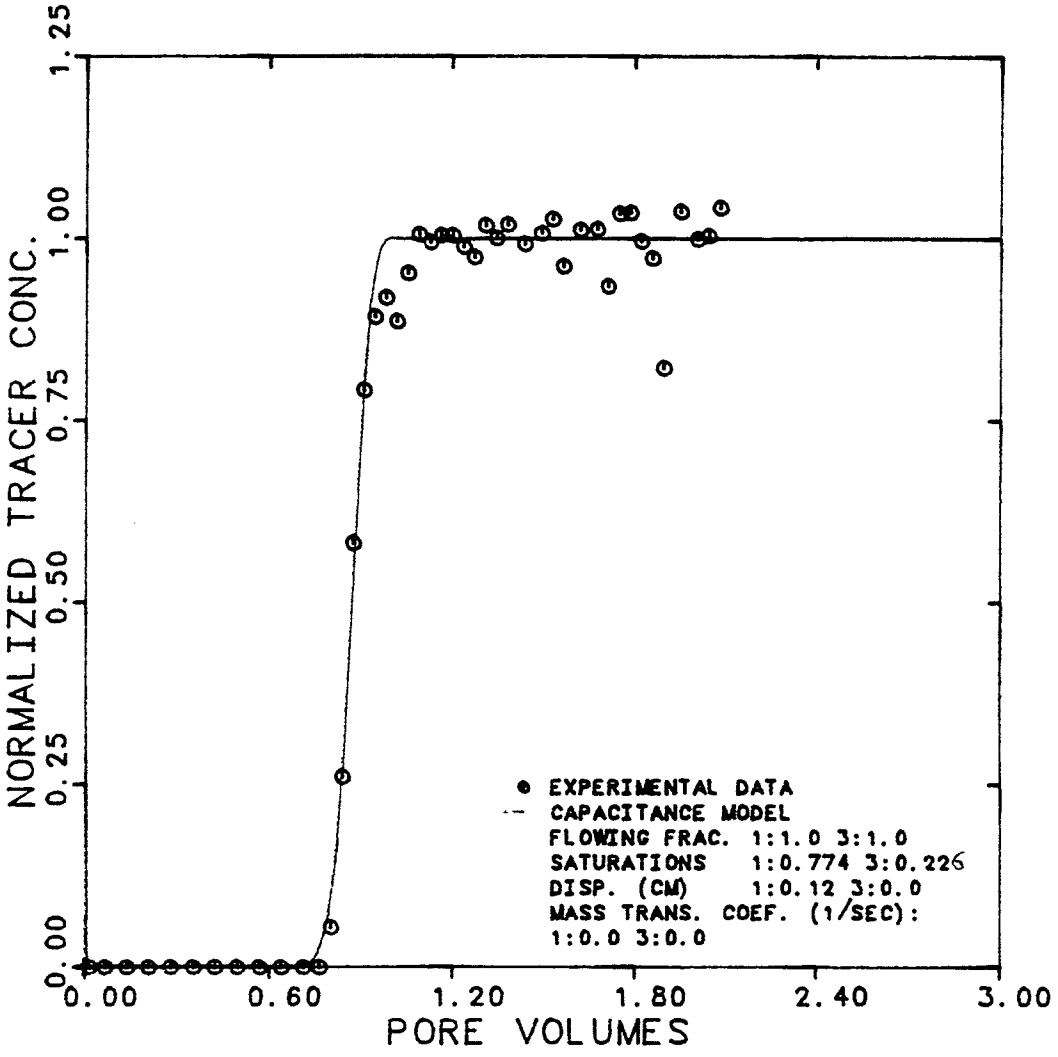

Figure 6.2.6 Effluent History for Tritiated Water in Brine for Single-Phase Brine Flow at 0.134 cc/min

EXPERIMENT NUMBER		CDC3-14
TRACER & PHASE		TRITIUM BRINE
FRACTIONAL FLOW		1:1.0
MAX. & INJ. CONC.	(DPM/CC)	56800 56800
FLOW RATE		2.86 CC/MIN.

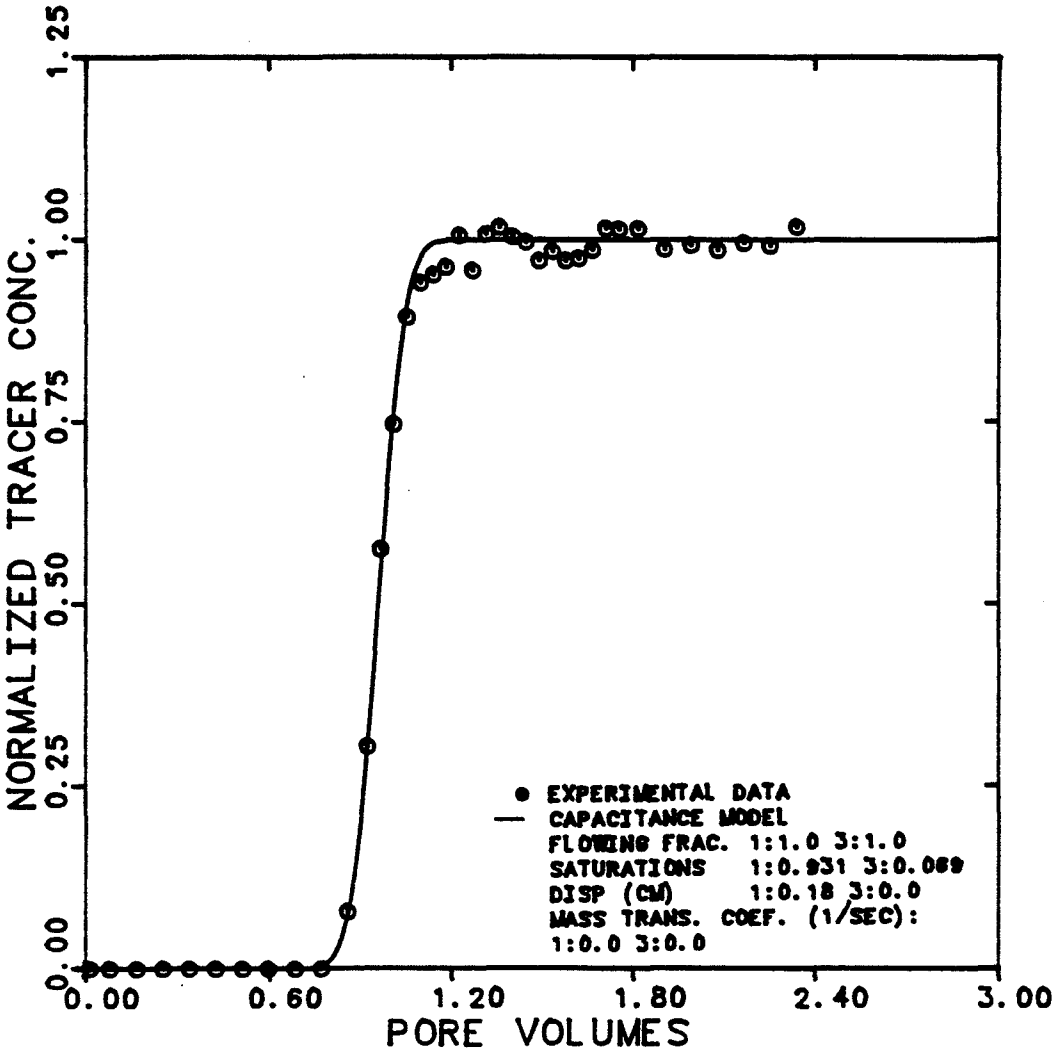

Figure 6.2.7 Effluent History for Tritiated Water in Brine for Single-Phase Brine Flow at 2.86 cc/min

EXPERIMENT NUMBER		CDC3-16
TRACER & PHASE		TRITIUM BRINE
FRACTIONAL FLOW		1:1.0
MAX. & INJ. CONC.	(DPM/CC)	61200 61200
FLOW RATE		51.0 CC/MIN.

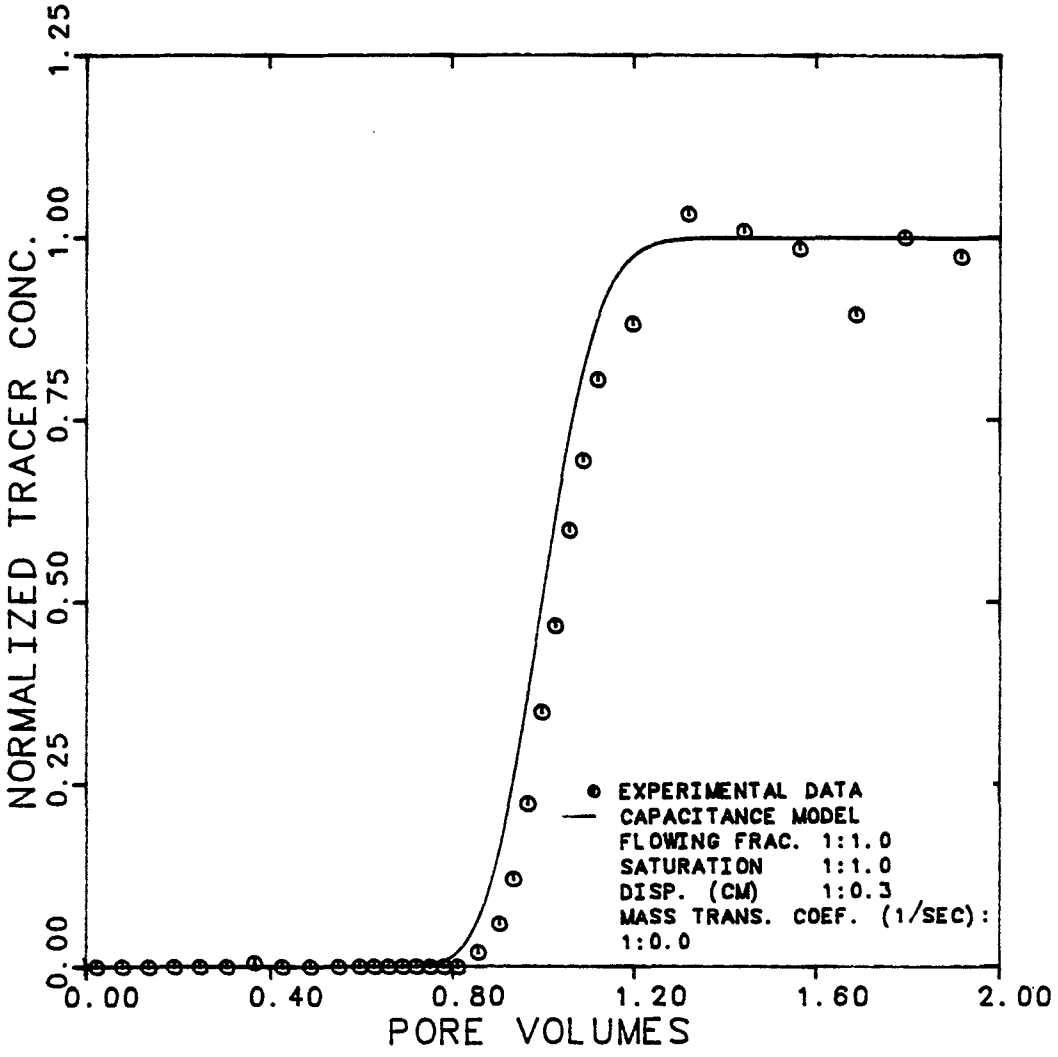

Figure 6.2.8 Effluent History for Tritiated Water in Brine for Single-Phase Brine Flow at 51 cc/min

EXPERIMENT NUMBER		CDC3-18
TRACER & PHASE		TRITIUM BRINE
FRACTIONAL FLOW		1:1.0
MAX. & INJ. CONC.	(DPM/CC)	59200 59200
FLOW RATE		2.06 CC/MIN.

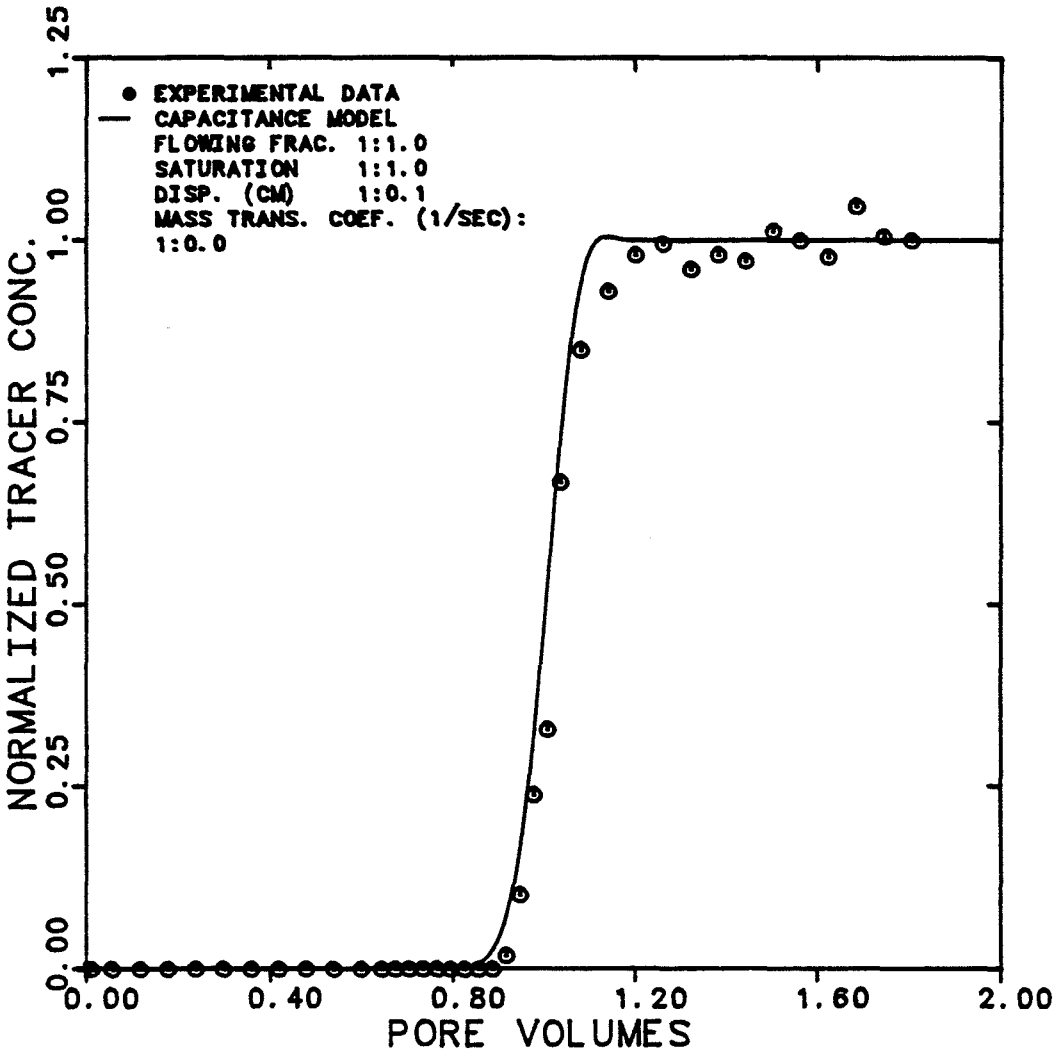

Figure 6.2.9 Effluent History of Tritiated Water for Single-Phase Brine Flow at 2.06 cc/min

EXPERIMENT NUMBER	CDC3-20		
TRACER & PHASE	TRITIUM	M.E.	
FRACTIONAL FLOW	3: 1.0		
MAX. & INJ. CONC.	22000	22000	DPM/CC
FLOW RATE	0.031		CC/MIN.

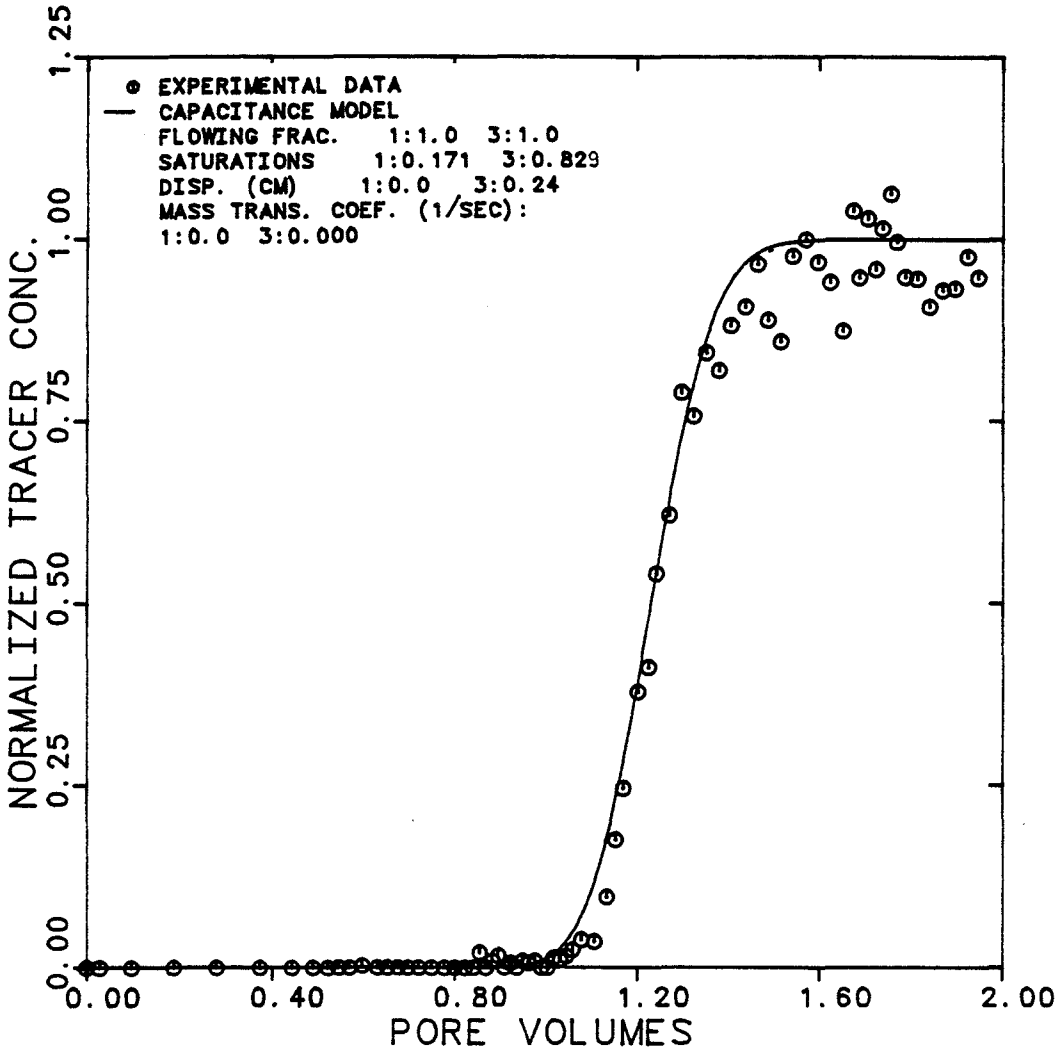

Figure 6.2.10 Effluent History for Tritiated Water in M.E. for Single-Phase Flow of M.E. at 0.031 cc/min

EXPERIMENT NUMBER	CDC3-20
TRACER & PHASE	CARBON-14 M.E.
FRACTIONAL FLOW	3: 1.0
MAX. & INJ. CONC.	4440 4440 DPM/CC
FLOW RATE	0.031 CC/MIN.

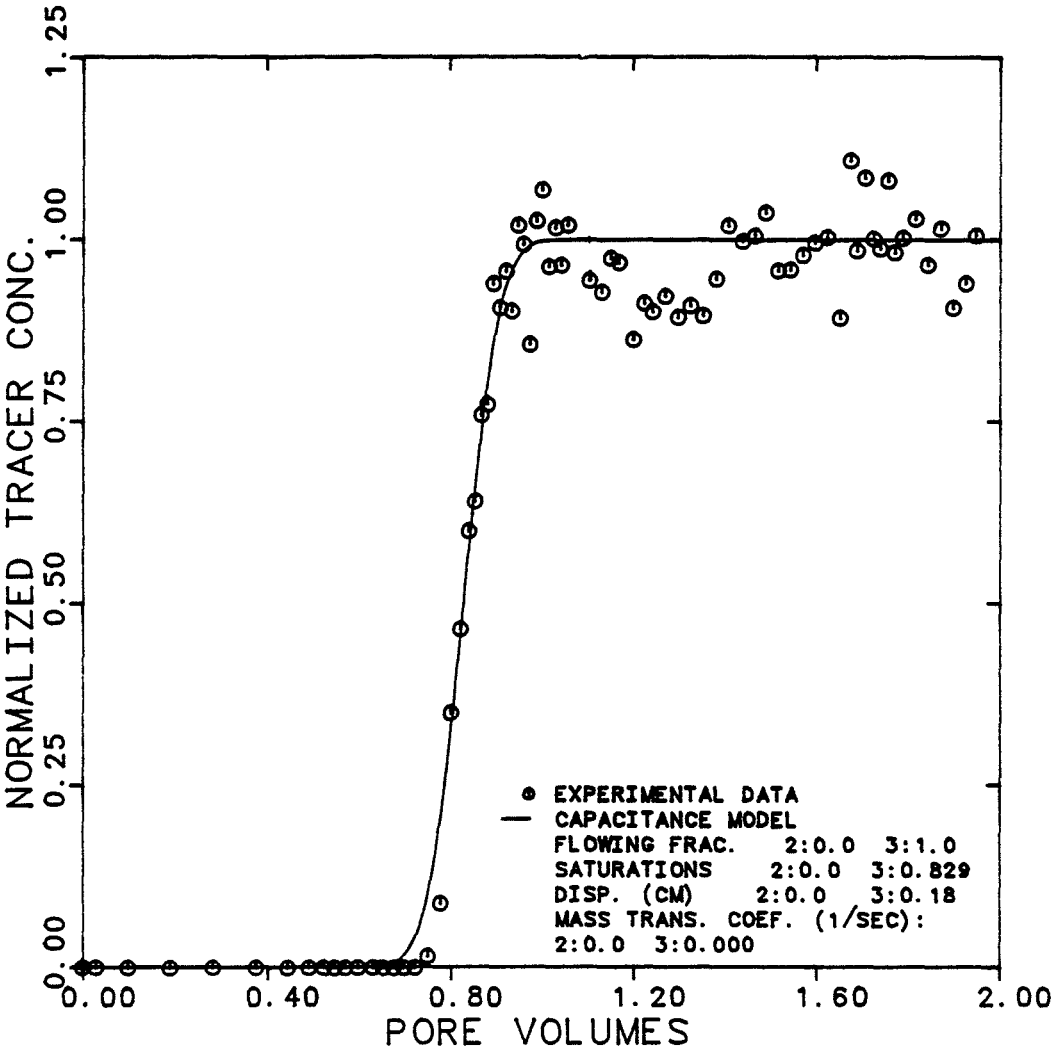

Figure 6.2.11 Effluent History for Carbon-14 in M.E. for Single-Phase Flow of M.E. at 0.031 cc/min

EXPERIMENT NUMBER	CDC3-22
TRACER & PHASE	CARBON-14 M.E.
FRACTIONAL FLOW	3: 1.0
MAX. & INJ. CONC.	4200 4200 DPM/CC
FLOW RATE	0.26 CC/MIN.

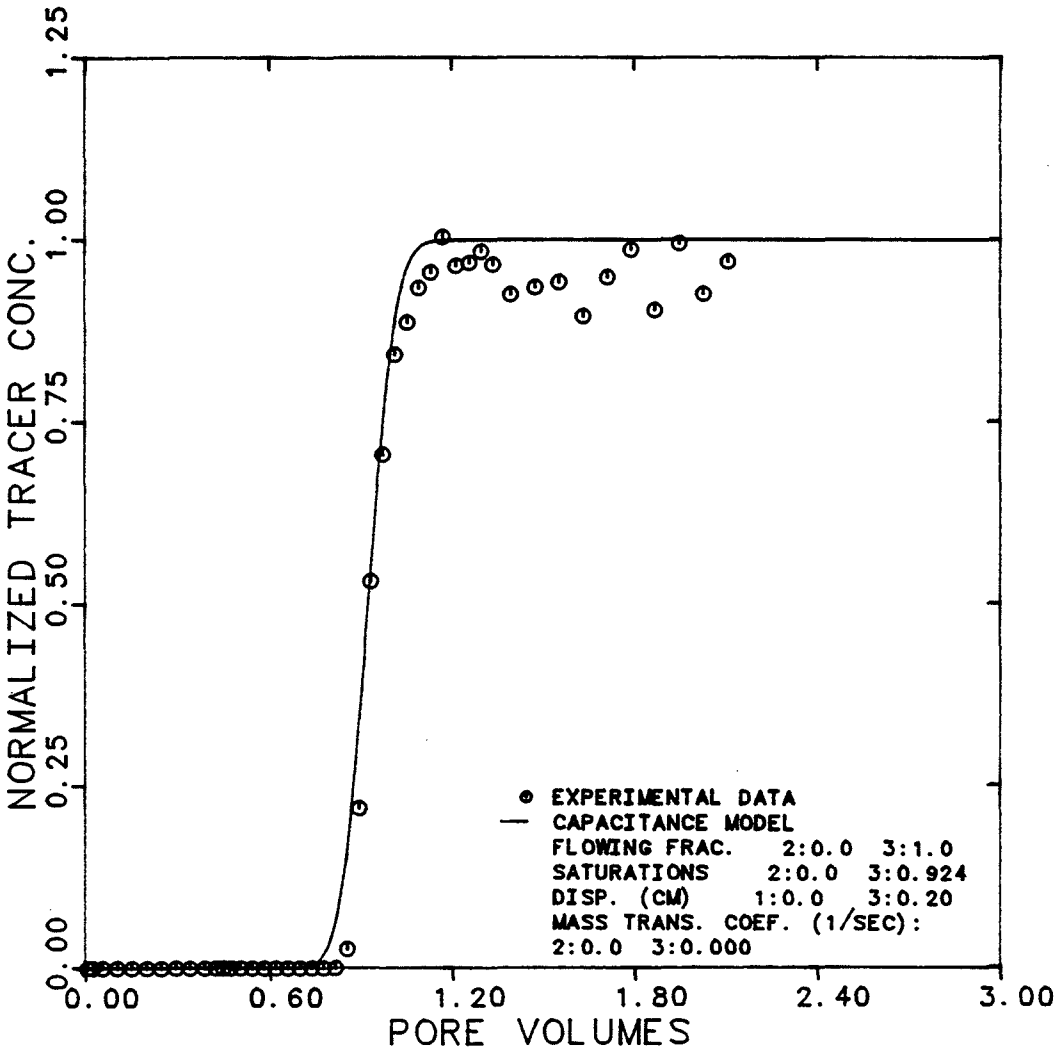

Figure 6.2.12 Effluent History for Carbon-14 in M.E. for Single-Phase M.E. Flow at 0.26 cc/min

EXPERIMENT NUMBER	CDC3-22		
TRACER & PHASE	TRITIUM	M.E.	
FRACTIONAL FLOW	3: 1.0		
MAX. & INJ. CONC.	21200	21200	DPM/CC
FLOW RATE	0.26		CC/MIN.

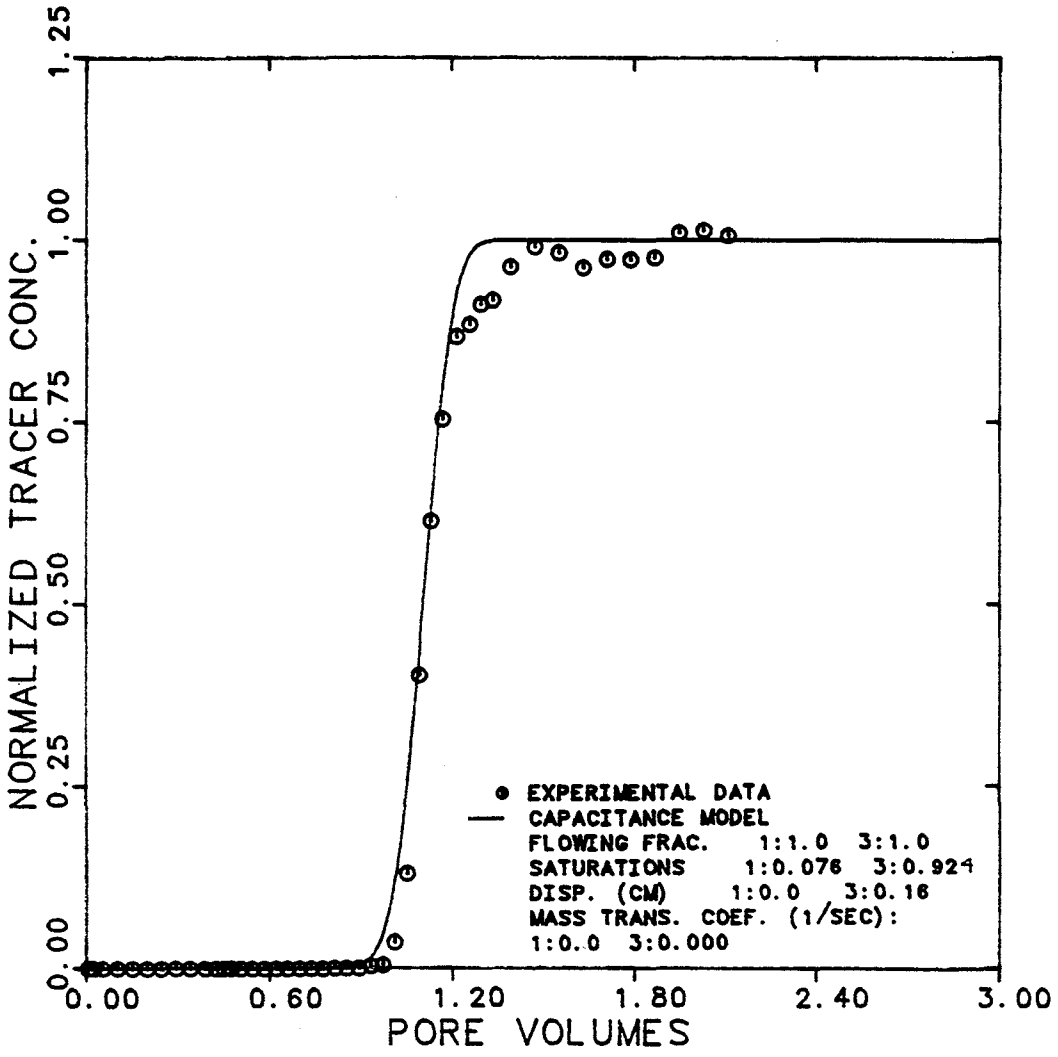

Figure 6.2.13 Effluent History for Tritiated WAter in M.E. for Single-Phase Flow of M.E. at 0.26 cc/min

EXPERIMENT NUMBER	CDC3-24
TRACER & PHASE	CARBON-14 M.E.
FRACTIONAL FLOW	3: 1.0
MAX. & INJ. CONC.	4000 4000 DPM/CC
FLOW RATE	2.83 CC/MIN.

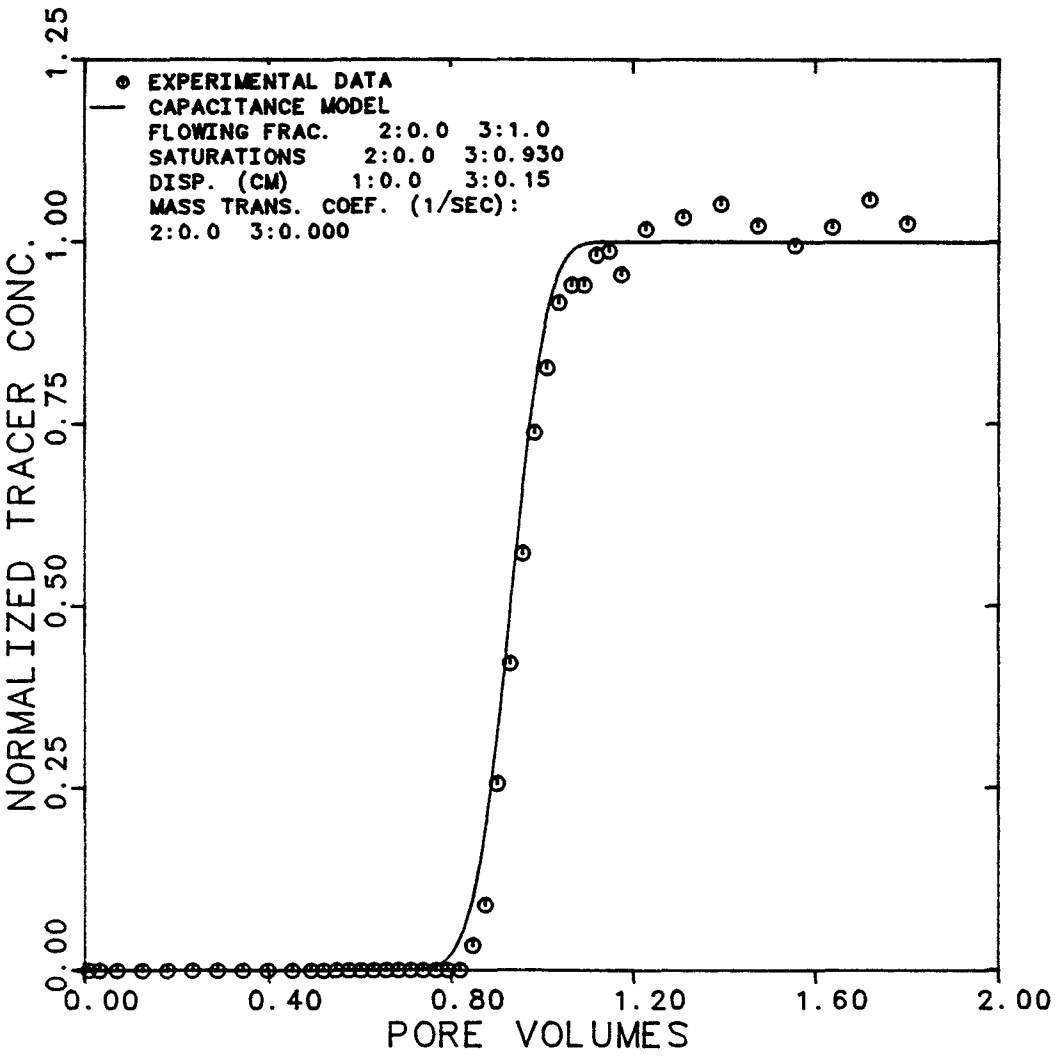

Figure 6.2.14 Effluent History for Carbon-14 in M.E. for Single-Phase Flow of M.E. at 2.83 cc/min

EXPERIMENT NUMBER	CDC3-24
TRACER & PHASE	TRITIUM M.E.
FRACTIONAL FLOW	3: 1.0
MAX. & INJ. CONC.	21000 21000 DPM/CC
FLOW RATE	2.83 CC/MIN.

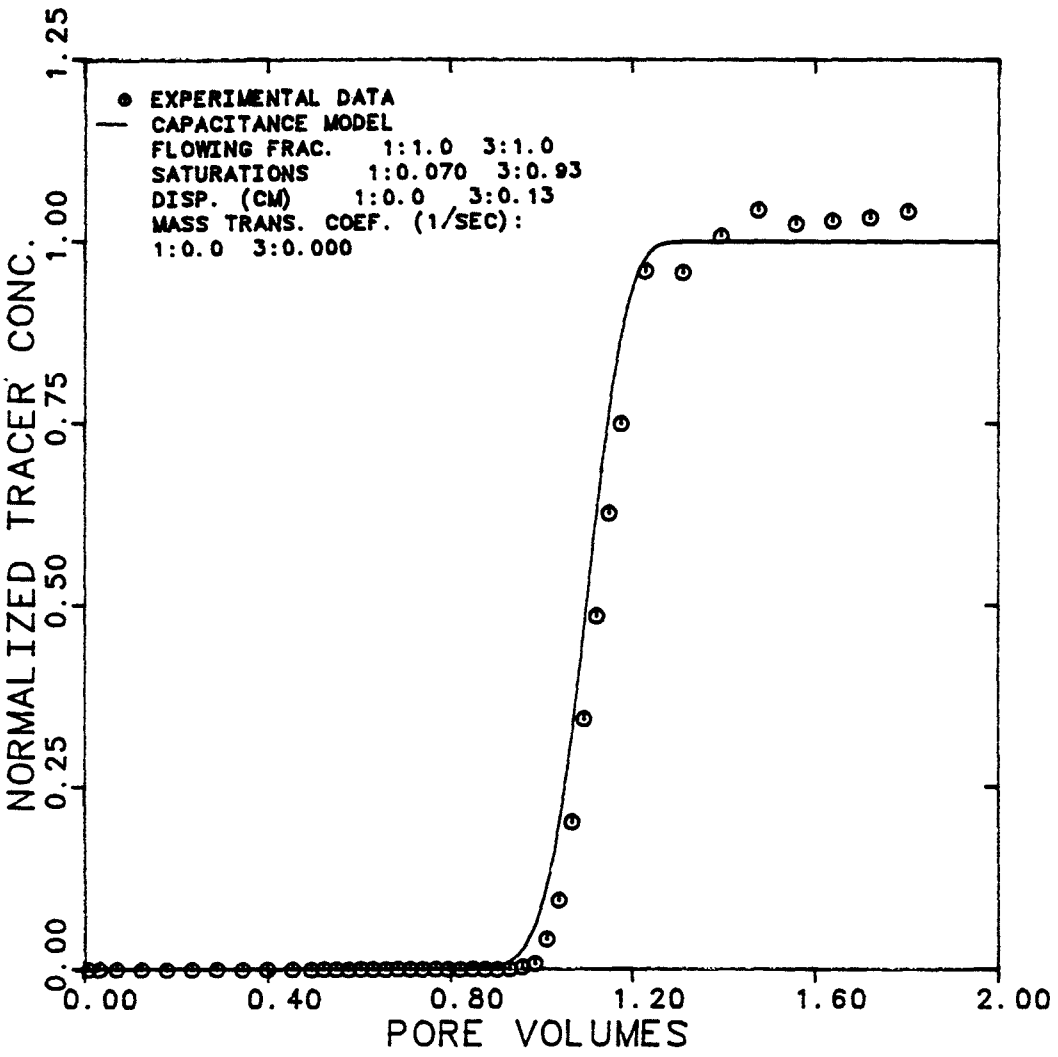

Figure 6.2.15 Effluent History for Tritiated Water in M.E. for Single-Phase Flow of M.E. at 2.83 cc/min

EXPERIMENT NUMBER	CDC3-26
TRACER & PHASE	CARBON-14 M.E.
FRACTIONAL FLOW	3: 1.0
MAX. & INJ. CONC.	4200 4200 DPM/CC
FLOW RATE	11.7 CC/MIN.

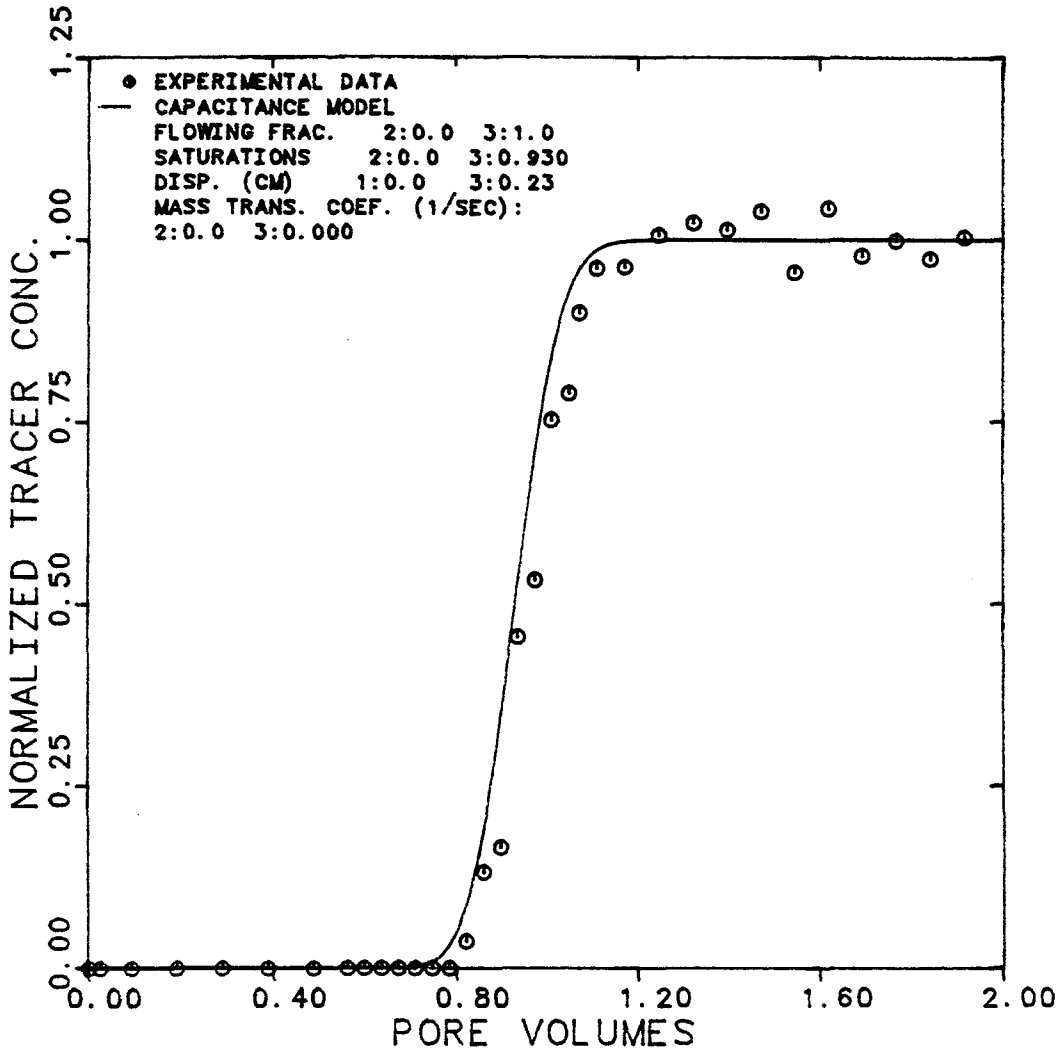

Figure 6.2.16 Effluent History for Carbon-14 in M.E. for Single-Phase Flow of M.E. at 11.7 cc/min

EXPERIMENT NUMBER	CDC3-26
TRACER & PHASE	TRITIUM M.E.
FRACTIONAL FLOW	3: 1.0
MAX. & INJ. CONC.	21000 21000 DPM/CC
FLOW RATE	11.7 CC/MIN.

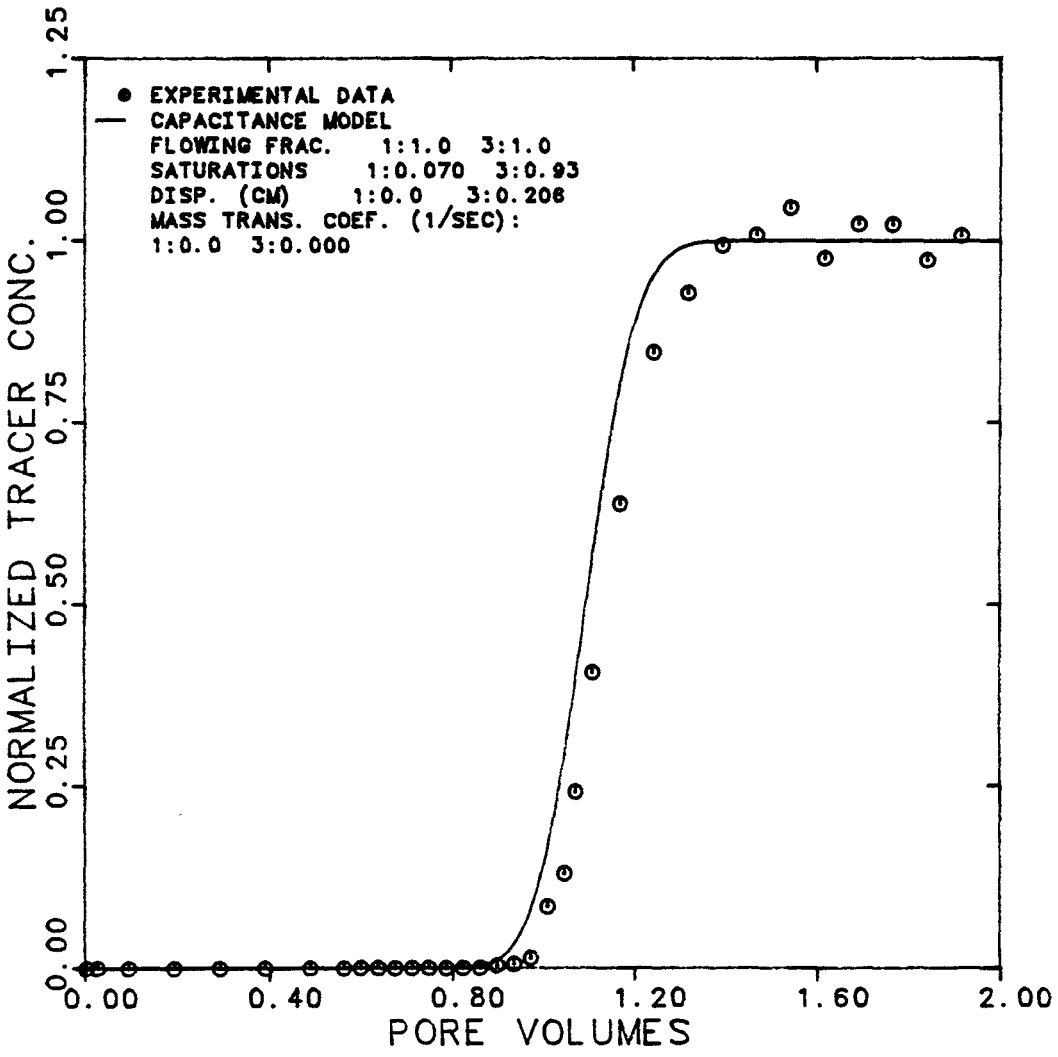

Figure 6.2.17 Effluent History for Tritiated Water in M.E. for Single-Phase Flow of M.E. at 11.7 cc/min

EXPERIMENT NUMBER		CDC3-28
TRACER & PHASE		CARBON-14 OIL
FRACTIONAL FLOW		2:1.0
MAX. & INJ. CONC.	(DPM/CC)	7760 7760
FLOW RATE		0.195 CC/MIN.

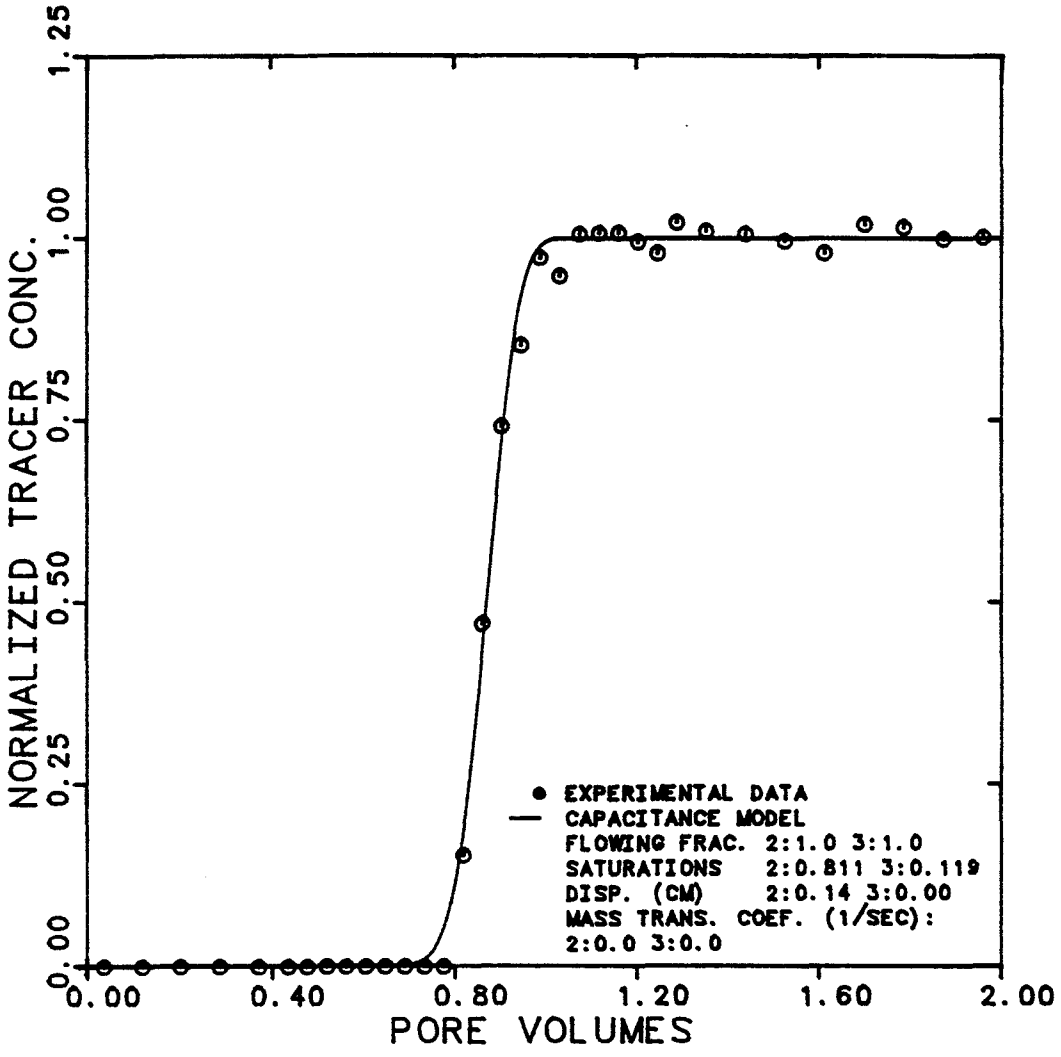

Figure 6.2.18 Effluent History for Carbon-14 in Oil for Single-Phase Flow of Oil at 0.195 cc/min

EXPERIMENT NUMBER		CDC3-30
TRACER & PHASE		CARBON-14 OIL
FRACTIONAL FLOW		2:1.0
MAX. & INJ. CONC.	(DPM/CC)	7940 7940
FLOW RATE		0.875 CC/MIN.

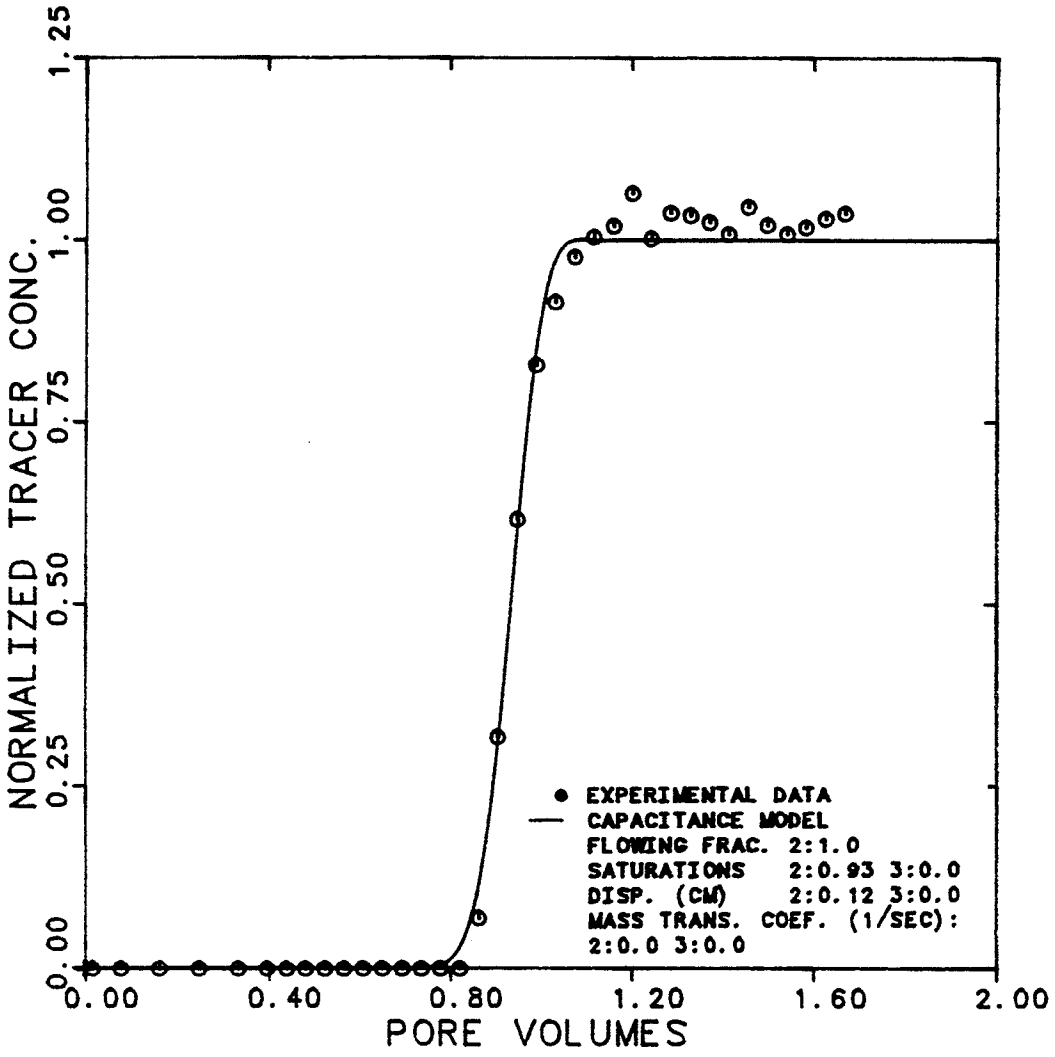

Figure 6.2.19 Effluent History for Carbon-14 in Oil for Single-Phase Flow at 0.875 cc/min

EXPERIMENT NUMBER		CDC3-32
TRACER & PHASE		CARBON-14 OIL
FRACTIONAL FLOW		2:1.0
MAX. & INJ. CONC.	(DPM/CC)	7940 7940
FLOW RATE		47.5 CC/MIN.

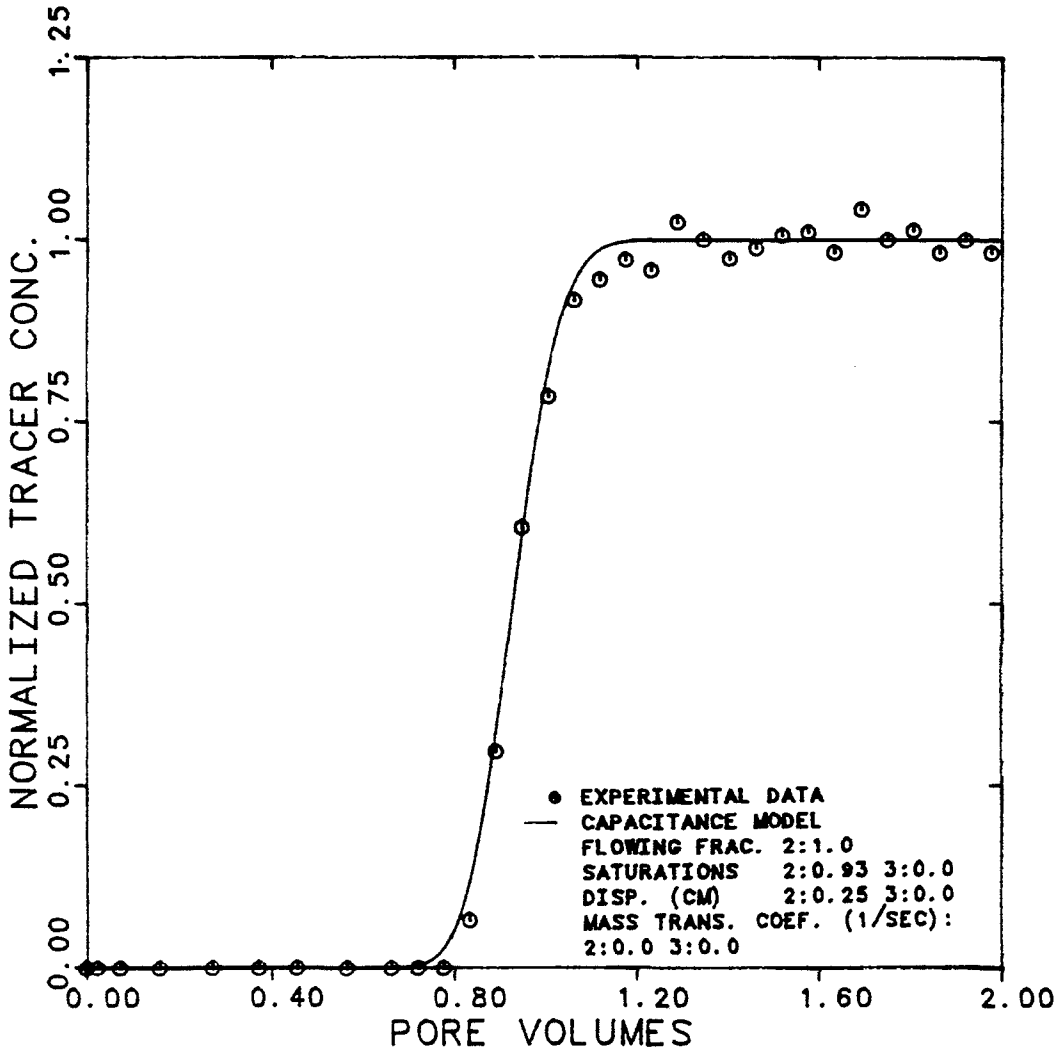

Figure 6.2.20 Effluent History for Carbon-14 in Oil for Single-Phase Flow at 47.5 cc/min

EXPERIMENT NUMBER	CDC3-34		
TRACER & PHASE	TRITIUM	M.E.	
FRACTIONAL FLOW	3: 1.0		
MAX. & INJ. CONC.	21284	21284	DPM/CC
FLOW RATE	0.056		CC/MIN.

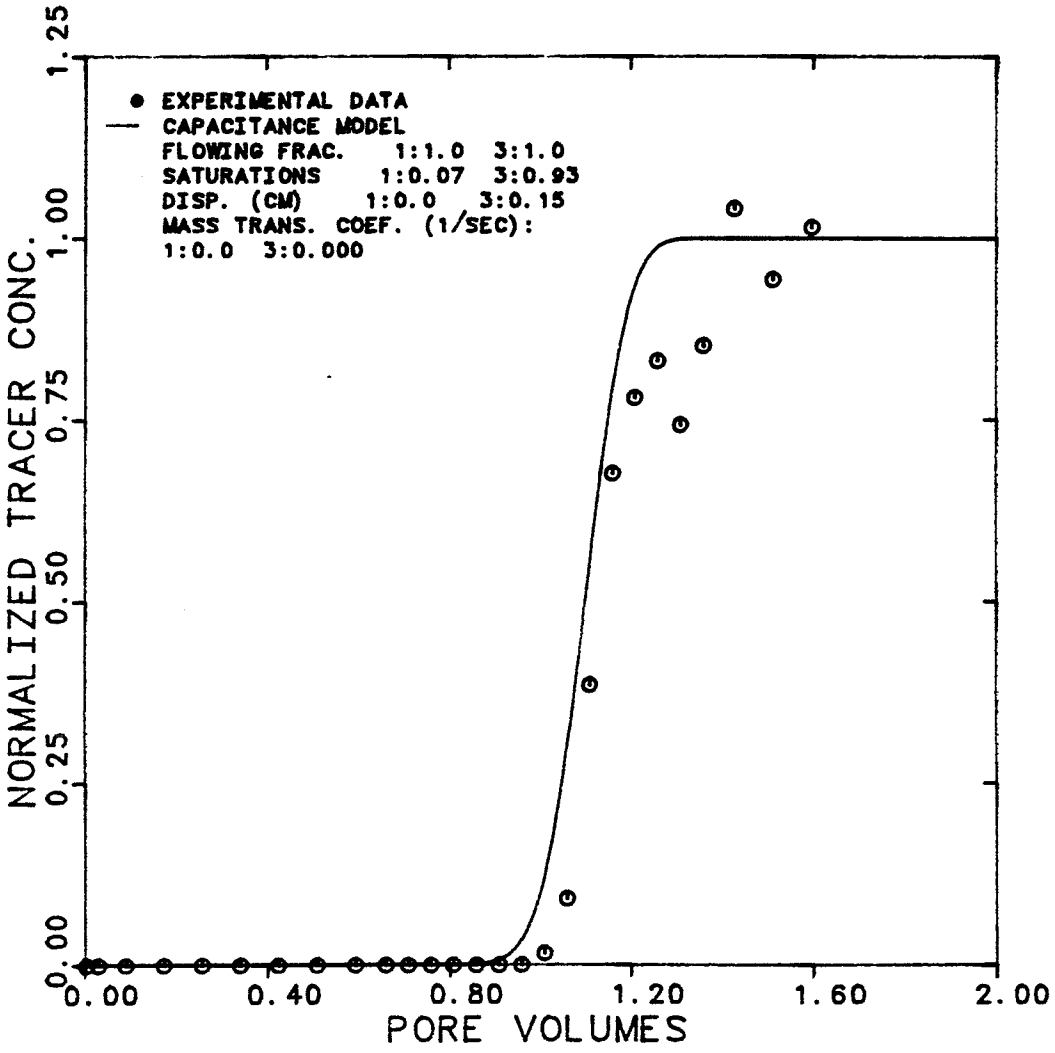

Figure 6.2.21 Effluent History for Tritiated Water in M.E. for Single-Phase M.E. Flow at 0.056 cc/min

EXPERIMENT NUMBER		CDC3-34
TRACER & PHASE		CARBON-14 M.E.
FRACTIONAL FLOW		3:1.0
MAX. & INJ. CONC.	(DPM/CC)	4000 4000
FLOW RATE		0.056 CC/MIN.

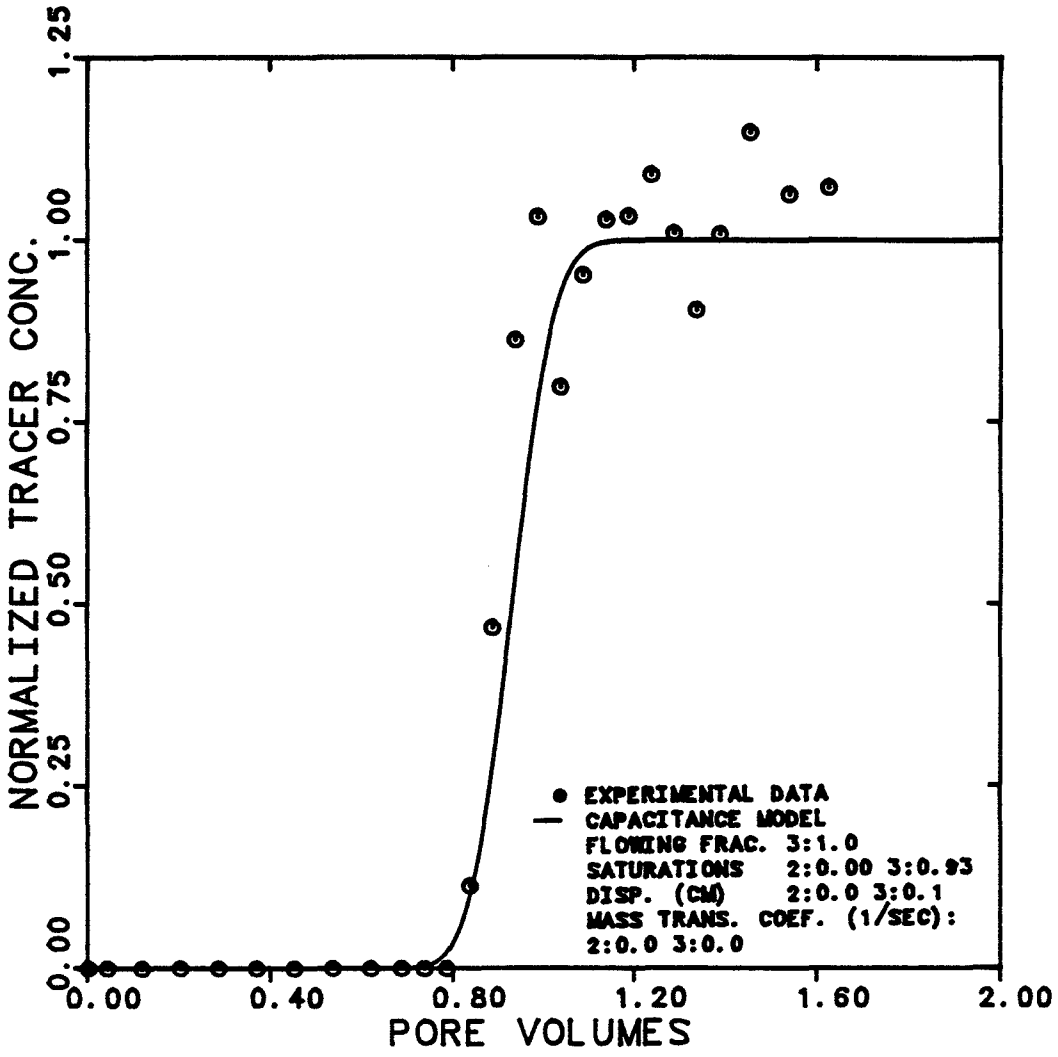

Figure 6.2.22 Effluent History for Carbon-14 in M.E. for Single-Phase M.E. Flow at 0.056 cc/min

EXPERIMENT NUMBER		CDC3-36
TRACER & PHASE		CARBON-14 M.E.
FRACTIONAL FLOW		3:1.0
MAX. & INJ. CONC.	(DPM/CC)	4000 4000
FLOW RATE		0.94 CC/MIN.

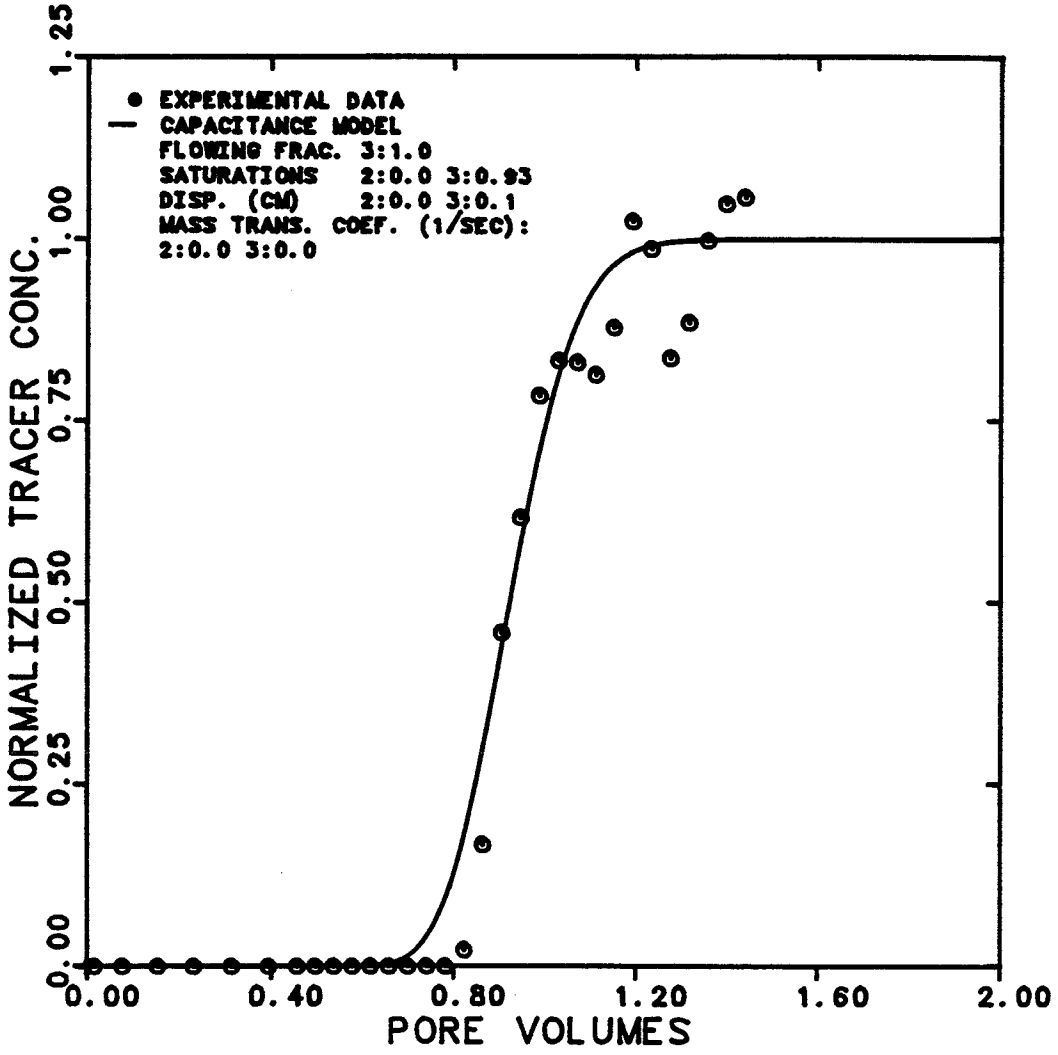

Figure 6.2.23 Effluent History for Carbon-14 in M.E. for Single-Phase M.E. Flow at 0.94 cc/min

EXPERIMENT NUMBER		CDC3-36
TRACER & PHASE		TRITIUM M.E.
FRACTIONAL FLOW		3:1.0
MAX. & INJ. CONC.	(DPM/CC)	20000 20000
FLOW RATE		0.94 CC/MIN.

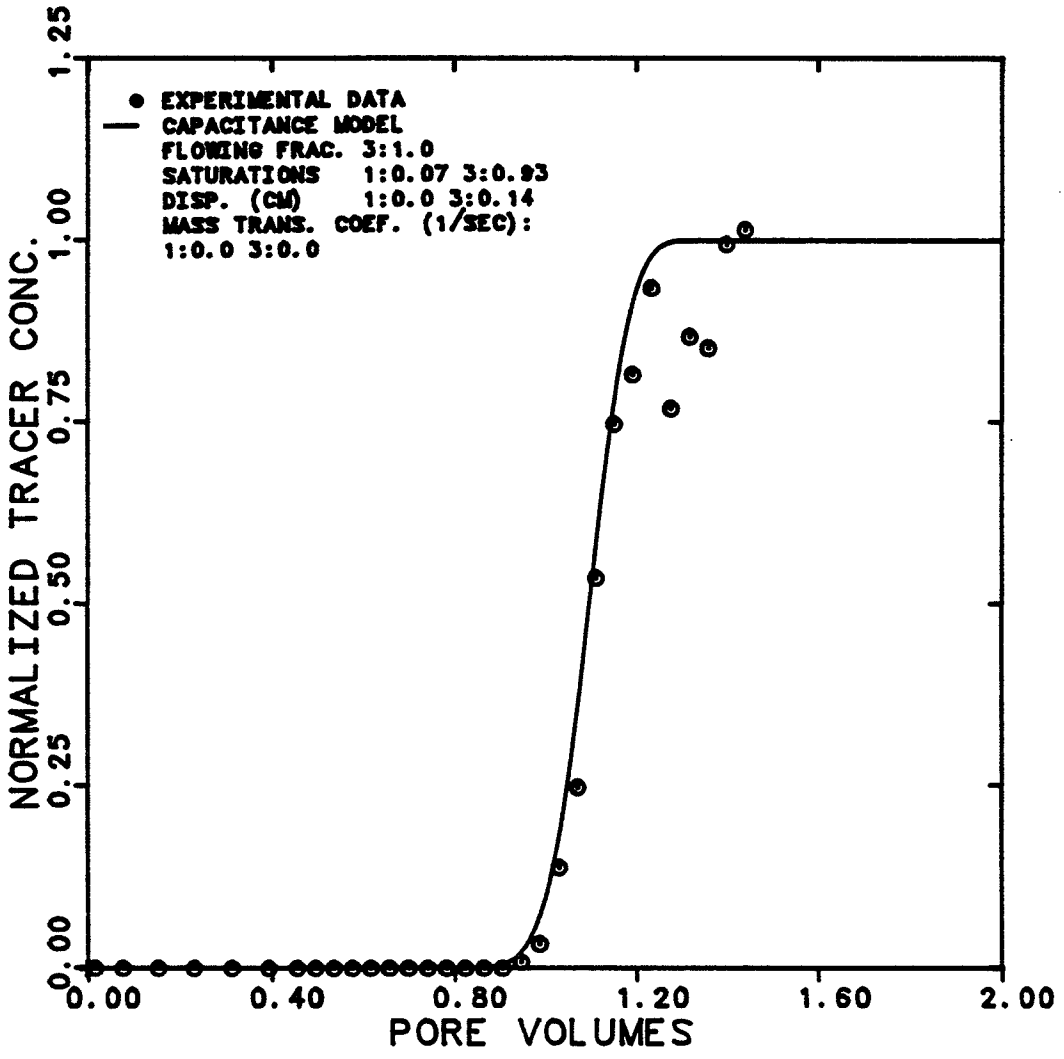

Figure 6.2.24 Effluent History for Tritiated Water in M.E. for Single-Phase M.E. Flow at 0.94 cc/min

EXPERIMENT NUMBER	CDC3-38
TRACER & PHASE	TRITIUM M.E.
FRACTIONAL FLOW	3: 1.0
MAX. & INJ. CONC.	20400 20400 DPM/CC
FLOW RATE	12.81 CC/MIN.

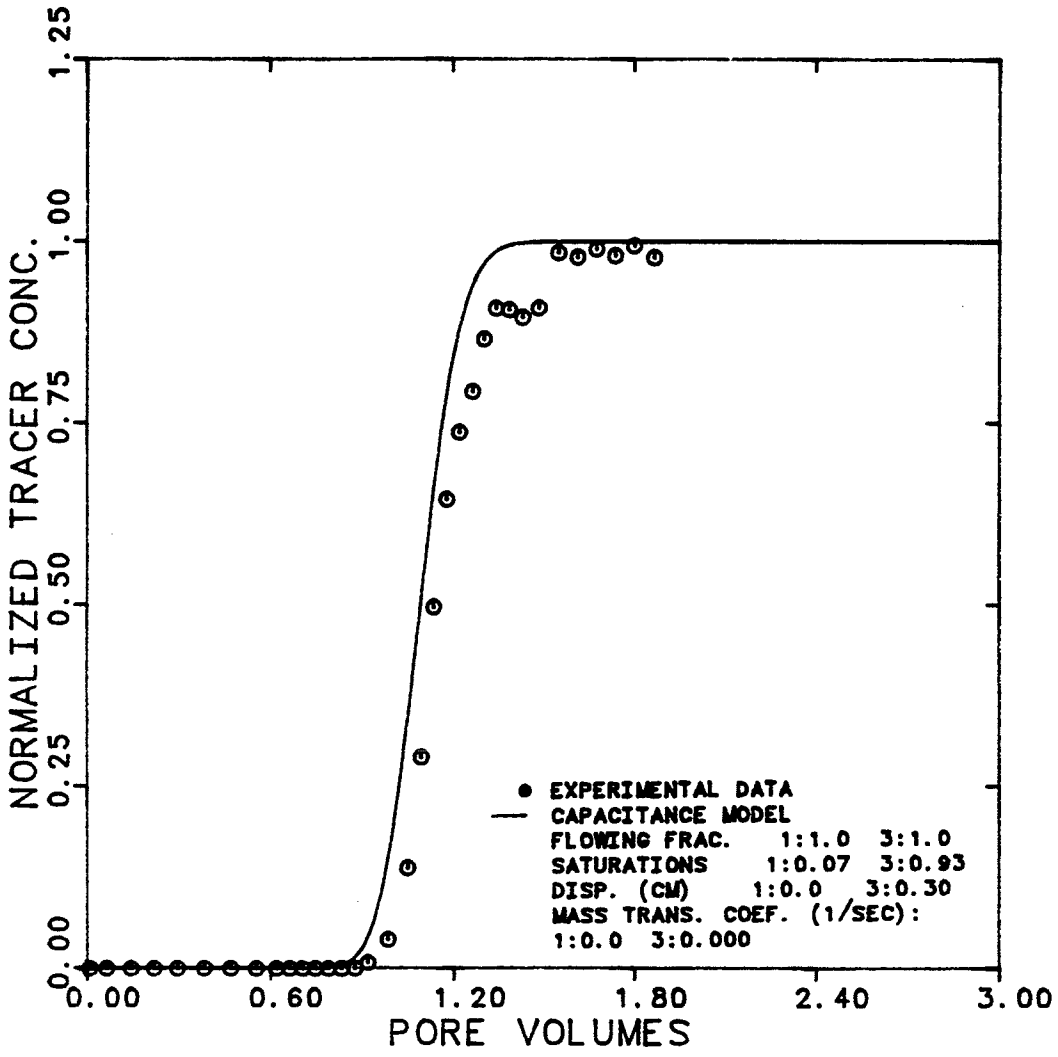

Figure 6.2.25 Effluent History for Tritiated Water in M.E. for Single-Phase M.E. Flow at 12.81 cc/min

EXPERIMENT NUMBER		CDC3-38
TRACER & PHASE		CARBON-14 M.E.
FRACTIONAL FLOW		3:1.0
MAX. & INJ. CONC.	(DPM/CC)	3960 3960
FLOW RATE		12.81 CC/MIN.

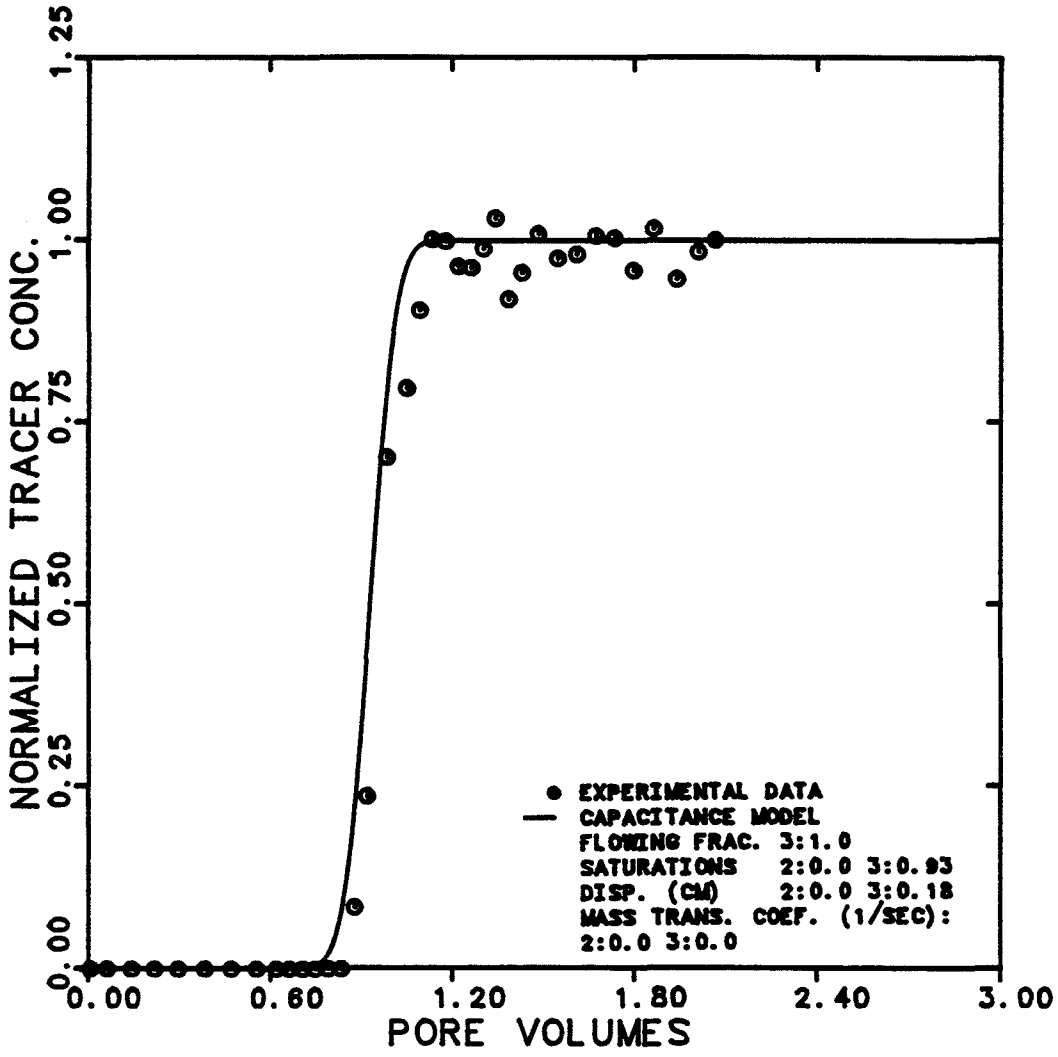

Figure 6.2.26 Effluent History for Carbon-14 in M.E. for Single-Phase M.E. Flow at 12.81 cc/min

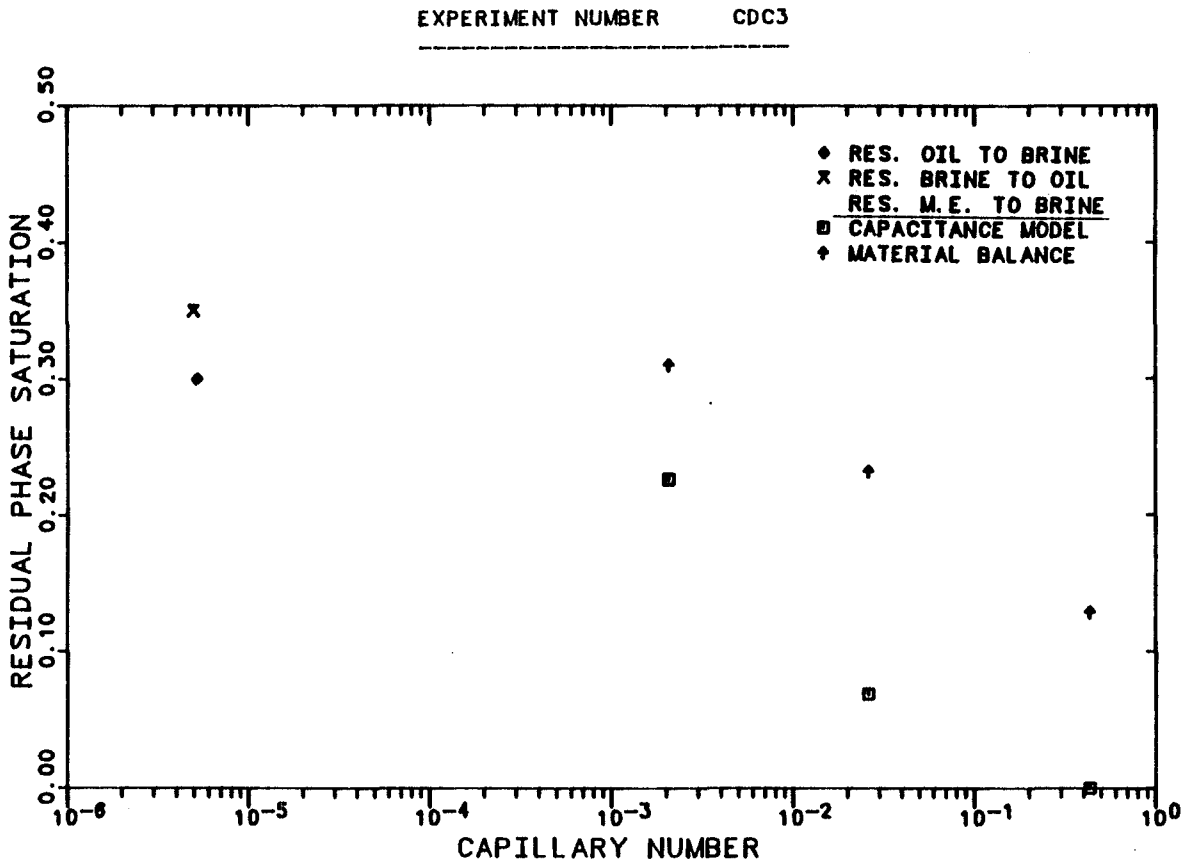

Figure 6.2.27 Comparison Between the Capacitance Model and Material Balance Estimates of Residual M.E. to Brine as a Function of Capillary Number

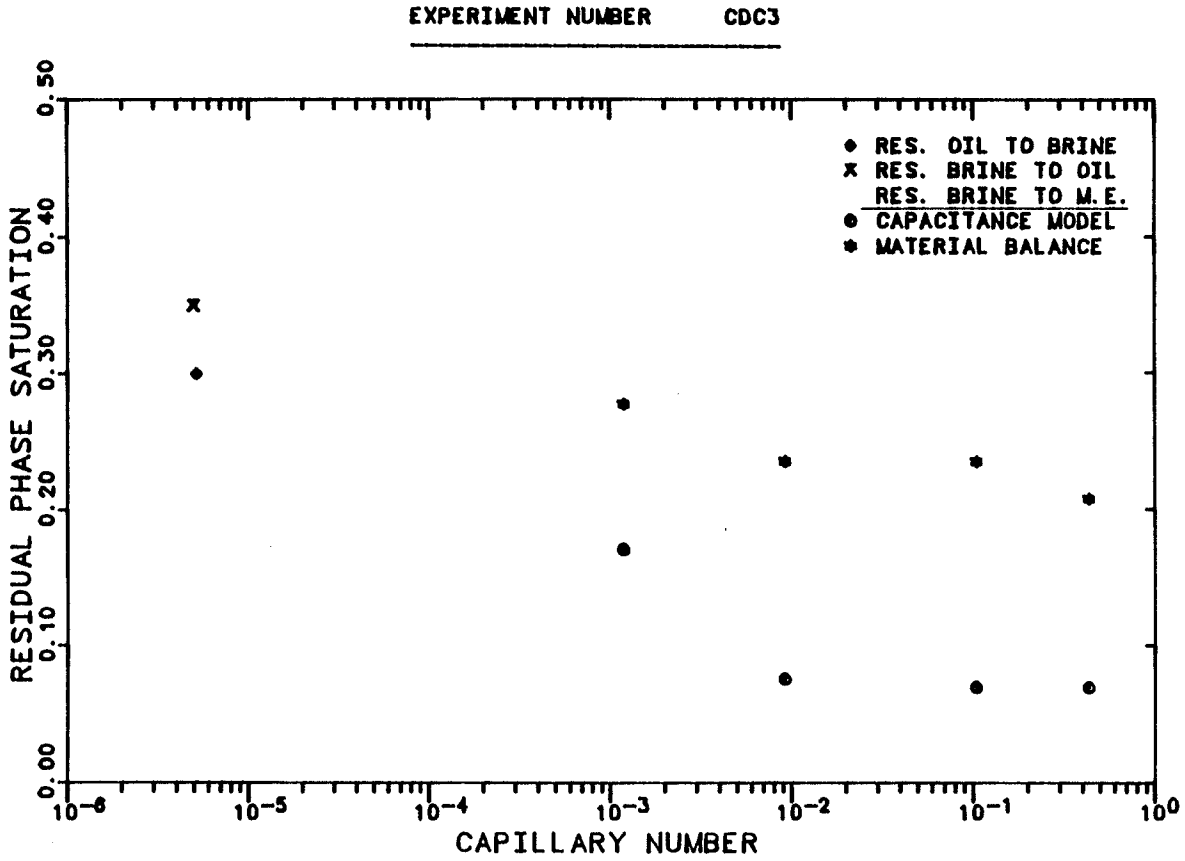

Figure 6.2.28 Comparison Between the Capacitance Model and Material Balance Estimates of Residual Brine to M.E. as a Function of Capillary Number

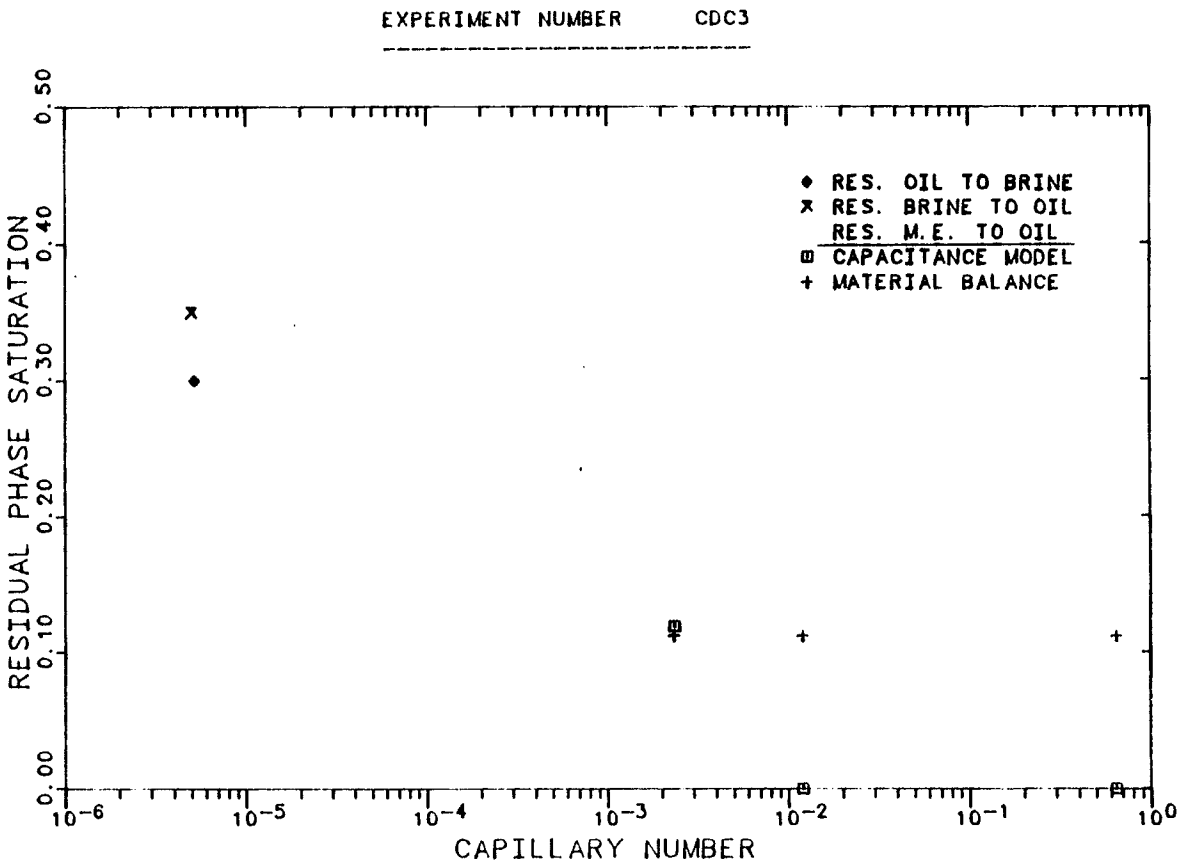

Figure 6.2.29 Comparison Between the Capacitance Model and Material Balance Estimates of Residual M.E. to Oil as a Function of Capillary Number

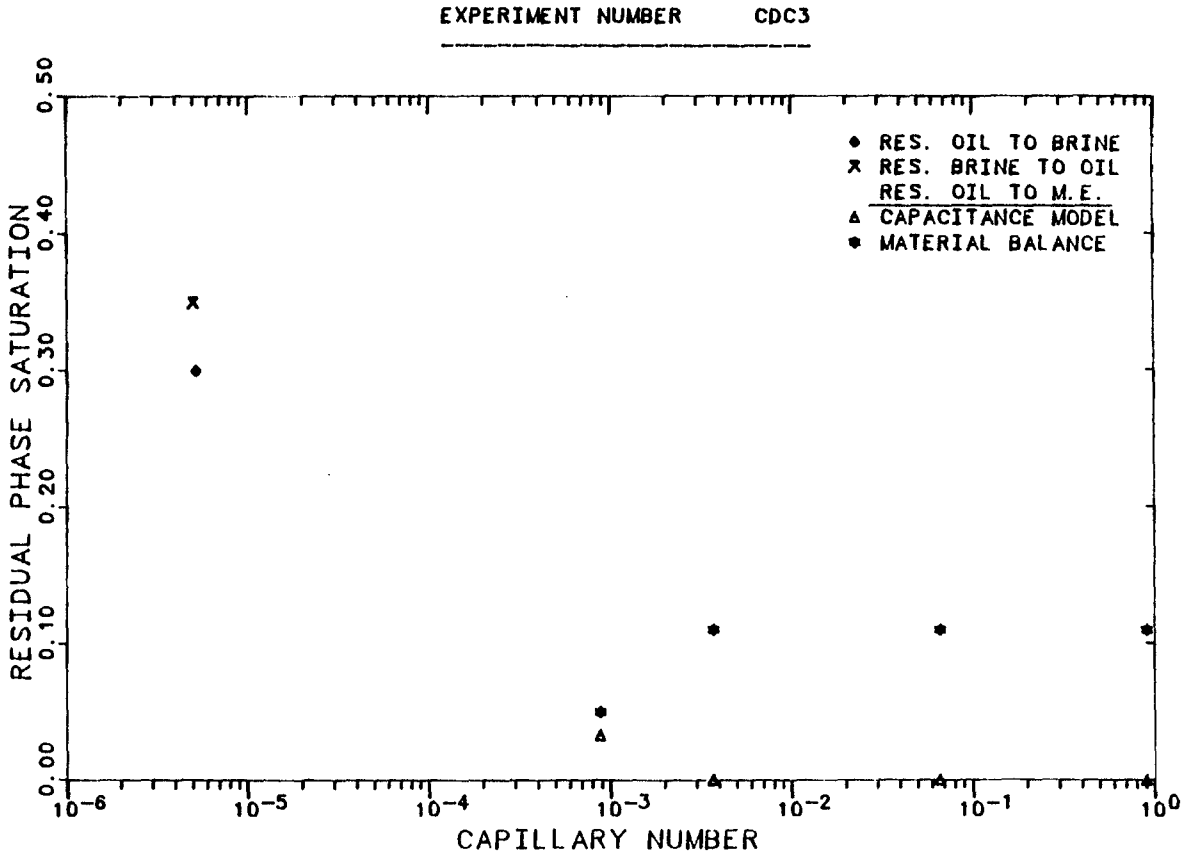

Figure 6.2.30 Comparison Between the Capacitance Model and Material Balance Estimates of Residual Oil to M.E. as a Function of Capillary Number

COMPOSITION OF INJECTED MICROEMULSION

WATER	39	VOL.%
OIL	55	VOL.%
IBA	1.8	VOL.%
TRS 10-410	3.5	VOL.%

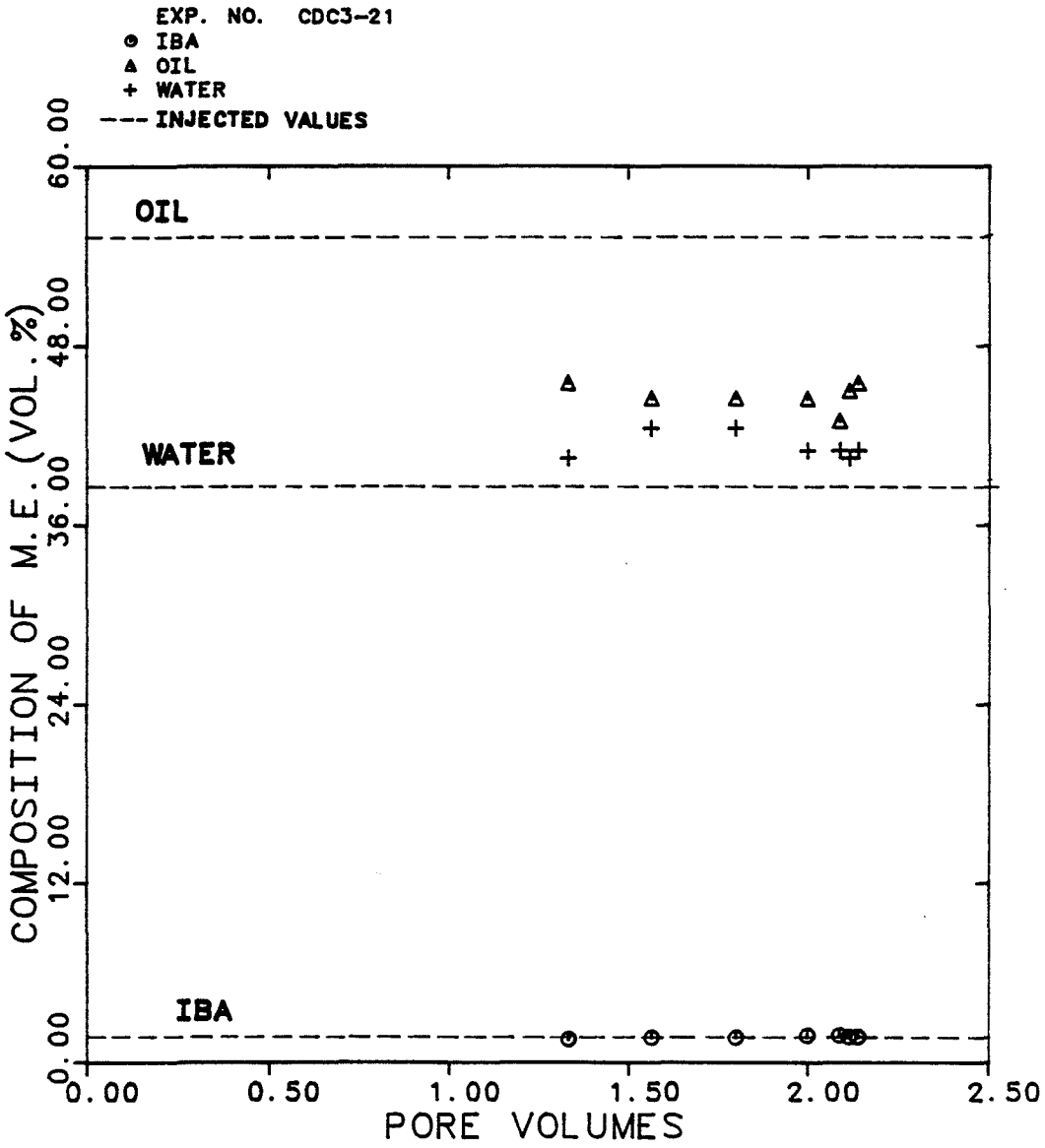

Figure 6.2.31 Composition of M.E. in Steady-State Effluent Samples as a Function of Pore Volumes (Exp. CDC3-21)

COMPOSITION OF INJECTED MICROEMULSION

WATER	39 VOL.%
OIL	55 VOL.%
IBA	1.8 VOL.%
TRS 10-410	3.5 VOL.%

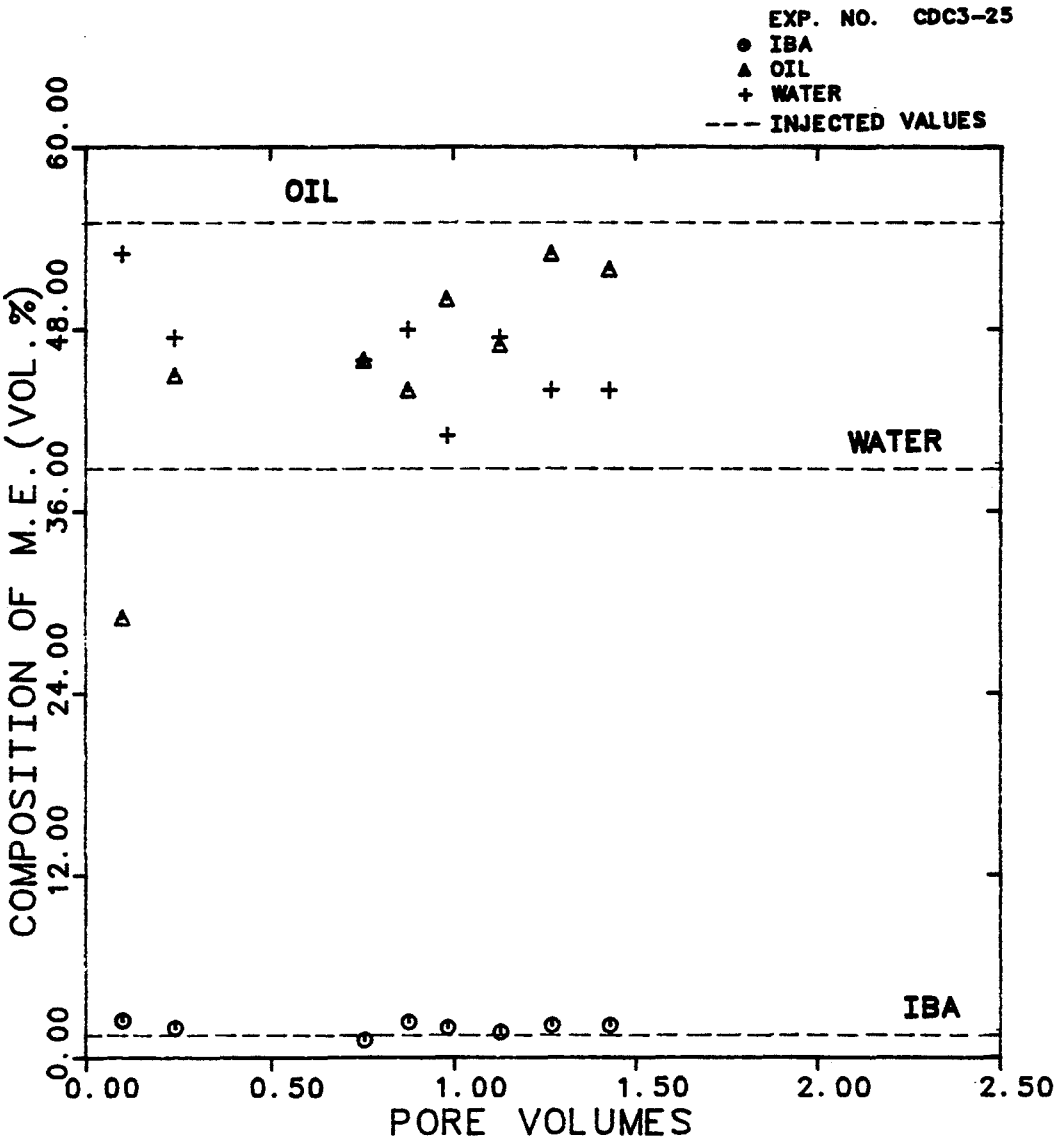

Figure 6.2.32 Composition of M.E. in Steady-State Effluent Samples as a Function of Pore Volumes (Exp. CDC3-25)

EXPERIMENT NUMBER		CDC3-51
TRACER & PHASE		CARBON-14 OIL
FRACTIONAL FLOW		2:1.0
MAX. & INJ. CONC.	(DPM/CC)	13800 13800
FLOW RATE		1.00 CC/MIN.

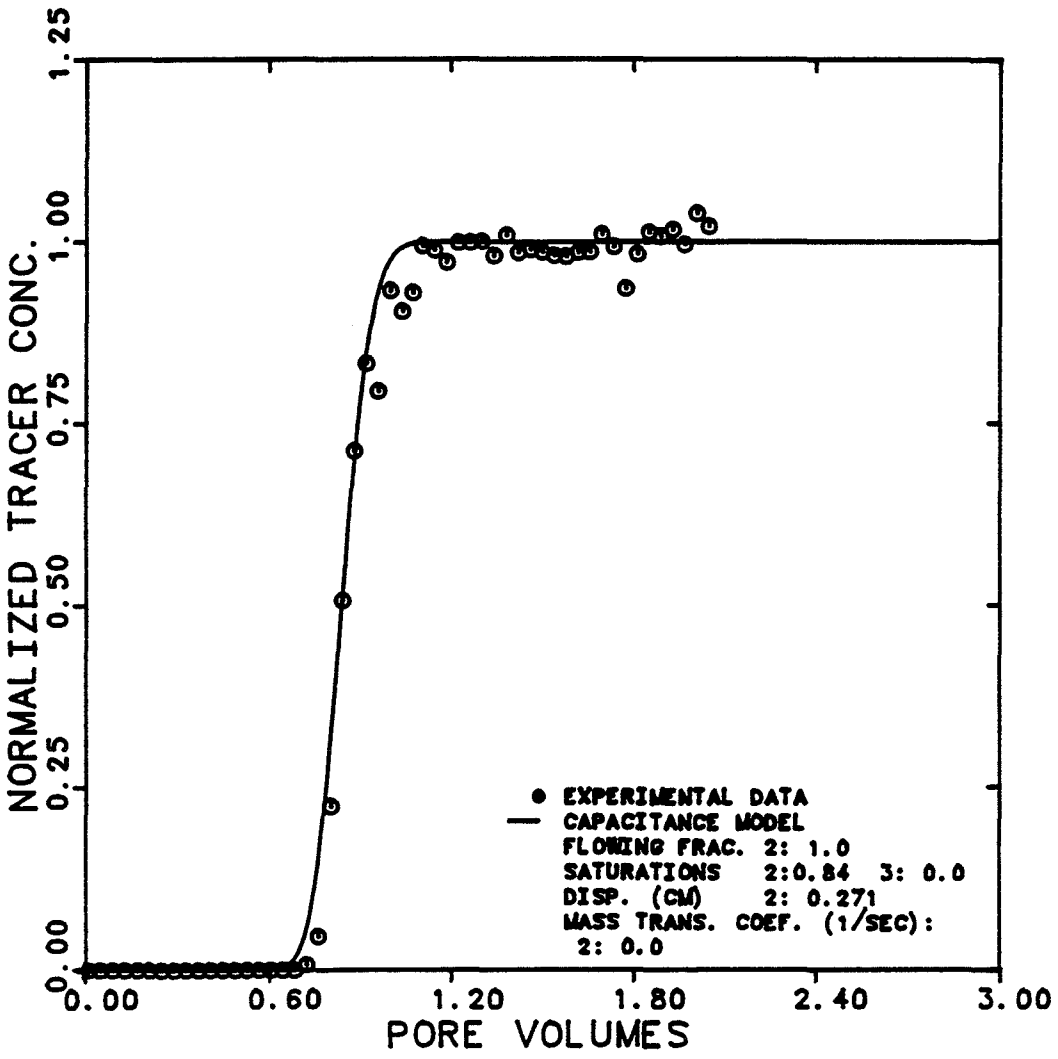

Figure 6.2.33 Effluent History for Carbon-14 in Oil for Single-Phase Oil Flow at 1 cc/min

EXPERIMENT NUMBER		CDC3-54
TRACER & PHASE		TAGG. SULF. M.E.
FRACTIONAL FLOW		3:1.0
MAX. & INJ. CONC.	(DPM/CC)	49800 49800
FLOW RATE		0.0095 CC/MIN.

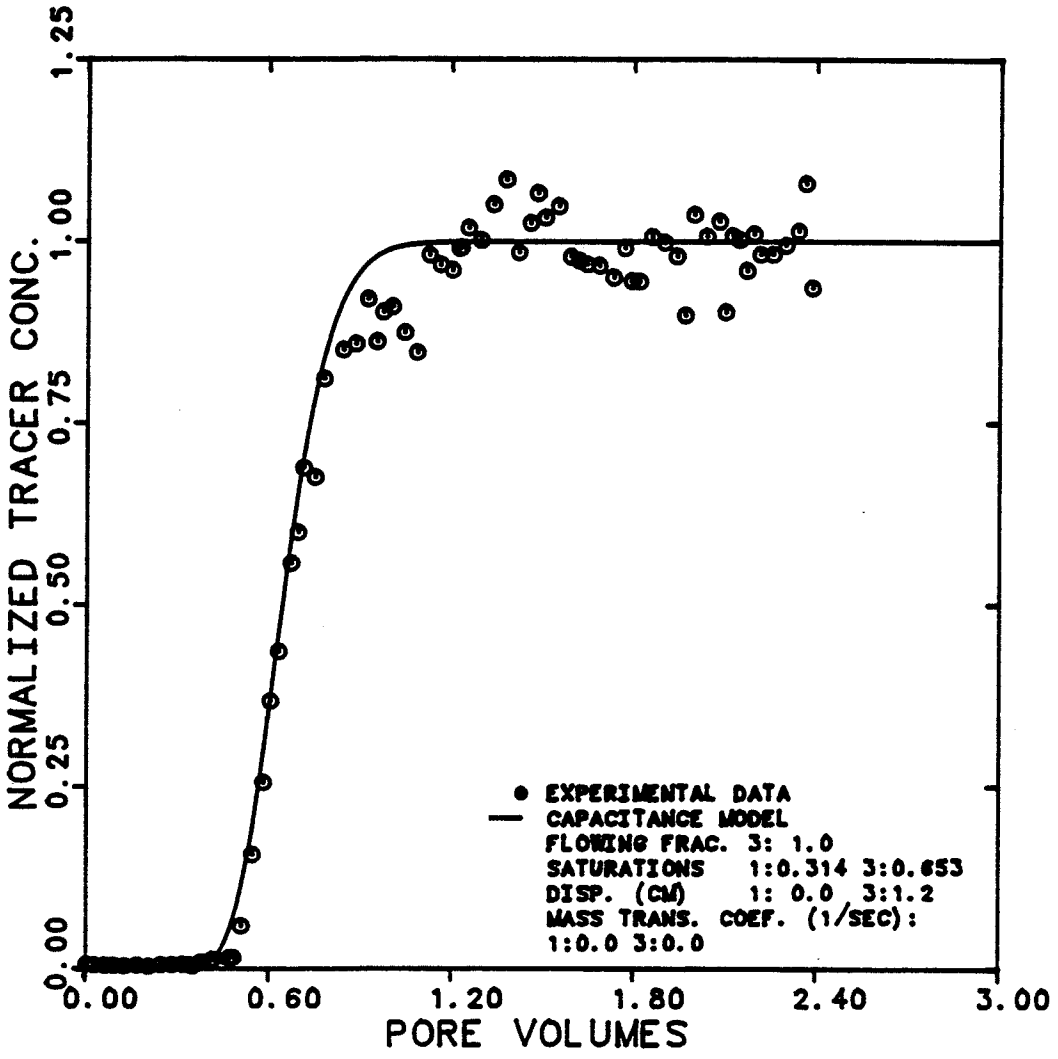

Figure 6.2.34 Effluent History for Tritium Labelled Sulfonate in M.E. for Single-Phase M.E. Flow at 0.0095 cc/min

EXPERIMENT NUMBER	CDC3-54	
TRACER & PHASE	CHLORIDE-36	M.E.
FRACTIONAL FLOW	1: 1.0	
MAX. & INJ. CONC.	670 670	DPM/CC
FLOW RATE	0.0095	CC/MIN

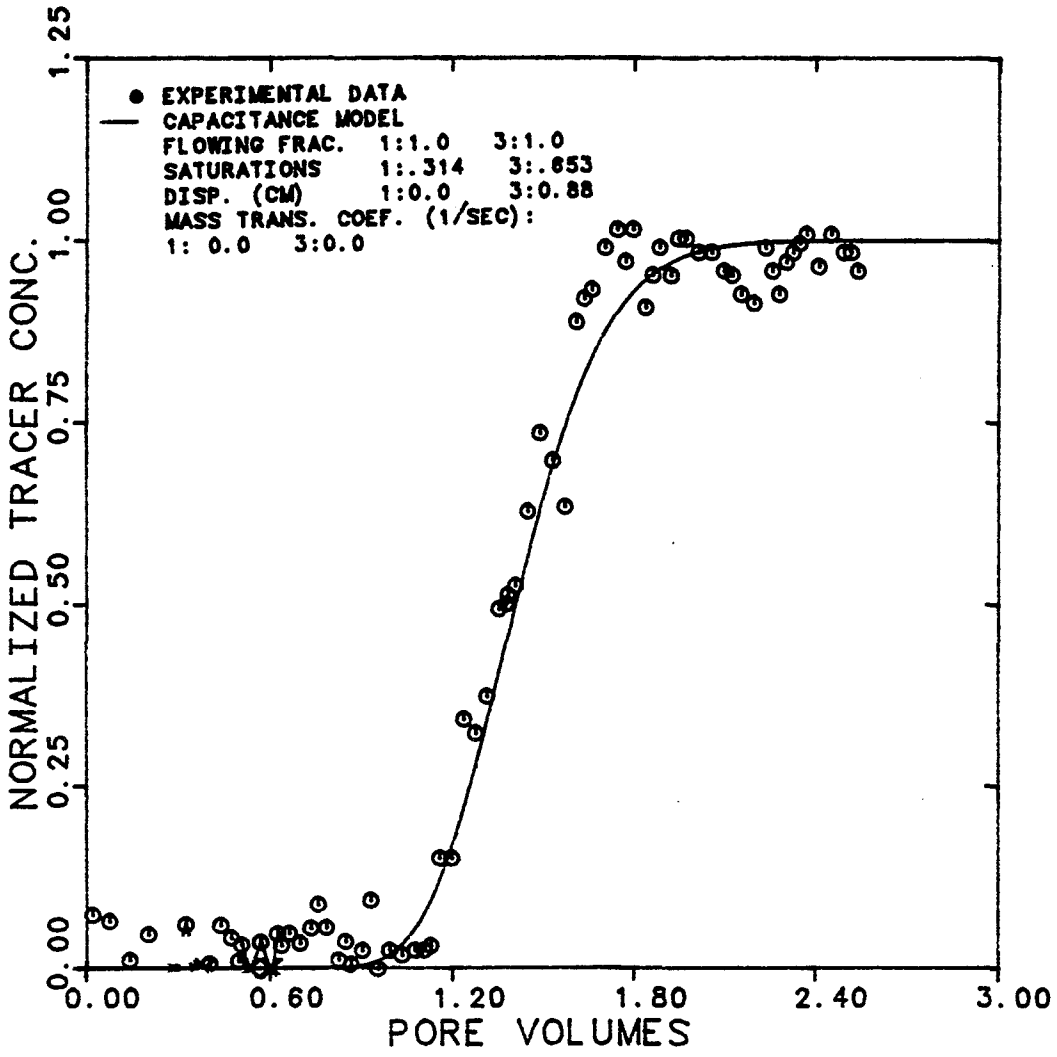

Figure 6.2.35 Effluent History for Chloride-36 in M.E for Single-Phase M.E. Flow at 0.0095 cc/min

EXPERIMENT NUMBER	CDC3-54
TRACER & PHASE	CARBON-14 M.E.
FRACTIONAL FLOW	3: 1.0
MAX. & INJ. CONC.	7400 7400 DPM/CC
FLOW RATE	0.0095 CC/MIN.

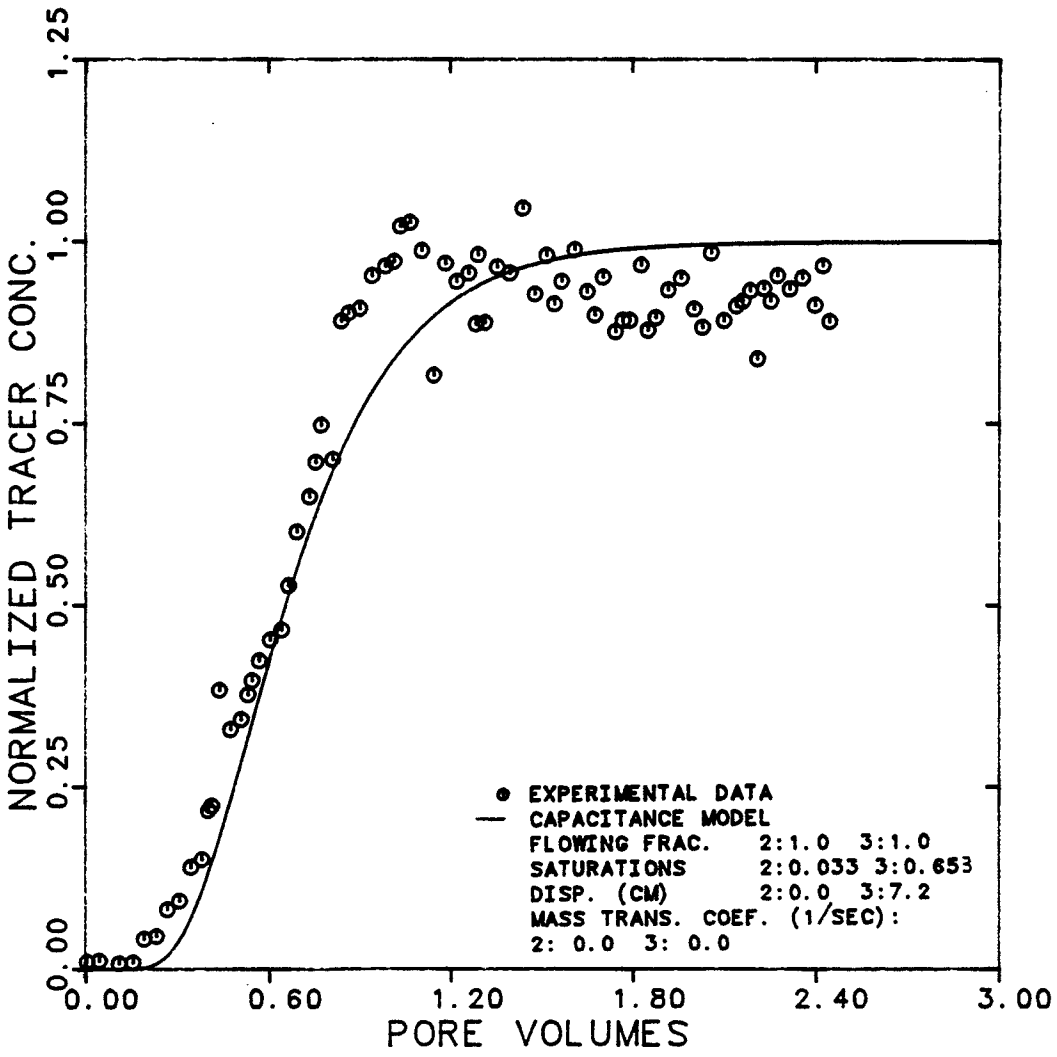

Figure 6.2.36 Effluent History for Carbon-14 in M.E. for Single-Phase M.E. Flow at 0.0095 cc/min

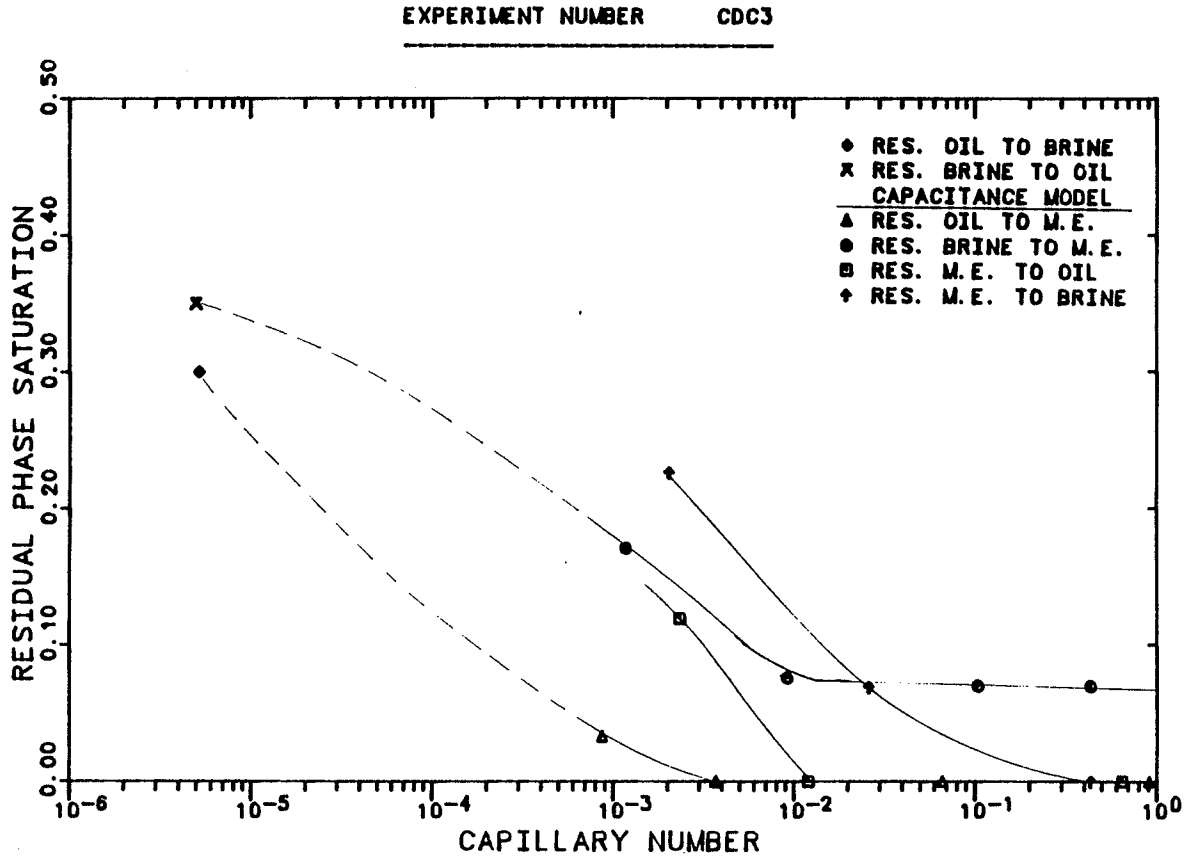

Figure 6.2.37 Capillary Desaturation Curves for M.E., Oil, and Brine Phases

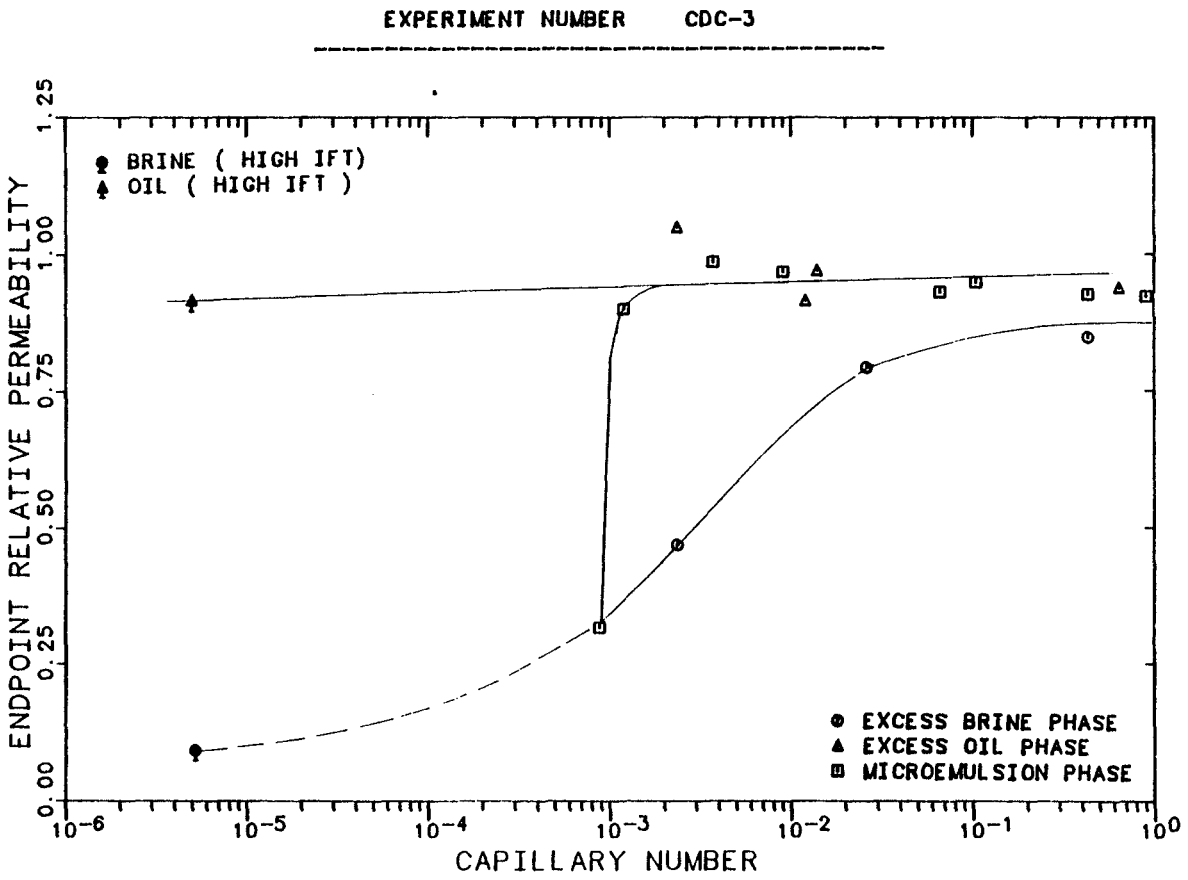

Figure 6.2.38 Endpoint Relative Permeabilities as a Function of Capillary Number

EXPERIMENT NUMBER CDC3

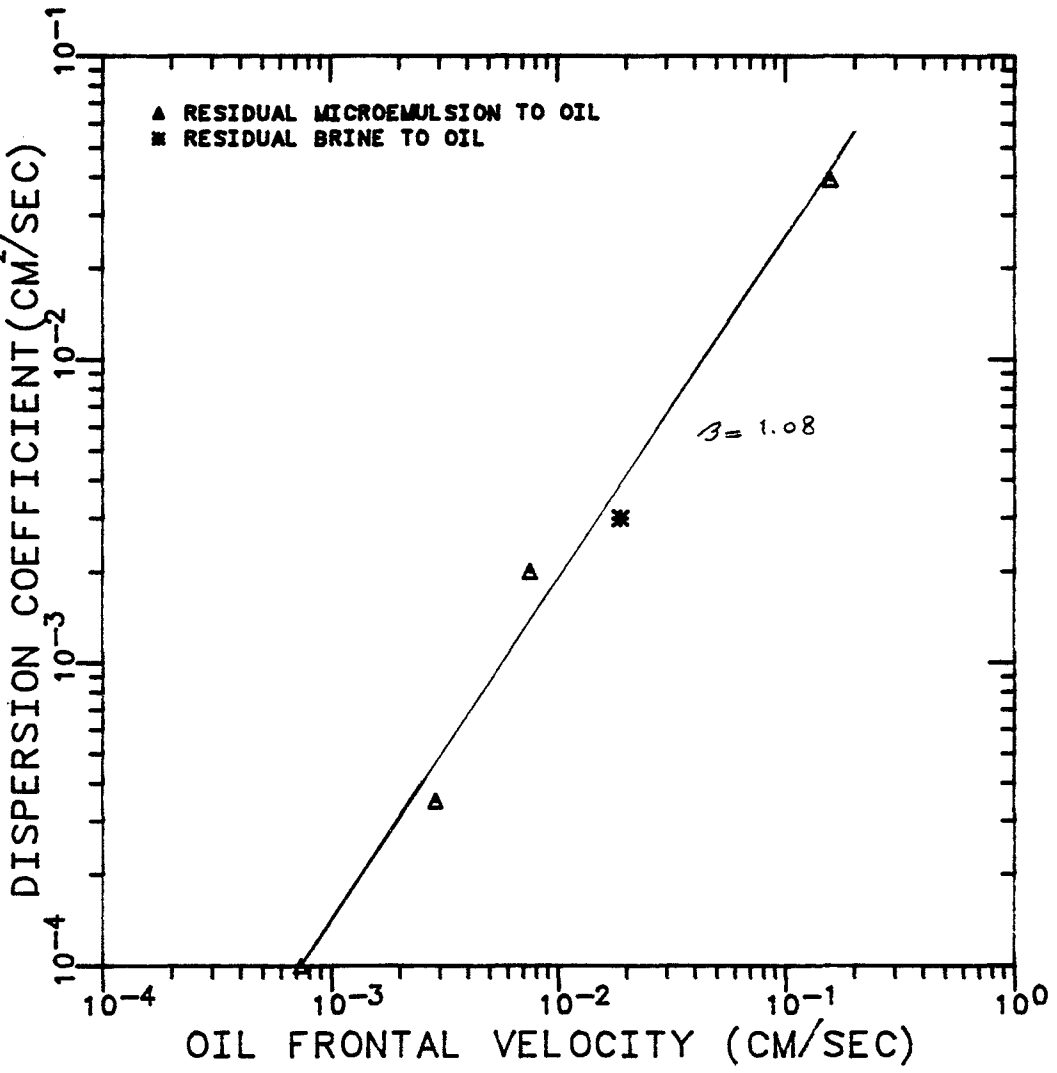

Figure 6.2.39 Dispersion Coefficient of Carbon-14 in Oil as a Function of Oil Frontal Velocity

EXPERIMENT NUMBER CDC3

RESIDUAL OIL AND BRINE TO MICROEMULSION

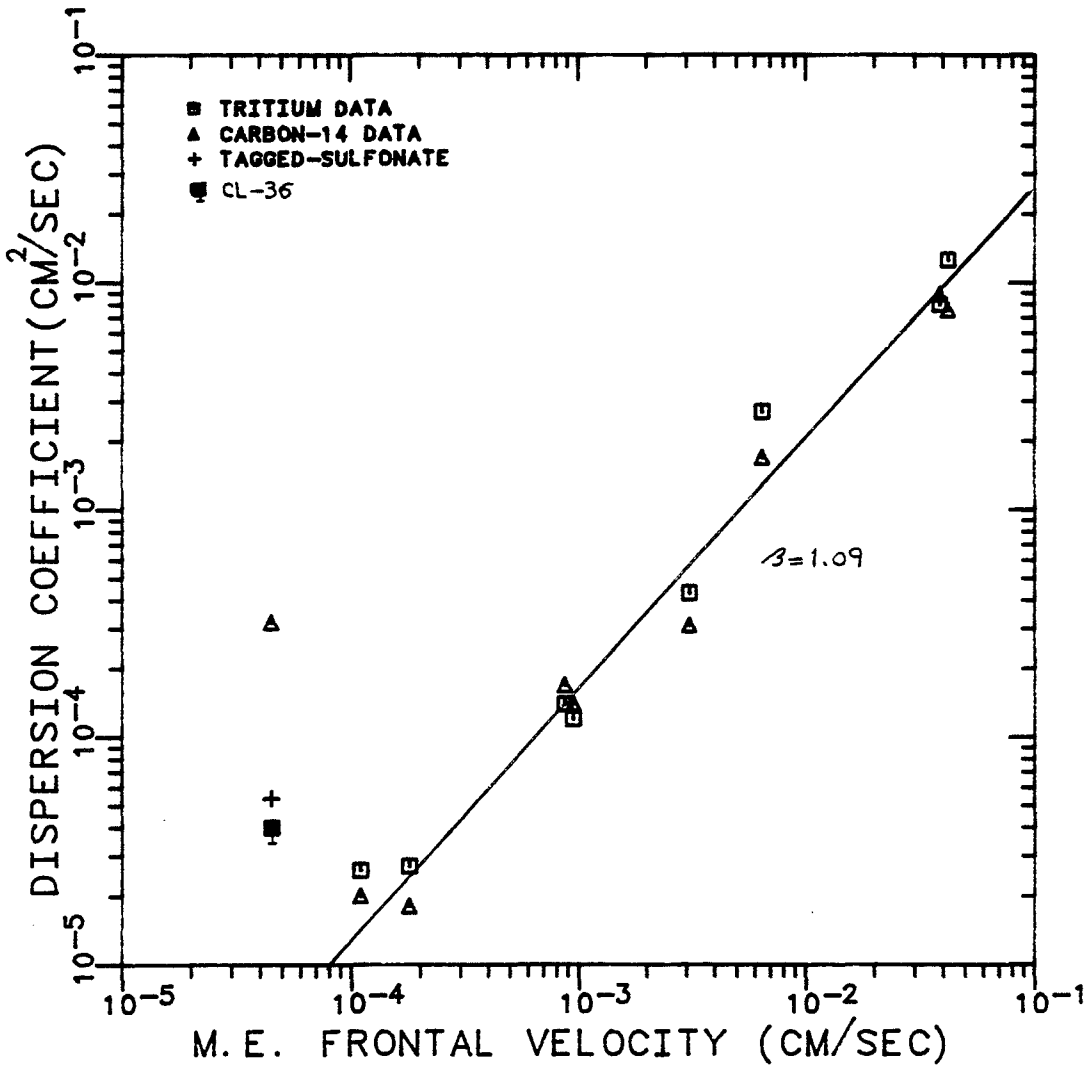

Figure 6.2.40 Dispersion Coefficient of Tracers in M.E. Phase as a Function of M.E. Frontal Velocity

EXPERIMENT NUMBER CDC3

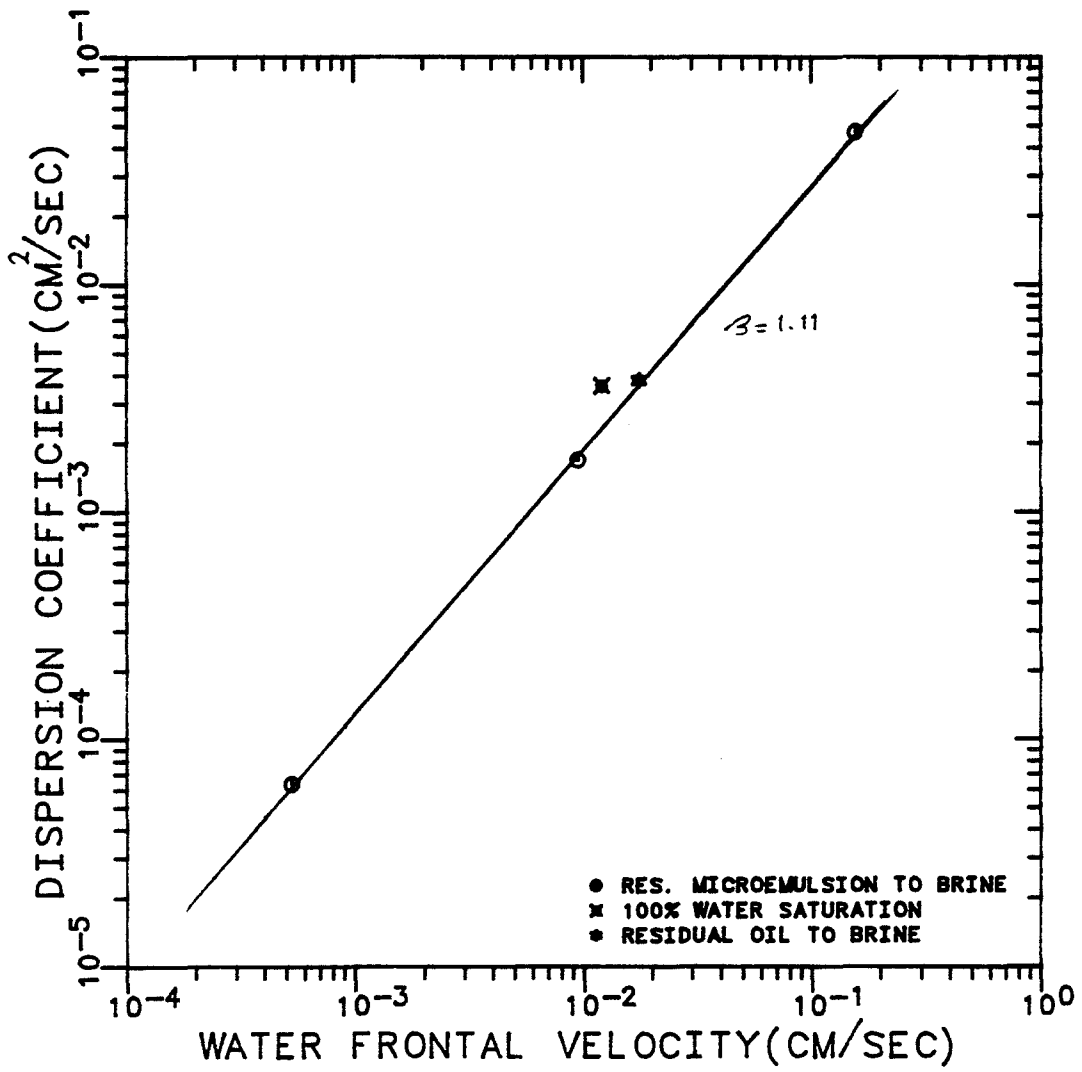

Figure 6.2.41 Dispersion Coefficient of Tritiated Water in Brine as a Function of Brine Frontal Velocity

EXPERIMENT NUMBER CDC3

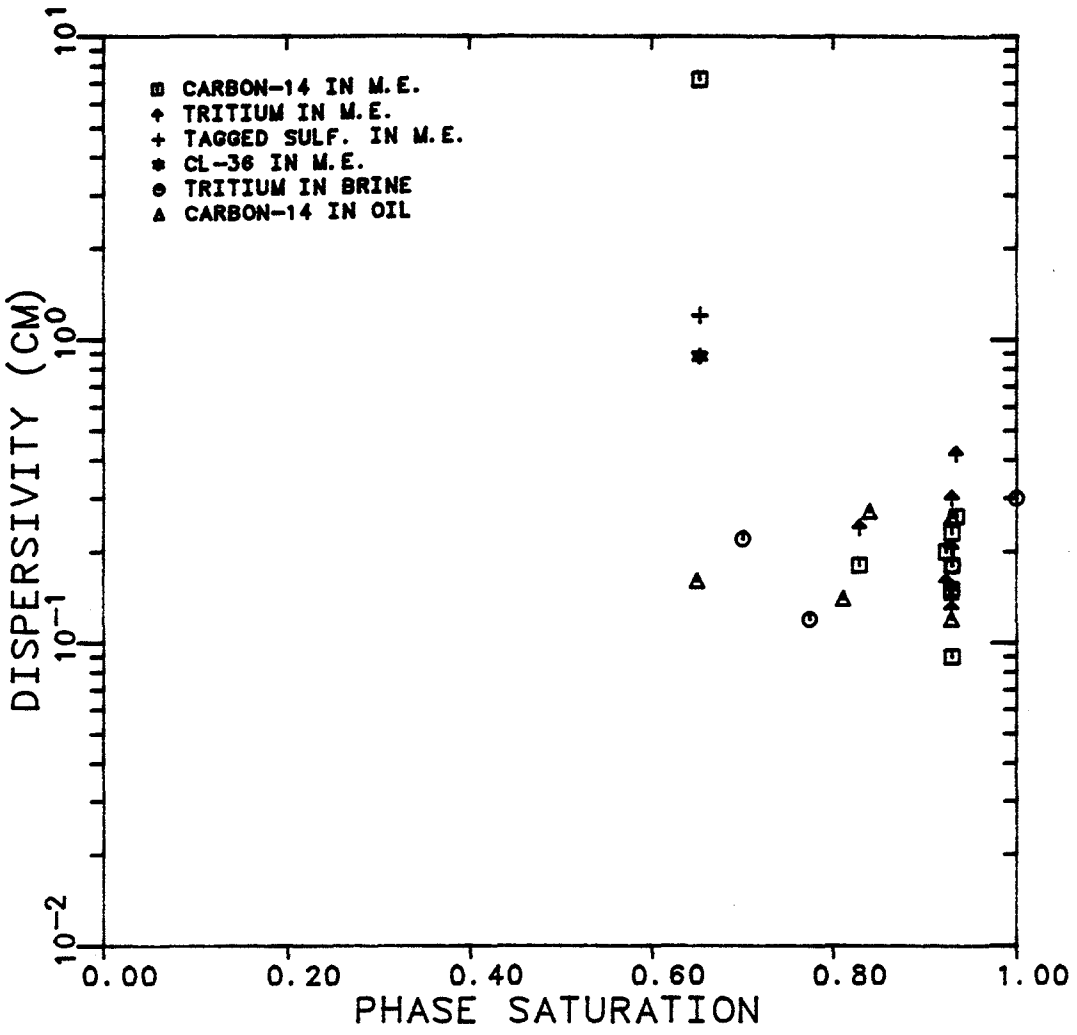

Figure 6.2.42 Dispersivities of Tracers in Single-Phase Flow of M.E., Oil, and Brine as a Function of Phase Saturation

6.2.1 Comparison of Capillary Desaturation Curves

A large number of experimental data have been published which relates removal of residual wetting and non-wetting phases to applied flow conditions and fluid and rock properties. The few selected examples are the experiments of Gupta and Trushenski [G.4], Abrams [A.1], Amaefule and Handy [A.2], Chatzis and Morrow [C.4], Mohanty and Salter [M.2], and Bhuyan [B.5]. The porous media used were all Berea sandstone. Information on the fluids are in Chapter 2 (section 2.2).

Shown in Figures 6.2.43 and 6.2.44 are the capillary desaturation curves for non-wetting oil phase using the definitions of capillary number $N_c = \frac{u\mu}{\sigma}$ and $N_c = \frac{k\Delta P}{L\sigma}$, respectively. Excellent agreement is observed for the data of Amaefule and Gupta in Figure 6.2.43 and Amaefule; Abrams; Chatzis, and Mohanty in Figure 6.2.44. Higher values of capillary number are required to initiate mobilization in Amaefule's results than those reported by others. The normalized residual oil from Exp. No. CDC agrees very well with the non-wetting curve of Bhuyan. The capillary desaturation data measured by Bhuyan are on the left side of those reported by Abrams, Amaefule, Gupta, Mohanty, and Chatzis.

Figure 6.2.45 shows the normalized wetting

saturation as a function of $N_c = \frac{u\mu}{\sigma}$. There is an excellent agreement among the data of Amaefule, Bhuyan and the residual microemulsion to oil and brine of this study. The data reported by Gupta and residual brine to microemulsion of Exp. CDC require lower values of capillary number for mobilization than those reported by others.

The capillary desaturation data for the wetting phase (residual oil in an oil-wet core for Mohanty) using the definition of $N_c = \frac{k\Delta P}{L\sigma}$ (Figure 6.2.46) suggest the following,

- The data reported by Amaefule and the residual microemulsion to brine of this study are in a fair agreement. These data are all to the right of the remaining points.

- Excellent agreement is observed for the results of Bhuyan, Mohanty and this study (residual brine to m.e.).

- The results of this study are the only data measured at $N_c > 10^{-2}$.

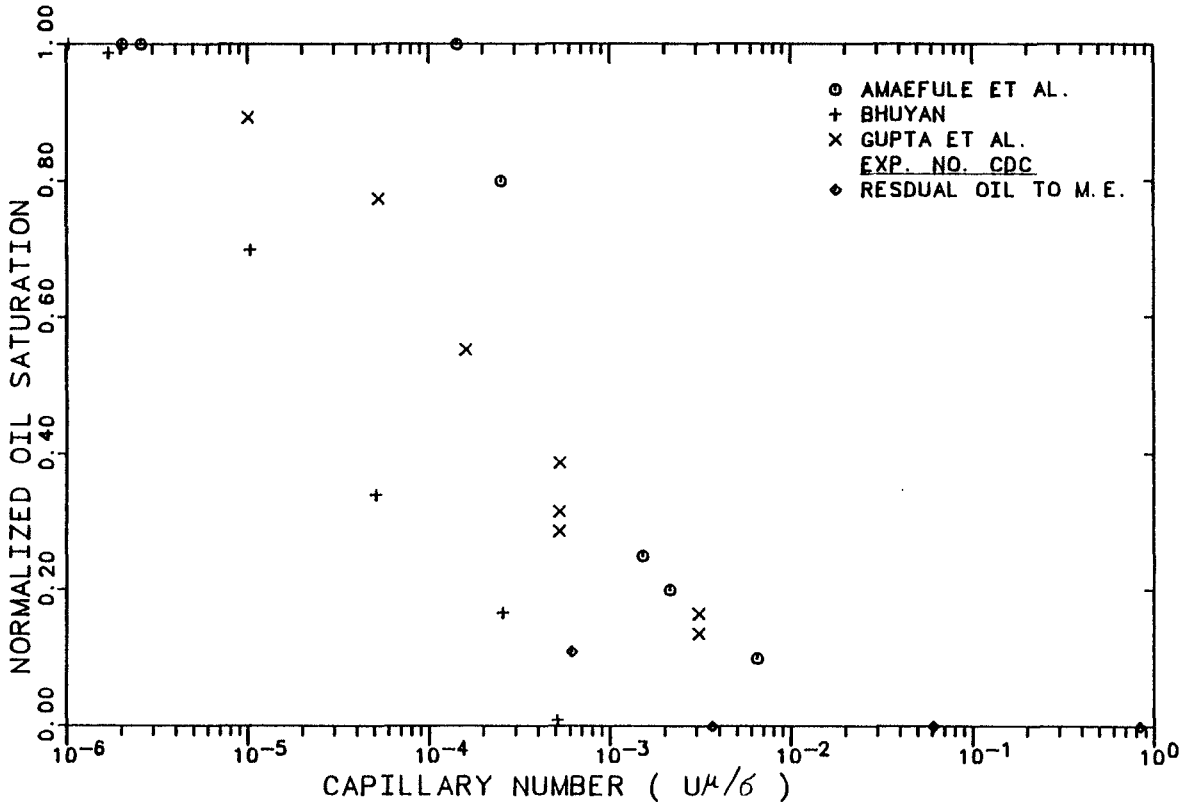

Figure 6.2.43 Normalized Residual Oil Saturation as a Function of Capillary Number (N_C=uμ/σ)

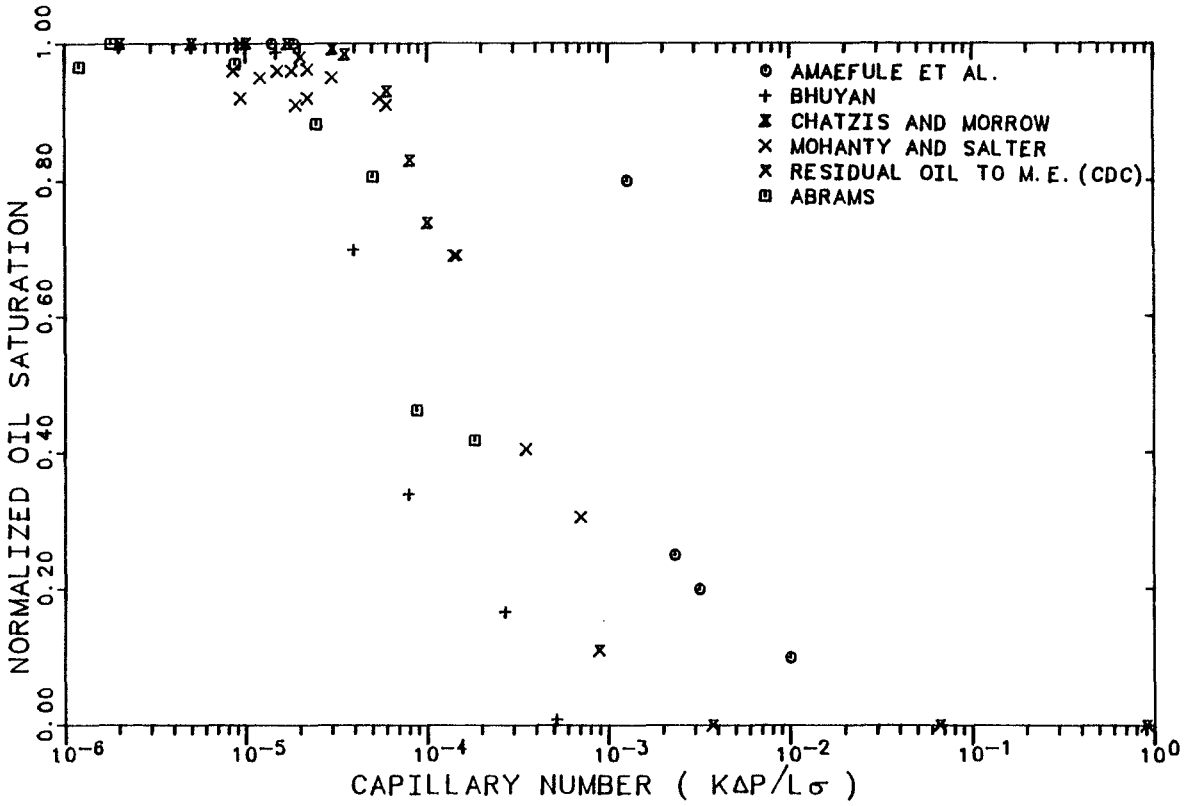

Figure 6.2.44 Normalized Residual Oil Saturation as a Function of Capillary Number ($N_C=k\Delta p/L\sigma$)

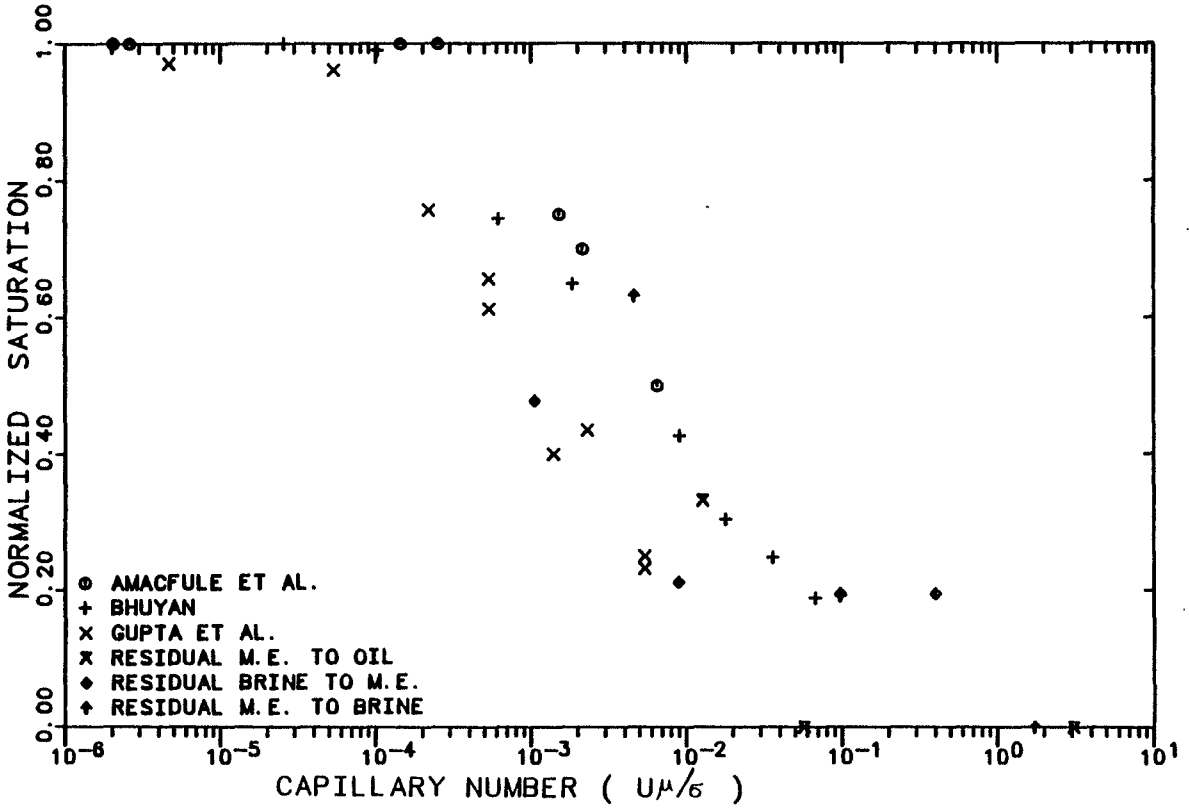

Figure 6.2.45 Normalized Residual Wetting Saturation as a Function of Capillary Number ($N_C=u\mu/\sigma$)

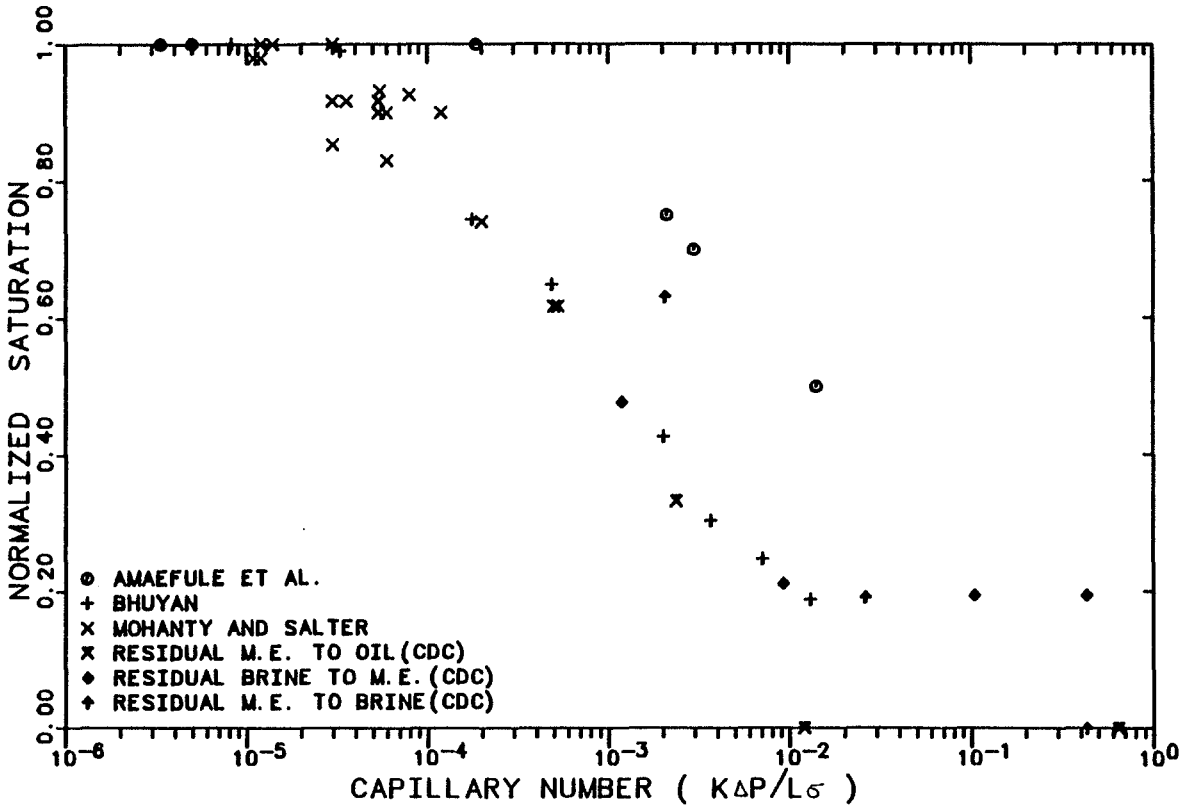

Figure 6.2.46 Normalized Residual Wetting Saturation as a Function of Capillary Number (N_C=kΔp/Lσ)

6.2.2 Comparison of Single-Phase Dispersion Coefficients

Gupta [G.4], Shuler [S.10], Delshad [D.8], and Salter and Mohanty [S.3] measured dispersion coefficients as a function of frontal velocity. These results were all performed in 100% water saturated media.

Figure 6.2.47 shows a comparison of results of the above mentioned investigators with those obtained in this study. Although, the results of Exp. No. CDC3 (Figure 6.2.41) are at different water saturation, but the independency of dispersivity (Figure 6.2.42) on water saturation makes this comparison possible.

The results are in fair agreement considering the differences in the porous medium used. All curves show the well known increased with velocity. The slope corresponding to the exponent given in the classical equation (Eq. 2.19) for dispersion coefficient is about 1.17. These measurements were all made at velocities high enough that diffusion was negligible, so the usual approach to $D/F\phi$ at low velocity is not apparent on the plot.

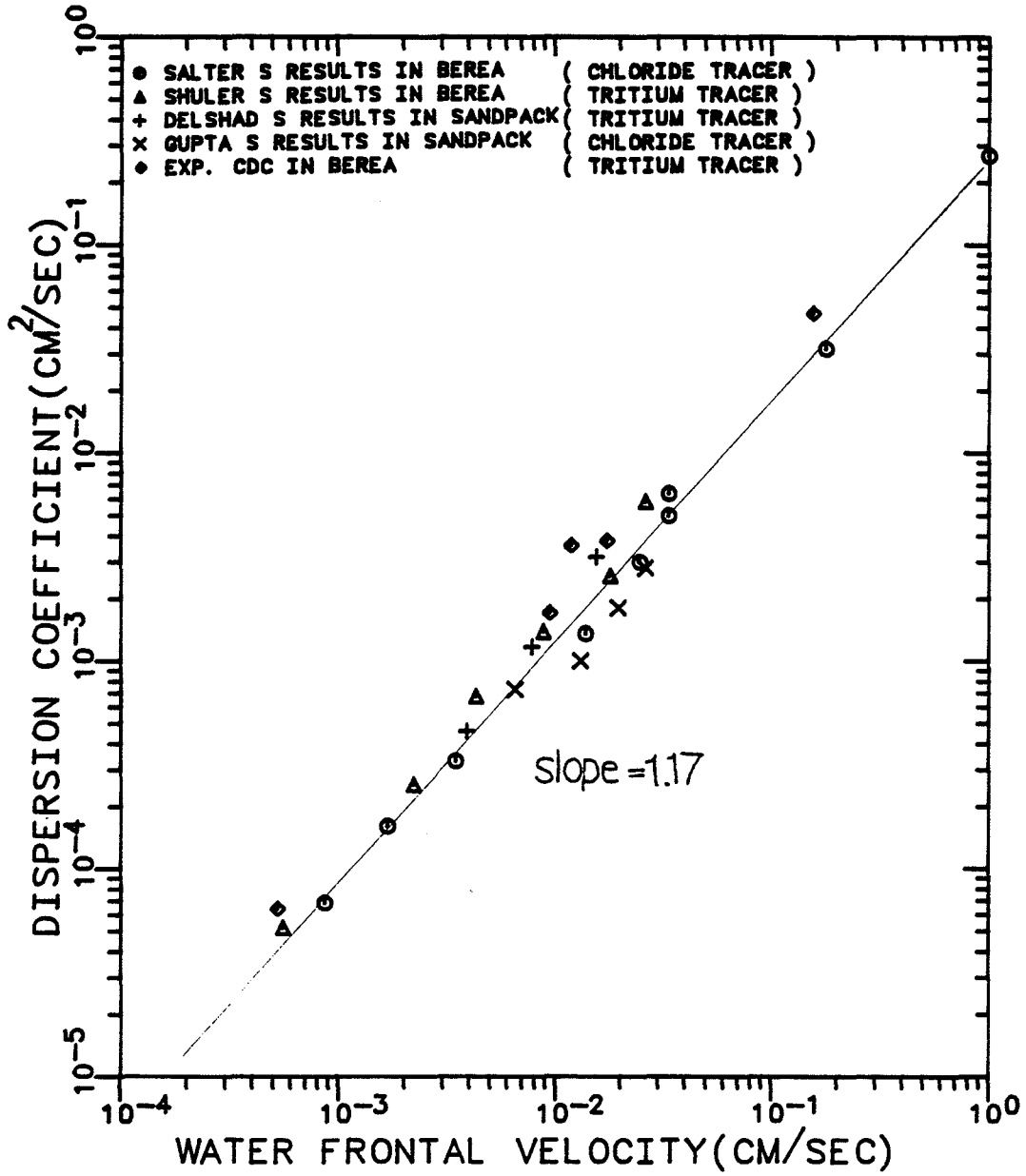

Figure 6.2.47 Comparison of the Dispersion Coefficient of Tritiated Water in Brine with Literature Values

6.3 Two-Phase Flow Relative Permeability and Dispersion Experiments

6.3.1 Microemulsion/Excess Oil (Exp. No. SMO)

The purpose of this experiment was to measure relative permeability and dispersion at a constant capillary number of 10^{-2} for the upper phase excess oil and middle phase microemulsion of a three-phase micellar solution.

The main difference between this experiment and those previously reported [D.8] is that at each cut the flow rate was adjusted to obtain a constant potential drop and thus a constant capillary number. Appendix D gives a numerical example of how the fractional flow (cuts) and the total flow rates were planned

The experiment was conducted at 30°C in the same core as experiment CDC-3 (Table 6.2.1) except it was vertical, with injection at the top, to prevent phase segregation. The schematic diagram of the experimental apparatus is shown in Figure 5.1.8. A new batch (Stock 2) of micellar solution (hot and cold) with the same composition was made and the properties are listed in Table 6.1.1.

The procedure followed in this experiment was to:

- Saturate the core with microemulsion at 0.955 cm^3/min until the produced samples showed single phase microemulsion, the pressure drop was constant and the composition of injected and produced became identical. The concentration of calcium and magnesium after injection of 0.65 pore volumes were about 10 and 3 ppm, respectively.

- Inject the microemulsion containing both carbon-14 and tritium at the same velocity. The tracer breakthrough curve were matched using the C-D equation. The residual saturations were S_{1r} = 0.117 and S_{2r} = 0.0 (Figures 6.3.1.1 and 6.3.1.2).

- Flood the core with excess oil to steady-state at 0.647 cm^3/min and then

- Inject oil containing carbon-14 at the same velocity. The residual saturations from the dispersion data were determined to be S_{1r} = 0.117 and S_{3r} = 0.043 (Figure 6.3.1.3).

- Inject microemulsion cuts of 4.7%, 9.9%, 22%, 57.2%, and 100%.

At steady-state for each cut, tritium and carbon-14 were used in the microemulsion and carbon-14 in oil to measure microemulsion and oleic phase dispersions.

In this experiment, because of a constant

residual brine (S_{1r} = 0.117), both tracers are partitioning. The values of partition coefficients were 0.407 and 0.555 (see table 6.1.1) for tritium and carbon-14, respectively.

The calculated saturations by means of material balance, relative permeabilities, relative mobilities, capillary number, total fluids injected to steady-state, and the potential drop across all the three sections of the core are shown in Table 6.3.1.1. The potential drop measured across the inlet and outlet sections of the core are generally higher than that of the middle section. The maximum end-effect (0.14 psi/ft at the outlet) was during oil flood. The relative permeabilities were calculated from Darcy's law taking into consideration the effect of gravity head.

Figures 6.3.1.4 through 6.3.1.12 show the normalized tracer concentration curves versus injected pore volumes. Breakthrough curves were first compared with the solution of the C-D equation for saturation determination. The sum of saturations obtained in this manner was less than one. The microemulsion saturation estimate from matching the tritium breakthrough curve against the C-D equation was consistently in good agreement with the material balance estimate. The

saturation of excess oil was thought to be low because of microscoping bypassing (or capacitance). The carbon-14 breakthrough curves in both oil and microemulsion phases were then compared with theoretical curves for both the C-D equation (shown as dashed curves) and the capacitance-dispersion model (solid curves). The breakthrough curves were matched against both models with the restriction that sum of saturations should add to unity. The matching parameters (shown in Figures) for the capacitance model are: flowing fraction, saturation, dispersivity, and mass transfer coefficient (M.T.C.) for phases 2 (oil) and 3 (microemulsion). While the parameters for the C-D equation are only saturation and dispersivity of these phases.

The saturations and dispersivities estimated from both carbon-14 and tritium breakthrough curves using the C-D equation are shown in Table 6.3.1.2.

Table 6.3.1.3 presents the estimated values for the matching parameters of the capacitance model. The calculated flowing phase velocities ($v_j^f = \frac{q_j}{A\phi S_j F_j}$) and dispersion coefficients ($K_{ij} = \alpha_{ij} v_j$), and percent tracer recoveries are also shown in Table 6.3.1.3.

The results obtained from the three analyses indicate that

- Saturations of the excess oil phase (non-wetting) estimated from carbon-14 breakthrough curve without capacitance are in error by typically 8%.

- The saturations obtained from material balance and the capacitance model are in good agreement.

- Capacitance model estimates flowing fraction of 0.9 for the excess oil phase implying that only 90% of the in-situ oil saturation is flowing.

- The dispersivities estimated from the capacitance model are lower than those estimated from the C-D equation.

- The carbon-14 breakthrough curves are all matched with a single value of mass transfer coefficient ($M_{22} = 10^{-6}$ sec^{-1}).

Consistent with the previous results (Exp. CDC) the single-phase breakthrough curves are matched well with the C-D equation.

The relative permeabilities for excess oil and microemulsion are plotted versus microemulsion saturation estimated from both material balance and the capacitance model in Figure 6.3.1.13. Material balance and the capacitance model estimates of saturation are in good agreement.

The relative permeabilities for each phase were

matched with an exponential functional form similar to those used by Pope and Nelson [P.2], and Hirasaki, et al. [H.4],

$$k_{rj} = k^{\circ}_{rj} (\bar{S}_j)^{n_j} \qquad (6.5)$$

where

$$\bar{S}_j = \frac{S_j - S_{jr}}{1 - \sum_{j=1}^{3} S_{jr}} \quad , \quad j=1,2,3 \qquad (6.6)$$

The exponents (n_j) were the matching parameters to fit the relative permeabilities to experimental data since the S_{jr} and the k°_{rj} were measured quantities.

The experimentally obtained relative permeabilities were matched using equation 6.5. Figure 6.3.1.13 also shows the computed curves for parameters listed in Table 6.3.1.4.

Phase relative permeabilities are also plotted versus phase saturations and flowing phase saturations ($S^f_j = S_j F_j$) obtained from the capacitance model in Figures 6.3.1.14 and 6.3.1.15. The flowing saturation is the part of the in-situ phase saturation which contributes to the permeability of the phase. The

microemulsion phase has higher relative permeabilities than those of excess oil at the same saturation. Relative permeability data show significant curvature. The microemulsion relative permeability curve is concave downward ($n_3 < 1$) as compared to that of excess brine and excess oil phases which are concave upward (n_1 and $n_2 > 1.0$). The exponent of the microemulsion relative permeability curve is less than one. This implies that it can not be estimated by interpolation from low to high capillary number [H.4, L.1]. Relative permeabilities are closer to each other when flowing saturations are used.

Total relative mobility (λ_{rT}) as a function of microemulsion saturation is shown in Figure 6.3.1.16. The total mobility decreases as more microemulsion is introduced in the core.

Fractional flow (cuts) versus phase saturations estimated from the capacitance model are shown for both phases in Figure 6.3.1.17. The fractional flow curve for oil does not show a typical behavior, but this anomaly is mainly caused by the data at the lowest non-zero oil saturation.

Dispersivities of carbon-14 in both oil and microemulsion phases and tritium in the microemulsion are plotted as a function of microemulsion saturation in

Figure 6.3.1.18. Dispersivities and saturations are the capacitance model estimates. The dispersivities of tracers in both phases show a strong decrease with increasing saturation.

Dispersion coefficients of carbon-14 in both microemulsion and oil phases and tritium in microemulsion are plotted as a function of phase velocity in Figure 6.3.1.19. The dispersion coefficient of carbon-14, partitioning tracer between two flowing phases, as a function of velocity is very erratic. But the data of tritium in microemulsion show an increase in dispersion coefficient with increasing velocity similar to that observed for single-phase flow. No conclusion can be made whether there exists a linear relationship between dispersion coefficient and velocity since

1- Each point on Figure 6.3.1.19 is at a different phase saturation and

2- Dispersivities are strong functions of phase saturation (Figure 6.3.1.18).

The concentration of both Ca^{++} and Mg^{++} in the effluent microemulsion samples were measured (by Atomic Absorption) and are plotted as a function of pore volumes in Figure 6.3.1.20. The concentration of both calcium and magnesium was on the same level as that of injected

at early times, but the Mg^{++} concentration decreased while Ca^{++} concentration increased as more fluids were introduced into the core.

Figure 6.3.1.21 shows the composition (by Gas Chromatography) of effluent microemulsion phase at steady-state. A comparison between the composition of injected and effluent microemulsion phase indicates that

- The concentration of IBA is about the same.
- The concentration of oil is consistently lower than that of the injected, and
- The concentration of water shows a lot of scatter.

The scatter in the data can be partly explained by the error involved in GC analysis. The sum of volume percent of n-decane, water, IBA (Figure 6.3.1.21) and surfactant (Table 6.1.1) do not add up to 100 but to an averaged value of 88 percent.

Experimental Difficulties

Due to the low fractional flow rate of microemulsion in experiment SMO-2 and in consequence small volume in effluent samples, the tracer analysis of microemulsion phase was not performed. The volume of microemulsion in each test tube was about 0.70 cm^3 and by the time the excess oil was completely separated from the sample the remaining microemulsion was not enough for the

tracer concentration analysis.

TABLE 6.3.1.1

Excess Oil/Microemulsion Relative Permeabilities
Material Balance Results (Steady-State)
(Experiment SMO)

Experiment Number	Phase Fractional Flow		Total Flow Rate cm^3/min	Phase Potential Drop (1) (psi/ft)		Phase Potential Drop (2) (psi/ft)		Phase Potential Drop (3) (psi/ft)		Total Pore Volumes Inj. (P.V.)	Capillary Number $N_{cj} = \frac{k\Delta\Phi_j}{L\sigma}$	
	Oil	M.E.		Oil	M.E.	Oil	M.E.	Oil	M.E.		Oil	M.E.
SMO-2	0.0	1.0	0.955	-	1.69	-	1.52	-	1.60	3.73	-	0.093
SMO-4	1.0	0.0	0.647	0.22	-	0.26	-	0.36	-	6.77	0.012	-
SMO-6	0.953	0.047	0.716	0.25	0.308	0.36	0.418	0.28	0.338	4.0	0.0137	0.0169
SMO-8	0.901	0.099	0.671	0.27	0.328	0.34	0.398	0.32	0.398	2.64	0.0148	0.0179
SMO-10	0.78	0.22	0.507	0.27	0.328	0.31	0.368	0.29	0.348	2.94	0.0148	0.0179
SMO-12	0.428	0.572	0.256	0.26	0.318	0.21	0.268	0.28	0.338	2.40	0.0142	0.0173
SMO-14	0.0	1.0	0.141	-	0.248	-	0.258	-	0.248	2.29	-	0.0136

(1) pressure drop measured across the center section of the core (1.0 foot)
(2) pressure drop measured across the inlet (0.5 foot)
(3) pressure drop measured across the outlet (0.5 foot)

Density of fluid in the line = 0.725 g/cm^3
Micellar solution batch no. 2 was used

TABLE 6.3.1.1 (continued)

Experiment Number	Phase Saturation (1)		Phase Relative Permeability (2)		Relative Mobility (cp^{-1})		
	Oil	M.E.	Oil	M.E.	Oil	M.E.	Total
SMO-2	0.0	0.883	0.0	1.0	0.0	0.224	0.224
SMO-4	0.839	0.044	0.955	0.0	1.165	0.0	0.165
SMO-6	0.768	0.115	0.890	0.194	1.08	0.043	1.123
SMO-8	0.717	0.166	0.727	0.361	0.886	0.08	0.966
SMO-10	0.644	0.239	0.476	0.606	0.580	0.135	0.715
SMO-12	0.366	0.517	0.137	0.821	0.167	0.182	0.349
SMO-14	0.108	0.775	0.0	1.02	0.0	0.226	0.226

(1) Irreducible brine saturation = 0.117 (constant)
(2) Permeabilities are normalized with permeability to 100% brine saturation or to M.E. permeability (k = 0.739 Darcy)

TABLE 6.3.1.2
Dispersion Data of Excess Oil/Microemulsion Experiments
Convection-Dispersion Results
(Experiment SMO)

Experiment Number	Phase Saturation (1) ^{14}C		Dispersivity (cm)			Total Pore Volumes Inj. (P.V.)	Phase Saturation (1) T_2O	
	Oil	M.E.	^{14}C in Oil	^{14}C in M.E.	T_2O in M.E.	(P.V.)	Oil	M.E.
SMO-2	0.0	0.883	-	0.10	0.10	1.98	0.0	0.883
SMO-4	0.840	0.043	0.10	-	-	2.12	-	-
SMO-6	0.755	0.128	0.45	0.45	-	2.17	-	-
SMO-8	0.654	0.229	3.0	3.0	1.50	8.0	0.783	0.100
SMO-10	0.603	0.280	2.9	2.9	1.03	4.5	0.640	0.243
SMO-12	0.122	0.761	13.0	13.0	0.35	3.3	0.203	0.680
SMO-14	0.033	0.850	-	0.11	0.14	1.96	0.033	0.85

(1) Irreducible brine saturation = 0.117 (constant)

TABLE 6.3.1.3
Dispersion Data of Excess Oil/Microemulsion Experiments
Capacitance Results
(Experiment SMO)

Experiment Number	Phase Saturation (1)		Phase Flowing Fraction		^{14}C Mass Transfer Coefficient (sec^{-1})	Dispersivity (cm)			Dispersion Coefficient (cm^2/sec)			Flowing Phase Velocity (cm/sec)		Tracer Recovery (%)	
	Oil	M.E.	Oil	M.E.		^{14}C in oil	^{14}C in M.E.	T_2O in M.E.	^{14}C in Oil	^{14}C in M.E.	T_2O in M.E.	Oil	M.E.	^{14}C	T_2O
SMO-2	0.0	0.883	-	1.0	0.0	-	0.10	0.10	-	0.00033	0.00033		0.0033	-	99.7
SMO-4	0.840	0.043	1.0	-	0.0	0.10	-	-	0.00024	-	-	0.0024	-	97.3	-
SMO-6	0.813	0.070	0.95	1.0	10^{-6}	0.21	0.20	-	0.00056	0.0003	-	0.0028	0.0015	-	-
SMO-8	0.783	0.10	0.90	1.0	10^{-6}	0.56	0.50	1.5	0.00126	0.0010	0.0031	0.0026	0.00205	86.0	96.3
SMO-10	0.640	0.243	0.90	1.0	10^{-6}	1.11	1.0	1.03	0.00207	0.0014	0.0015	0.0021	0.0014	92.0	92.0
SMO-12	0.203	0.680	0.8	1.0	10^{-6}	10	8.0	0.35	0.0168	0.0053	0.00023	0.0021	0.00066	97.0	94.2
SMO-14	0.033	0.850	-	1.0	0.0	-	0.11	0.14	-	0.000056	0.00007	-	0.00051	97.0	98.0

(1) Irreducible brine saturation = 0.117 (constant)

Table 6.3.1.4

Parameters for Two-Phase Relative Permeability Curves

Fluids	Phase (j)	Residual Saturation (S_{jr})	End-point Relative Permeability (k°_{rj})	Exponent (n_j)
oil/brine (high IFT)	1	0.35	0.09	1.50
	2	0.30	0.92	1.41
microemulsion/oil	1	0.117	-	-
	2	0.033	0.95	1.98
	3	0.043	1.0	0.48
microemulsion/brine	1	0.117	0.85	1.50
	2	0.033	-	-
	3	0.120	1.0	0.58

EXPERIMENT NUMBER		SMO-2
TRACER & PHASE		TRITIUM M.E.
FRACTIONAL FLOW		3:1.0
MAX. & INJ. CONC.	(DPM/CC)	17680 17680
FLOW RATE		0.955 CC/MIN.

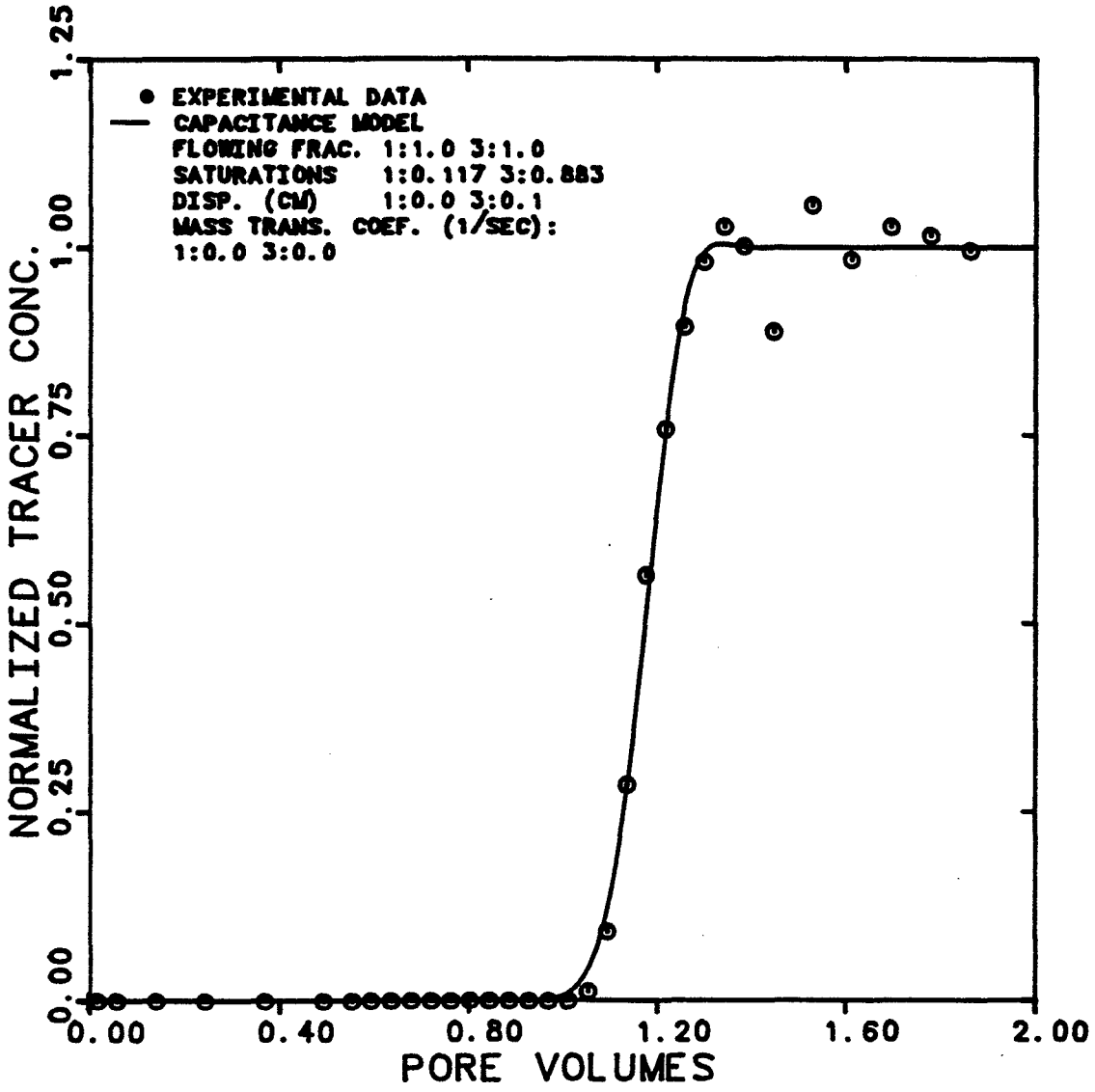

Figure 6.3.1.1 Effluent History for Tritiated Water in M.E. for Single-Phase M.E. Flow

EXPERIMENT NUMBER	SMO-2
TRACER & PHASE	CARBON-14 M.E.
FRACTIONAL FLOW	3: 1.0
MAX. & INJ. CONC.	2680 2680 DPM/CC
FLOW RATE	0.955 CC/MIN

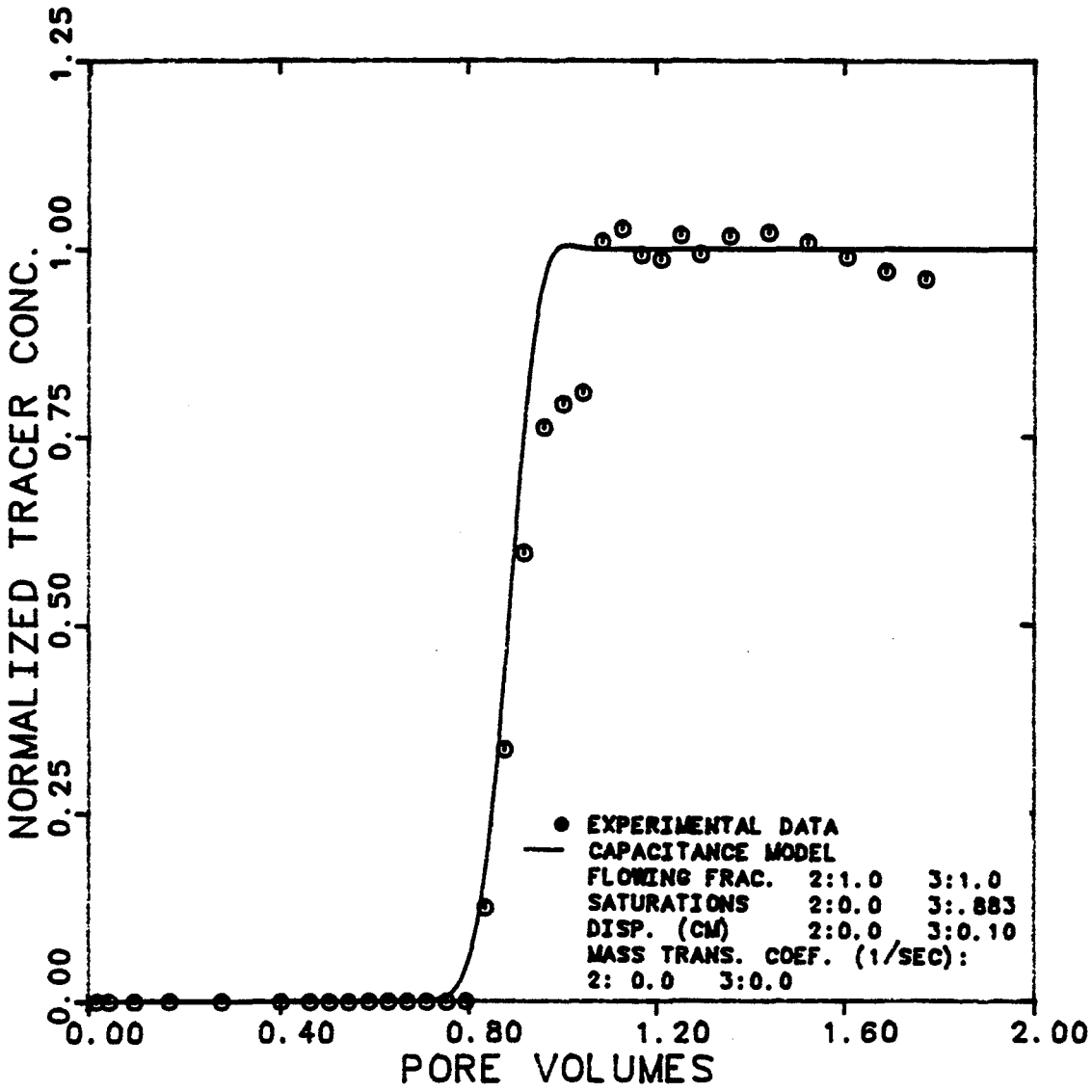

Figure 6.3.1.2 Effluent History for Carbon-14 in M.E. for Single-Phase M.E. Flow

EXPERIMENT NUMBER		SMO-4
TRACER & PHASE		CARBON-14 OIL
FRACTIONAL FLOW		2:1.0
MAX. & INJ. CONC.	(DPM/CC)	5400 5400
FLOW RATE		0.647 CC/MIN.

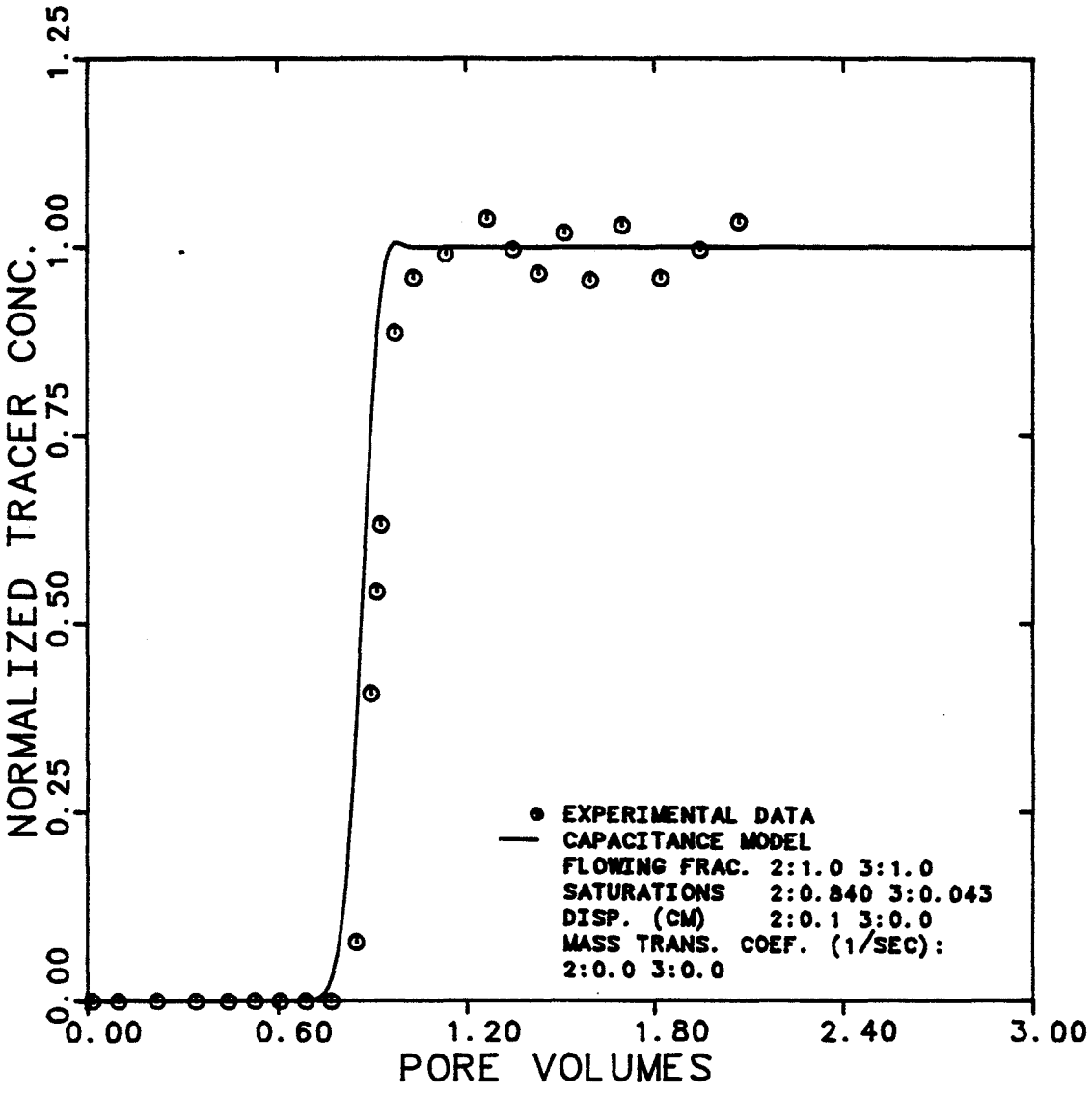

Figure 6.3.1.3 Effluent History for Carbon-14 in Oil for Single-Phase Oil Flow

EXPERIMENT NUMBER	SMO-6		
TRACER & PHASE	CARBON-14	OIL	
FRACTIONAL FLOW	2:0.953	3:0.047	
MAX. & INJ. CONC.	4600	4600	DPM/CC
FLOW RATE	0.716		CC/MIN.

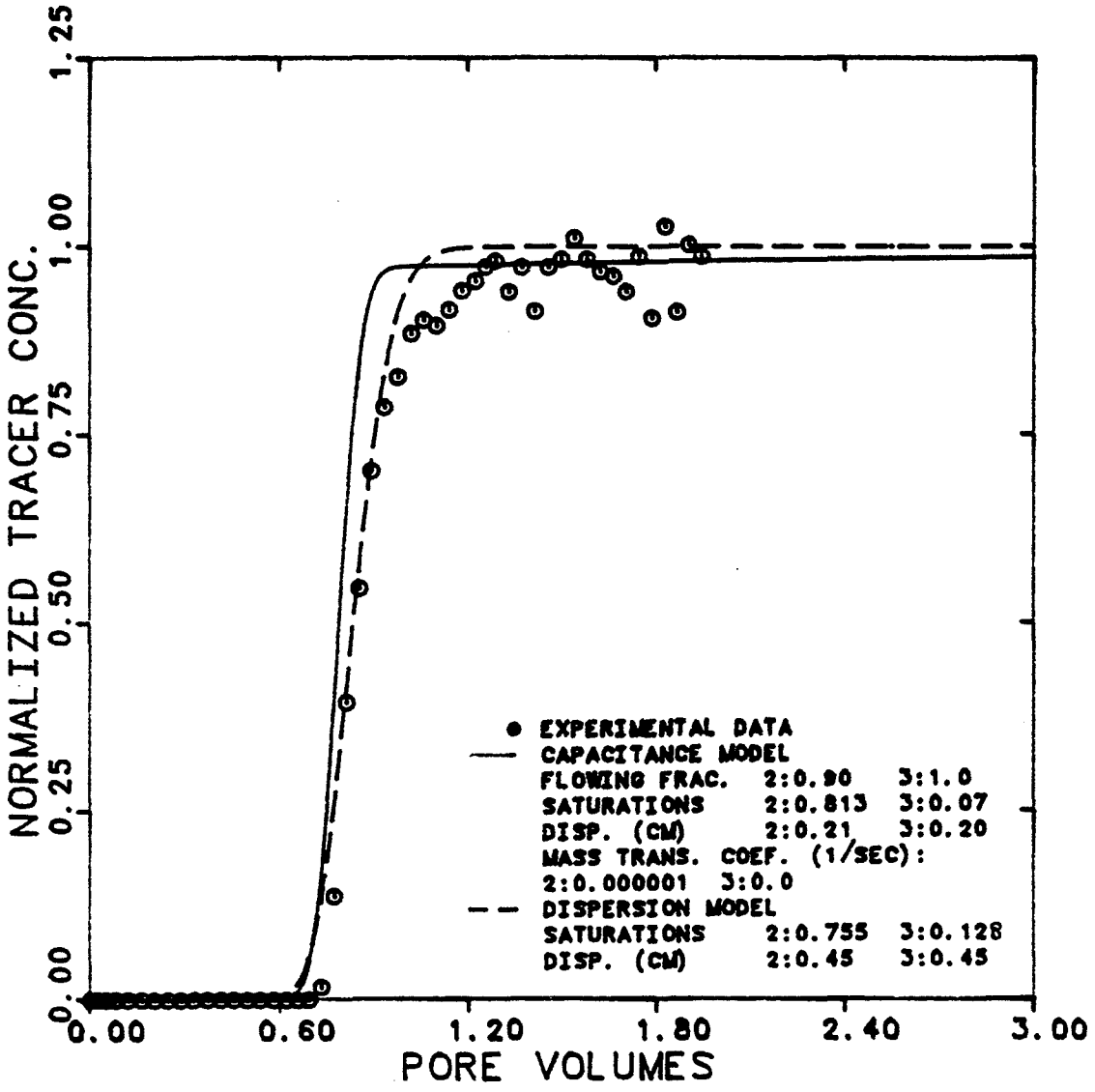

Figure 6.3.1.4 Effluent History for Carbon-14 in Oil at 95.3% Oil and 4.7% M.E. Cuts

EXPERIMENT NUMBER	SMO-8	
TRACER & PHASE	TRITIUM M.E.	
FRACTIONAL FLOW	2: 0.901 3:0.099	
MAX. & INJ. CONC.	18900 22300	DPM/CC
FLOW RATE	0.671	CC/MIN.

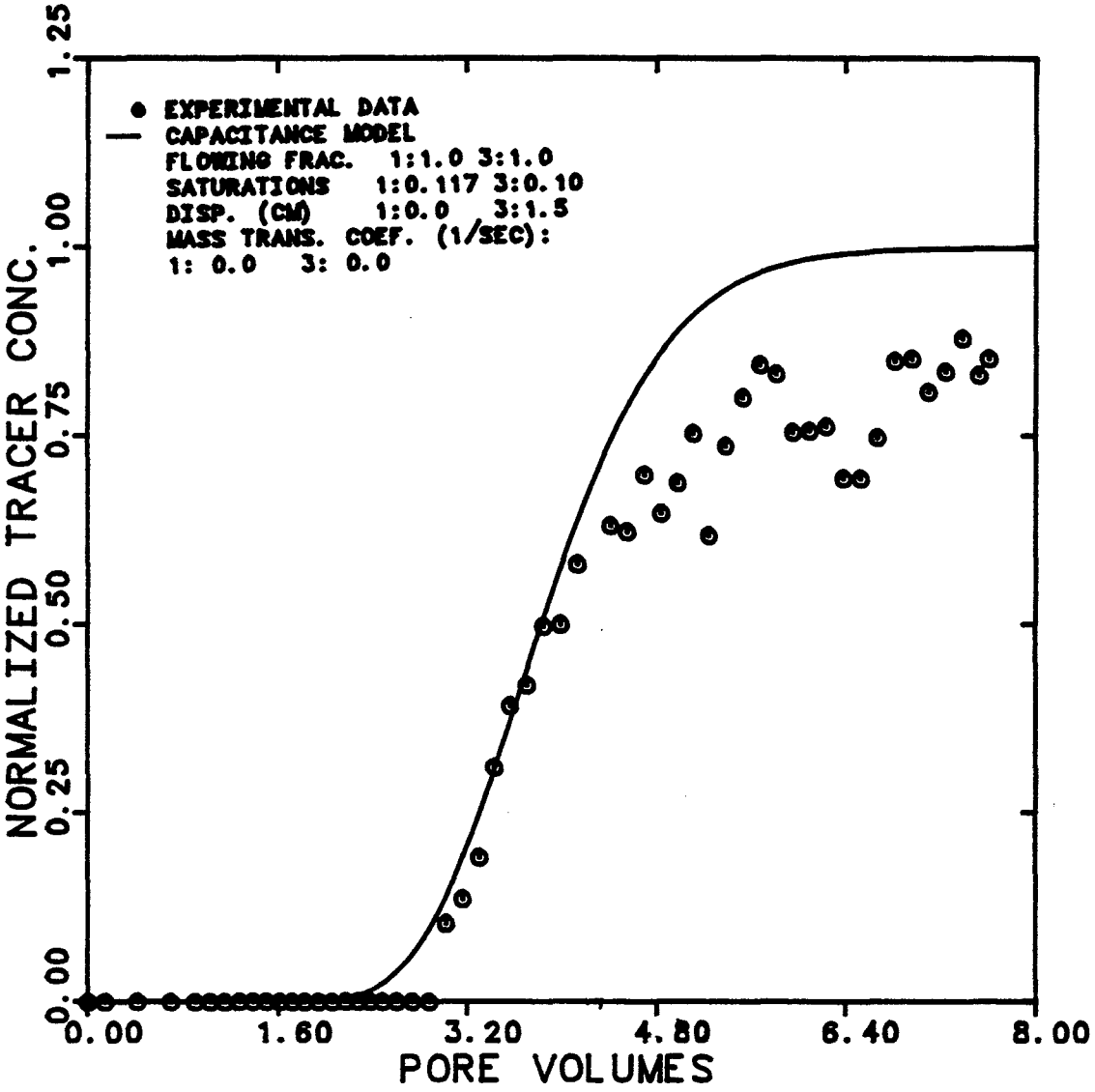

Figure 6.3.1.5 Effluent History for Tritiated Water in M.E. at 90.1% Oil and 9.9% M.E. Cuts

EXPERIMENT NUMBER	SMO-8		
TRACER & PHASES	CARBON-14		OIL&M.E.
MAX. & INJ. CONC. (OIL)	4520	4600	DPM/CC
MAX. & INJ. CONC. (M.E.)	3200	3200	DPM/CC
FLOW RATE	0.671		CC/MIN.

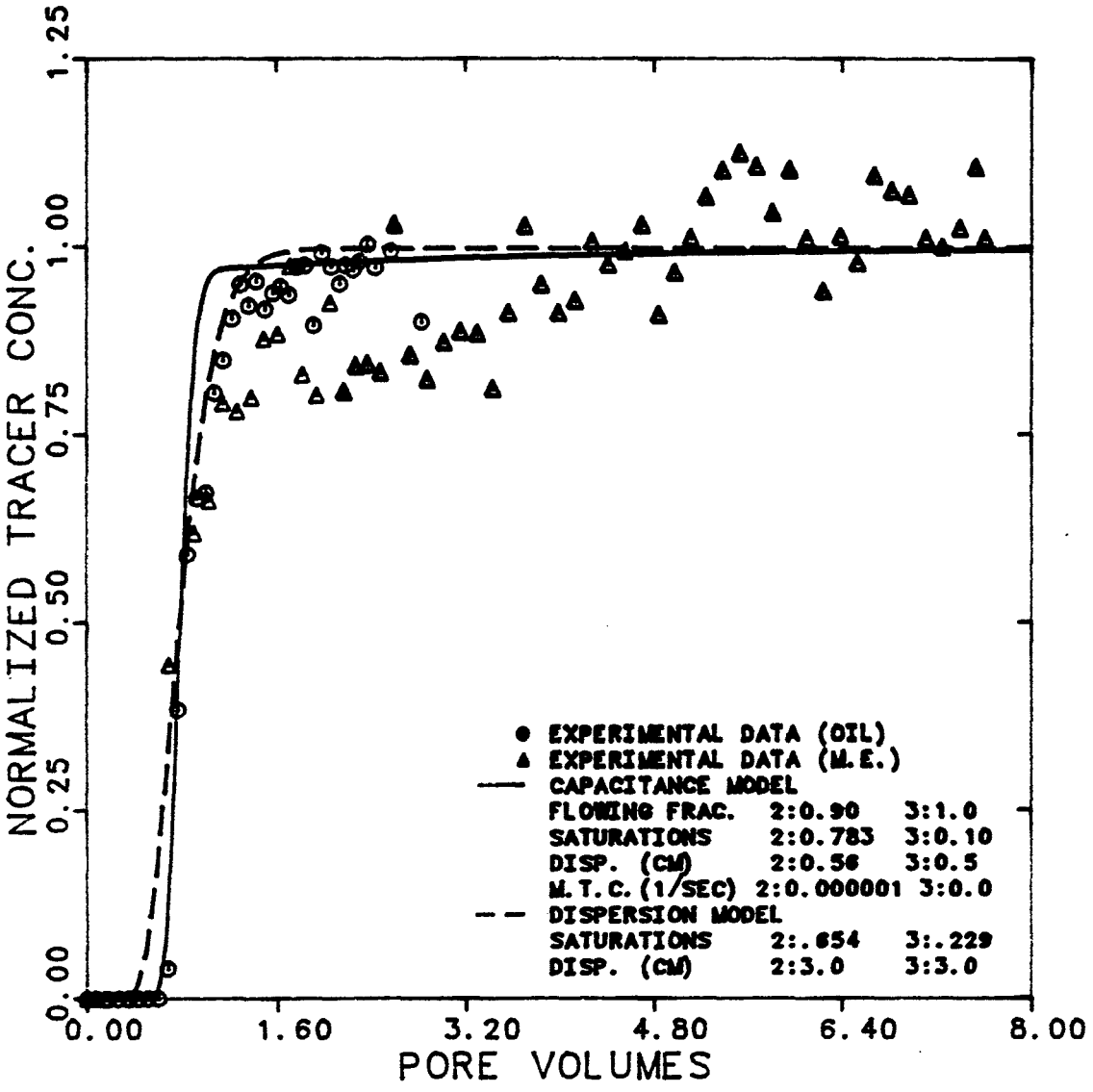

Figure 6.3.1.6 Effluent Histories for Carbon-14 in Oil and M.E. at 90.1% Oil and 9.9% M.E. Cuts

EXPERIMENT NUMBER	SMO-10	
TRACER & PHASE	TRITIUM M.E.	
FRACTIONAL FLOW	2: 0.78 3: 0.22	
MAX. & INJ. CONC.	15400 16800	DPM/CC
FLOW RATE	0.507	CC/MIN.

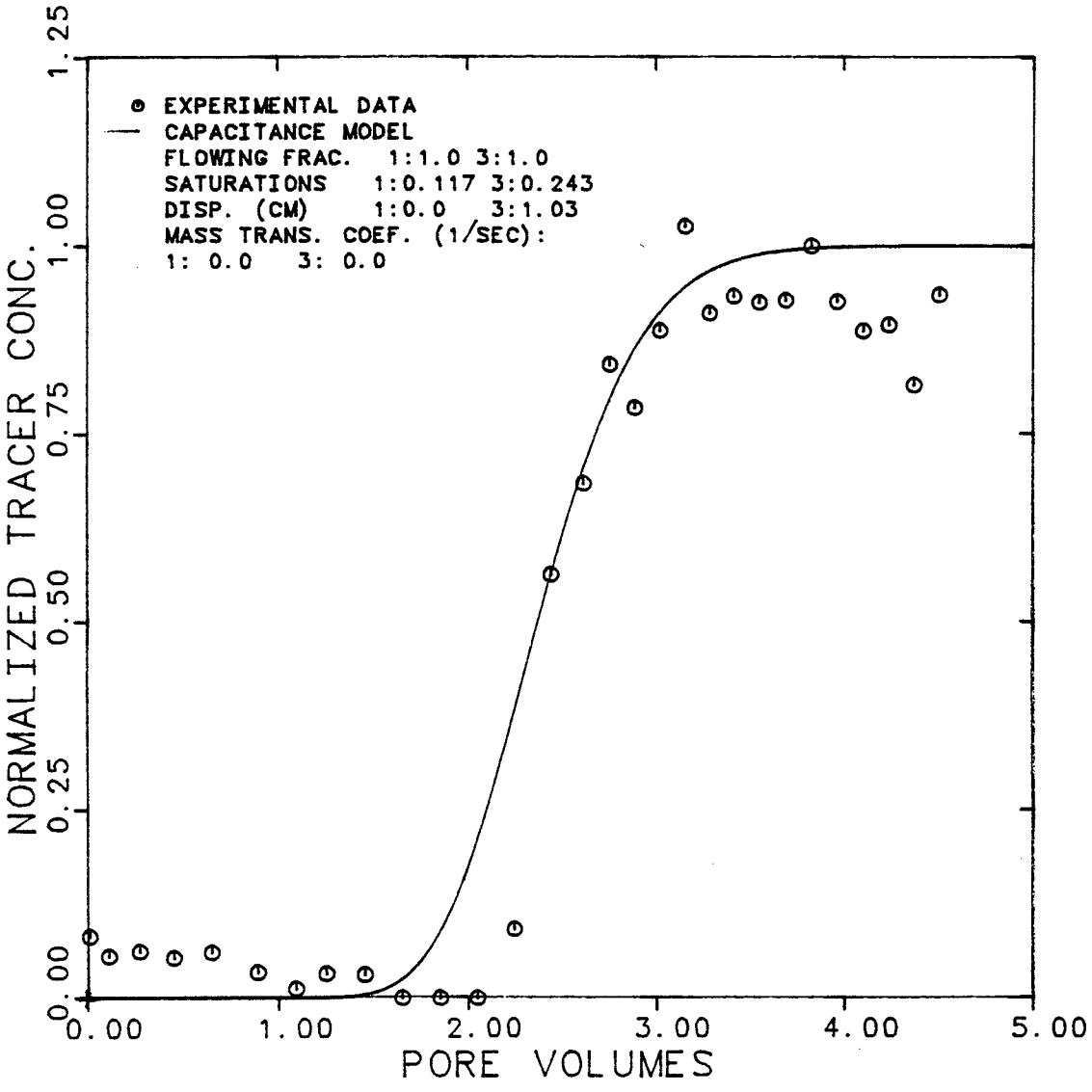

Figure 6.3.1.7 Effluent History for Tritiated Water in M.E. at 78% Oil and 22% M.E. Cuts

EXPERIMENT NUMBER	SMO-10		
TRACER & PHASES	CARBON-14		OIL&M.E.
MAX. & INJ. CONC. (OIL)	8480	8800	DPM/CC
MAX. & INJ. CONC. (M.E.)	2800	2900	DPM/CC
FLOW RATE	0.507		CC/MIN.

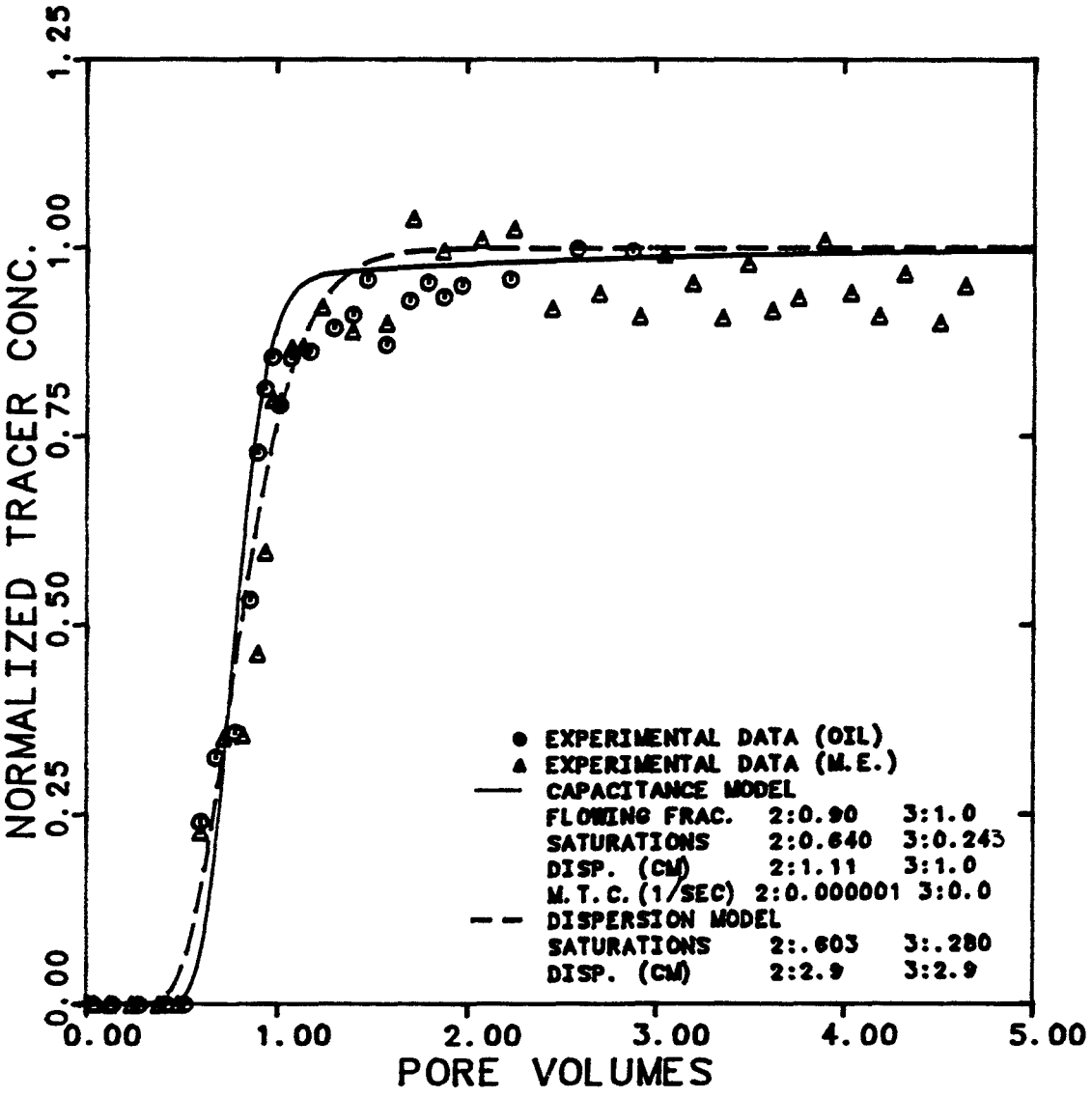

Figure 6.3.1.8 Effluent Histories for Carbon-14 in Oil and M.E. at 78% Oil and 22% M.E. Cuts

EXPERIMENT NUMBER	SMO-12	
TRACER & PHASE	TRITIUM M.E.	
FRACTIONAL FLOW	2:0.428 3:0.572	
MAX. & INJ. CONC.	19400 20400	DPM/CC
FLOW RATE	0.256	CC/MIN.

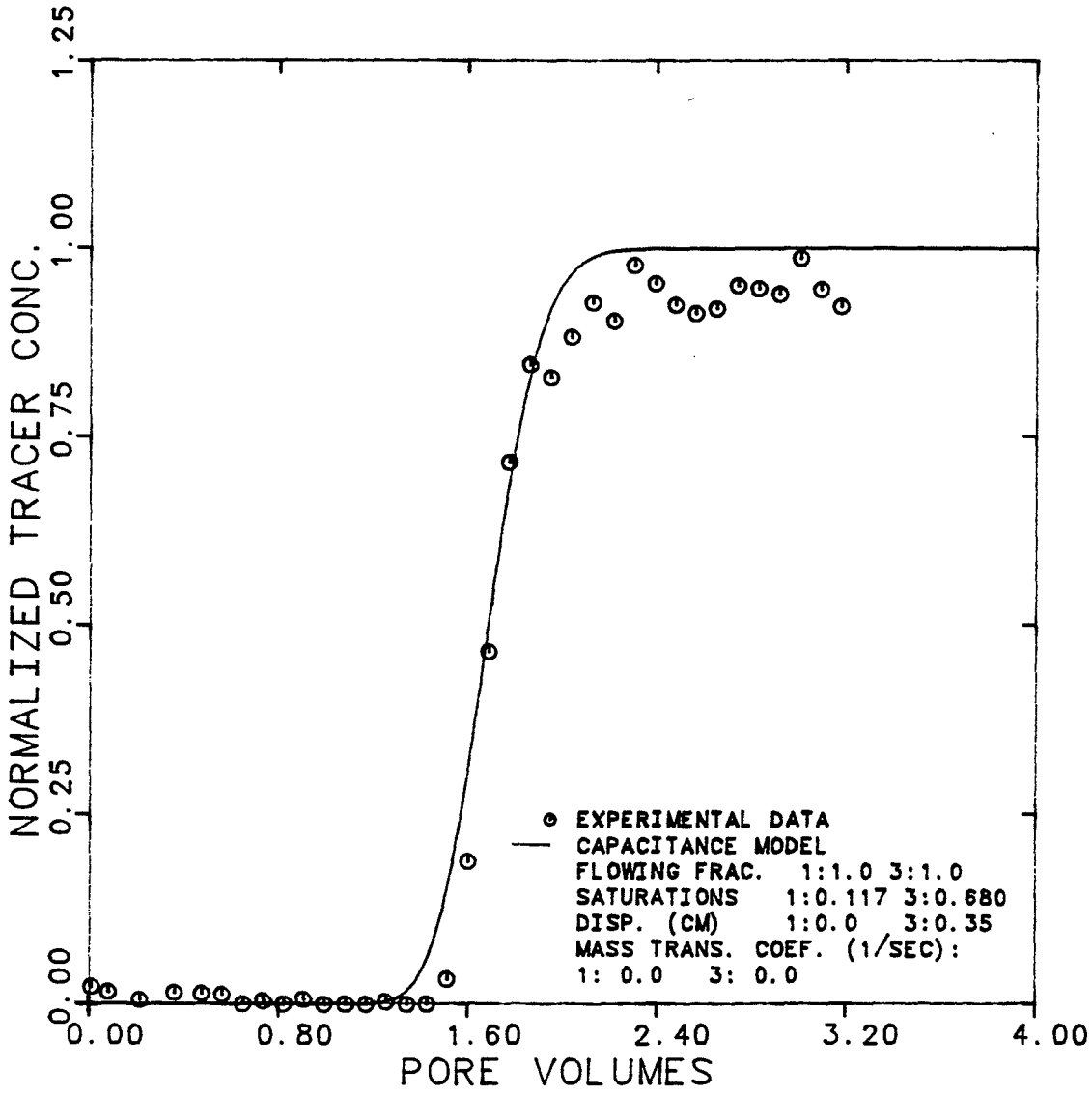

Figure 6.3.1.9 Effluent History for Tritiated Water in M.E. at 42.8% Oil and 57.2% M.E. Cuts

EXPERIMENT NUMBER	SMO-12		
TRACER & PHASES	CARBON-14		OIL&M.E.
MAX. & INJ. CONC. (OIL)	4640	4640	DPM/CC
MAX. & INJ. CONC. (M.E.)	2640	2640	DPM/CC
FLOW RATE	0.250		CC/MIN.

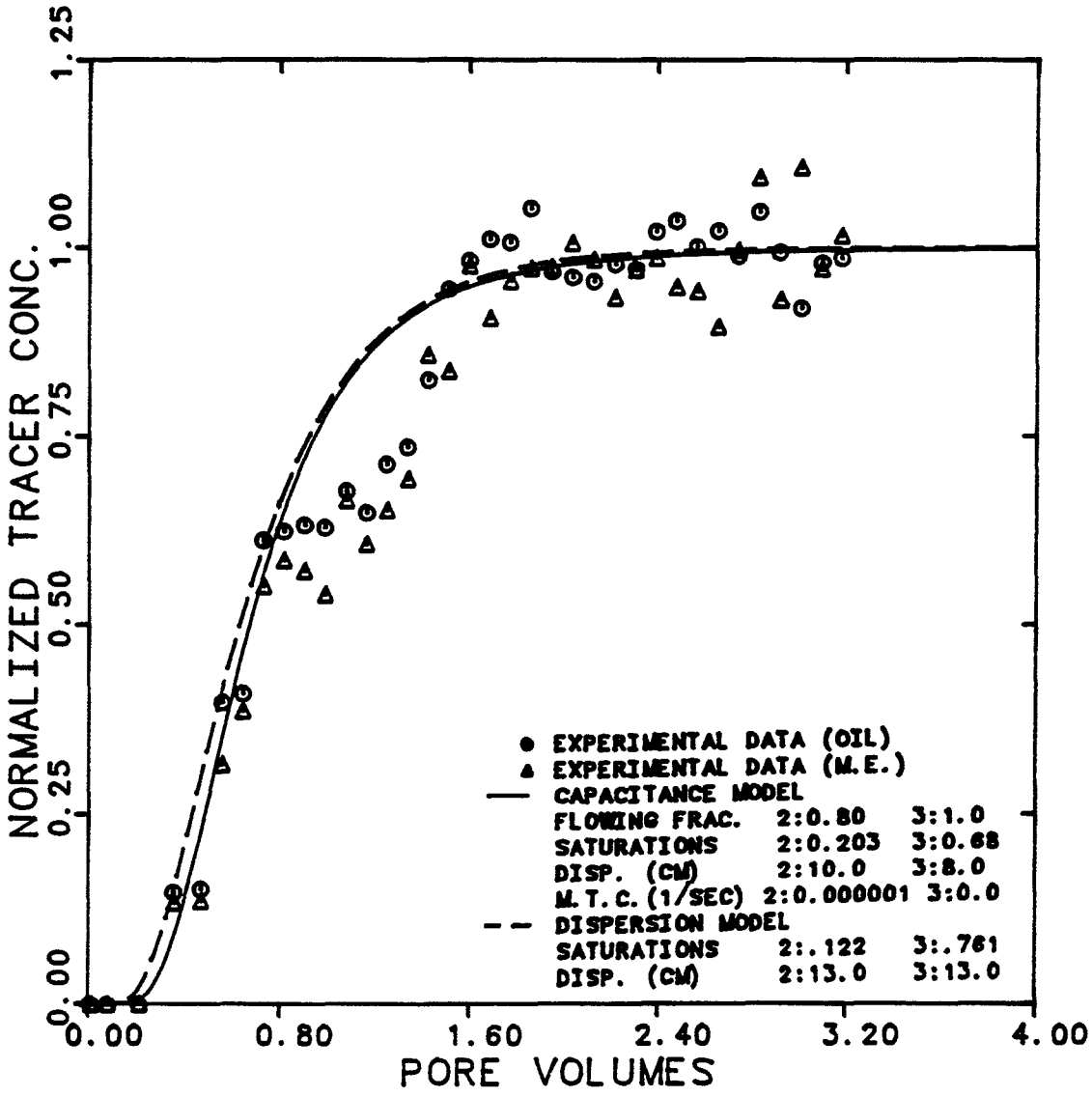

Figure 6.3.1.10 Effluent Histories for Carbon-14 in Oil and M.E. at 42.8% Oil and 57.2% M.E. Cuts

EXPERIMENT NUMBER		SMO-14
TRACER & PHASE		TRITIUM M.E.
FRACTIONAL FLOW		3:1.0
MAX. & INJ. CONC.	(DPM/CC)	18400 18400
FLOW RATE		0.15 CC/MIN.

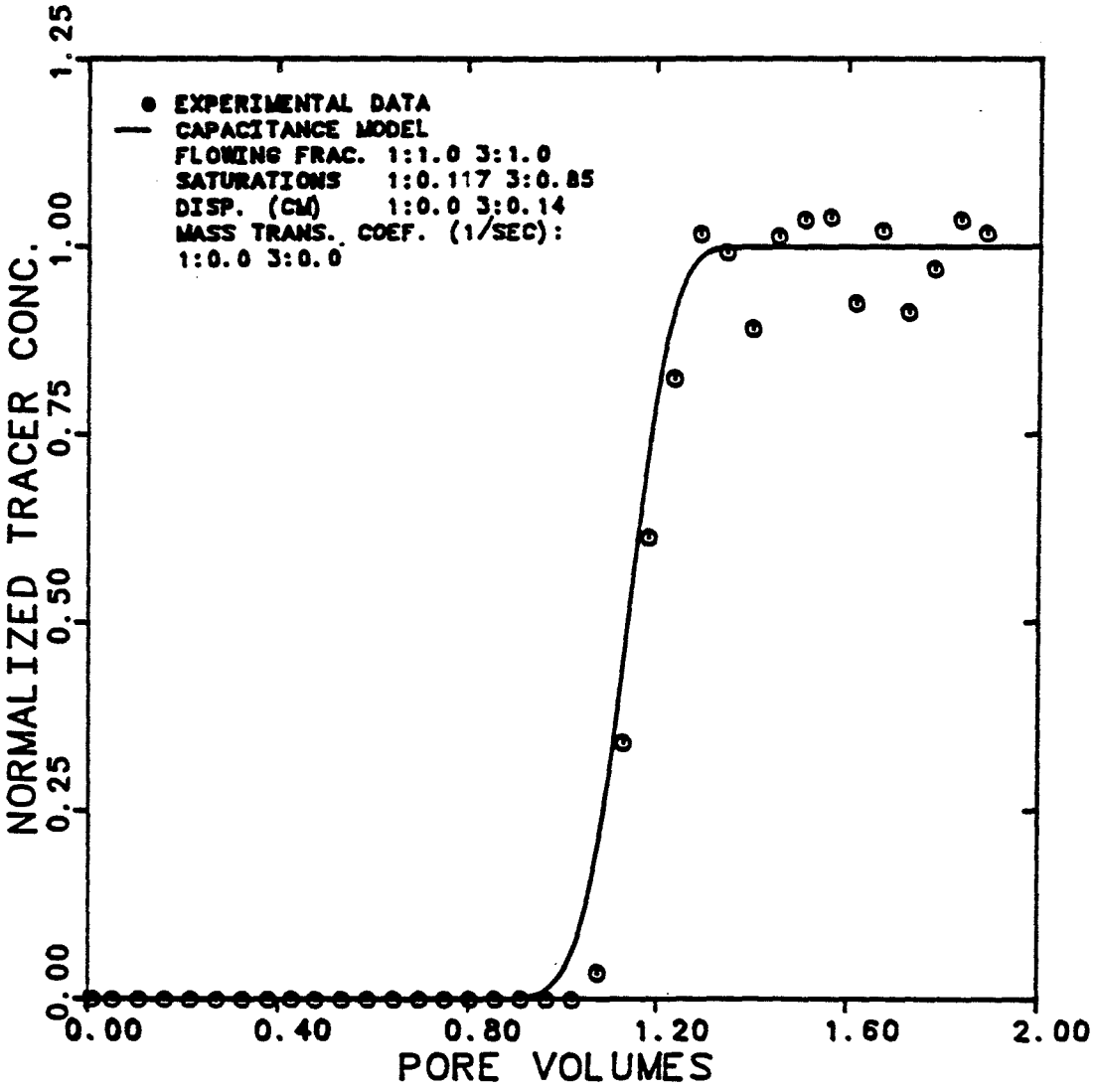

Figure 6.3.1.11 Effluent History for Tritiated Water in M.E. for Single-Phase M.E. Flow

EXPERIMENT NUMBER		SMO-14
TRACER & PHASE		CARBON-14 M.E.
FRACTIONAL FLOW		3:1.0
MAX. & INJ. CONC.	(DPM/CC)	2812 2812
FLOW RATE		0.15 CC/MIN.

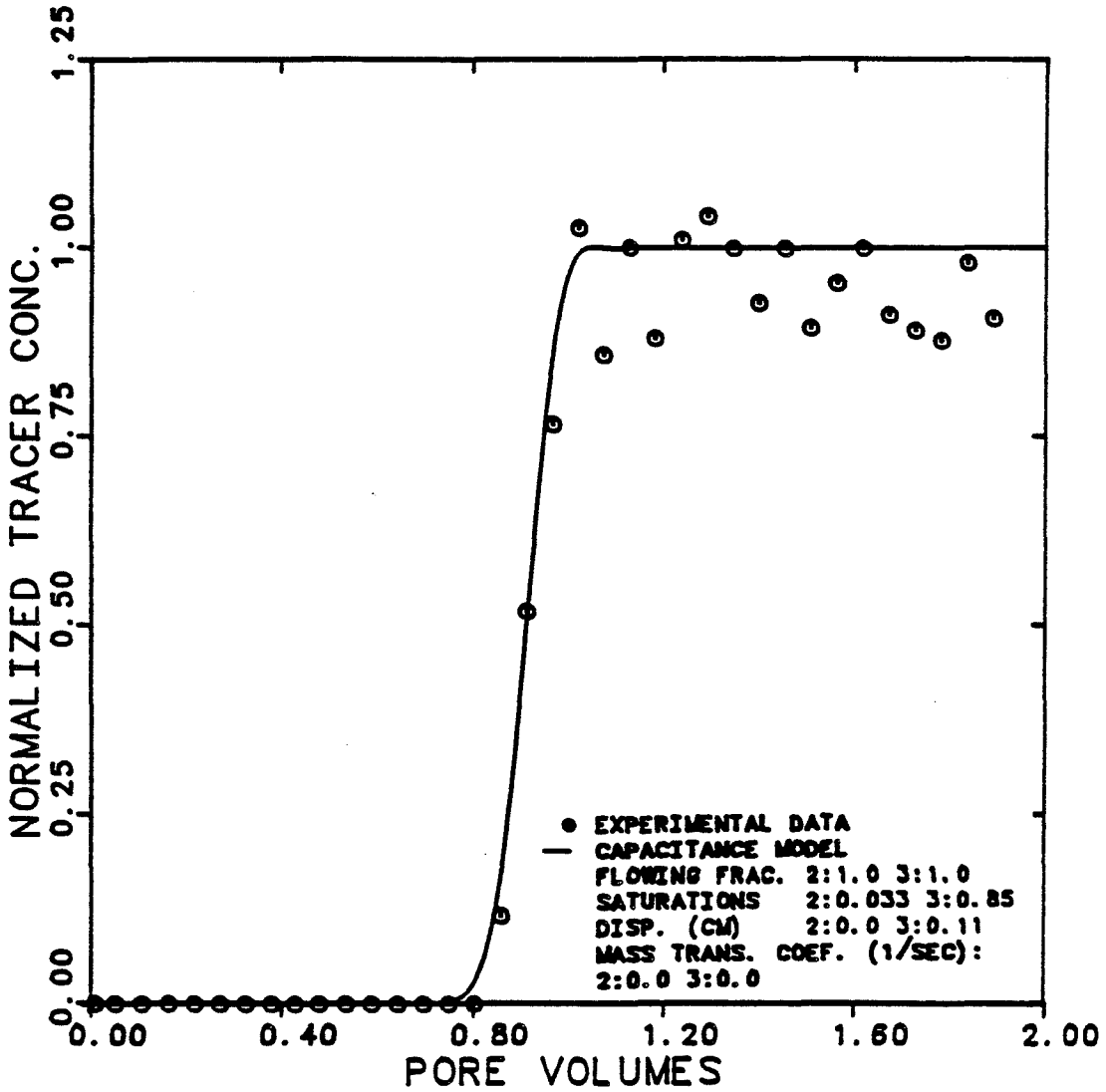

Figure 6.3.1.12 Effluent History for Carbon-14 in M.E. for Single-Phase M.E. Flow

EXPERIMENT NUMBER	SMO
CAPILLARY NUMBER	0.01
TEMPERATURE	30° C
RESIDUAL BRINE	0.117

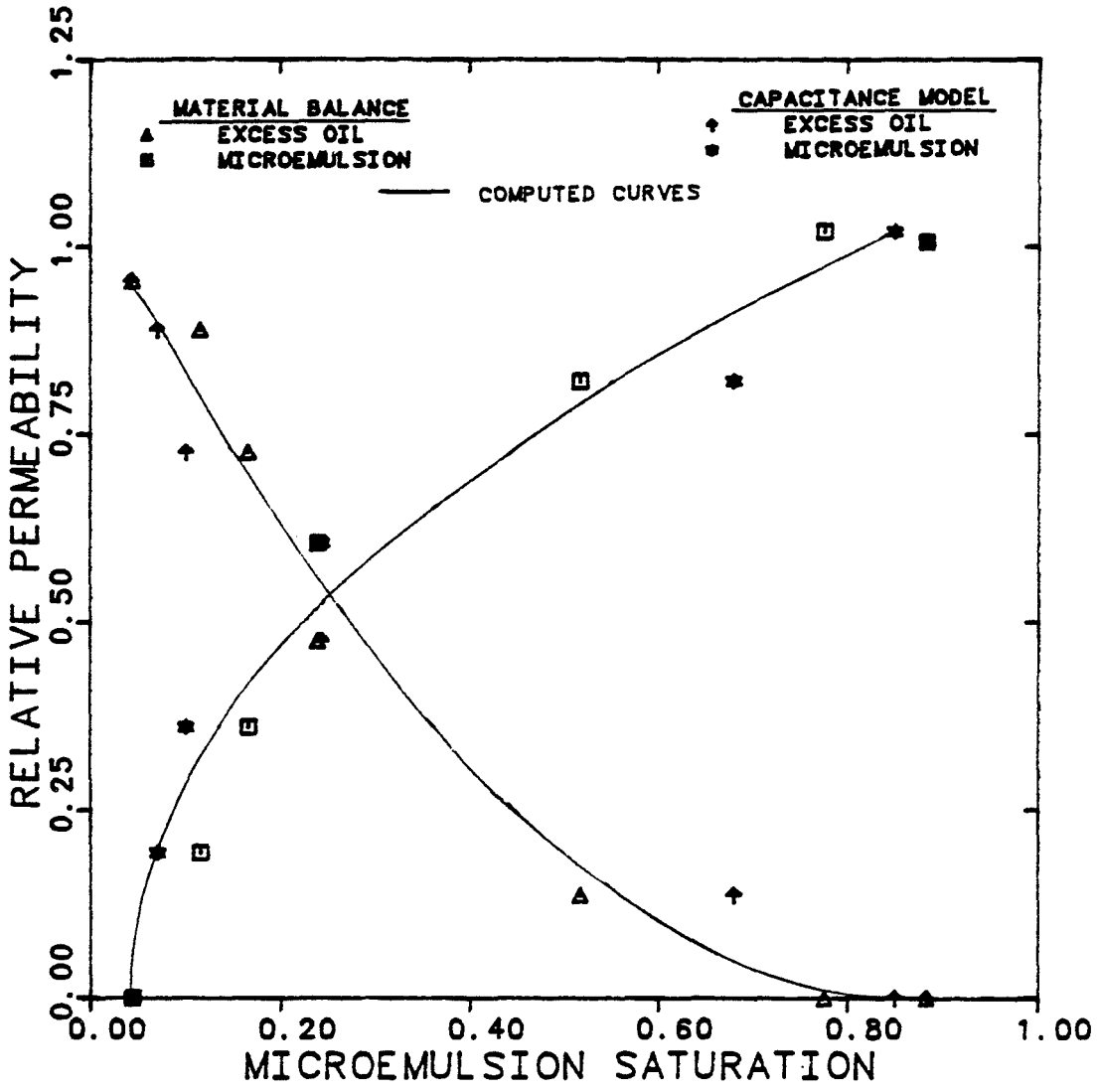

Figure 6.3.1.13 Computed and Experimental Oil/M.E. Relative Permeabilities as a Function of M.E. Saturation

EXPERIMENT NUMBER	SMO
CAPILLARY NUMBER	0.01
TEMPERATURE	30° C
RESIDUAL BRINE	0.117

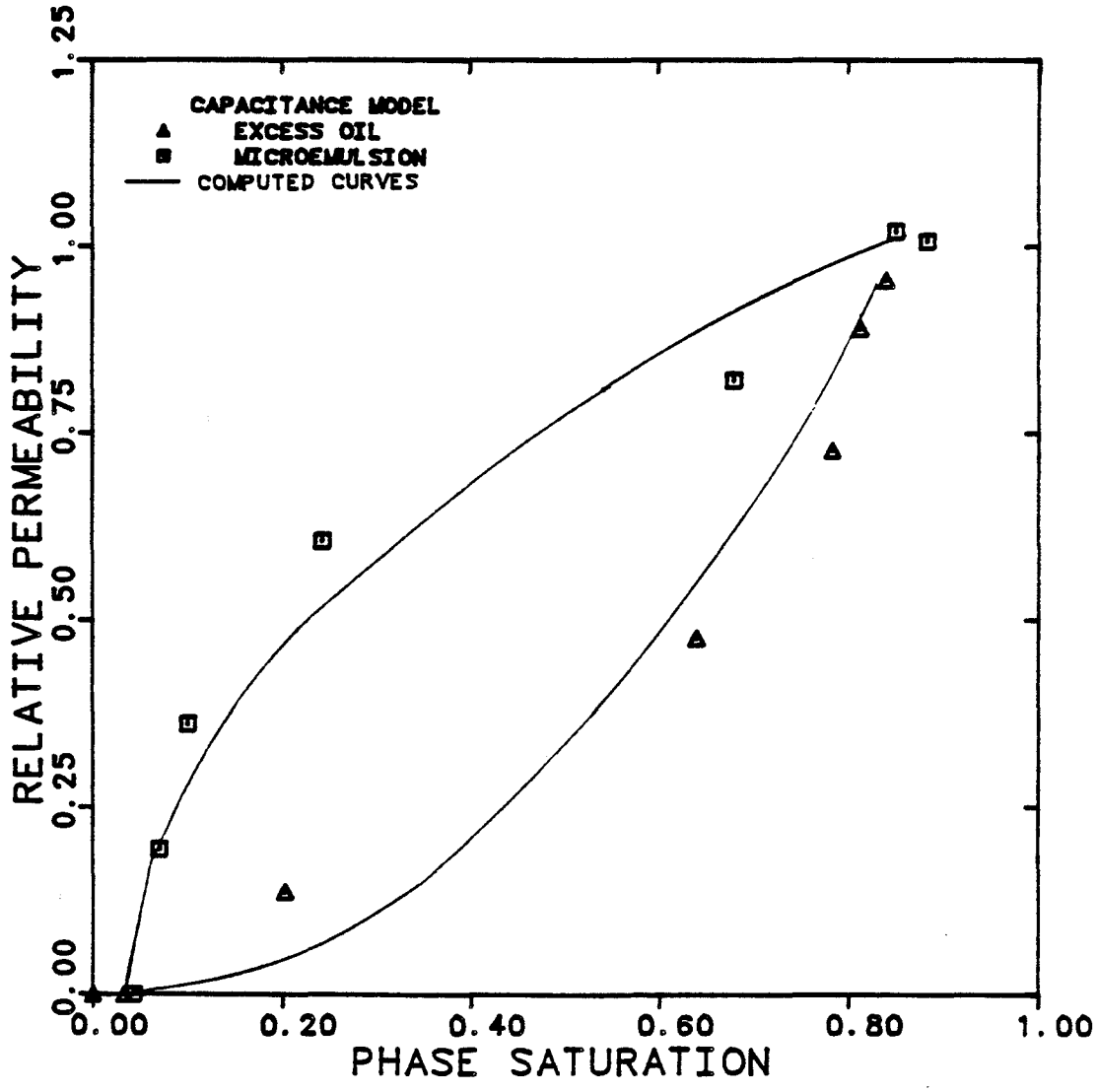

Figure 6.3.1.14 Oil/M.E. Relative Permeabilities as a Function of Phase Saturation Estimated by the Capacitance Model

EXPERIMENT NUMBER	SMO
CAPILLARY NUMBER	0.01
TEMPERATURE	30° C
RESIDUAL BRINE	0.117

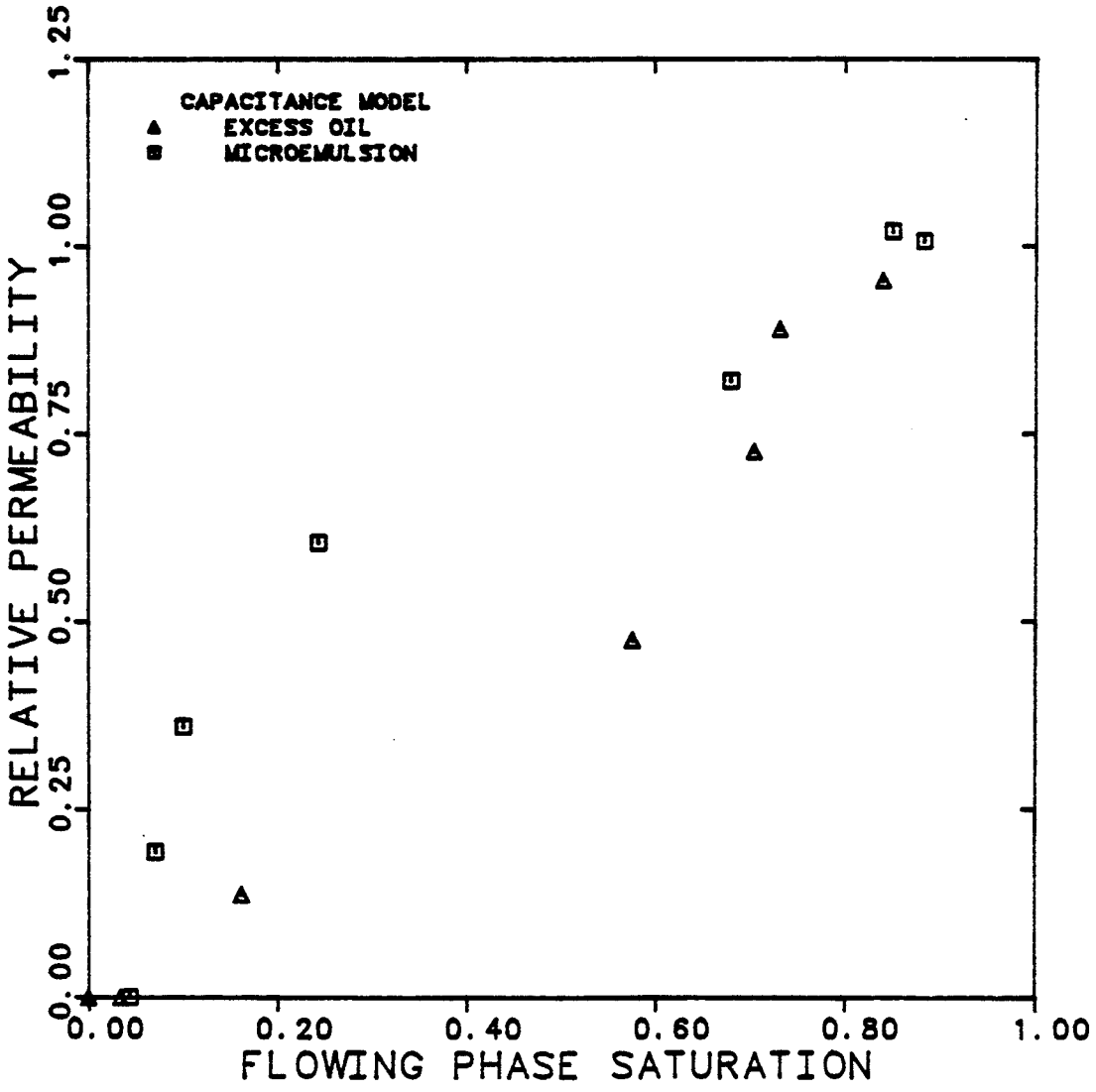

Figure 6.3.1.15 Oil/M.E. Relative Permeabilities as a Function of Flowing Phase Saturations

EXPERIMENT NUMBER	SMO
CAPILLARY NUMBER	0.01
TEMPERATURE	30°C
RESIDUAL BRINE	0.117

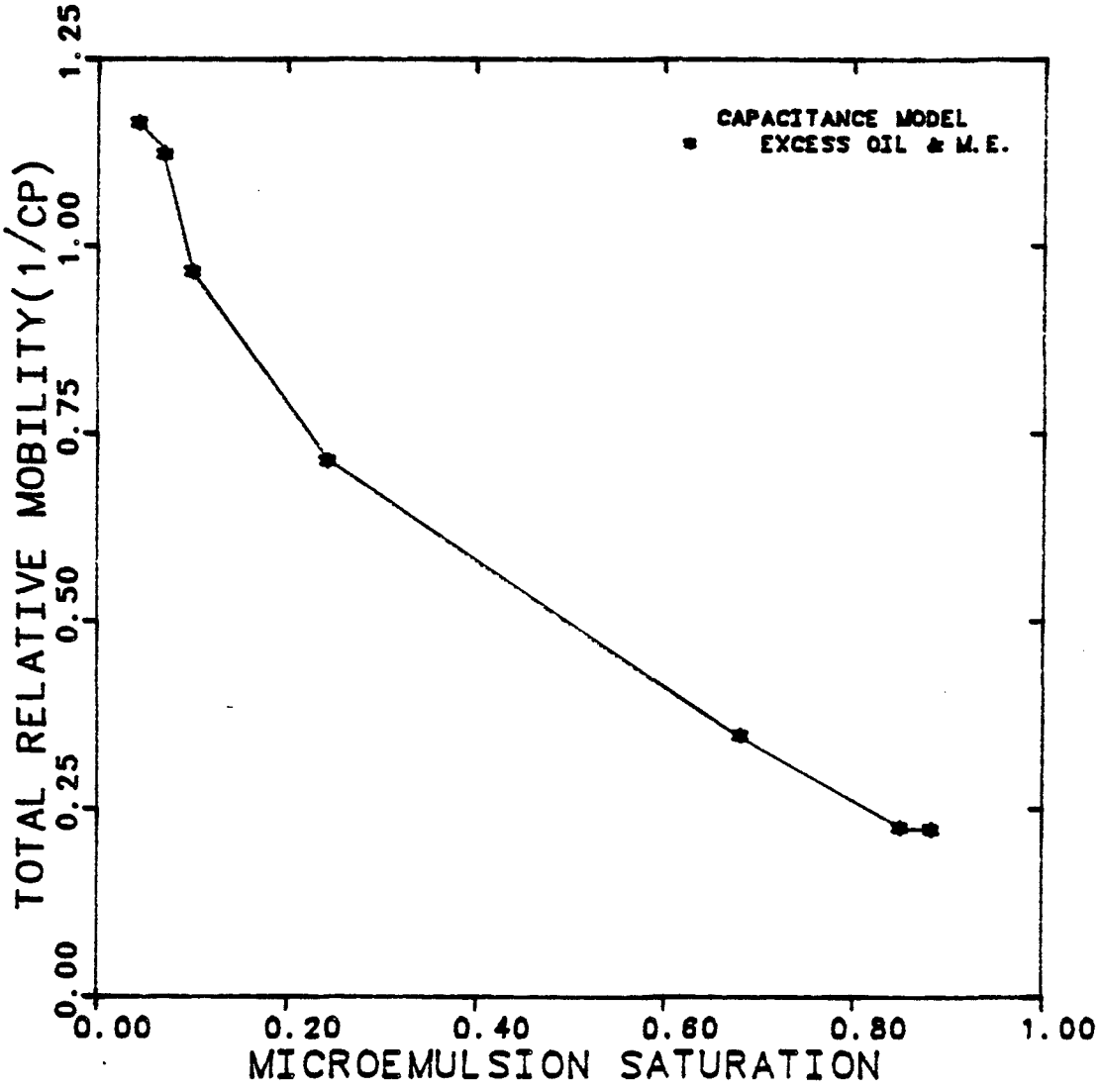

Figure 6.3.1.16 Total Relative Mobility Curve for Two-Phase Oil/M.E. Flow Experiment

EXPERIMENT NUMBER	SMO
CAPILLARY NUMBER	0.01
TEMPERATURE	30°C
RESIDUAL BRINE	0.117

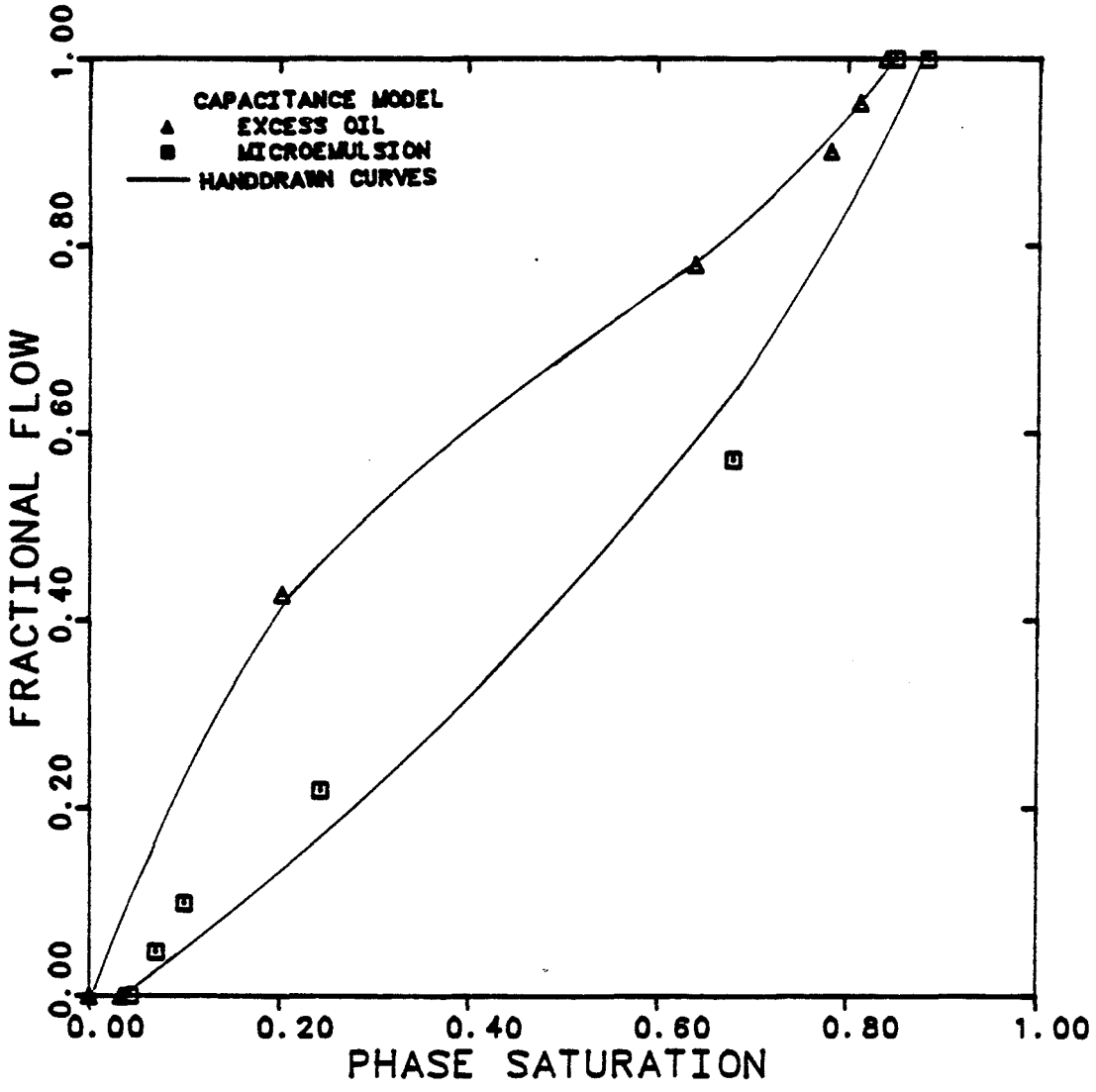

Figure 6.3.1.17 Fractional Flow Curves for M.E. and Oil Phases

EXPERIMENT NUMBER	SMO
CAPILLARY NUMBER	0.01
TEMPERATURE	30°C
RESIDUAL BRINE	0.117

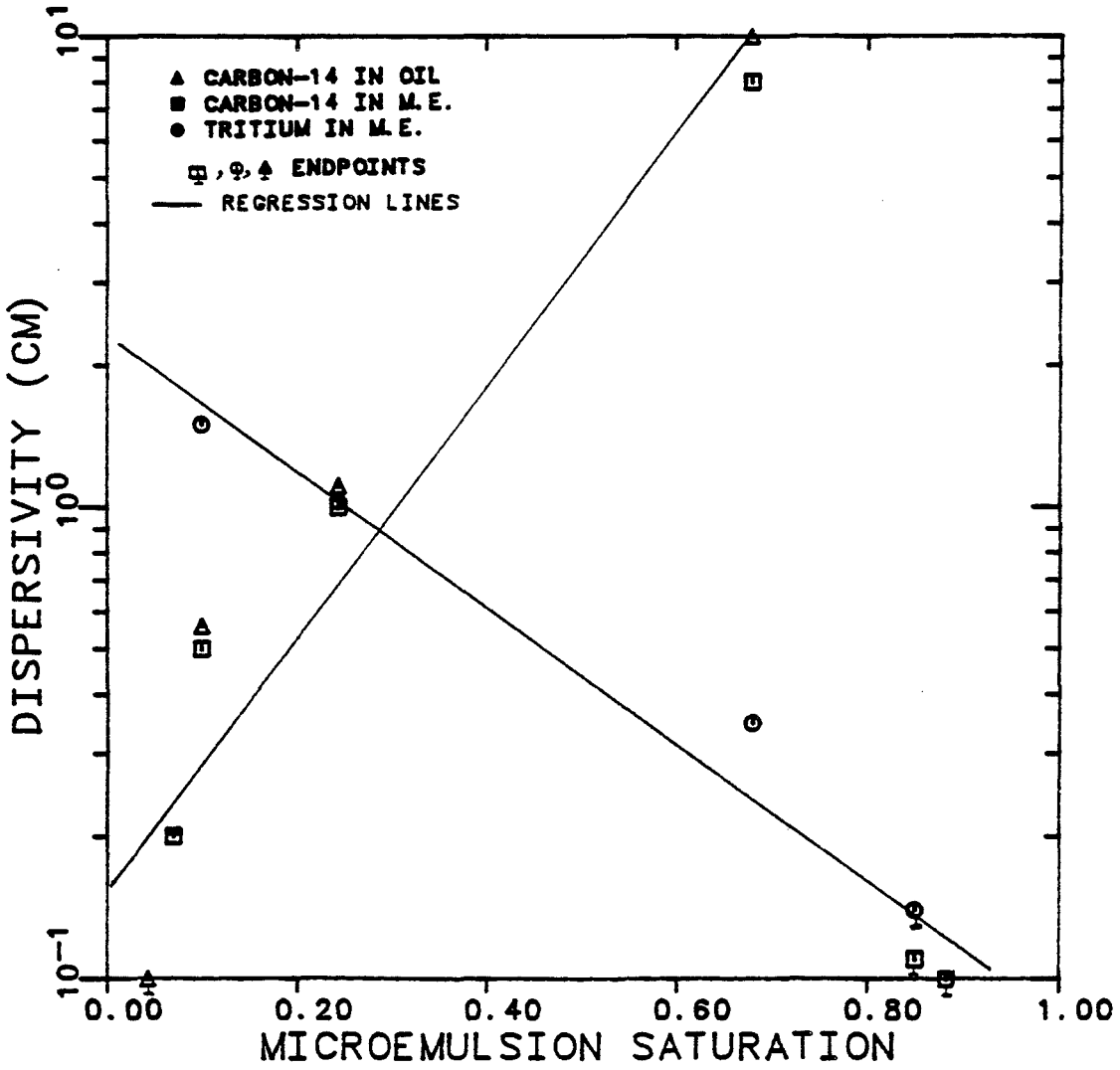

Figure 6.3.1.18 Dispersivity of Tracers in Oil and M.E. Phases as a Function of M.E. Saturation

EXPERIMENT NUMBER	SMO
CAPILLARY NUMBER	0.01
TEMPERATURE	30° C
RESIDUAL BRINE	0.117

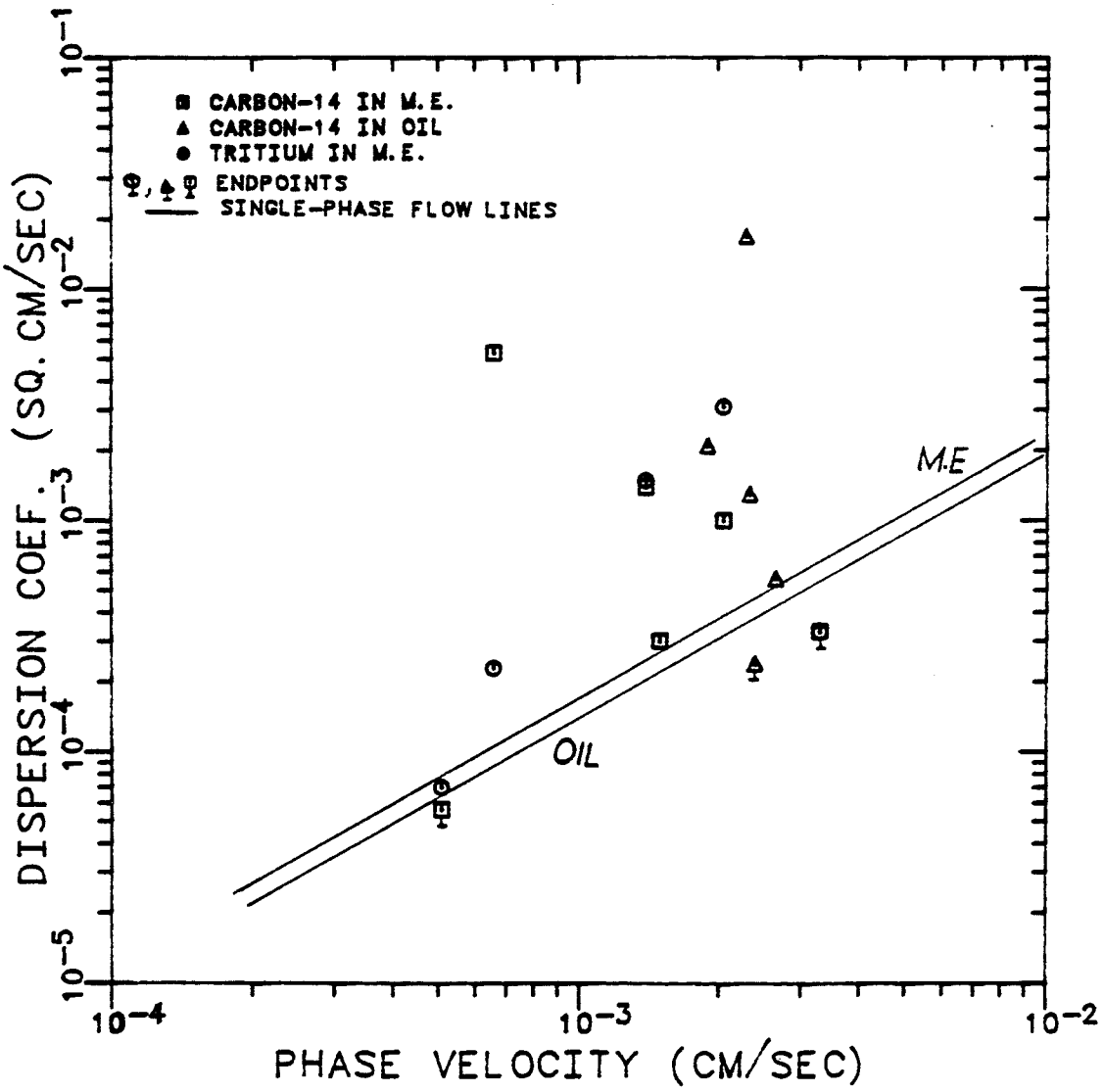

Figure 6.3.1.19 Dispersion Coefficient of Tracers in Oil and M.E. During Two-Phase Flow Versus Phase Velocity

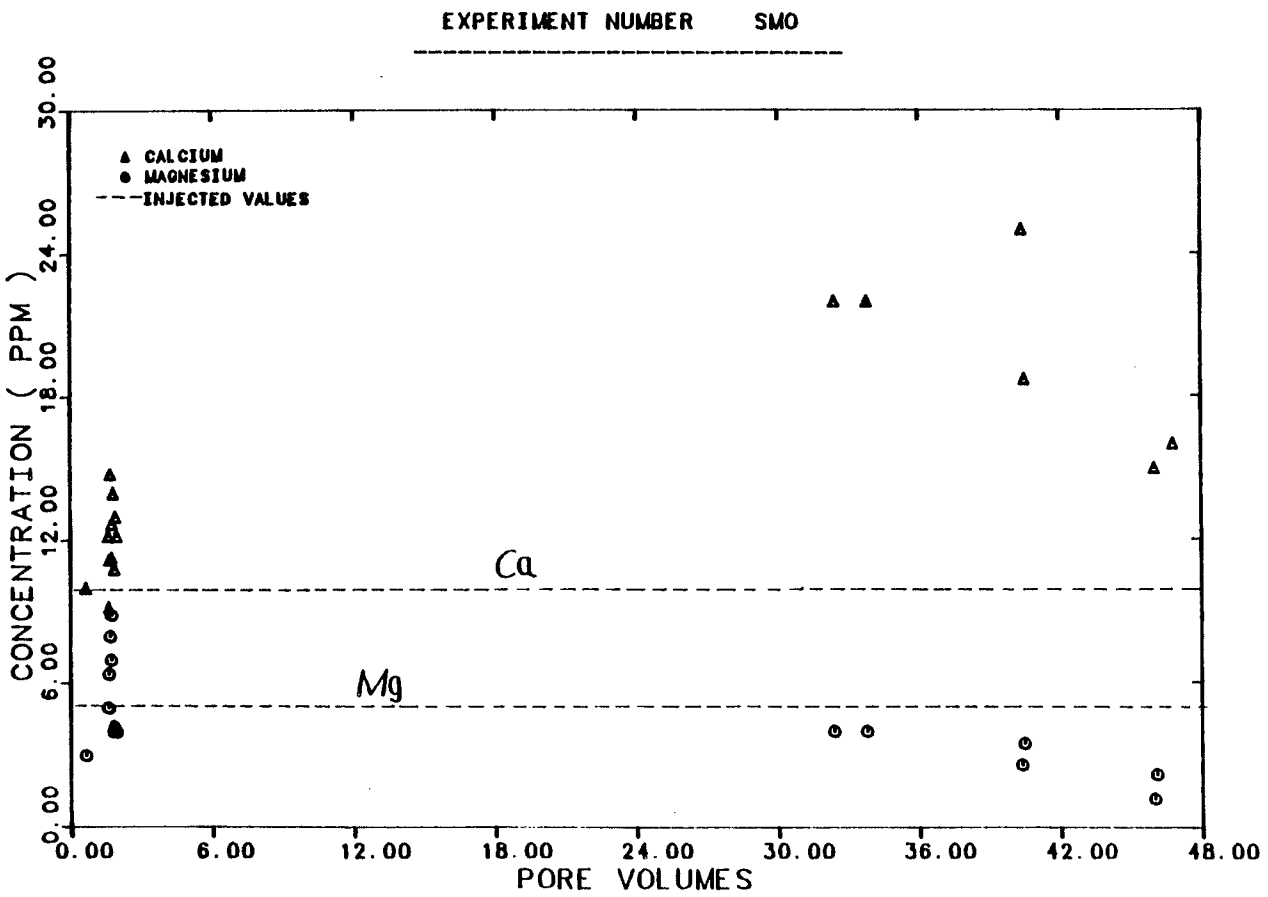

Figure 6.3.1.20 Concentration of Calcium and Magnesium in Effluent M.E. as a Function of Pore Volumes Injected

COMPOSITION OF INJECTED MICROEMULSION

WATER	40.7 VOL.%
N-DECANE	55.5 VOL.%
IBA	1.81 VOL.%
TRS 10-410	3.2 VOL.%

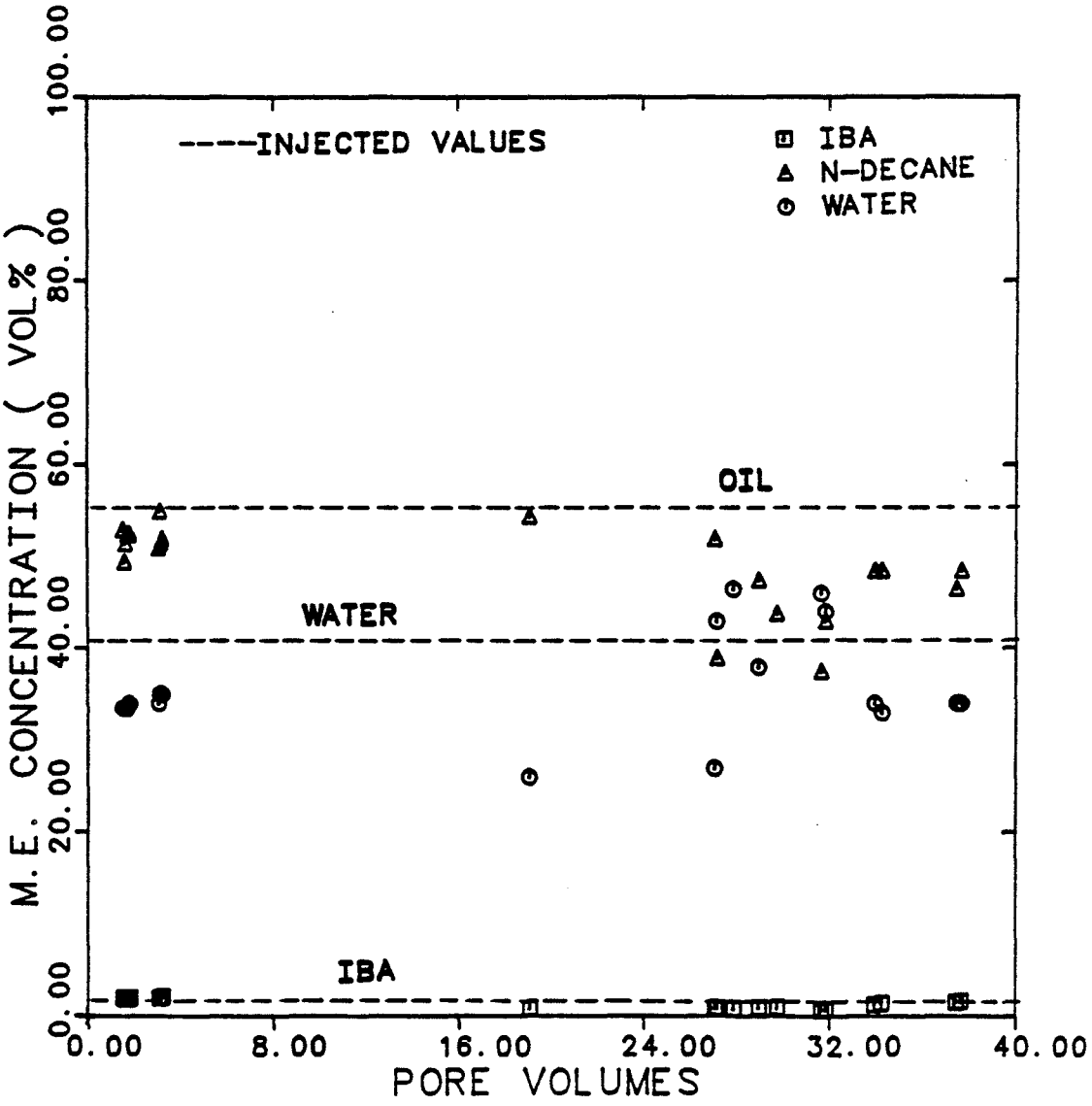

Figure 6.3.1.21 Composition of Effluent M.E. as a Function of Pore Volumes Injected

6.3.2 Microemulsion/Excess Brine (Exp. No. SMW)

The objective of this experiment was to measure the relative permeability and dispersion for middle-phase microemulsion and lower-phase brine at a constant nominal capillary number of 10^{-2}. A numerical example of how the fractional flow (cuts) and the total flow rates were planned is given in Appendix D.

The same core, micellar solution (stock 2), and apparatus were used as in previous experiment (see Tables 6.2.1, 6.1.1, and Figure 5.1.8). The tracers used in this experiment were carbon-14 and tritium in microemulsion, and tritium in the brine phase.

The procedure for the experiment was to

- Flood the core, which is at the known saturations of $S_{1r} = 0.117$, $S_{2r} = 0.033$, $S_3 = 0.849$, with 22.5% brine and 77.5% microemulsion to steady-state.

- Flood the core with labelled microemulsion and brine at the same cut and flow rate.

- Inject 67.5% and 83.4% brine cuts. At each cut, after reaching the steady-state, inject a 15.6% pore volume slug of tracers.

- Inject 93.3% brine cut to steady-state followed by continuous injection of labelled brine and microemulsion at steady-state.

There were three tasks involved in running a slug type experiment: the establishment of steady-state at the specific cut; the injection of a certain size (15.6% P.V.'s) of radioactive tracers in both phases; and finally, displacement of the slug with the same fluids (without tracers) at the same cut and flow rate.

For continuous injection of tracers in two-phase flow, at some of the cuts the concentration increases rapidly to a 50% concentration, after which the effluent concentration rises only slowly to that of the injected fluid. Thus, it was thought that the slug type run might decrease the time required and the quantity of fluid injected to perform the dispersion run. As discussed later, the slug concentration profiles have long tails. Therefore, it takes nearly as long to produce the entire slug as the complete profile using continuous injection. The advantage of this type of run is found to be that the concentration histories for tracers are readily distinguishable from each other.

In this experiment, because of a constant residual oil ($S_{2r} = 0.033$), both tracers are partitioning. The values of partition coefficients were 0.407 and 0.555 for tritium and carbon-14, respectively.

The calculated saturations (material balance),

relative permeabilities, relative mobilities, capillary number, total fluids injected to reach steady-state, and the potential drop across all the three sections of the core are tabulated in Table 6.3.2.1. The potential drop measured across the middle section was used for calculation to avoid end-effects. The values of potential drop across the inlet and outlet are higher than those for the middle section by maximum of 22%.

Figures 6.3.2.1 through 6.3.2.8 show the normalized tracer concentration versus injected pore volumes. Breakthrough curve were first compared with the solution of the C-D equation (Equation 3.14 for continuous and 3.19 for slug injection) for saturation determination. The sum of saturations obtained was less than one. The microemulsion saturation estimate from matching of carbon-14 breakthrough curve against the C-D equation was in good agreement with the material balance. The saturation of excess brine estimated from the C-D equation was thought to be low in comparison with the material balance estimate because of capacitance (non-equilibrium) effect. The tritium breakthrough curves of both brine and microemulsion phases were then compared with a theoretical curve of capacitance-dispersion model.

Dispersion curves computed from the C-D

equation are more symmetric in comparison with that of the capacitance-dispersion model, and they estimate only the flowing saturation ($S_j^f = S_j F_j$) and not the in-situ saturation. For example in experiment SMW-6, from tritium breakthrough curve the C-D equation estimates the following

$$S_1 = 0.448, \quad F_1 = 1.0, \quad M_{11} = 0.0, \quad \alpha_{11} = 1.22 \text{ cm}$$

and the capacitance-dispersion model estimates are

$$S_1 = 0.607, \; F_1 = 0.70, \; M_{11} = 3\text{x}10^{-6} \text{ sec}^{-1}, \; \alpha_{11} = 1.86 \text{ cm}.$$

This implies that the flowing saturation of brine is $F_1 S_1 = 0.42$, almost the same estimate of saturation given by the C-D equation. Therefore, the excess brine saturation estimates for tritium dispersion without capacitance are in error by as high as 16 percent.

The capacitance model estimates a lower flowing fraction (0.50 or 0.70) for the excess brine during finite slug displacements. Finite slug breakthrough curves have more character to their shape, and it was more difficult to estimate the parameters in the capacitance-dispersion model which give good agreement

between the theoretical and experimental curves. The peak breakthrough time, peak height, and tail of the slug are much more sensitive than the 50% breakthrough time and plateau of a continuous curve to the capacitance parameters.

The saturations and dispersivities estimated from both carbon-14 and tritium breakthrough curves using the C-D equation are shown in Table 6.3.2.2.

Table 6.3.2.3 shows the parameters used in the capacitance model such as saturations, flowing fractions, dispersivities, and mass transfer coefficients. The calculated flowing phase velocities ($v_j^f = \frac{q_j}{A\phi S_j F_j}$) and dispersion coefficients ($K_{ij} = \alpha_{ij} v_j$), and percent recovery of tracers are also shown in Table 6.3.2.3.

The relative permeabilities for excess brine and microemulsion are plotted versus microemulsion saturation estimated from both material balance and the capacitance model in Figure 6.3.2.9.

The relative permeabilities (using capacitance estimates of saturation) for each phase were matched against Equation 6.5. The exponent (n_j) was found by fitting the data while S_{jr} and k°_{rj} were estimated by extrapolation of experimental curves. Figure 6.3.2.9 also shows the computed curves for parameters listed in

Table 6.3.1.4. The exponent of the microemulsion relative permeability curve is less than one. This is similar to what was observed in the microemulsion-oil flow experiment (SMO).

Phase relative permeabilities are also plotted versus phase saturation and flowing phase saturations ($S_j^f = S_j F_j$) obtained from the capacitance model in Figures 6.3.2.10 and 6.3.2.11. Once again microemulsion has higher relative permeabilities than those of excess phase at the same saturation. Relative permeability curves are not straight and show curvature even at this high capillary number of 0.0066. Relative permeabilities are closer to each other when flowing saturations are used.

Total relative mobility as a function of microemulsion saturation is shown in Figure 6.3.1.12. The total mobility decreases as more microemulsion is introduced in the core.

Fractional flows versus phase saturations estimated from the capacitance model are shown for both phases in Figure 6.3.2.13. The figure indicates that the saturation of microemulsion is much higher than that of excess brine phase corresponding to the same fractional flow.

Figure 6.3.2.14 shows the dispersivities of carbon-14 in microemulsion and tritium in both microemulsion and brine phases as a function of microemulsion saturation. Dispersivities and saturations are the capacitance model estimates. The dispersivities of both tracers, with the exception of one point, are close and fairly constant over entire range of saturation investigated. Shown in Figure 6.3.2.15 are the dispersion coefficients of carbon-14 in microemulsion and tritium in both water and microemulsion phases as a function of phase velocity ($v_j = \frac{q_j}{A\phi S_j}$). No conclusion can be made for the tracer data in the microemulsion phase since the velocity varies over a very narrow range. The dispersion coefficients of tritium in brine show no specific trend with the brine velocity.

The concentration of divalents were measured in effluent microemulsion and brine phases (Figures 6.3.2.16 and 6.3.2.17). The concentration of Ca^{++} and Mg^{++} in excess brine was about 1.8 and 0.6 ppm while that of the microemulsion was 22 and 4 ppm. It seems that the concentration of Ca^{++} in effluent microemulsion samples is at steady level but higher than the injected value.

The composition of effluent microemulsion was measured at each steady-state cut. Figure 6.3.2.18 shows

the concentration of IBA, water, and oil in microemulsion which indicates that, within the experimental error, the concentrations are close to those of the injected values.

TABLE 6.3.2.1

Excess Brine/Microemulsion Relative Permeabilities
Material Balance Results (Steady-State)
(Experiment SMW)

Experiment Number	Phase Fractional Flow		Total Flow Rate cm^3/min	Phase Potential Drop (1) (psi/ft)		Phase Potential Drop (2) (psi/ft)		Phase Potential Drop (3) (psi/ft)		Total Pore Volumes Inj. (P.V.)	Capillary Number	
	Brine	M.E.		Brine	M.E.	Brine	M.E.	Brine	M.E.		Brine	M.E.
SMW-2	0.225	0.775	0.177	0.311	0.25	0.34	0.28	0.34	0.28	2.09	0.00665	0.0053
SMW-4	0.675	0.325	0.310	0.311	0.25	0.38	0.32	0.34	0.28	3.12	0.00665	0.0053
SMW-6	0.834	0.166	0.453	0.311	0.25	0.36	0.30	0.34	0.28	2.92	0.00665	0.0053
SMW-8	0.933	0.067	0.593	0.301	0.24	0.34	0.28	0.30	0.24	2.83	0.0064	0.0051

Pressure drop measured: (1) across the center of the core (1.0 foot)
(2) across the inlet (0.5 foot)
(3) across the outlet (0.5 foot)

Density of fluid in the line = 0.860 g/cm^3
Micellar solution batch no. 2 was used

TABLE 6.3.2.1 (continued)

Experiment Number	Phase Saturation (1)		Phase Relative Permeability (2)		Relative Mobility (cp^{-1})		
	Brine	M.E.	Brine	M.E.	Brine	M.E.	Total
SMW-2	0.28	0.687	0.045	0.978	0.05	0.217	0.267
SMW-4	0.536	0.430	0.237	0.718	0.266	0.159	0.425
SMW-6	0.701	0.266	0.428	0.536	0.481	0.119	0.60
SMW-8	0.83	0.137	0.648	0.295	0.728	0.066	0.794
SMW-4	0.536	0.430	0.237	0.718	0.266	0.159	0.425
SMW-6	0.701	0.266	0.428	0.536	0.481	0.119	0.60
SMW-8	0.83	0.137	0.648	0.295	0.728	0.066	0.794

(1) Irreducible oil saturation = 0.033 (constant)
(2) Permeabilities are normalized with permeability to 100% brine saturation (k = 0.739 Darcy)

TABLE 6.3.2.2
Dispersion Data of Excess Brine/Microemulsion Experiments
Convection-Dispersion Results
(Experiment SMW)

Experiment Number	Phase Saturation (1)		Dispersivity (cm)			Total Pore Volumes Inj. (P.V.)	Type of Dispersion	Slug Size (P.V.)
	Brine	M.E.	T_2O in Brine	T_2O in M.E.	^{14}C in M.E.			
SMW-2	0.183	0.754	5.55	5.55	0.980	2.0	continuous	-
SMW-4	0.321	0.519	1.35	1.35	0.60	2.50	slug	0.156
SMW-6	0.448	0.360	1.22	1.22	1.0	3.65	slug	0.156
SMW-8	0.630	0.210	3.03	3.03	0.80	4.91	continuous	-

(1) Irreducible oil saturation = 0.033 (constant)

TABLE 6.3.2.3
Dispersion Data of Excess Brine/Microemulsion Experiment
Capacitance Results
(Experiment SMW)

Experiment Number	Phase Saturation (1)		Phase Flowing Fraction		T_2O Mass Transfer Coefficient (sec^{-1})	Dispersivity (cm)			Dispersion Coefficient (cm^2/sec)			Flowing Phase Velocity (cm/sec)		Tracer Recovery (%)	
	Brine	M.E.	Brine	M.E.		T_2O in Brine	T_2O in M.E.	^{14}C in M.E.	T_2O in Brine	T_2O in M.E.	^{14}C in M.E.	Brine	M.E.	T_2O	^{14}C
SMW-2	0.213	0.754	0.90	1.0	$1x10^{-6}$	6.66	6.0	0.98	0.0038	0.0033	0.00055	0.00064	0.00056	100	97.6
SMW-4	0.448	0.519	0.50	1.0	$9x10^{-6}$	1.0	0.50	1.30	0.00014	0.00030	0.00035	0.00028	0.00059	97.8	82.0
SMW-6	0.607	0.360	0.70	1.0	$3x10^{-6}$	1.86	1.30	1.0	0.0036	0.00083	0.00064	0.0027	0.00064	87.5	70.0
SMW-8	0.757	0.210	0.90	1.0	$7x10^{-6}$	1.0	0.90	0.80	0.00225	0.00052	0.00046	0.0025	0.00058	95.0	97.3

(1) Irreducible oil saturation = 0.033 (constant)

EXPERIMENT NUMBER	SMW-2	
TRACER & PHASE	CARBON-14 M.E.	
FRACTIONAL FLOW	1:0.225 3:0.775	
MAX. & INJ. CONC.	2560 2560	DPM/CC
FLOW RATE	0.177	CC/MIN.

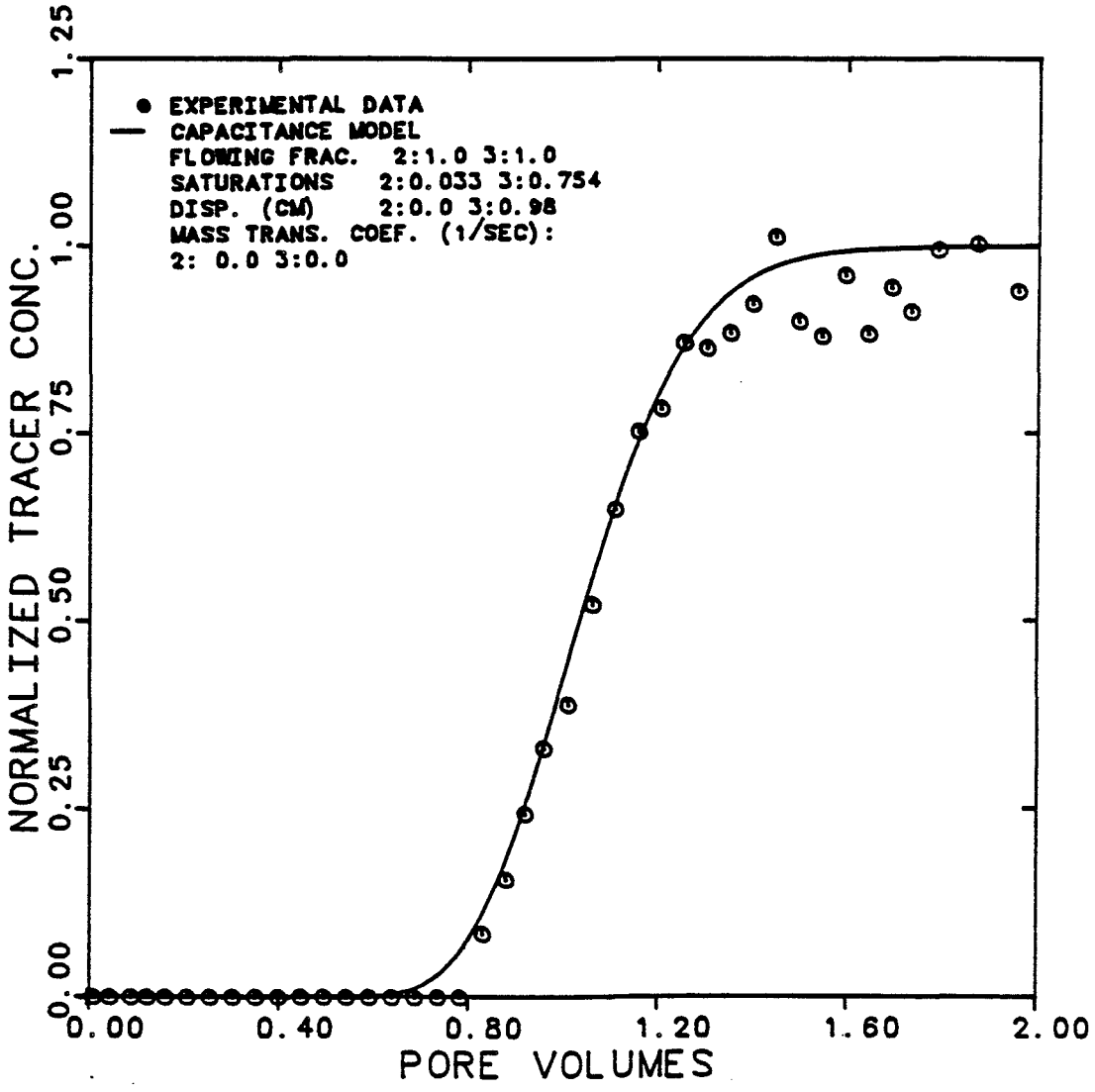

Figure 6.3.2.1 Effluent History for Carbon-14 in M.E. at 22.5% Brine and 77.5% M.E. Cuts

EXPERIMENT NUMBER	SMW-2		
TRACER & PHASES	TRITIUM	BRINE&M.E.	
MAX. & INJ. CONC. (BRINE)	48400	48400	DPM/CC
MAX. & INJ. CONC. (M.E.)	20400	20400	DPM/CC
FLOW RATE	0.177		CC/MIN.

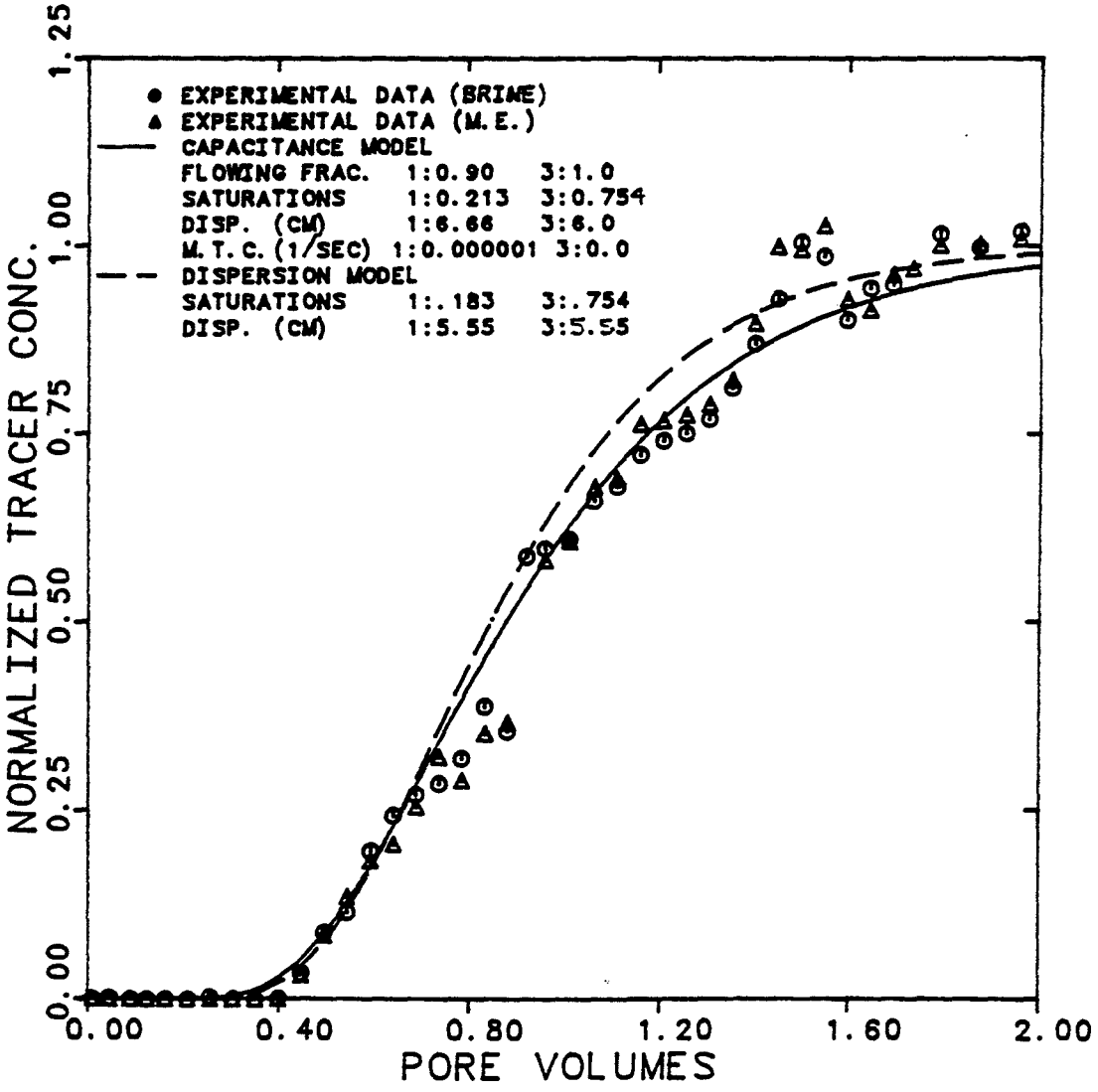

Figure 6.3.2.2 Effluent Histories for Tritiated Water in M.E. and Brine at 22.5% and 77.5% M.E. Cuts

EXPERIMENT NUMBER	SMW-4
TRACER & PHASE	CARBON-14 M.E.
FRACTIONAL FLOW	1:0.675 3:0.325
MAX. & INJ. CONC.	571 2214 DPM/CC
FLOW RATE & SLUG SIZE	0.307 CC/MIN. 0.156 P.V.

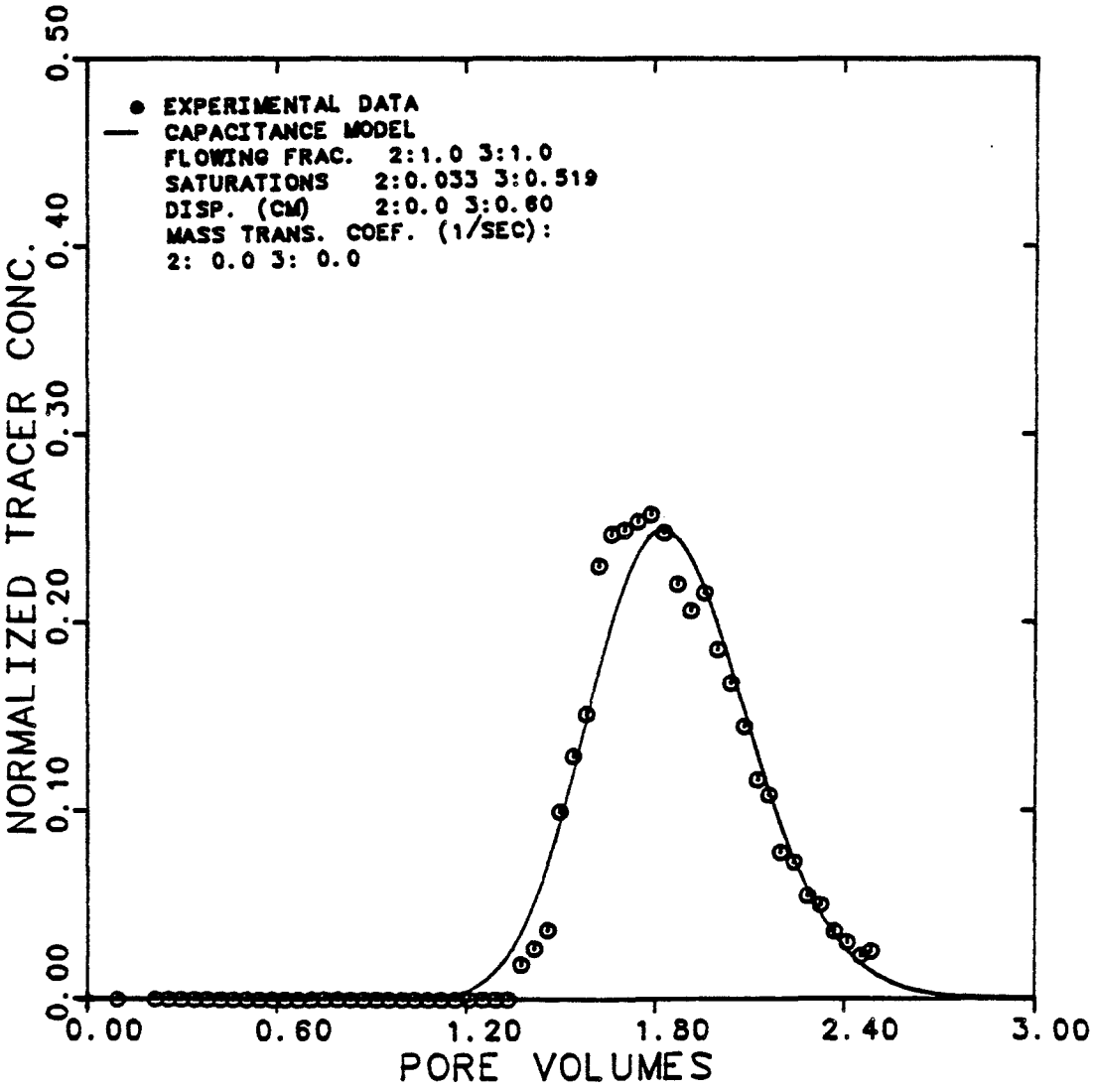

Figure 6.3.2.3 Effluent History for a Finite Slug of Carbon-14 in M.E. at 67.5% Brine and 32.5% M.E. Cuts

EXPERIMENT NUMBER	SMW-4		
TRACER & PHASES	TRITIUM	BRINE & M.E.	
MAX. & INJ. CONC. (BRINE)	22034	52146	DPM/CC
MAX. & INJ. CONC. (M.E.)	8161	17826	DPM/CC
FLOW RATE & SLUG SIZE	0.307 CC/MIN	.156 P.V.	

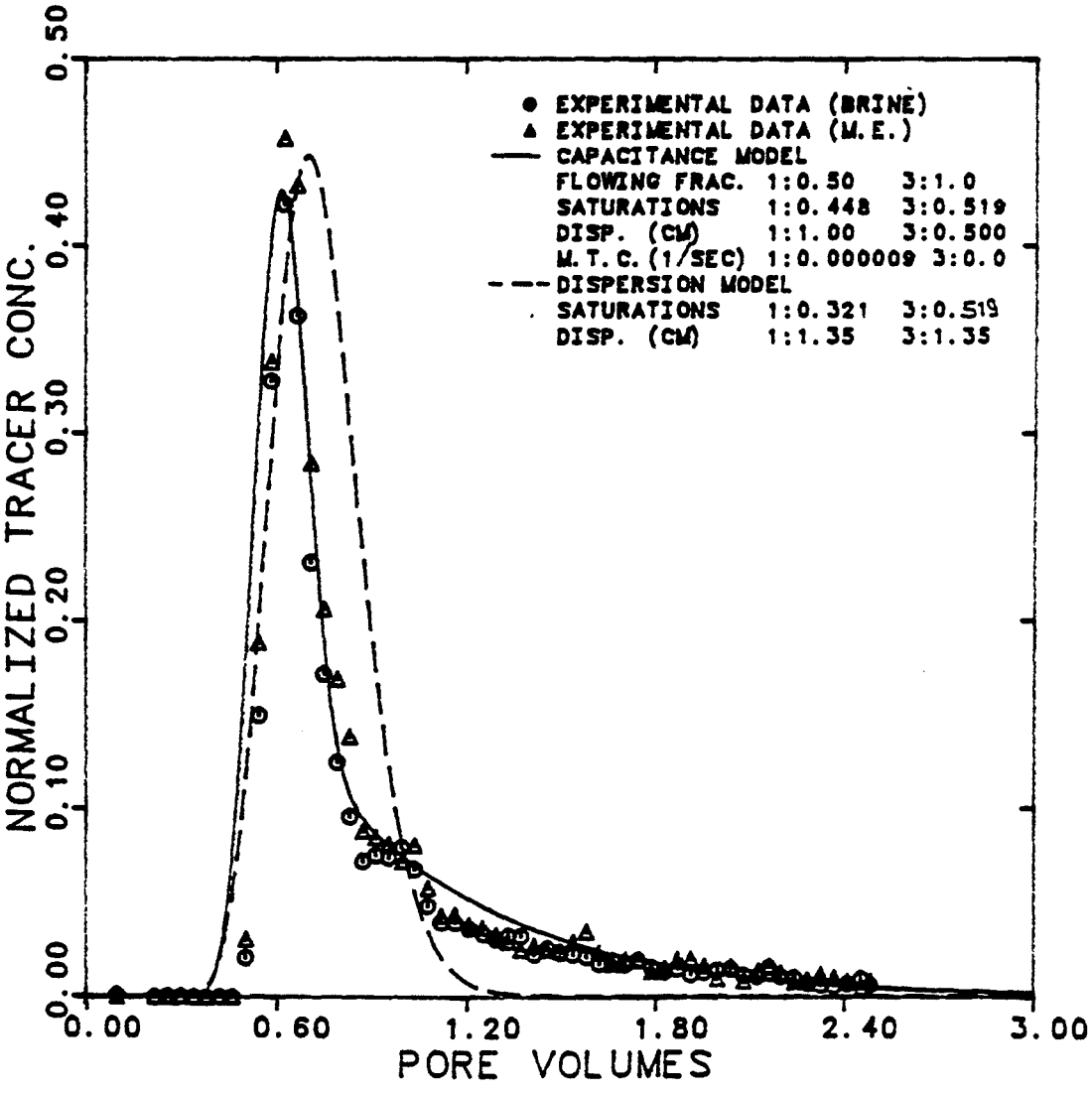

Figure 6.3.2.4 Effluent Histories for a Finite Slug of Tritium in M.E. and Brine at 67.5% Brine and 32.5% M.E. Cuts

EXPERIMENT NUMBER	SMW-6
TRACER & PHASE	CARBON-14 M.E.
FRACTIONAL FLOW	1:0.834 3:0.166
MAX. & INJ. CONC.	374 2448 DPM/CC
FLOW RATE & SLUG SIZE	0.453 CC/MIN. 0.156 P.V.

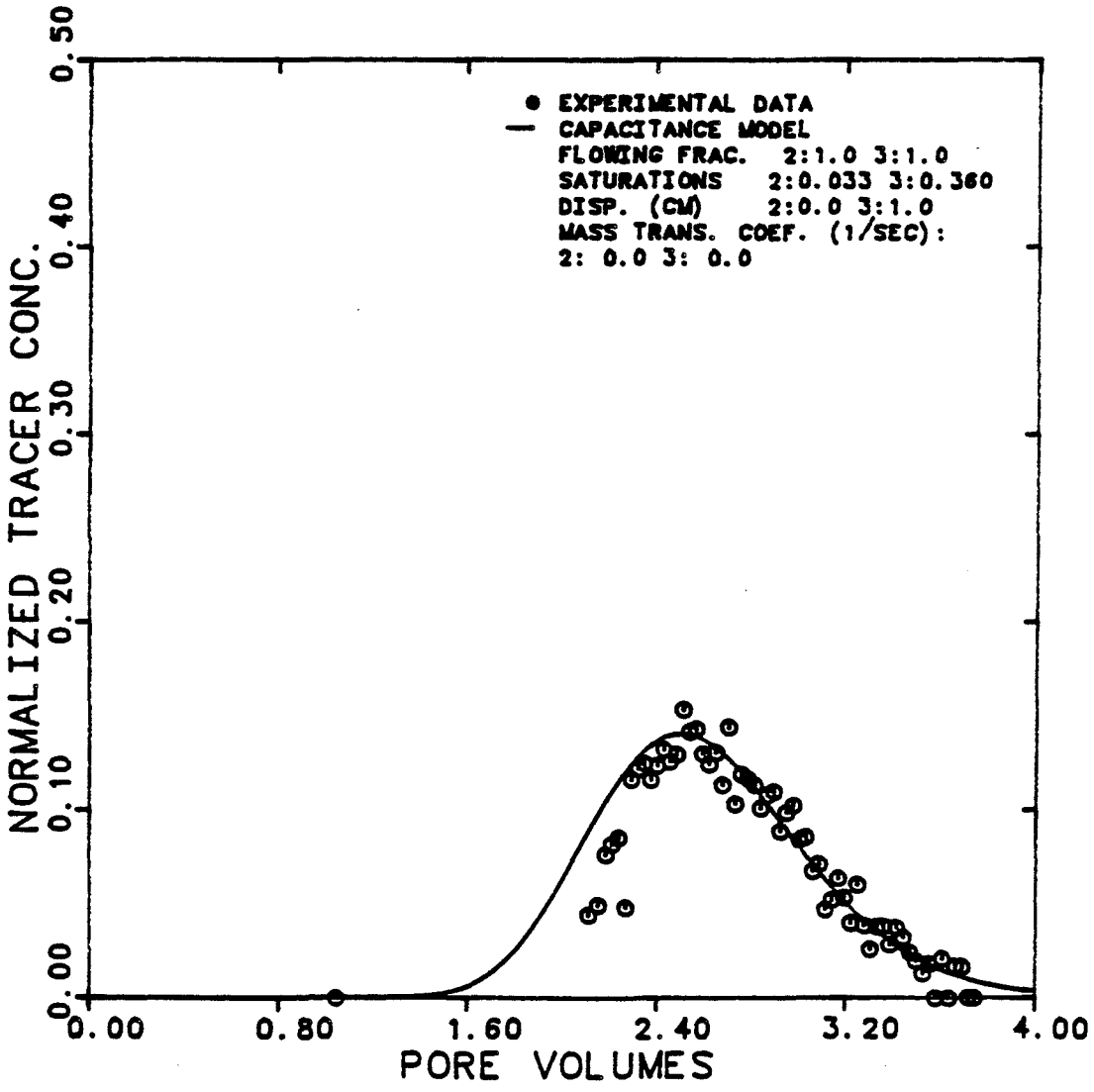

Figure 6.3.2.5 Effluent History for a Finite Slug of Carbon-14 in M.E. at 83.4% Brine and 16.6% M.E. Cuts

EXPERIMENT NUMBER	SMW-6		
TRACER & PHASES	TRITIUM	BRINE & M.E.	
MAX. & INJ. CONC. (BRINE)	20376	50996	DPM/CC
MAX. & INJ. CONC. (M.E.)	8750	18752	DPM/CC
FLOW RATE & SLUG SIZE	0.453 CC/MIN	..156 P.V.	

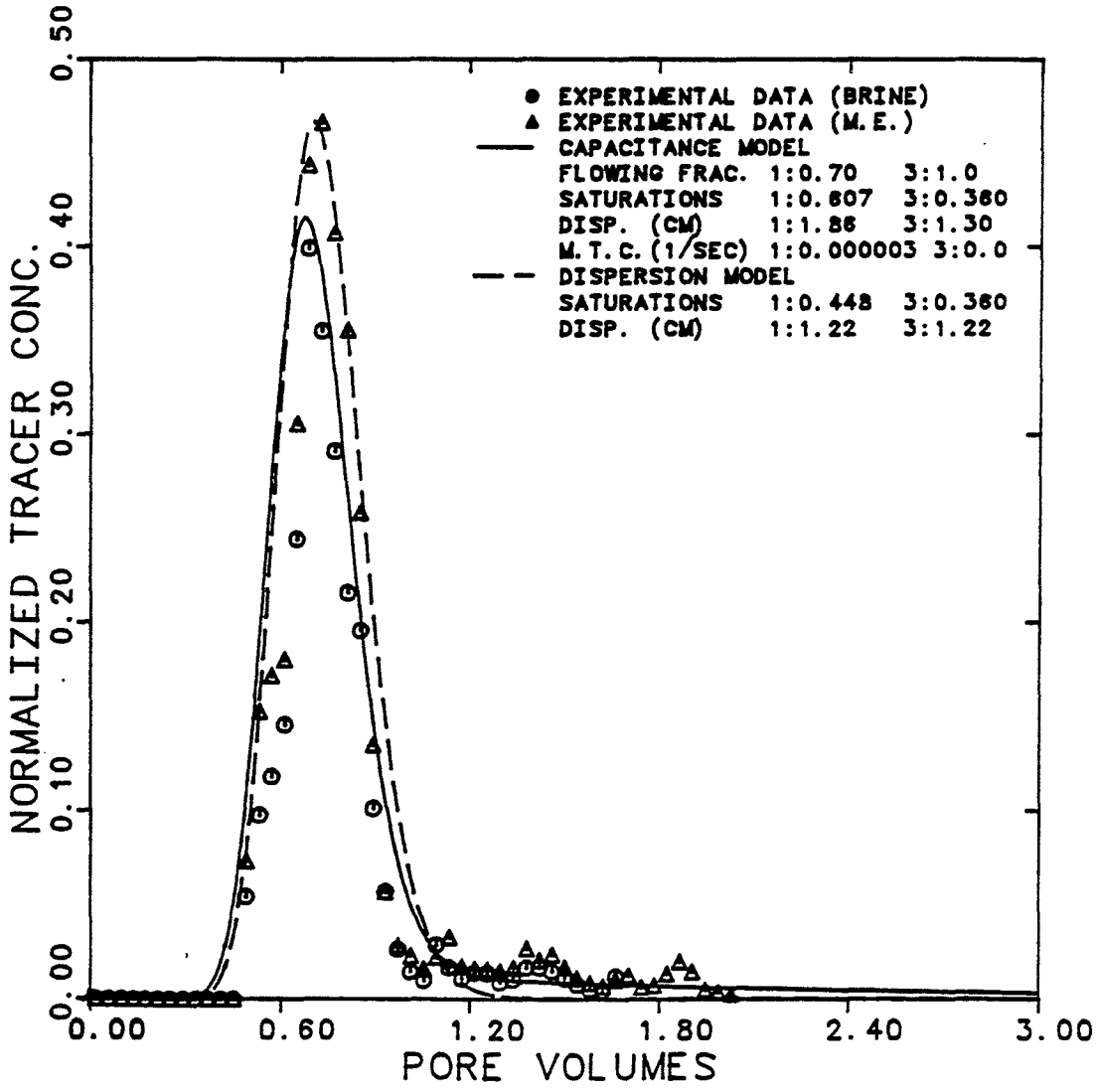

Figure 6.3.2.6 Effluent Histories for a Finite Slug of Tritiated Water in M.E. and Brine at 83.4% Brine and 16.6% M.E. Cuts

EXPERIMENT NUMBER	SMW-8	
TRACER & PHASE	CARBON-14 M.E.	
FRACTIONAL FLOW	1:0.933 3:0.067	
MAX. & INJ. CONC.	2040 2220	DPM/CC
FLOW RATE	0.593	CC/MIN.

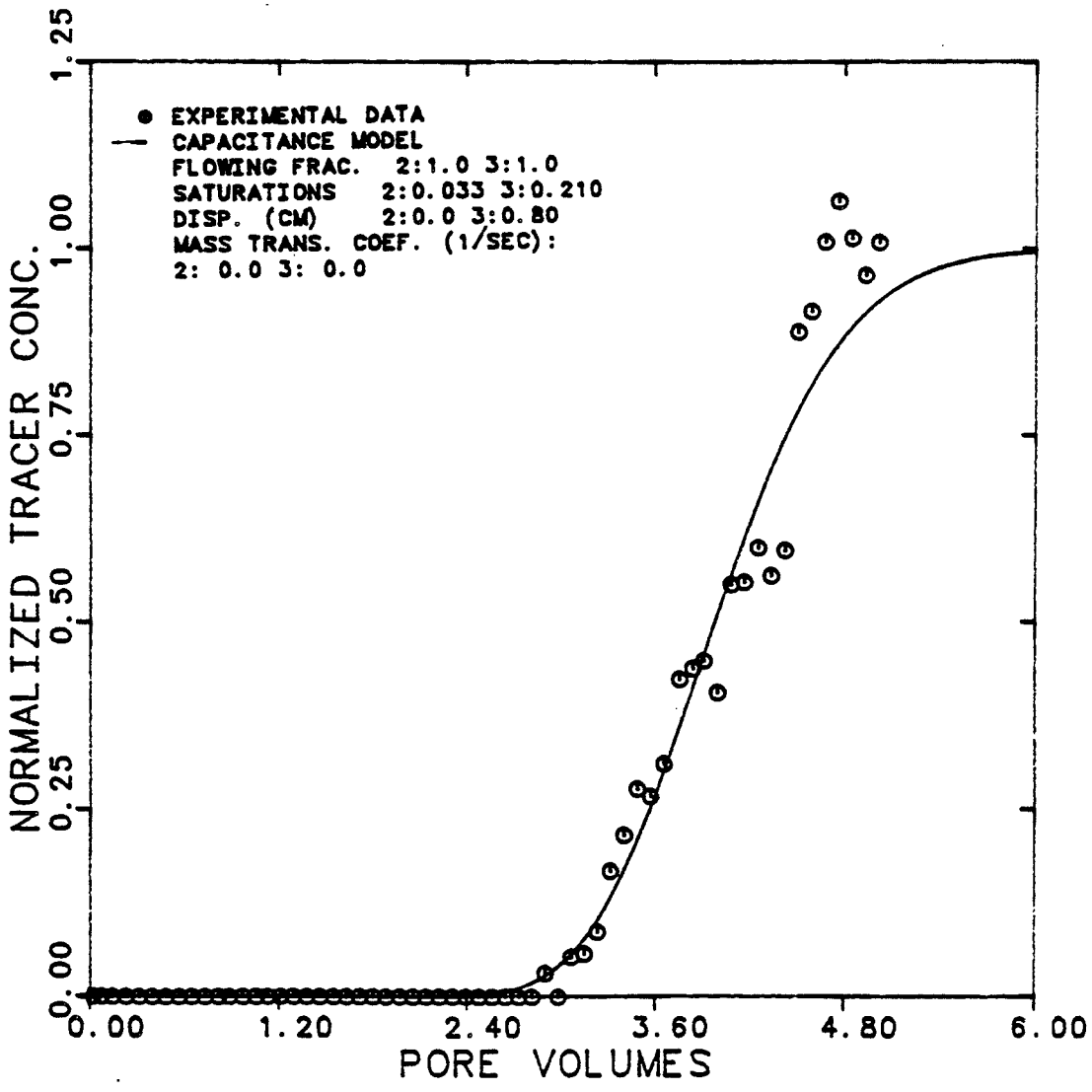

Figure 6.3.2.7 Effluent History for Carbon-14 in M.E. at 93.3% Brine and 6.7% M.E. Cuts

EXPERIMENT NUMBER	SMW-8		
TRACER & PHASES	TRITIUM	BRINE&M.E.	
MAX. & INJ. CONC. (BRINE)	42000	42000	DPM/CC
MAX. & INJ. CONC. (M.E.)	17600	17600	DPM/CC
FLOW RATE	0.593		CC/MIN.

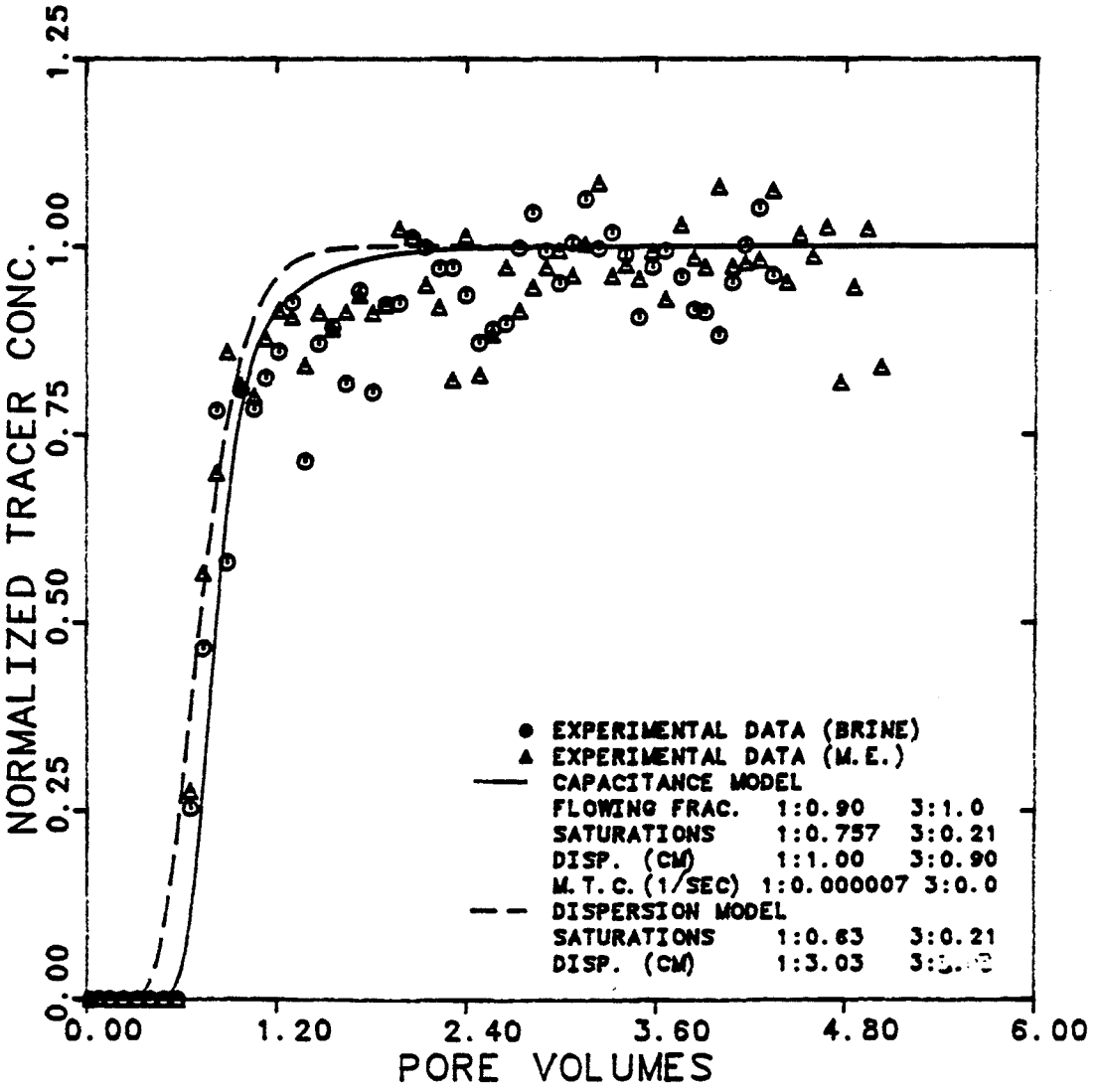

Figure 6.3.2.8 Effluent Histories for Tritiated Water in Brine and M.E. at 93.3% Brine and 6.7% M.E. Cuts

EXPERIMENT NUMBER	SMW
CAPILLARY NUMBER	0.0066
TEMPERATURE	30° C
RESIDUAL OIL	0.033

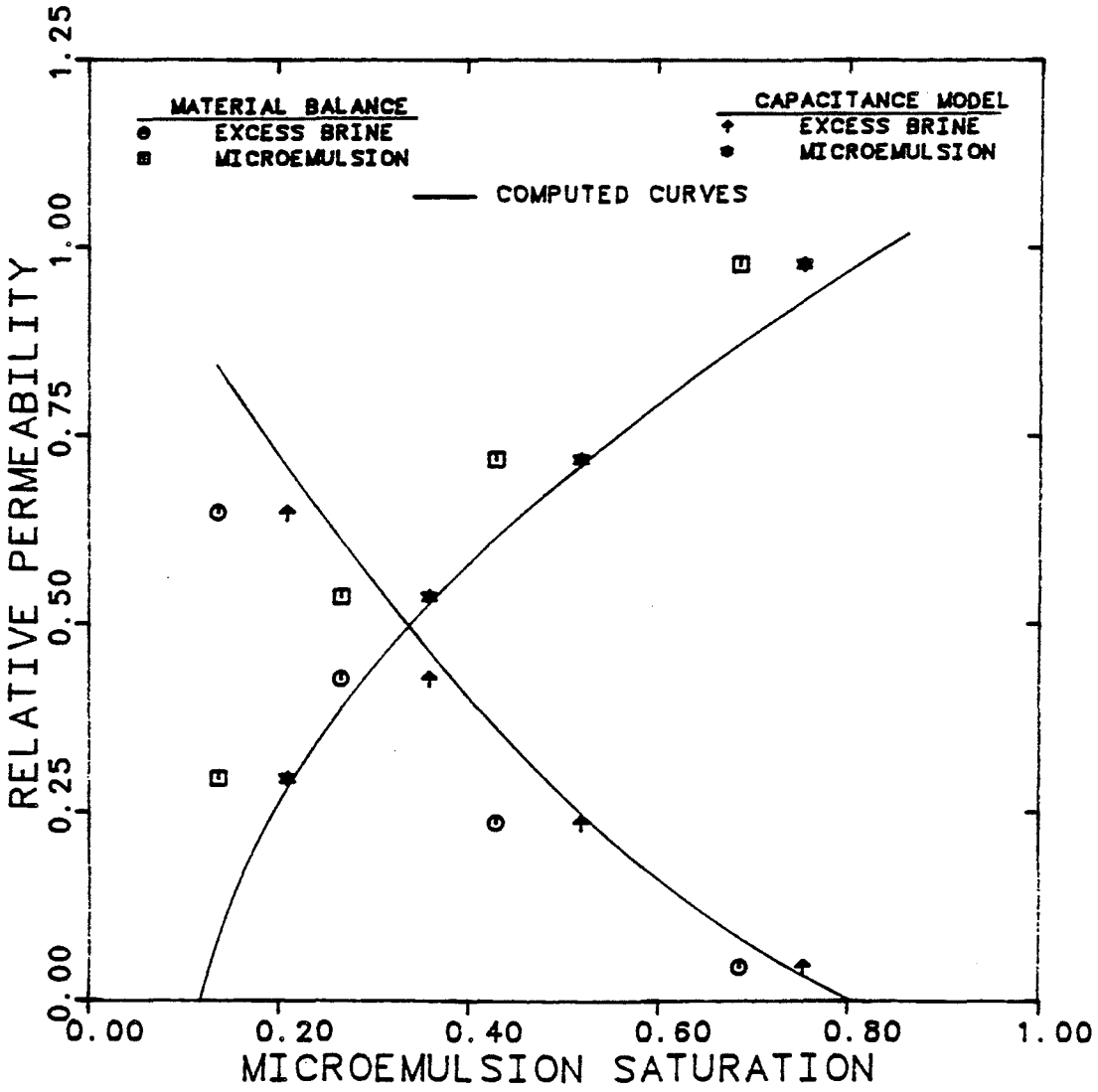

Figure 6.3.2.9 Computed and Experimental Brine/M.E. Relative Permeabilities as a Function of Saturation

EXPERIMENT NUMBER	SMW
CAPILLARY NUMBER	0.0066
TEMPERATURE	30°C
RESIDUAL OIL	0.033

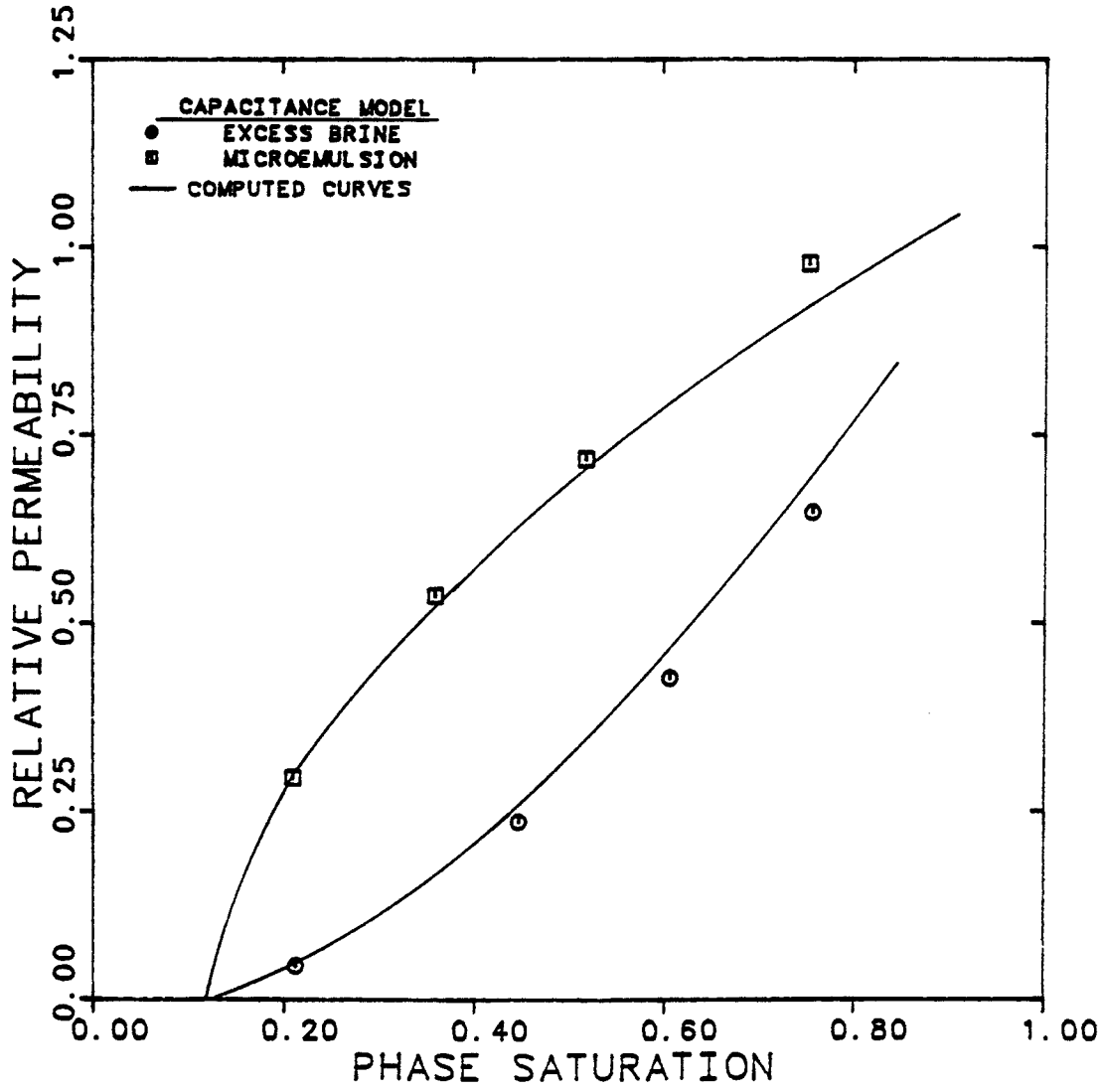

Figure 6.3.2.10 Brine/M.E. Relative Permeabilities as a Function of Phase Saturation Estimated from the Capacitance Model

EXPERIMENT NUMBER	SMW
CAPILLARY NUMBER	0.0066
TEMPERATURE	30° C
RESIDUAL OIL	0.033

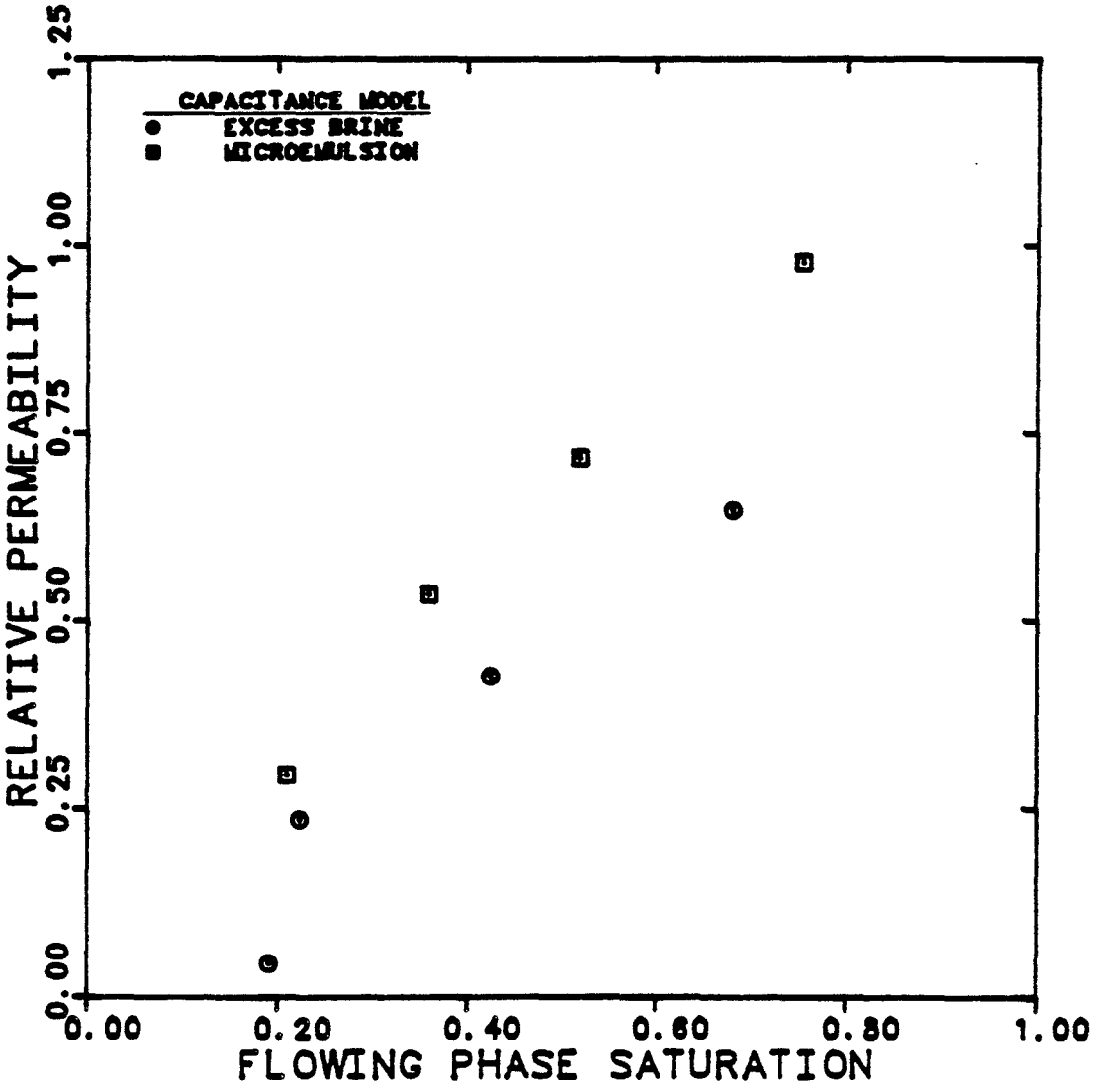

Figure 6.3.2.11 Brine/M.E. Relative Permeabilities Versus Flowing Phase Saturation

EXPERIMENT NUMBER	SMW
CAPILLARY NUMBER	0.0066
TEMPERATURE	30° C
RESIDUAL OIL	0.033

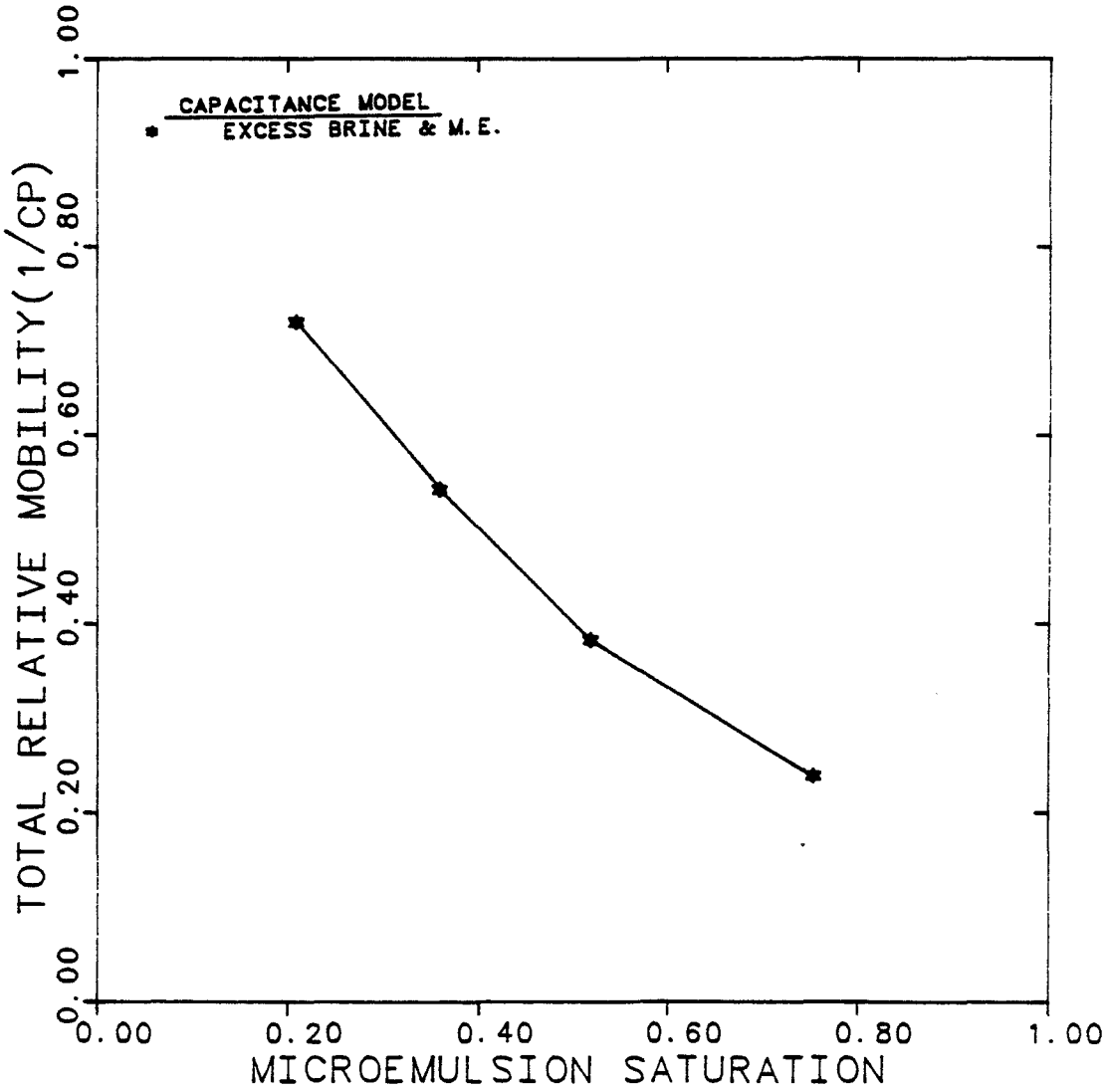

Figure 6.3.2.12 Total Relative Mobility Curve for Brine/ M.E. Flow Experiment

EXPERIMENT NUMBER	SMW
CAPILLARY NUMBER	0.0066
TEMPERATURE	30° C
RESIDUAL OIL	0.033

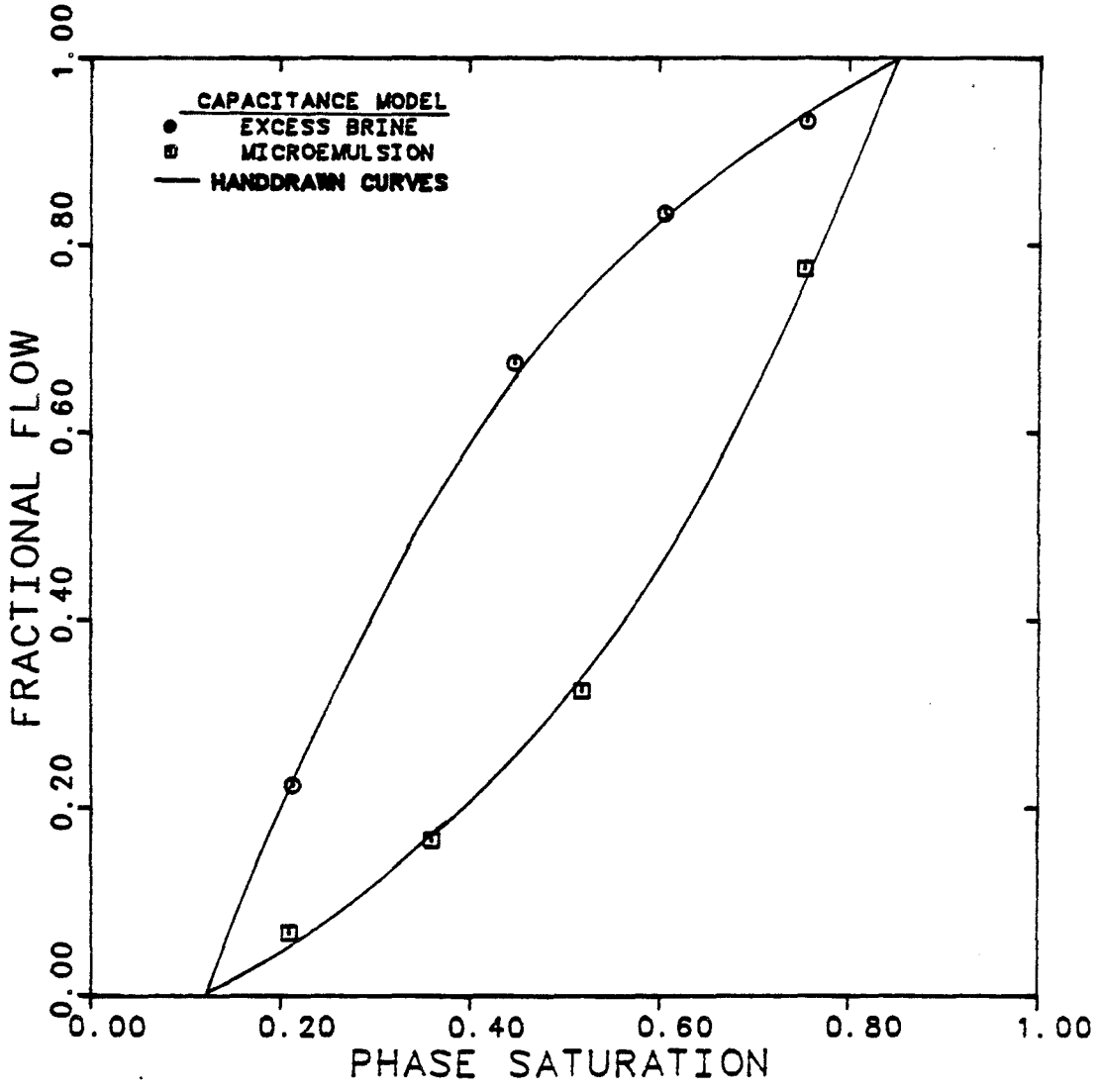

Figure 6.3.2.13 Brine/M.E. Fractional Flow Curves

EXPERIMENT NUMBER	SMW
CAPILLARY NUMBER	0.0066
TEMPERATURE	30° C
RESIDUAL OIL	0.033

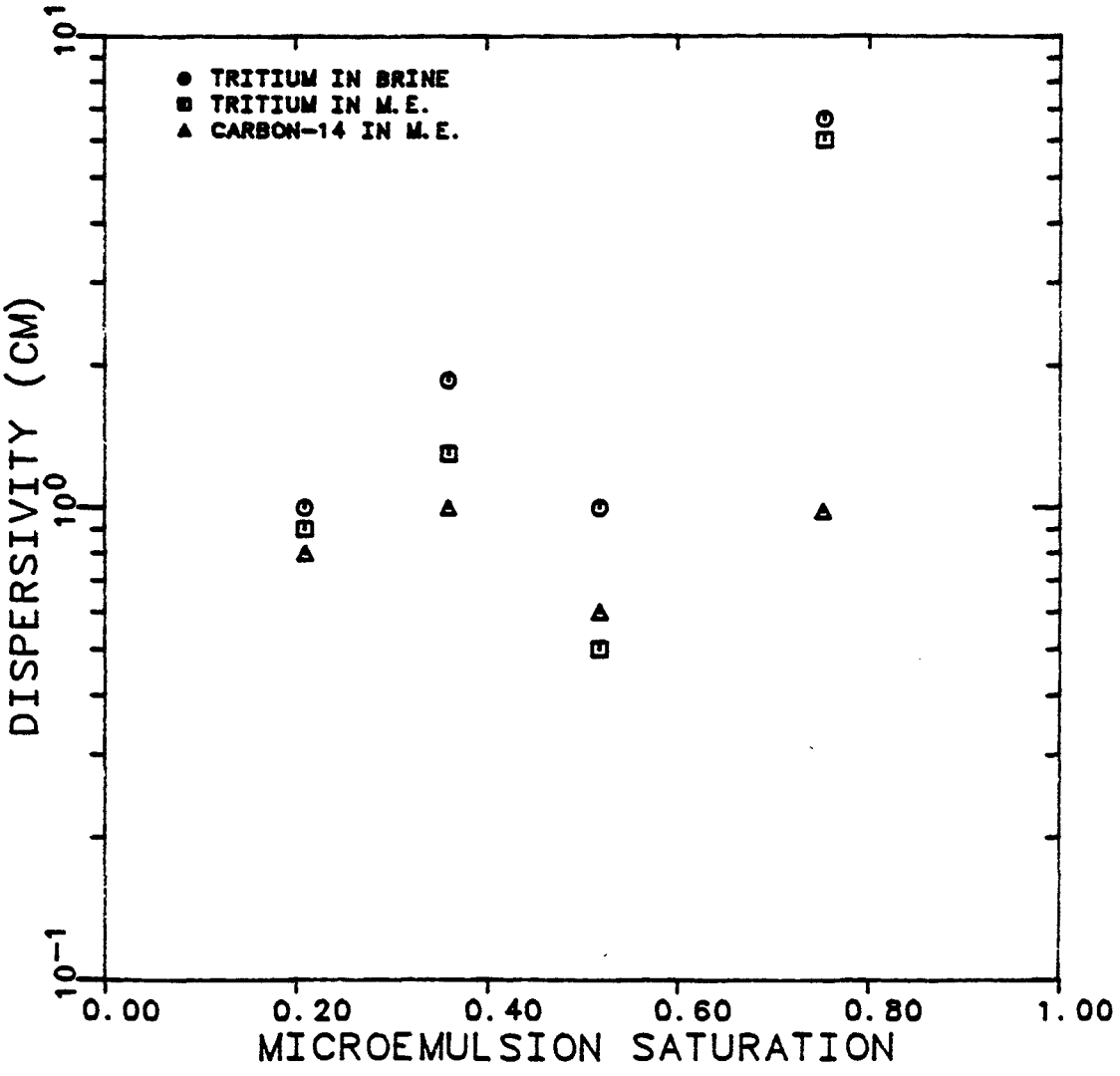

Figure 6.3.2.14 Dispersivities of Tracers in M.E. and Brine During Two-Phase Flow as a Function of M.E. Saturation

EXPERIMENT NUMBER	SMW
CAPILLARY NUMBER	0.0066
TEMPERATURE	30° C
RESIDUAL OIL	0.033

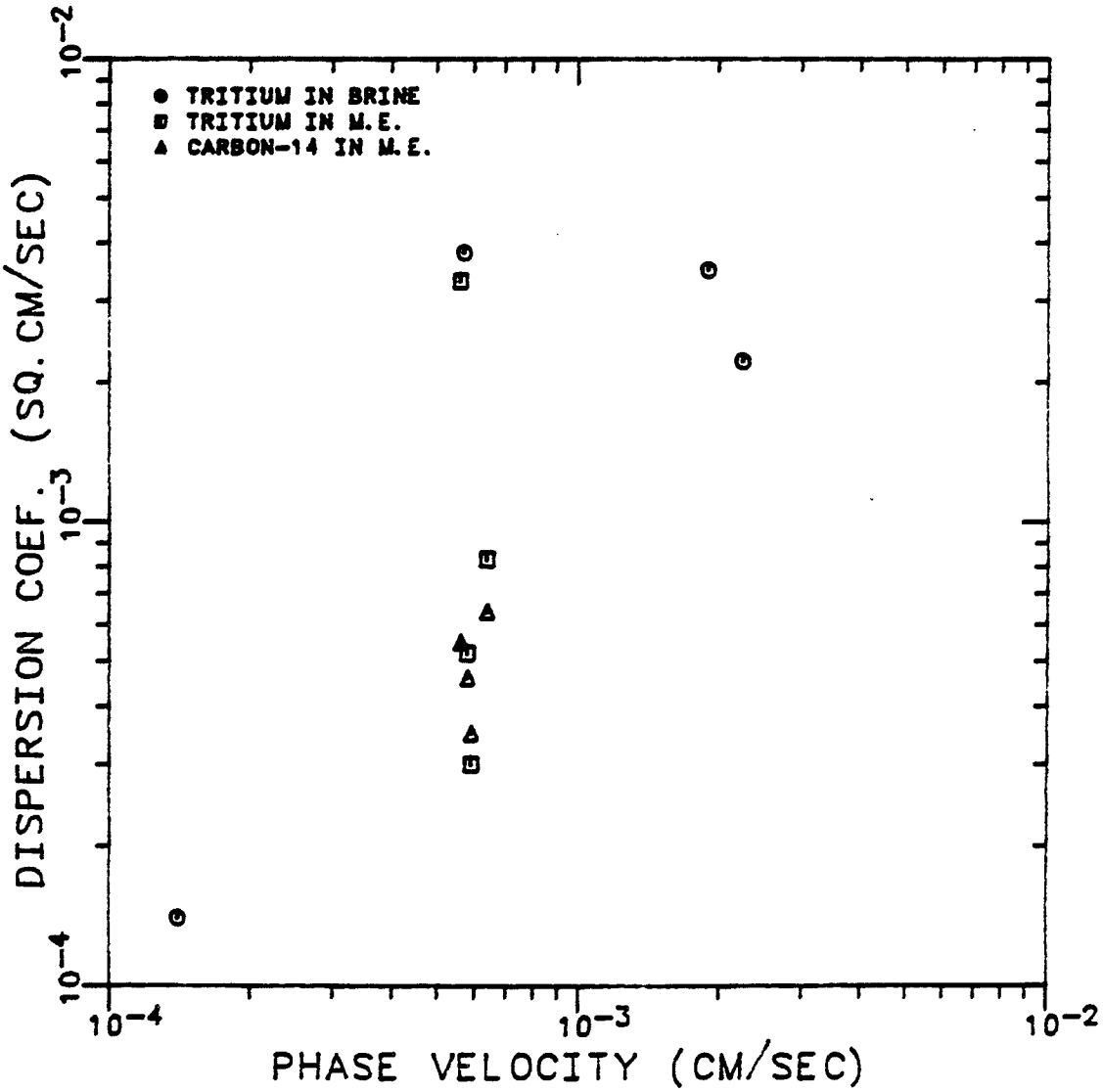

Figure 6.3.2.15 Dispersion Coefficient of Tracers in M.E. and Brine During Two-Phase Flow as a Function of Phase Velocity

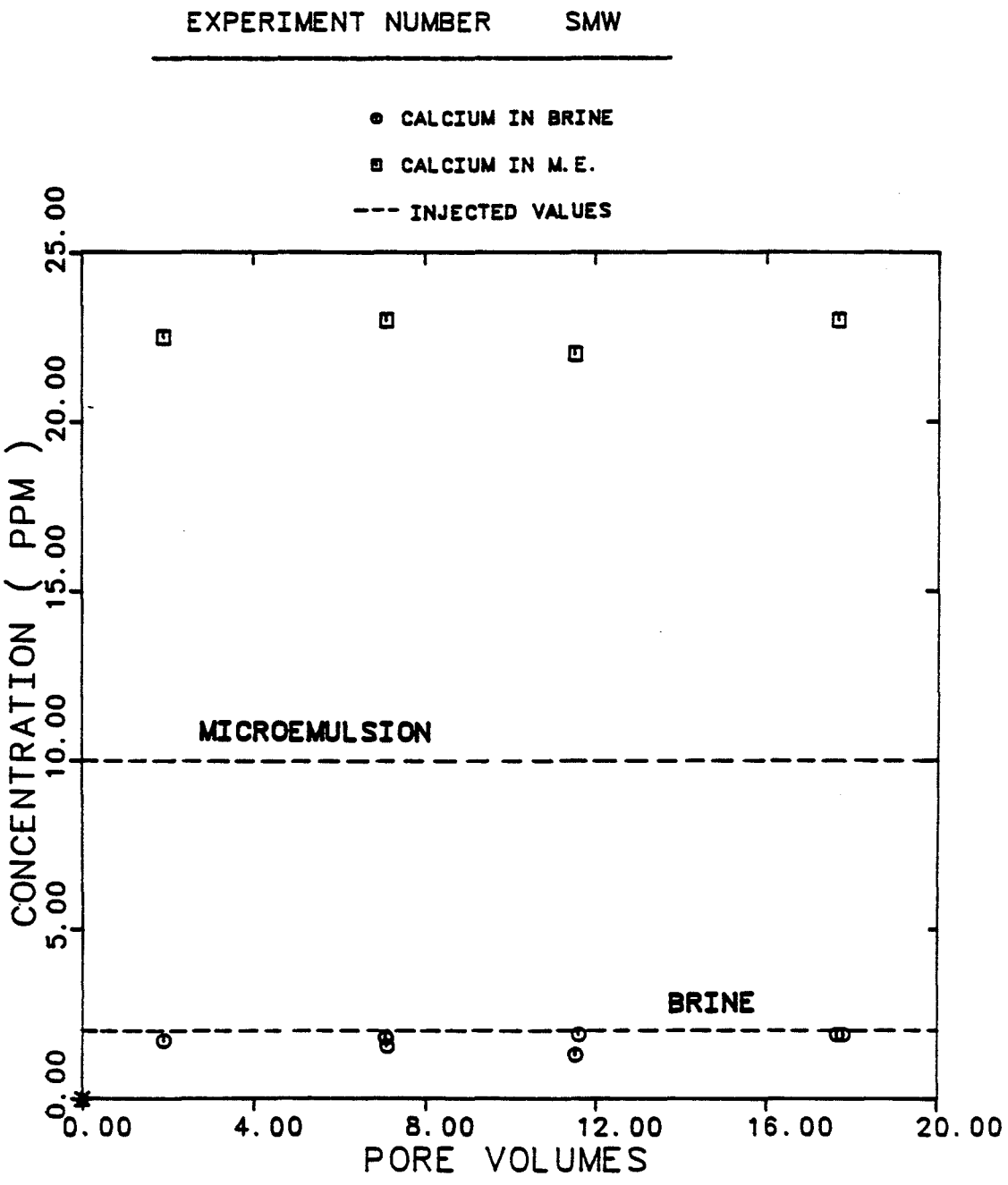

Figure 6.3.1.16 Calcium Concentration in Effluent M.E. and Brine as a Function of Pore Volumes Injected

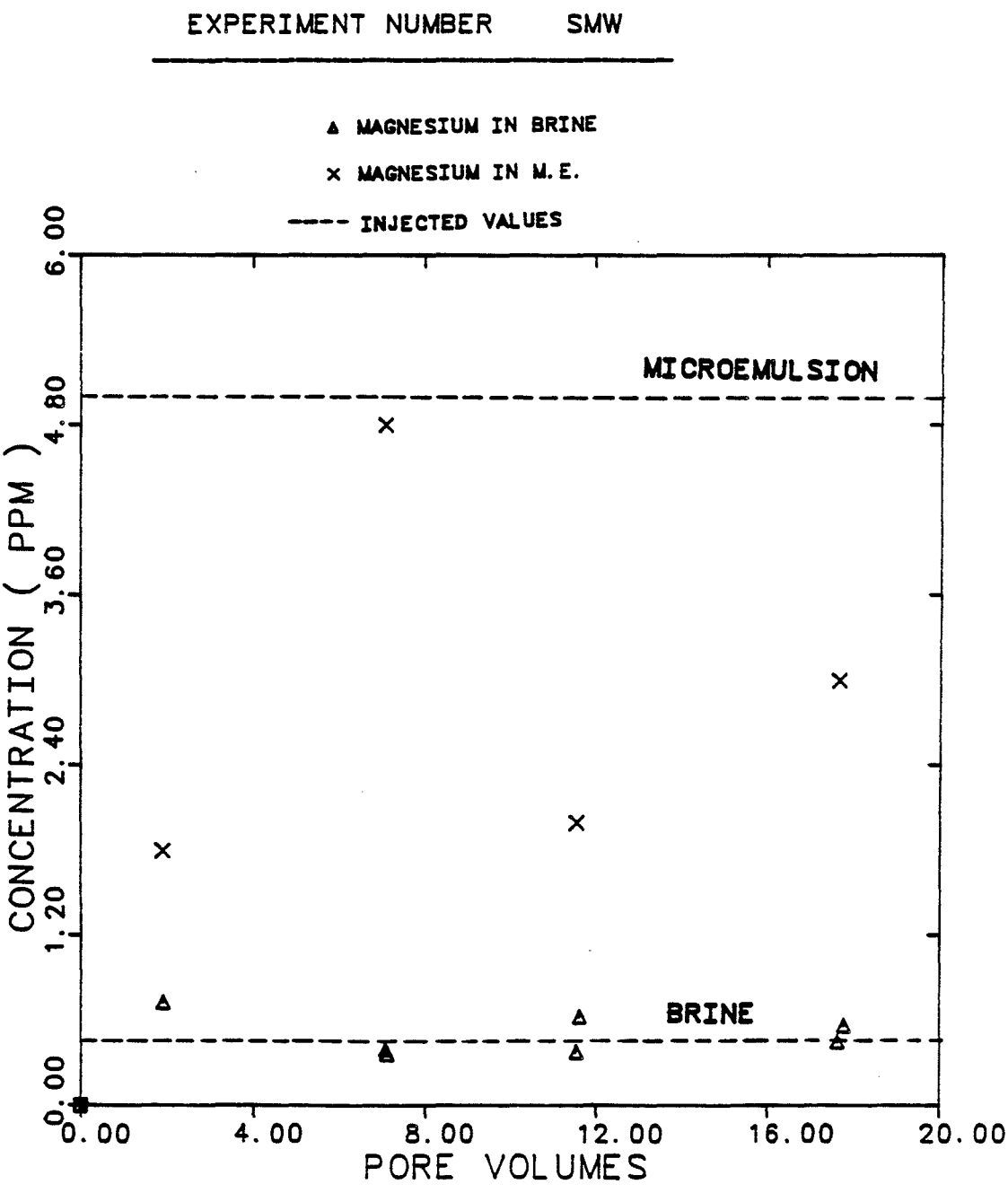

Figure 6.3.2.17 Magnesium Concentration in Effluent M.E. and Brine as a Function of Pore Volumes Injected

COMPOSITION OF INJECTED MICROEMULSION

WATER	40.7 VOL.%
N-DECANE	55.5 VOL.%
IBA	1.81 VOL.%
TRS 10-410	3.2 VOL.%

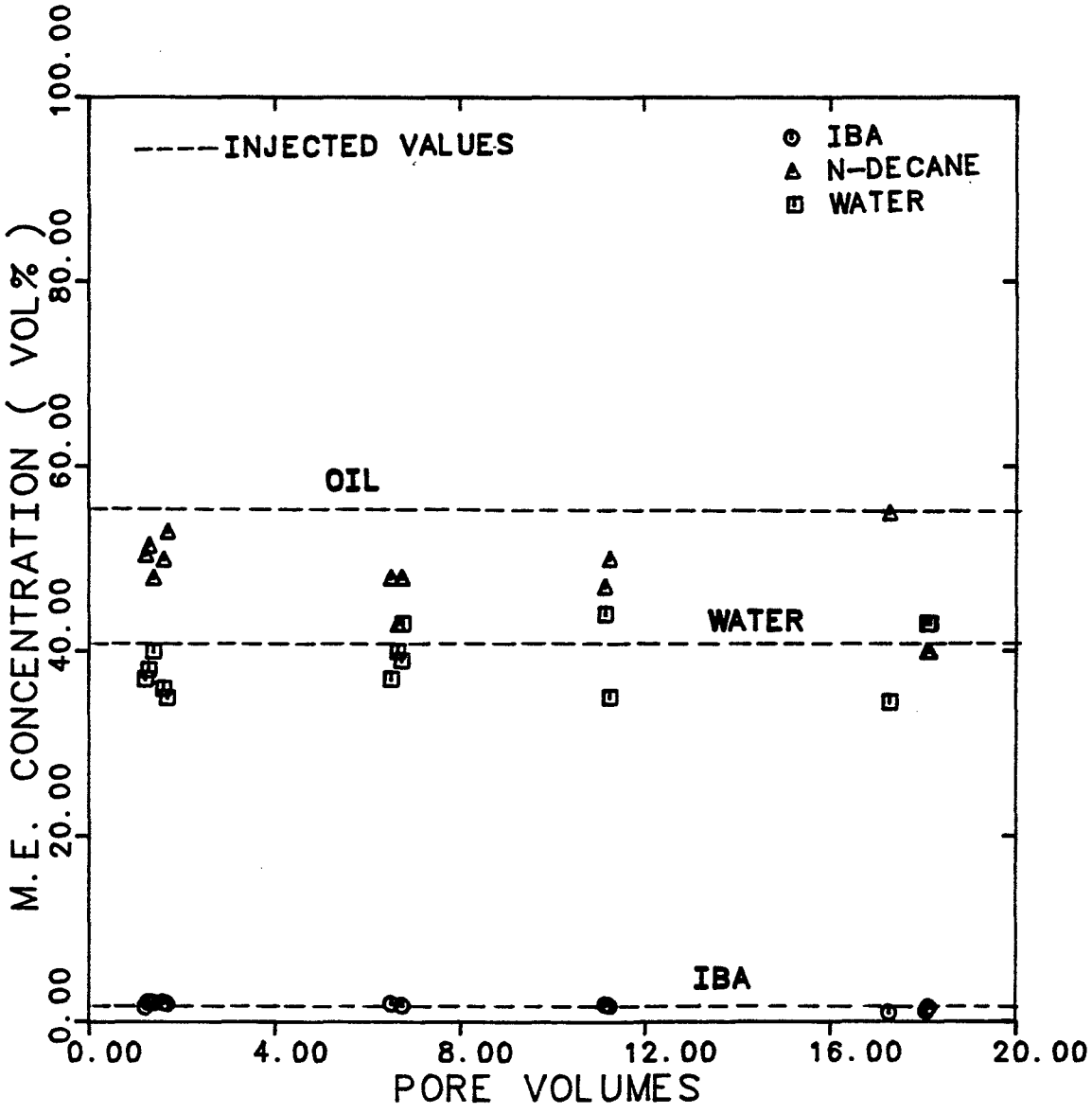

Figure 6.3.2.18 Composition of Effluent M.E. at Steady-State as a Function of Pore Volumes Injected

6.3.3 Comparison of Two-Phase Relative Permeability Data - Microemulsion (or Aqueous)/Oil

Delshad [D.8], Fulcher et al. [F.4], and Torabzadeh and Handy [T.7] performed similar two-phase oil and microemulsion experiments for water-wet Berea sandstone cores. They conducted all experiments at a constant total flow rate in the group $\frac{u\mu}{\sigma}$ rather than a constant $\frac{k\Delta\Phi}{L\sigma}$. In order to make some comparisons, however, those data with no significant change in capillary number (Table 6.3.3.1) were used.

The basic properties of the Berea cores, fluid system and the capillary number ($N_c = \frac{k\Delta\Phi}{L\sigma}$) used in these experiments are in Table 6.3.3.1. The capillary numbers were calculated only for the end-point of the relative permeability curves (single-phase flow at the residual saturation of the other phase). Only steady-state experimental data are compared.

Relative permeabilities versus normalized phase saturations (Equation 6.6) of experiment SMO are compared with the results obtained by the above mentioned investigators in Figures 6.3.3.1 and 6.3.3.2. The normalized saturations were used for the comparison since the residual phase saturations were different in these experiments.

A comparison of the oil relative permeabilities (Figure 6.3.3.1) shows that the data are close and show the same trend with the exception of those of Torabzadeh and Handy [T.7]. This discrepancy may be because of an order of magnitude lower capillary numbers used in their experiment.

The microemulsion (or aqueous) phase relative permeabilities (Figure 6.3.3.2), on the other hand, are very different in these experiments. Once again, the data of Torabzadeh and Handy show the lowest relative permeabilities for the aqueous phase. There is a fair agreement between the data of Fulcher and Exp. II-MM/D, whereas the results of Exp. SMO show the highest m.e. relative permeability at normalized saturations of less than 0.60. The discrepancies in Figure 6.3.3.2 may be because of the variation in the capillary number or the differences in the degree of wettability of these fluids in the Berea cores used.

The relative permeability data were also matched against the exponential relative permeability function (Equation 6.5) to obtain the exponent for each of the aforementioned relative permeability data. Table 6.3.3.2 presents the values of the parameters, exponent, endpoint relative permeability, residual saturation, used

in Equation 6.5.

The parameters found by matching the low capillary number (high IFT) relative permeability data obtained by the same investigators are listed in Table 6.3.3.3.

Comparing two-phase high and low IFT results (Tables 6.3.1.4, 6.3.3.2, 6.3.3.3) suggest that

- The residual saturations depend strongly on capillary number.

- The exponent and endpoint of the oil relative permeability curves do not strongly depend on N_c with the exception of Torabzadeh's data.

- The exponent of the aqueous phase is independent of capillary number with the exception of Delshad's [D.8] data. The latter may be partly because of comparison of the microemulsion phases in two different phase environment since they have totally different composition and behavior.

- The endpoint relative permeability of the aqueous phase is a strong function of the N_c.

- Microemulsion/Excess Brine

Similar two-phase excess brine/microemulsion flow experiments have been performed by Delshad [D.8] (experiments III-MM/B and IV-MM/B); Amaefule and Handy

[A.2], and Delshad [D.6] (experiment MB) for water-wet Berea sandstone cores. Experiments III-MM/B and IV-MM/B, and those by Amaefule were conducted at a constant total flow rate, while experiment MB was performed at a constant capillary number of 0.02.

The basic properties of the Berea cores and fluid system used in these experiments are shown in Table 6.3.3.4. The fluid formulation and phase compositions in Experiments III-MM/B, IV-MM/B and MB were almost the same as those used in experiment SMW. Table 6.3.3.4 lists the capillary number ($N_c = \frac{k\Delta\Phi}{L\sigma}$) used in these experiments and the residual phase saturations. The capillary numbers for Amaefule's data and Experiments III-MM/B and IV-MM1B shown in the table are the values calculated for the endpoints. Figures 6.3.3.3 and 6.3.3.4 compare the relative permeabilities versus normalized phase saturations (Eq. 6.6) of experiment SMW with the results of the above mentioned experiments. The agreement for excess brine phases is excellent. A comparison of the microemulsion relative permeabilities shows that the data are close and show the same trend with the exception of those of Amaefule.

The relative permeabilities were then matched against the exponential relative permeability function

(Eq. 6.5). Table 6.3.3.2 gives the obtained parameters such as exponent, endpoint relative permeability and residual saturation. A comparison among these results indicate that

- There are some variation in endpoint relative permeability and residual saturation of excess brine and microemulsion which may be because of the variation in capillary number. The residual microemulsion saturation of Amaefule is the lowest among these data.

- The exponent for the excess brine phase varies from 1.29 - 2.05 where the highest value is that of Amaefule.

- The exponent of the microemulsion phase is less than 1.0 (n_3 = 0.4 - 0.6) with the exception of that of Amaefule (n_3 = 1.43).

The above discrepancies may be because of comparison of microemulsion phases in two different phase environment, type II(+) in Amaefule's experiment and type III for others. The microemulsion in different phase environment may have different wettability in the core.

The data of microemulsion/excess brine including polymer obtained by Delshad [D.6] were also matched against the relative permeability function. The parameters found are listed in Table 6.3.3.2 which are in

good agreement with those without polymer.

A comparison of brine phase parameters of low and high IFT (Tables 6.3.1.4, 6.3.3.2 and 6.3.3.3) suggests that

- The residual saturation and endpoint relative permeability depend strongly on the capillary number.

- The exponent seems independent of the N_c.

Table 6.3.3.1

Properties of Berea Cores and Fluids Used in Similar Microemulsion (or Aqueous)/Oil Experiments

	Delshad [D.8]	Fulcher [F.4]	Torabzadeh [T.7]
Porous Medium	Berea	Fired Berea	Fired Berea
Length (cm)	60.96	60.96	21.60
Porosity (fraction)	0.193	0.224	0.243
Pore Volume (cm^3)	304.75	279.00	26.60
Ref. Permeability (Darcy)	0.231	0.433	0.629
Total Flow Rate (cm^3/min)	0.64	0.84	2.0
Temperature (°C)	30	25	27
Core Orientation	vertical	horizontal	horizontal
Fluid System	three-phase	two-phase	two-phase
Interfacial Tension (IFT), (dyne/cm)	0.0008	0.039	0.187
IFT reducer	TRS 10-410	IPA	Petrostep 465
Capillary Number $N_c = \frac{k\Delta\Phi}{L\sigma}$	0.0048-0.0214	0.009-0.011	0.0006-0.0017
Residual Excess Oil Saturation	0.0	0.0	0.236
Residual Excess Brine Saturation	0.112	-	-
Residual M.E. or Aqueous Saturation	0.151	0.32	0.213

Table 6.3.3.2

Parameters for High Capillary Number Relative Permeability Curves

Experimentalist	Phase	Exponent	Residual Saturation	End-Point	Capillary Number
Delshad [D.8]	Brine Oil M.E.	- 1.25 0.77	0.112 0.0 0.151	- 0.632 1.0	- 0.0048-0.0214
Amaefule [A.2]	Aqueous Oil (M.E.)	2.05 1.43	0.20 0.02	0.96 1.0	0.010-0.014
Fulcher [F.4]	Aqueous (M.E.) Oil	1.01 1.35	0.320 0.0	0.90 1.0	0.009-0.011
Torabzadeh [T.7]	Aqueous (M.E.) Oil	1.94 3.75	0.213 0.236	0.180 0.823	0.0006-0.0017
Delshad [D.8]	Brine Oil M.E.	1.29 - 0.63	0.108 0.0 0.354	0.634 - 1.0	0.0089-0.023
Delshad [D.8]	Brine Oil M.E.	1.30 - 0.56	0.170 0.0 0.287	0.714 - 1.0	0.0073-0.033
Delshad [D.6]	Brine Oil M.E.	1.65 - 0.40	0.079 0.015 0.203	0.85 - 1.077	0.020
Delshad [D.6] with polymer	Brine Oil M.E.	1.37 - 0.603	0.033 0.015 0.165	0.887 - 1.187	0.0070

Table 6.3.3.3

Parameters for Low Capillary Number Relative Permeability Curves

Experimentalist	Phase	Exponent	Residual Saturation	End-Point	Capillary Number
Delshad [D.8]	Brine	1.50	0.40	0.062	10^{-6}
	Oil	1.41	0.352	0.80	
Amaefule [A.2]	Brine	2.09	0.40	0.150	3.4×10^{-6}-1.4×10^{-5}
	Oil	2.59	0.20	0.840	
Fulcher [F.4]	Brine	1.26	0.33	0.10	2.4×10^{-6}-6.7×10^{-6}
	Oil	1.37	0.368	0.70	
Torabzadeh [T.7]	Brine	1.42	0.279	0.089	4.4×10^{-6}-1.8×10^{-5}
	Oil	1.47	0.317	0.713	

Table 6.3.3.4

Properties of Berea Cores and Fluids used in Similar Microemulsion/Excess Brine Experiments

	Delshad [D.8] III-MM/B	Delshad [D.8] IV-MM/B	Delshad [D.6] MB	Amaefule [A.2]
Porous Medium	Berea	Berea	Berea	Fired Berea
Length (cm)	60.96	60.96	60.96	9.60
Porosity (fraction)	0.193	0.193	0.230	0.214
Pore Volume (cm^3)	304.75	304.75	363.00	10.43
Ref. Permeability (Darcy)	0.231	0.231	0.826	0.231
Total Flow Rate (cm^3/min)	0.66	0.64	variable	2.0
Temperature (°C)	30	30	30	25
Core Orientation	vertical	vertical	vertical	horizontal
Fluid System	three-phase	three-phase	three-phase	two-phase
IFT (dyne/cm)	0.0009	0.00028	0.00094	0.01
IFT reducer	TRS 10-410	TRS 10-410	TRS 10-410	Igepal CO430
Capillary Number	0.0089-0.023	0.0073-0.033	0.02	0.010-0.014
Residual Excess Brine Saturation	0.108	0.170	0.079	0.20
Residual Excess Oil Saturation	0.0	0.0	0.015	-
Residual Microemulsion Saturation	0.354	0.287	0.203	0.020

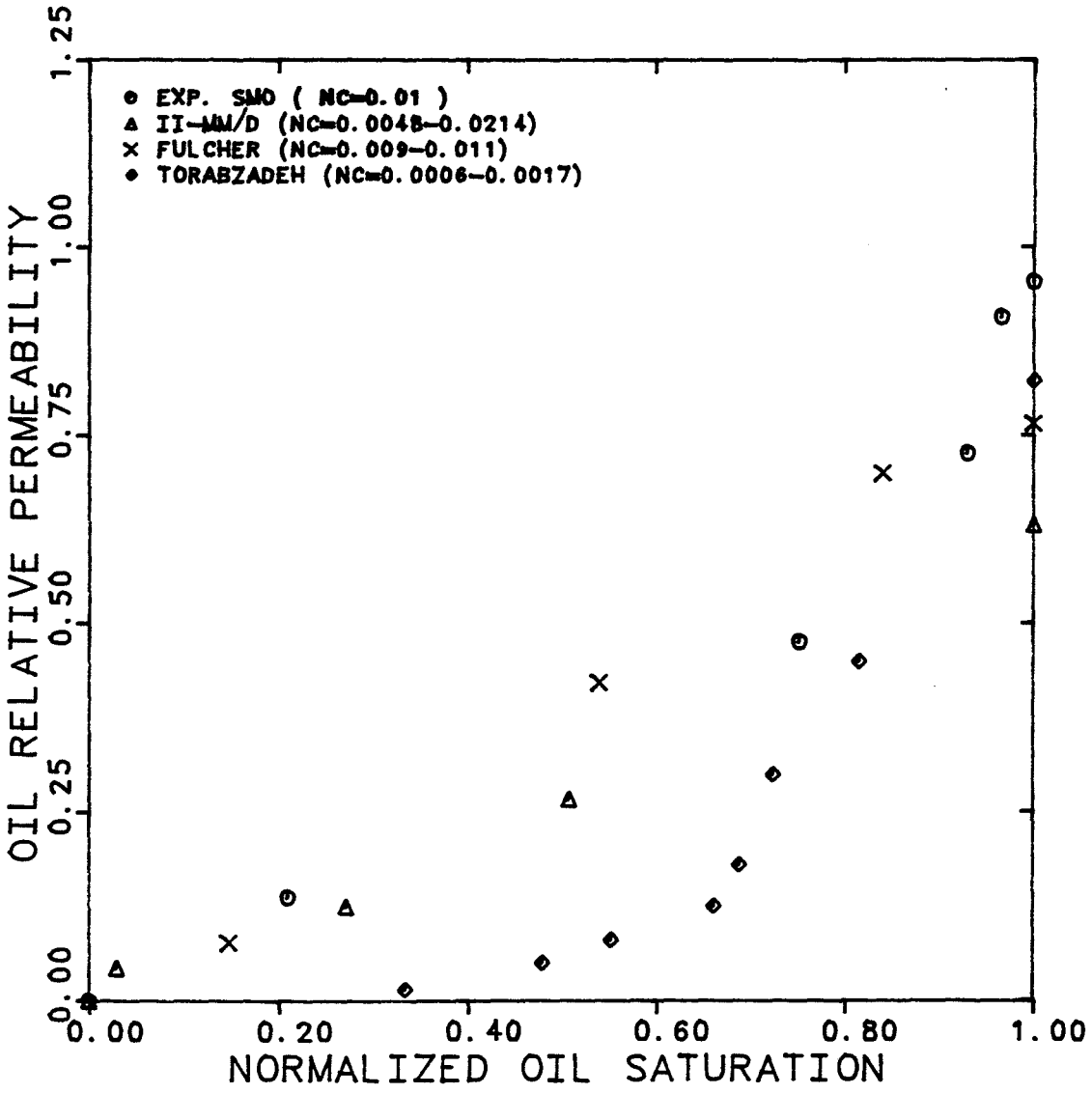

Figure 6.3.3.1 Comparison of Oil Relative Permeability Curves for Two-Phase M.E. or Aqueous/ Oil Experiments

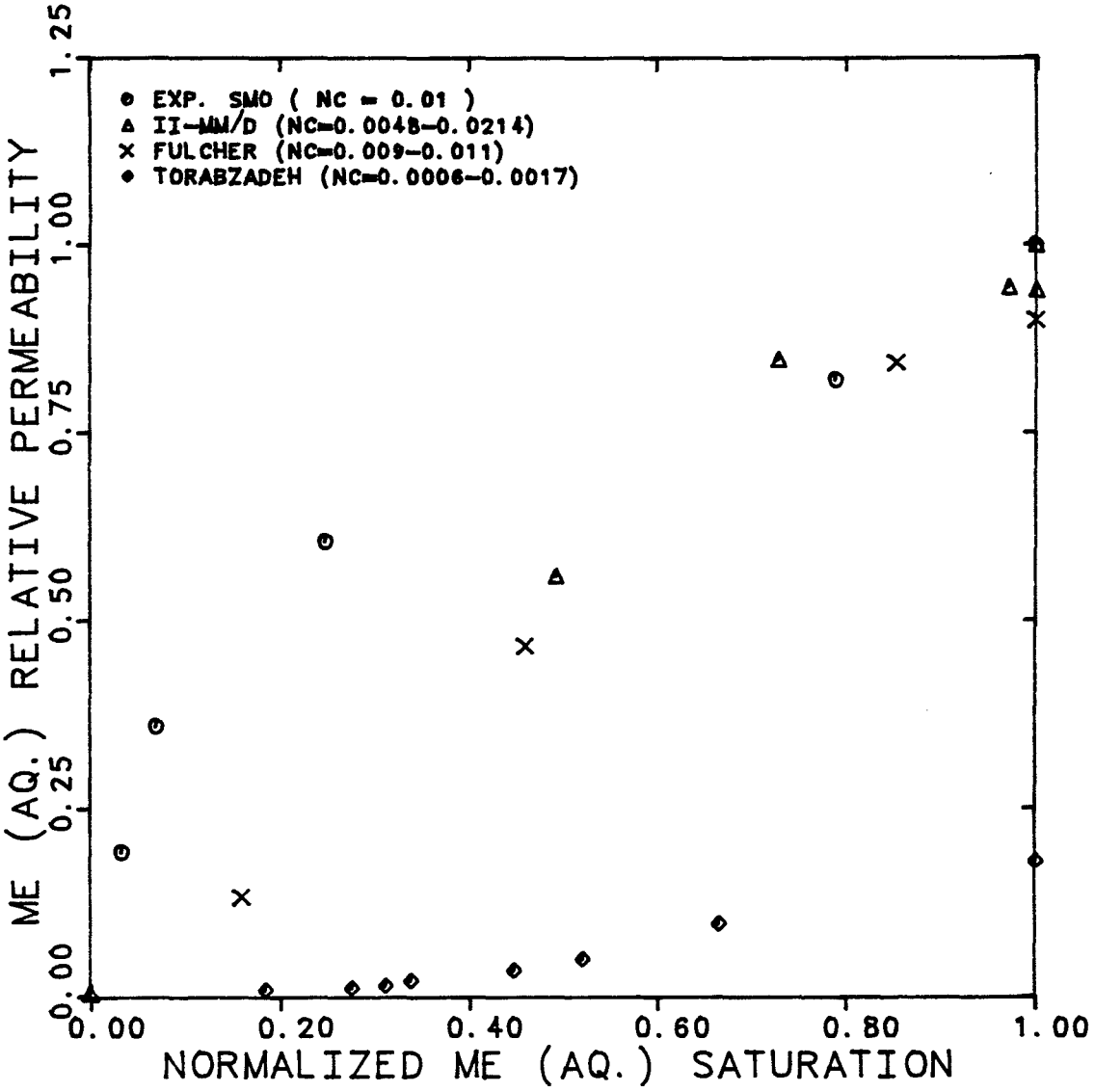

Figure 6.3.3.2 Comparison of M.E. or Aqueous Relative Permeability Curves for Two-Phase M.E. or Aqueous/Oil Flow

MICROEMULSION / EXCESS BRINE

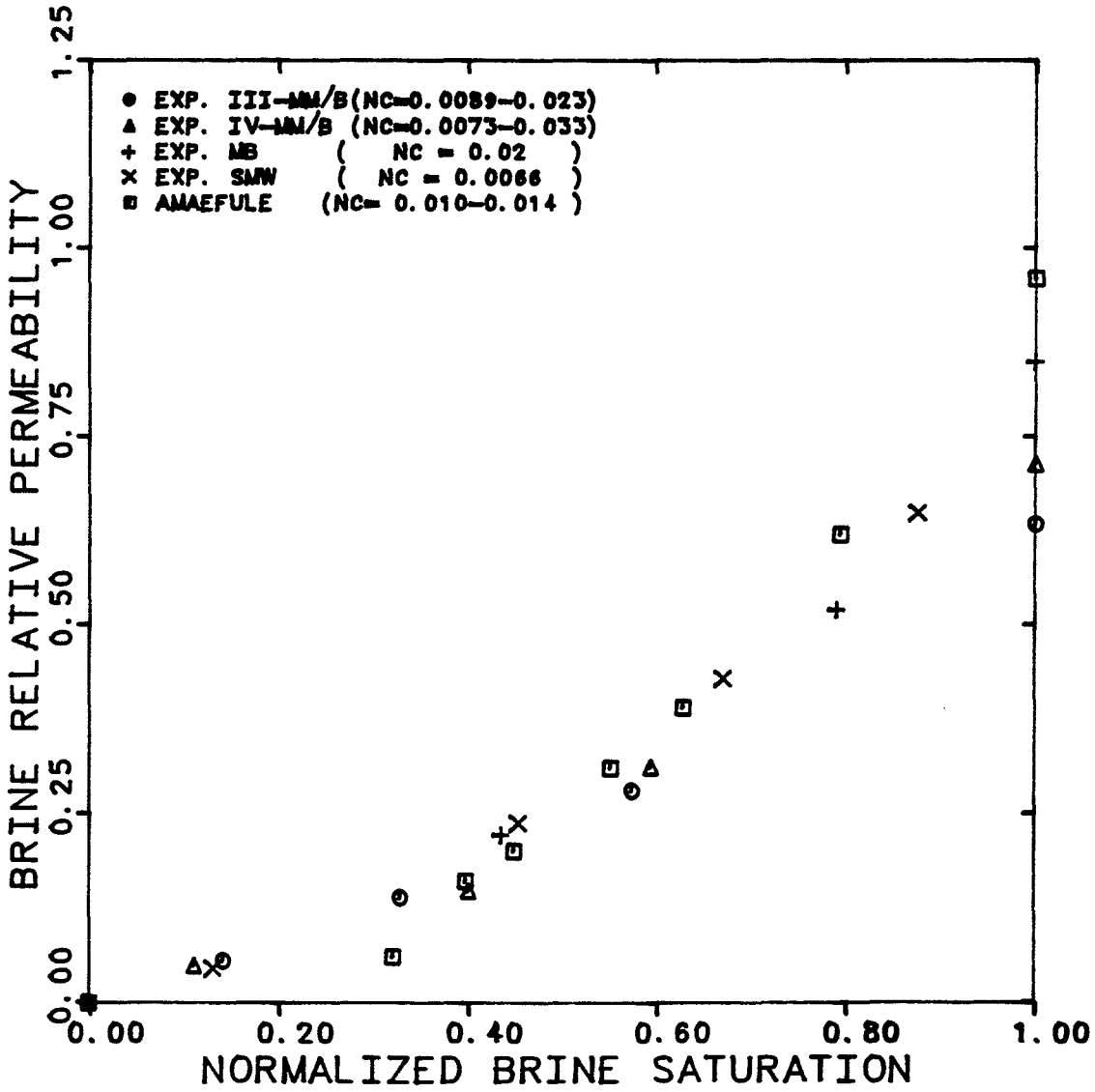

Figure 6.3.3.3 Comparison of Brine Relative Permeability Curves for Two-Phase M.E./Excess Brine Experiments

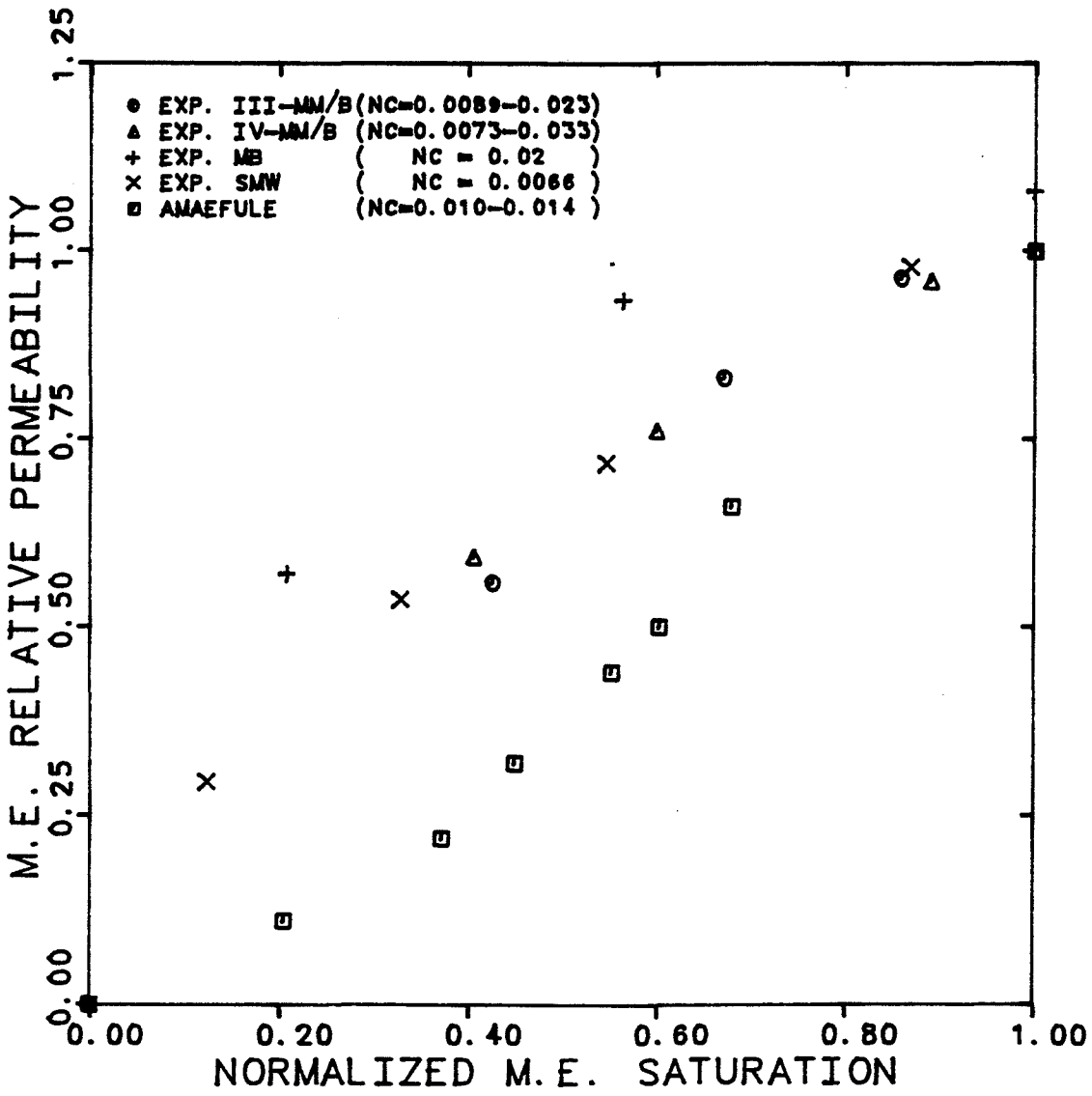

Figure 6.3.3.4 Comparison of M.E. Relative Permeability Curves for Two-Phase M.E./Excess Brine Experiments

6.3.4 A Comparison of the Computed Two-Phase Relative Permeabilities using Amaefule's Expression and Experimental Data

In addition to the exponential relative permeaiblity function (Eq. 6.5) discussed in Section 6.3.1, the microemulsion/oil and microemulsion/brine relative permeability curves were matched against the relative permeability expression used by Amaefule and Handy [A.2]. These relative permeability relationships (Eqs. 2.1 and 2.2) discussed in Chapter 2 (Section 2.1.1) have two matching parameters for each phase. Parameters n and b are for the wetting phase whereas p and a are selected for the non-wetting phase. For the microemulsion/oil data (Exp. SMO) these values are $n = 0.50$, $b = 1.34$, $p = 3.0$, and $a = 0.89$. Figure 6.3.4.1 compares the experimental data with the computed oil and microemulsion relative permeabilities using Equations 2.1 and 2.2 with the above matching parameters.

The matching parameters for the microemulsion/brine relative permeabilities (Exp. SMW) are $n = 0.6$, $b = 1.47$ for the microemulsion phase and $p = 3.0$, $a = 0.695$ for the excess brine phase. A comparison of the computed and experimental microemulsion and excess brine phases is in Figure 6.3.4.2.

An statistical analysis of the two, two-parameter relative permeability expressions showed that

- The expression used by Amaefule and Handy fits the data of both oil and microemulsion better (with smaller standard deviation) than the exponential relative permeability function.

- The data of both excess brine and microemulsion were matched better with the exponential function than the parametric expression used by Amaefule and Handy.

- The exponents found for the microemulsion relative permeability curve in both SMW and SMO experiments are nearly the same in both models (Table 6.3.1.4).

EXPERIMENT NUMBER	SMO
CAPILLARY NUMBER	0.01
TEMPERATURE	30°C
RESIDUAL BRINE	0.117

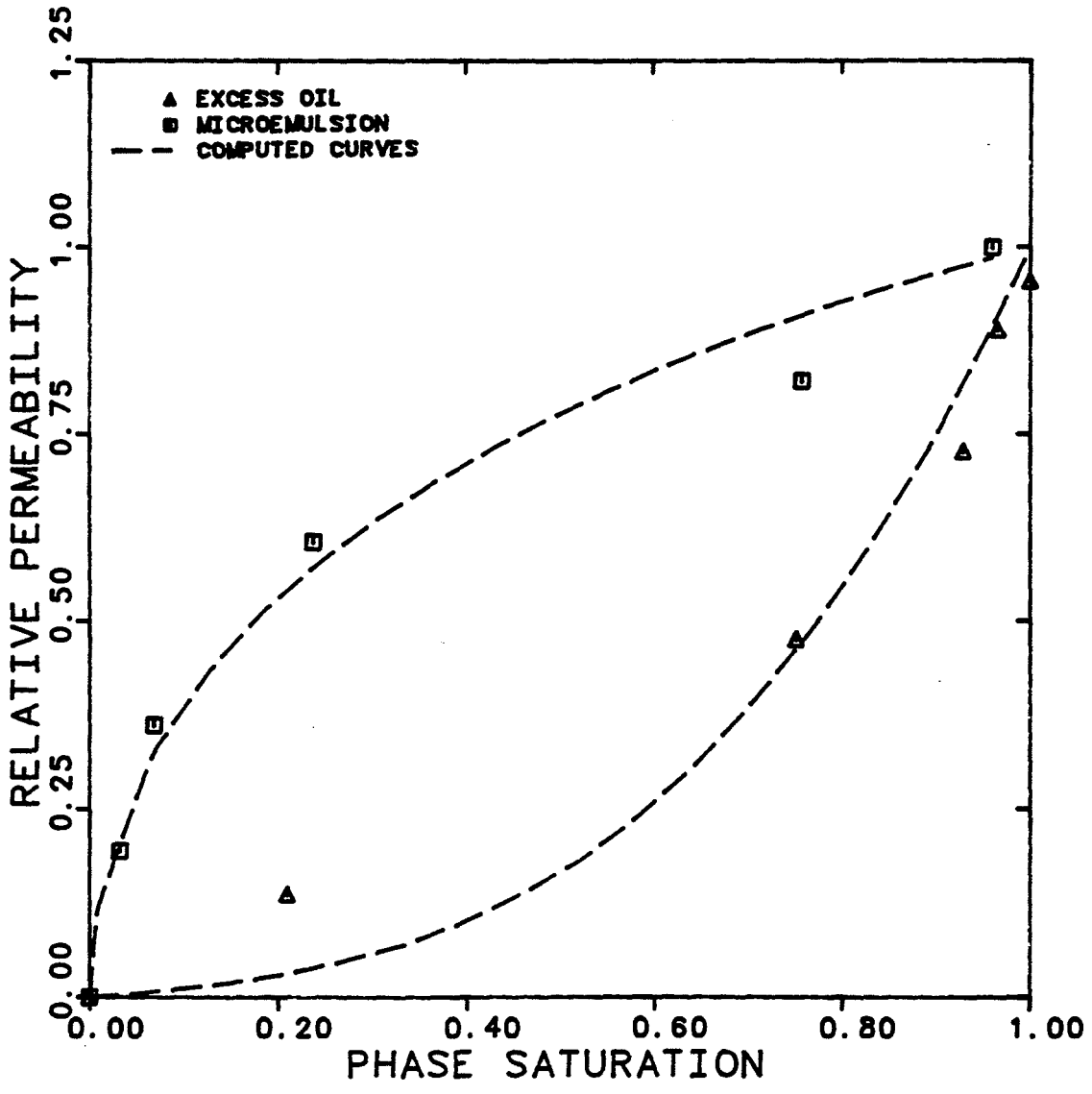

Figure 6.3.4.1 Comparison of Computed M.E./Excess Oil Relative Permeabilities using Amaefule's Expression with the Experimental Data

EXPERIMENT NUMBER	SMW
CAPILLARY NUMBER	0.0066
TEMPERATURE	30° C
RESIDUAL OIL	0.033

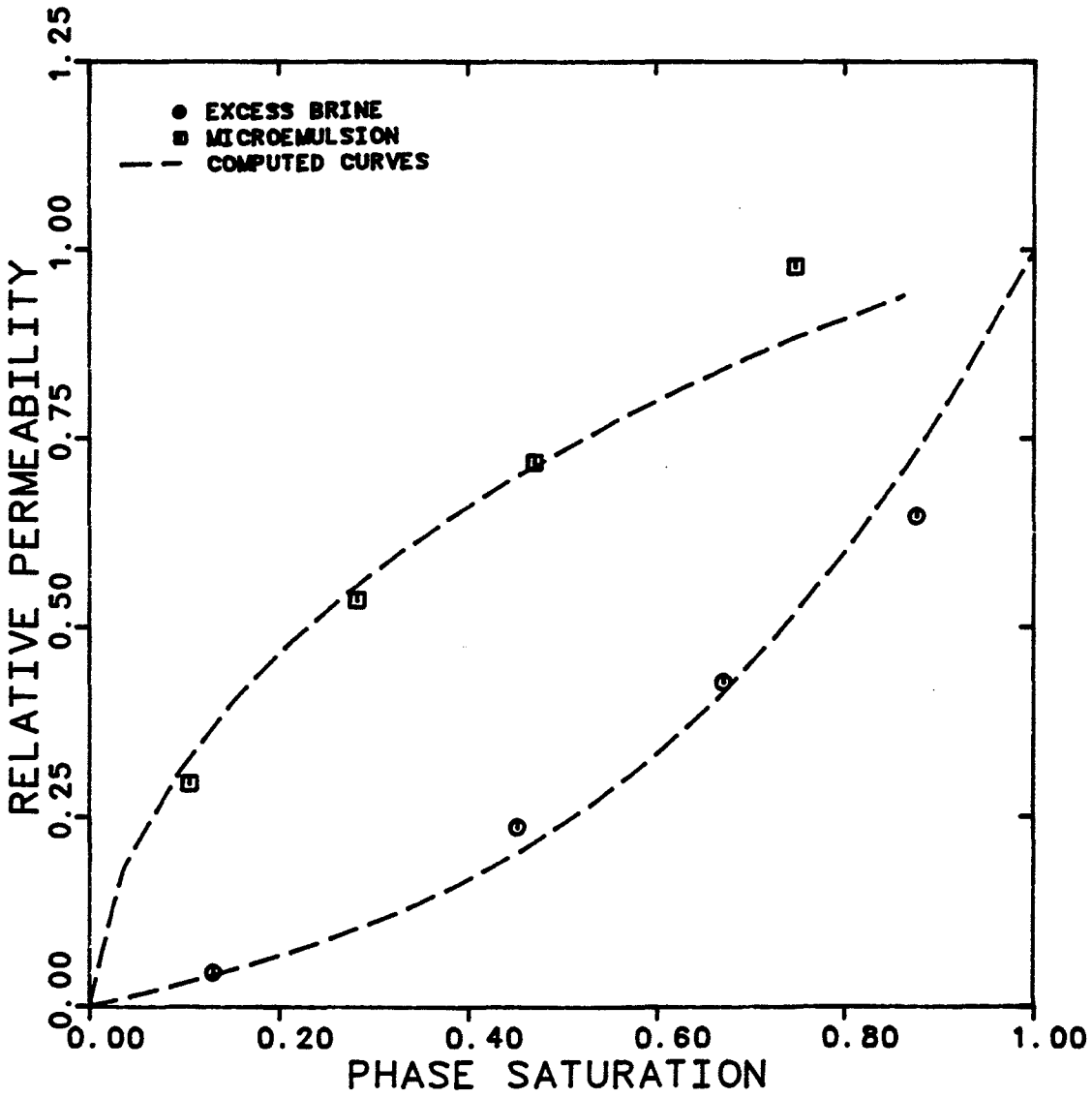

Figure 6.3.4.2 Comparison of Computed M.E./Excess Brine Relative Permeabilities using Amaefule's Expression with the Experimental Data

6.4 Three-Phase Flow Experiments

Three-phase flow experiments were performed at a constant nominal capillary number of 10^{-2}. To design the floods such that the capillary number remains constant, the following was done:

1- Select the saturation sequence for the experiment.

2- Read the endpoint relative permeabilities and residual phase saturations from the results of capillary desaturation experiment (Figures 6.2.37 and 6.2.38) at the selected capillary number.

3- Find the exponents of microemulsion and excess oil phase relative permeability curves from two-phase data [D.8].

4- Estimate the microemulsion and excess oil relative permeabilities using Equation 6.5. The exponents, saturations, residual saturations and endpoint relative permeabilities are known from the previous steps.

5- Estimate the excess brine relative permeabilities using a modified version of Lake's three-phase relative permeability model.

6- Estimate the potential drop for each phase from

$$\Delta\Phi_j = \frac{N_{cj} L \sigma_{ij}}{k} \qquad i \neq j$$

7- Estimate the fractional flows (cuts) and total flow rate for the selected saturations using Darcy's equation. These values were then used as the nominal flow rates injected.

Appendix C gives a numerical example.

6.4.1 Excess Brine/Microemulsion/Excess Oil (Exp. No. BMO1)

- Cut Numbers BMO1-2 and BMO1-4

The same core and coreflood setup were used as in the previous experiments (Table 6.2.1 and Figure 5.1.8). A new batch (number 4) of micellar solution with the salinity of 1.2 wt% NaCl was made up. Table 6.1.1 gives the properties of this batch. Tracers used in this experiment were tritium and carbon-14 labelled n-decane.

The three-phase flow experiments, using the estimated fractional flows (cuts) and total flow rate were begun and run for the predicted saturations. The experimental protocol was as follow:

- Inject the fluids at the pre-selected nominal cuts until steady-state is attained. One can calculate the actual phase cut using the volume of steady-state

effluent samples.

- Verify the steady-state condition by comparing the composition of the effluent samples with that of the injected fluids.

- Inject radioactive-labelled phases at steady-state. Analyze the effluent samples to determine the dispersion curve characteristics.

- Match the dispersion curves against the theoretical curves of both the C-D equation and capacitance-dispersion model to estimate the saturations and dispersivities.

Table 6.4.1.1 gives the actual cuts, total flow rates, material balance estimate of phase saturations and relative permeabilities. Listed in Table 6.4.1.2 are the total fluids injected (PV) to reach steady-state and flush out the tracers in the core from the previous dispersion run and the potential drop across all the sections of the core measured at steady-state.

The potential drop across the middle section was used to calculate the relative permeabilities and capillary numbers. Given in Table 6.4.1.3 are the capillary numbers and relative mobilities calculated for all three phases.

The dispersion results of these two experiments

(BMO1-2, BMO1-4) are in Figures 6.4.1.1 through 6.4.1.4. For reasons discussed later, the dispersion curves for the microemulsion phases in these experiments are not available. Breakthrough curves were first compared with the solution of the C-D equation (dashed curves). The saturations obtained once again did not add up to one. Table 6.4.1.4 presents the saturations and dispersion estimated using the C-D equation. The total fluids injected for the dispersion runs are also in Table 6.4.1.4.

The breakthrough curves were then compared with the theoretical curve of capacitance-dispersion model (solid curves). The parameters used in the model such as phase saturations, phase flowing fractions, mass transfer coefficients, and dispersivities are shown in Table 6.4.1.5. The sum of saturations estimated from the capacitance model do add up to one. The saturations of excess brine and oil estimated from the C-D equation are lower than the actual values (capacitance or material balance estimates) since this equation does not allow for non-equilibrium or microscopic bypassing effects. Therefore, the C-D equation estimates only the flowing saturation ($S_j^f = F_j S_j$) not the in-situ saturation (S_j). The flowing saturations calculated using the flowing

fractions and saturations estimate of capacitance model agree remarkably well with the total saturations estimate of the C-D equation.

Calculated dispersion coefficients, frontal flowing velocities and percent tracer recoveries are in Table 6.4.1.5. The breakthrough curves of carbon-14 and tritium were both matched with a mass transfer coefficient of 10^{-7} sec^{-1}. The flowing fractions of microemulsion, excess brine, and excess oil in these two cuts were constant and equal to 1.0, 0.9, and 0.7 consecutively. Or in other words, there is no capacitance associated with the microemulsion phase, but only about 90% and 70% of the in-situ excess brine and excess oil saturations are flowing, respectively.

Relative permeabilities and relative mobilities are plotted and shown with the data of experiment BMO2 in the next subsection.

- Experimental Difficulties and Observations

There was about 30 days of time lag between the previous experiment (SMW-8) and experiment BMO1-2. Because of this time lag and the change in phase behavior due to calcium leaching, material balance saturations for the cut BMO1-2 were based on the dispersion results of this specific cut.

The dispersion analysis of the middle phase for these experiments could not be accomplished due to the extremely low microemulsion-phase cut used in the experiments (0.045 and 0.035). The produced volumes of microemulsion were not large enough to allow removal of a sufficient volume for analysis without contamination by an adjacent phase.

When tracers used are only two partitioning ones, the trial and error procedure to match the tracer histories against the capacitance model can be very time consuming. There are a total of twelve parameters that must be estimated in order to obtain good agreement between experimental and theoretical breakthrough curves. These parameters are phase saturations (2) since $\sum_{j=1}^{3} S_j = 1.0$, phase flowing fractions (3), dispersivities (3), and mass transfer coefficients (4). The number of parameters reduces to nine by making the assumption that the microemulsion phase has no capacitance ($F_3 = 1.0$, $M_{13} = M_{23} = 0.0$) since it is the apparent wetting phase based on capillary desaturation data. To further investigate the possibility that microemulsion does not show any capacitance, a non-partitioning surfactant tracer is required in the microemulsion phase. This would also speed up the matching procedure.

- Cut Numbers BMO1-6 and BMO1-8

A new batch (number 6) of cold micellar solution was made up at 1.2 wt% NaCl with the properties listed in Table 6.1.1. Due to the reasons discussed in the previous cuts (BMO1-2, BMO1-4), a 2-liter batch of micellar solution with three tracers was made up. The tracers were carbon-14 labelled decane, chloride-36 labelled sodium chloride, and tritium labelled sulfonate. The properties of this batch (number 6) are in Table 6.1.1. The partition coefficients for chloride-36, carbon-14 and tritium were 0.496, 0.465, and 0.05, consecutively. Tritium labelled sulfonate is a non-partitioning tracer for the microemulsion phase due to the low concentration of sulfonate in excess brine and oil phases (0.27 and 0.04 percent).

The three-phase flow experiment continued with the same experimental protocol as in the previous experiment. There was a lag time of about 30 days between the previous cuts and these new cuts.

Table 6.4.1.1 gives the fractional flows, total flow rate, material balance estimate of saturations and relative permeabilities. The total fluids injected to steady-state, the potential drops, the capillary numbers, and the relative mobilities are in Tables 6.4.1.2 and

6.4.1.3.

Figures 6.4.1.5 through 6.4.1.10 show the breakthrough curves. Five sets of breakthrough curves are presented for each cut which are carbon-14 in the excess oil and microemulsion, chloride-36 in the excess brine and microemulsion and tritium labelled sulfonate in the microemulsion phase. The theoretical curves of both the C-D equation and the capacitance-dispersion model are shown in these figures.

Table 6.4.1.4 shows the total fluids injected for the dispersion runs and phase saturations and dispersivities estimated from the C-D equation.

Chloride-36 and carbon-14 breakthrough curves deviate somewhat from the usual s-shaped curve and show capacitance behavior. The labelled sulfonate histories, on the other hand, are fairly symmetric and s-shaped.

Table 6.4.1.5 lists the capacitance parameters which gave the best agreement between the theoretical curves and experimental breakthrough curves. The calculated dispersion coefficients, flowing phase velocities, and tracer recoveries are in Table 6.4.1.5.

The microemulsion saturation estimated from matching the tritium breakthrough curve of experiment BMO1-8 with the C-D equation was in good agreement with

the material balance estimate. But, the saturation estimate of the C-D equation for both excess oil and excess brine were low when compared with the material balance estimate. Microscopic bypassing was considered as the prime possibility for this anomaly. Therefore, in order to better fit the data and improve the estimate of saturations the breakthrough curves were matched with the capacitance model.

The breakthrough curves of the partitioning tracers (carbon-14 or chloride-36) in the microemulsion and excess phases are almost identical since we are plotting the concentration of these tracers in the flowing portion of the phase. The breakthrough curves of carbon-14 and chloride-36 were both matched with a mass transfer coefficient of 10^{-7} sec^{-1}. The flowing fractions of the excess brine and excess oil in these two cuts were found to be 0.9 and 0.7 respectively.

Relative permeabilities and mobilities are plotted and shown along with the data of experiment BMO2 in the next subsection.

The concentration of Ca^{++} and Mg^{++} in both microemulsion and excess brine phases are measured and plotted as a function of total pore volumes fluid injected in Figures 6.4.1.11 and 6.4.1.12. When the core

was shut in for 30 days, the concentration of calcium and magnesium in both microemulsion and excess brine phases increased over its initial value. For example, the concentration of calcium in the effluent microemulsion sample after about 2 pore volumes was 53 ppm but it reduced to about 25 ppm after 6 pore volumes fluid injection.

Alcohol, water, and n-decane concentrations in the produced microemulsion phase were measured by Gas Chromatography (Figure 6.4.1.13). The concentration of water in the microemulsion phase before steady-state (about 2 pore volumes) was much lower than that of the injected value. This might be because of the change in phase behavior due to the very high concentration of Ca^{++} (see Figure 6.4.1.11). The concentration of IBA, water, and n-decane in the effluent microemulsion samples at steady-state are close to those of the injected values.

TABLE 6.4.1.1
Excess Brine/Microemulsion/Excess Oil Relative Permeabilities
Material Balance Results (Steady-State)
(Experiment BMO)

Experiment Number	Phase Fractional Flow			Total Flow Rate (cm^3/min)	Phase Saturation			Phase Relative Permeability (1)		
	Brine	Oil	M.E.		Brine	Oil	M.E.	Brine	Oil	M.E.
BMO1-2*	0.771	0.185	0.044	0.766	0.580	0.280	0.140	0.448	0.147	0.156
BMO1-4	0.510	0.455	0.035	0.689	0.487	0.398	0.115	0.278	0.347	0.119
BMO1-6*	0.375	0.334	0.291	0.40	0.20	0.323	0.477	0.132	0.166	0.589
BMO1-8	0.586	0.249	0.165	0.532	0.440	0.290	0.270	0.302	0.190	0.494
BMO2-2	0.0	0.0	1.0	1.02	0.032	0.0	0.968	0.0	0.0	0.932
BMO2-4	0.772	0.088	0.140	0.906	0.448	0.229	0.323	0.429	0.061	0.439
BMO2-6	0.676	0.190	0.134	0.887	0.365	0.342	0.293	0.374	0.130	0.418
BMO2-8	0.260	0.630	0.110	1.11	0.215	0.546	0.239	0.151	0.437	0.353
BMO2-10	0.263	0.436	0.301	0.678	0.231	0.321	0.448	0.113	0.236	0.732
BMO2-12	0.167	0.144	0.689	0.45	0.207	0.221	0.572	0.041	0.042	0.931
BMO2-14	0.56	0.07	0.370	0.604	0.430	0.170	0.399	0.221	0.043	0.797
BMO2-16	0.40	0.120	0.480	0.480	0.215	0.090	0.695	0.124	0.047	0.845
BMO2-18	0.564	0.104	0.332	0.620	0.430	0.169	0.401	0.219	0.051	0.734
BMO2-20	0.697	0.08	0.223	0.75	0.542	0.231	0.227	0.330	0.047	0.596
BMO2-22	0.831	0.035	0.134	0.789	0.730	0.046	0.224	0.413	0.022	0.377
BMO3-3*	0.0	1.0	0.0	0.997	0.150	0.820	0.03	0.0	0.940	0.0
BMO3-6	0.0	0.0	1.0	0.50	0.120	0.0	0.880	0.0	0.0	1.0
BMO3-8	0.289	0.653	0.058	1.73	0.371	0.436	0.193	0.211	0.541	0.220
BMO3-10	0.359	0.294	0.347	1.04	0.314	0.214	0.472	0.158	0.174	0.668
BMO3-12	0.50	0.027	0.473	0.827	0.373	0.157	0.470	0.178	0.011	0.868
BMO3-14	0.719	0.013	0.268	1.11	0.467	0.159	0.374	0.349	0.007	0.671
BMO3-16	0.84	0.015	0.145	1.45	0.577	0.159	0.264	0.524	0.010	0.467
BMO3-18*	0.89	0.013	0.097	1.494	0.705	0.065	0.230	0.582	0.0095	0.327
BMO3-20	1.0	0.0	0.0	1.575	0.880	0.037	0.048	0.931	0.0	0.0

(1) Permeabilities were normalized to M.E. permeability (k = 0.936 D)
* Saturations are from the capacitance model

TABLE 6.4.1.2
Excess Brine/Microemulsion/Excess Oil Relative Permeabilities
Pressure Drop Results (Steady-State)
(Experiment BMO)

Experiment Number	Phase Potential Drop (1) (psi/ft)			Phase Potential Drop (2) (psi/ft)			Phase Potential Drop (3) (psi/ft)			Total Pore Volumes Inj. (P.V.)
	Brine	Oil	M.E.	Brine	Oil	M.E.	Brine	Oil	M.E.	
BMO1-2	0.371	0.253	0.30	0.45	0.332	0.38	0.351	0.233	0.28	4.6
BMO1-4	0.356	0.237	0.285	0.43	0.312	0.36	0.351	0.233	0.28	3.65
BMO1-6	0.350	0.230	0.297	0.36	0.24	0.31	0.36	0.24	0.31	6.86
BMO1-8	0.319	0.20	0.267	0.42	0.30	0.37	0.32	0.20	0.27	5.49
BMO2-2	-	-	1.64	-	-	1.70	-	-	1.76	3.48
BMO2-4	0.502	0.382	0.442	0.58	0.46	0.52	0.46	0.34	0.40	5.33
BMO2-6	0.494	0.375	0.435	0.58	0.46	0.52	0.48	0.36	0.42	4.58
BMO2-8	0.589	0.470	0.530	0.66	0.54	0.60	0.60	0.48	0.54	4.62
BMO2-10	0.486	0.367	0.427	0.60	0.48	0.54	0.54	0.42	0.48	3.78
BMO2-12	0.568	0.450	0.510	0.68	0.56	0.62	0.60	0.48	0.54	4.12
BMO2-14	0.475	0.355	0.415	0.66	0.54	0.60	0.50	0.38	0.44	3.94
BMO2-16	0.475	0.355	0.415	0.66	0.54	0.60	0.50	0.38	0.44	3.20
BMO2-18	0.49	0.37	0.43	0.68	0.56	0.62	0.51	0.39	0.45	3.17
BMO2-20	0.49	0.37	0.43	0.66	0.54	0.60	0.50	0.38	0.44	4.40
BMO2-22	0.49	0.37	0.43	0.66	0.54	0.60	0.54	0.42	0.48	7.10
BMO3-3	-	0.290	-	-	0.34	-	-	0.30	-	5.40
BMO3-6	-	-	0.704	-	-	0.744	-	-	0.704	4.74
BMO3-8	0.70	0.58	0.644	0.76	0.64	0.70	0.72	0.60	0.66	4.32
BMO3-10	0.70	0.58	0.644	0.74	0.62	0.68	0.66	0.54	0.60	2.60
BMO3-12	0.69	0.57	0.634	0.72	0.60	0.66	0.62	0.50	0.58	3.15
BMO3-14	0.68	0.56	0.624	0.72	0.60	0.66	0.65	0.53	0.59	4.69
BMO3-16	0.69	0.57	0.634	0.74	0.62	0.68	0.69	0.57	0.63	2.0
BMO3-18	0.68	0.56	0.624	0.72	0.60	0.66	0.66	0.54	0.60	4.32
BMO3-20	0.50	-	-	0.56	-	-	0.48	-	-	2.0

(1) Pressure drop measured across the center section of the core (1.0 foot)
(2) Pressure drop measured across the inlet (0.5 foot)
(3) Pressure drop measured across the outlet (0.5 foot)

Density of fluid in the line = 0.725 g/cc

TABLE 6.4.1.3
Excess Brine/Microemulsion/Excess Oil Relative Mobilities
(Experiment BMO)

Experiment Number	Relative Mobility (cp^{-1})				Capillary Number $N_{cj} = \frac{k\Lambda\Phi_j}{L\sigma}$					Phase Viscosity (cp)		
							M.E. using					
	Brine	Oil	M.E.	Total	Brine	Oil	σ_{mw}	σ_{mo}	σ_{ave}	Brine	Oil	M.E.
BMO1-2	0.498	0.175	0.0346	0707	0.0076	0.0138	0.006	0.016	0.011	0.900	0.84	4.5
BMO1-4	0.309	0.413	0.0264	0748	0.0073	0.0129	0.0058	0.0156	0.0107	0.900	0.84	4.5
BMO1-6	0.133	0.180	0.122	0.435	0.0057	0.0047	0.0049	0.006	0.0055	0.990	0.92	4.81
BMO1-8	0.305	0.206	0.103	0.614	0.0052	0.0041	0.0044	0.0055	0.0050	0.990	0.92	4.81
BMO2-2	-	-	0.194	0.194	-	-	0.033	0.033	0.033	-	-	4.81
BMO2-4	0.435	0.065	0.089	0.589	0.0107	0.0082	0.0095	0.0095	0.0095	0.986	0.94	4.9
BMO2-6	0.379	0.138	0.085	0.602	0.0105	0.0080	0.0093	0.0093	0.0093	0.986	0.94	4.9
BMO2-8	0.153	0.465	0.072	0.690	0.0126	0.010	0.011	0.011	0.011	0.986	0.94	4.9
BMO2-10	0.115	0.251	0.149	0.515	0.0104	0.0078	0.009	0.009	0.009	0.986	0.94	4.9
BMO2-12	0.041	0.0446	0.190	0.275	0.0120	0.0096	0.0109	0.0109	0.0109	0.986	0.94	4.9
BMO2-14	0.224	0.046	0.162	0.433	0.0106	0.0076	0.009	0.009	0.009	0.986	0.94	4.9
BMO2-16	0.126	0.050	0.172	0.348	0.0106	0.0076	0.009	0.009	0.009	0.983	0.94	4.9
BMO2-18	0.223	0.054	0.149	0.426	0.0109	0.0079	0.0093	0.0093	0.0093	0.983	0.94	4.9
BMO2-20	0.335	0.050	0.121	0.506	0.0109	0.0079	0.0093	0.0093	0.0093	0.983	0.94	4.9
BMO2-22	0.420	0.023	0.077	0.520	0.0109	0.0079	0.0093	0.0093	0.0093	0.983	0.94	4.9
BMO3-3	-	1.05	-	1.050	-	0.033	-	-	-	-	0.89	4.5
BMO3-6	-	-	0.205	0.205	-	-	0.014	-	0.014	-	0.89	4.5
BMO3-8	0.222	0.608	0.049	0.879	0.0144	0.010	0.013	0.011	0.012	0.950	0.89	4.5
BMO3-10	0.166	0.195	0.148	0.509	0.0144	0.010	0.013	0.011	0.012	0.950	0.89	4.5
BMO3-12	0.187	0.0123	0.193	0.392	0.0144	0.010	0.013	0.011	0.012	0.950	0.89	4.5
BMO3-14	0.367	0.0078	0.149	0.524	0.0140	0.0098	0.0128	0.0109	0.00118	0.950	0.89	4.5
BMO3-16	0.551	0.011	0.104	0.665	0.0144	0.010	0.013	0.011	0.012	0.950	0.89	4.5
BMO3-18	0.612	0.0106	0.0726	0.695	0.0140	0.0098	0.0128	0.0109	0.0118	0.950	0.89	4.5
BMO3-20	0.980	-	-	0.980	0.0100	-	-	-	-	0.950	-	-

Micellar batch nos. 4, 5, 7, 9, 13, 14 used

Table 6.4.1.4
Dispersion Data of Excess Brine/Microemulsion/Excess Oil Experiment
Convection-Dispersion Results
(Experiment BMO)

Experiment Number	Phase Saturation				Dispersivity (cm)				Total Pore Volumes Inj. (P.V.)
	Brine	Oil	M.E.	Total	T_2O	^{36}Cl	^{14}C	T.S.	
BMO1-2	0.560	0.190	0.140	0.890	0.890	-	9.2	-	4.90
BMO1-4	0.360	0.334	0.130	0.824	1.0	-	1.0	-	2.87
BMO1-6	0.160	0.20	0.477	0.837	-	6.10	12.10	1.34	3.31
BMO1-8	0.310	0.20	0.290	0.80	-	3.3	17.0	1.95	5.68
BMO2-2	0.03	0.0	0.970	1.0	-	0.140	0.23	0.29	2.85
BMO2-4	0.445	0.166	0.294	0.905	-	2.50	2.90	1.47	5.86
BMO2-6	0.397	0.180	0.277	0.854	-	5.60	10.8	1.75	5.98
BMO2-8	0.220	0.371	0.208	0.799	-	9.30	12.30	2.65	5.89
BMO2-10	0.240	0.240	0.433	0.913	-	10.2	8.0	2.32	2.98
BMO2-12	0.220	0.087	0.654	0.961	-	13.0	4.50	1.64	3.30
BMO2-14	0.30	0.072	0.547	0.919	-	19.9	4.80	1.51	2.89
BMO2-16	0.210	0.104	0.615	0.929	-	12.5	5.0	2.33	3.75
BMO2-18	0.290	0.131	0.461	0.882	-	10.2	4.40	1.31	4.43
BMO2-20	0.383	0.143	0.379	0.905	-	4.5	1.20	1.78	4.94
BMO2-22	0.484	0.062	0.280	0.826	-	3.40	3.20	1.38	6.42
BMO3-3	0.150	0.820	0.030	1.0	-	-	0.190	-	3.38
BMO3-6	0.027	0.0	0.973	1.0	-	0.08	0.140	0.27	2.35
BMO3-8	0.248	0.385	0.180	0.813	-	2.60	1.20	3.20	8.15
BMO3-10	0.260	0.110	0.519	0.889	-	15.0	5.60	3.0	3.43
BMO3-12	0.260	0.045	0.648	0.953	-	13.0	4.50	3.98	3.35
BMO3-14	0.306	0.041	0.493	0.840	-	4.0	2.10	3.25	3.81
BMO3-16	0.496	0.043	0.327	0.866	-	4.0	1.0	2.19	4.20
BMO3-18	0.600	0.048	0.230	0.878	-	3.5	1.4	2.89	5.60
BMO3-20	0.880	0.0	0.120	1.0	-	0.10	-	-	2.30

TABLE 6.4.1.5

Dispersion Data of Excess Brine/Microemulsion/Excess Oil Experiments
Capacitance Results
(Experiment BMO)

Experiment Number	Phase Saturation			Phase Flowing Fraction			Mass Transfer Coefficient (sec^{-1})		
	Brine	Oil	M.E.	Brine	Oil	M.E.	^{14}C	^{36}Cl or T_2O	S_1/S_2
BMO1-2	0.580	0.280	0.140	0.90	0.70	1.0	$1x10^{-7}$	$1x10^{-7}$	2.07
BMO1-4	0.402	0.468	0.130	0.90	0.70	1.0	$1x10^{-7}$	$1x10^{-7}$	0.86
BMO1-6	0.200	0.323	0.477	0.90	0.70	1.0	$1x10^{-7}$	$1x10^{-7}$	0.62
BMO1-8	0.400	0.310	0.290	0.90	0.70	1.0	$1x10^{-7}$	$1x10^{-7}$	1.27
BMO2-2	0.030	0.0	0.970	1.0	-	1.0	-	-	-
BMO2-4	0.497	0.209	0.294	0.90	0.70	1.0	$1x10^{-7}$	$1x10^{-7}$	2.37
BMO2-6	0.440	0.283	0.277	0.90	0.70	1.0	$1x10^{-7}$	$1x10^{-7}$	1.55
BMO2-8	0.292	0.50	0.208	0.90	0.70	1.0	$1x10^{-7}$	$1x10^{-7}$	0.58
BMO2-10	0.273	0.294	0.433	0.90	0.70	1.0	$1x10^{-7}$	$1x10^{-7}$	0.93
BMO2-12	0.243	0.103	0.654	0.90	0.70	1.0	$1x10^{-7}$	$1x10^{-7}$	2.35
BMO2-14	0.350	0.103	0.547	0.90	0.70	1.0	$1x10^{-7}$	$1x10^{-7}$	3.39
BMO2-16	0.246	0.139	0.615	0.90	0.70	1.0	$1x10^{-7}$	$1x10^{-7}$	1.77
BMO2-18	0.351	0.188	0.461	0.90	0.70	1.0	$1x10^{-7}$	$1x10^{-7}$	1.86
BMO2-20	0.428	0.193	0.379	0.90	0.70	1.0	$1x10^{-7}$	$1x10^{-7}$	2.22
BMO2-22	0.645	0.075	0.280	0.90	0.70	1.0	$1x10^{-7}$	$1x10^{-7}$	8.60
BMO3-3	0.150	0.820	0.030	-	1.0	1.0	0.0	-	0.18
BMO3-6	0.027	0.0	0.973	1.0	-	1.0	0.0	0.0	-
BMO3-8	0.280	0.540	0.180	0.90	0.70	1.0	$1x10^{-7}$	$1x10^{-7}$	0.52
BMO3-10	0.300	0.181	0.519	0.90	0.70	1.0	$1x10^{-6}$	$4x10^{-7}$	1.66
BMO3-12	0.300	0.052	0.648	0.90	0.70	1.0	$1x10^{-7}$	$1x10^{-7}$	5.77
BMO3-14	0.450	0.057	0.493	0.90	0.70	1.0	$1x10^{-7}$	$2x10^{-6}$	7.89
BMO3-16	0.623	0.050	0.327	0.90	0.70	1.0	$1x10^{-7}$	$1x10^{-7}$	12.46
BMO3-18	0.705	0.065	0.230	0.90	0.70	1.0	$1x10^{-7}$	$1x10^{-7}$	10.84
BMO3-20	0.880	0.0	0.120	1.0	-	1.0	-	0.0	-

TABLE 6.4.1.5 (continued)

Experiment Number	Dispersivity (cm)					Dispersion Coefficient (cm^2/sec)				
	T_2O or ^{36}Cl		^{14}C		T.S.	T_2O or ^{36}Cl		^{14}C		T.S.
	Brine	M.E.	Oil	M.E.	M.E.	Brine	M.E.	Oil	M.E.	M.E.
BMO1-2	1.11	1.0	5.7	4.0	-	0.0035	0.0007	0.0088	0.0029	-
BMO1-4	0.45	0.40	0.57	0.40	-	0.0012	0.0002	0.00028	0.0002	-
BMO1-6	6.66	6.0	10.0	7.0	1.34	0.015	0.0045	0.0160	0.0067	0.0010
BMO1-8	3.40	3.0	12.9	9.0	1.95	0.0077	0.0028	0.0133	0.0065	0.0018
BMO2-2	-	0.14	-	0.23	0.29	-	0.0004	-	0.0007	0.0009
BMO2-4	1.50	1.35	2.80	1.90	1.47	0.0012	0.0019	0.0024	0.0032	0.0019
BMO2-6	6.10	5.50	11.4	8.0	1.75	0.0252	0.0072	0.0210	0.0105	0.0023
BMO2-8	5.5	5.0	2.90	2.0	2.65	0.0171	0.0090	0.012	0.0036	0.0047
BMO2-10	10.0	9.0	5.0	3.5	2.32	0.020	0.0126	0.017	0.0050	0.0032
BMO2-12	12.0	10.8	4.5	3.1	1.64	0.010	0.0154	0.008	0.0043	0.0023
BMO2-14	16.7	15.0	5.70	4.0	1.51	0.0495	0.0180	0.0072	0.0048	0.0018
BMO2-16	11.1	10.0	5.70	4.0	2.33	0.033	0.0150	0.0072	0.0060	0.0035
BMO2-18	4.5	4.0	5.70	4.0	1.31	0.0135	0.0055	0.0059	0.0055	0.0018
BMO2-20	4.5	4.0	1.60	1.10	1.78	0.0167	0.0052	0.0016	0.0014	0.0023
BMO2-22	3.40	3.0	4.30	3.0	1.38	0.0099	0.0036	0.0047	0.0036	0.0016
BMO3-3	-	-	0.19	-	-	-	-	0.0007	-	-
BMO3-6	-	0.08	-	0.14	0.27	-	0.0001	-	0.0002	0.0004
BMO3-8	2.2	2.0	1.4	1.0	3.20	0.0121	0.0034	0.009	0.0024	0.0054
BMO3-10	11.1	10.0	4.30	3.0	3.0	0.0432	0.0210	0.009	0.0063	0.0063
BMO3-12	8.9	8.0	5.7	4.0	3.98	0.037	0.0149	0.007	0.0074	0.0074
BMO3-14	3.3	3.0	2.9	2.0	3.25	0.0204	0.0054	0.0022	0.0036	0.0058
BMO3-16	3.3	3.0	1.1	0.8	2.19	0.0201	0.0057	0.0015	0.0015	0.0042
BMO3-18	2.2	2.0	1.4	1.0	2.89	0.0130	0.0038	0.0013	0.0019	0.0055
BMO3-20	0.10	-	-	-	-	0.00055	-	-	-	-

TABLE 6.4.1.5 (continued)

Experiment Number	Flowing Phase Velocity (cm/sec) $v_j^f = \frac{qf_j}{A\phi S_j F_j}$ Brine	Oil	M.E.	Tracer Recovery (%) T_2O or ^{36}Cl	^{14}C	T.S.	# on Ternary
BMO1-2	0.0035	0.0022	0.00073	97.0	99.7	-	1
BMO1-4	0.0030	0.00073	0.00057	97.1	100.0	-	2
BMO1-6	0.0025	0.0018	0.00075	97.0	100.0	93.0	3
BMO1-8	0.0026	0.0019	0.00093	100.0	100.0	85.3	4
BMO2-2	-	-	0.0032	97.0	97.5	98.3	5
BMO2-4	0.00081	0.0012	0.0013	98.0	97.0	95.4	6
BMO2-6	0.0047	0.0026	0.00132	96.3	100.0	100.0	7
BMO2-8	0.0034	0.006	0.0018	96.5	100.0	83.0	8
BMO2-10	0.0022	0.0050	0.0014	100.0	97.6	94.0	9
BMO2-12	0.0009	0.0027	0.0014	97.2	91.0	93.0	10
BMO2-14	0.0033	0.0018	0.0012	96.0	100.0	87.0	11
BMO2-16	0.0026	0.0018	0.00154	98.3	100.0	90.0	12
BMO2-18	0.0034	0.0015	0.00137	94.0	97.6	92.5	13
BMO2-20	0.0042	0.0014	0.0013	95.0	100	98.1	14
BMO2-22	0.0035	0.0016	0.0012	94.0	78.8	94.0	15
BMO3-3	-	0.0037	-	-	100.0	-	16
BMO3-6	-	-	0.0016	100.0	100.0	100.0	17
BMO3-8	0.0061	0.0092	0.0017	97.6	100.0	90.0	18
BMO3-10	0.0043	0.0074	0.0021	114.0	78.2	108.0	19
BMO3-12	0.0047	0.0019	0.00186	97.3	99.8	96.3	20
BMO3-14	0.0068	0.0011	0.0018	100.0	100.0	99.0	21
BMO3-16	0.0067	0.0019	0.0019	96.0	94.5	97.5	22
BMO3-18	0.0065	0.0013	0.0019	100.0	100.0	89.0	23
BMO3-20	0.0055	-	-	100.0	-	-	24

EXPERIMENT NUMBER	BMO1-2		
TRACER & PHASE	TRITIUM		BRINE
FRACTIONAL FLOW	1:.772	2:.185	3:.043
MAX. & INJ. CONC.	76000	76000	DPM/CC
FLOW RATE	0.766		CC/MIN.

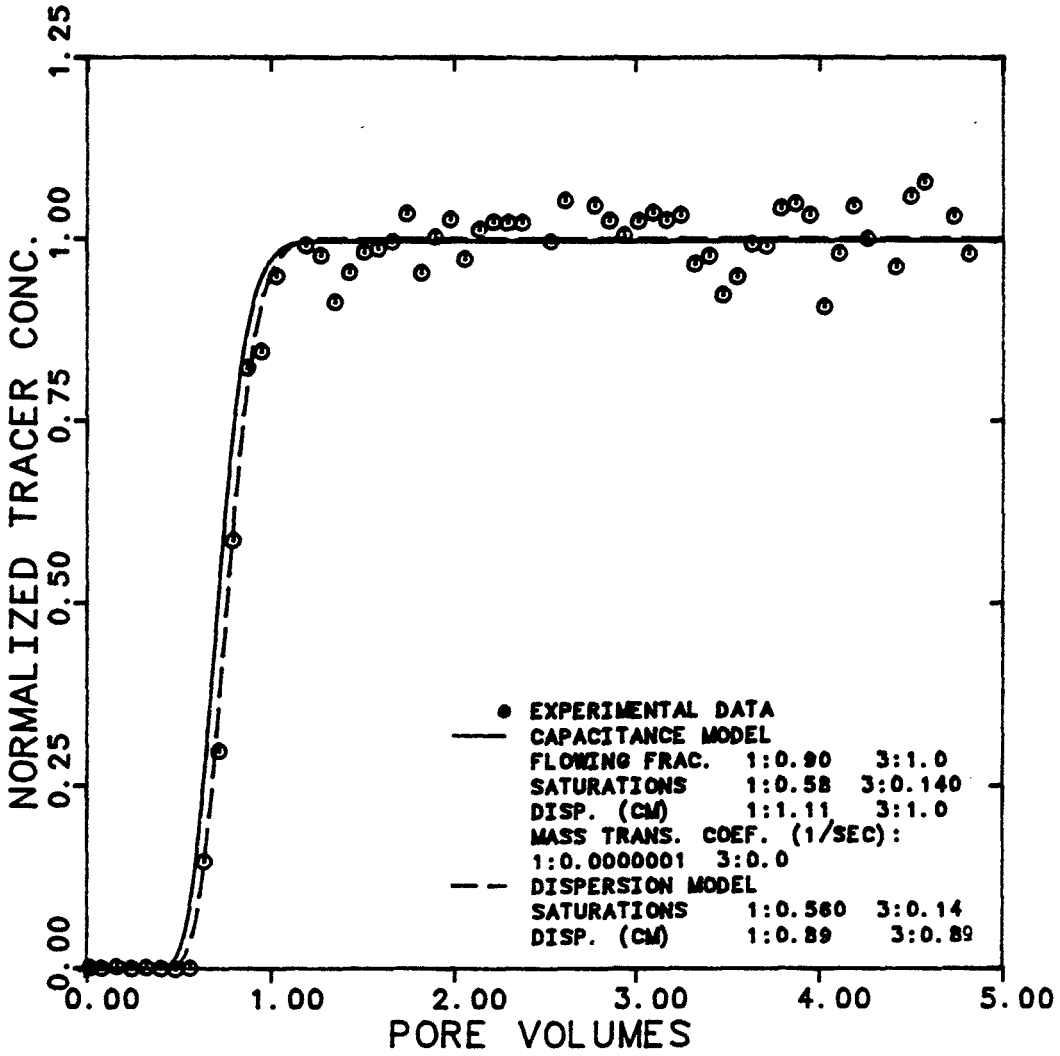

Figure 6.4.1.1 Effluent History for Tritiated Water in Brine for 77.2% Brine, 18.5% Oil, and 4.3% M.E. Cuts

EXPERIMENT NUMBER	BM01-2		
TRACER & PHASE	CARBON-14		OIL
FRACTIONAL FLOW	1:.772	2:.185	3:.043
MAX. & INJ. CONC.	14200	14200	DPM/CC
FLOW RATE	0.766		CC/MIN.

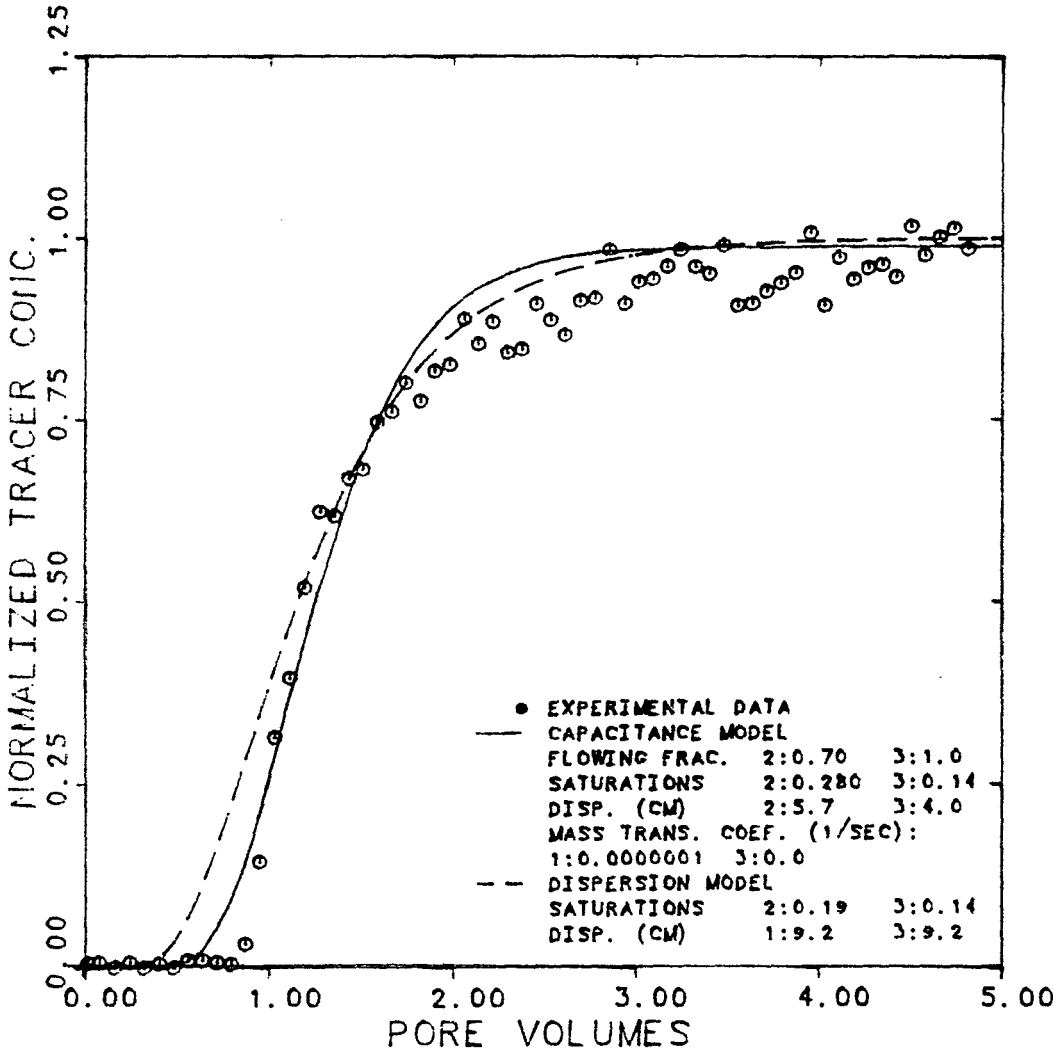

Figure 6.4.1.2 Effluent History for Carbon-14 in Oil for 77.2% Brine, 18.5% Oil, and 4.3% M.E. Cuts

EXPERIMENT NUMBER	BM01-4			
TRACER & PHASE	TRITIUM			BRINE
FRACTIONAL FLOW	1:.510	2:.455	3:.035	
MAX. & INJ. CONC.	82000	83752		DPM/CC
FLOW RATE	0.689			CC/MIN.

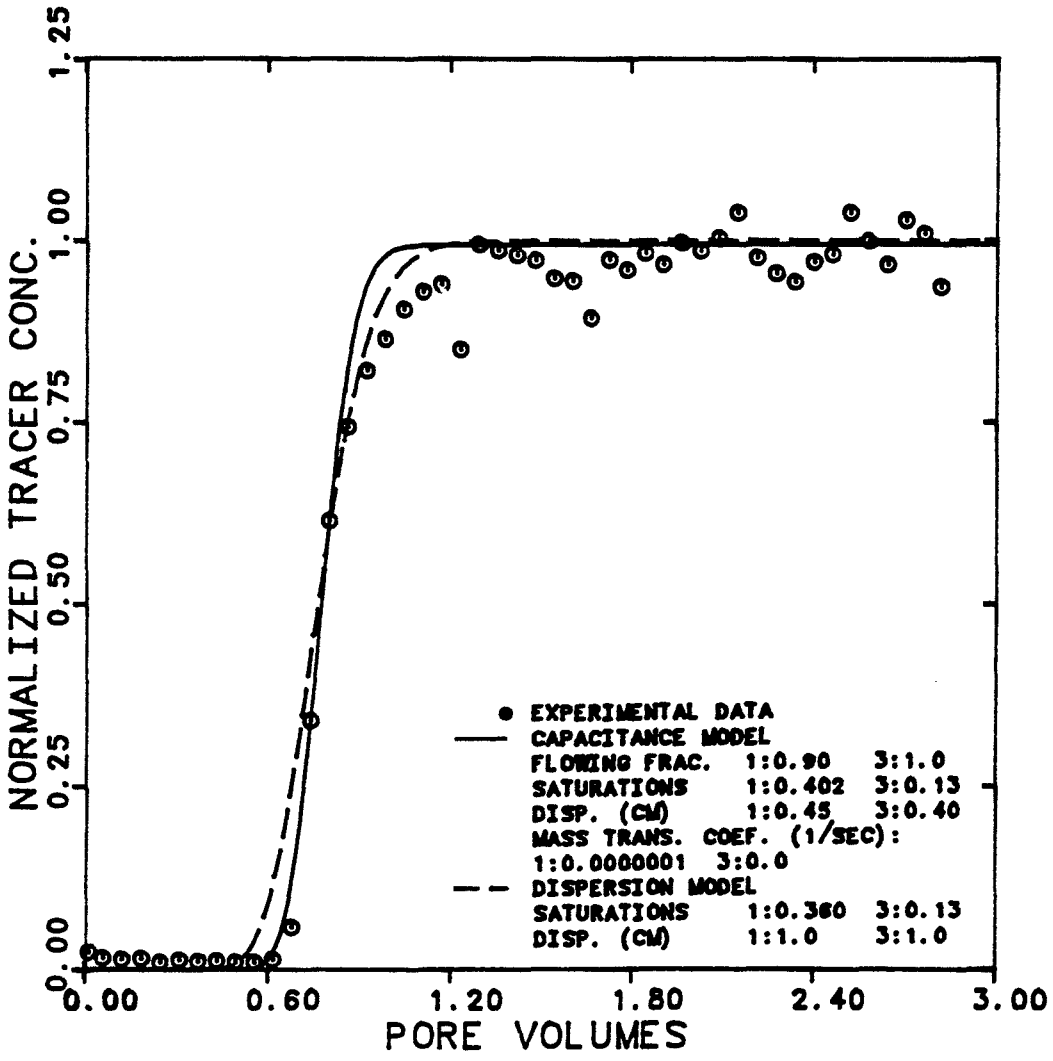

Figure 6.4.1.3 Effluent History for Tritiated Water in Brine for 51% Brine, 45.5% Oil, and 3.5% M.E. Cuts

EXPERIMENT NUMBER	BM01-4			
TRACER & PHASE	CARBON-14		OIL	
FRACTIONAL FLOW	1:.510	2:.455	3:.035	
MAX. & INJ. CONC.	11600	11600	DPM/CC	
FLOW RATE	0.689		CC/MIN.	

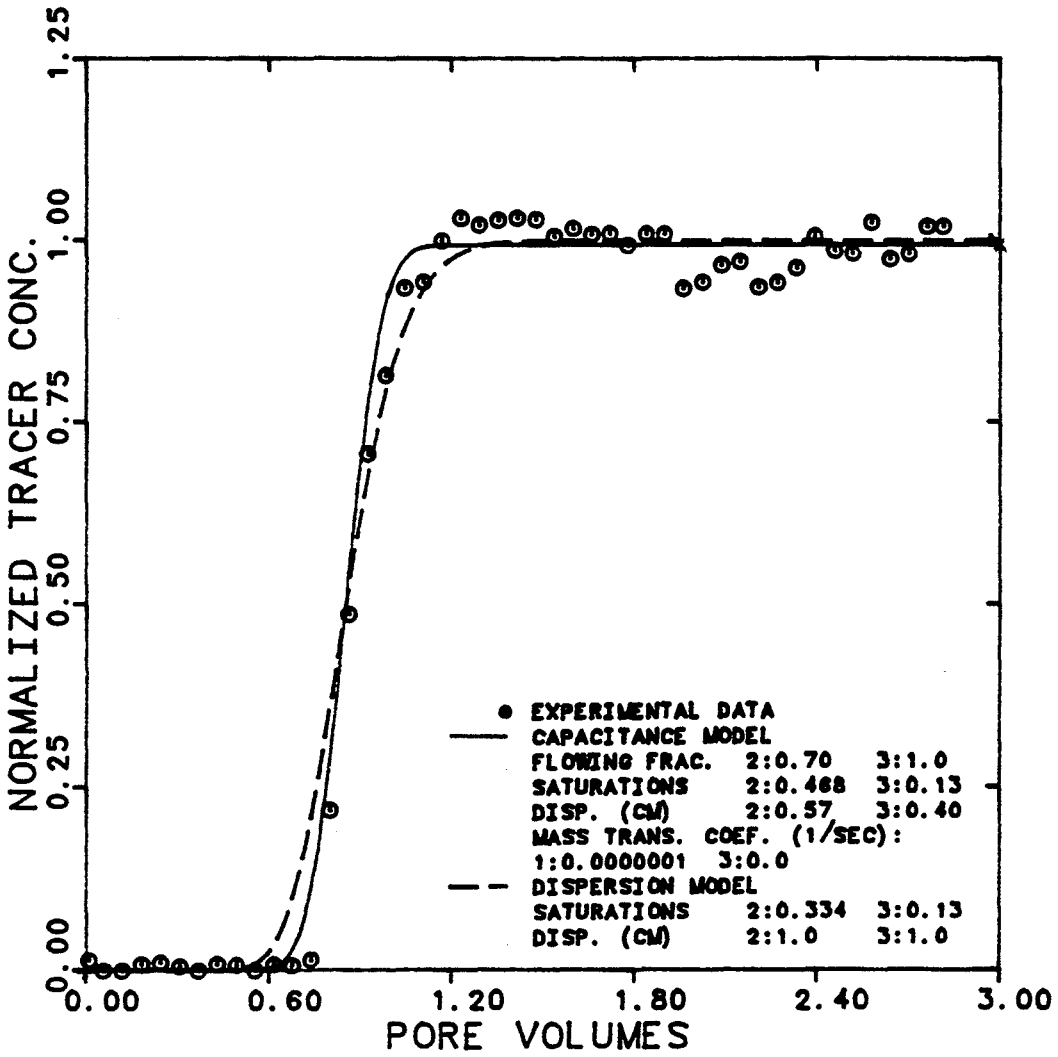

Figure 6.4.1.4 Effluent History for Carbon-14 in Oil for 51% Brine, 45.5% Oil, and 3.5% M.E Cuts

EXPERIMENT NUMBER	BM01-6
TRACER & PHASE	TAG. SULF. M.E.
FRACTIONAL FLOW	3: 0.291
MAX. & INJ. CONC.	10613 11500 DPM/CC
FLOW RATE	0.40 CC/MIN.

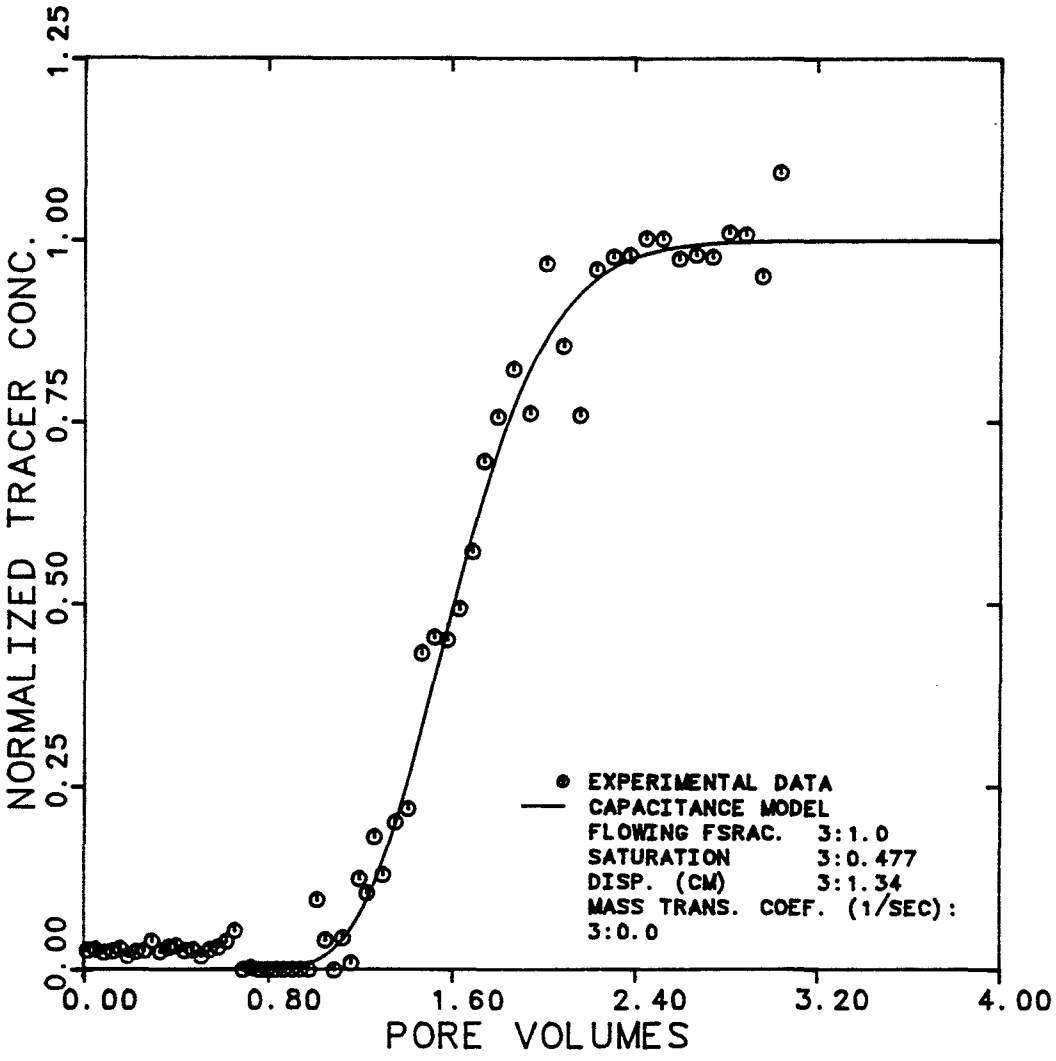

Figure 6.4.1.5 Effluent History for Labelled Sulfonate in M.E. at 37.5% Brine, 33.4% Oil, and 29.1% M.E. Cuts

EXPERIMENT NUMBER	BM01-6		
TRACER & PHASES	CHLORIDE-36	BRINE& M.E.	
MAX. & INJ. CONC. (BRINE)	3744	3744	DPM/CC
MAX. & INJ. CONC. (M.E.)	1822	1900	DPM/CC
FLOW RATE	0.400		CC/MIN.

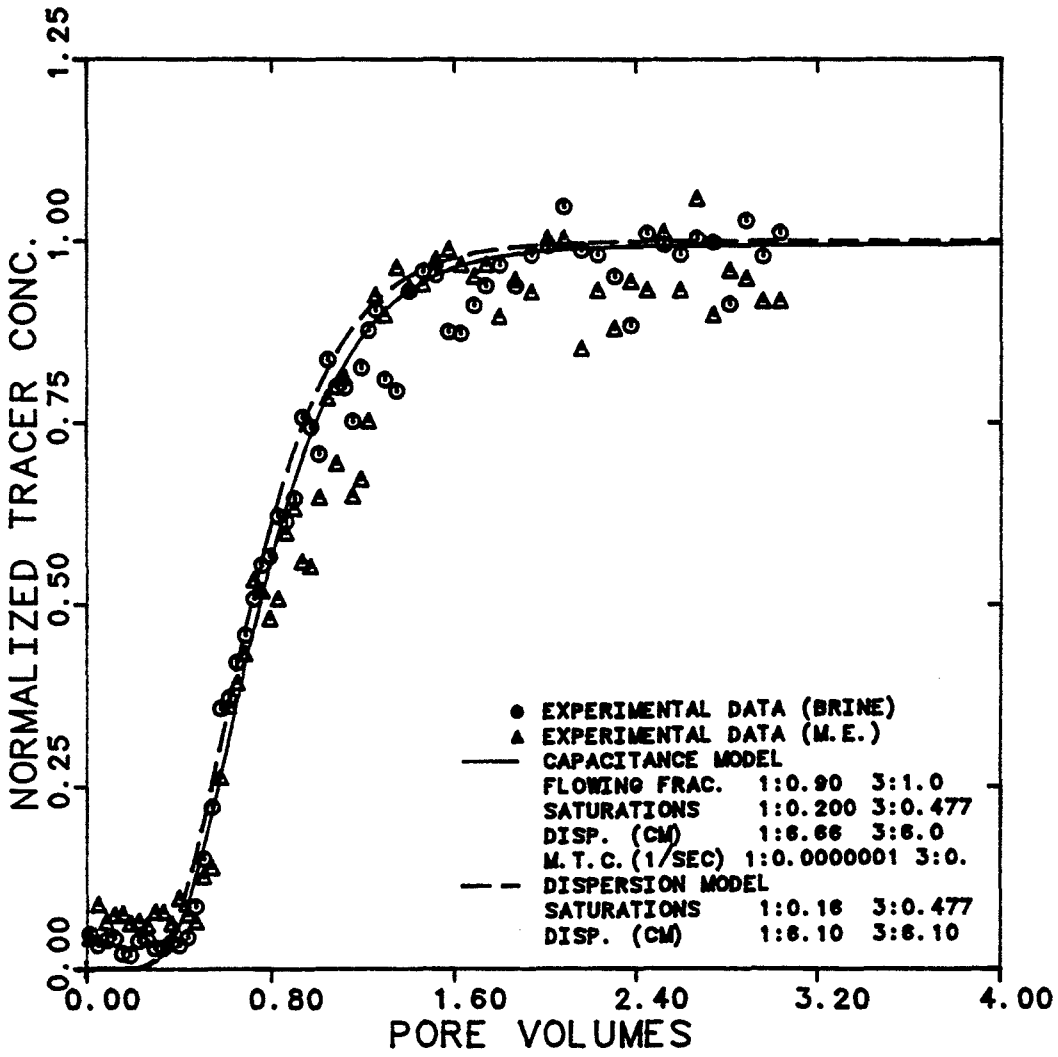

Figure 6.4.1.6 Effluent Histories for Chloride-36 in M.E. and Brine at 37.5% Brine, 33.4% Oil, and 29.1% M.E. Cuts

EXPERIMENT NUMBER	BM01-6		
TRACER & PHASES	CARBON-14 OIL & M.E.		
MAX. & INJ. CONC. (OIL)	32264	33000	DPM/CC
MAX. & INJ. CONC. (M.E.)	13713	14000	DPM/CC
FLOW RATE	0.400		CC/MIN.

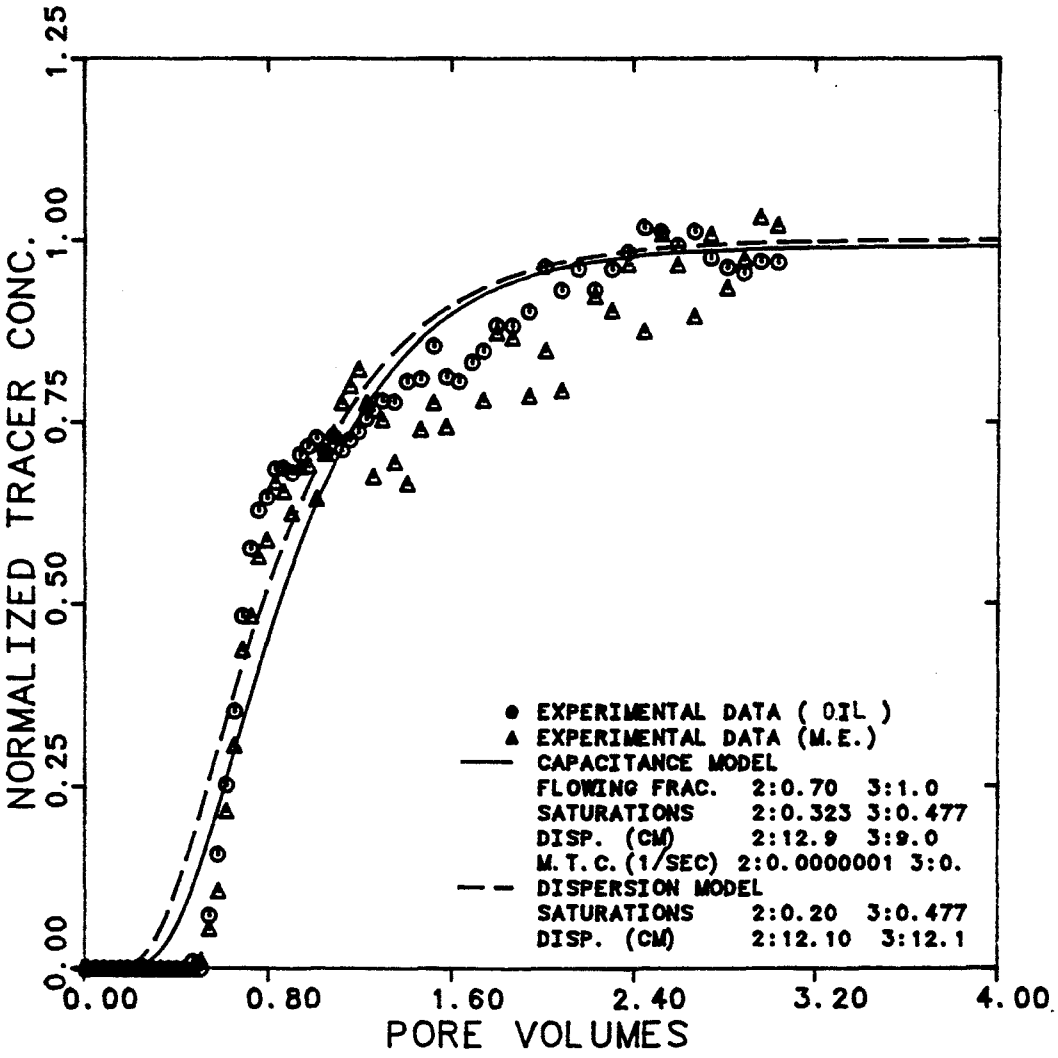

Figure 6.4.1.7 Effluent Histories for Carbon-14 in M.E. and Oil at 37.5% Brine, 33.4% Oil, and 29.1% M.E. Cuts

EXPERIMENT NUMBER	BM01-8	
TRACER & PHASE	TAG. SULF.	M.E.
FRACTIONAL FLOW	3: 0.165	
MAX. & INJ. CONC.	16000 18500	DPM/CC
FLOW RATE	0.532	CC/MIN.

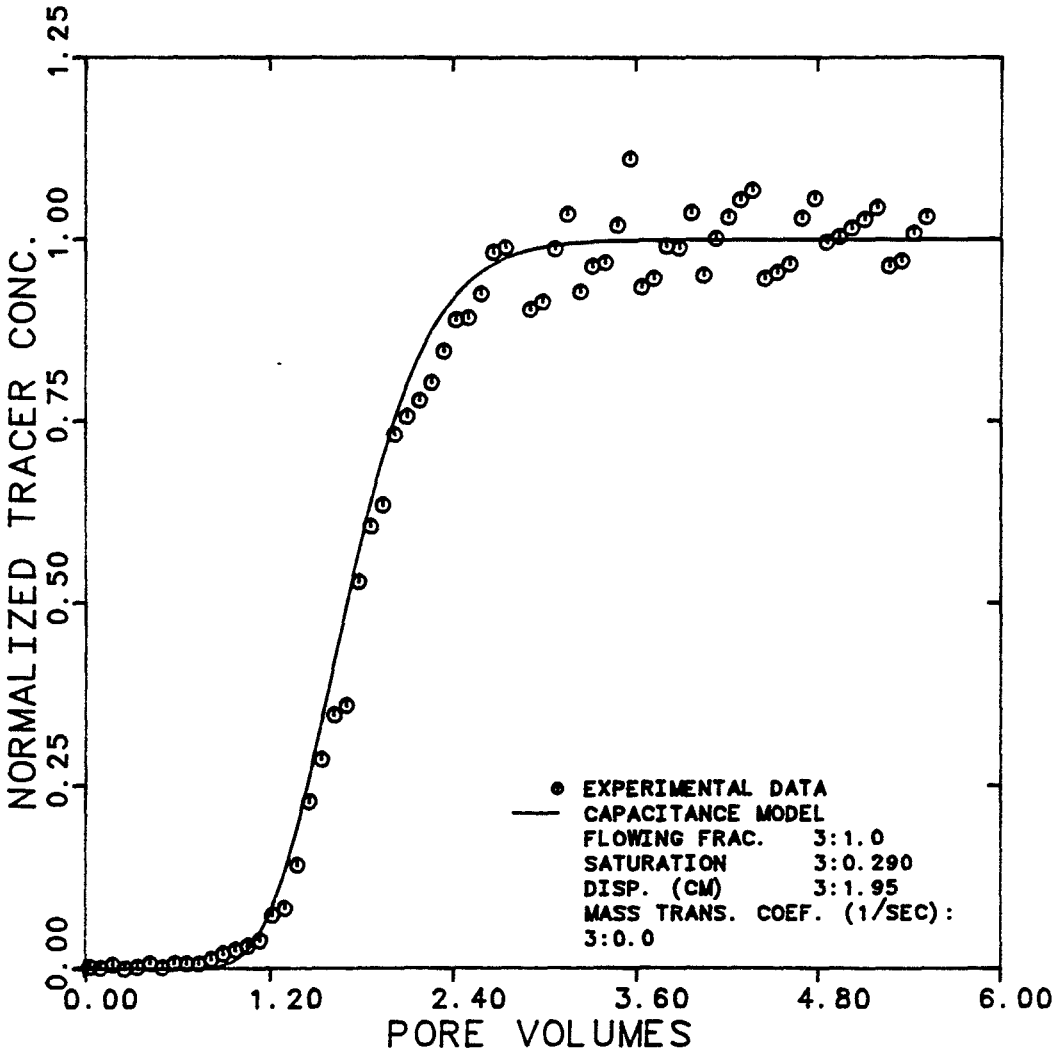

Figure 6.4.1.8 Effluent History for Labelled Sulfonate in M.E. at 58.6% Brine, 24.9% Oil, and 16.5% M.E. Cuts

EXPERIMENT NUMBER	BM01-8		
TRACER & PHASES	CHLORIDE-36 BRINE & M.E.		
MAX. & INJ. CONC. (BRINE)	2740	2740	DPM/CC
MAX. & INJ. CONC. (M.E.)	1477	1520	DPM/CC
FLOW RATE	0.532		CC/MIN.

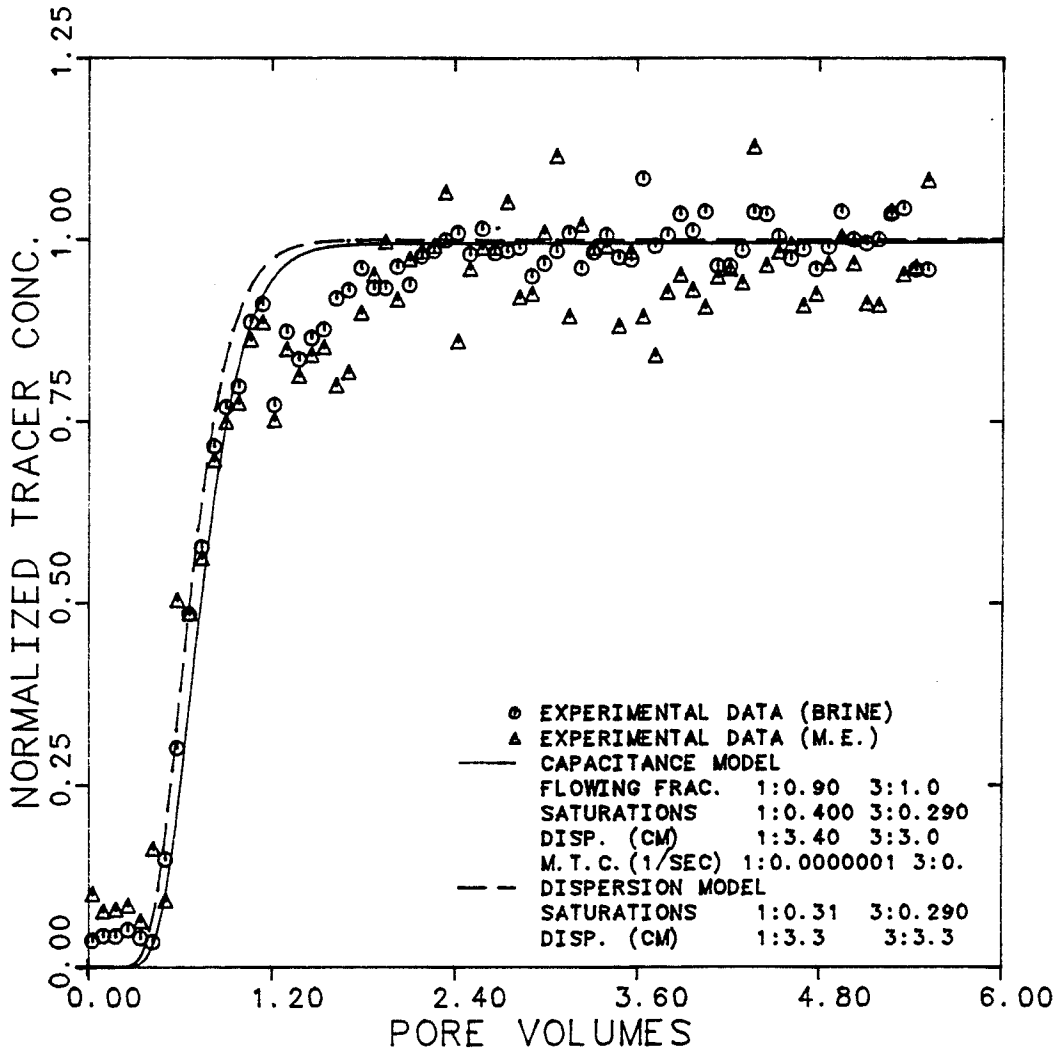

Figure 6.4.1.9 Effluent Histories for Chloride-36 in Brine and M.E. at 58.6% Brine, 24.9% Oil, and 16.5% M.E. Cuts

EXPERIMENT NUMBER	BMO1-8		
TRACER & PHASES	CARBON-14	OIL & M.E.	
MAX. & INJ. CONC. (OIL)	18000	19000	DPM/CC
MAX. & INJ. CONC. (M.E.)	5250.	5250.	DPM/CC
FLOW RATE	0.532		CC/MIN.

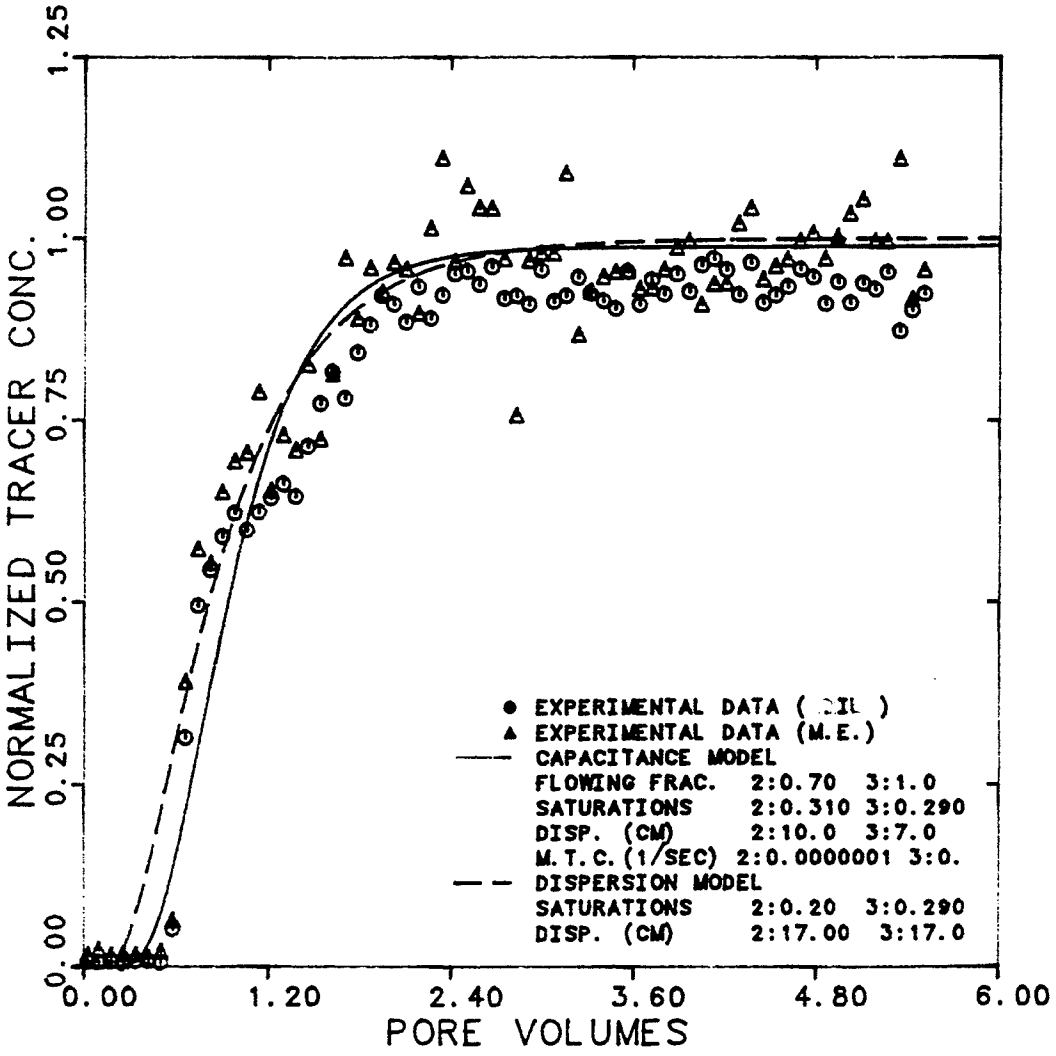

Figure 6.4.1.10 Effluent Histories for Carbon-14 in Oil and M.E. at 58.6% Brine, 24.9% Oil, and 16.5% M.E. Cuts

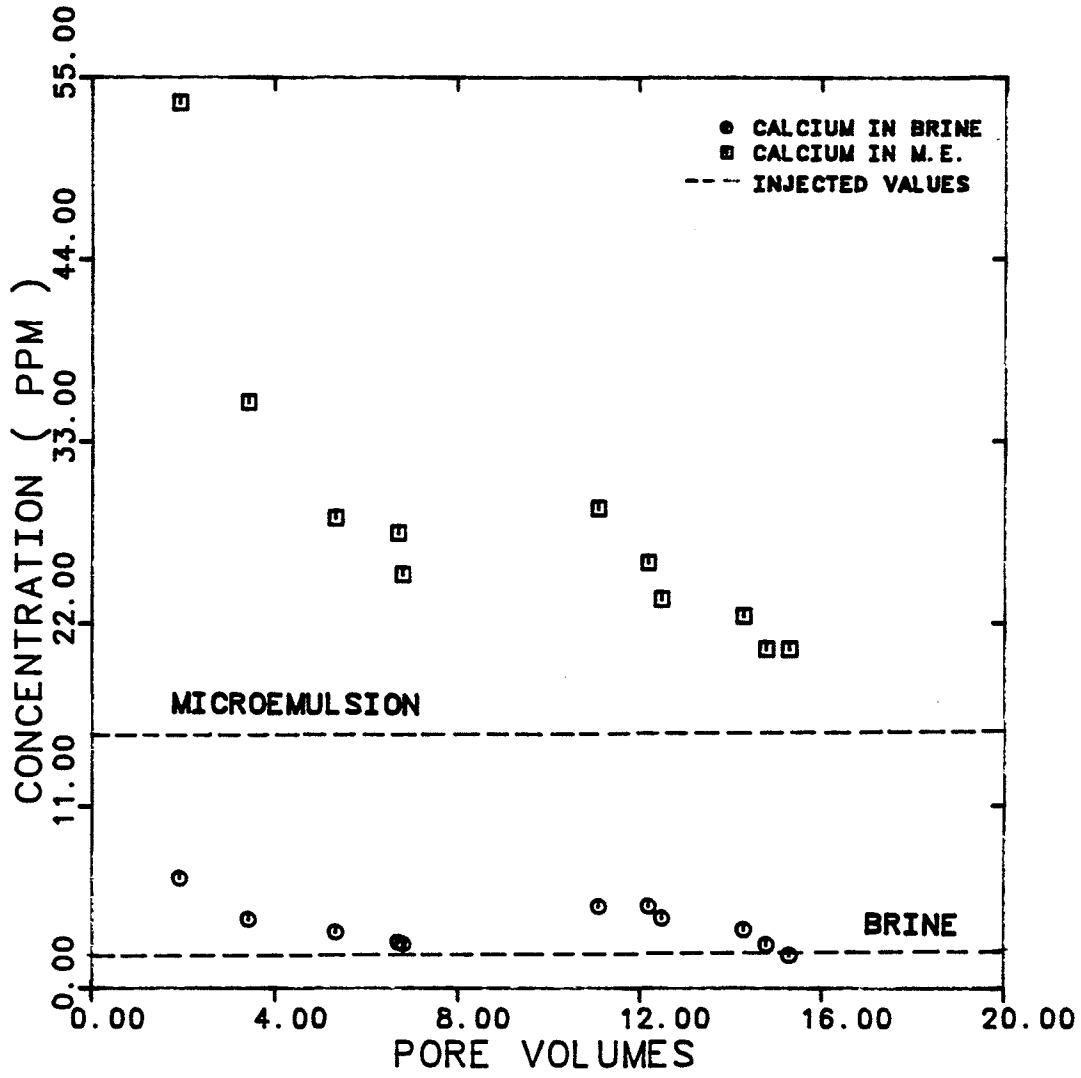

Figure 6.4.1.11 Calcium Concentration in Effluent Brine and M.E. During Three-Phase Flow (Exp. BMO1)

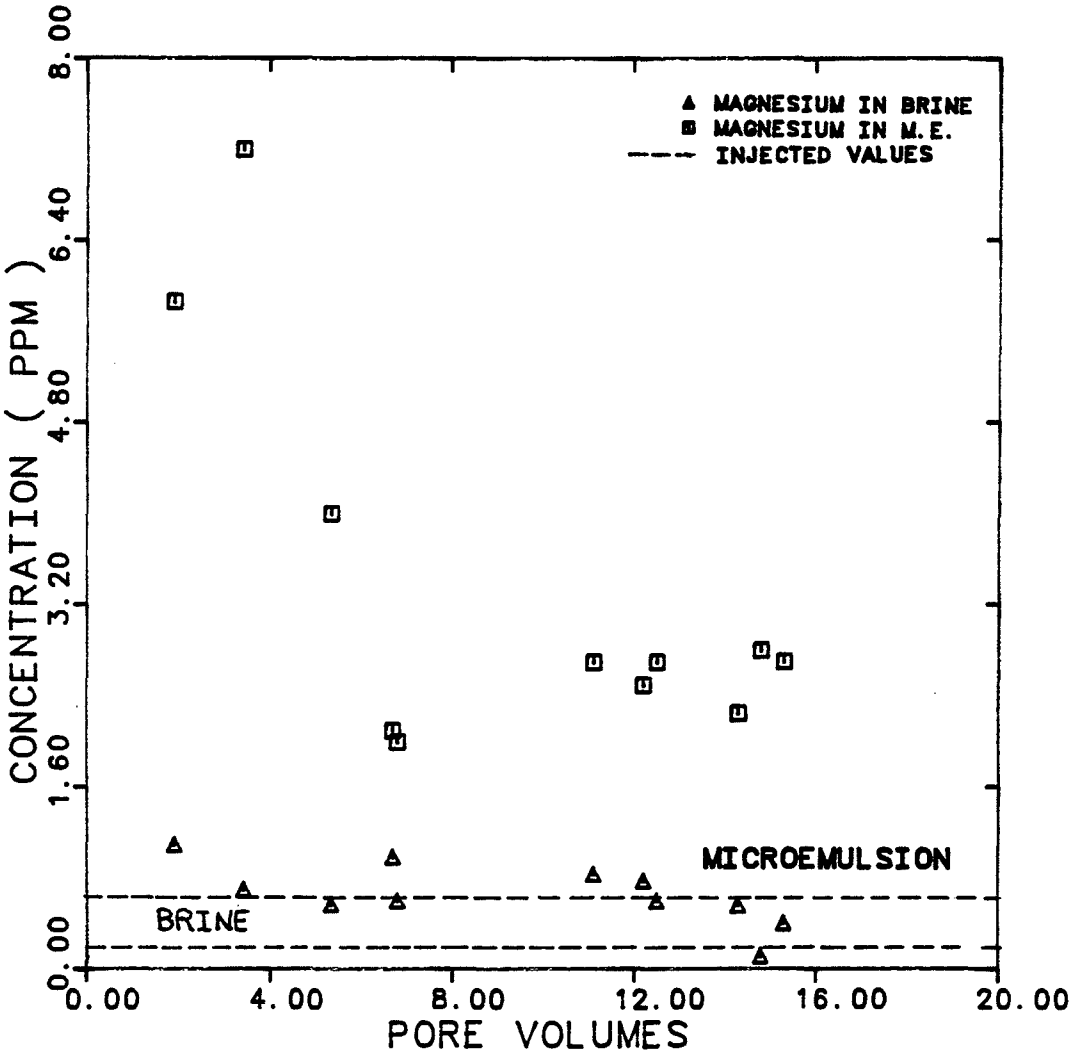

Figure 6.4.1.12 Magnesium Concentration in Effluent Brine and M.E. During Three-Phase Flow (Exp. BM01)

COMPOSITION OF INJECTED MICROEMULSION

WATER	49.6 VOL.%
OIL	46.5 VOL.%
IBA	2.2 VOL.%
TRS 10-410	3.6 VOL.%

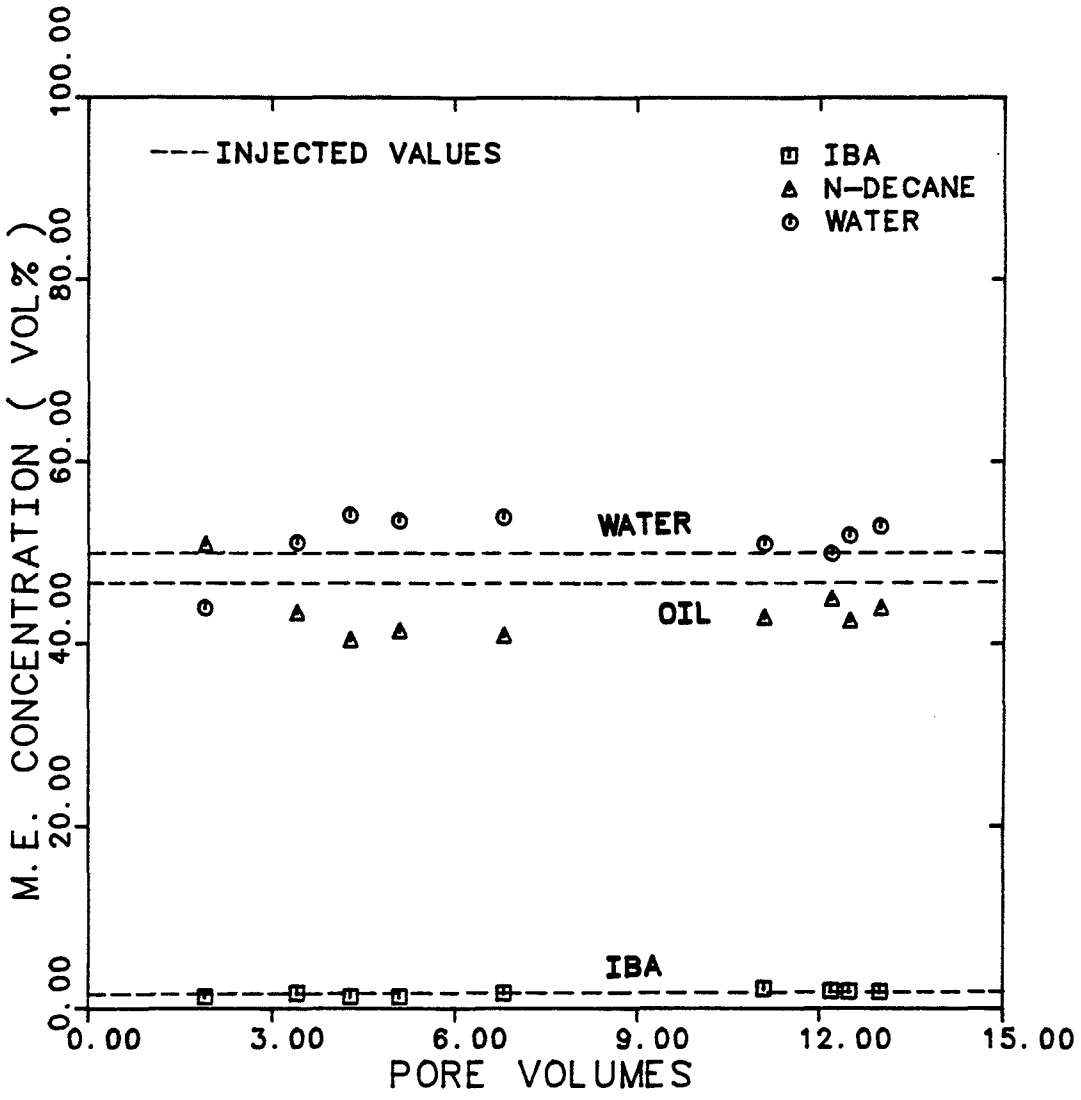

Figure 6.4.1.13 Composition of Effluent M.E. as a Function of Pore Volumes Injected

6.4.2 Excess Brine/Microemulsion/Excess Oil (Exp. No. BMO2)

The core with properties listed in Table 6.2.1 was used once more for this experiment. A new batch (number 7) of micellar solution with the salinity of 1.2 wt% NaCl was made up. The hot batch contained carbon-14, tritium labelled sulfonate, and chloride-36 as radioactive tracers. Table 6.1.1 shows the properties of both hot and cold stocks.

It was initially anticipated that the sequence of floods conducted would follow the saturation sequence shown in Figure 6.4.2.1. Shown in Figure 6.4.2.2 are the estimated fractional flows necessary to give the saturations. These same data were used to estimate the total flow rate necessary to maintain a constant capillary number of 10^{-2}. These were the values used as the nominal flow rates injected.

There was about 20 days of time lag between the experiment BMO1 and this experiment (the core was shut in). Therefore, 100% microemulsion at 1.02 cm^3/min was injected until steady-state was reached and followed by performing the dispersion run to re-establish the saturation state of the core.

The fluids (oil, microemulsion, excess brine)

were then injected at the pre-selected nominal flow rates to steady-state.

The actual cuts, total flow rates, material balance estimate of saturations and relative permeabilities are in Table 6.4.1.1. Given in Table 6.4.1.2 are the potential drops and the total fluids injected to steady-state. The steady-state potential drops ($\Delta\Phi$) measured were higher for the inlet than for the outlet section of the core. The inlet $\Delta\Phi$s were higher than those of the middle section by 20%, on the average. Table 6.4.1.3 shows the calculated capillary numbers and relative mobilities.

Tracer breakthrough data for tritium labelled sulfonate in the microemulsion, chloride-36 in the excess brine and microemulsion, and carbon-14 in the microemulsion and excess oil are in Figures 6.4.2.3 through 6.4.2.35.

The breakthrough curves of tritium labelled sulfonate are fairly smooth, symmetric and s-shaped while the breakthrough curves of carbon-14 and chloride-36 in the microemulsion phase show more scatter when compared with those of excess oil and excess brine phases.

The breakthrough curves were first compared with the solution of the C-D equation (dashed curves),

the saturations obtained did not add up to one. The microemulsion saturations obtained from the matching of tritium labelled sulfonate breakthrough curve against the C-D equation were consistently in good agreement with the material balance estimates. The saturations of excess brine and excess oil are lower than the material balance estimates because of non-equilibrium or microscopic bypassing. These observations are consistent with the previous findings obtained from capillary desaturation curves (Experiment CDC3), that microemulsion is probably the wetting phase, brine is the intermediate wetting phase, and oil is the non-wetting phase, since capacitance effects are known to be associated with the non-wetting phase.

The saturations and dispersivities estimated using the C-D equation are in Table 6.4.1.4. The total fluids injected for the dispersion runs are tabulated in Table 6.4.1.4. The breakthrough curves were then compared to the computed curves of the capacitance-dispersion model using microemulsion saturation obtained from the sulfonate breakthrough curve. The matching parameters such as saturations, flowing fractions, dispersivities, and mass transfer coefficients which gave the best agreement between the computed curves and

experimental breakthrough curves are in Table 6.4.1.5. This table also gives the calculated dispersion coefficients, flowing phase velocity, and tracer recoveries.

The flowing fraction for excess brine obtained from these matches was constant and equal to 0.90 for all the cuts. The flowing fraction of excess oil was also constant but equal to 0.70 for all the cuts. These imply that 90% of the in-situ brine saturation and only about 70% of the in-situ oil saturation are contributing to flow. The flowing fraction for the microemulsion phase was equal to one since no capacitance effect was needed to match the sulfonate tracer curve. The values for brine and oil are consistent with the interpretation that oil is the non-wetting phase and brine the intermediate wetting phase.

The carbon-14 and chloride-36 breakthrough curves were first matched against the capacitance model with no restriction on the values of mass transfer coefficient. The mass transfer coefficients obtained were ranged between 10^{-7} to 10^{-6} sec^{-1} for chloride-36 and 7×10^{-8} to 10^{-6} sec^{-1} for carbon-14. The dependency of mass transfer coefficient on the phase velocity has been observed and reported by some investigators

[B.1,S.10]. The mass transfer coefficients were anticipated to be constant in these experiments (BM02) since there was not significant variation in phase velocities (see Table 6.4.1.5). The breakthrough curves were then matched using a constant mass transfer coefficient of 10^{-7} sec^{-1} for both tracers, keeping the rest of parameters as before. The computed curves did not seem very sensitive to this change and there was no significant change in the quality of these matches.

Estimated dispersivities from the capacitance model are lower than those estimated from the C-D equation. The dispersivities of tritium labelled sulfonate in the microemulsion phase are lower than the dispersivities of either carbon-14 or chloride-36 in the microemulsion and excess phases.

Figures 6.4.2.36 through 6.4.2.38 show the relative permeability of each phase as a function of the saturation of that phase. Saturations estimated from both the material balance and capacitance model are compared for each phase in these figures. Material balance and capacitance model estimates of saturation are in fairly good agreement.

The excess brine and oil phase relative permeabilities are nearly the same, but the microemulsion

relative permeability is significantly higher than that of excess phases (Figure 6.4.2.39). Relative permeability curves again show curvature despite the very high capillary number of 10^{-2}. The shape, trend, and the curvature of relative permeability curves are very close to those of the two-phase flow experiments discussed in sections 6.3.1 and 6.3.2.

Phase relative permeabilities are also plotted versus flowing phase saturations ($S_j^f = S_j F_j$) obtained from the capacitance model in Figure 6.4.2.40. The flowing saturation is the part of the in-situ phase saturation which contributes to the permeability of the phase. Relative permeability curves are close to each other when flowing saturations are used.

Figures 6.4.2.41 and 6.4.2.42 show the measured concentrations of calcium and magnesium in both effluent microemulsion and excess brine phases. Table 6.1.1 contains data on the injected phase composition. Figure 6.4.2.43 shows the composition by GC of effluent microemulsion phase for steady-state determination. It appears, within experimental error and scatter in data, steady-state was achieved for this experiment.

Relative mobility, fractional flow, dispersivity and dispersion coefficient data are plotted

and presented in the following subsection (6.4.4).

- Experimental Difficulties and Observations

The breakthrough data of tritium labelled sulfonate (TS) in microemulsion phase are fairly smooth, but the plateau concentration during three-phase flow was only 93% of that of the injected value, on average. In other words, there is about 7% impurity of the excess phases in the microemulsion phase. The contamination occurs during the sampling of the microemulsion phase for the dispersion analysis. The degree of contamination is more severe when the microemulsion volume is low. Thus, we normalized the effluent TS concentration in the microemulsion by the plateau value (the average of last 10-20 samples) rather than the injected value.

The breakthrough data of carbon-14 and chloride-36 in the microemulsion phase show more scatter when compared to those of the excess phases. This may be partly a consequence of the above-mentioned observation (contamination problem) and due to the fact that the microemulsion contains all the three tracers and there is some overlap in the counting data.

The relative permeability data of the excess brine (Figure 6.4.2.36) show more scatter compared to those of the excess oil and microemulsion phases.

I calculated the ratio of brine to oil saturation (S_1/S_2) for the different cuts. This varied from 0.58 to 8.6 (Table 6.4.1.5). This variation was considered as the probable reason for the deviation of some of the brine data from the smooth trend apparent by the rest of the data. This observation was also consistent with the analysis of Lake's modified three-phase relative permeability model (Chapter 7, Figure 7.3.2) which incorporates the dependence of the intermediate wetting phase (brine) on two saturations.

Experiment BM03 (section 6.4.3) is therefore designed to test this aspect of the results.

SATURATION TERNARY

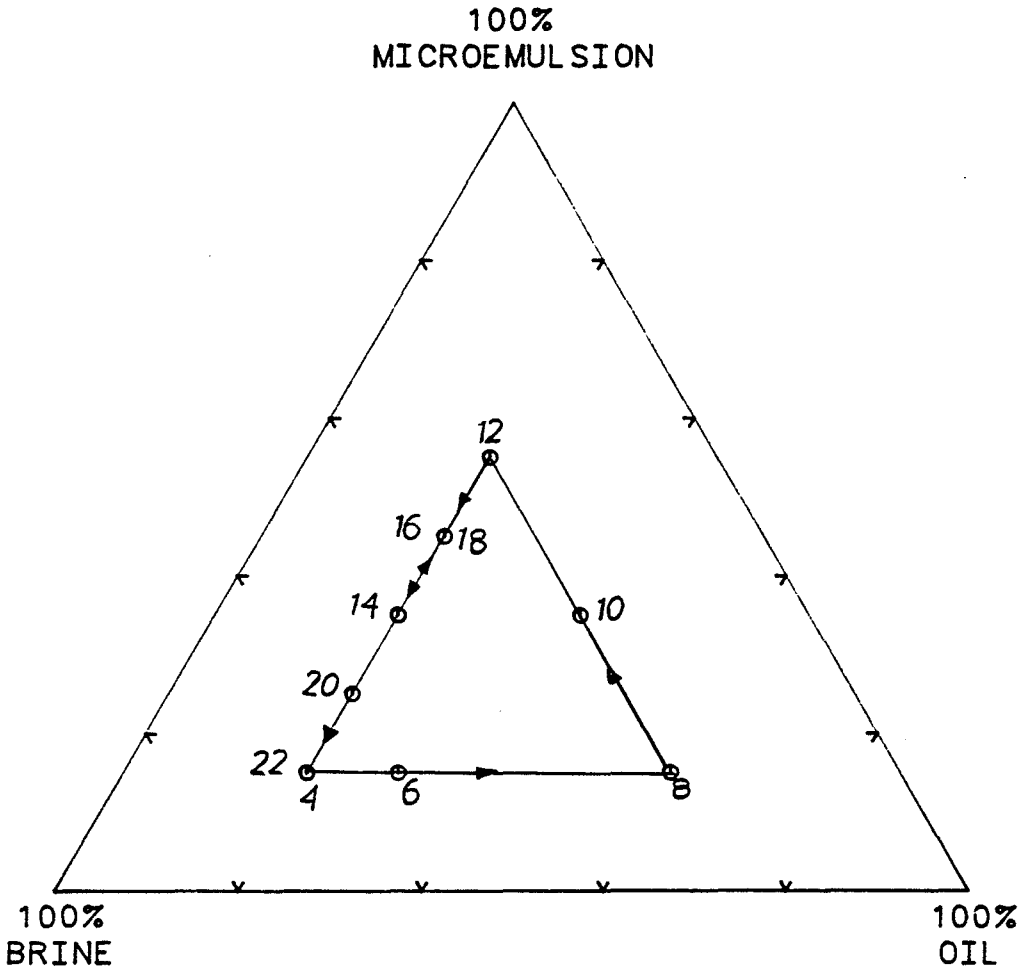

Figure 6.4.2.1 Planned Phase Saturation for Three-Phase Flow (Exp. BMO2)

FRACTIONAL FLOW TERNARY

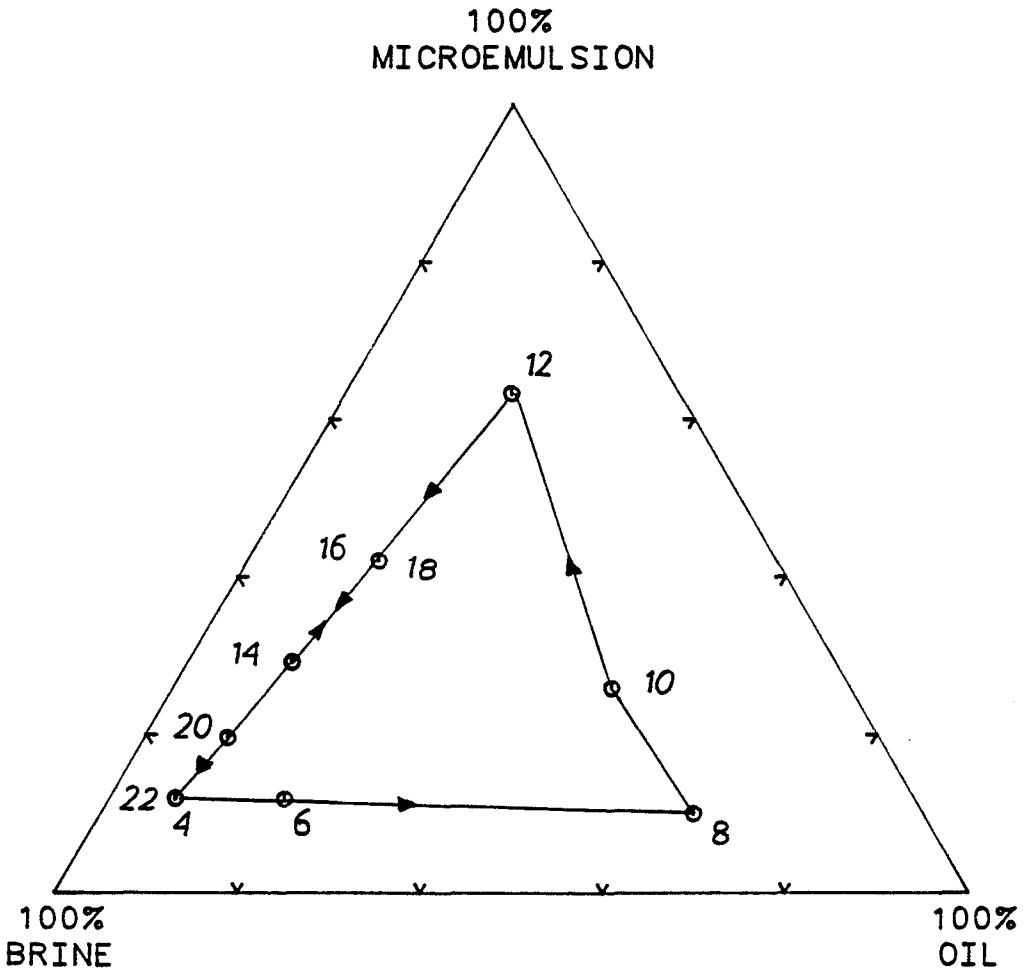

Figure 6.4.2.2 Planned Fractional Flow for Three-Phase Flow (Exp. BMO2)

EXPERIMENT NUMBER	BM02-2	
TRACER & PHASE	TAG. SULF.	M.E.
FRACTIONAL FLOW	3: 1.0	
MAX. & INJ. CONC.	28960 28960	DPM/CC
FLOW RATE	0.71	CC/MIN.

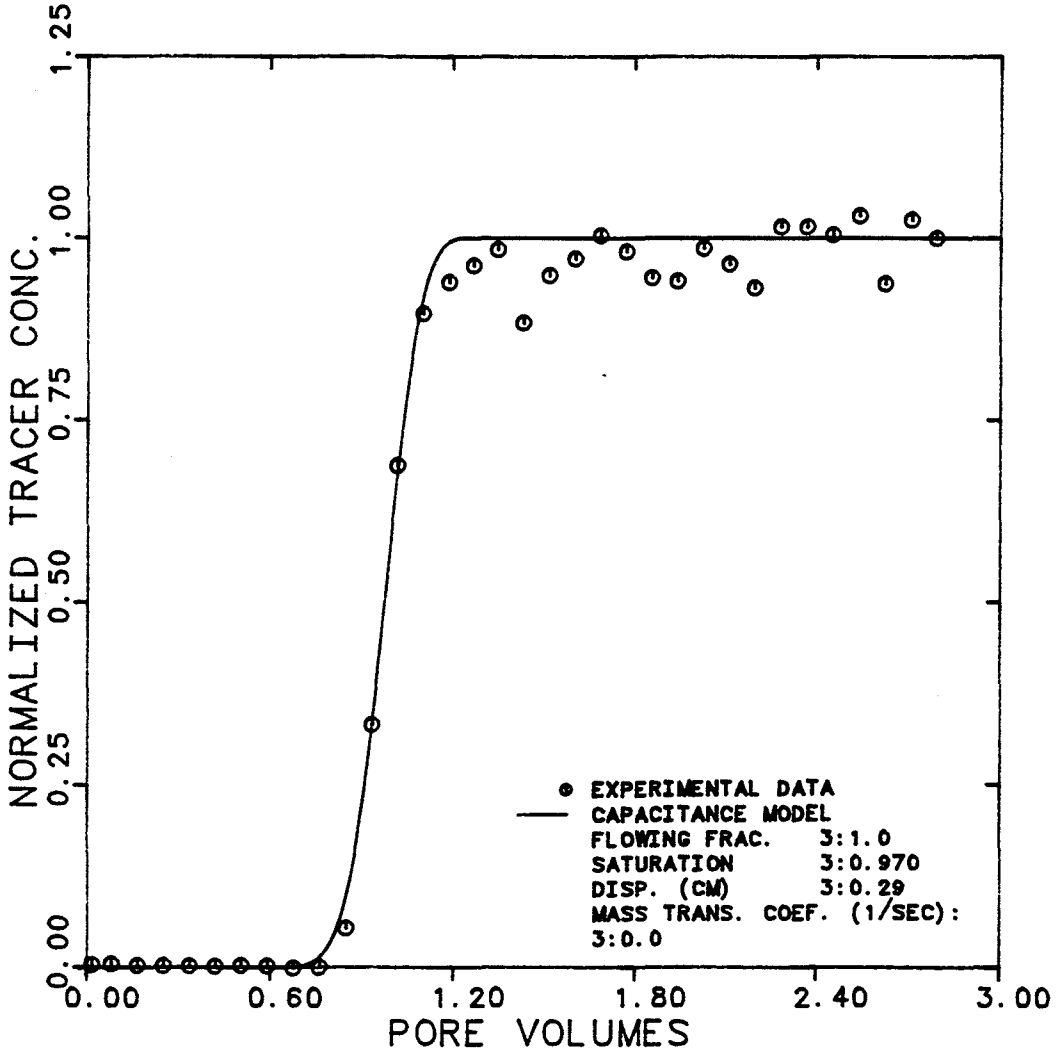

Figure 6.4.2.3 Effluent History for Labelled Sulfonate in M.E. During Single-Phase Flow of M.E.

EXPERIMENT NUMBER	BMO2-2		
TRACER & PHASE	CHLORIDE-36		M.E.
FRACTIONAL FLOW	100%		M.E.
MAX. & INJ. CONC.	840	840	DPM/CC
FLOW RATE	0.710		CC/MIN.

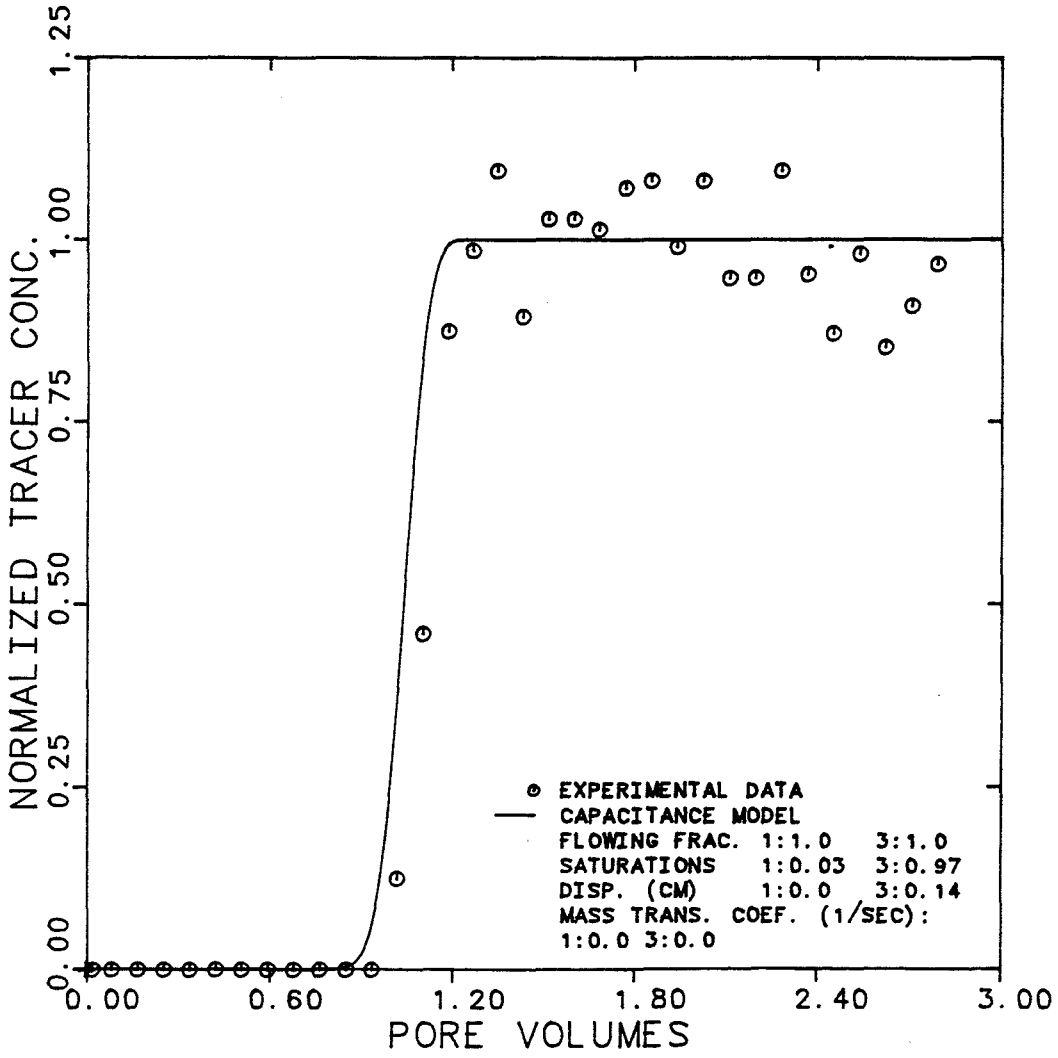

Figure 6.4.2.4 Effuent History for Chloride-36 in M.E. During Single-Phase Flow of M.E.

EXPERIMENT NUMBER	BM02-2		
TRACER & PHASE	CARBON-14		M.E.
FRACTIONAL FLOW	100%		M.E.
MAX. & INJ. CONC.	6400	6400	DPM/CC
FLOW RATE	0.710		CC/MIN.

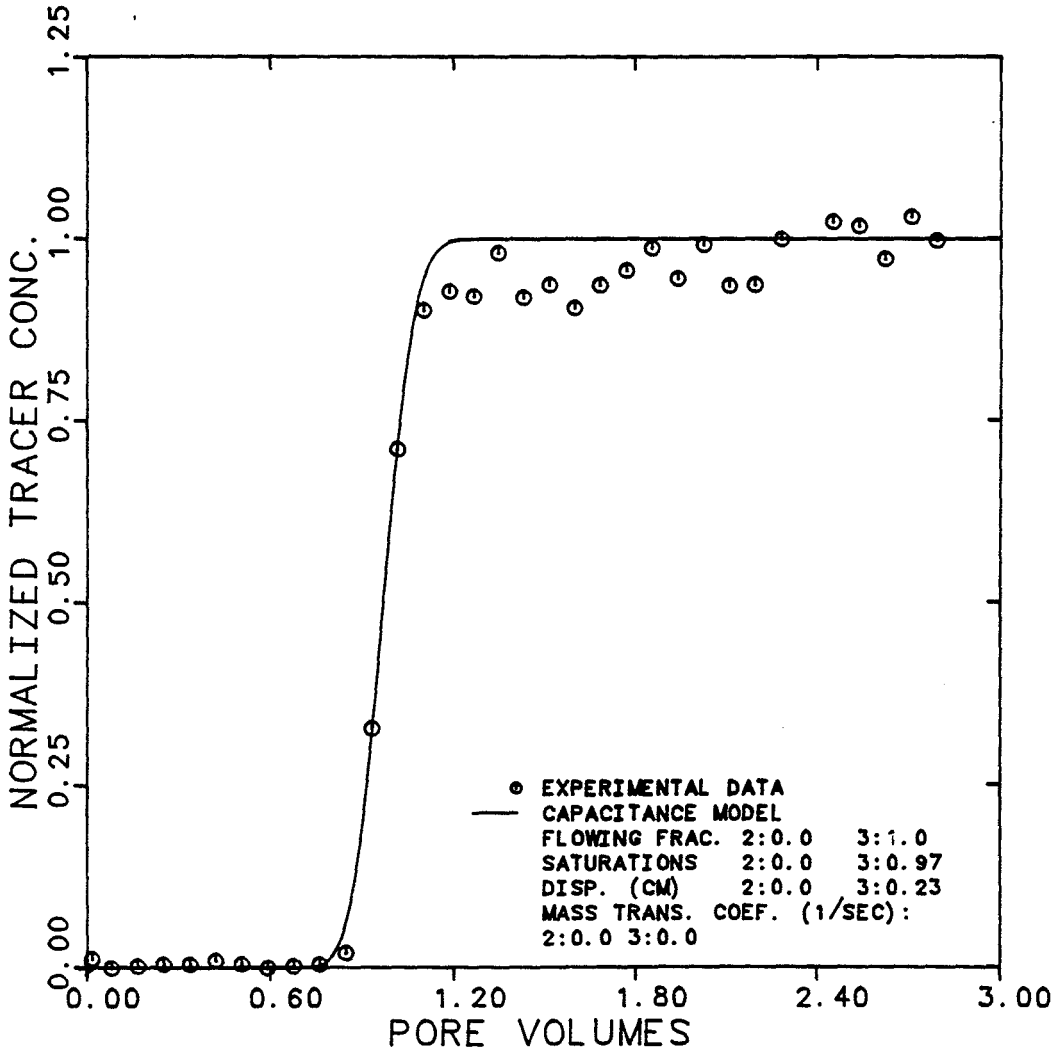

Figure 6.4.2.5 Effluent History for Carbon-14 in Oil During Single-Phase Flow of M.E.

EXPERIMENT NUMBER	BM02-4	
TRACER & PHASE	TAG. SULF.	M.E.
FRACTIONAL FLOW	3: 0.140	
MAX. & INJ. CONC.	28500 29500	DPM/CC
FLOW RATE	0.906	CC/MIN.

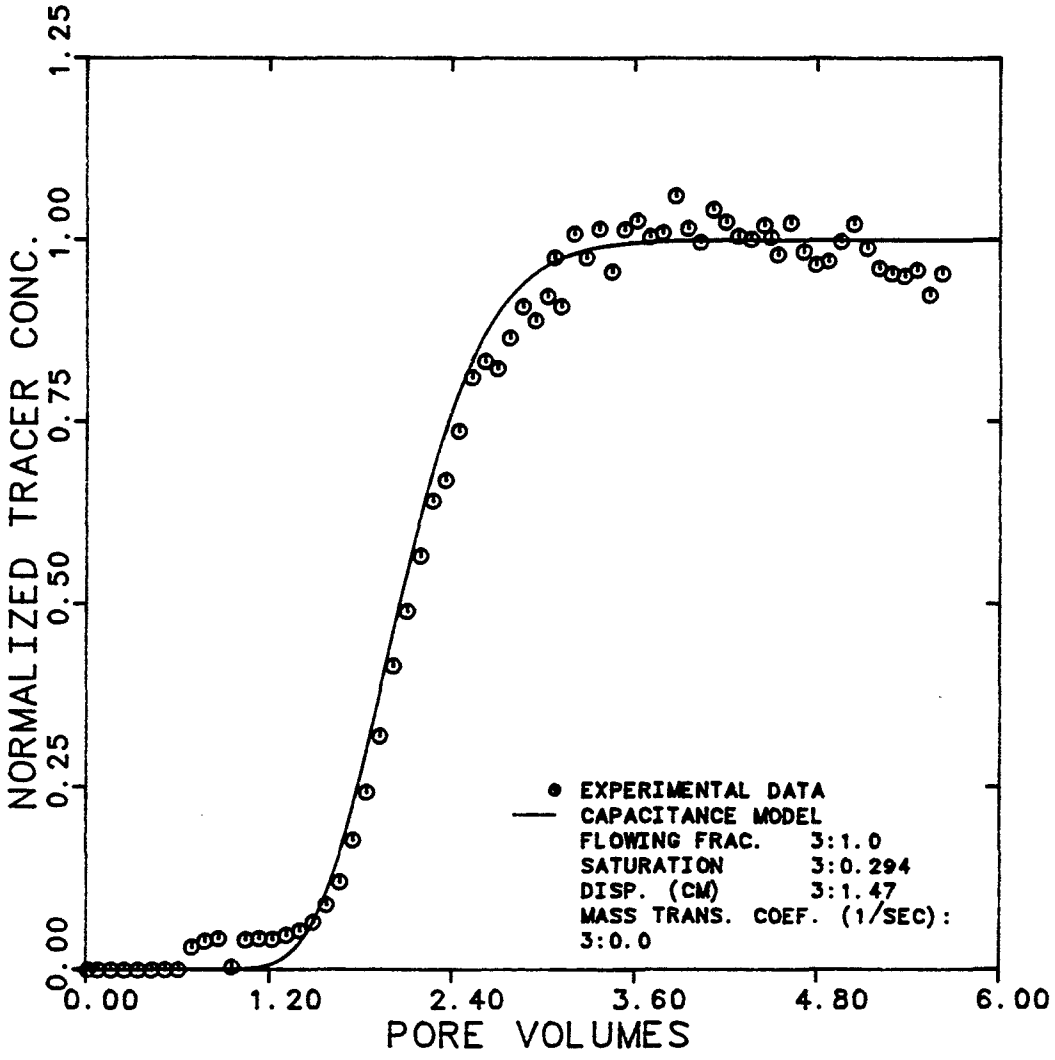

Figure 6.4.2.6 Effluent History for Labelled Sulfonate in M.E. for 77.2% Brine, 18.8% Oil, and 14% M.E. Cuts

EXPERIMENT NUMBER		BMO2-4	
TRACER & PHASES		CHLORIDE-36	BRINE & M.E.
MAX. & INJ. CONC.	(BRINE)	2034 2078	DPM/CC
MAX. & INJ. CONC.	(M.E.)	1100 1100	DPM/CC
FLOW RATE		0.906	CC/MIN

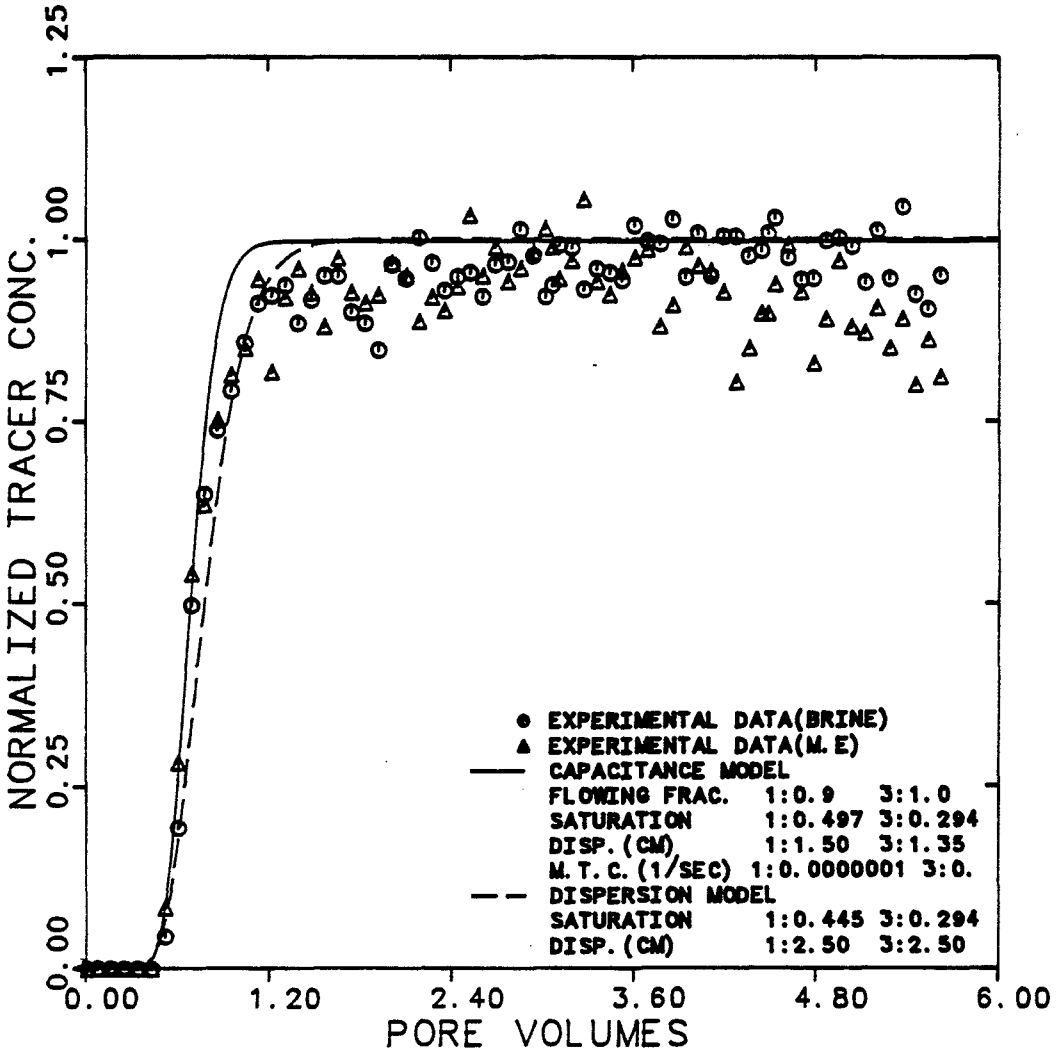

Figure 6.4.2.7 Effluent Histories for Chloride-36 in Brine and M.E. at 77.2% Brine, 8.8% Oil, ad 14% M.E. Cuts

EXPERIMENT NUMBER	BMO2-4		
TRACER & PHASES	CARBON-14	OIL &	M.E.
MAX. & INJ. CONC. (OIL)	14000	14354	DPM/CC
MAX. & INJ. CONC. (M.E.)	6650	6650	DPM/CC
FLOW RATE	0.906		CC/MIN

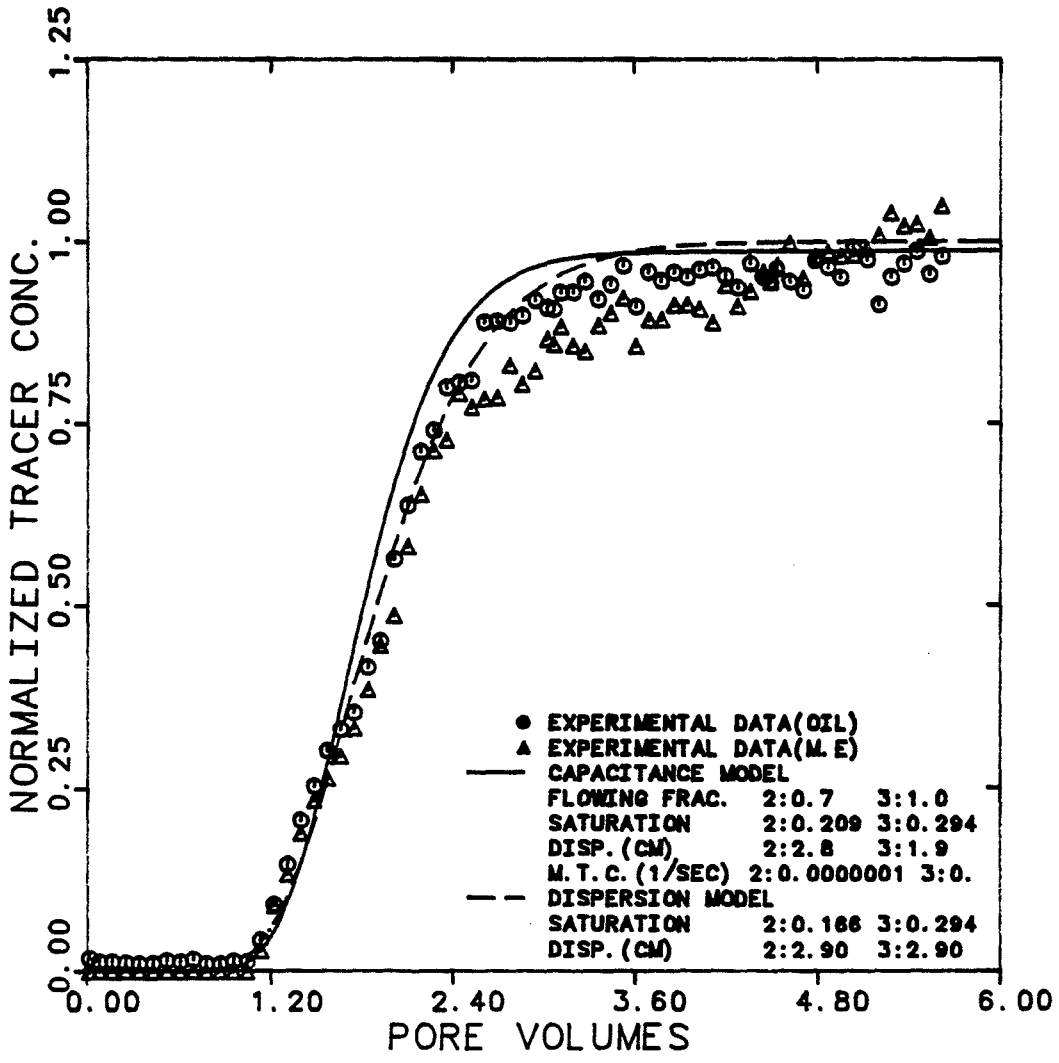

Figure 6.4.2.8 Effluent Histories for Carbon-14 in Oil and M.E. at 77.2% Brine, 8.8% Oil, and 14% M.E. Cuts

EXPERIMENT NUMBER	BM02-6	
TRACER & PHASE	TAGG. SULF.	M.E.
FRACTIONAL FLOW	3:0.134	
MAX. & INJ. CONC.	26200 27000	DPM/CC
FLOW RATE	0.8870	CC/MIN.

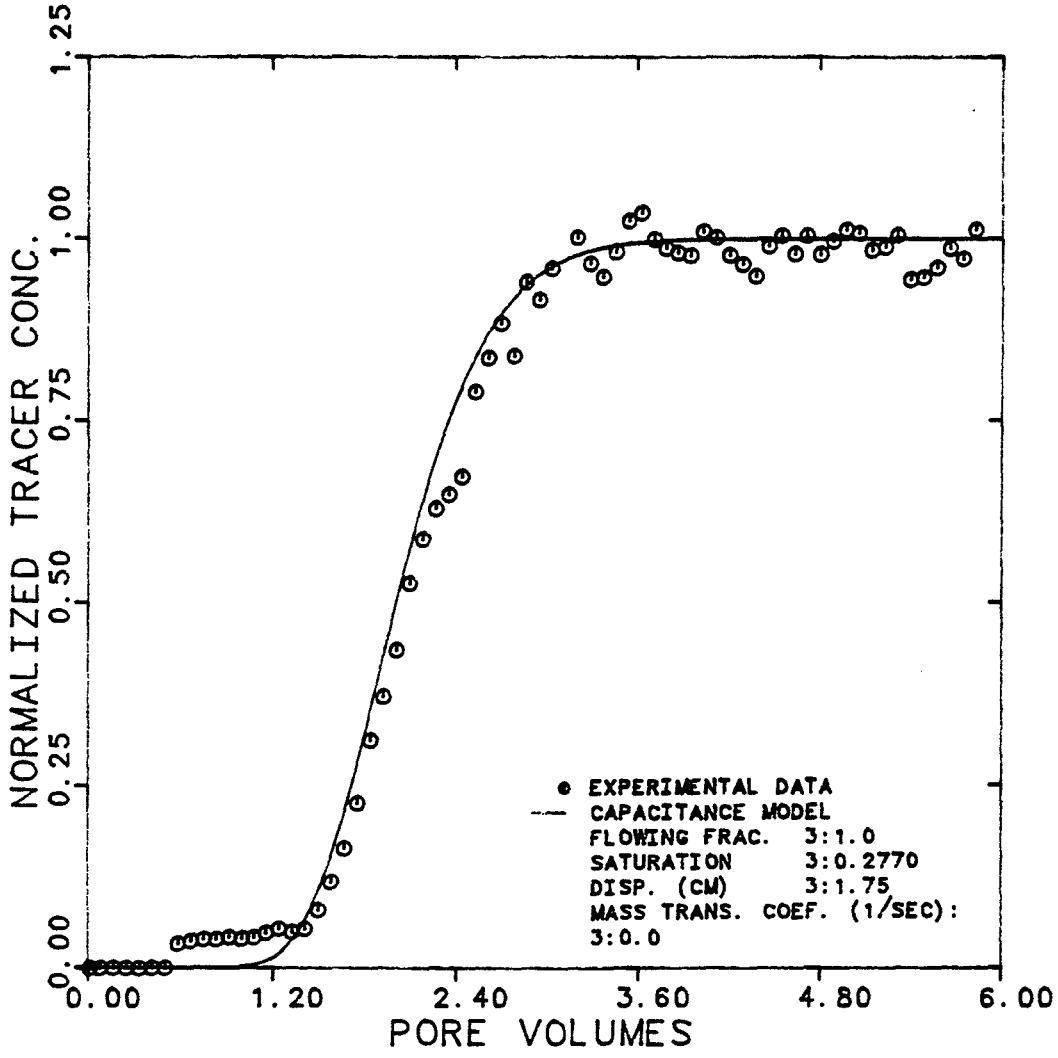

Figure 6.4.2.9 Effluent History for Labelled Sulfonate in M.E. at 67.6% Brine, 19% Oil, and 13.4% M.E. Cuts

EXPERIMENT NUMBER	BMO2-6		
TRACER & PHASES	CHLORIDE-36 BRINE & M.E.		
MAX. & INJ. CONC. (BRINE)	1998	2076	DPM/CC
MAX. & INJ. CONC. (M.E.)	907	907	DPM/CC
FLOW RATE	0.887		CC/MIN.

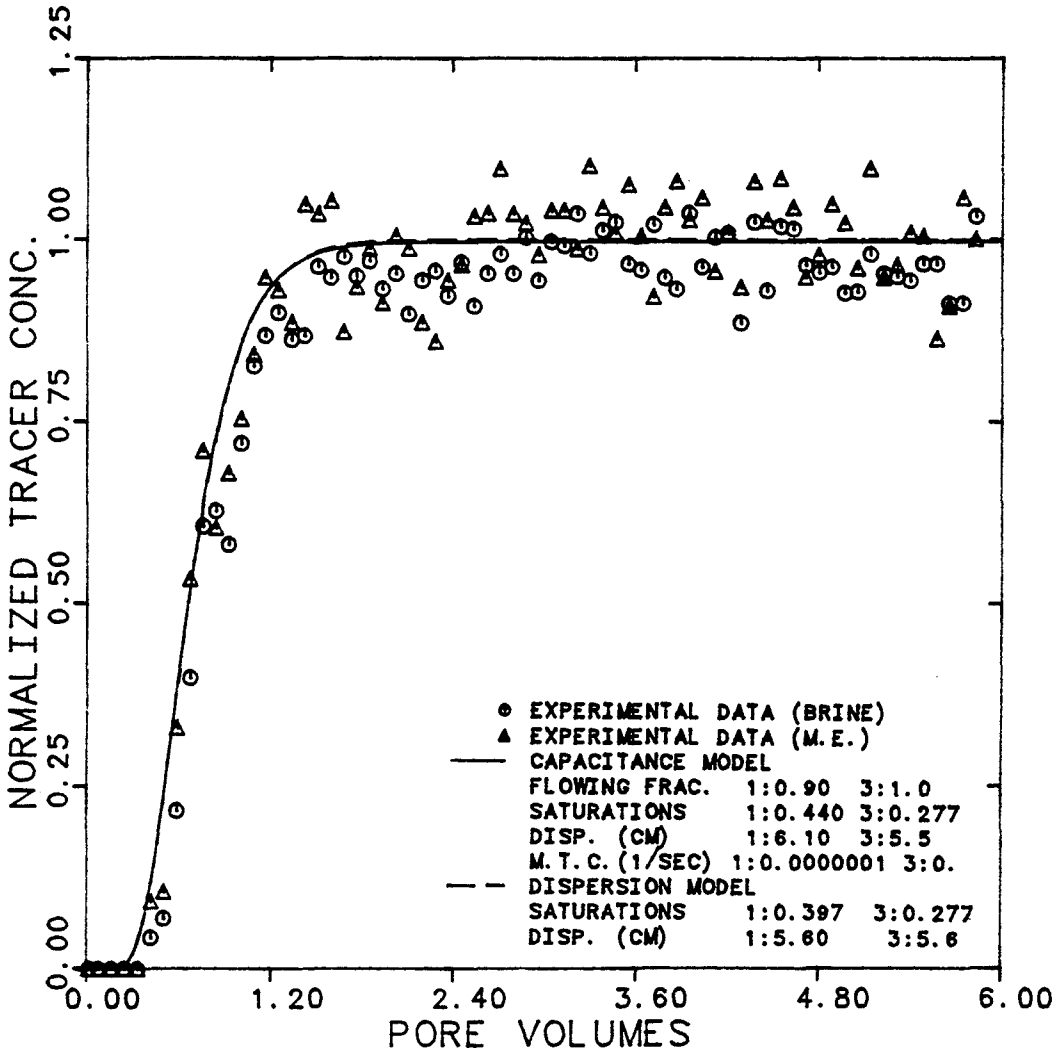

Figure 6.4.2.10 Effluent Histories for Chloride-36 in Brine and M.E. at 67.6% Brine, 19% Oil, and 13.4% M.E. Cuts

EXPERIMENT NUMBER		BM02-6	
TRACER & PHASES		CARBON-14 OIL & M.E.	
MAX. & INJ. CONC.	(OIL)	13897 14354	DPM/CC
MAX. & INJ. CONC.	(M.E.)	5900 5968	DPM/CC
FLOW RATE		0.887	CC/MIN.

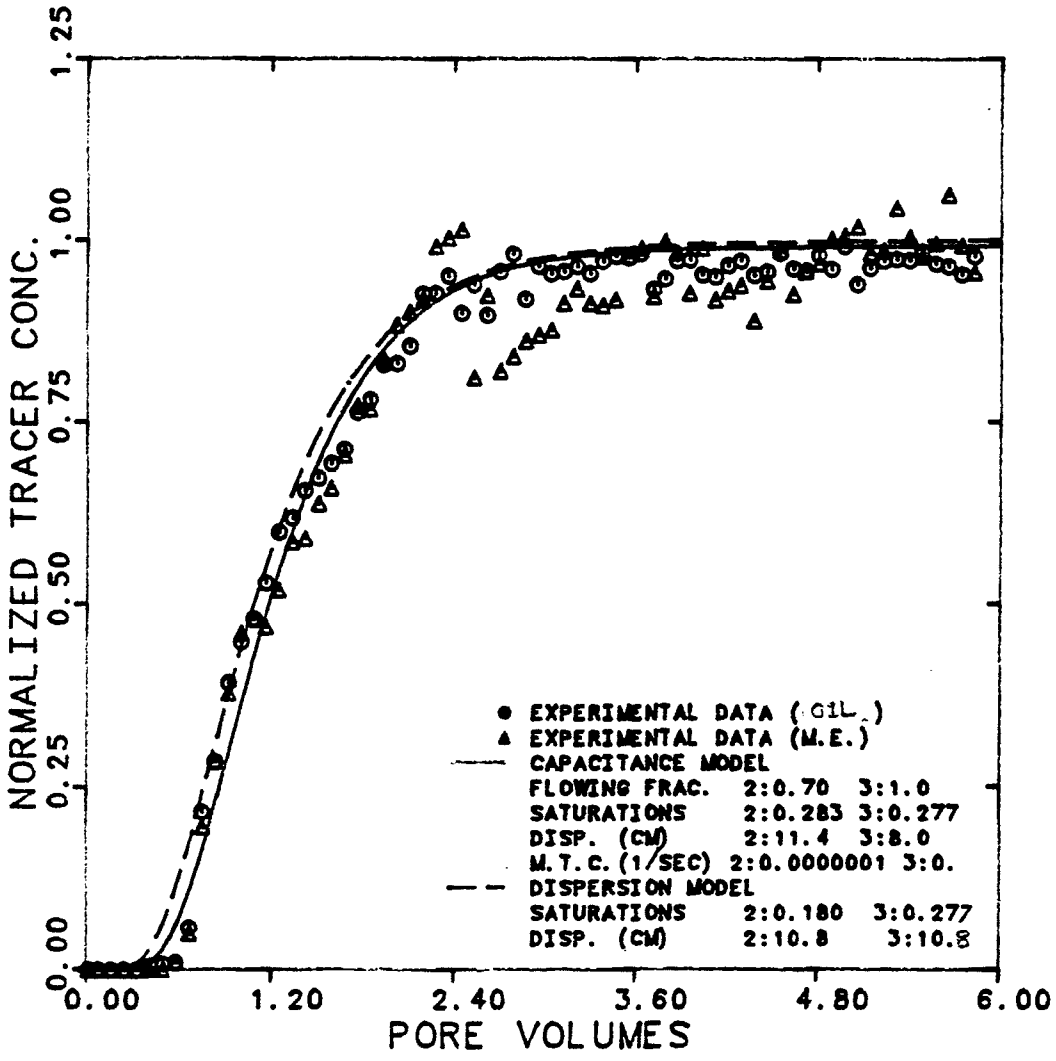

Figure 6.4.2.11 Effluent Histories for Carbon-14 in Oil and M.E. at 67.6% Brine, 19% Oil, and 13.4% M.E. Cuts

EXPERIMENT NUMBER	BM02-8	
TRACER & PHASE	TAG. SULF.	M.E.
FRACTIONAL FLOW	3: 0.110	
MAX. & INJ. CONC.	23200 27000	DPM/CC
FLOW RATE	1.110	CC/MIN.

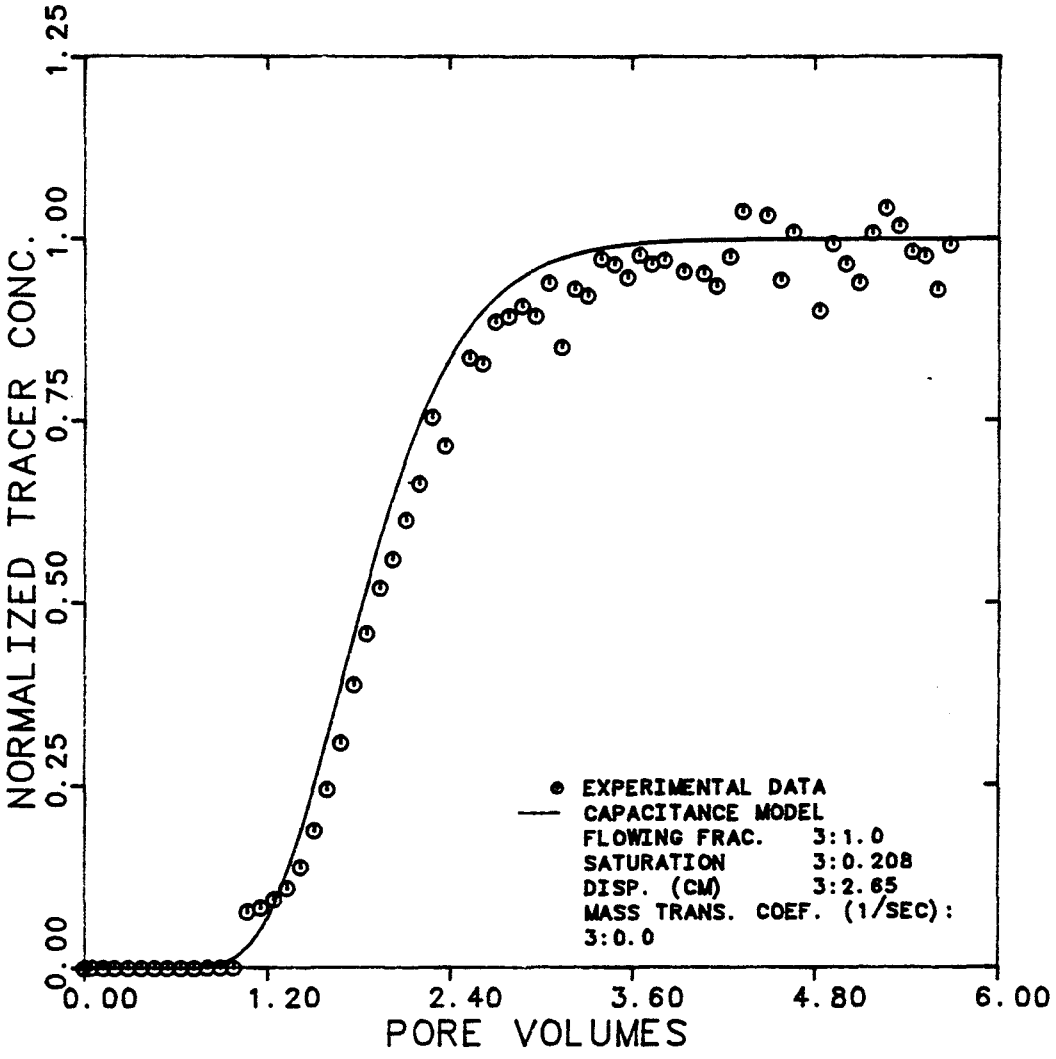

Figure 6.4.2.12 Effluent History for Labelled Sulfonate in M.E. at 26% Brine, 63% Oil, and 11% M.E. Cuts

EXPERIMENT NUMBER	BMO2-8		
TRACER & PHASES	CHLORIDE-36 BRINE & M.E.		
MAX. & INJ. CONC. (BRINE)	1983	2050	DPM/CC
MAX. & INJ. CONC. (M.E.)	880	880	DPM/CC
FLOW RATE	1.110		CC/MIN.

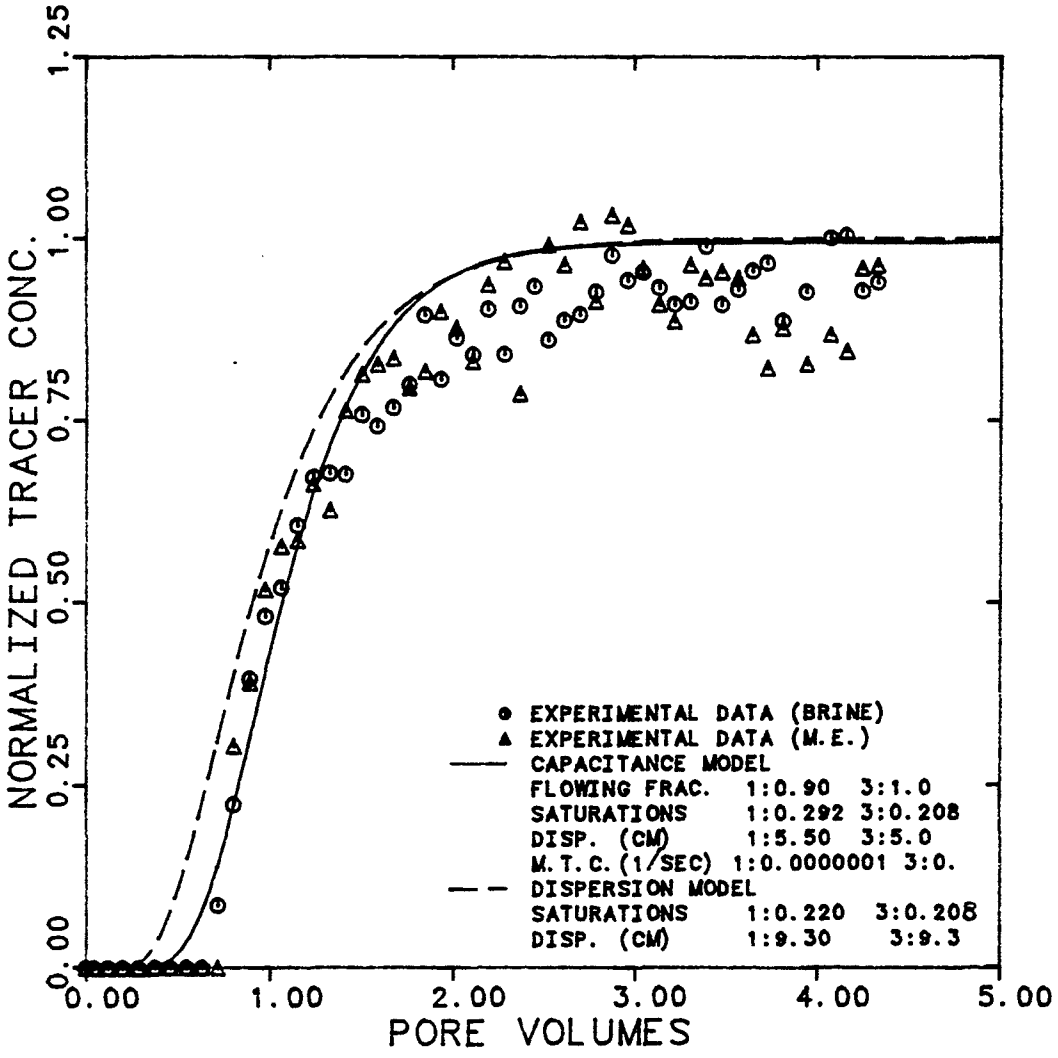

Figure 6.4.2.13 Effluent Histories for Chloride-36 in Brine and M.E. at 26% Brine, 63% Oil, and 11% M.E. Cuts

EXPERIMENT NUMBER	BMO2-8		
TRACER & PHASES	CARBON-14	OIL & M.E.	
MAX. & INJ. CONC. (OIL)	13962	14350	DPM/CC
MAX. & INJ. CONC. (M.E.)	6400	6500	DPM/CC
FLOW RATE	1.110		CC/MIN.

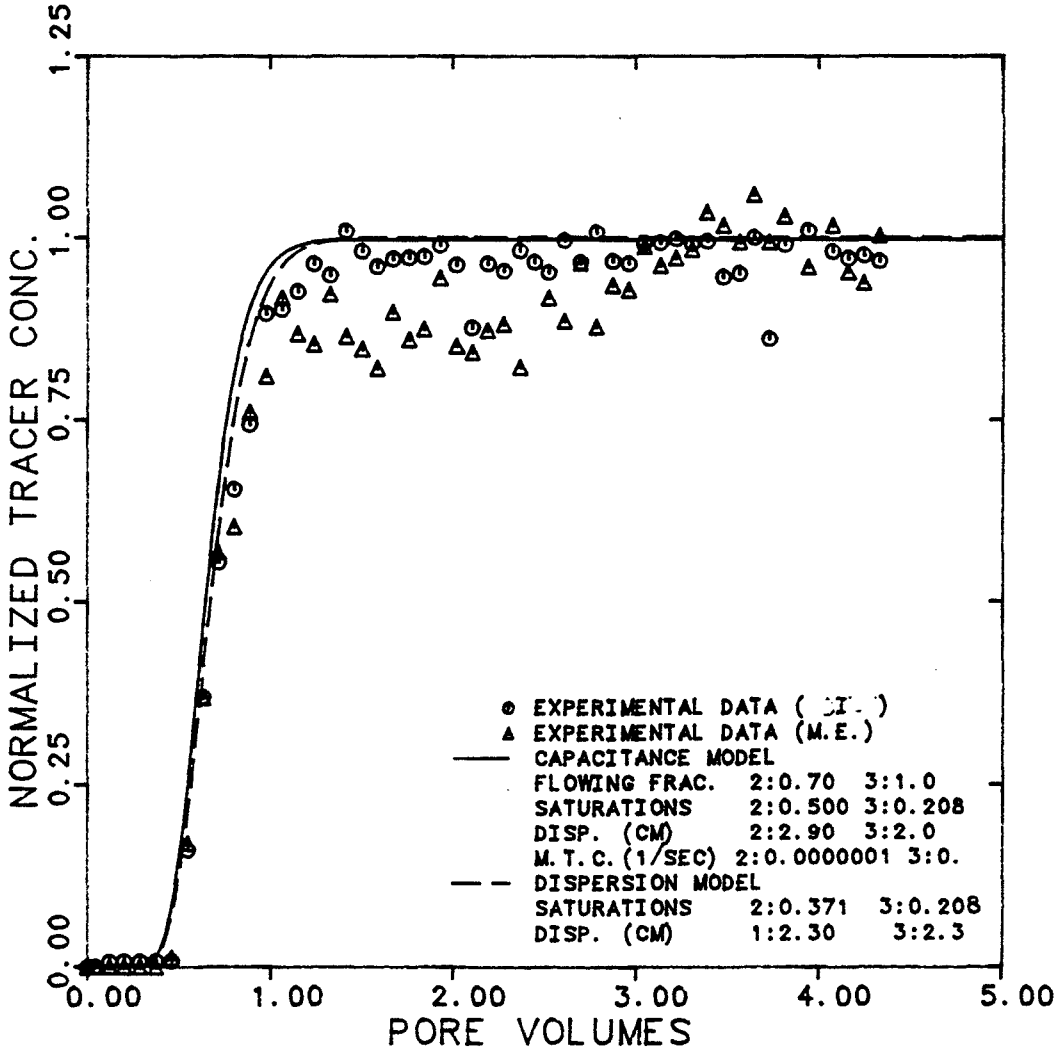

Figure 6.4.2.14 Effluent Histories for Carbon-14 in Oil and M.E. at 26% Brine, 63% Oil, and 11% M.E. Cuts

EXPERIMENT NUMBER	BMO2-10	
TRACER & PHASE	TAG. SULF.	M.E.
FRACTIONAL FLOW	3: 0.301	
MAX. & INJ. CONC.	24800 26000	DPM/CC
FLOW RATE	0.678	CC/MIN.

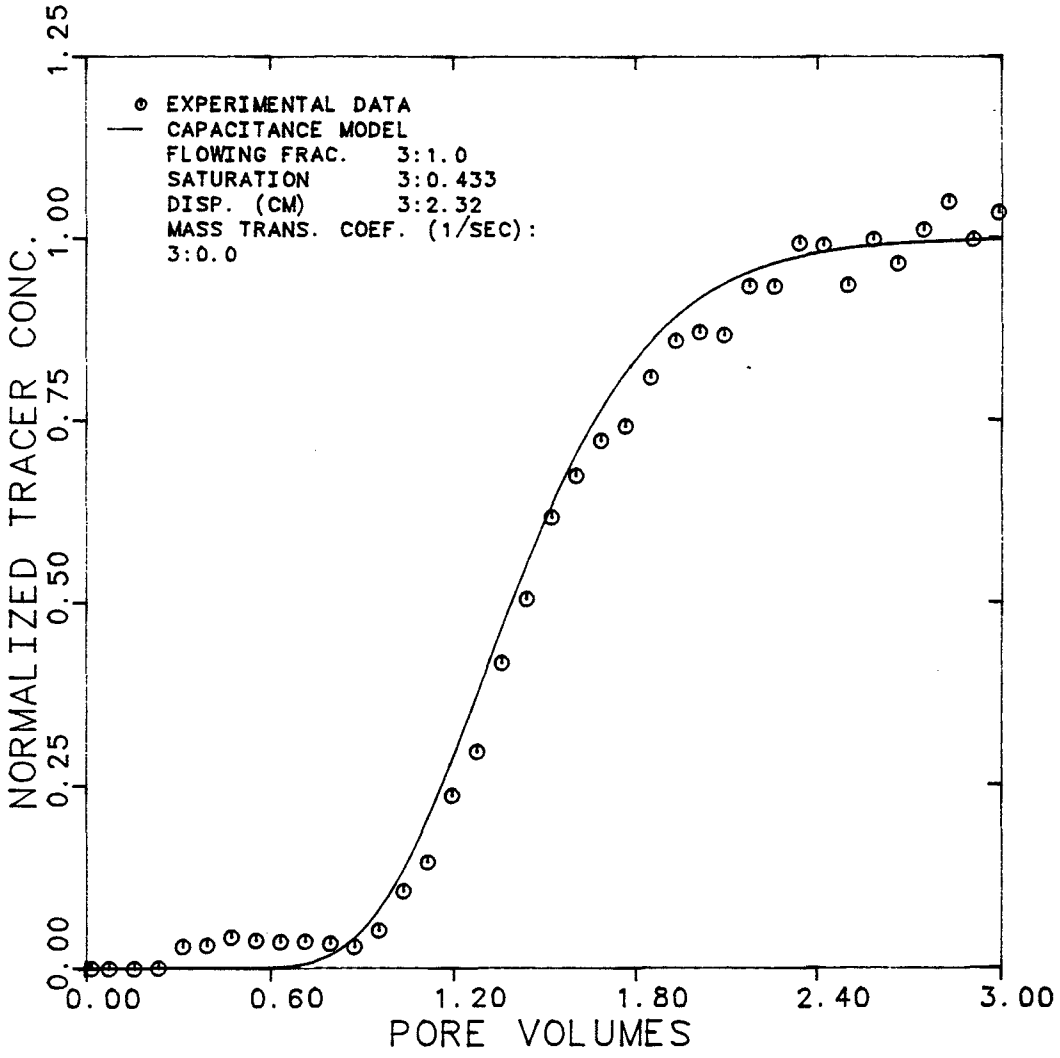

Figure 6.4.2.15 Effluent History for Labelled Sulfonate in M.E. at 26.3% Brine, 43.6% Oil, and 30.1% M.E. Cuts

EXPERIMENT NUMBER	BM02-10		
TRACER & PHASE	CHLORIDE-36 BRINE&M.E		
MAX. & INJ. CONC. (BRINE)	1880	1950	DPM/CC
MAX. & INJ. CONC. (M.E)	860	878	DPM/CC
FLOW RATE	0.678		CC/MIN

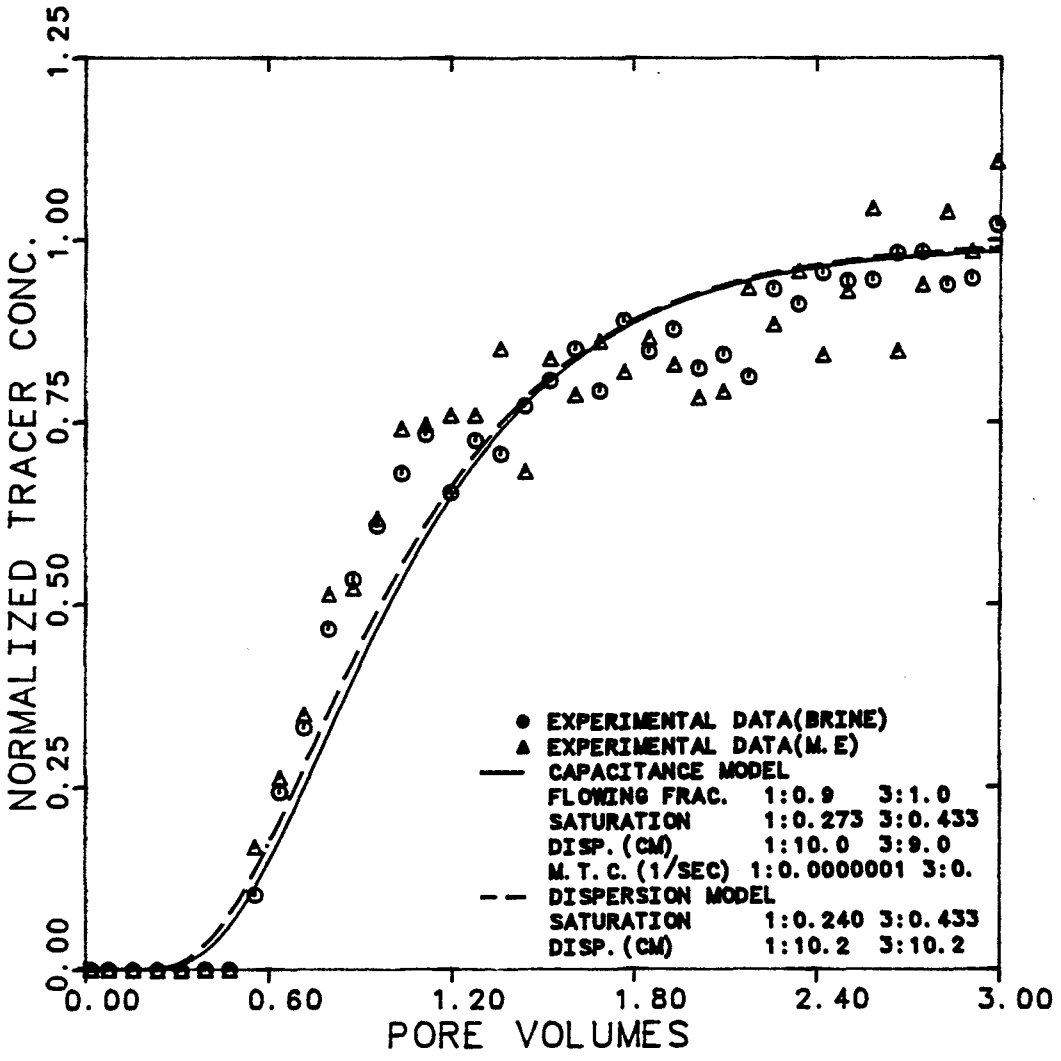

Figure 6.4.2.16 Effluent Histories for Chloride-36 in Brine and M.E. at 26.3% Brine, 43.6% Oil, and 30.1% M.E. Cuts

EXPERIMENT NUMBER	BM02-10		
TRACER & PHASE	CARBON-14	OIL & M.E	
MAX. & INJ. CONC. (OIL)	14000	14173	DPM/CC
MAX. & INJ. CONC. (M.E)	6200	6300	DPM/CC
FLOW RATE	0.678		CC/MIN

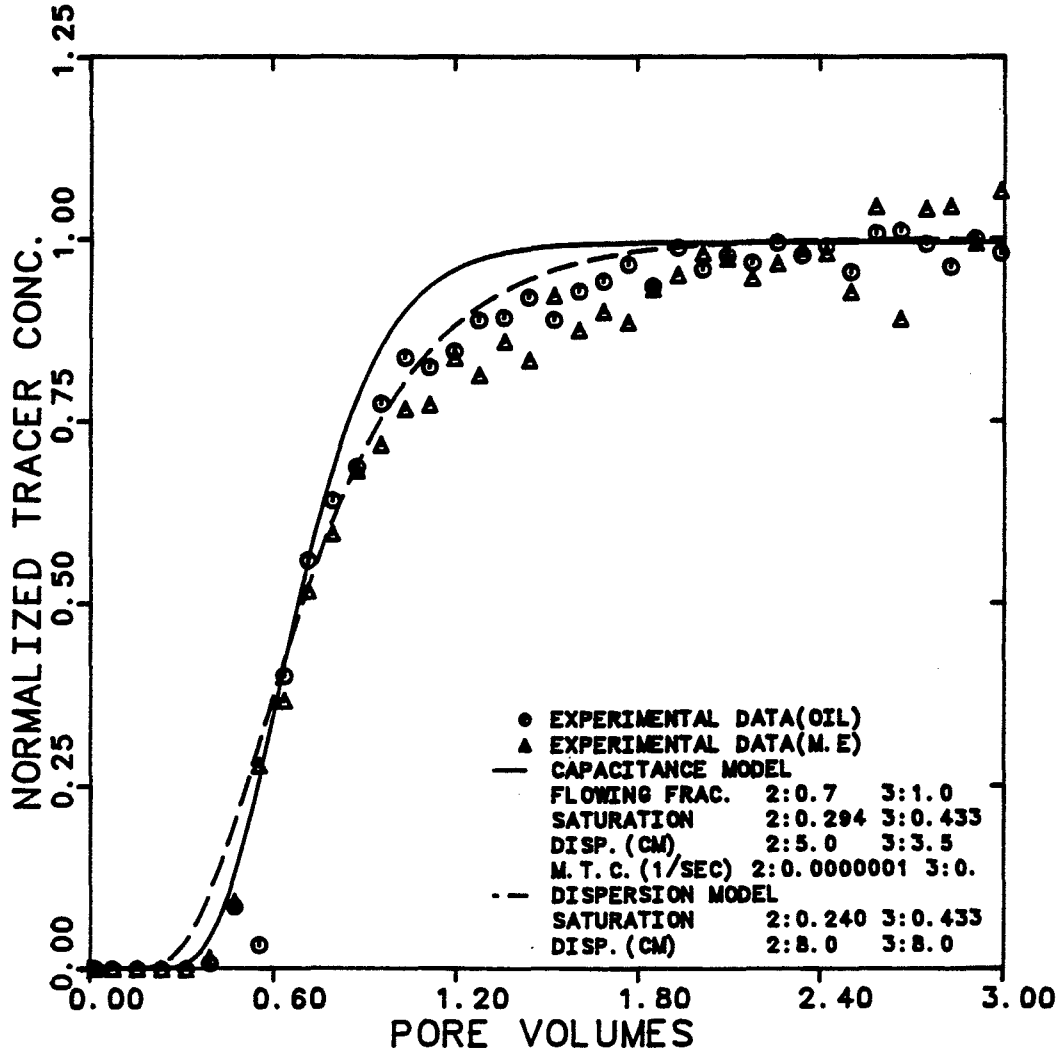

Figure 6.4.2.17 Effluent Histories for Carbon-14 in Oil and M.E. at 26.3% Brine, 43.6% Oil, and 30.1% M.E. Cuts

EXPERIMENT NUMBER	BMO2-12	
TRACER & PHASE	TAG. SULF.	M.E.
FRACTIONAL FLOW	3: 0.689	
MAX. & INJ. CONC.	24852 26000	DPM/CC
FLOW RATE	0.450	CC/MIN.

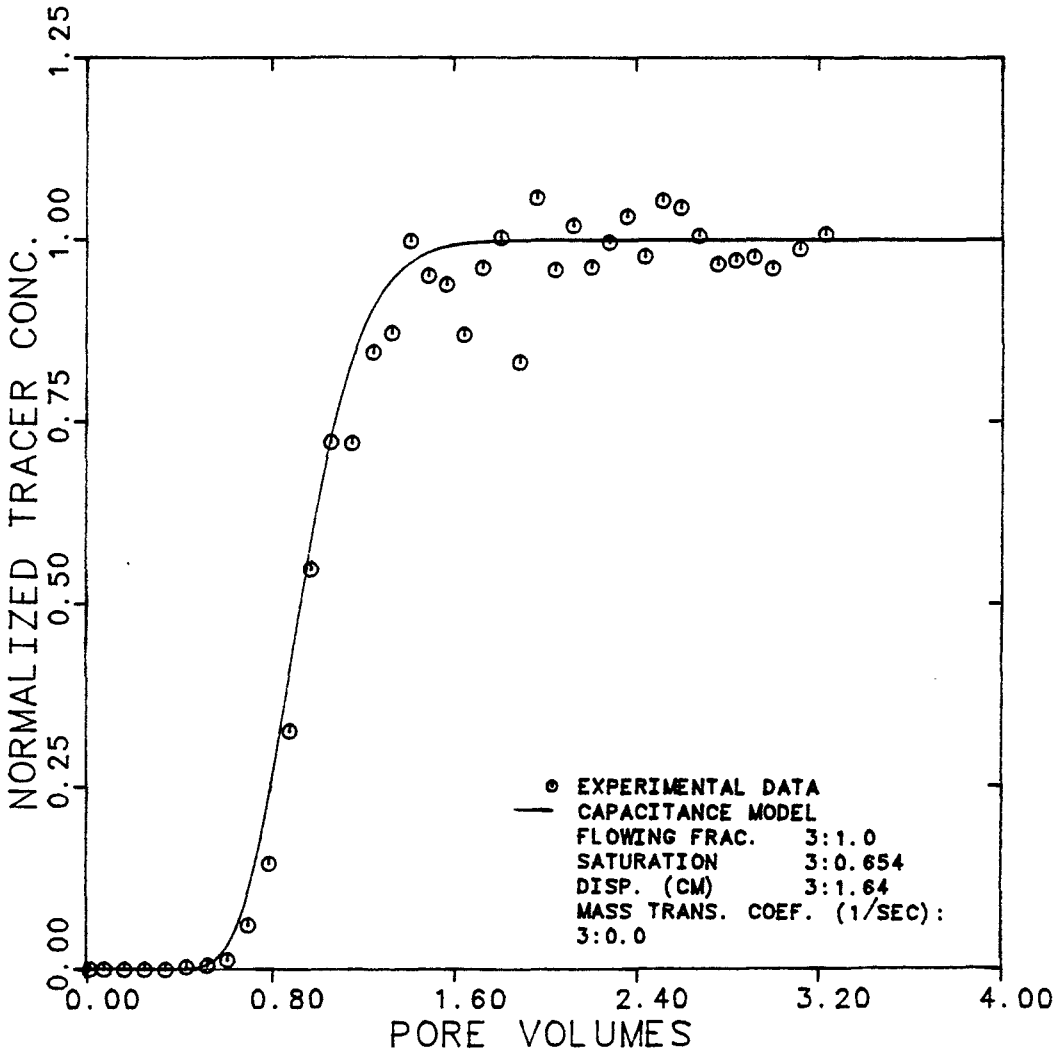

Figure 6.4.2.18 Effluent History for Labelled Sulfonate in M.E. for 16.7% Brine, 14.4% Oil, and 68.9% M.E. Cuts

EXPERIMENT NUMBER	BMO2-12		
TRACER & PHASE	CHLORIDE-36	BRINE&M.E	
MAX. & INJ. CONC. (BRINE)	1980	1980	DPM/CC
MAX. & INJ. CONC. (M.E)	940	1000	DPM/CC
FLOW RATE	0.45		CC/MIN

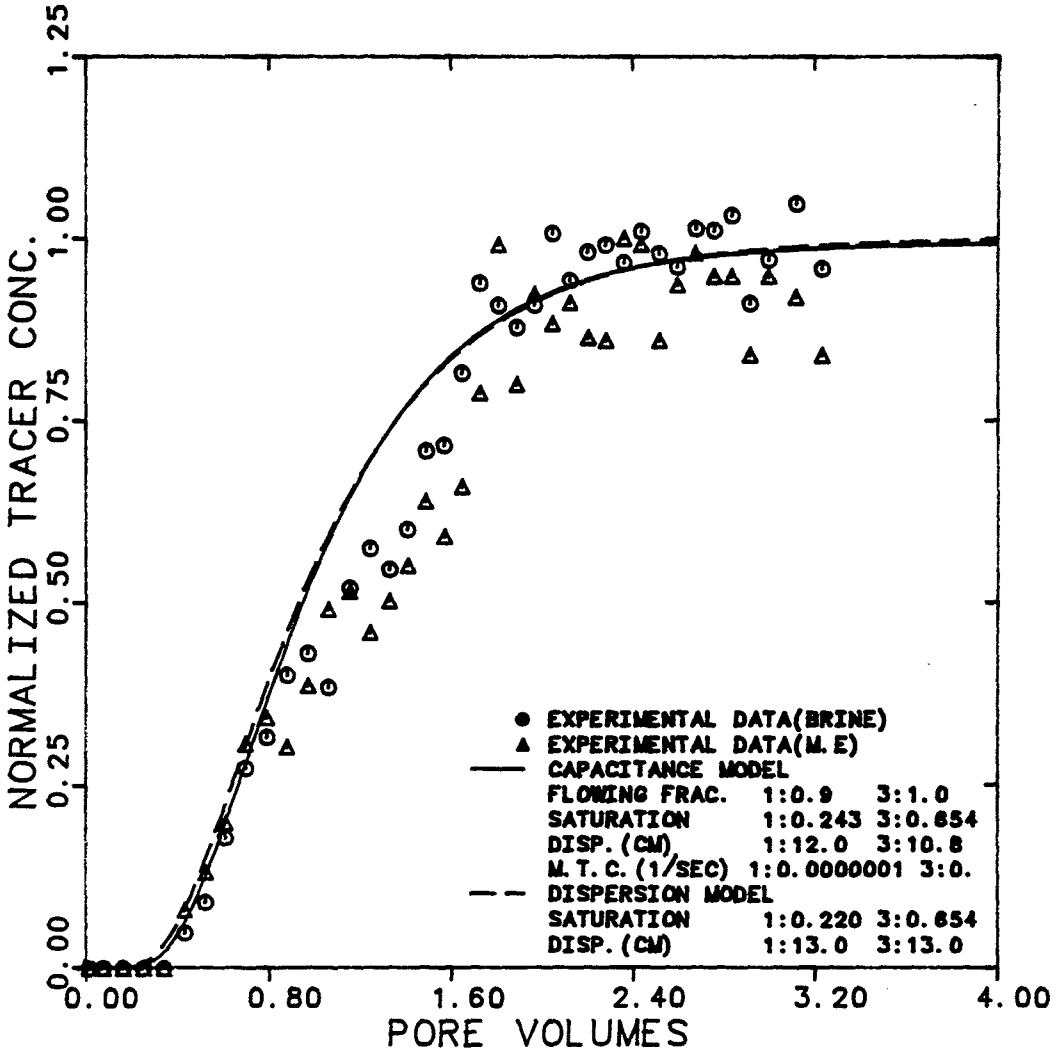

Figure 6.4.2.19 Effluent Histories for Chloride-36 in Brine and M.E. at 16.7% Brine, 14.4% Oil, and 68.9% M.E. Cuts

EXPERIMENT NUMBER	BM02-12		
TRACER & PHASE	CARBON-14	OIL & M.E	
MAX. & INJ. CONC. (OIL)	14000	14400	DPM/CC
MAX. & INJ. CONC. (M.E)	6020	6220	DPM/CC
FLOW RATE	0.45		CC/MIN

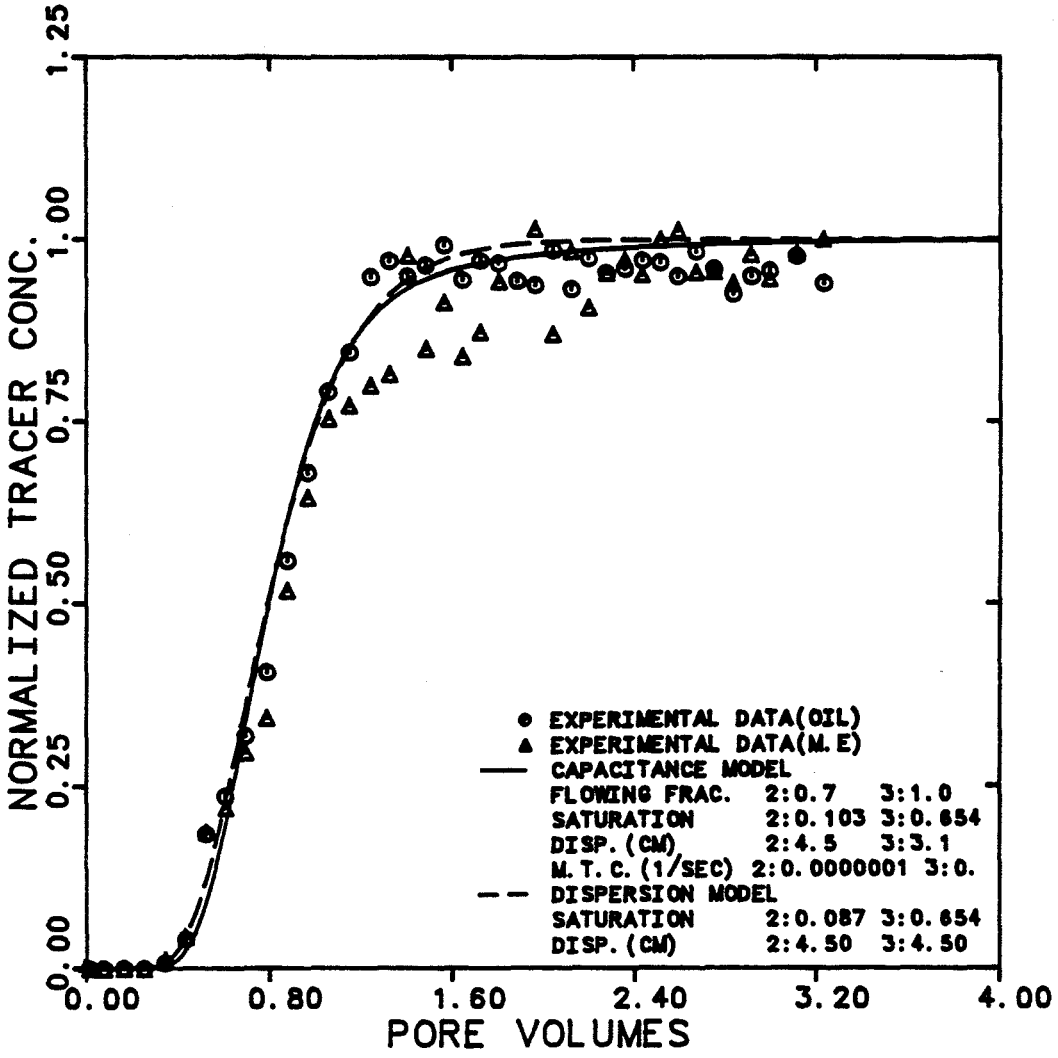

Figure 6.4.2.20 Effluent Histories for Carbon-14 in Oil and M.E. at 16.7% Brine, 14.4% Oil, and 68.9% M.E. Cuts

EXPERIMENT NUMBER	BM02-14	
TRACER & PHASE	TAGG. SULF.	M.E.
FRACTIONAL FLOW	3:.370	
MAX. & INJ. CONC.	22800 26000	DPM/CC
FLOW RATE	0.604	CC/MIN.

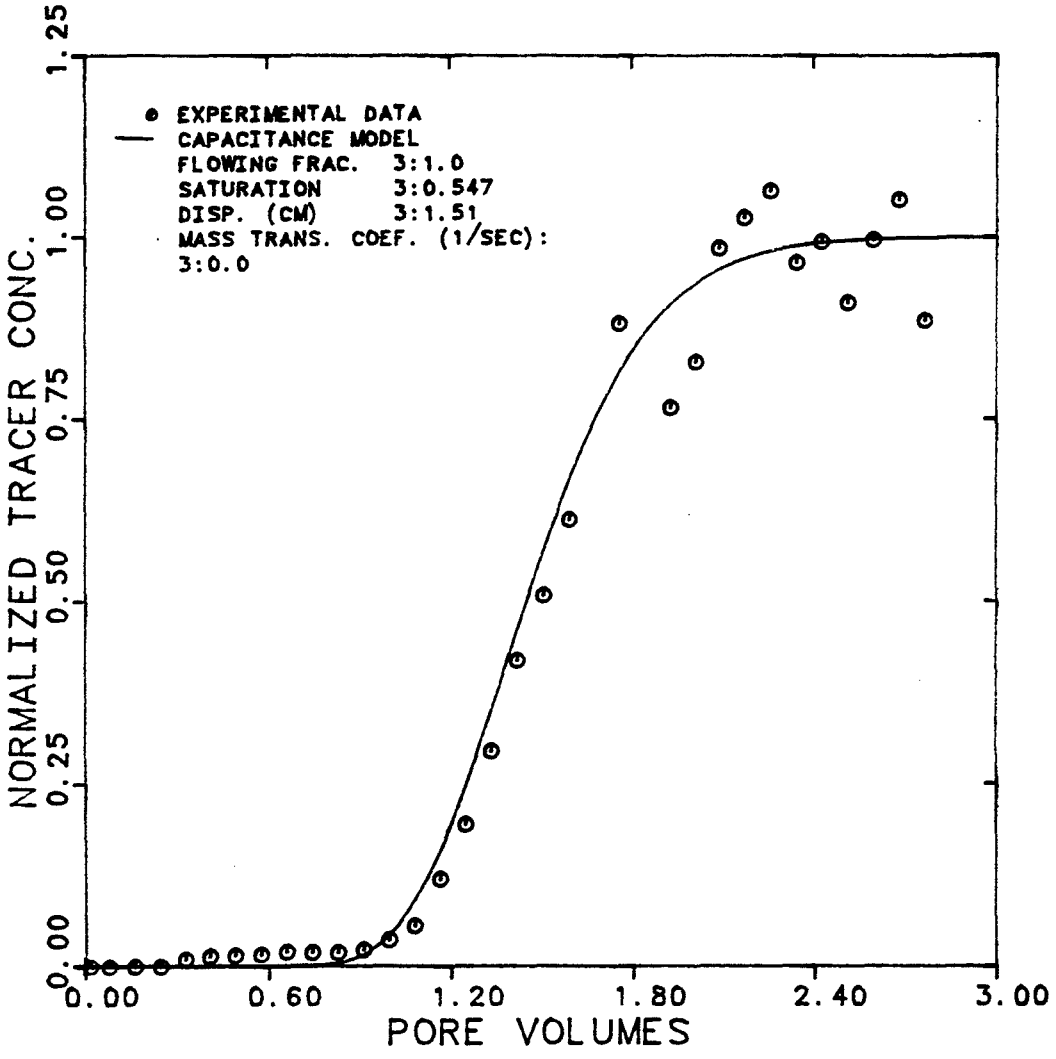

Figure 6.4.2.21 Effluent History for Labelled Sulfonate in M.E. at 56% Brine, 7% Oil, and 37% M.E. Cuts

EXPERIMENT NUMBER	BMO2-14		
TRACER & PHASES	CHLORIDE-36 BRINE & M.E.		
MAX. & INJ. CONC. (BRINE)	1960	2020	DPM/CC
MAX. & INJ. CONC. (M.E.)	887	952	DPM/CC
FLOW RATE	0.604		CC/MIN

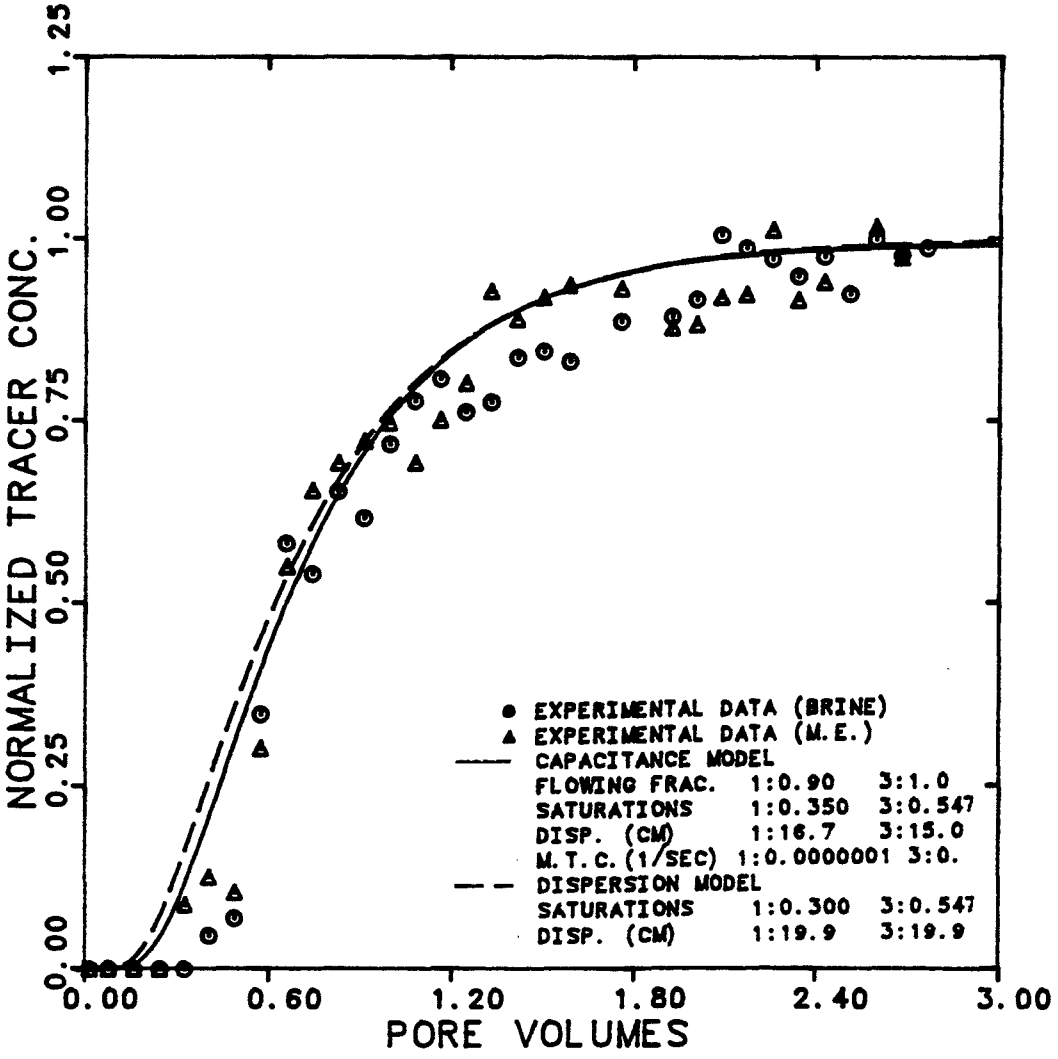

Figure 6.4.2.22 Effluent Histories for Chloride-36 in Brine and M.E. for 56% Brine, 7% Oil, and 37% M.E. Cuts

EXPERIMENT NUMBER	BM02-14		
TRACER & PHASES	CARBON-14	OIL	& M.E.
MAX. & INJ. CONC. (OIL)	13431	14235	DPM/CC
MAX. & INJ. CONC. (M.E.)	4795	4900	DPM/CC
FLOW RATE	0.604		CC/MIN

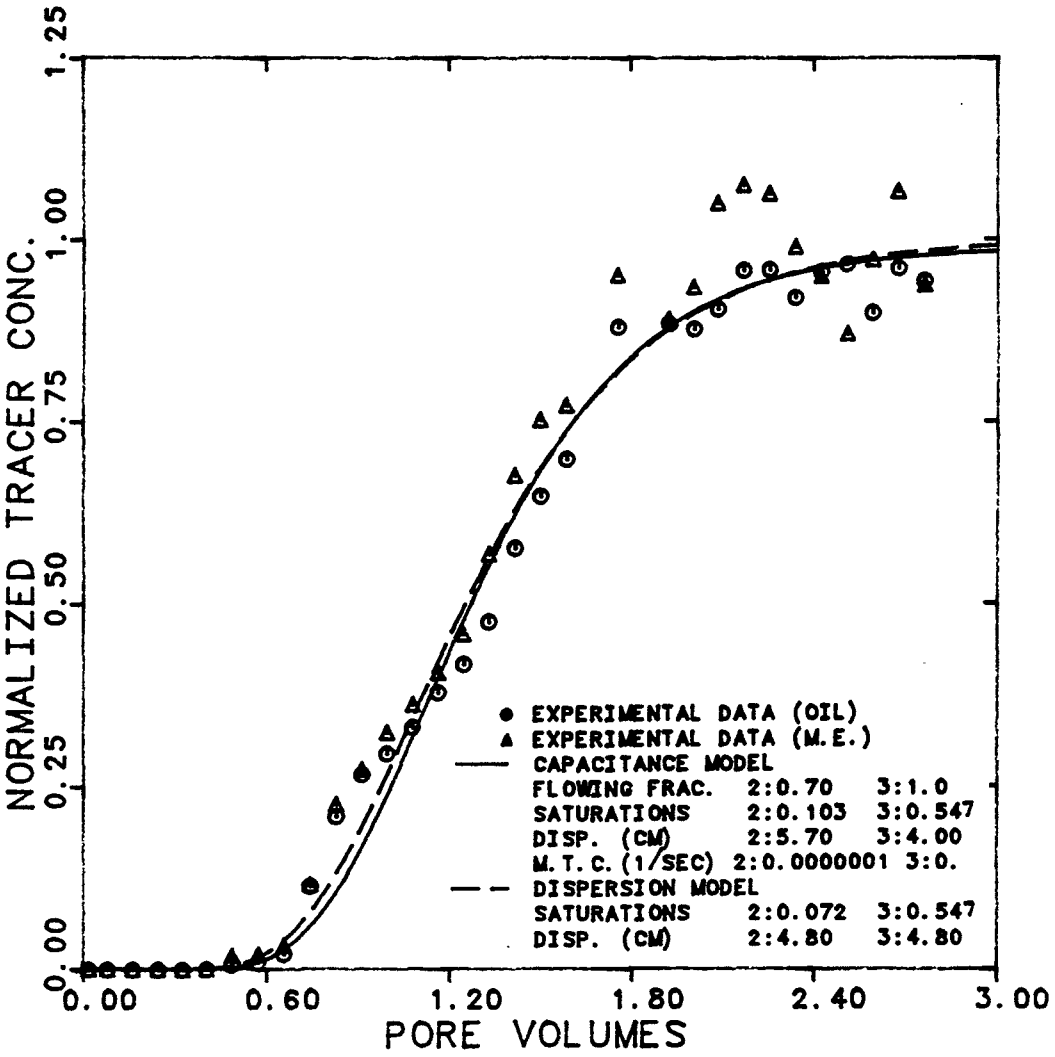

Figure 6.4.2.23 Effluent Histories for Carbon-14 in Oil and M.E. at 56% Brine, 7% Oil, and 37% M.E. Cuts

EXPERIMENT NUMBER	BMO2-16	
TRACER & PHASE	TAG. SULF.	M.E.
FRACTIONAL FLOW	3: 0.480	
MAX. & INJ. CONC.	24365 27140	DPM/CC
FLOW RATE	0.480	CC/MIN.

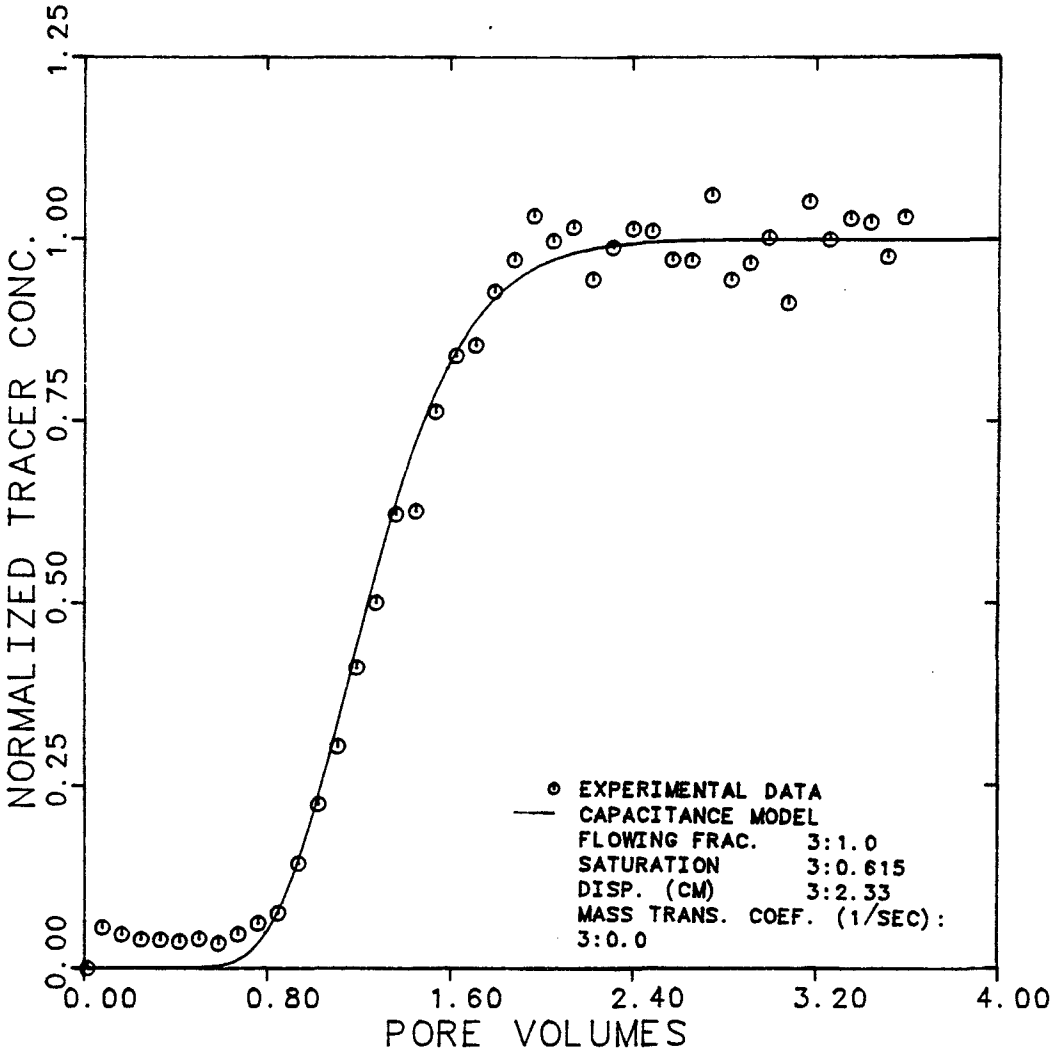

Figure 6.4.2.24 Effluent History for Labelled Sulfonate in M.E. at 40% Brine, 12% Oil, and 48% M.E. Cuts

EXPERIMENT NUMBER	BMO2- 16		
TRACER & PHASES	CHLORIDE-36 BRINE & M.E.		
MAX. & INJ. CONC. (BRINE)	1720	1720	DPM/CC
MAX. & INJ. CONC. (M.E.)	810	830	DPM/CC
FLOW RATE	0.480		CC/MIN

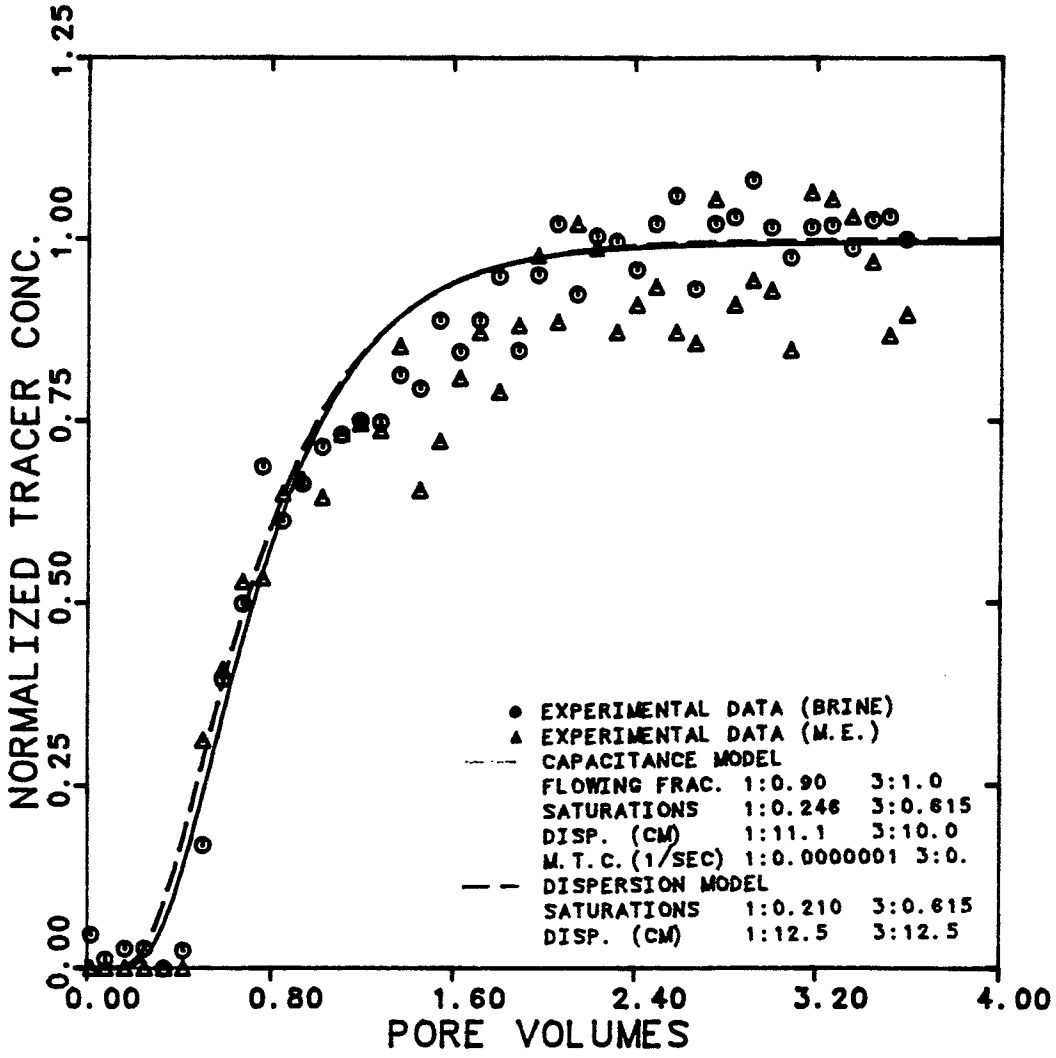

Figure 6.4.2.25 Effluent Histories for Chloride-36 in Brine and M.E. at 40% Brine, 12% Oil, and 48% M.E. Cuts

EXPERIMENT NUMBER	BM02-16		
TRACER & PHASES	CARBON-14	OIL	& M.E.
MAX. & INJ. CONC. (OIL)	14000	14600	DPM/CC
MAX. & INJ. CONC. (M.E.)	6047	6100	DPM/CC
FLOW RATE	0.480		CC/MIN

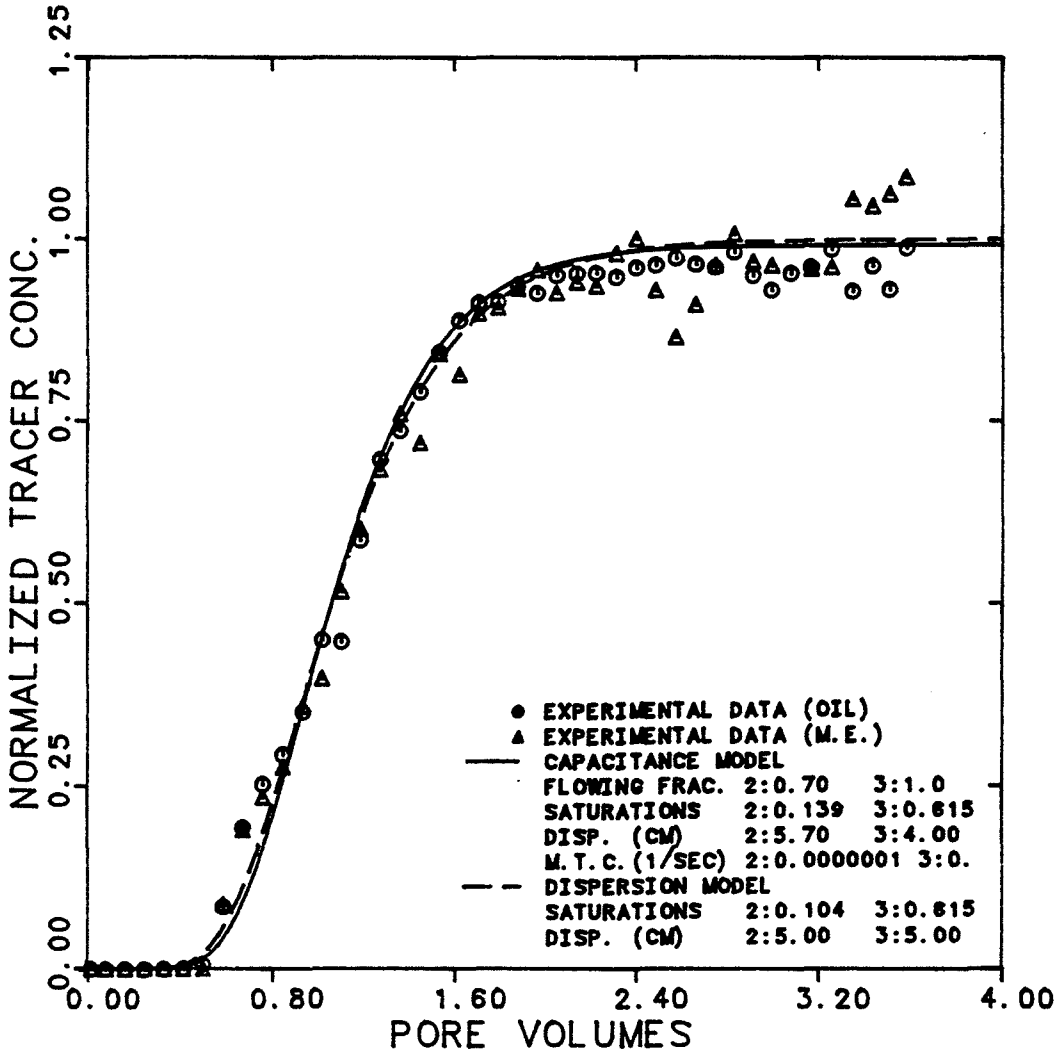

Figure 6.4.2.26 Effluent Histories for Carbon-14 in Oil and M.E. at 40% Brine, 12% Oil, and 48% M.E. Cuts

EXPERIMENT NUMBER	BMO2-18	
TRACER & PHASE	TAGG. SULF. M.E.	
FRACTIONAL FLOW	3: .332	
MAX. & INJ. CONC.	26022 27000	DPM/CC
FLOW RATE	0.620	CC/MIN.

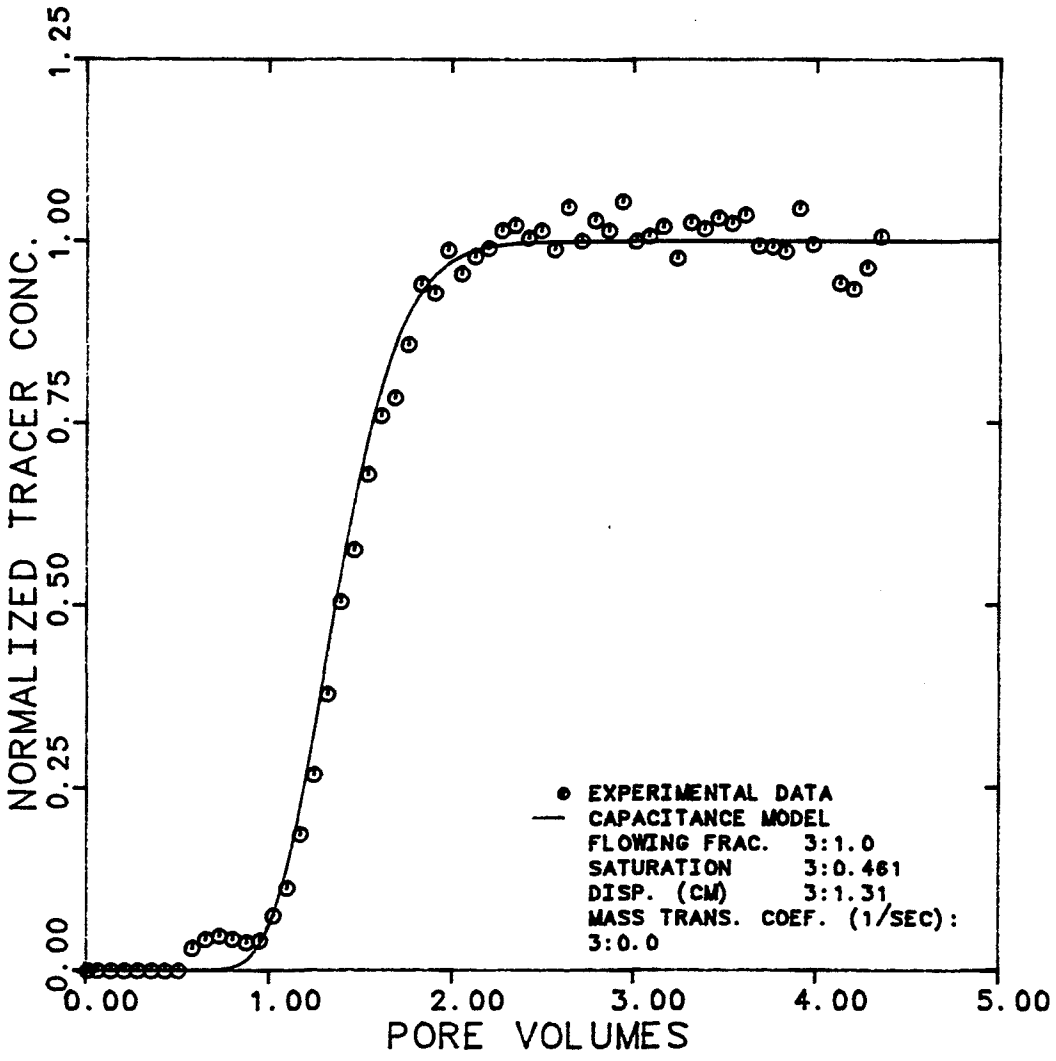

Figure 6.4.2.27 Effluent History for Labelled Sulfonate in M.E. at 56.4% Brine, 10.4% Oil, and 33.2% M.E. Cuts

EXPERIMENT NUMBER	BMO2-18		
TRACER & PHASES	CHLORIDE-36 BRINE & M.E.		
MAX. & INJ. CONC. (BRINE)	1740	1780	DPM/CC
MAX. & INJ. CONC. (M.E.)	820	820	DPM/CC
FLOW RATE	0.620		CC/MIN

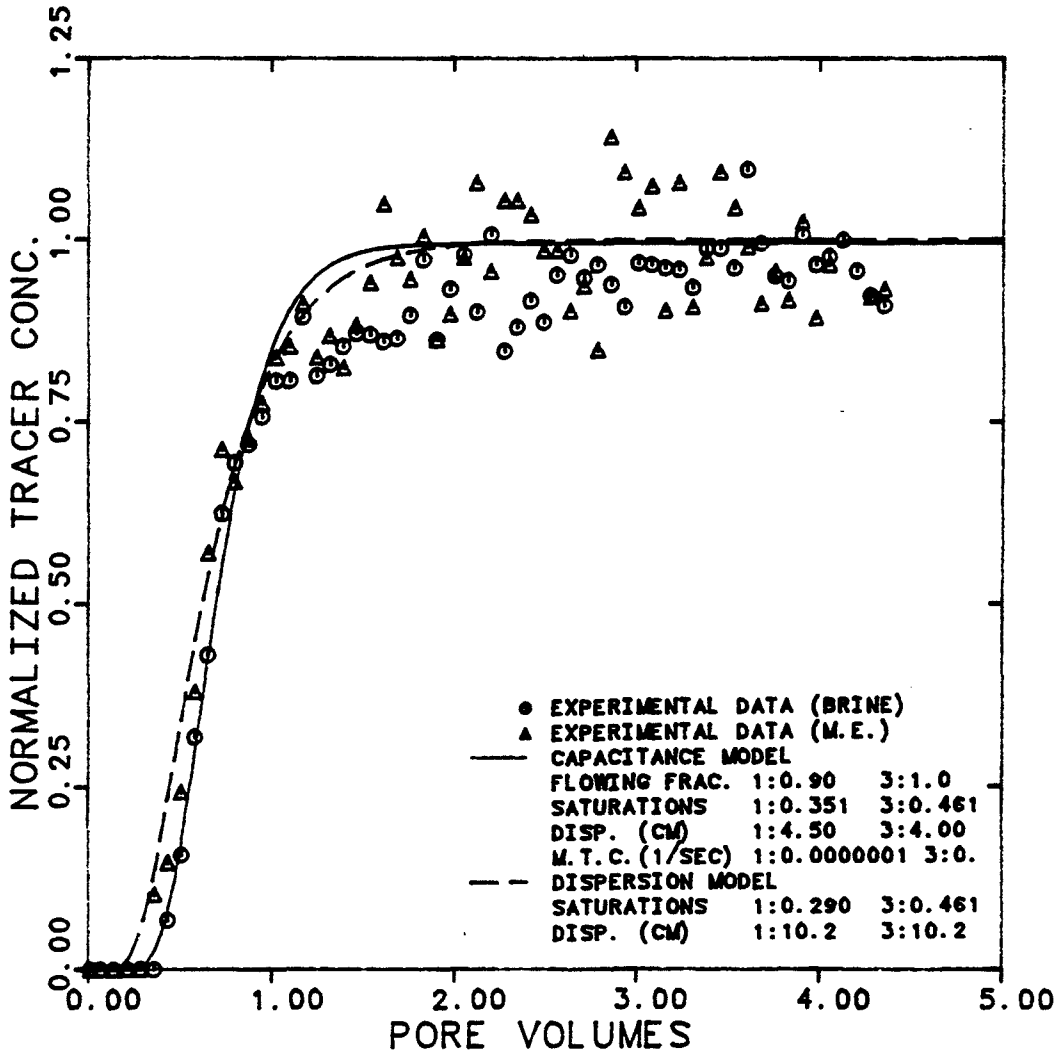

Figure 6.4.2.28 Effluent Histories for Chloride-36 in Brine and M.E. at 56.4% Brine, 10.4% Oil, and 33.2% M.E. Cuts

EXPERIMENT NUMBER	BM02-18		
TRACER & PHASES	CARBON-14	OIL	& M.E.
MAX. & INJ. CONC. (OIL)	14000	14370	DPM/CC
MAX. & INJ. CONC. (M.E.)	6300	6800	DPM/CC
FLOW RATE	0.620		CC/MIN

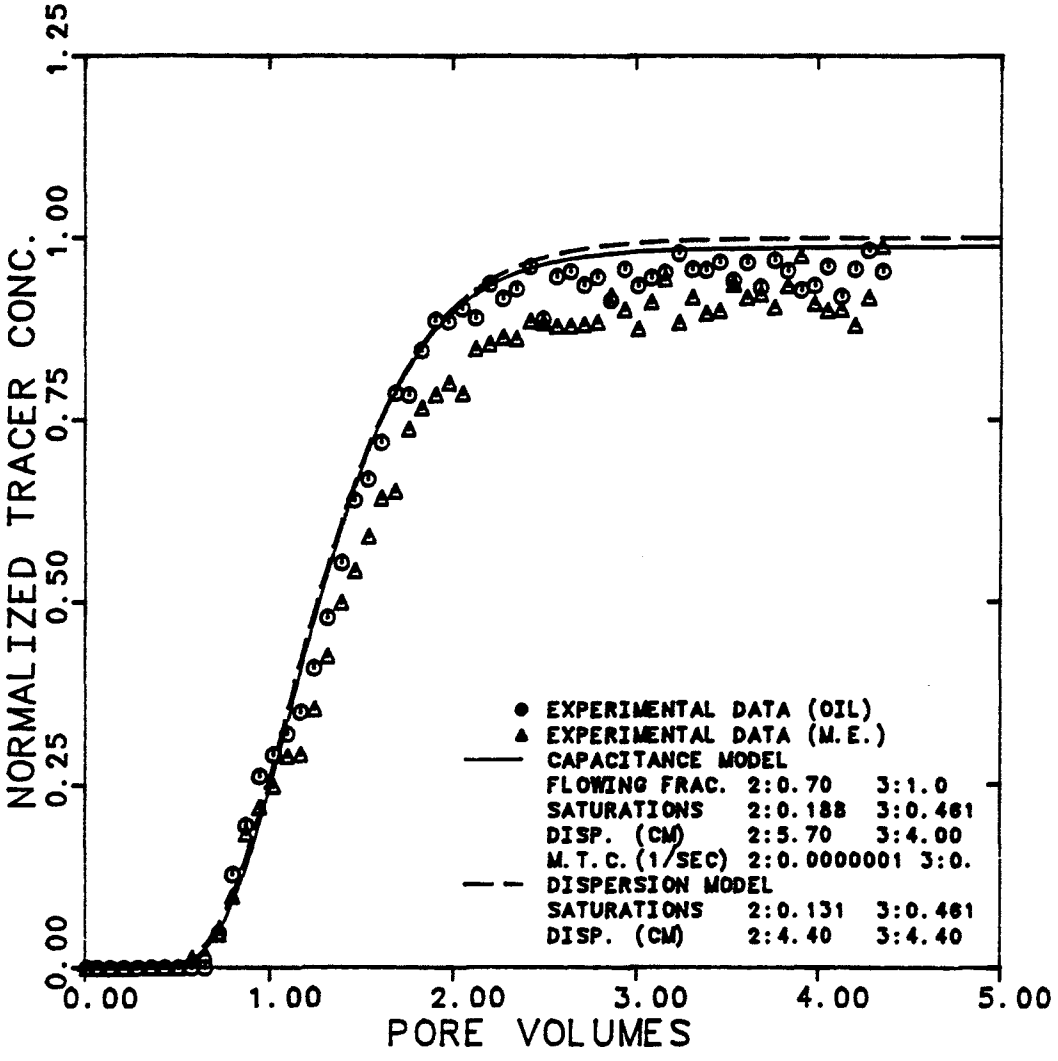

Figure 6.4.2.29 Effluent Histories for Carbon-14 in Oil and M.E. at 56.4% Brine, 10.4% Oil, and 33.2% M.E. Cuts

EXPERIMENT NUMBER	BM02-20	
TRACER & PHASE	TAGG. SULF. M.E.	
FRACTIONAL FLOW	3:.223	
MAX. & INJ. CONC.	26800 27000	DPM/CC
FLOW RATE	0.750	CC/MIN.

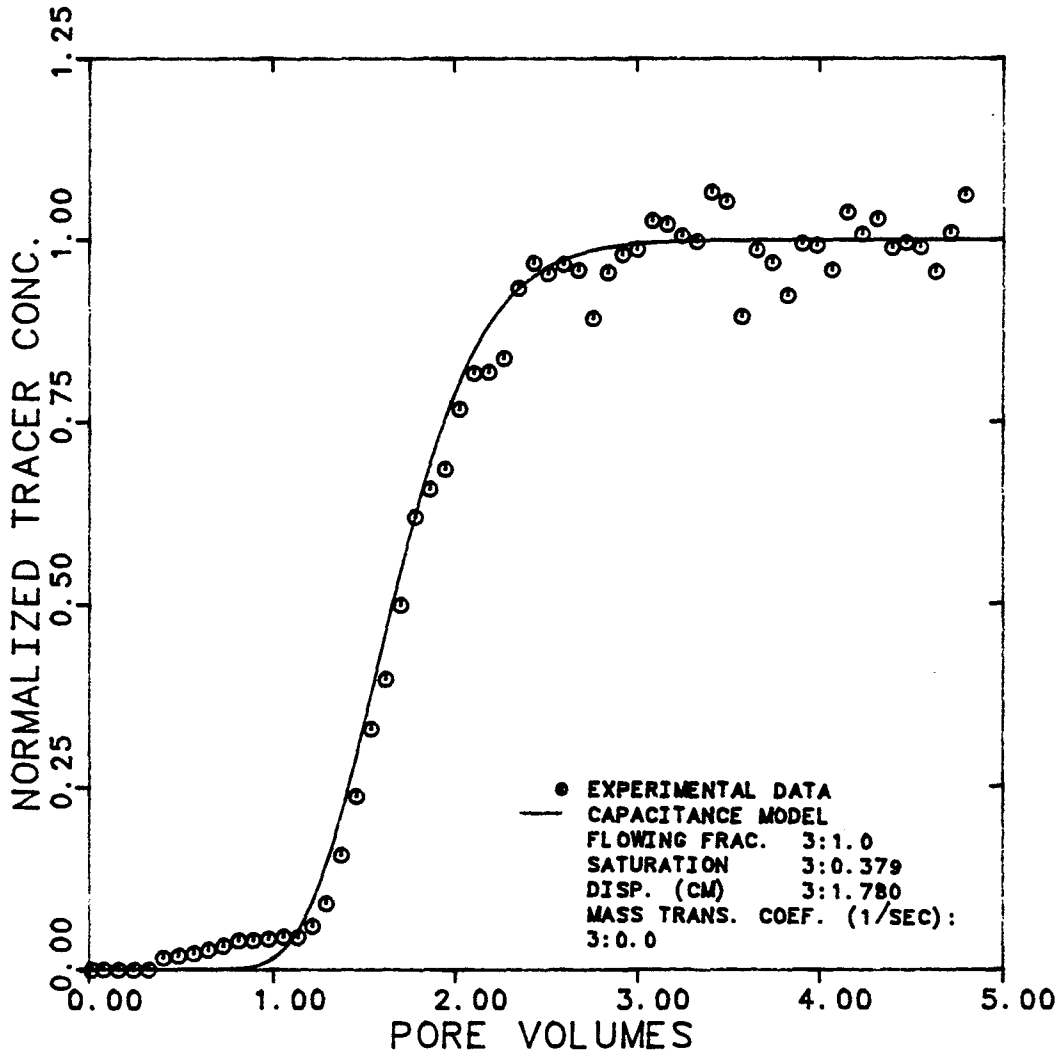

Figure 6.4.2.30 Effluent History for Labelled Sulfonate in M.E. at 69.7% Brine, 8% Oil, and 22.3% M.E. Cuts

EXPERIMENT NUMBER	BM02-20		
TRACER & PHASES	CHLORIDE-36 BRINE & M.E.		
MAX. & INJ. CONC. (BRINE)	1700	1800	DPM/CC
MAX. & INJ. CONC. (M.E.)	860	900	DPM/CC
FLOW RATE	0.750		CC/MIN

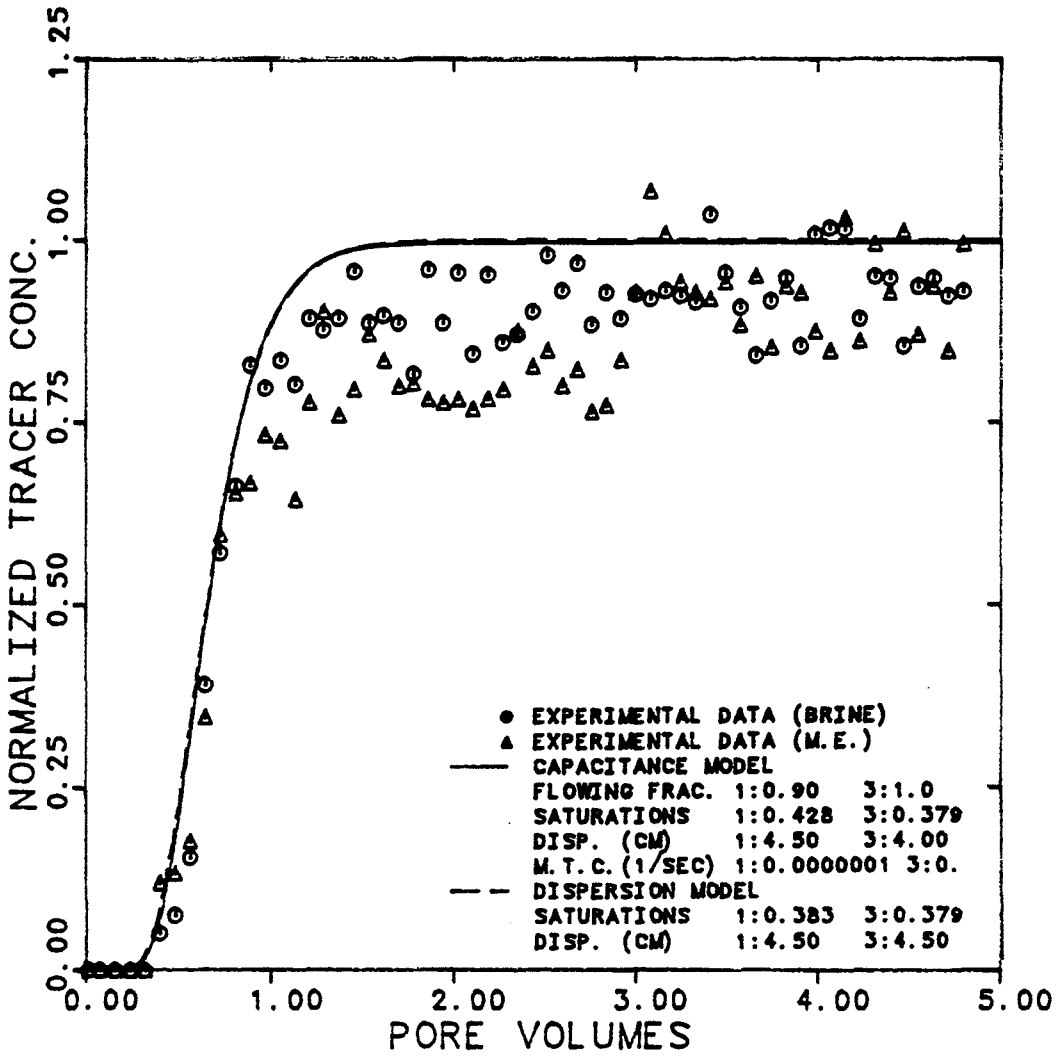

Figure 6.4.2.31 Effluent Histories for Chloride-36 in Brine and M.E. at 69.7% Brine, 8% Oil, and 22.3% M.E. Cuts

EXPERIMENT NUMBER	BM02-20		
TRACER & PHASES	CARBON-14	OIL	& M.E.
MAX. & INJ. CONC. (OIL)	14000	14370	DPM/CC
MAX. & INJ. CONC. (M.E.)	5600	5700	DPM/CC
FLOW RATE	0.750		CC/MIN

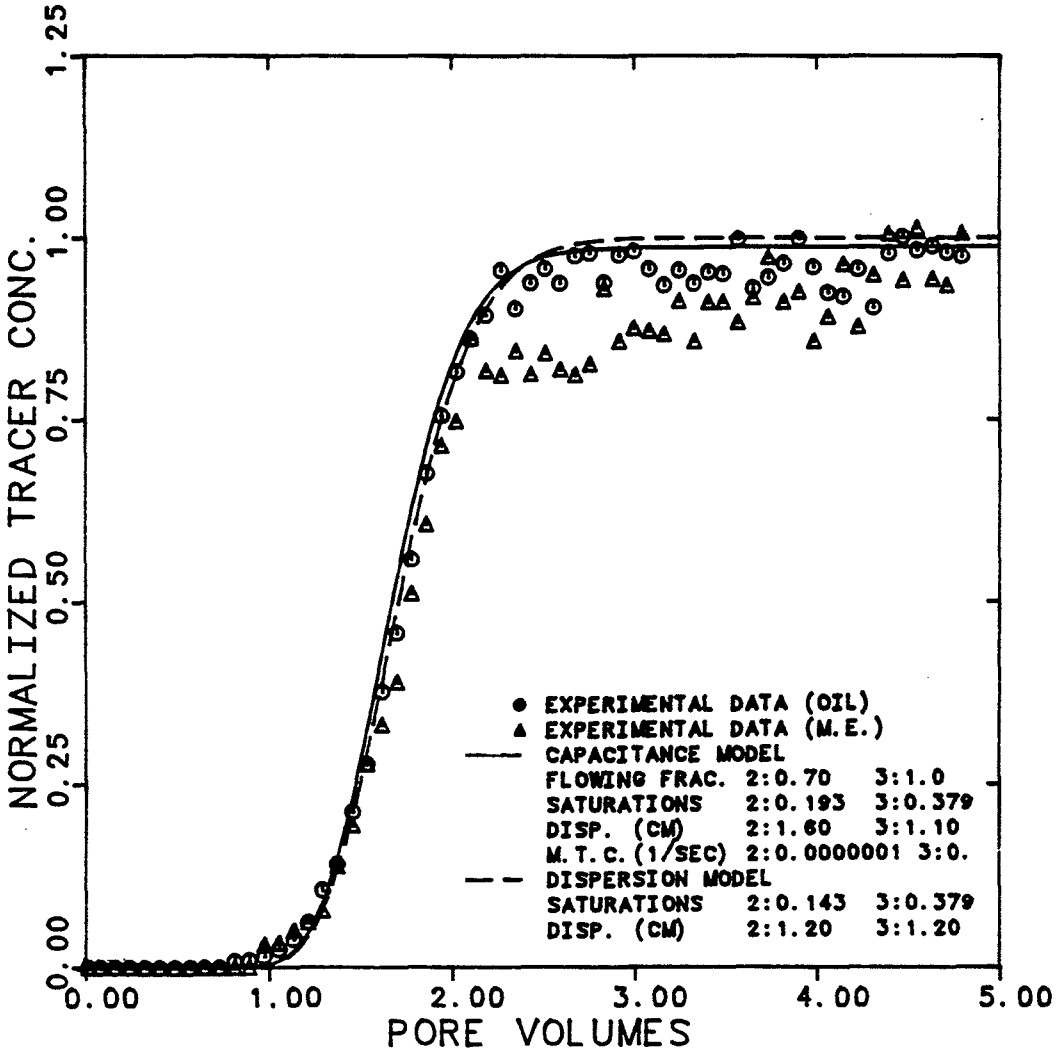

Figure 6.4.2.32 Effluent Histories for Carbon-14 in Oil and M.E. at 69.7% Brine, 8% Oil, and 22.3% M.E. Cuts

EXPERIMENT NUMBER	BMO2-22	
TRACER & PHASE	TAGG. SULF. M.E.	
FRACTIONAL FLOW	3:.134	
MAX. & INJ. CONC.	44000 46000	DPM/CC
FLOW RATE	0.789	CC/MIN.

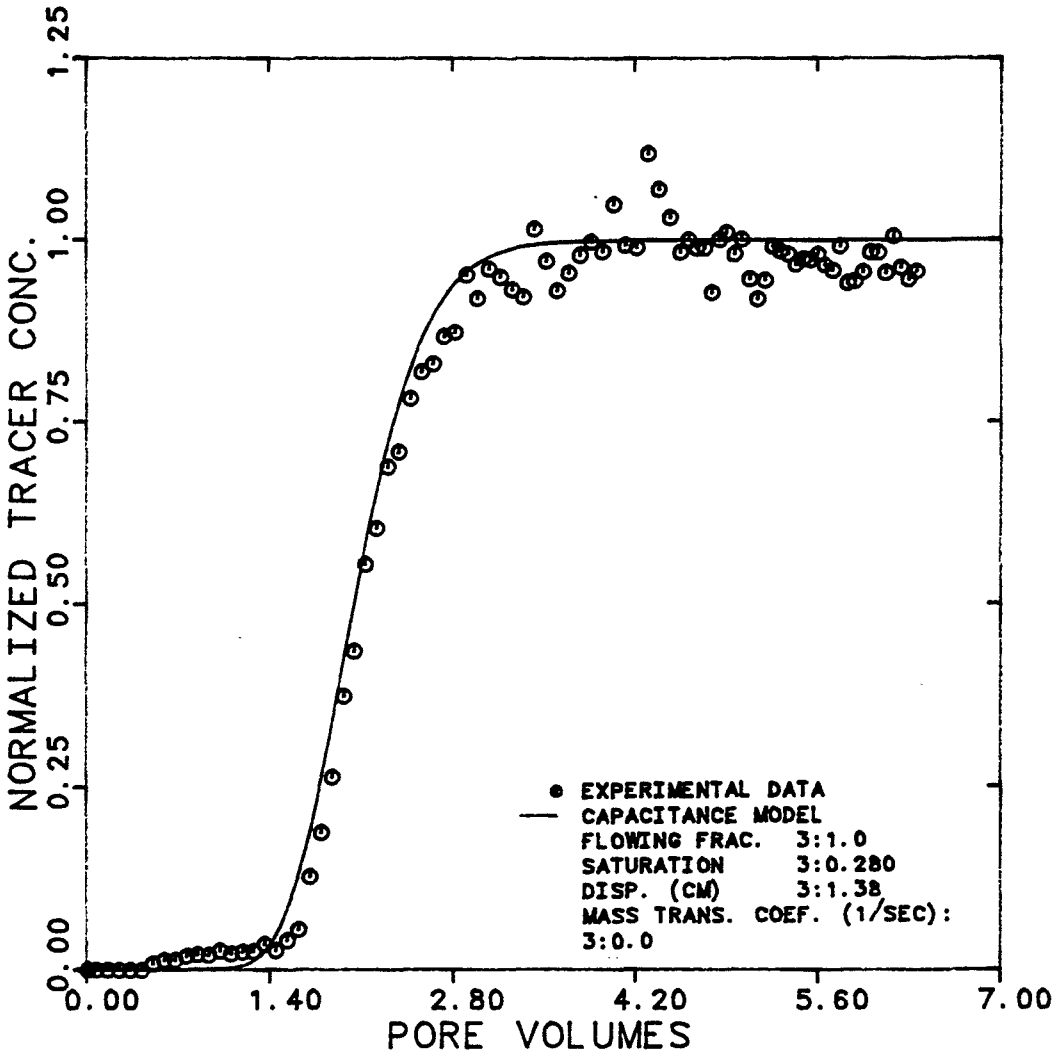

Figure 6.4.2.33 Effluent History for Labelled Sulfonate in M.E. at 83.1% Brine, 3.5% Oil, and 13.4% M.E. Cuts

EXPERIMENT NUMBER	BMO2-22		
TRACER & PHASES	CHLORIDE-36 BRINE & M.E.		
MAX. & INJ. CONC. (BRINE)	1320	1326	DPM/CC
MAX. & INJ. CONC. (M.E.)	640	680	DPM/CC
FLOW RATE	0.789		CC/MIN

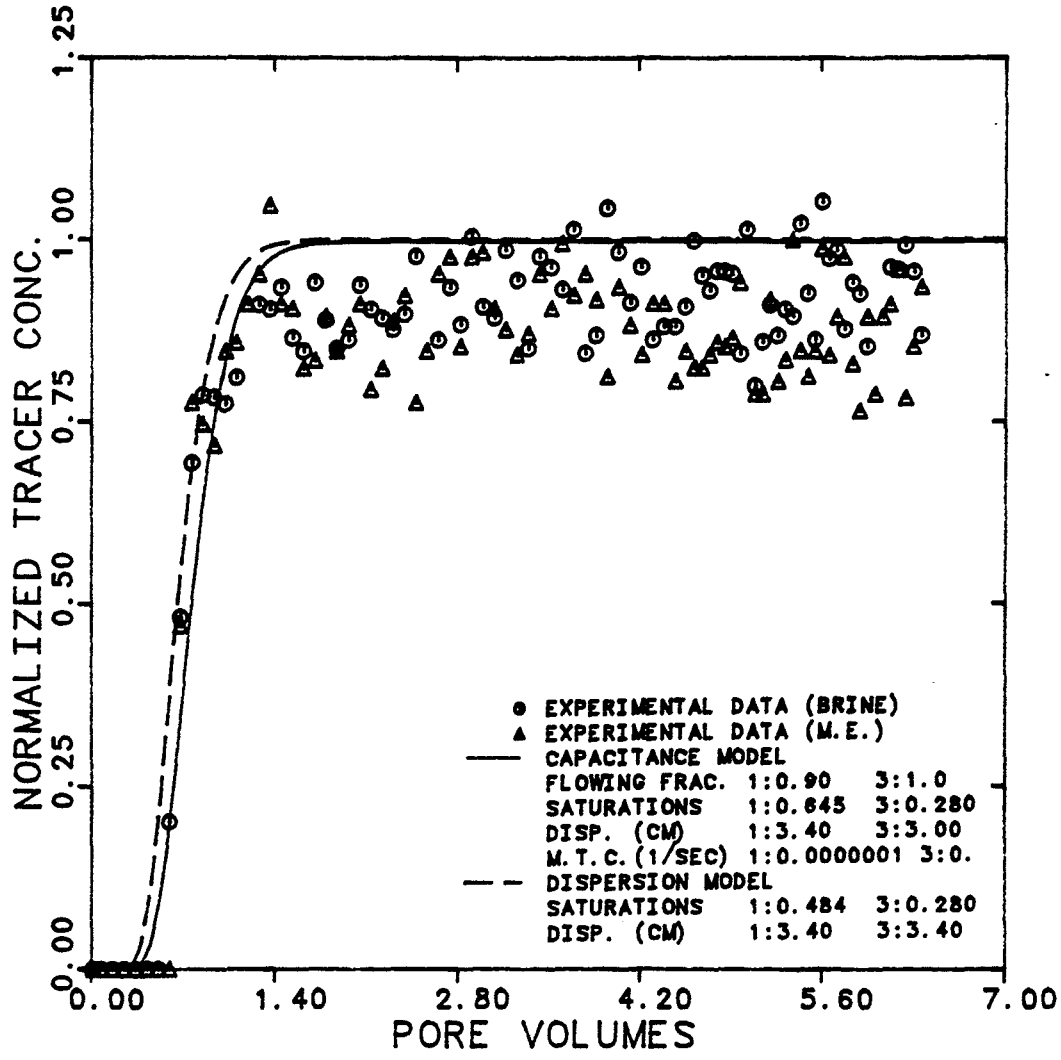

Figure 6.4.2.34 Effluent Histories for Chloride-36 in Brine and M.E. at 83.1% Brine, 3.5% Oil, and 13.4% M.E. Cuts

EXPERIMENT NUMBER	BM02-22		
TRACER & PHASES	CARBON-14	OIL	& M.E.
MAX. & INJ. CONC. (OIL)	14466	14680	DPM/CC
MAX. & INJ. CONC. (M.E.)	6000	6100	DPM/CC
FLOW RATE	0.789		CC/MIN

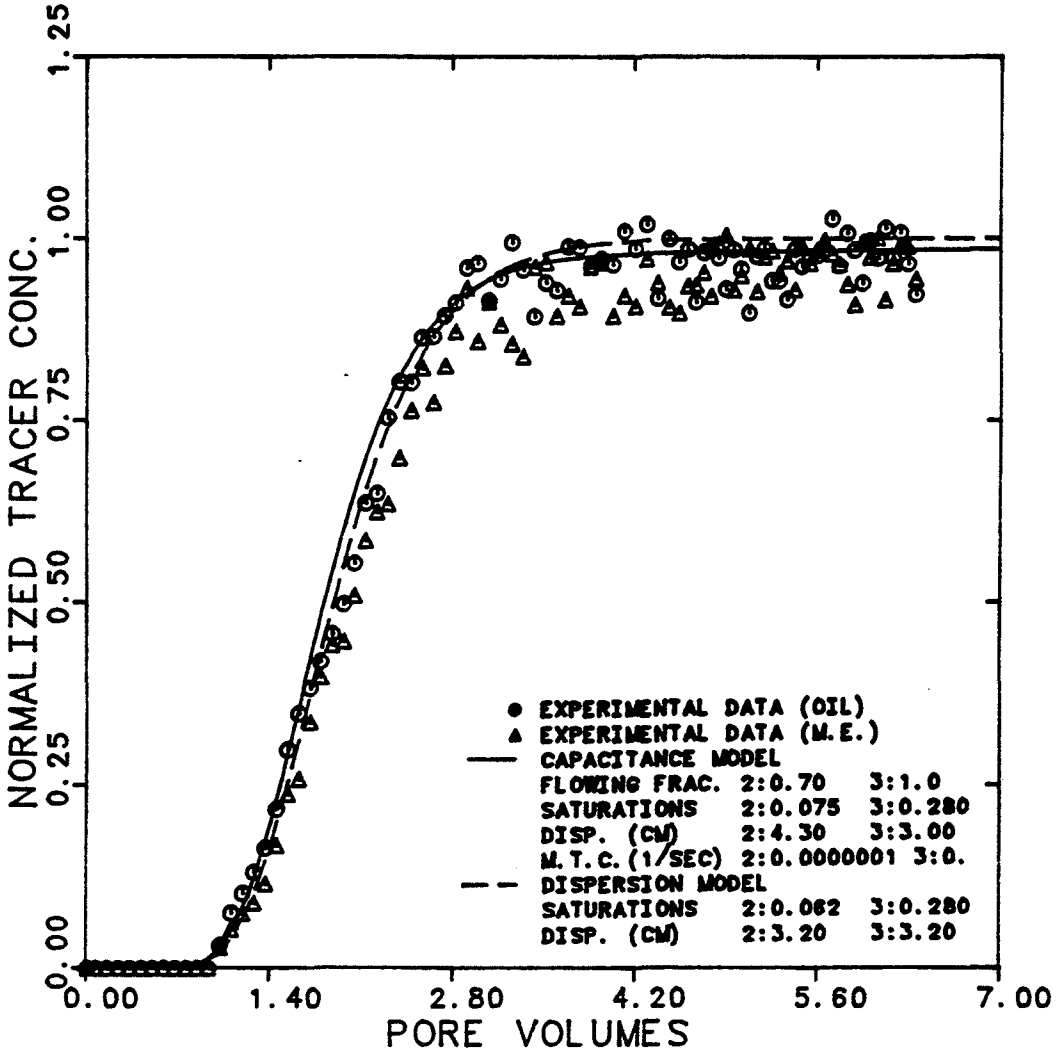

Figure 6.4.2.35 Effluent Histories for Carbon-14 in Oil and M.E. at 83.1% Brine, 3.5% Oil, and 13.4% M.E. Cuts

EXPERIMENT NUMBERS	BM01 & BM02
REF. PERMEABILITY	0.936 D
CAPILLARY NUMBER	0.01
TEMPERATURE	30° C

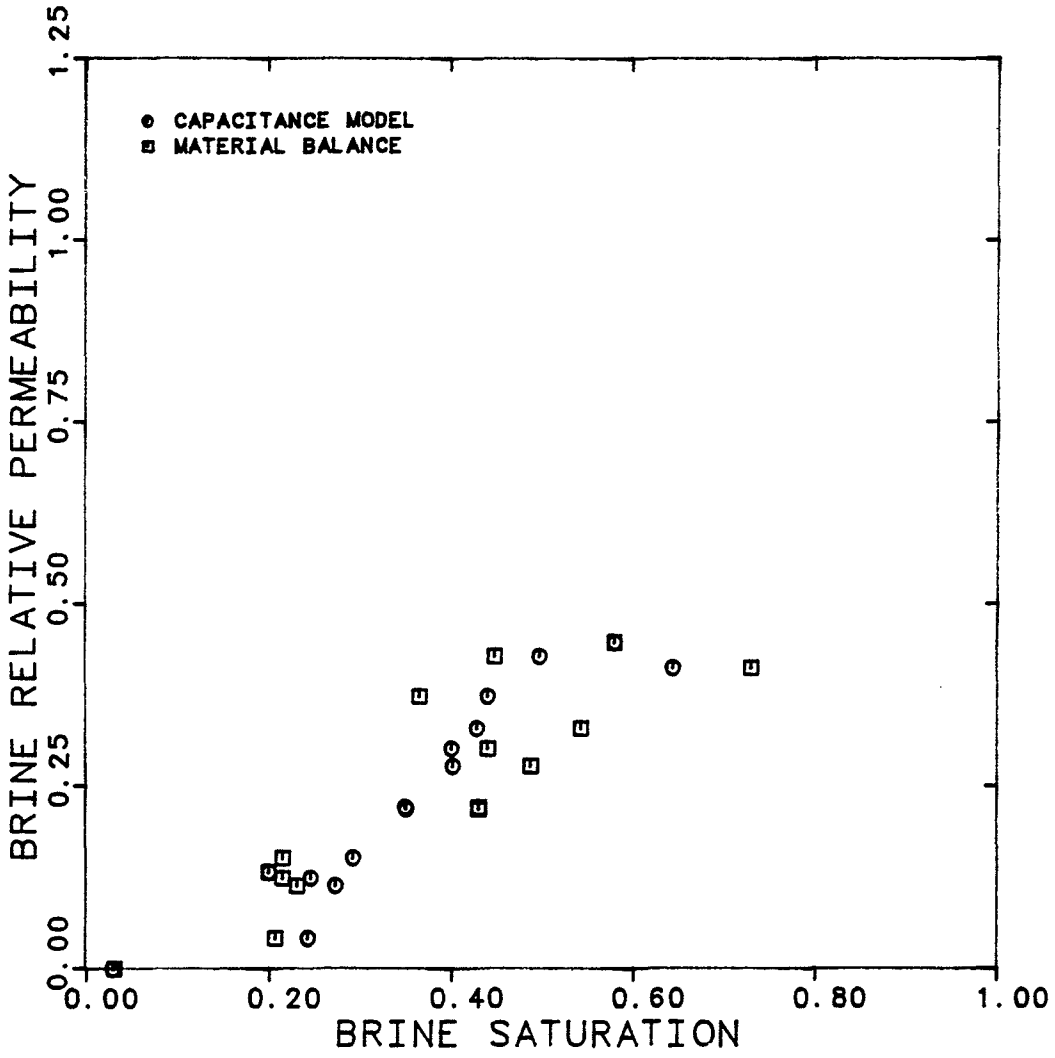

Figure 6.4.2.36 Comparison Between the Capacitance Model and Material Balance Estimates of Brine Saturation for Three-Phase Flow (Exp. BM01, BM02)

EXPERIMENT NUMBERS	BMO1 & BMO2
REF. PERMEABILITY	0.936 D
CAPILLARY NUMBER	0.01
TEMPERATURE	30°C

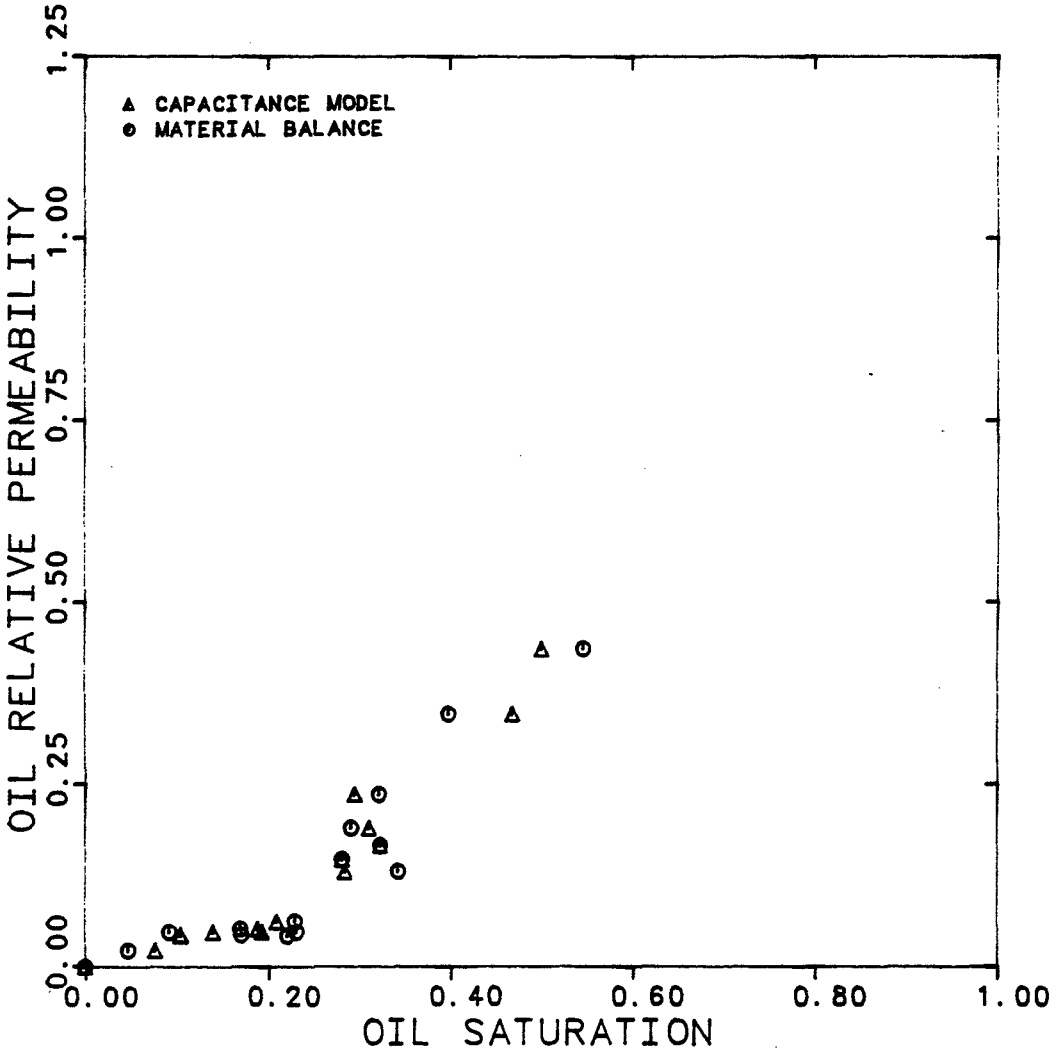

Figure 6.4.2.37 Comparison Between the Capacitance Model and Material Balance Estimates of Oil Saturation for Three-Phase Flow (Exp. BMO1, BMO2)

EXPERIMENT NUMBERS	BMO1&BMO2
REF. PERMEABILITY	0.936 D
CAPILLARY NUMBER	0.01
TEMPERATURE	30°C

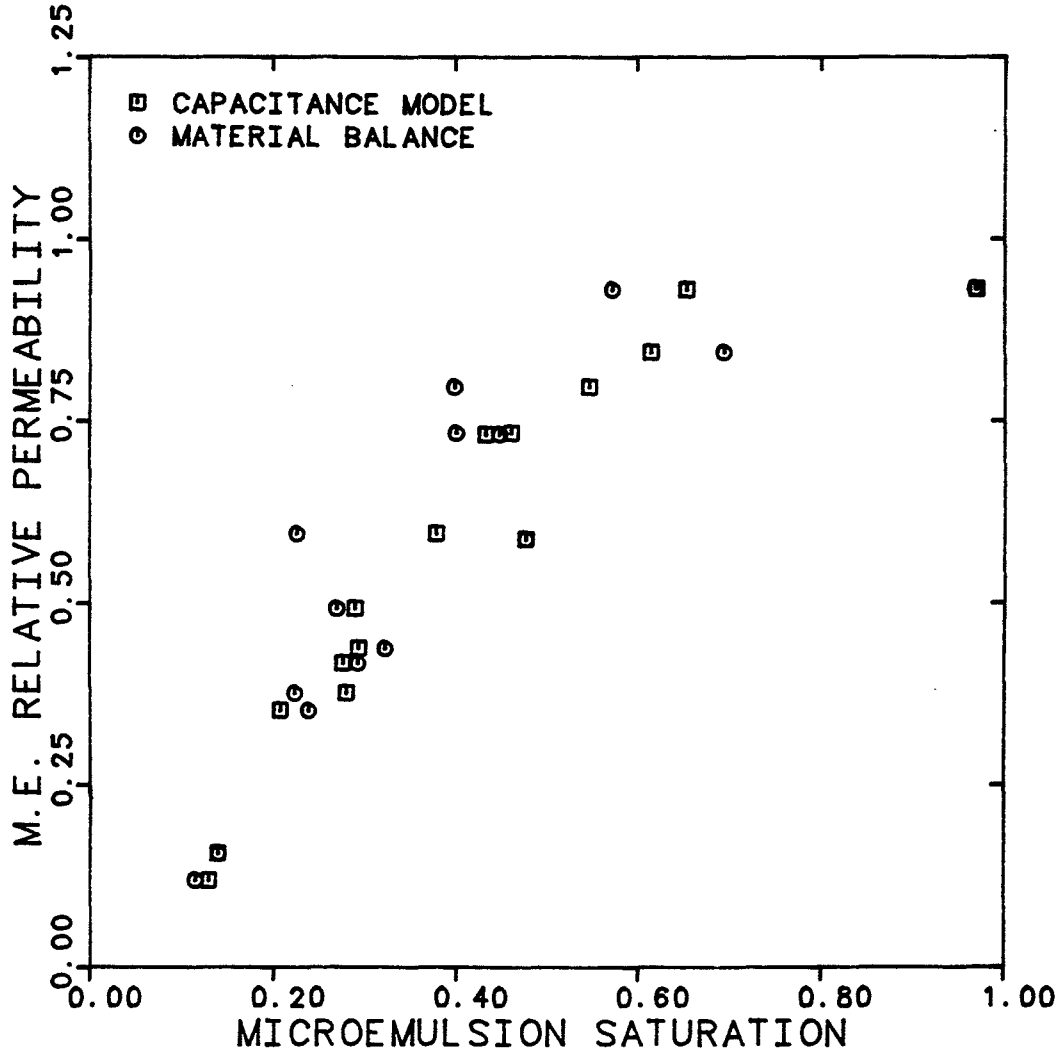

Figure 6.4.2.38 Comparison Between the Capacitance Model and Material Balance Estimates of M.E. Saturation for Three-Phase Flow (Exp. BMO1, BMO2)

EXPERIMENT NUMBERS	BMO1 & BMO2
REF. PERMEABILITY	0.936 D
CAPILLARY NUMBER	0.01
TEMPERATURE	30°C

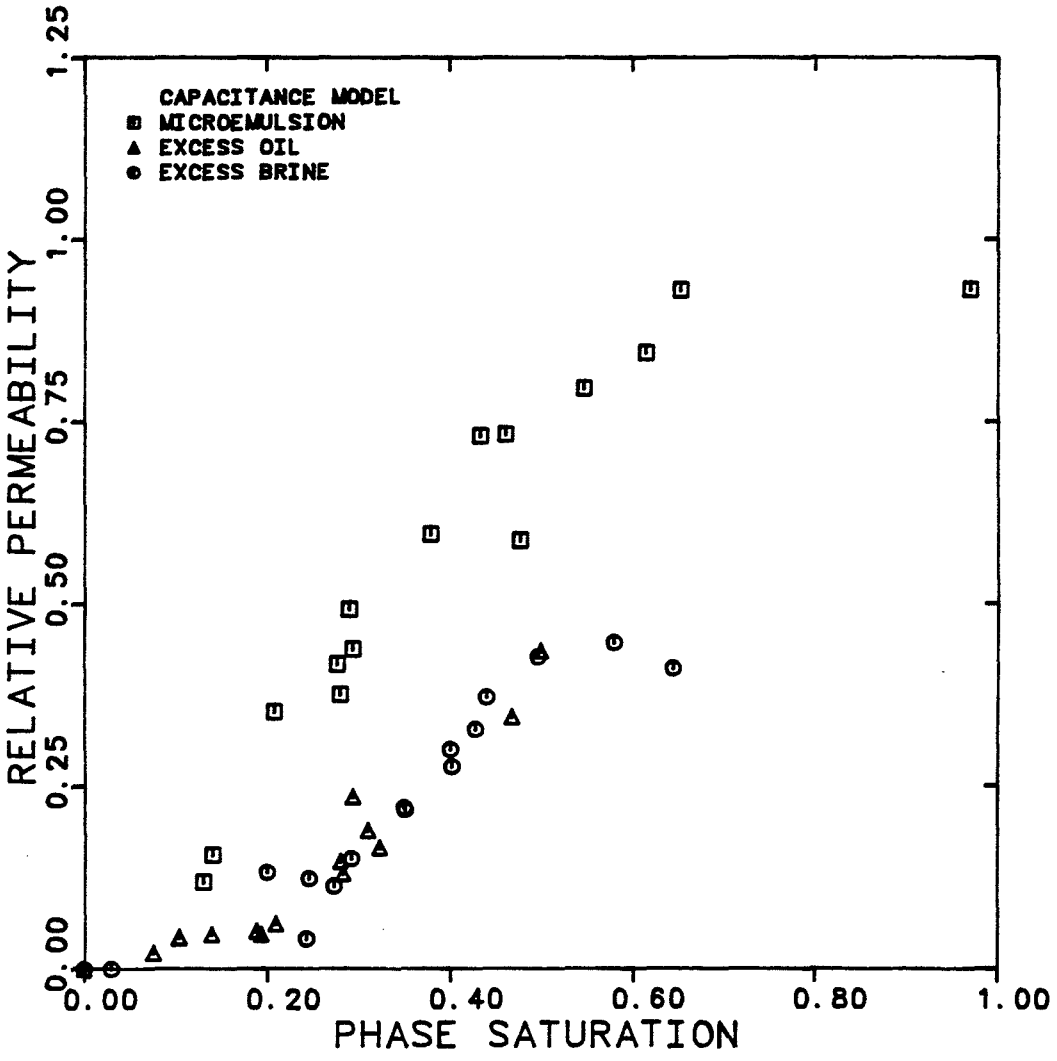

Figure 6.4.2.39 Phase Relative Permeabilities Versus Phase Saturation for Three-Phase Flow (Exp. BMO1, BMO2)

EXPERIMENT NUMBERS	BMO1 & BMO2
REF. PERMEABILITY	0.936 D
CAPILLARY NUMBER	0.01
TEMPERATURE	30°C

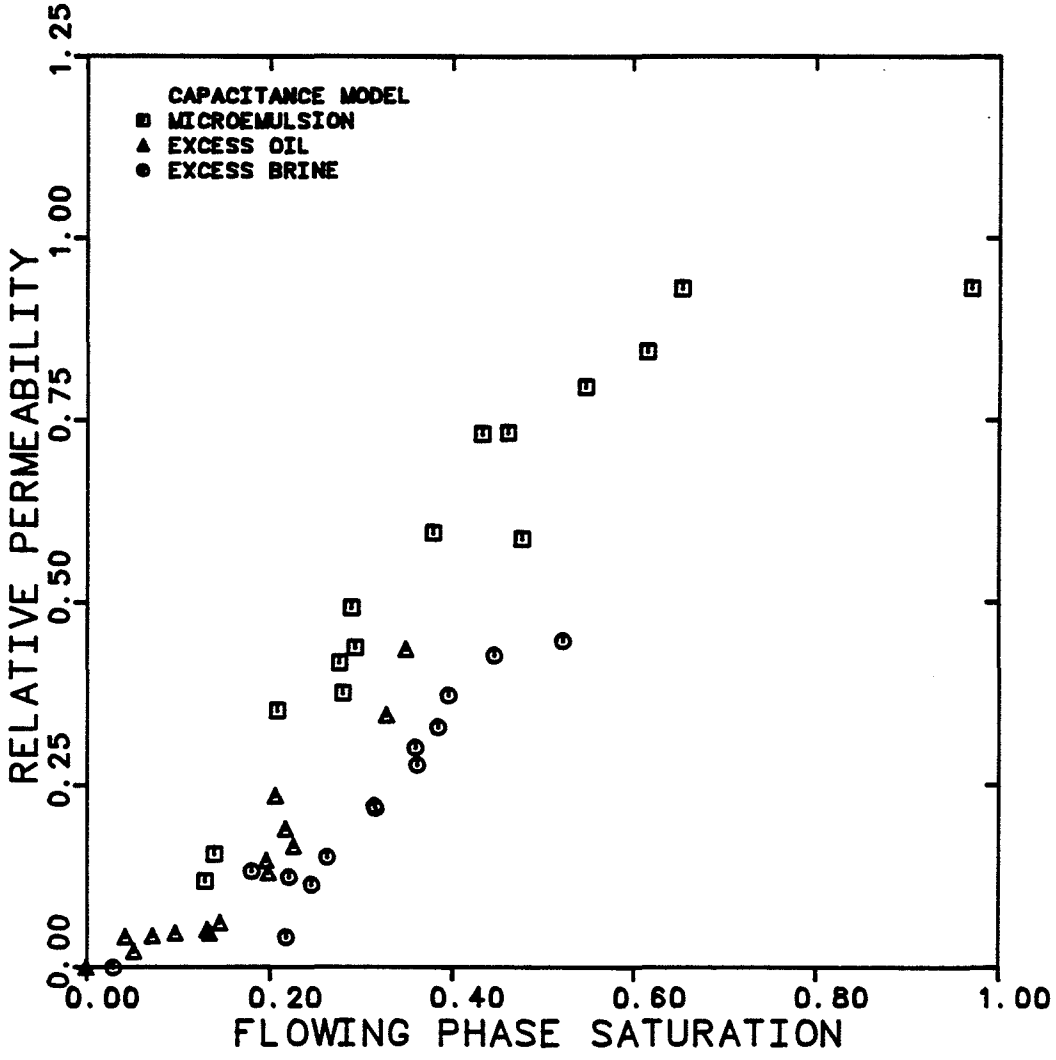

Figure 6.4.2.40 Phase Relative Permeabilities Versus Flowing Phase Saturation for Three-Phase Flow (Exp. BMO1, BMO2)

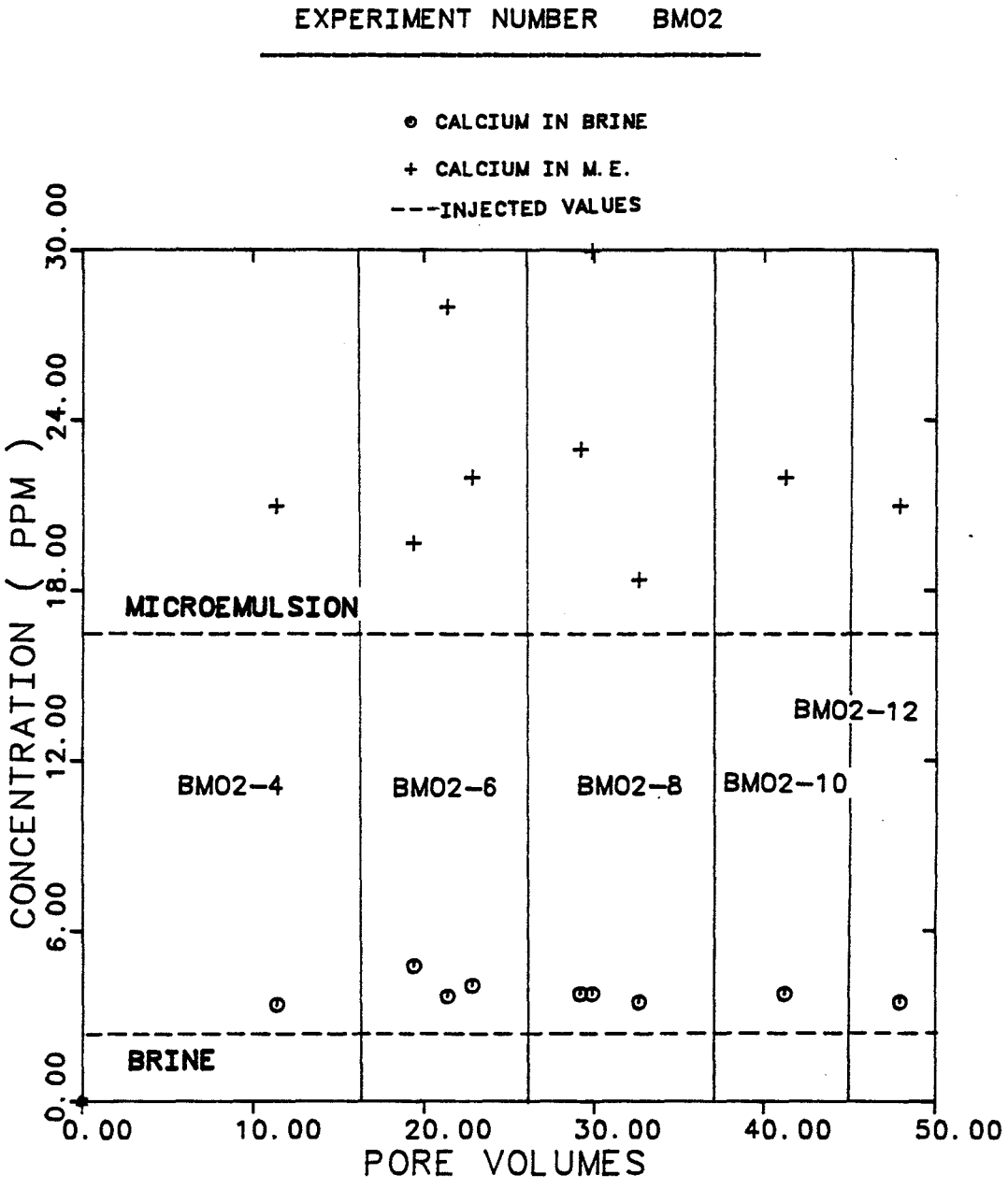

Figure 6.4.2.41 Calcium Concentration in Steady-State Effluent Brine and M.E. Phase as a Function of Pore Volumes Injected

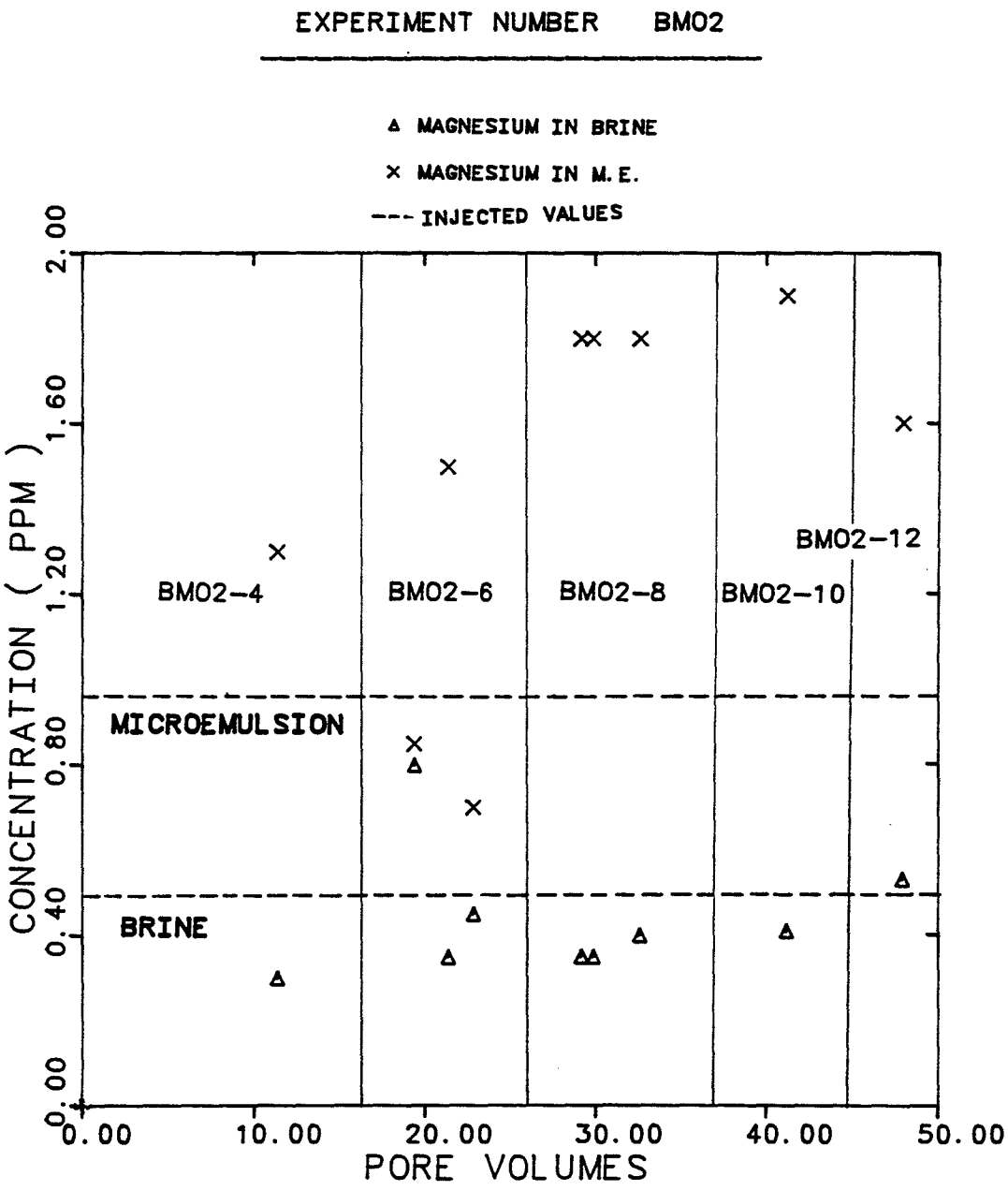

Figure 6.4.2.42 Magnesium Concentration in Steady-State Effluent Brine and M.E. as a Function of Pore Volumes Injected

COMPOSITION OF INJECTED MICROEMULSION

WATER	46.2 VOL.%
OIL	49.2 VOL.%
IBA	1.36 VOL.%
TRS 10-410	3.8 VOL.%

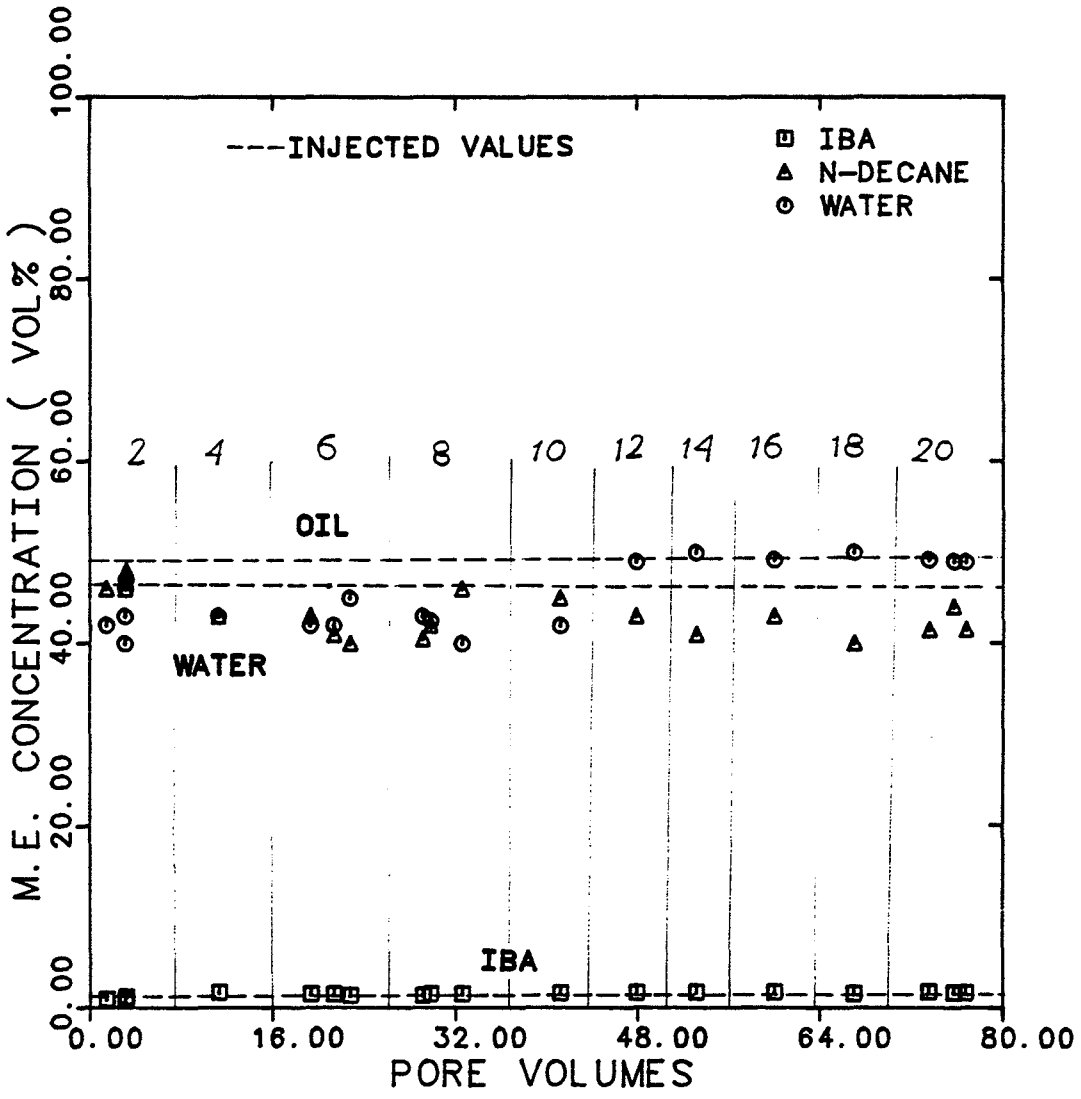

Figure 6.4.2.43 Composition of Steady-State Effluent M.E. Phase as a Function of Pore Volumes Injected

6.4.3 Excess Brine/Microemulsion/Excess Oil (Exp. No. BMO3)

The main objective of the experiment BMO3 was to further investigate the possibility that brine relative permeability is a function of two saturations. To accomplish this objective, the experiment was designed such that the brine saturation remained constant while the saturation of the other two phases were changed. The parameter chosen to indicate the change in saturations was the ratio of S_1/S_2.

Figure 6.4.3.1 shows the planned saturation sequence while the corresponding fractional flows (cuts) are plotted in Figure 6.4.3.2. The calculated fractional flow rates necessary to give the pre-determined saturations were then used to calculate the total flow rate necessary to maintain a constant capillary number of 10^{-2}. Appendix C demonstrates an example calculation for predicting the fractional flows and total flow rates.

The same core as in experiment BMO2 was used in this experiment. A new batch (number 13) of micellar solution with the salinity of 1.2 wt% NaCl was made up. The hot batch contained the partitioning tracers, carbon-14 and chloride-36, and the non-partitioning tracer, tritium labelled sulfonate. Table 6.1.1 presents the

properties of both stocks (with and without radioactive tracers).

There was a three-month time lag between the previous experiment (BMO2) and experiment BMO3 (no flow through the core in this period). Therefore,100% excess oil followed by 100% microemulsion were injected to re-establish the saturation state of the core.

The excess oil was injected at different flow rates and the potential drop was measured at steady-state. Figure 6.4.3.3 shows the plot of oil potential drop, output of the transducer in the middle section, versus flow rate.

At steady-state, oil containing radioactive tracer was injected at 1 cm^3/min (Fig. 6.4.3.4). This was then followed by the injection of cold oil at 0.997 cm^3/min to get the downside dispersion curve (Figure 6.4.3.5). The two breakthrough curves are identical and the saturations obtained from matching them against the theoretical curve of the convection-diffusion equation (C-D) were S_{1r} = 0.15, S_2 = 0.82, S_{3r}= 0.03.

Fluid injection was continued by switching to 100% microemulsion at 0.5 cm^3/min. The dispersion run was performed at the same steady-state rate. These were then followed by the injection of cold microemulsion

since some oil was produced during the first dispersion (upside curve) run. The saturations obtained by matching the three tracer breakthrough curves in the microemulsion phase against the C-D equation were S_{1r}= 0.027, S_{2r} = 0.0, and S_3 = 0.973.

The three phases (oil, microemulsion, brine) were then injected at the pre-selected flow rates to steady-state. This was then followed by the injection of radioactive labelled phases to determine the dispersion curves.

The dispersion experiments were performed in either increasing or decreasing concentration direction, so it would enable us to measure the concentration of radioactive components during the transient period before reaching the steady-state as well as those at steady-state. These concentration data may give some indication of whether there is a phase behavior change during the transient time.

The first three-phase flow experiment was at number BMO3-8 which was started with the injection of cold fluids to steady-state and then followed by flooding the core with labelled fluids to get the upside dispersion curves. The injection of labelled fluids was continued but at the new flow rate and fractional flows

(Exp. BMO3-10) to steady-state. This was followed by the injection of cold fluids to obtain the declining dispersion curves. Therefore, all the effluent samples from the start of the new cut to the end of the dispersion run were analyzed for tracer concentration.

The last three-phase cut was followed by flooding the core with 100% brine (Exp. BMO3-20). The residual saturations obtained from the tracer data were $S_{2r} = 0.0$ and $S_{3r} = 0.120$.

The actual cuts, total flow rates, material balance estimate of saturations and relative permeabilities are presented in Table 6.4.1.1. The total fluids injected to reach steady-state and potential drop measured across all three sections are listed in Table 6.4.1.2. Consistent with the previous three-phase flow results, the inlet potential drops are higher than those measured across the outlet section. The inlet potential drops are higher than the values across the middle section by 6.3%, on the average. Table 6.4.1.3 shows the calculated relative mobilities, total mobility, and capillary numbers.

The breakthrough curves of tritium labelled sulfonate in the microemulsion, chloride-36 in the excess brine and microemulsion, and carbon-14 in the

microemulsion and excess oil are shown in Figures 6.4.3.9 through 6.4.3.32.

The breakthrough curves of tritium labelled sulfonate were again fairly smooth, symmetrical and s-shaped while the breakthrough curves of chloride-36 and carbon-14 were asymmetric with long tails. The data of both chloride-36 and carbon-14 in the microemulsion showed more scatter but the trends were almost identical to those in the excess phases.

The theoretical curves of the C-D equation (dashed curves) were first used to match the breakthrough curves and determine the flowing saturations and apparent dispersivities. Table 6.4.1.4 presents the phase saturations and dispersivities estimated by the C-D equation. The total fluids injected for the dispersion experiment are also tabulated in Table 6.4.1.4.

The breakthrough curves were then compared with the computed curves of the capacitance-dispersion model to obtain the best estimates of the capacitance parameters. The estimate of matching parameters, (saturations, flowing fractions, dispersivities, and mass transfer coefficients) are shown in Table 6.4.1.5. This table also lists the calculated dispersion coefficients, flowing phase velocities, and tracer recoveries.

The tracer data obtained during the transient period (before steady-state) of experiments BMO3-10 and BMO3-14 are in Figures 6.4.3.12 - 6.4.3.14 and 6.4.3.21 - 6.4.3.23. The phase cuts as a function of pore volumes injected are also plotted on these figures. The tracer concentration data in the excess oil and brine are fairly constant and smooth in both experiments. On the other hand, the concentration of tracers in the microemulsion phase in experiment BMO3-10 show considerable scatter. The scatter might be because of a possible change in phase behavior due to the significant increase in the microemulsion saturation ($\Delta S_3 = +0.339$) from cut BMO3-8 to BMO3-10. The concentration of tracers in the microemulsion phase decreases and this drop coincides with the pore volume at which the microemulsion fractional flow increases to the new steady-state cut ($f_3 = 0.347$). The scatter is not evident in the result of cut BMO3-14 since (1) the change in the microemulsion saturation ($\Delta S_3 = -0.155$) is not as significant as that in the BMO3-10, and (2) the change is in the decreasing direction of saturation. More data of this type as well as analysis on the composition of effluent microemulsion samples is required to confirm that the tracer analysis during transient period actually detects the change in

phase behavior. Such results may have a big impact on the validity of the material balance calculations.

Figures 6.4.3.34 through 6.4.3.36 show the relative permeability of each phase as a function of the respective saturation estimated from both material balance and the capacitance model. The material balance and capacitance estimates of saturation are in reasonable agreement. Brine relative permeability is a function of its own saturation since the relative permeabilities measured for three different S_1/S_2 ratios at constant brine saturation of around 0.30 were fairly constant.

The relative permeabilities of excess brine, excess oil, and microemulsion compared in Figure 6.4.3.37 indicate that

1- The relative permeability data of the excess oil and brine phases are nearly the same.

2- The microemulsion relative permeability is higher than that of the excess phases at the same saturation.

3- The relative permeabilities are far from the straight lines at this high capillary number of 10^{-2}.

4- Consistent with the two-phase flow results, the microemulsion relative permeabilities show a concave upward curvature ($n_3 < 1$).

The composition of the steady-state effluent

samples measured by GC, presented in Figure 6.4.3.38, indicates that within the experimental uncertainty and scatter of data, steady-state is achieved in each cut.

- Experimental Difficulties and Observations

The effective permeability to single phase oil and microemulsion measured in experiments BMO3-3 and BMO3-6 were k_2 = 0.880 Darcy and k_3 = 0.936 Darcy as compared to the values of k_2 = 0.705 Darcy and k_3 = 0.739 Darcy obtained during two-phase flow of microemulsion and excess oil (experiment SMO). An error in pressure data was first considered as the probable reason for this increase in permeabilities. But, the pressure data measured versus flow rate (Figure 6.4.3.3) eliminated this possibility. The pressure versus flow rate is linear as ideally should be with the intercept at the origin (see Chapter 5, section 5.1.3.1). Thus, for the purpose of comparing the three-phase data, permeabilities were normalized with the microemulsion permeability of 0.936 Darcy since we could not find a good explanation for this discrepancy.

SATURATION TERNARY

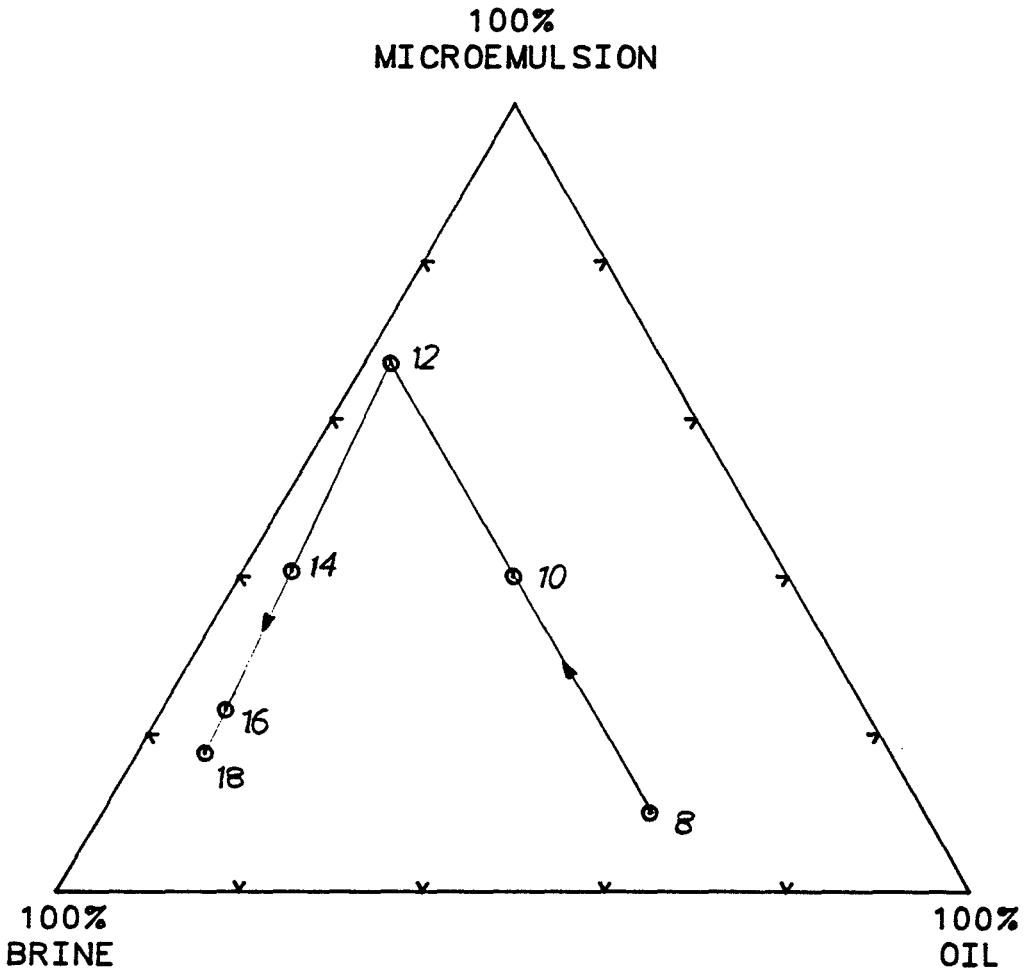

Figure 6.4.3.1 The Planned Saturation Sequence for Three-Phase Flow Experiment (BMO3)

FRACTIONAL FLOW TERNARY

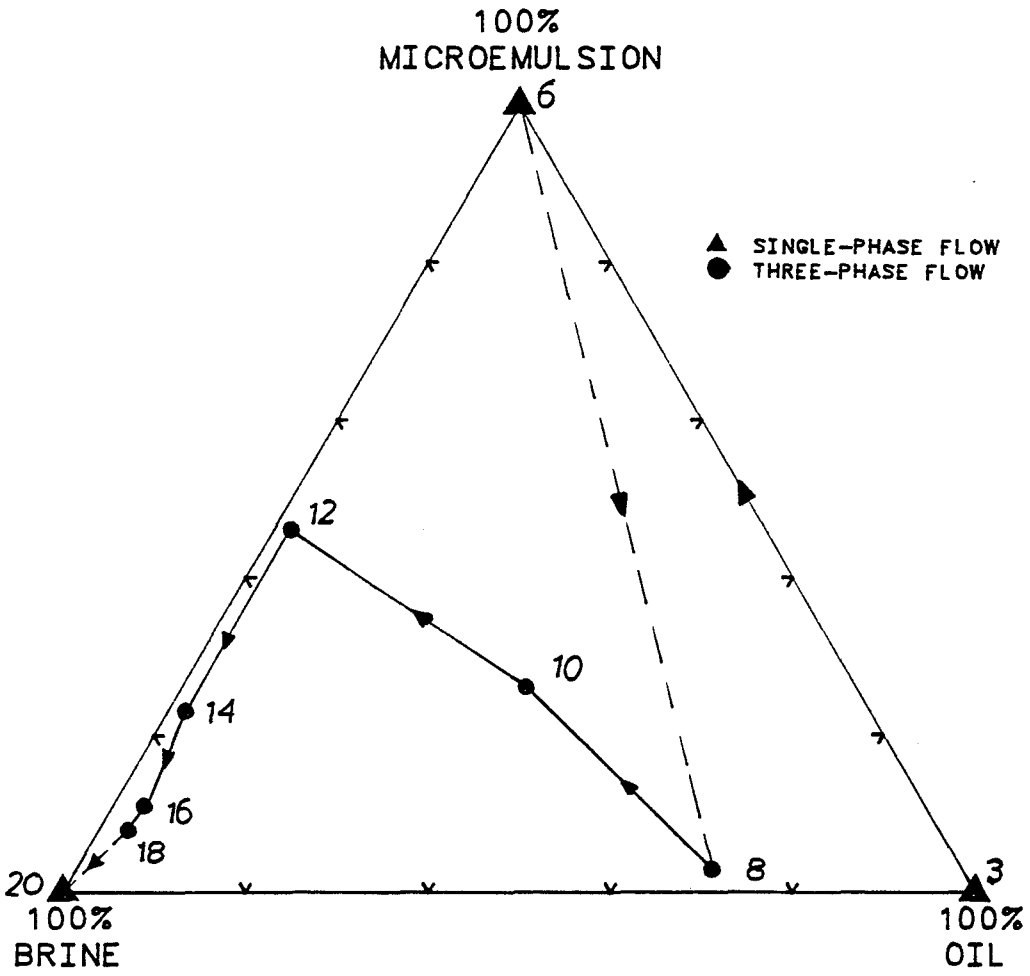

Figure 6.4.3.2 The Predicted Fractional Flows for Experiment BM03

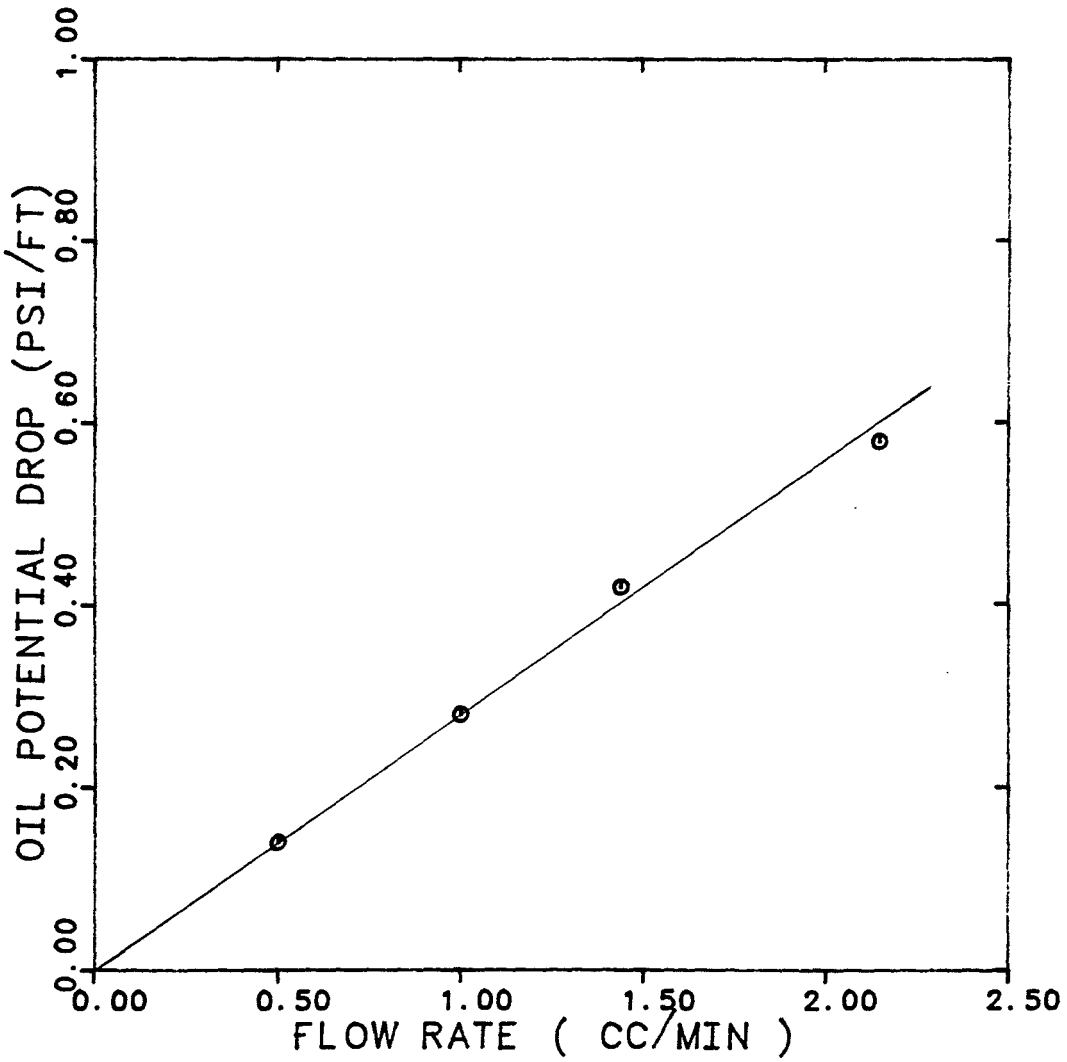

Figure 6.4.3.3 Steady-State Pressure Drop as a Function of Flow Rate

EXPERIMENT NUMBER	BM03-2
TRACER & PHASE	CARBON-14 OIL
FRACTIONAL FLOW	100% OIL
MAX. & INJ. CONC.	23559 23735 DPM/CC
FLOW RATE	1.0 CC/MIN

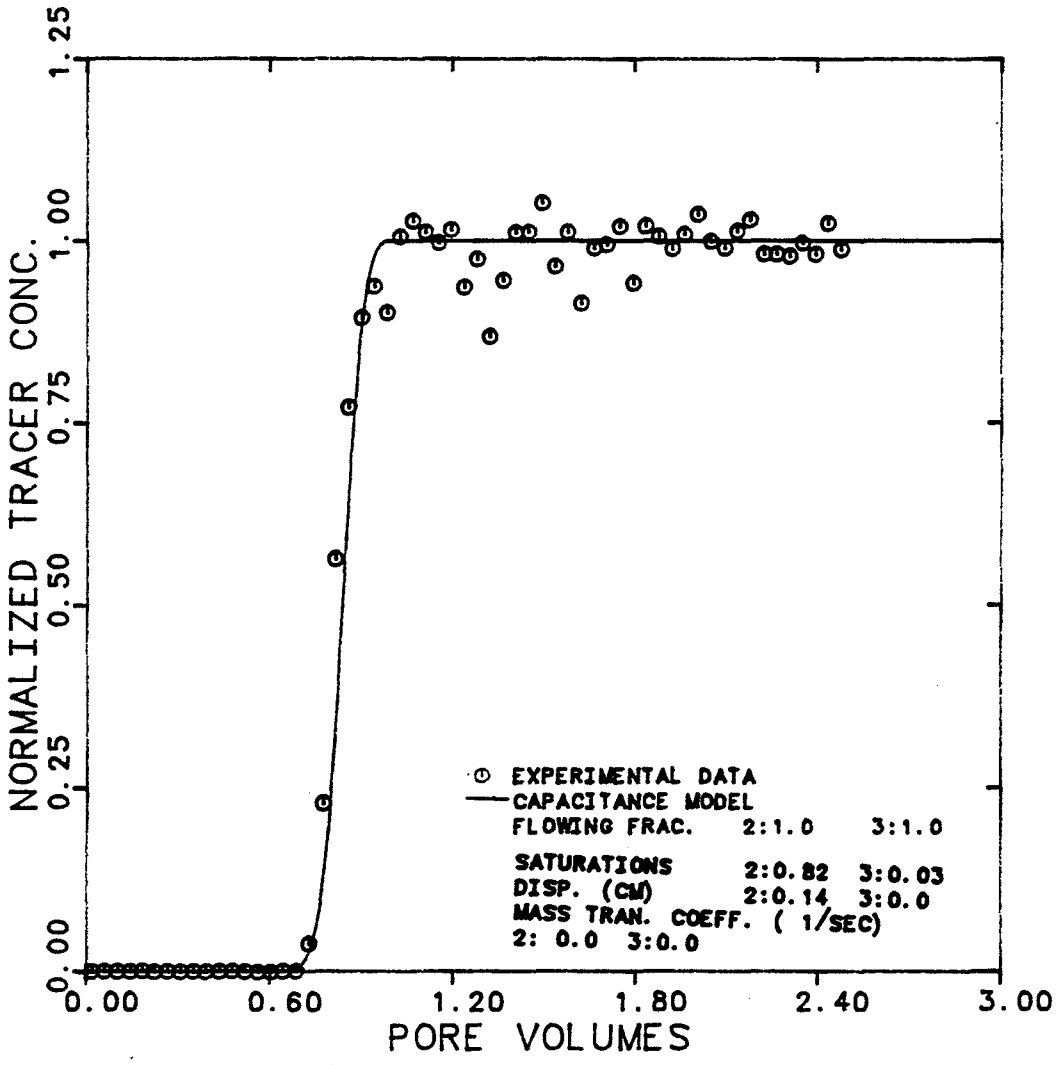

Figure 6.4.3.4 Effluent History for Carbon-14 in Oil for Single-Phase Flow of Oil (upside curve)

EXPERIMENT NUMBER	BM03-3		
TRACER & PHASE	CARBON-14		OIL
FRACTIONAL FLOW	100%		OIL
MAX. & INJ. CONC.	23150	0.0	DPM/CC
FLOW RATE	0.997		CC/MIN.

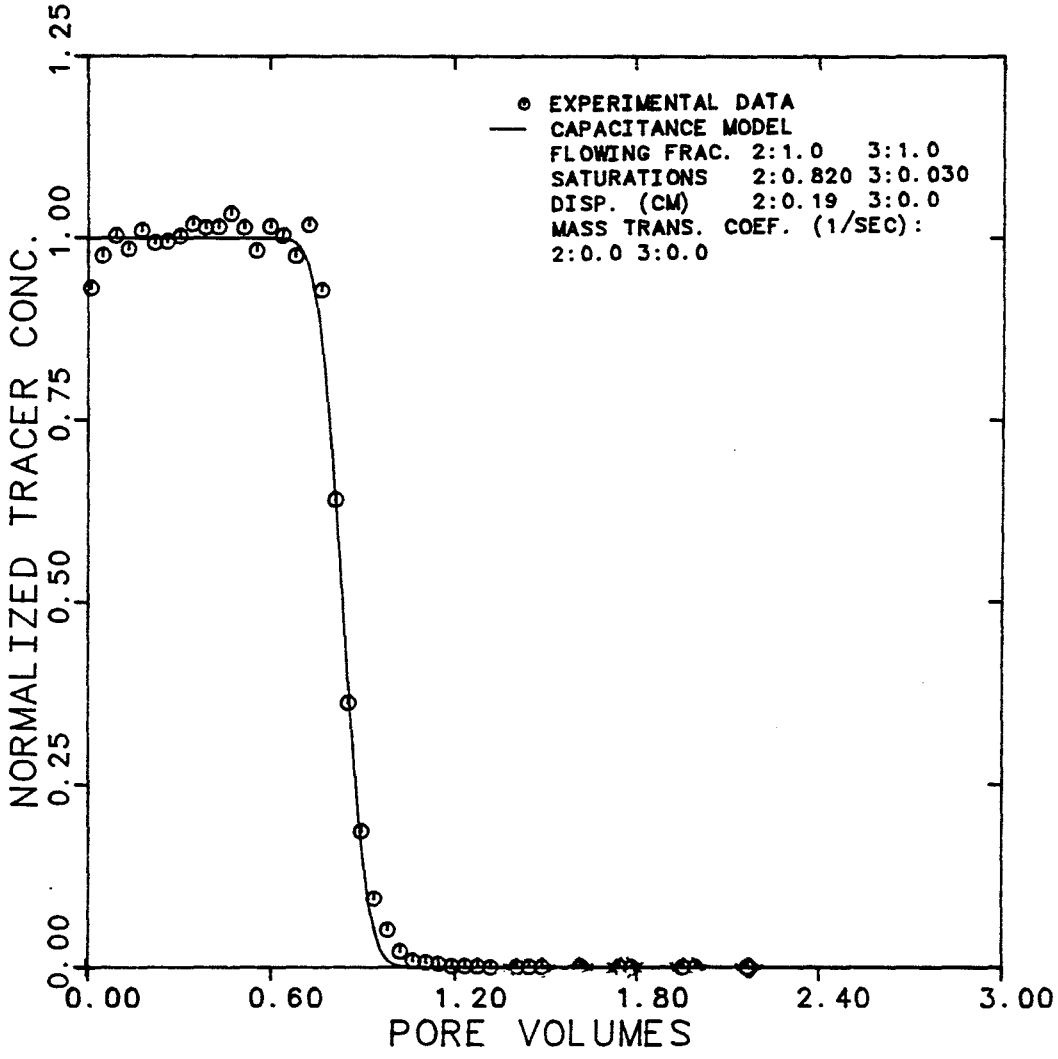

Figure 6.4.3.5 Effluent History for Carbon-14 in Oil for Single-Phase Flow of Oil (downside)

EXPERIMENT NUMBER	BM03-6	
TRACER & PHASE	TAGG. SULF.	M.E.
FRACTIONAL FLOW	3:1.00	
MAX. & INJ. CONC.	30259 0.0	DPM/CC
FLOW RATE	0.500	CC/MIN.

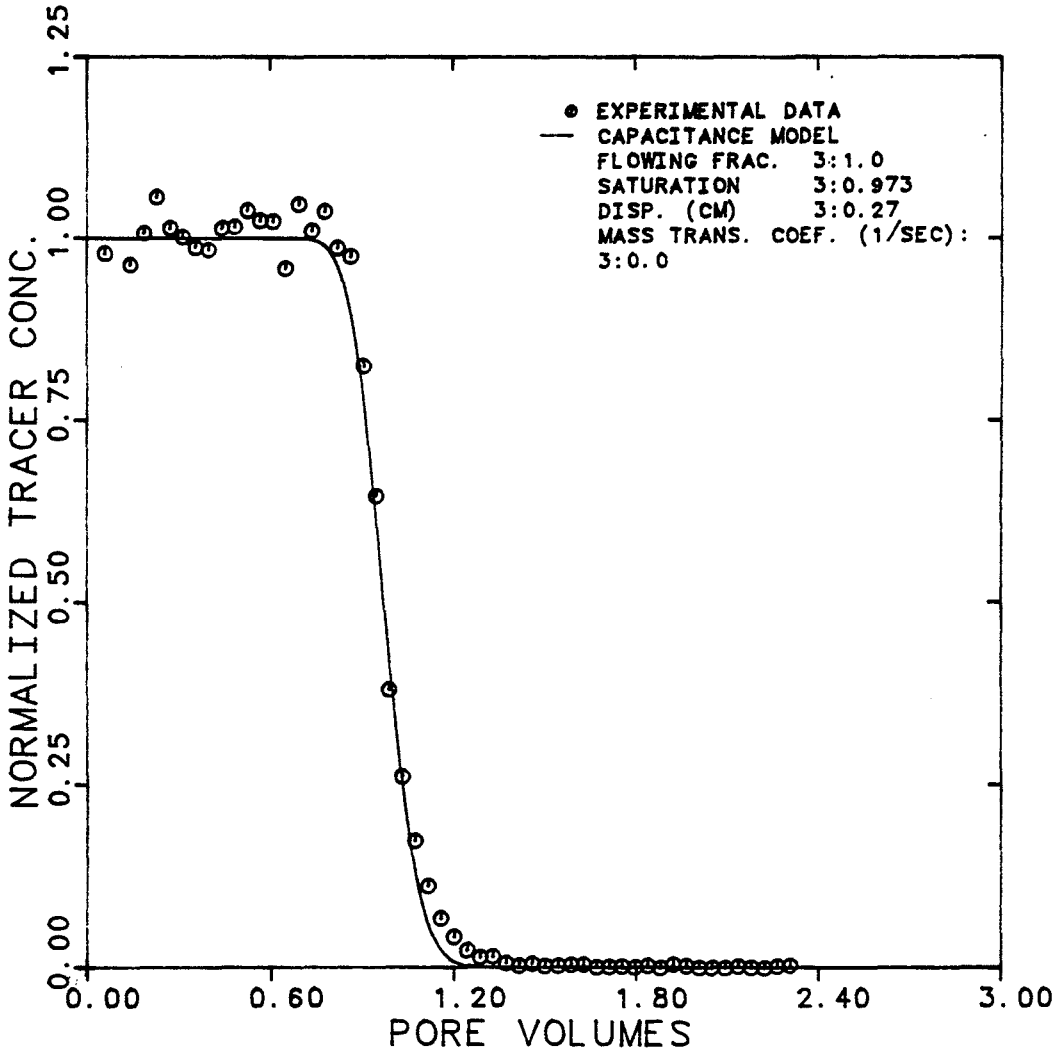

Figure 6.4.3.6 Effluent History for Labelled Sulfonate in M.E. for Single-Phase M.E. Flow

EXPERIMENT NUMBER	BM03-6	
TRACER & PHASE	CHLORIDE-36 M.E.	
FRACTIONAL FLOW	3:1.0	
MAX. & INJ. CONC.	3174 0.0	DPM/CC
FLOW RATE	0.50	CC/MIN.

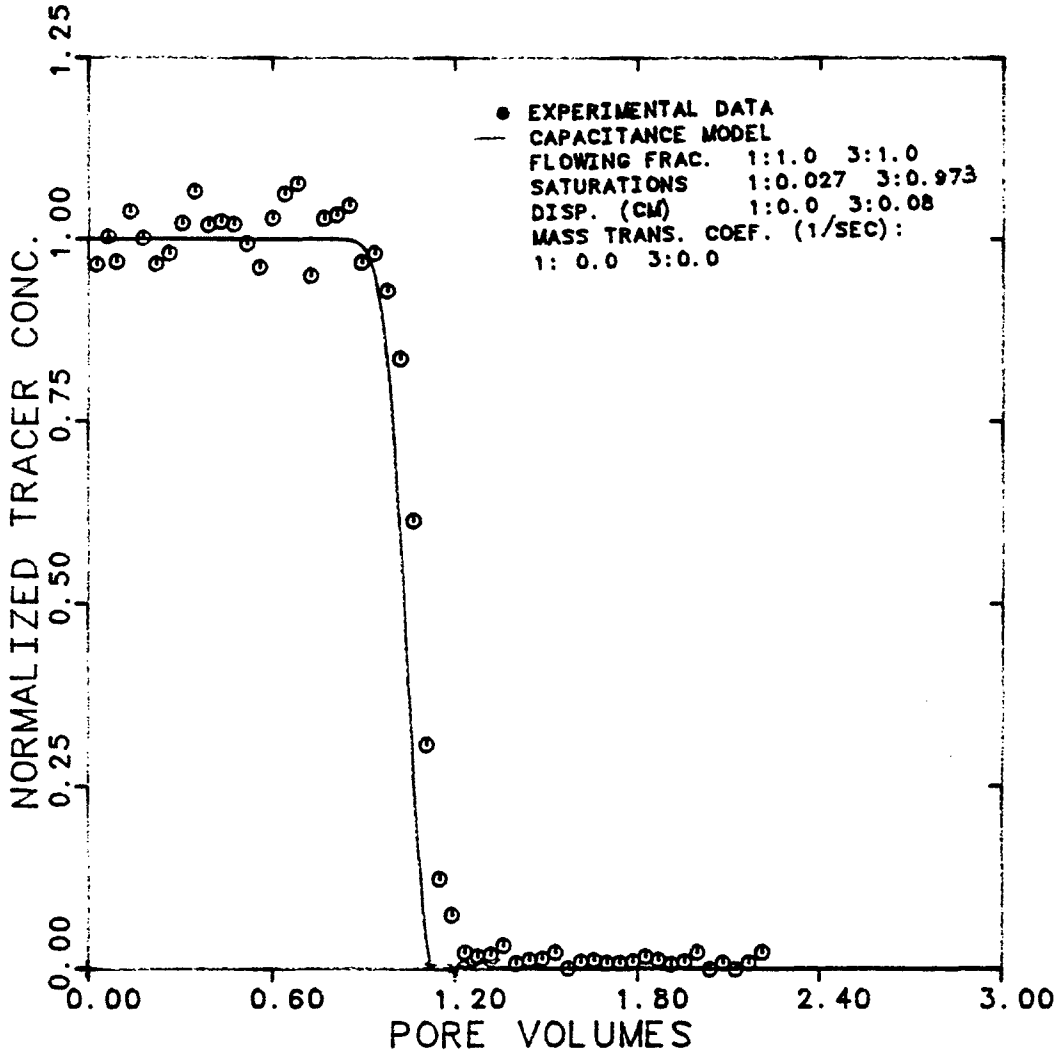

Figure 6.4.3.7 Effluent History for Chloride-36 in M.E. for Single-Phase M.E. Flow

EXPERIMENT NUMBER	BM03-6		
TRACER & PHASE	CARBON-14		M.E.
FRACTIONAL FLOW	100%		M.E.
MAX. & INJ. CONC.	10145	0.0	DPM/CC
FLOW RATE	0.500		CC/MIN.

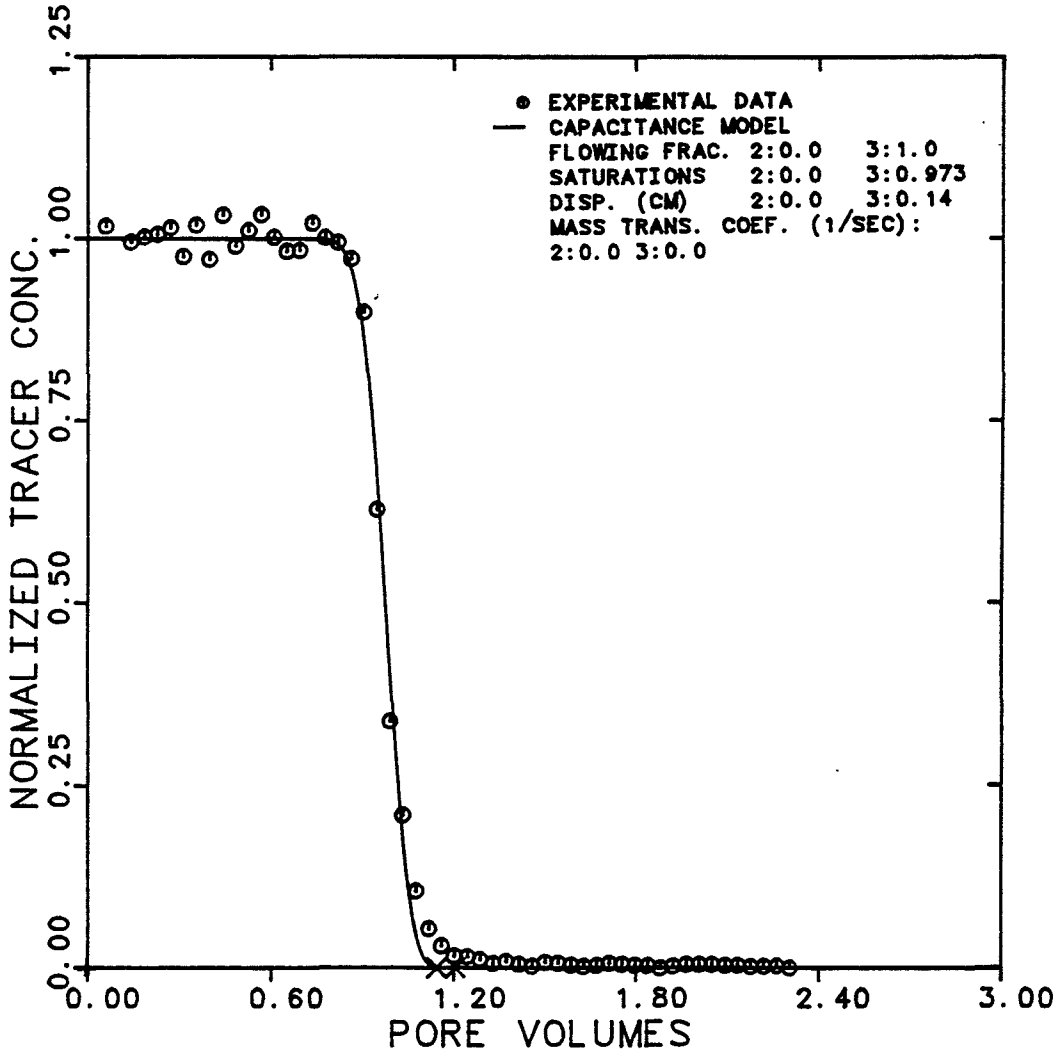

Figure 6.4.3.8 Effluent History for Carbon-14 in M.E. for Single-Phase M.E. Flow

EXPERIMENT NUMBER	BM03-8	
TRACER & PHASE	TAGG. SULF.	M.E.
FRACTIONAL FLOW	3:0.058	
MAX. & INJ. CONC.	22000 23000	DPM/CC
FLOW RATE	1.730	CC/MIN.

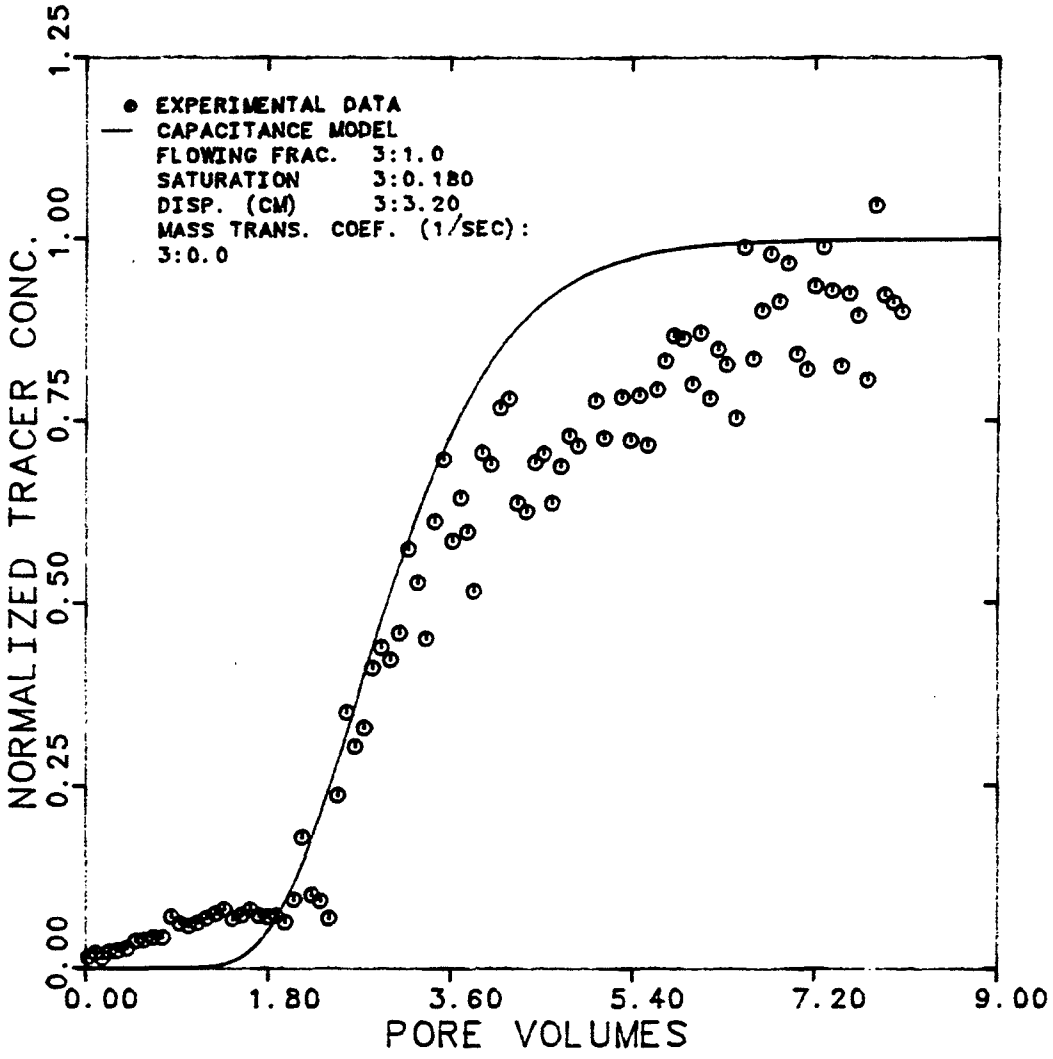

Figure 6.4.3.9 Effluent History for Labelled Sulfonate in M.E. at 28.9% Brine, 65.3% Oil, and 5.8% M.E.Cuts

EXPERIMENT NUMBER	BM03-8		
TRACER & PHASES	CHLORIDE-36 BRINE & M.E.		
MAX. & INJ. CONC. (BRINE)	7080	7080	DPM/CC
MAX. & INJ. CONC. (M.E.)	3300	3300	DPM/CC
FLOW RATE	1.730		CC/MIN

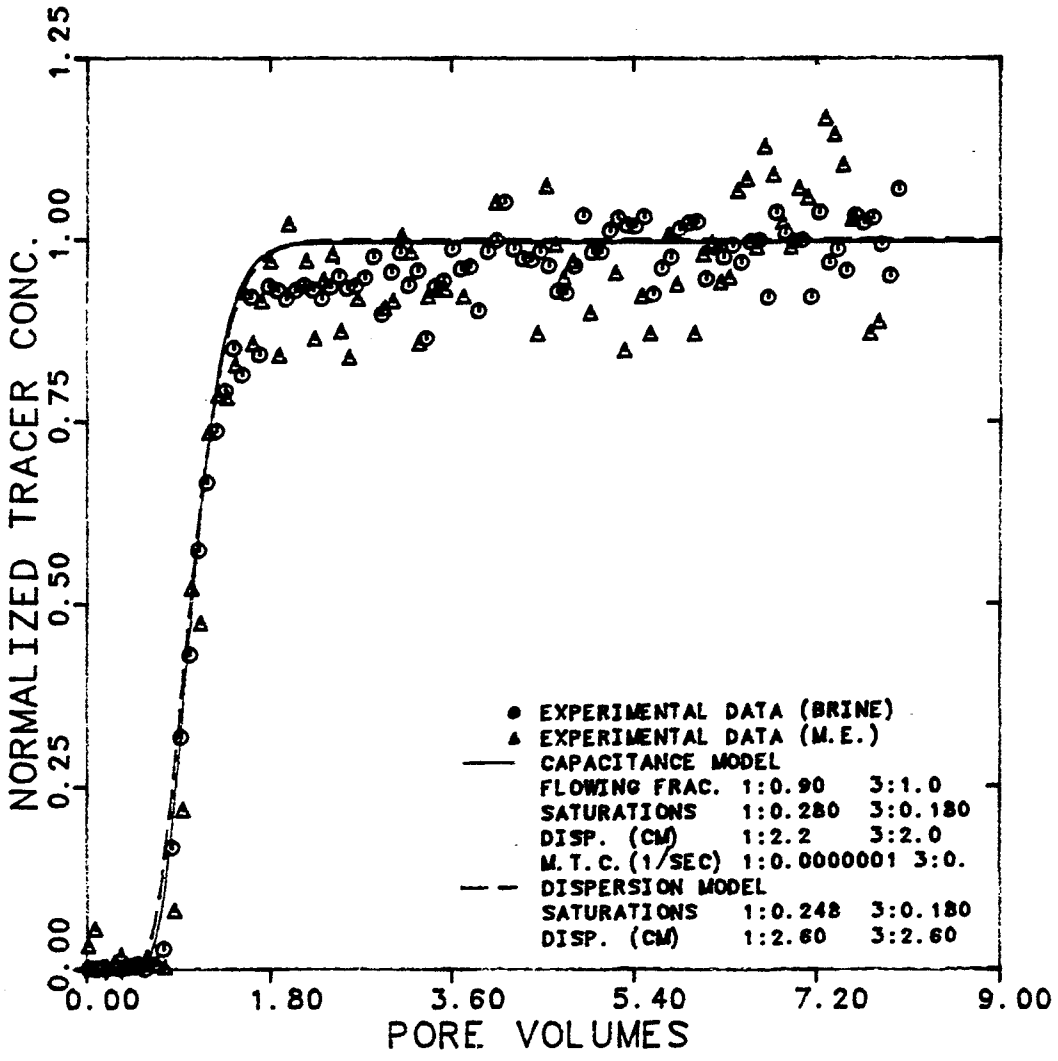

Figure 6.4.3.10 Effluent Histories for Chloride-36 in Brine and M.E. at 28.9% Brine, 65.3% Oil, and 5.8% M.E. Cuts

EXPERIMENT NUMBER	BM03-8		
TRACER & PHASES	CARBON-14	OIL & M.E.	
MAX. & INJ. CONC. (OIL)	23600	23720	DPM/CC
MAX. & INJ. CONC. (M.E.)	12000	12000	DPM/CC
FLOW RATE	1.730		CC/MIN

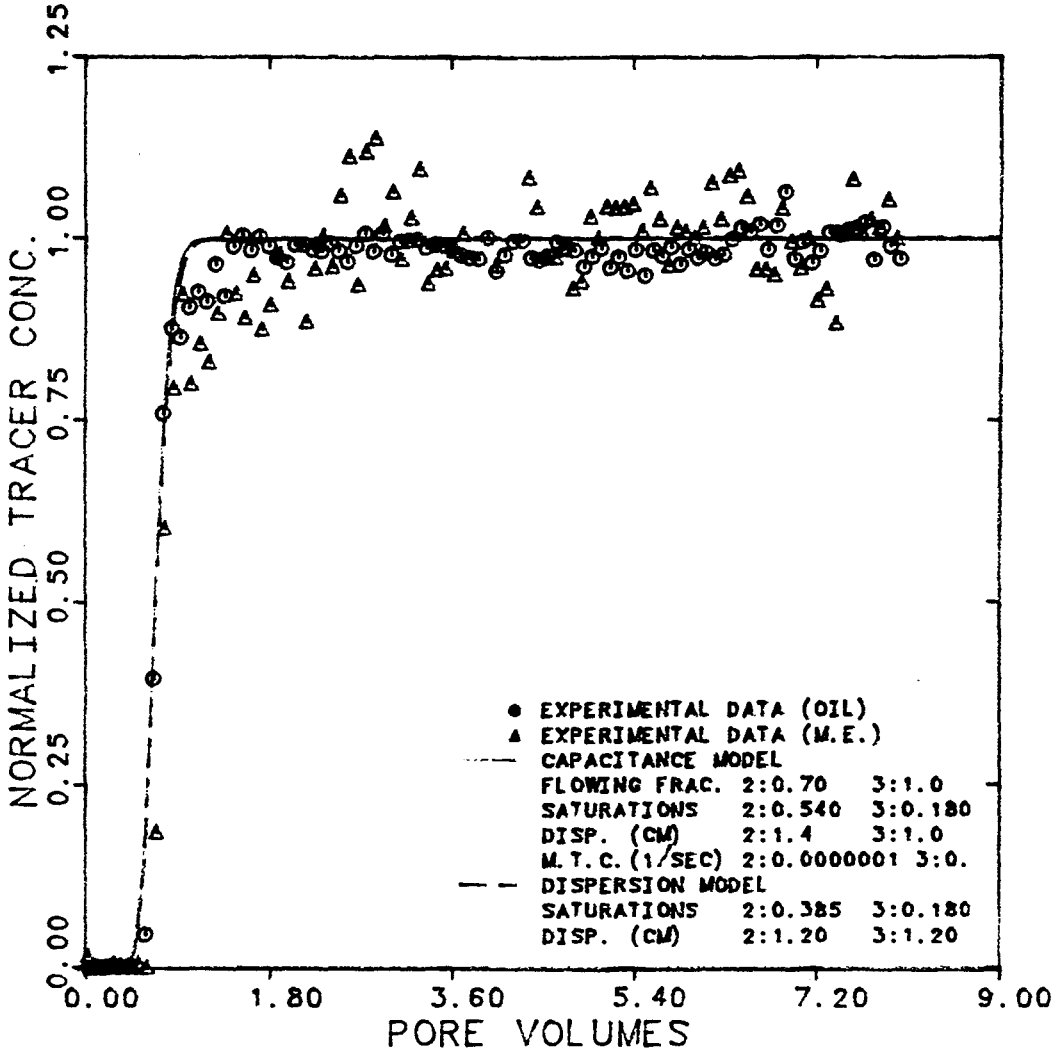

Figure 6.4.3.11 Effluent Histories for Carbon-14 in Oil and M.E. at 28.9% Brine, 65.3% Oil, and 5.8% M.E. Cuts

EXPERIMENT NUMBER	BMO3-10
TRACER & PHASE	TAGG. SULF. M.E.
INJECTED CONC.	23500 DPM/CC
FLOW RATE	1.04 CC/MIN

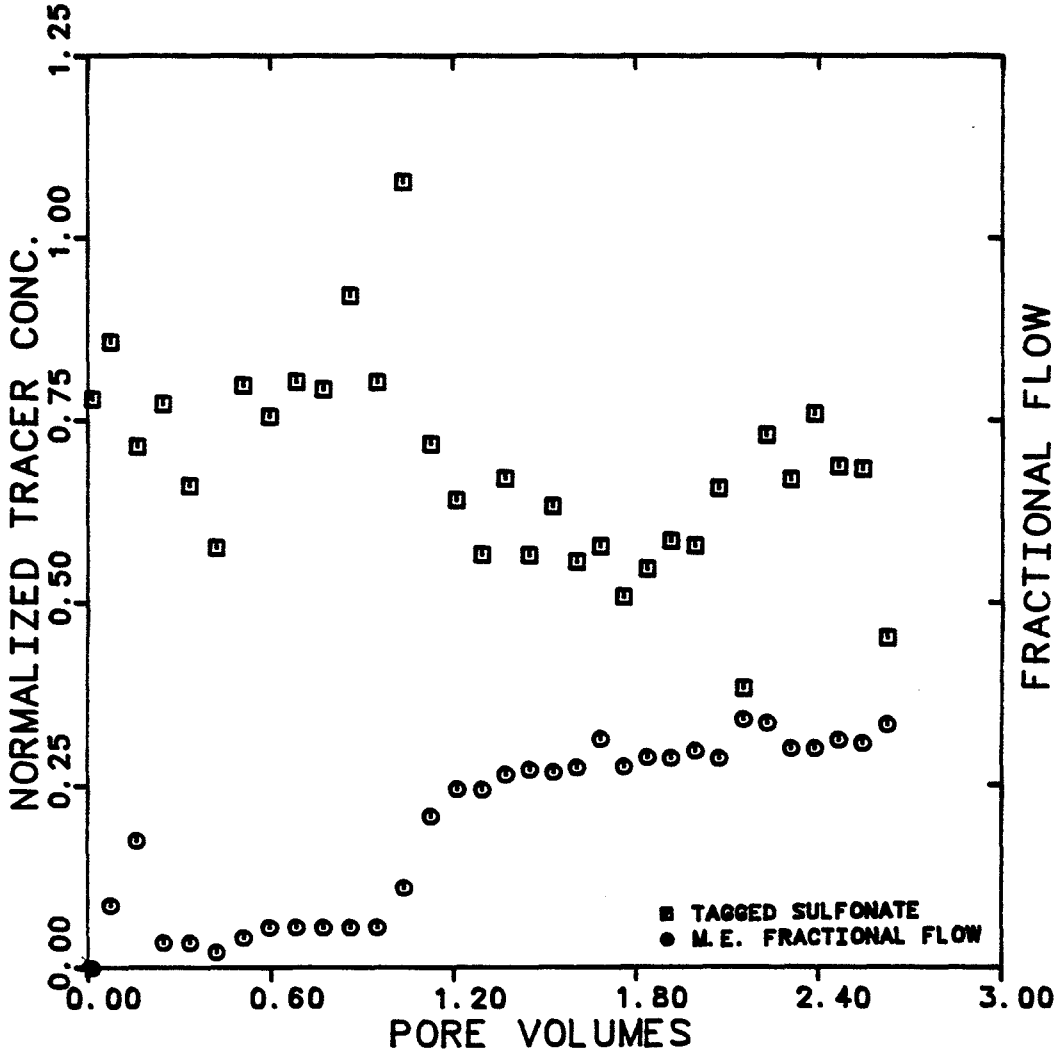

Figure 6.4.3.12 Concentration of Labelled Sulfonate in M.E. and M.E. Cut During Transient Period as a Function of Pore Volumes Injected (cut BMO3-10)

EXPEIMENT NUMBER	BMO3-10	
TRACER & PHASE	CHLORIDE-36	BRINE& M.E.
INJECTED CONC. (BRINE)	7444	DPM/CC
INJECTED CONC. (M.E.)	3300	DPM/CC
FLOW RATE	1.04	CC/MIN

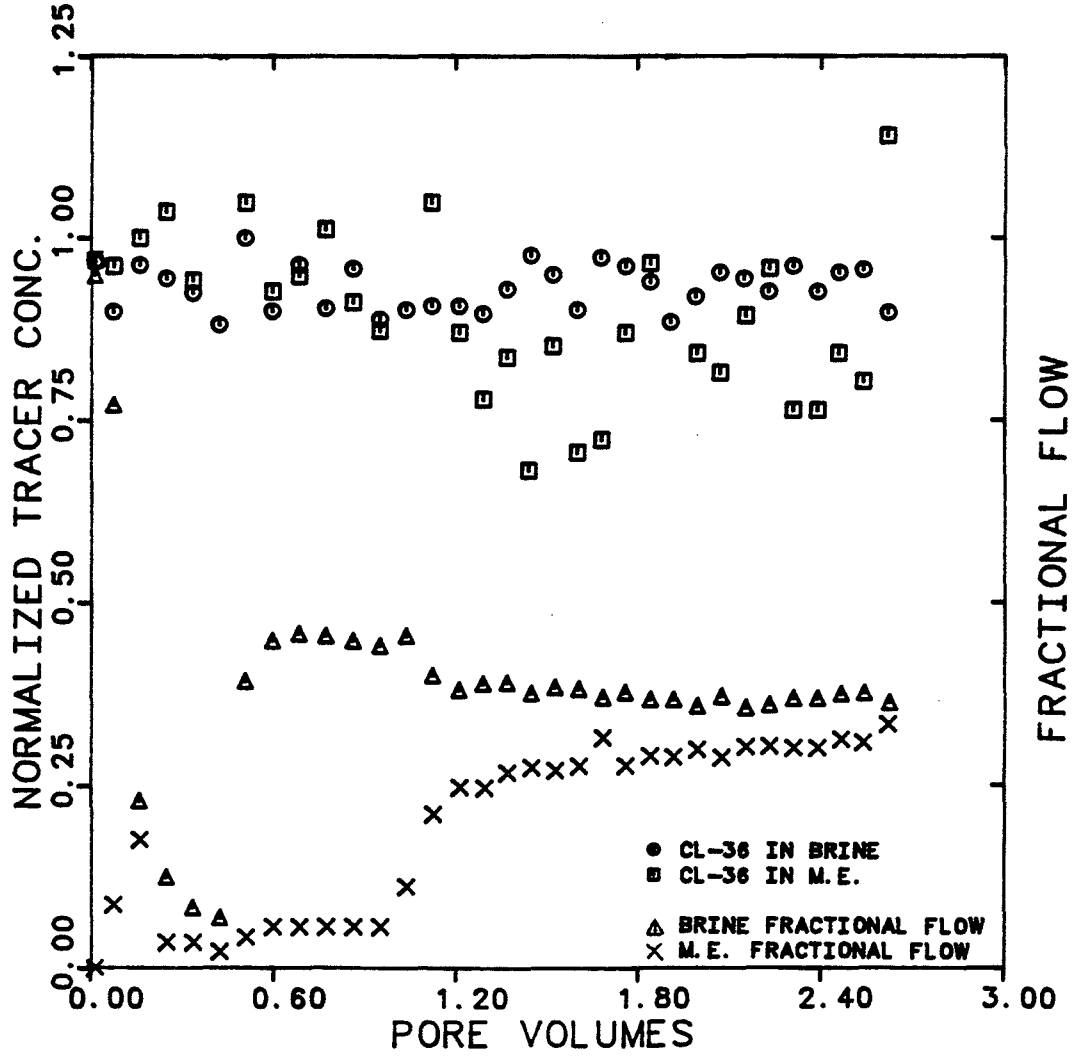

Figure 6.4.3.13 Concentration of Chloride-36 in Brine and M.E. and their Cuts During Transient Period as a Function of Pore Volumes Injected (cut BMO3-10)

EXPEIMENT NUMBER	BMO3-10	
TRACER & PHASE	CARBON-14	OIL & M.E.
INJECTED CONC. (OIL)	23720	DPM/CC
INJECTED CONC. (M.E.)	11690	DPM/CC
FLOW RATE	1.04	CC/MIN

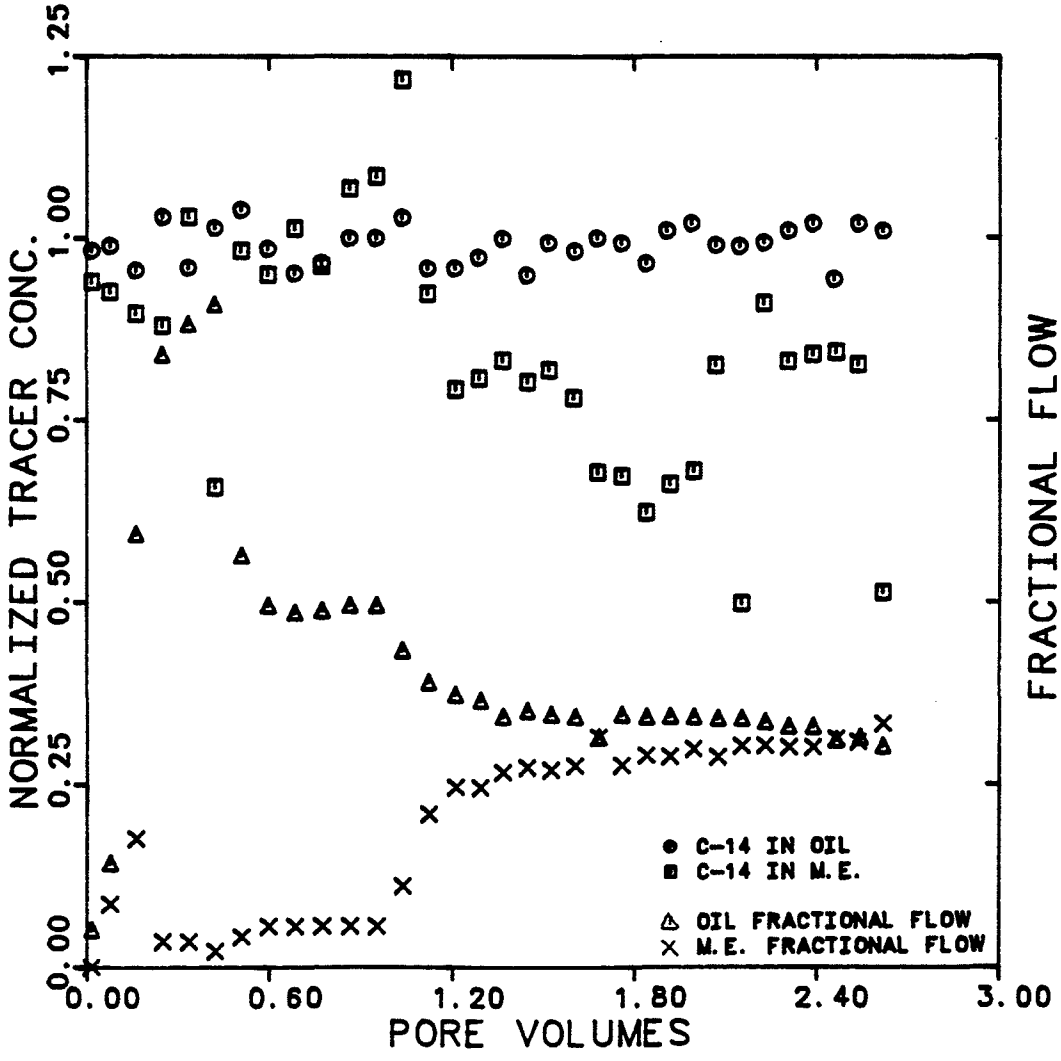

Figure 6.4.3.14 Concentration of Carbon-14 in Oil and M.E. and their Cuts During Transient Period as a Function of Pore Volumes Injected (cut BMO3-10)

EXPERIMENT NUMBER	BM03-10	
TRACER & PHASE	TAGG. SULF.	M.E.
FRACTIONAL FLOW	3:0.347	
MAX. & INJ. CONC.	20517 0.0	DPM/CC
FLOW RATE	1.040	CC/MIN.

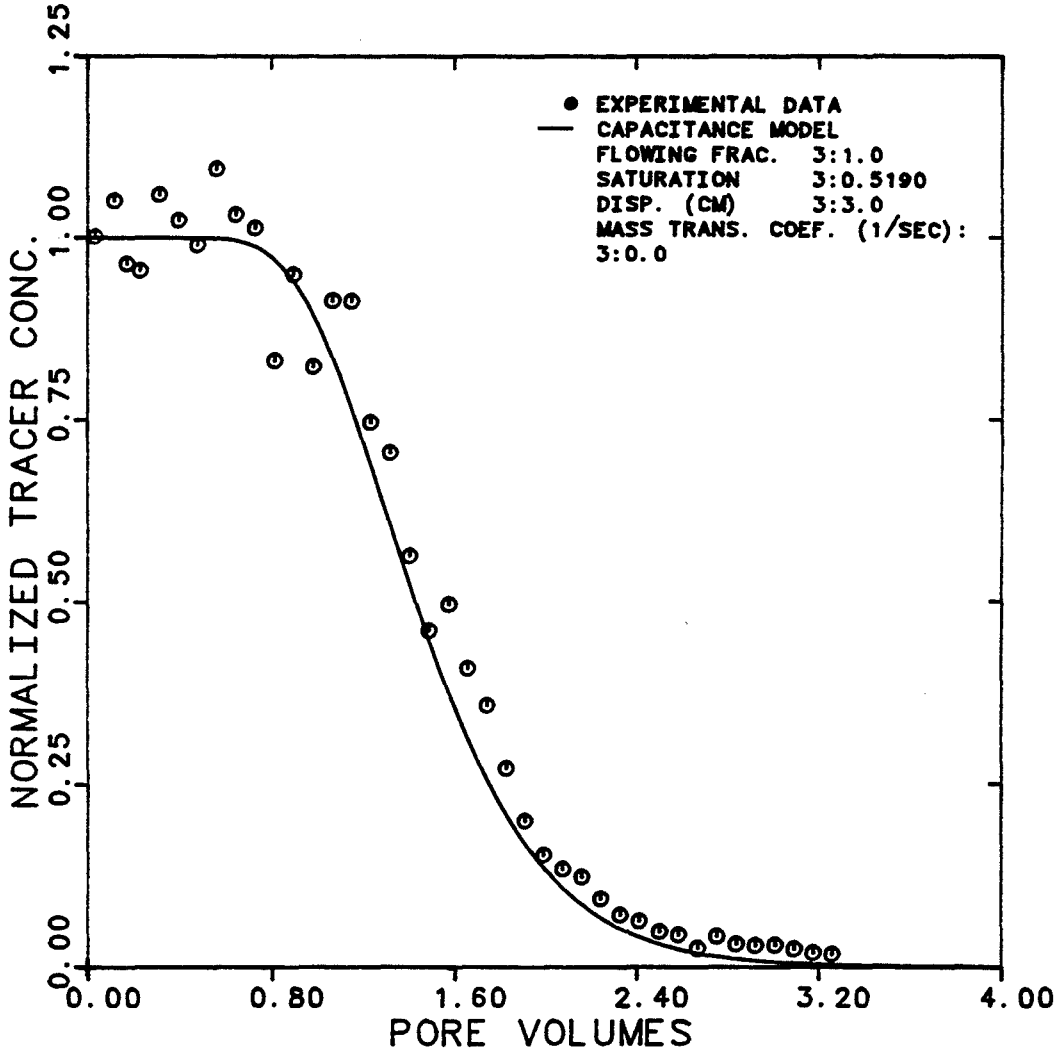

Figure 6.5.3.15 Effluent History for Labelled Sulfonate in M.E. at 35.9% Brine, 29.4% Oil, and 34.7% M.E. Cuts

EXPERIMENT NUMBER	BM03-10		
TRACER & PHASES	CHLORIDE-36		BRINE & M.E
MAX. & INJ. CONC. (BRINE)	6872	0.0	DPM/CC
MAX. & INJ. CONC. (M.E.)	2482	0.0	DPM/CC
FLOW RATE	1.040		CC/MIN

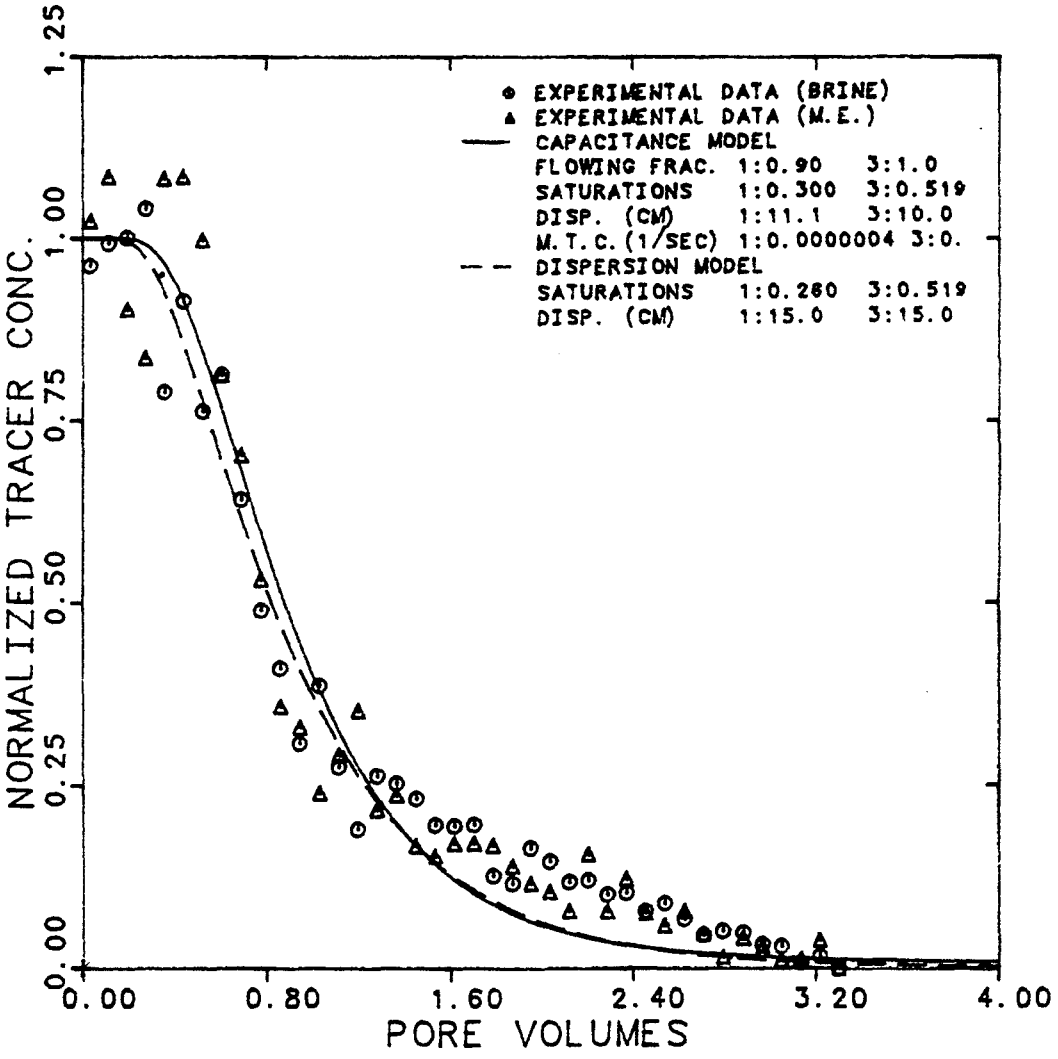

Figure 6.4.3.16 Effluent Histories for Chloride-36 in Brine and M.E. at 35.9% Brine, 29.4% Oil, and 34.7% M.E. Cuts

EXPERIMENT NUMBER	BM03- 10		
TRACER & PHASE	CARBON-14		OIL & M.E.
MAX. & INJ. CONC. (OIL)	22752	0.0	DPM/CC
MAX. & INJ. CONC. (M.E.)	8240	0.0	DPM/CC
FLOW RATE	1.04		CC/MIN

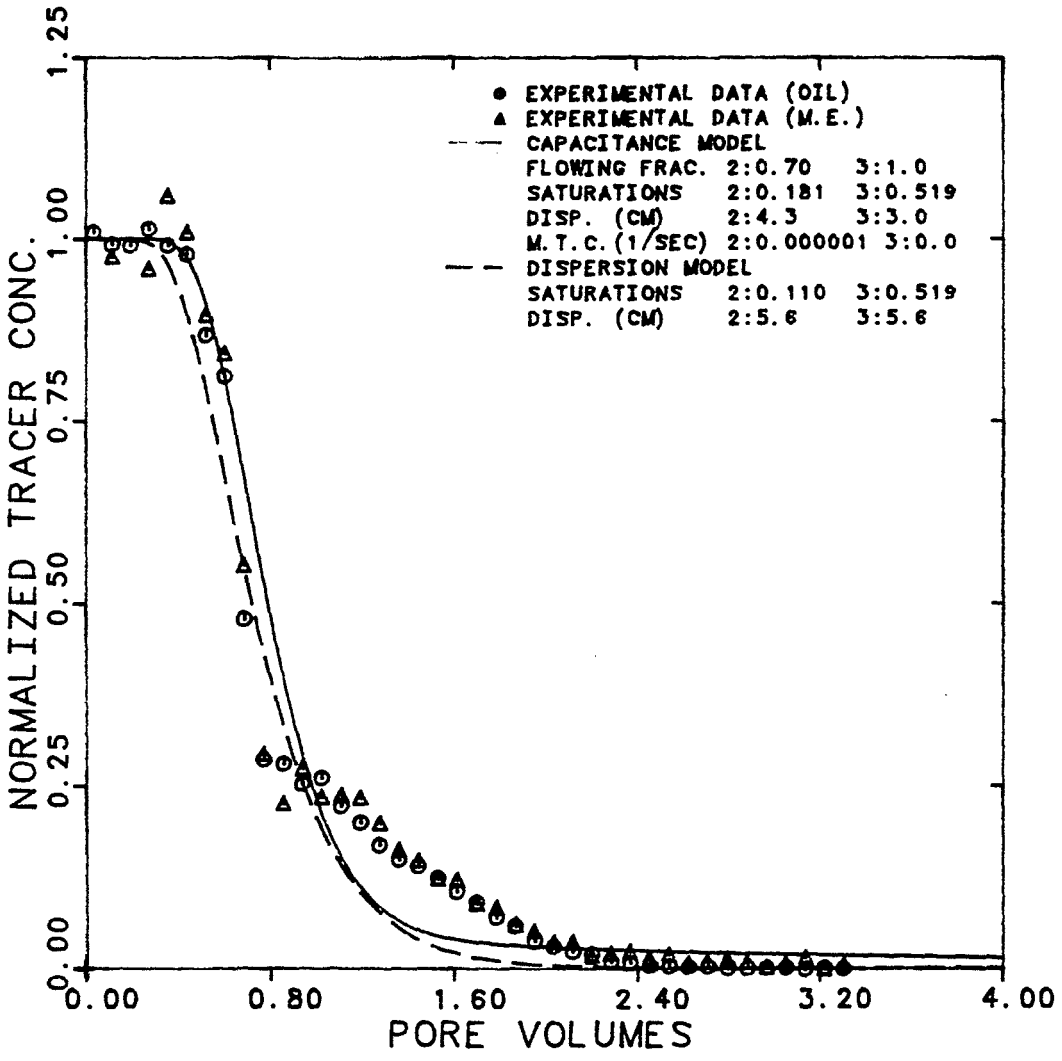

Figure 6.4.3.17 Effluent Histories for Carbon-14 in Oil and M.E. at 35.9% Brine, 29.4% Oil, and 34.7% M.E. Cuts

EXPERIMENT NUMBER	BM03-12	
TRACER & PHASE	TAGG. SULF.	M.E.
FRACTIONAL FLOW	3:0.473	
MAX. & INJ. CONC.	22158 23236	DPM/CC
FLOW RATE	0.8278	CC/MIN.

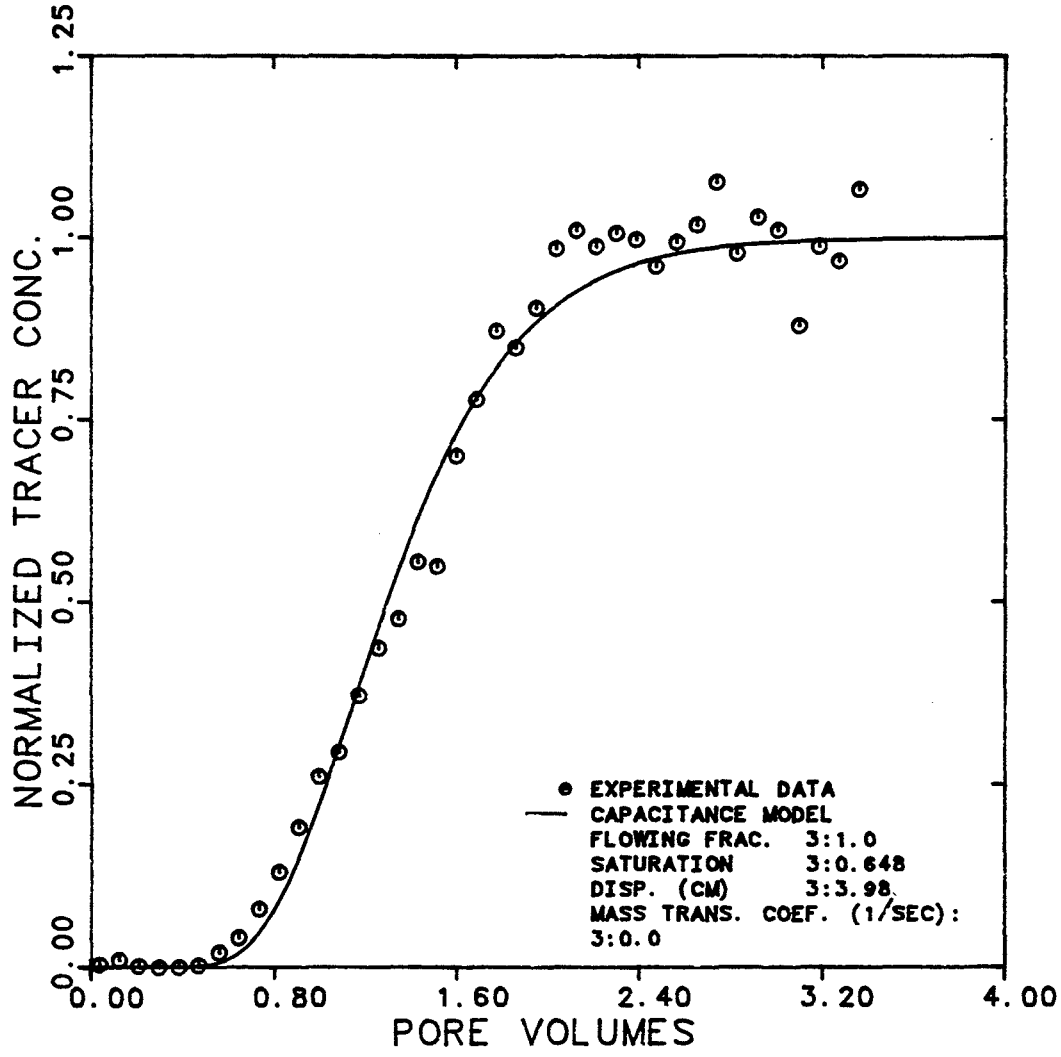

Figure 6.4.3.18 Effluent Histories for Labelled Sulfonate in M.E. at 50% Brine, 2.7% Oil, and 47.3% M.E. Cuts

EXPERIMENT NUMBER	BM03-12		
TRACER & PHASES	CHLORIDE-36 BRINE & M.E.		
MAX. & INJ. CONC. (BRINE)	6703	6868	DPM/CC
MAX. & INJ. CONC. (M.E.)	2746	2746	DPM/CC
FLOW RATE	0.8278		CC/MIN

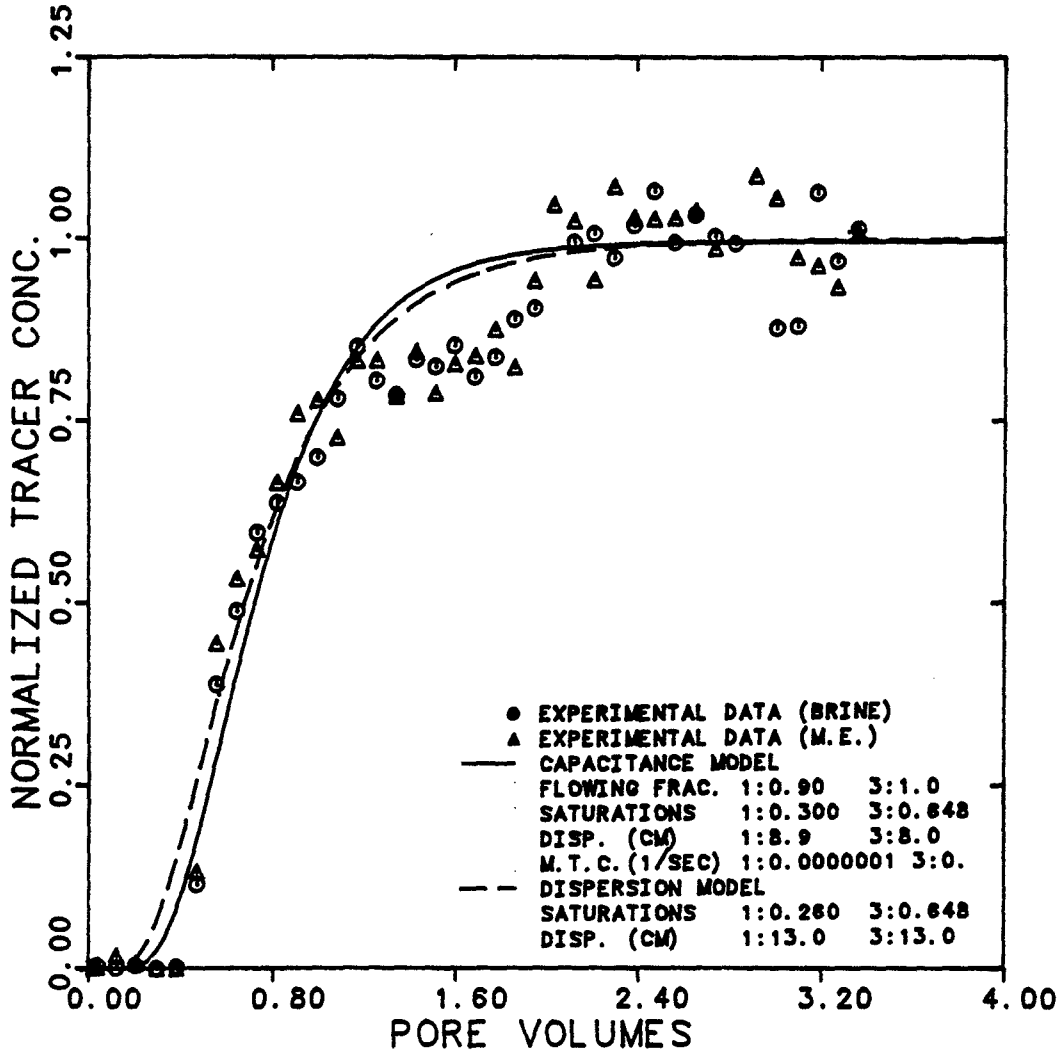

Figure 6.4.3.19 Effluent Histories for Chloride-36 in Brine and M.E. at 50% Brine, 2.7% Oil, and 47.3% M.E. Cuts

EXPERIMENT NUMBER	BM03-12	
TRACER & PHASE	CARBON-14	M.E.
FRACTIONAL FLOW	1:.500 2:.027	3:.473
MAX. & INJ. CONC.	8961 8961	DPM/CC
FLOW RATE	0.8278	CC/MIN.

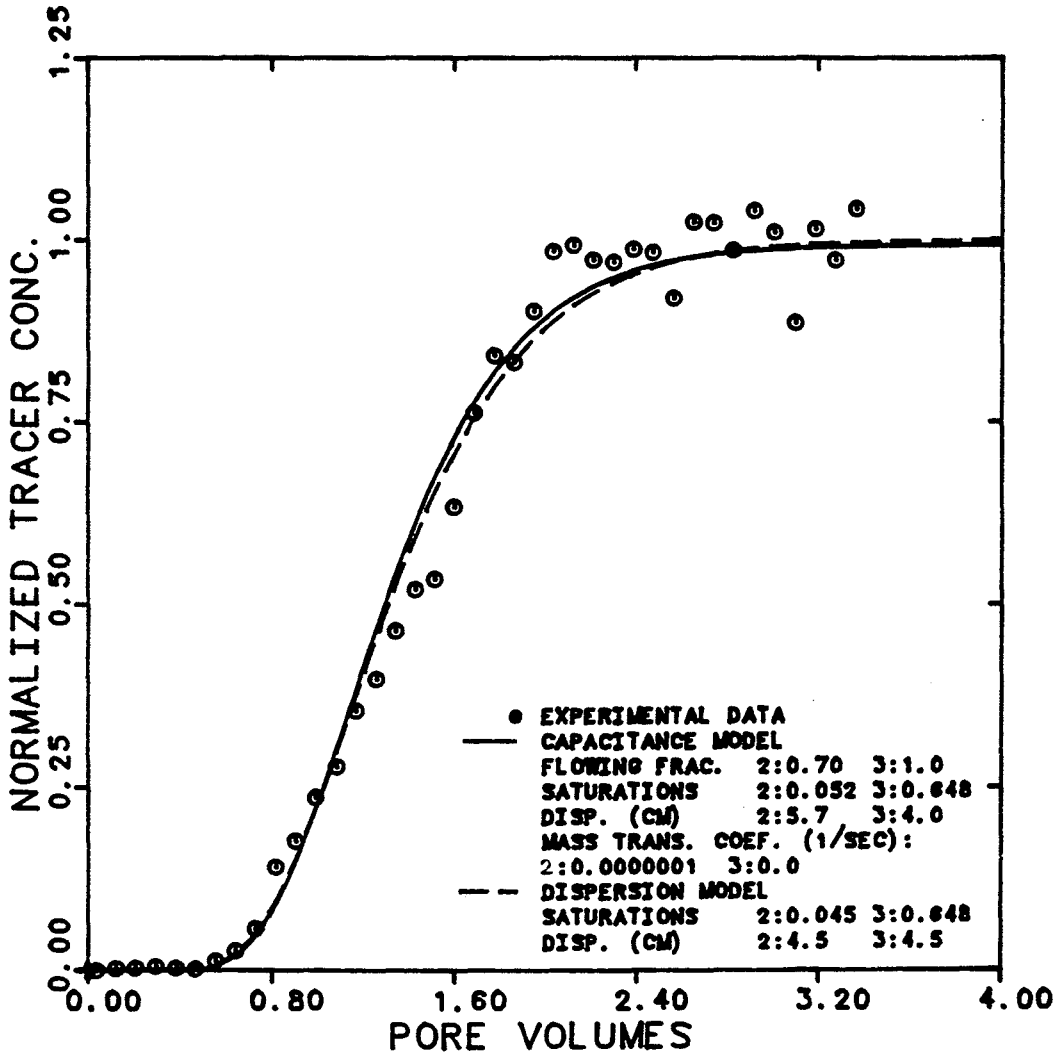

Figure 6.4.3.20 Effluent History for Carbon-14 in M.E. at 50% Brine, 2.7% Oil, and 47.3% M.E. Cuts

EXPERIMENT NUMBER	BMO3-14
TRACER & PHASE	TAGG. SULF. M.E.
INJECTED CONC.	23240 DPM/CC
FLOW RATE	1.11 CC/MIN

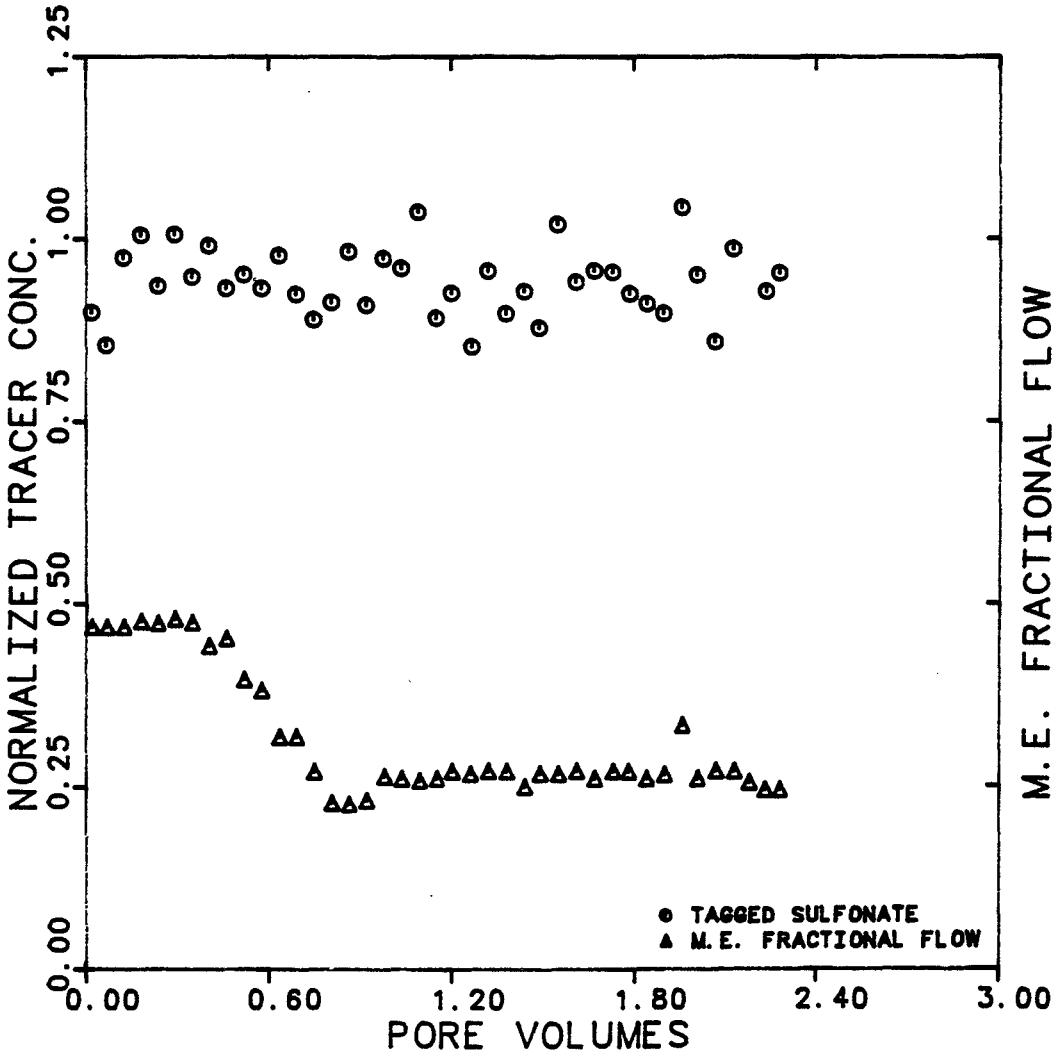

Figure 6.4.3.21 Concentration of Labelled Sulfonate in M.E. and M.E. Cut During Transient Period as a Function of Pore Volumes Injected (cut BMO3-14)

EXPERIMENT NUMBER	BMO3-14
TRACER & PHASE	CHLORIDE-36 BR. & M.E.
INJECTED CONC. (BRINE)	6870 DPM/CC
INJECTED CONC. (M.E.)	2550 DPM/CC
FLOW RATE	1.11 CC/MIN

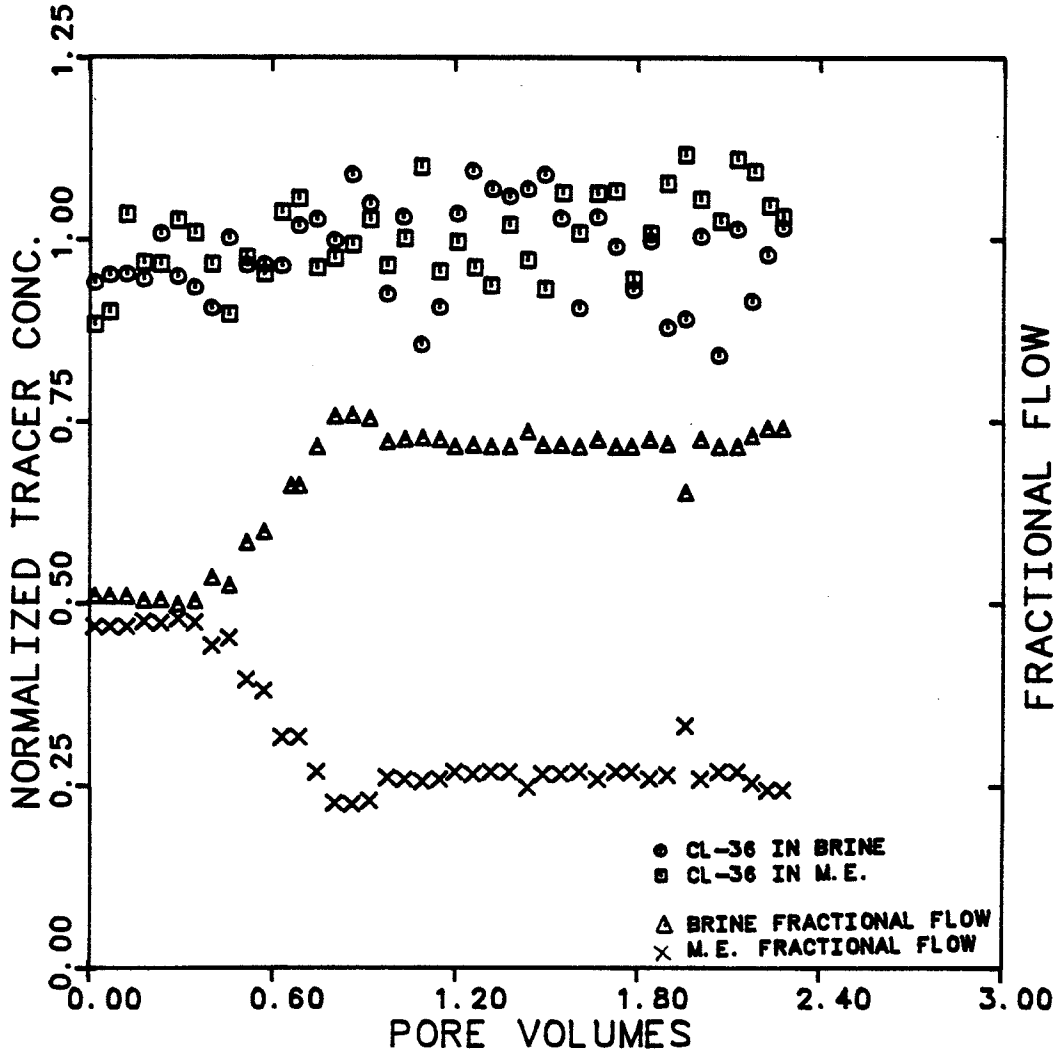

Figure 6.4.3.22 Concentration of Chloride-36 in Brine and M.E. and their Cuts During Transient Period as a Function of Pore Volumes Injected (cut BMO3-14)

EXPERIMENT NUMBER	BMO3-14
TRACER & PHASE	CARBON-14 M.E.
INJECTED CONC.	8960 DPM/CC
FLOW RATE	1.031 CC/MIN

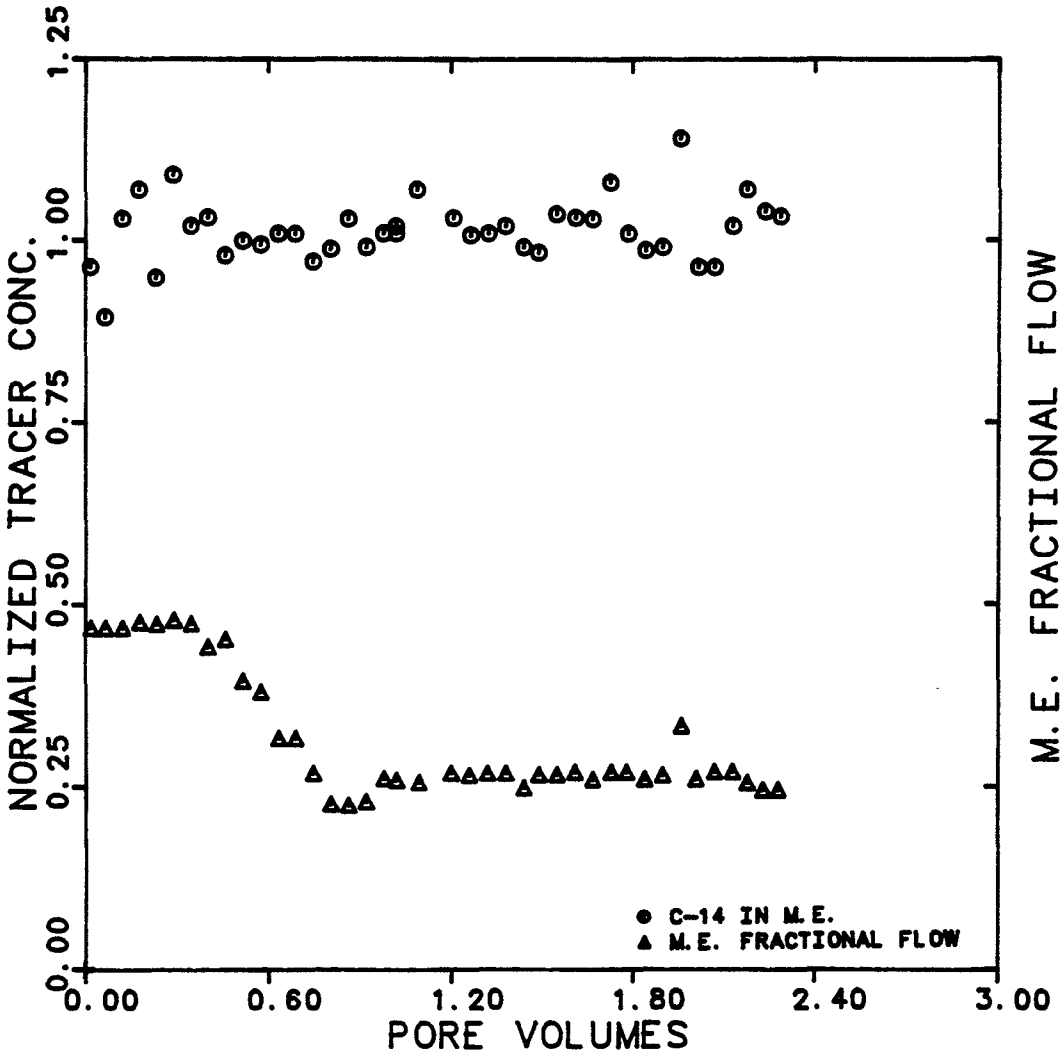

Figure 6.4.3.23 Concentration of Carbon-14 in M.E. and M.E. Cut During Transient Period as a Function of Pore Volumes Injected (cut BMO3-14)

EXPERIMENT NUMBER	BM03-14	
TRACER & PHASE	TAGG. SULF.	M.E.
FRACTIONAL FLOW	3:0.268	
MAX. & INJ. CONC.	22110 0.0	DPM/CC
FLOW RATE	1.110	CC/MIN.

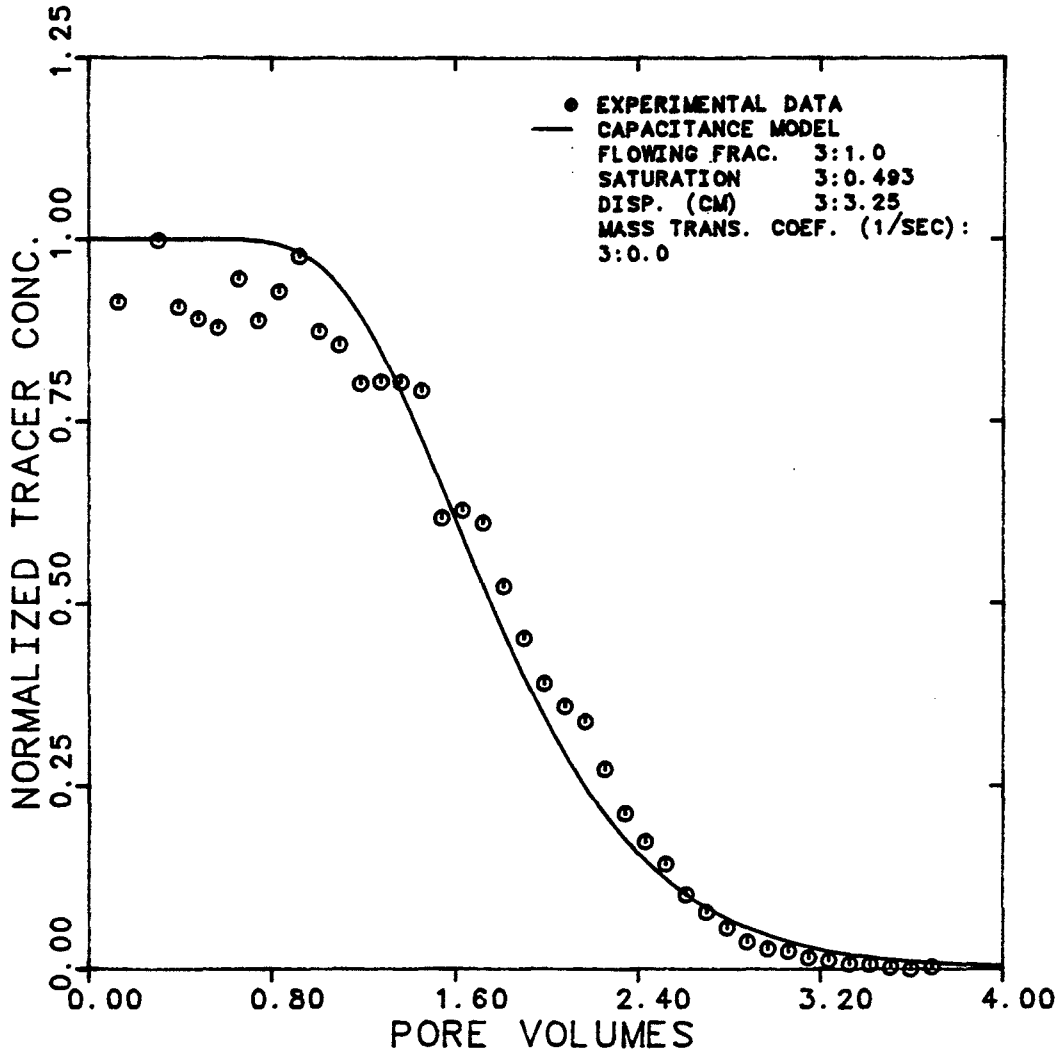

Figure 6.4.3.24 Effluent History for Labelled Sulfonate in ME. at 71.9% Brine, 1.3% Oil, and 26.8% M.E.Cuts

EXPERIMENT NUMBER	BM03-14		
TRACER & PHASES	CHLORIDE-36		BRINE & M.E
MAX. & INJ. CONC. (BRINE)	6800	0.0	DPM/CC
MAX. & INJ. CONC. (M.E.)	2625	0.0	DPM/CC
FLOW RATE	1.110		CC/MIN

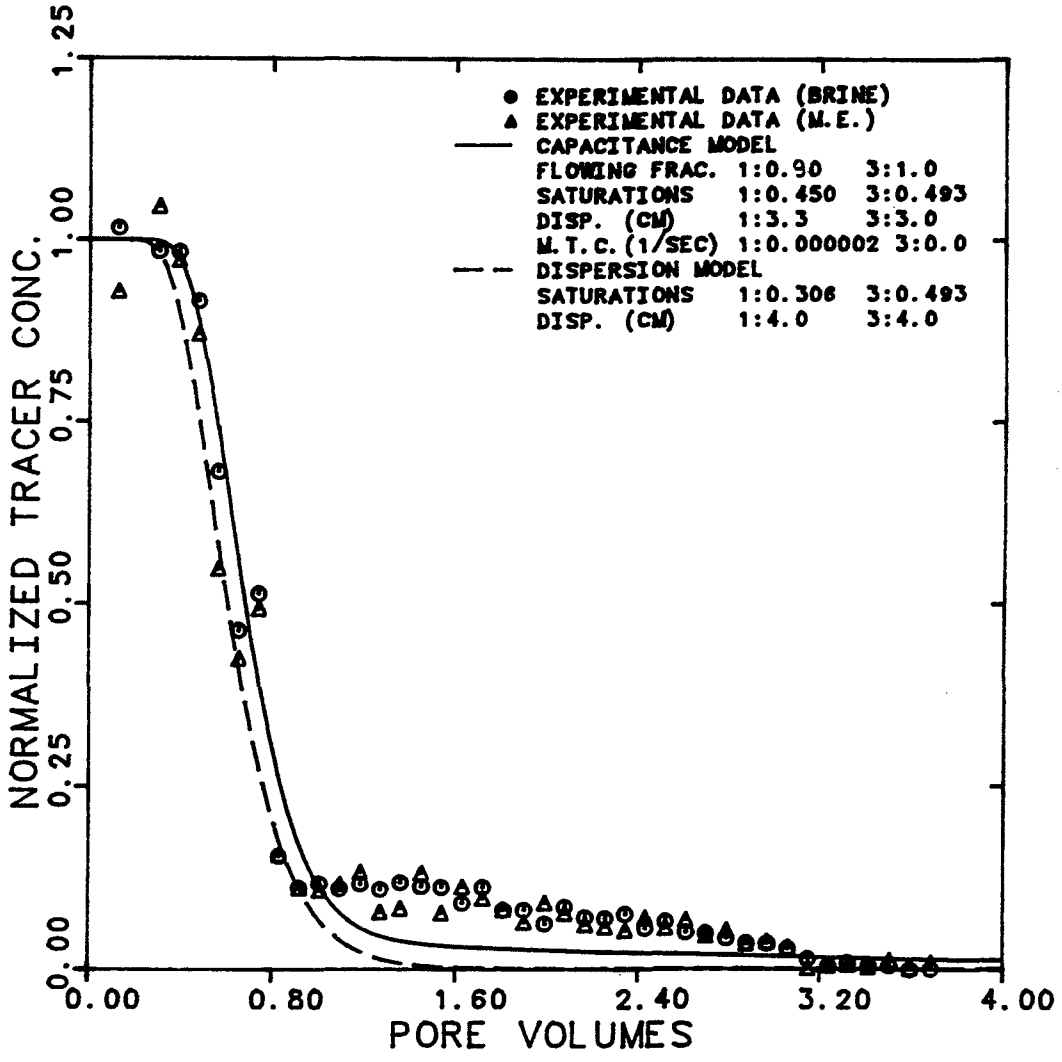

Figure 6.4.3.25 Effluent Histories for Chloride-36 in Brine and M.E. for 71.9% Brine, 1.3% Oil, and 26.8% M.E. Cuts

EXPERIMENT NUMBER	BM03-14		
TRACER & PHASE	CARBON-14		M.E.
FRACTIONAL FLOW	1:.719	2:.013	3:.268
MAX. & INJ. CONC.	8805	0.0	DPM/CC
FLOW RATE	1.110		CC/MIN.

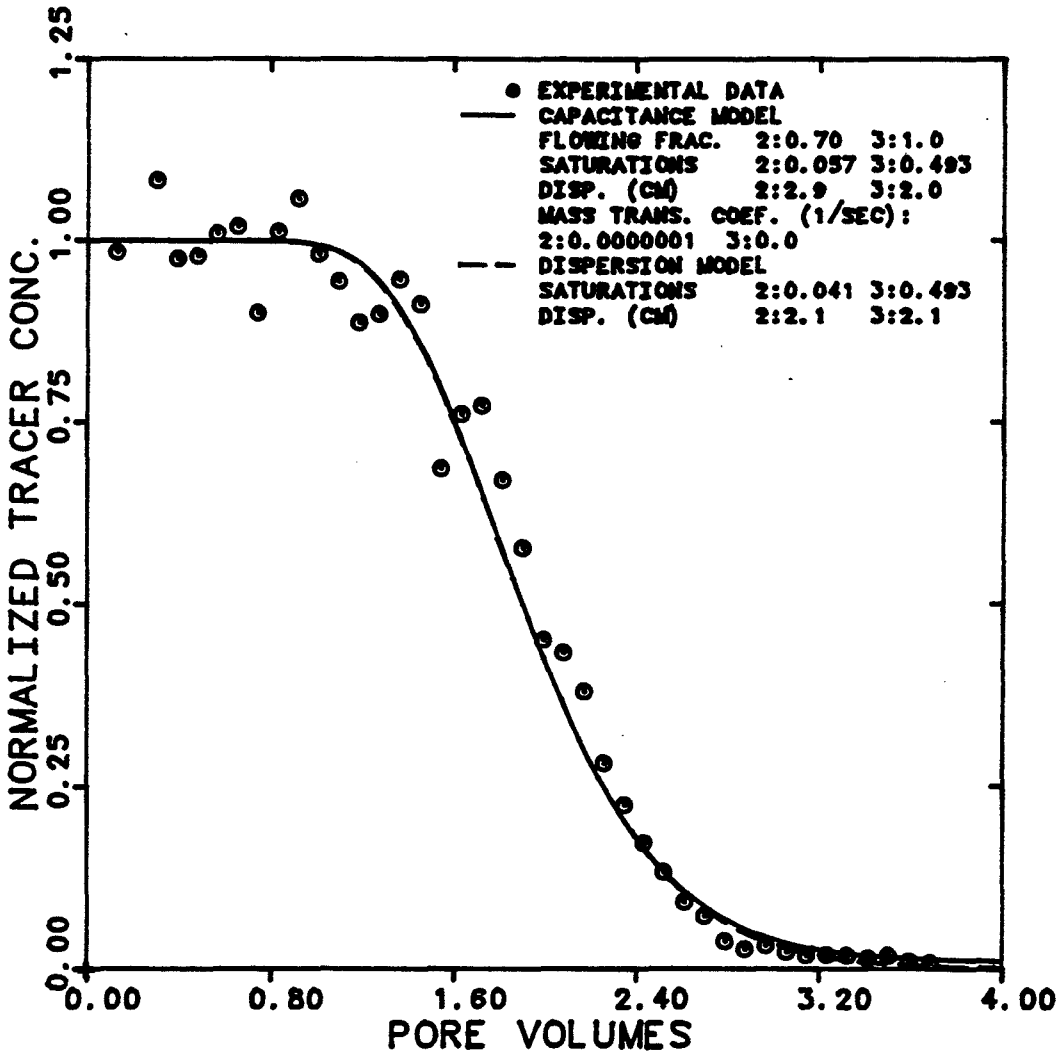

Figure 6.4.3.26 Effluent History for Carbon-14 in M.E. at 71.9% Brine, 1.3% Oil, and 26.8% M.E. Cuts

EXPERIMENT NUMBER	BM03-16	
TRACER & PHASE	TAGG. SULF.	M.E.
FRACTIONAL FLOW	3:0.145	
MAX. & INJ. CONC.	22400 23000	DPM/CC
FLOW RATE	1.450	CC/MIN.

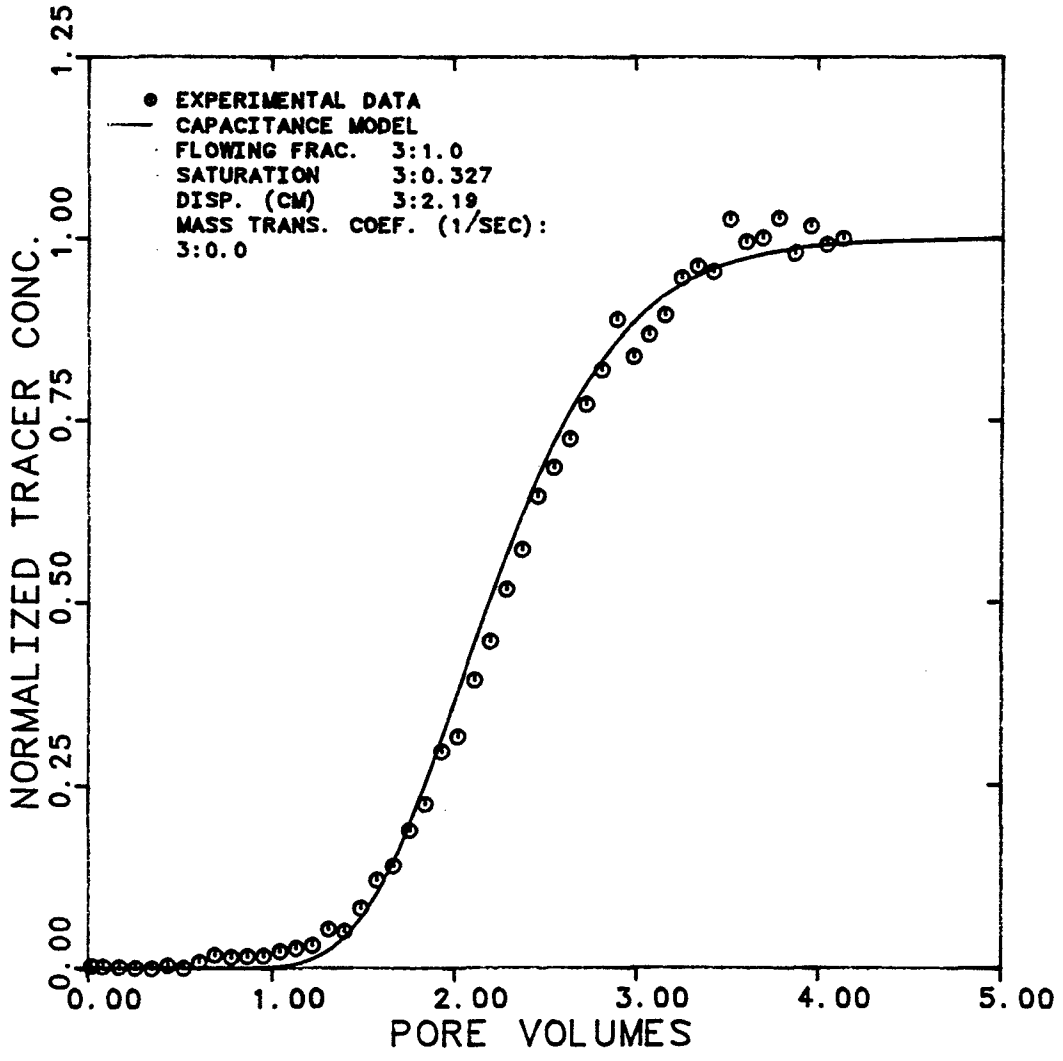

Figure 6.4.3.27 Effluent History for Labelled Sulfonate in M.E. at 84% Brine, 1.5% Oil, and 14.5% M.E. Cuts

EXPERIMENT NUMBER	BM03-16		
TRACER & PHASES	CHLORIDE-36 BRINE & M.E.		
MAX. & INJ. CONC. (BRINE)	6759	7080	DPM/CC
MAX. & INJ. CONC. (M.E.)	3097	3240	DPM/CC
FLOW RATE	1.450		CC/MIN

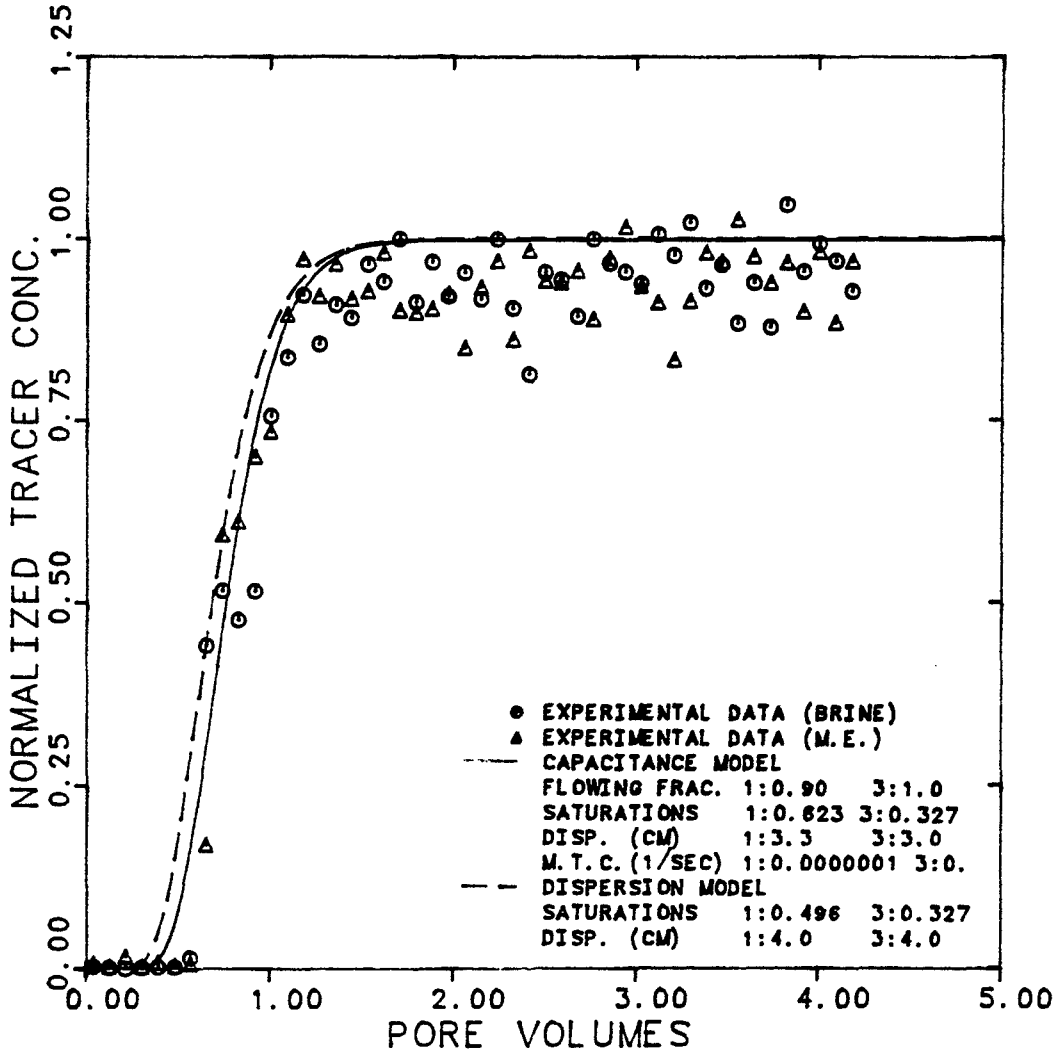

Figure 6.4.3.28 Effluent Histories for Chloride-36 in Brine and M.E. at 84% Brine, 1.5% Oil, and 14.5% M.E. Cuts

EXPERIMENT NUMBER	BM03-16	
TRACER & PHASES	CARBON-14	OIL & M.E.
MAX. & INJ. CONC. (OIL)	22000 23000	DPM/CC
MAX. & INJ. CONC. (M.E.)	10000 10500	DPM/CC
FLOW RATE	1.450	CC/MIN

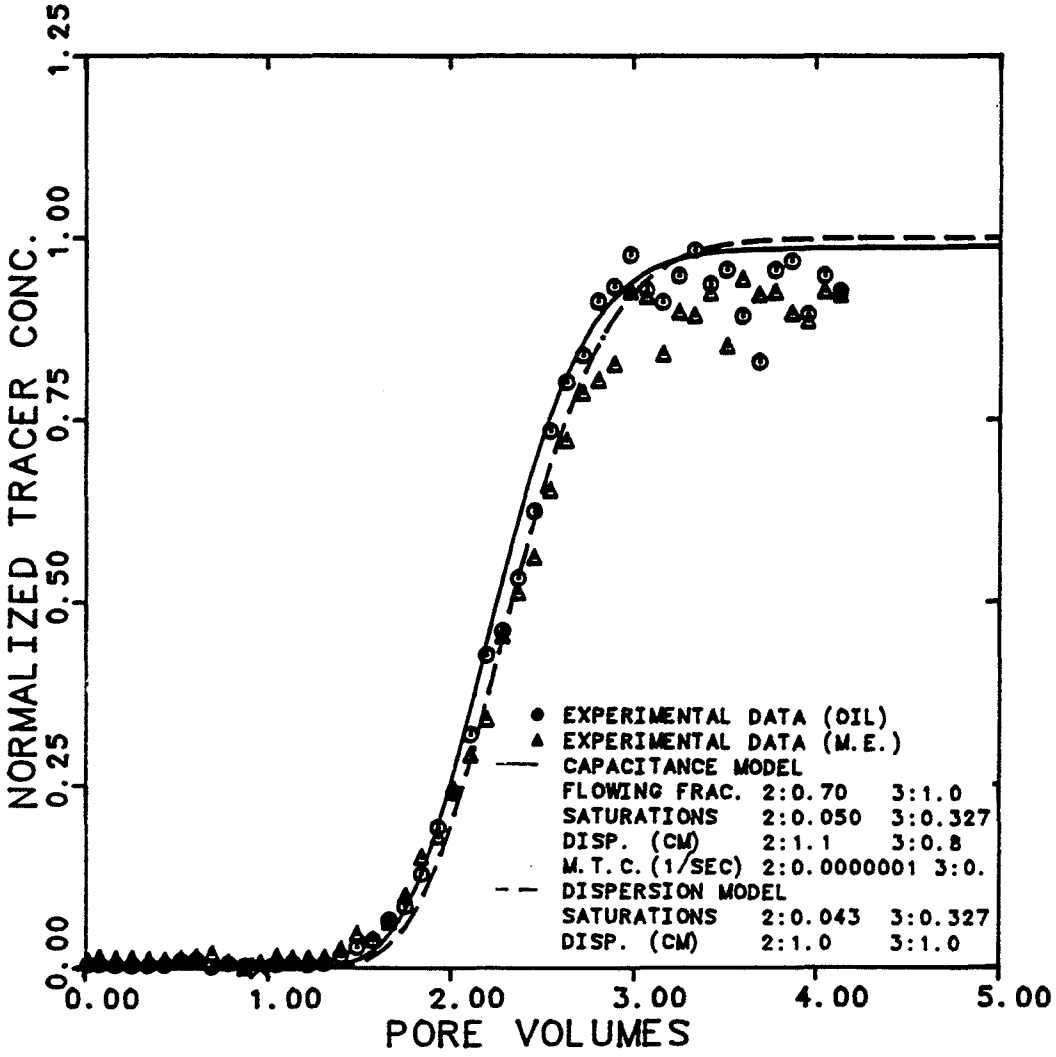

Figure 6.4.3.29 Effluent Histories for Carbon-14 in Oil and M.E. at 84% Brine, 1.5% Oil, and 14.5% M.E. Cuts

EXPERIMENT NUMBER	BM03-18	
TRACER & PHASE	TAGG. SULF.	M.E.
FRACTIONAL FLOW	3:0.097	
MAX. & INJ. CONC.	20710 22980	DPM/CC
FLOW RATE	1.494	CC/MIN.

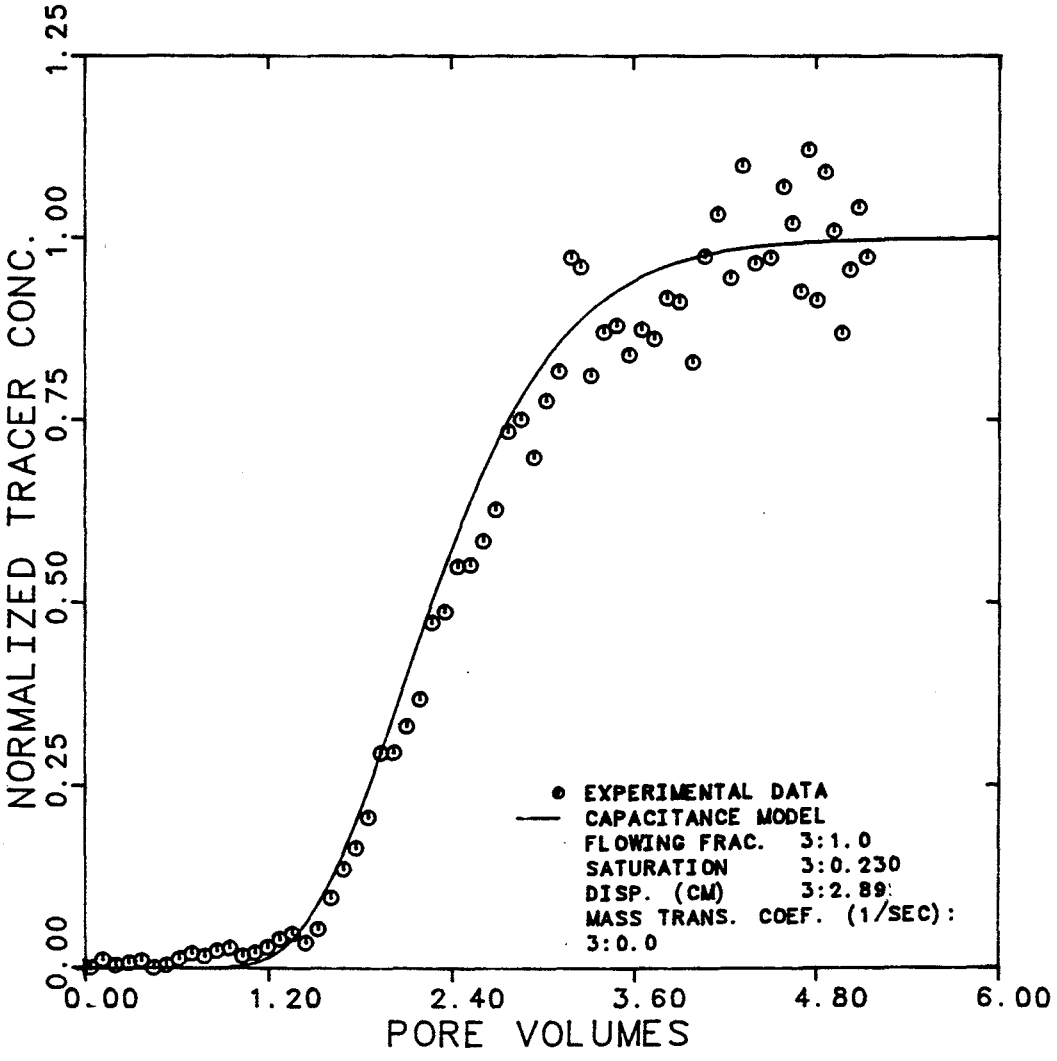

Figure 6.4.3.30 Effluent History for Labelled Sulfonate in M.E. at 89% Brine, 1.3% Oil, and 9.7% M.E. Cuts

EXPERIMENT NUMBER	BM03-18		
TRACER & PHASES	CHLORIDE-36	BRINE & M.E	
MAX. & INJ. CONC. (BRINE)	5589	5589	DPM/CC
MAX. & INJ. CONC. (M.E.)	2274	2274	DPM/CC
FLOW RATE	1.494		CC/MIN

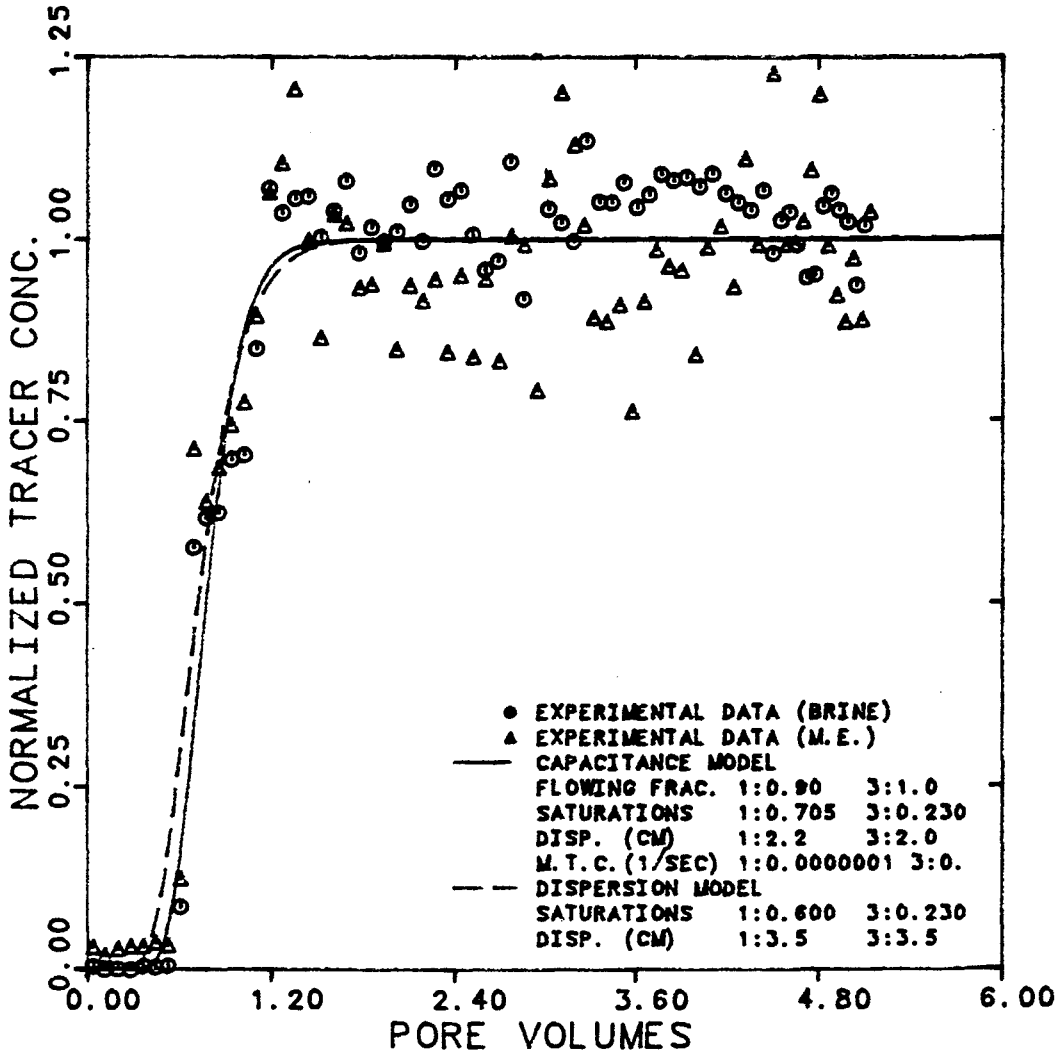

Figure 6.4.3.31 Effluent Histories for Chloride-36 in Brine and M.E. at 89% Brine, 1.3% Oil, and 9.7% M.E. Cuts

EXPERIMENT NUMBER	BM03-18		
TRACER & PHASES	CARBON-14	OIL & M.E.	
MAX. & INJ. CONC. (OIL)	21500	21530	DPM/CC
MAX. & INJ. CONC. (M.E.)	8190	8190	DPM/CC
FLOW RATE	1.494		CC/MIN

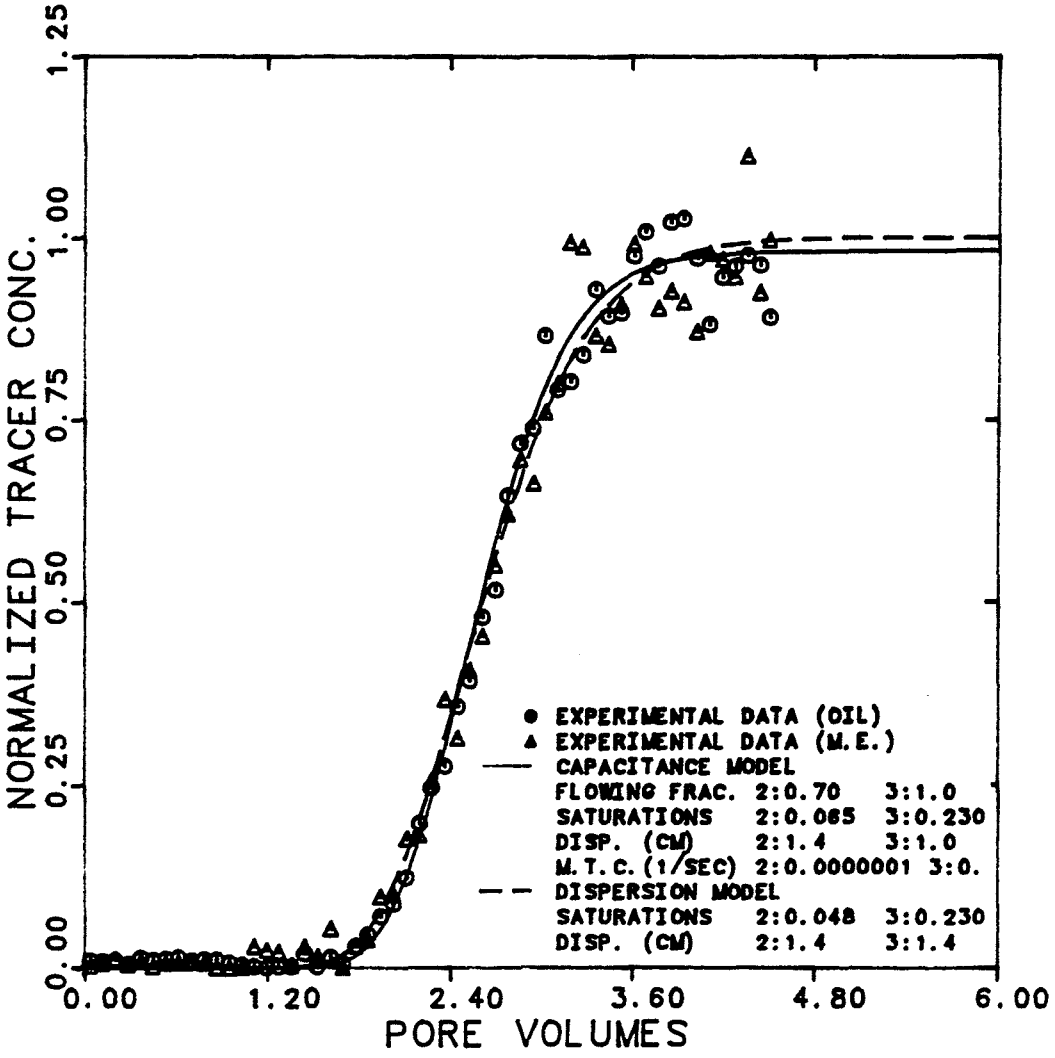

Figure 6.4.3.32 Effluent History for Carbon-14 in M.E. at 89% Brine, 1.3% Oil, and 9.7% M.E. Cuts

EXPERIMENT NUMBER	BM03-20		
TRACER & PHASE	CHLORIDE-36		BRINE
FRACTIONAL FLOW	100%		BRINE
MAX. & INJ. CONC.	5745	0.0	DPM/CC
FLOW RATE	1.575		CC/MIN.

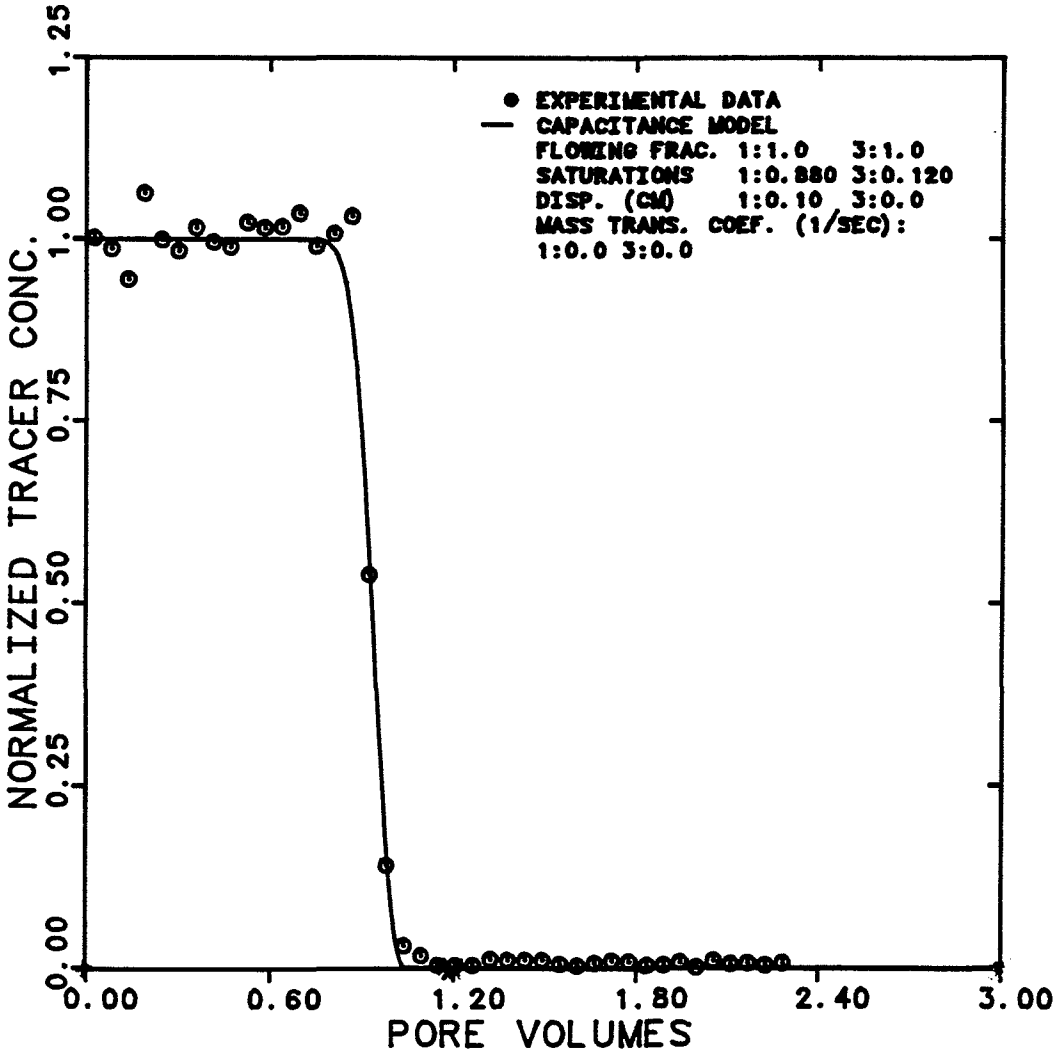

Figure 6.4.3.33 Effluent History for Chloride-36 in Brine for Single-Phase Flow

EXPERIMENT NUMBER	BM03
REF. PERMEABILITY	0.936 D
CAPILLARY NUMBER	0.01
TEMPERATURE	30°C

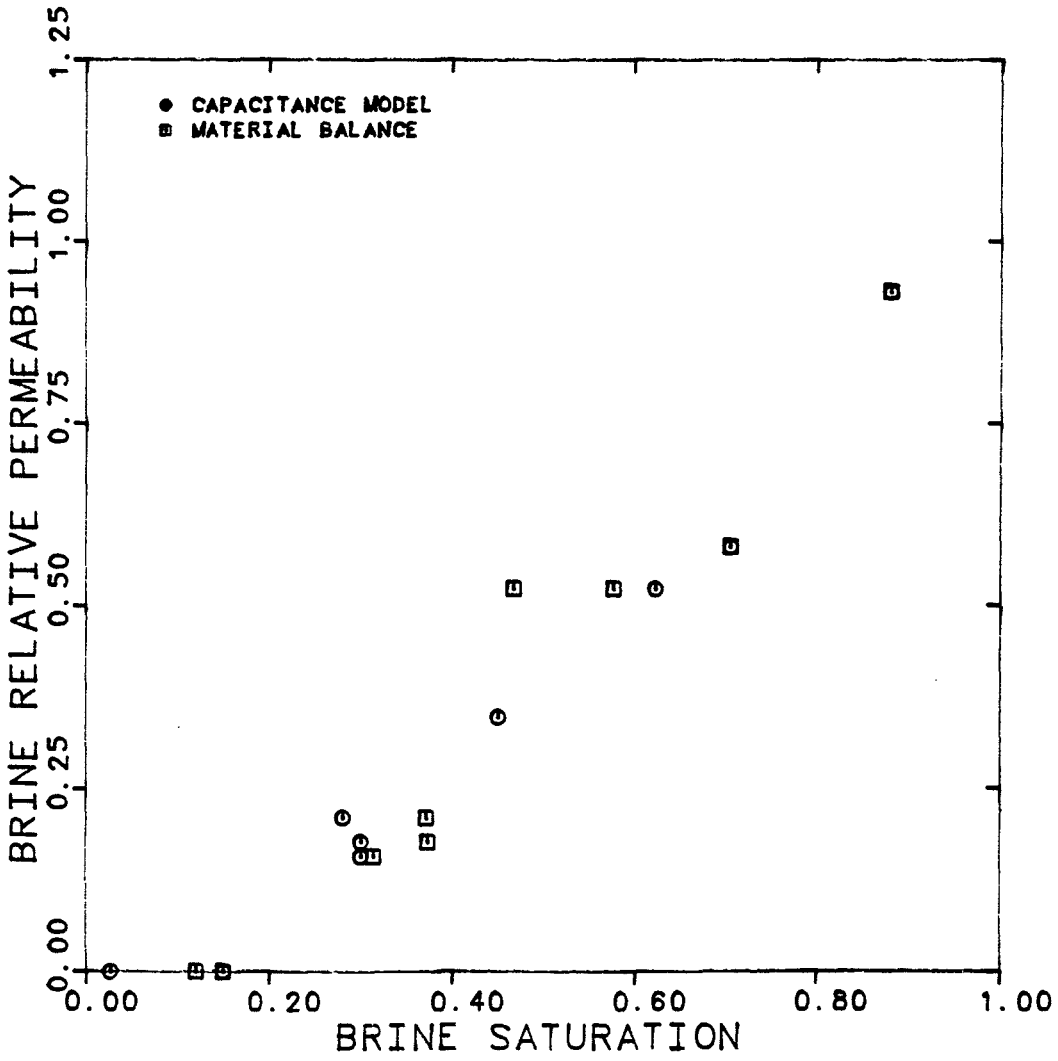

Figure 6.4.3.34 Comparison Between the Capacitance Model and Material Balance Estimates of Brine Saturation for Three-Phase Flow (Exp. BM03)

EXPERIMENT NUMBER	BM03
REF. PERMEABILITY	0.936 D
CAPILLARY NUMBER	0.01
TEMPERATURE	30°C

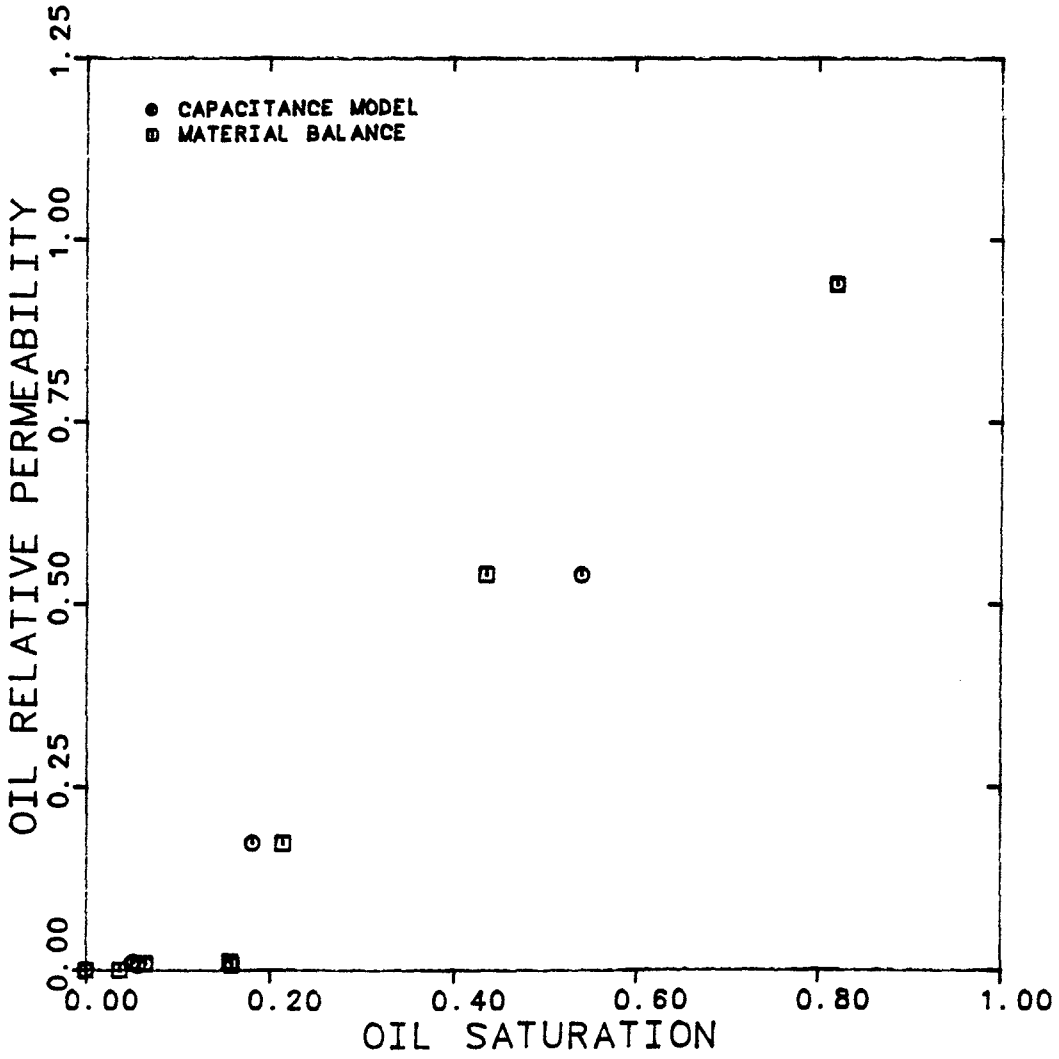

Figure 6.4.3.35 Comparison Between the Capacitance Model and Material Balance Estimates of Oil Saturation for Three-Phase Flow (Exp. BM03)

EXPERIMENT NUMBER	BMO3
REF. PERMEABILITY	0.936 D
CAPILLARY NUMBER	0.01
TEMPERATURE	30°C

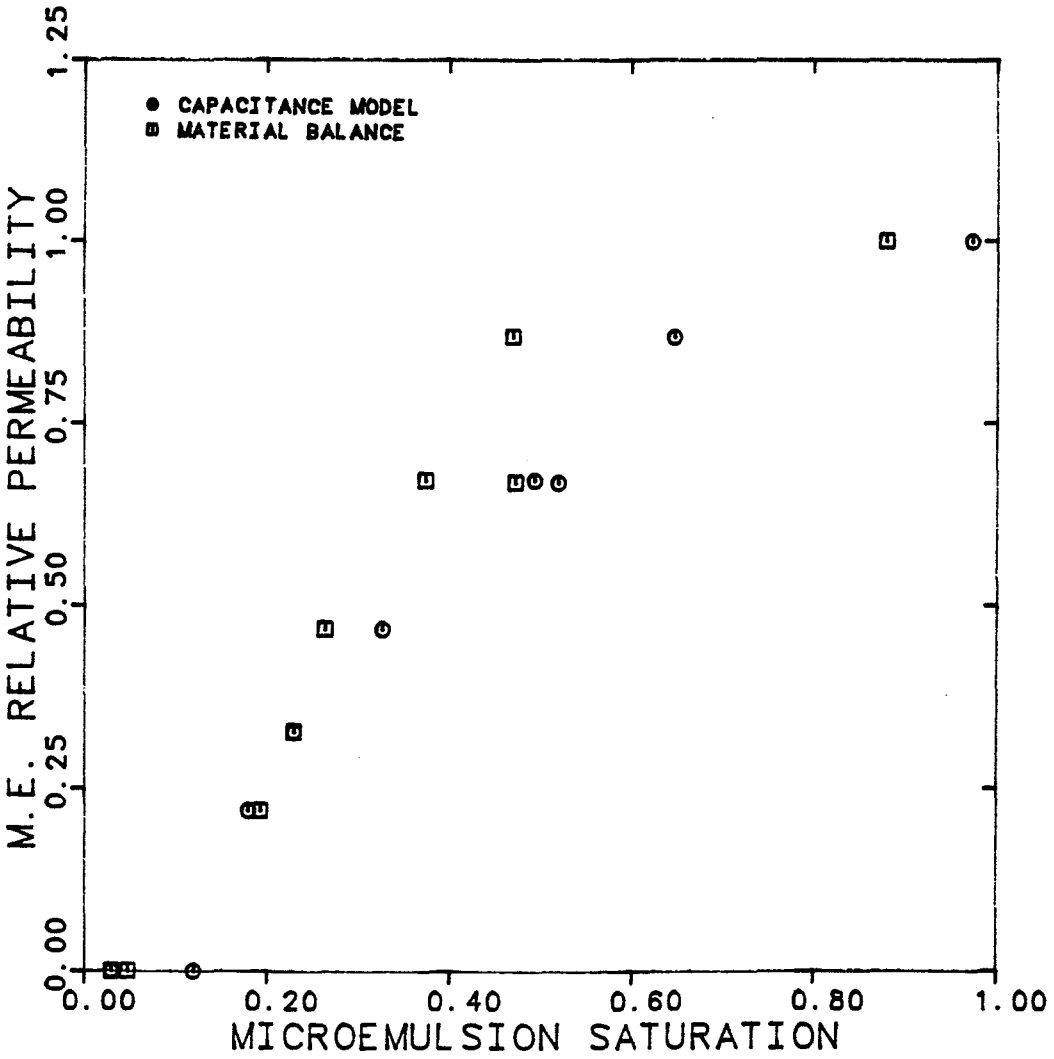

Figure 6.4.3.36 Comparison Between the Capacitance Model and Material Balance Estimates of M.E. Saturation for Three-Phase Flow (Exp. BMO3)

EXPERIMENT NUMBER	BMO3
REF. PERMEABILITY	0.936 D
CAPILLARY NUMBER	0.01
TEMPERATURE	30° C

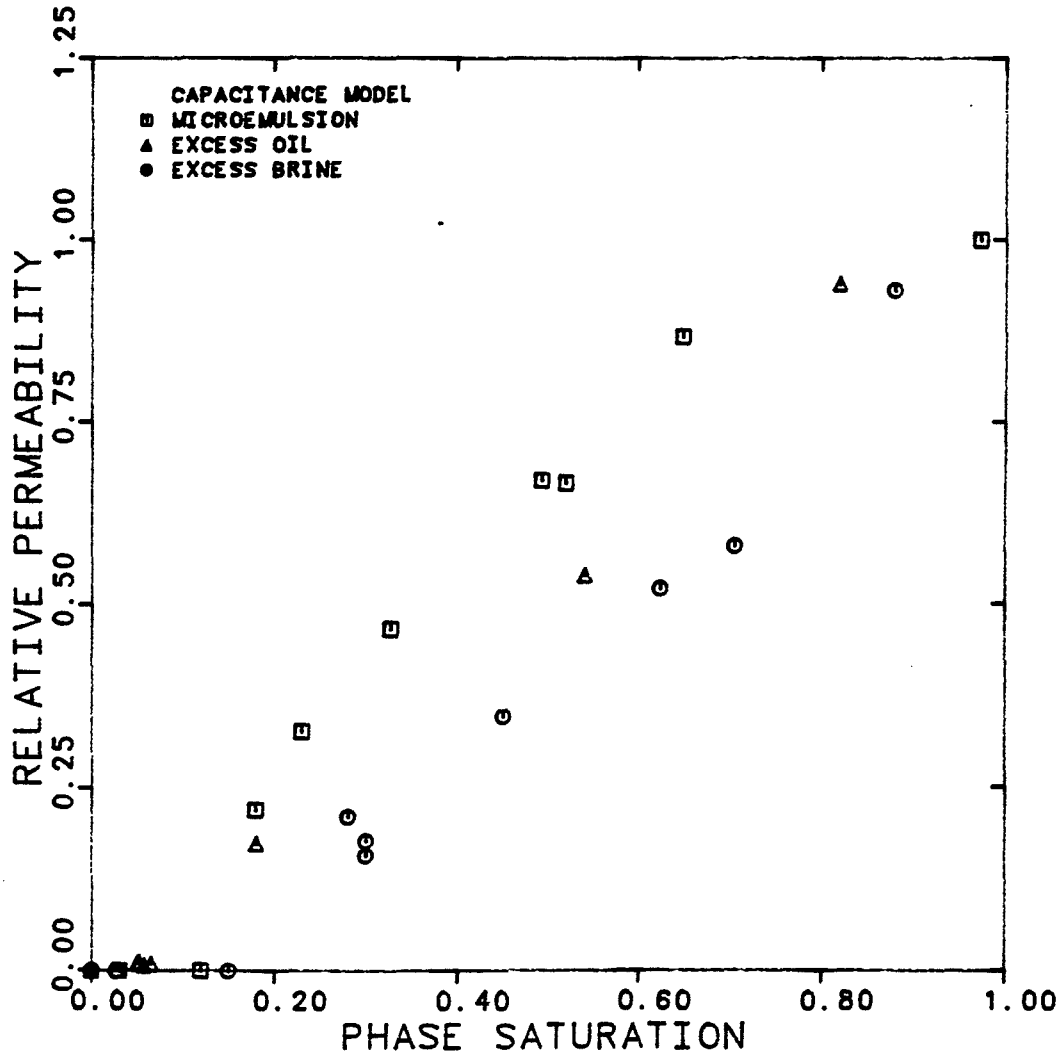

Figure 6.4.3.37 Phase Relative Permeabilities Versus Phase Saturation for Three-Phase Flow (Exp. BMO3)

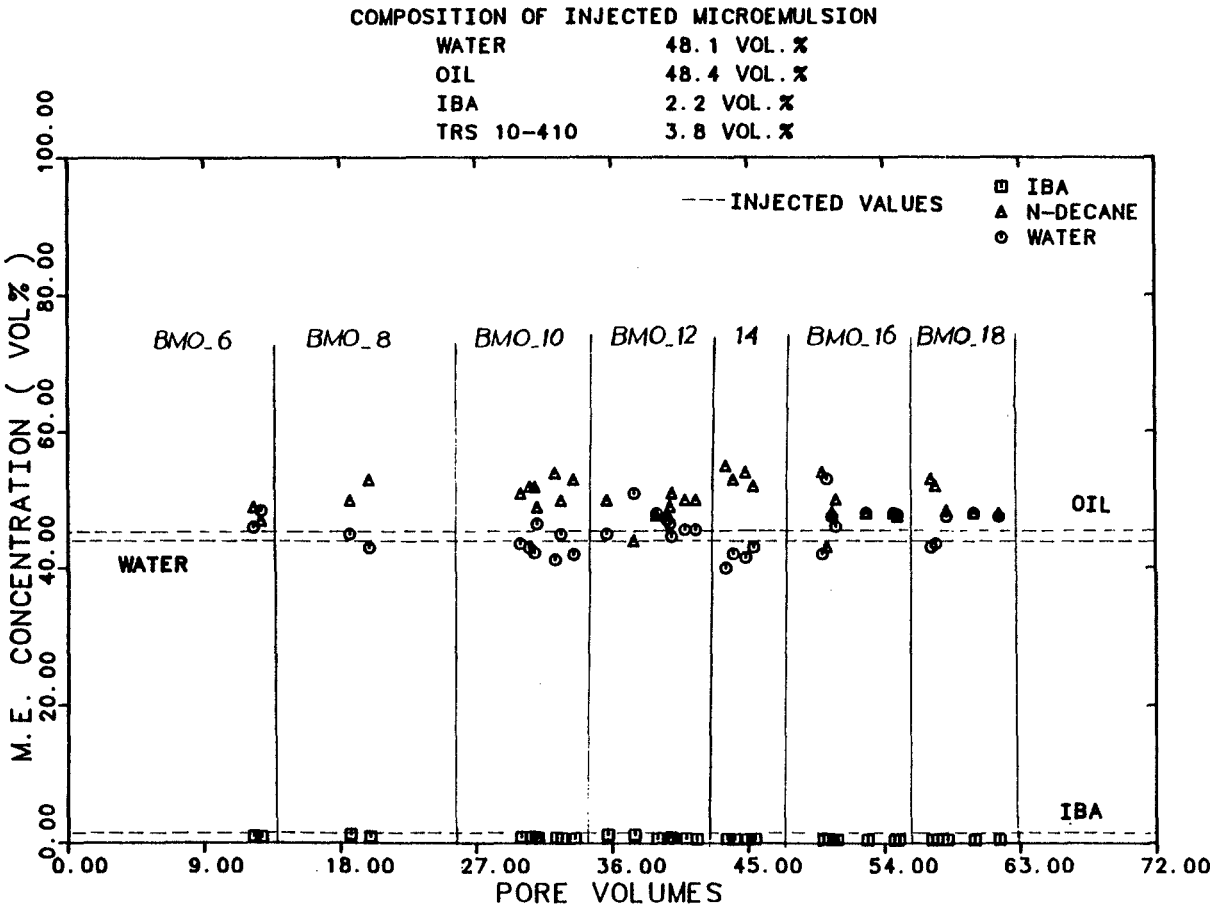

Figure 6.4.3.38 Composition of Steady-State Effluent M.E. Versus Pore Volumes Injected

6.4.4 Comparison of Three-Phase Data

6.4.4.1 Experiment BMO1, BMO2, BMO3 [BMO]

This subsection summarizes and compares the capacitance results of the three three-phase relative permeability experiments performed in one core and at a constant capillary number of 10^{-2}.

Figure 6.4.4.1 shows the region of saturation space covered in these experiments. The numbers in this figure corresponds to the specific three-phase flow cut as indicated in Table 6.4.1.5. The residual phase saturations obtained during single-phase flow experiments (points 5, 16, 17, 24) are also plotted in Figure 6.4.4.1. The dashed lines on the saturation ternary indicate a constant residual saturation which is an arithmetic average of the two endpoints (for example, the residual brine to oil and the residual brine to microemulsion). These constant residual saturations were used as an approximation for residual saturation in the three-phase relative permeability model (see Chapter 7, section 7.4).

Shown in Figures 6.4.4.2 through 6.4.4.4 are the phase fractional flow (cut) as a function of the respective saturation. The fractional flows are also plotted on a saturation ternary of the brine, oil, and

microemulsion phases (Figures 6.4.4.5 through 6.4.4.7).

The relative permeabilities as function of both total saturation and flowing saturation are in Figures 6.4.4.8 through 6.4.4.9. The relative permeabilities are closer when plotted as a function of flowing saturation. Figures 6.4.4.10 through 6.4.4.12 shows the relative permeabilities on a ternary saturation. The numbers on these figures are the values of relative permeability. There are not enough data in order to draw the oil, brine, and microemulsion isoperms.

Figures 6.4.4.13 through 6.4.4.15 present the total relative mobility (λ_{rT}) as a function of phase saturation. The total mobility decreases as more microemulsion is introduced in the core, it increases by increasing the oil saturation, while the trend for brine is not obvious due to scatter in data. Shown in Figure 6.4.4.16 are the total relative mobilities on a ternary saturation.

Dispersivities of tracers in each phase as a function of the respective saturation are plotted in Figures 6.4.4.17 through 6.4.4.19. Dispersivities and saturations are the capacitance model estimates. The following observations are made from these data,

1- The dispersivities estimated for three-phase flow

are an order of magnitude higher than those obtained in single-phase flow.

2- The dispersivities seem very insensitive to saturation for values of saturation of less than 0.65 ($S_j < 0.65$).

3- There is no significant difference among the dispersivities of tracers used in the three-phases.

Figure 6.4.4.20 through 6.4.4.23 show the calculated dispersion coefficient ($K_{ij} = \alpha_{ij} v_j$) as a function of phase velocity. These data demonstrate that

1- The three-phase data do not lie on a straight line with a slope of about 1.1 as observed for single-phase flow.

2- The increase in dispersion coefficient by increasing the phase velocity is apparent in data of all three phases.

3- The data of labelled sulfonate in microemulsion are smooth and lie on a straight line with the slope of about 2.10.

6.4.4.2 Experiments BMO and BMD

Delshad [D.6] performed a similar three-phase flow experiment, BMD, also at a capillary number of 10^{-2}. Basic properties of the Berea core and fluids used in his experiment are listed in Table 6.3.3.1.

Figures 6.4.4.24 through 6.4.4.26 compare the relative permeabilities of experiment BMO and BMD. The relative mobility for each phase is also compared and shown in Figures 6.4.4.27 through 6.4.4.29. Only the capacitance results of experiments BMO and BMD are compared in these figures. Although two different core samples were used, relative permeability and mobility data are in surprisingly good agreement.

SATURATION TERNARY

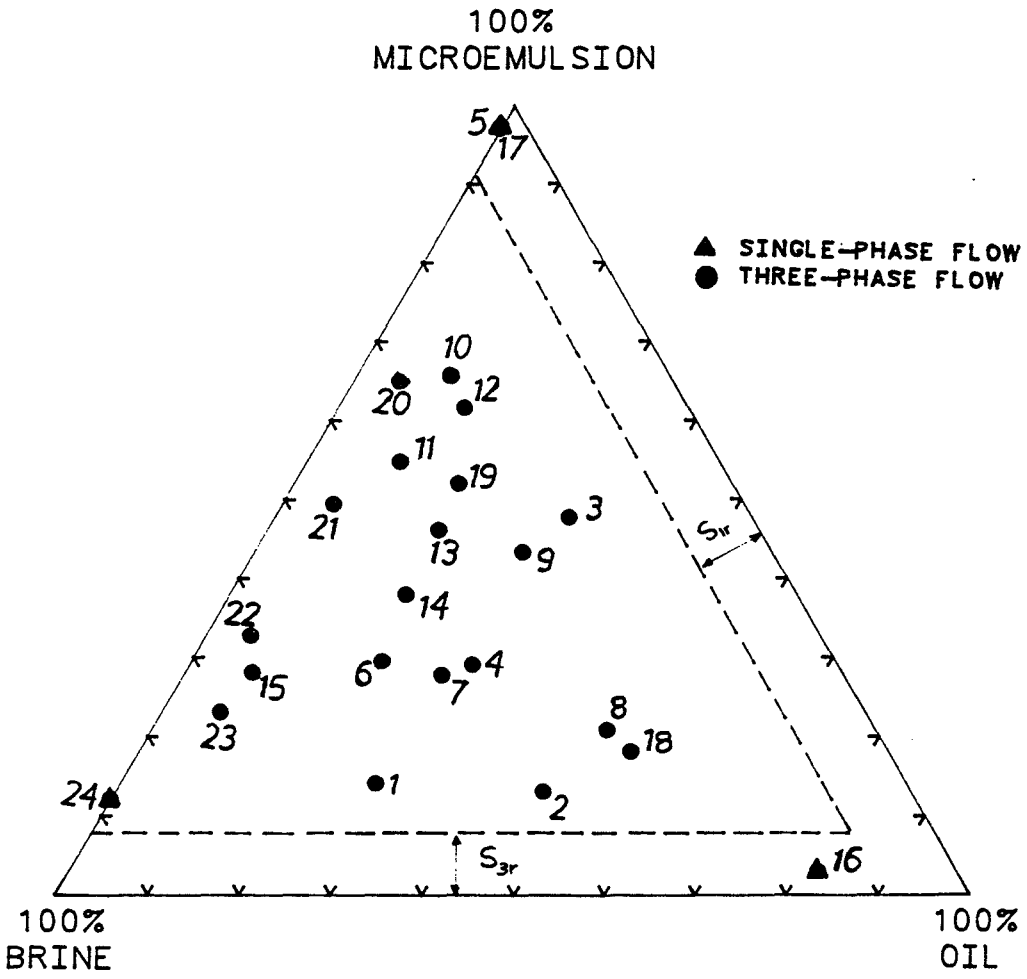

Figure 6.4.4.1 Saturation Data Covered by the Three-Phase Flow Experiments (BMO)

EXPERIMENT NUMBER	BMO
REF. PERMEABILITY	0.936 D
CAPILLARY NUMBER	0.01
TEMPERATURE	30°C

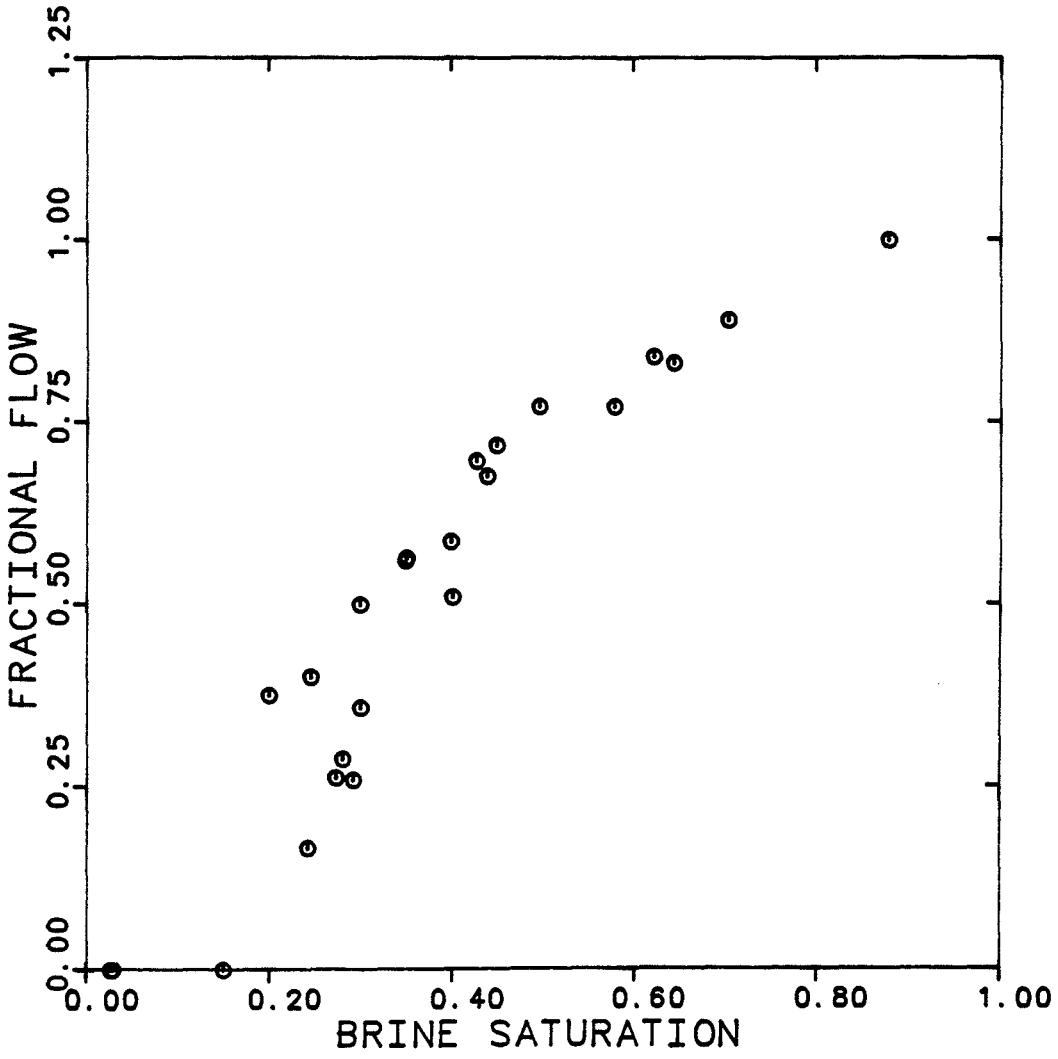

Figure 6.4.4.2 The Excess Brine Fractional Flow Curve for Three-Phase Flow Experiment (BMO)

EXPERIMENT NUMBER	BMO
REF. PERMEABILITY	0.936 D
CAPILLARY NUMBER	0.01
TEMPERATURE	30° C

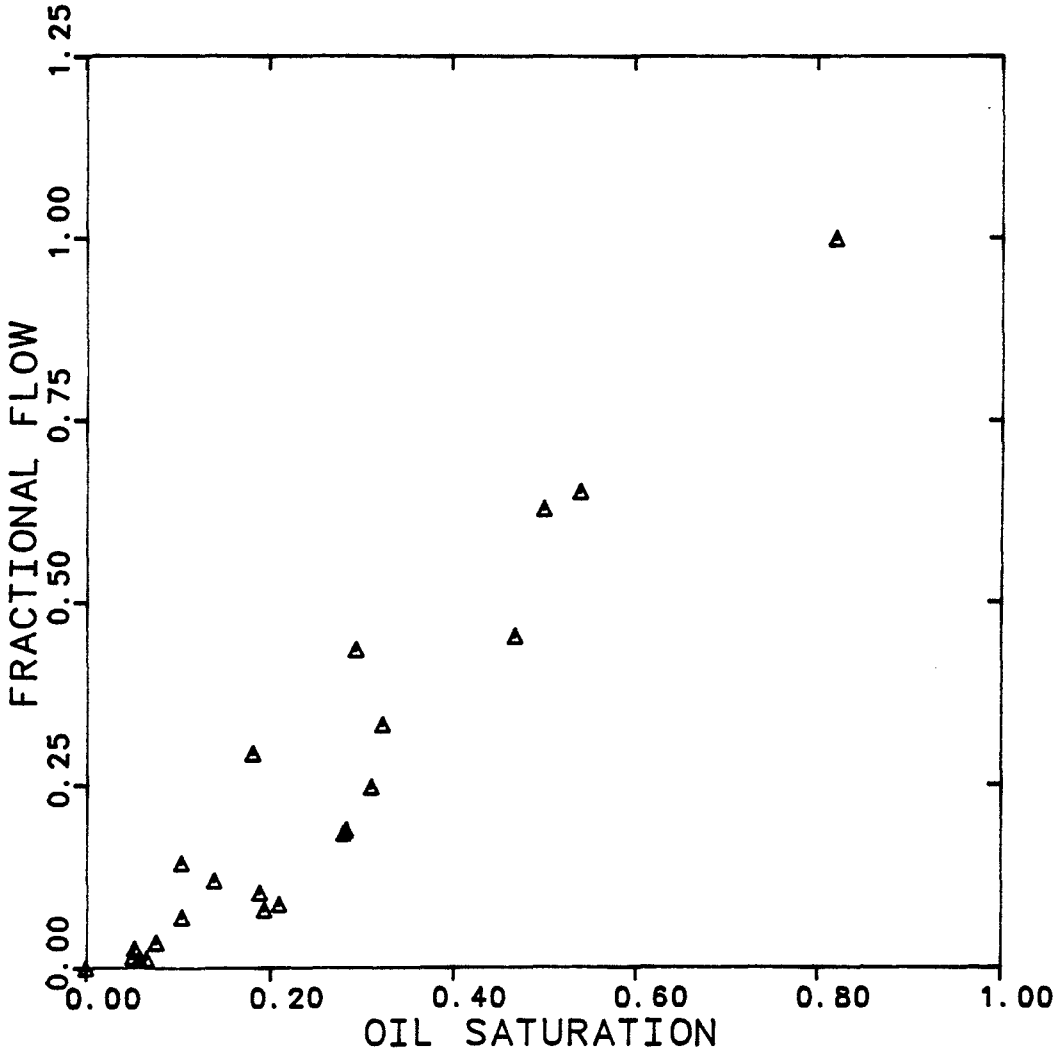

Figure 6.4.4.3 The Excess Oil Fractional Flow Curve for Three-Phase Flow Experiment (BMO)

EXPERIMENT NUMBER	BMO
REF. PERMEABILITY	0.936 D
CAPILLARY NUMBER	0.01
TEMPERATURE	30°C

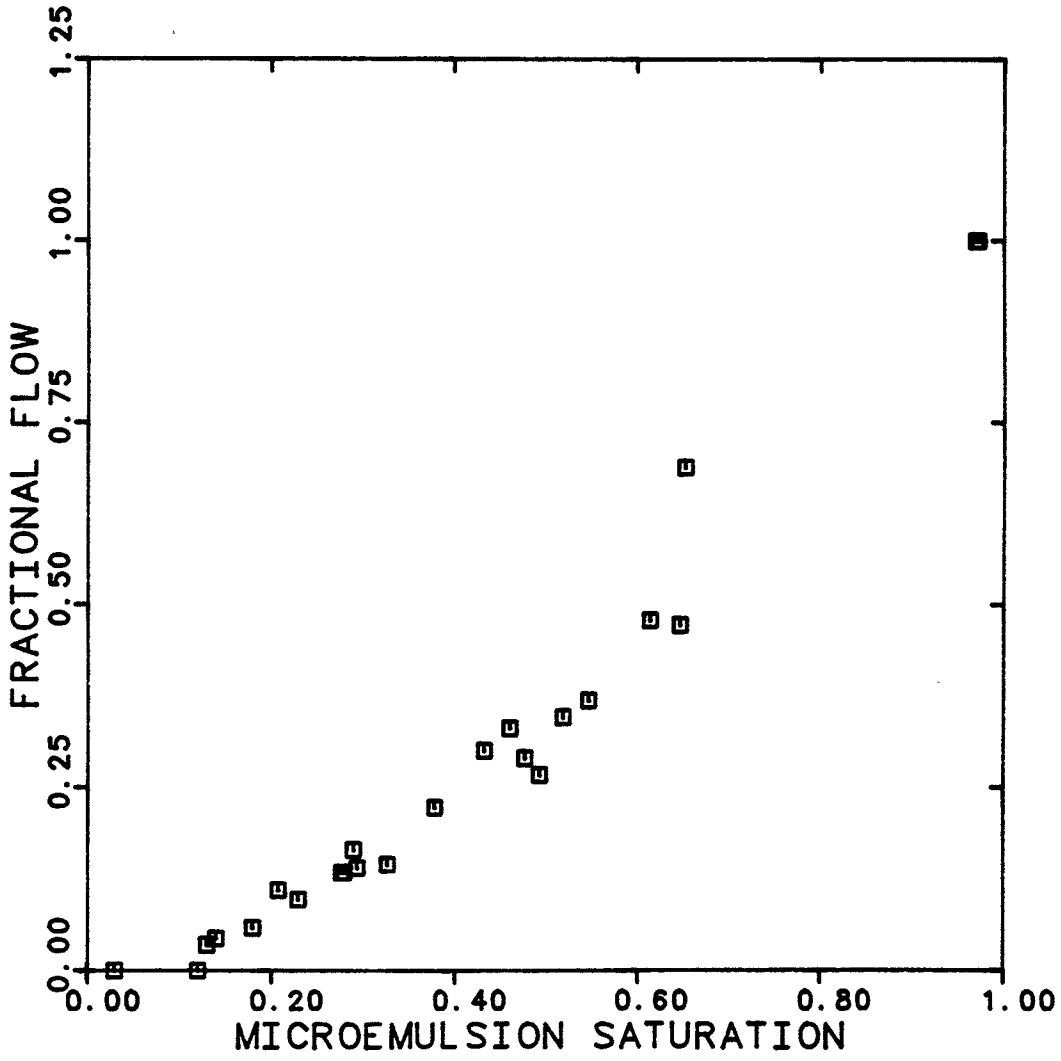

Figure 6.4.4.4 The M.E. Fractional Flow Curve for Three-Phase Flow Experiment (BMO)

SATURATION TERNARY

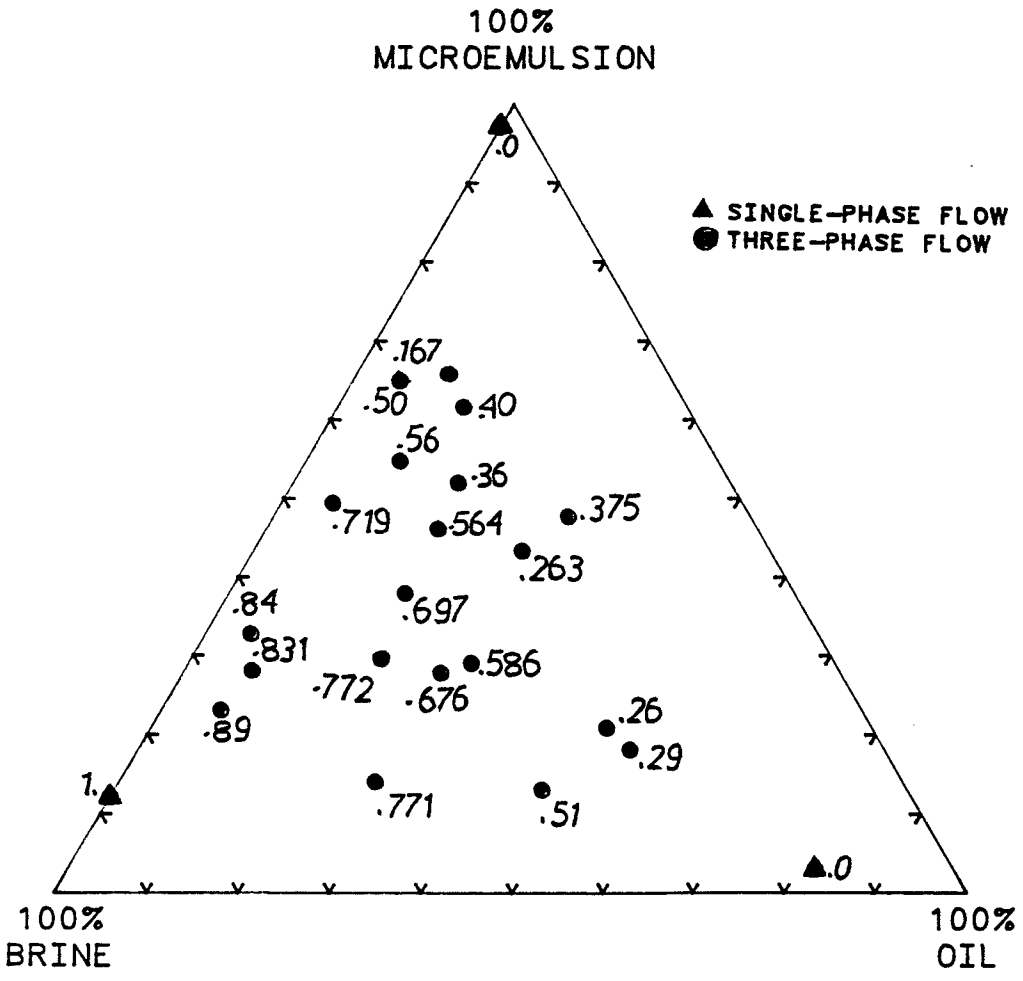

Figure 6.4.4.5 Brine Fractional Flow on Saturation Ternary

SATURATION TERNARY

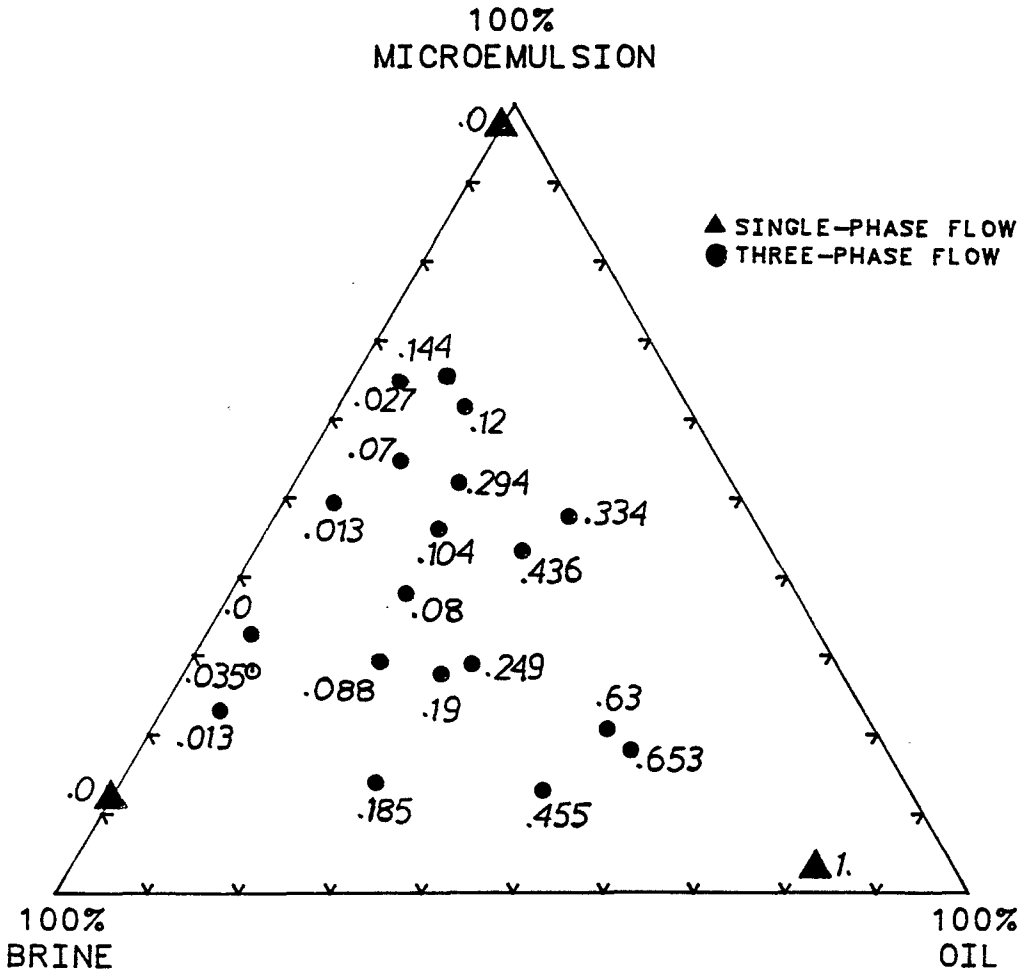

Figure 6.4.4.6 Oil Fractional Flow on Saturation Ternary

SATURATION TERNARY

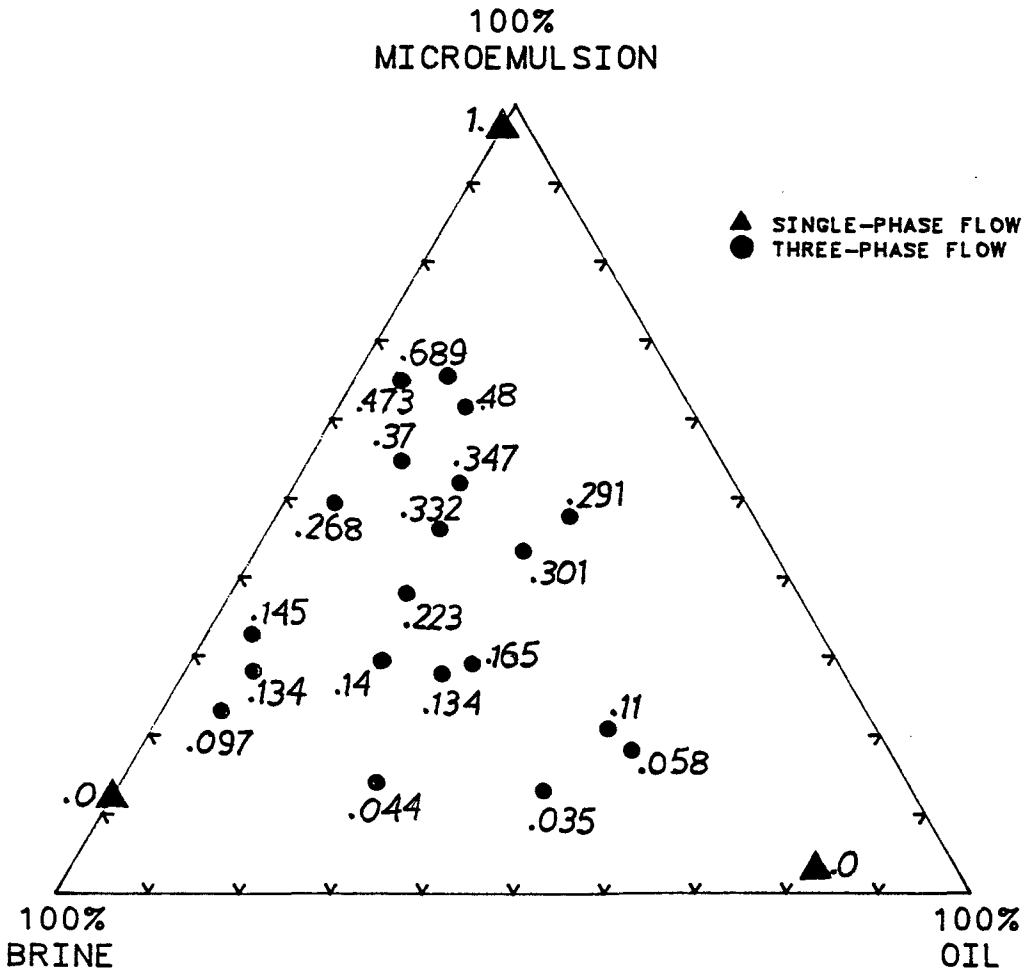

Figure 6.4.4.7 M.E. Fractional Flow on Saturation Ternary

EXPERIMENT NUMBER	BMO
REF. PERMEABILITY	0.936 D
CAPILLARY NUMBER	0.01
TEMPERATURE	30° C

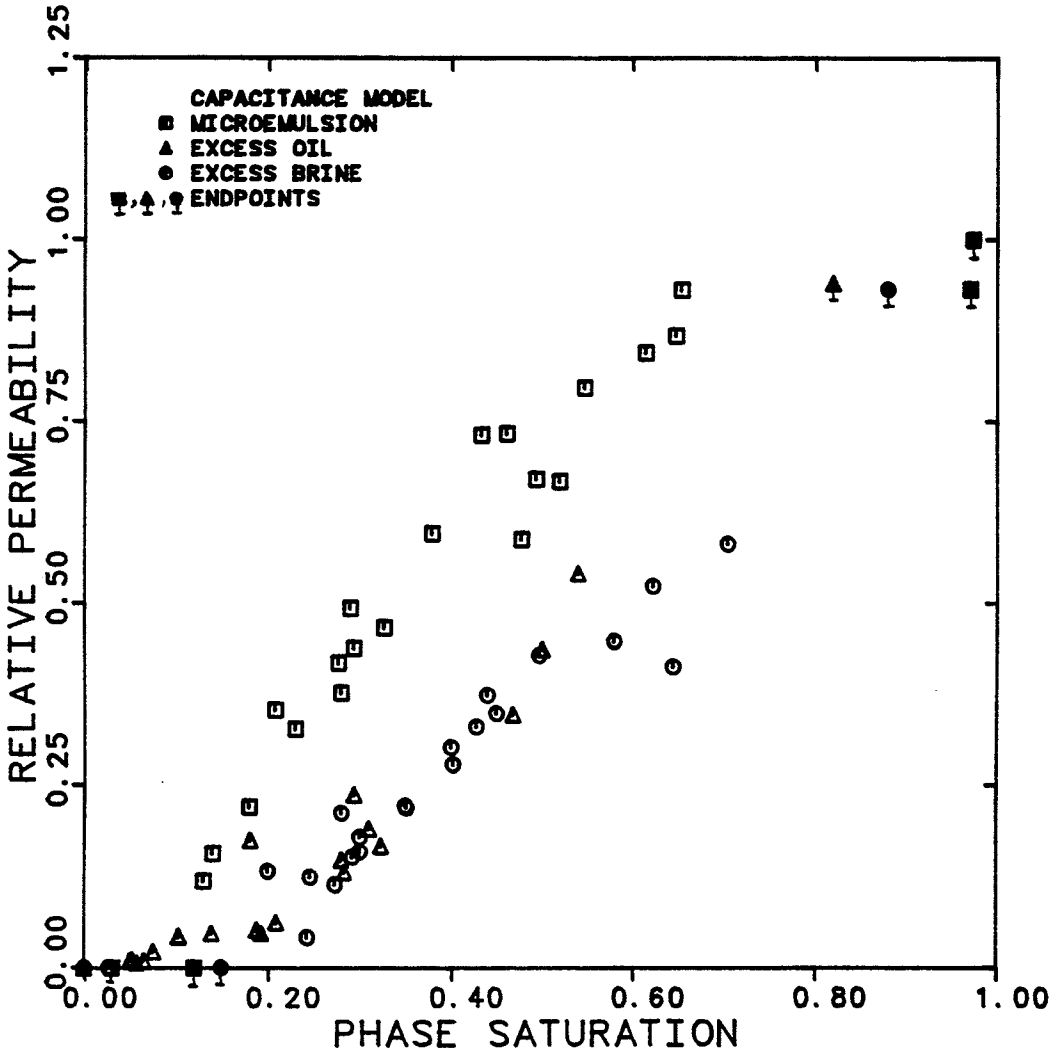

Figure 6.4.4.8 The Phase Relative Permeabilities Versus Phase Saturations for Three-Phase Flow Experiments

EXPERIMENT NUMBER	BMO
REF. PERMEABILITY	0.936 D
CAPILLARY NUMBER	0.01
TEMPERATURE	30° C

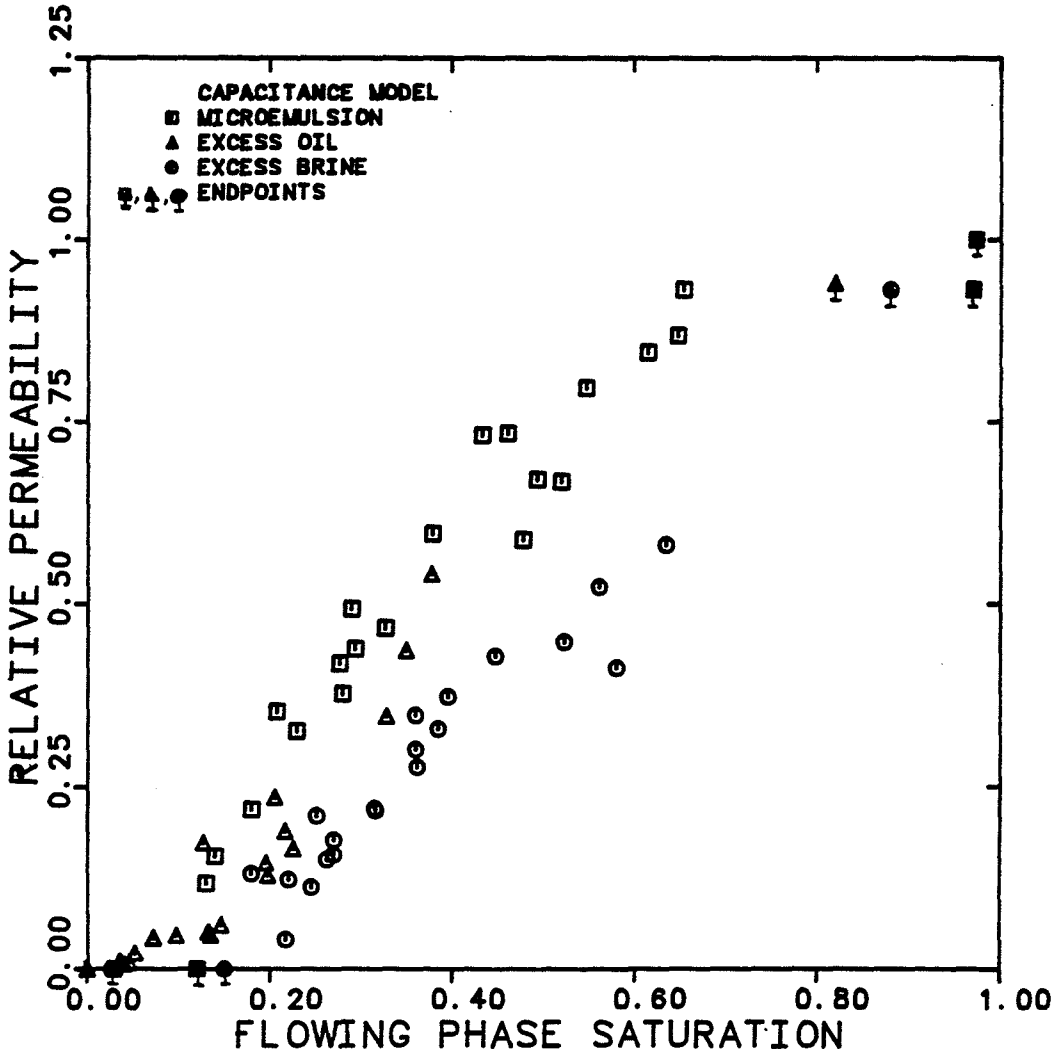

Figure 6.4.4.9 The Phase Relative Permeabilities Versus Flowing Phase Saturations for Three-Phase Flow Experiments

SATURATION TERNARY

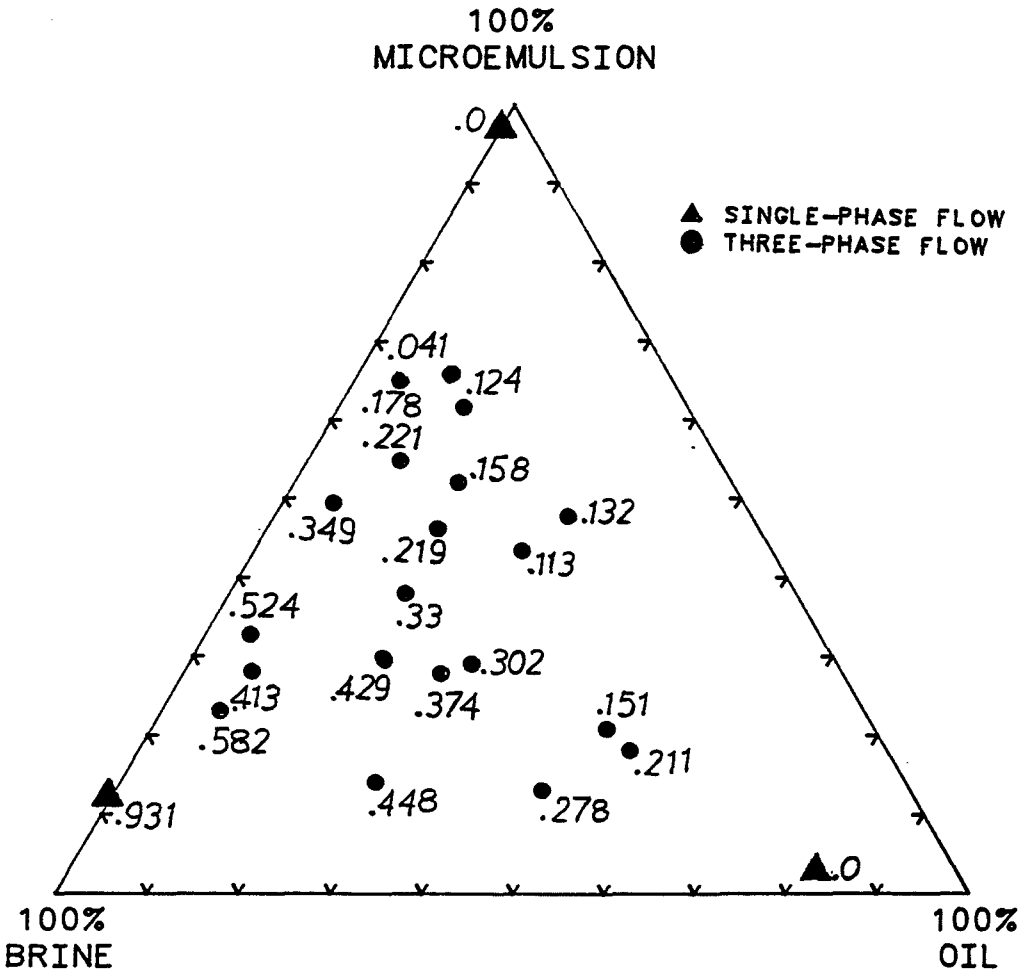

Figure 6.4.4.10 Brine Relative Permeabilities on Saturation Ternary

SATURATION TERNARY

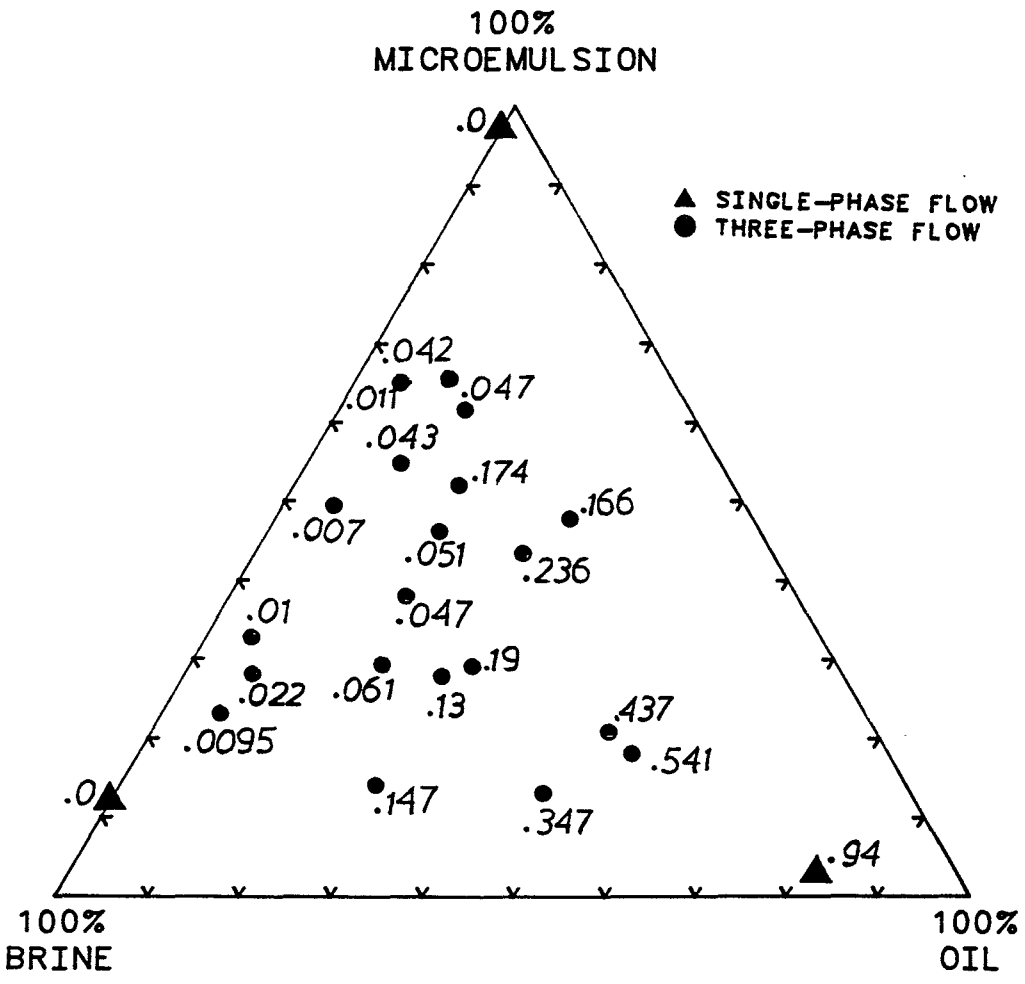

Figure 6.4.4.11 Oil Relative Permeabilities on Saturation Ternary

SATURATION TERNARY

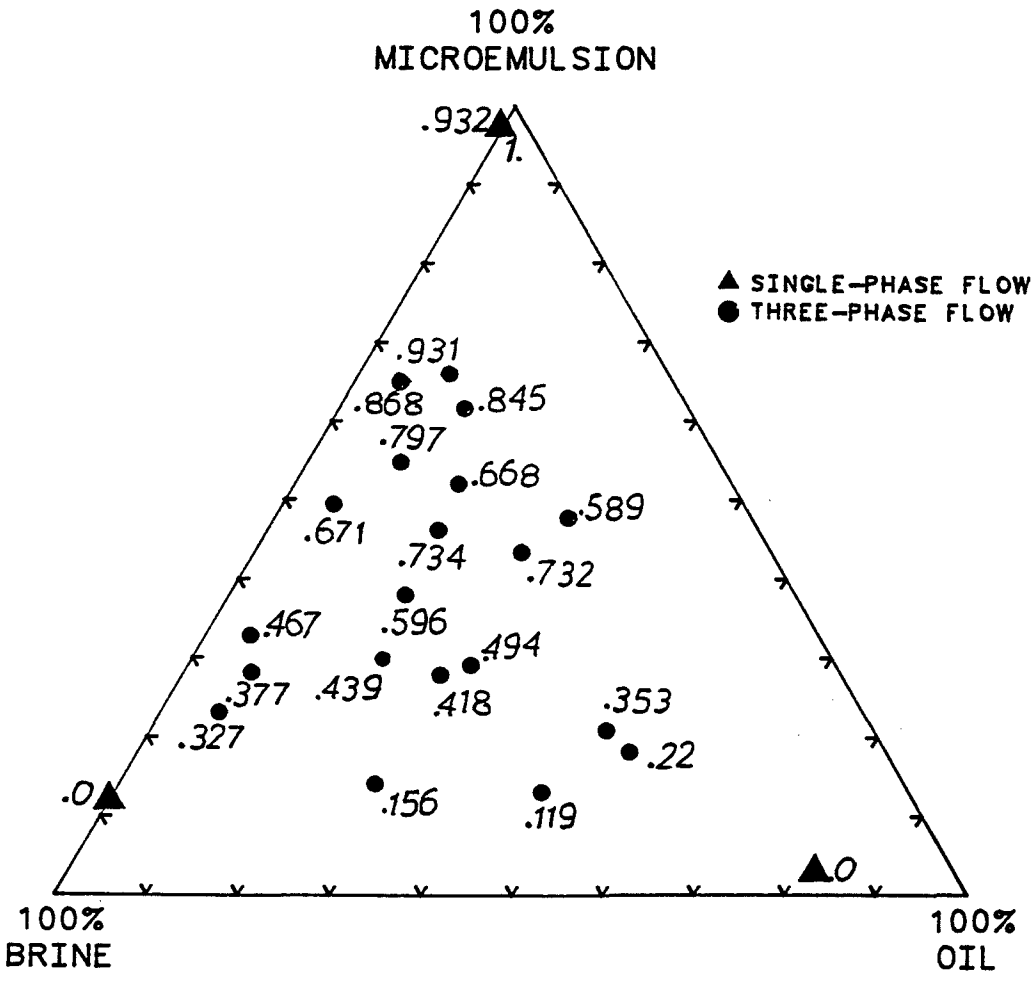

Figure 6.4.4.12 M.E. Relative Permeability on Saturation Ternary

EXPERIMENT NUMBER	BMO
REF. PERMEABILITY	0.936 D
CAPILLARY NUMBER	0.01
TEMPERATURE	30° C

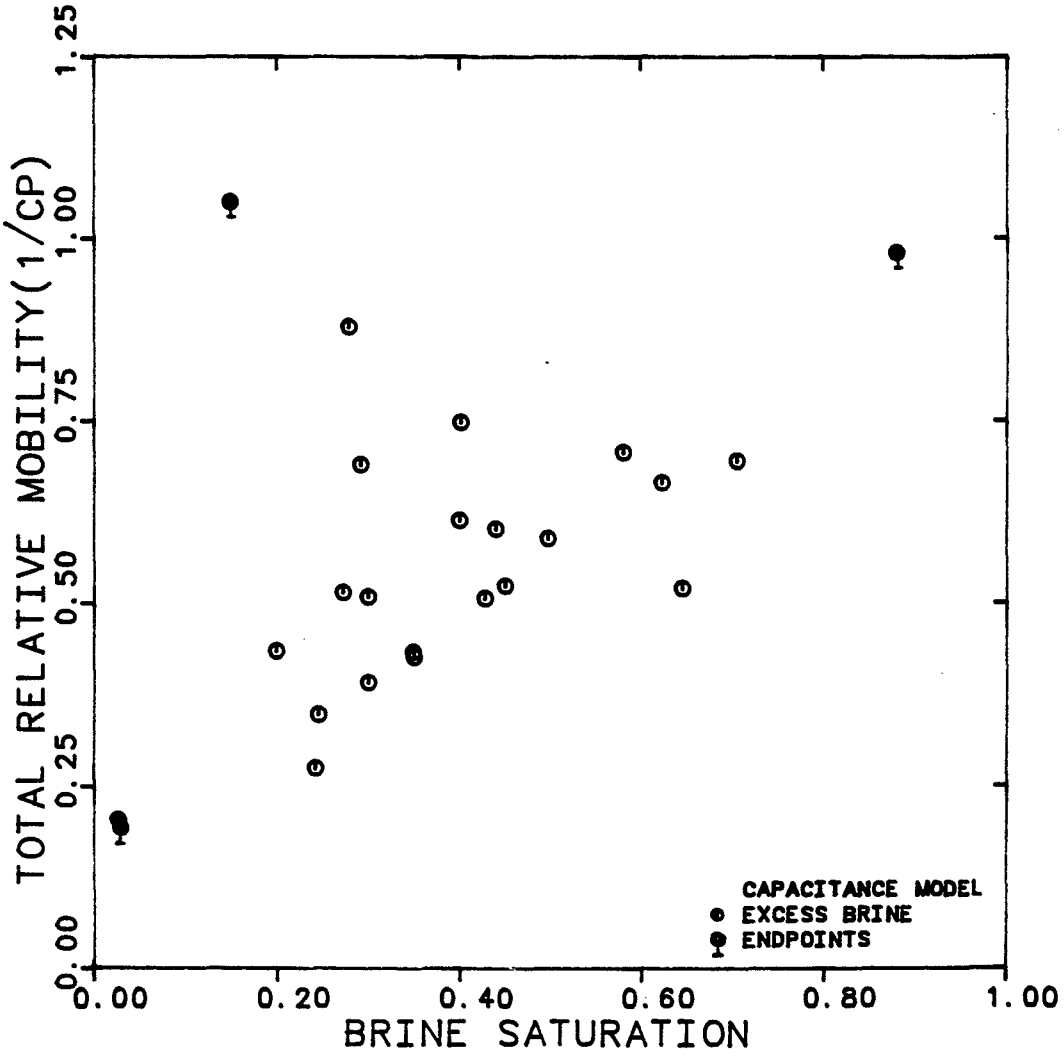

Figure 6.4.4.13 The Total Relative Mobility Versus Brine Saturation for Three-Phase Flow Experiments

EXPERIMENT NUMBER	BMO
REF. PERMEABILITY	0.936 D
CAPILLARY NUMBER	0.01
TEMPERATURE	30° C

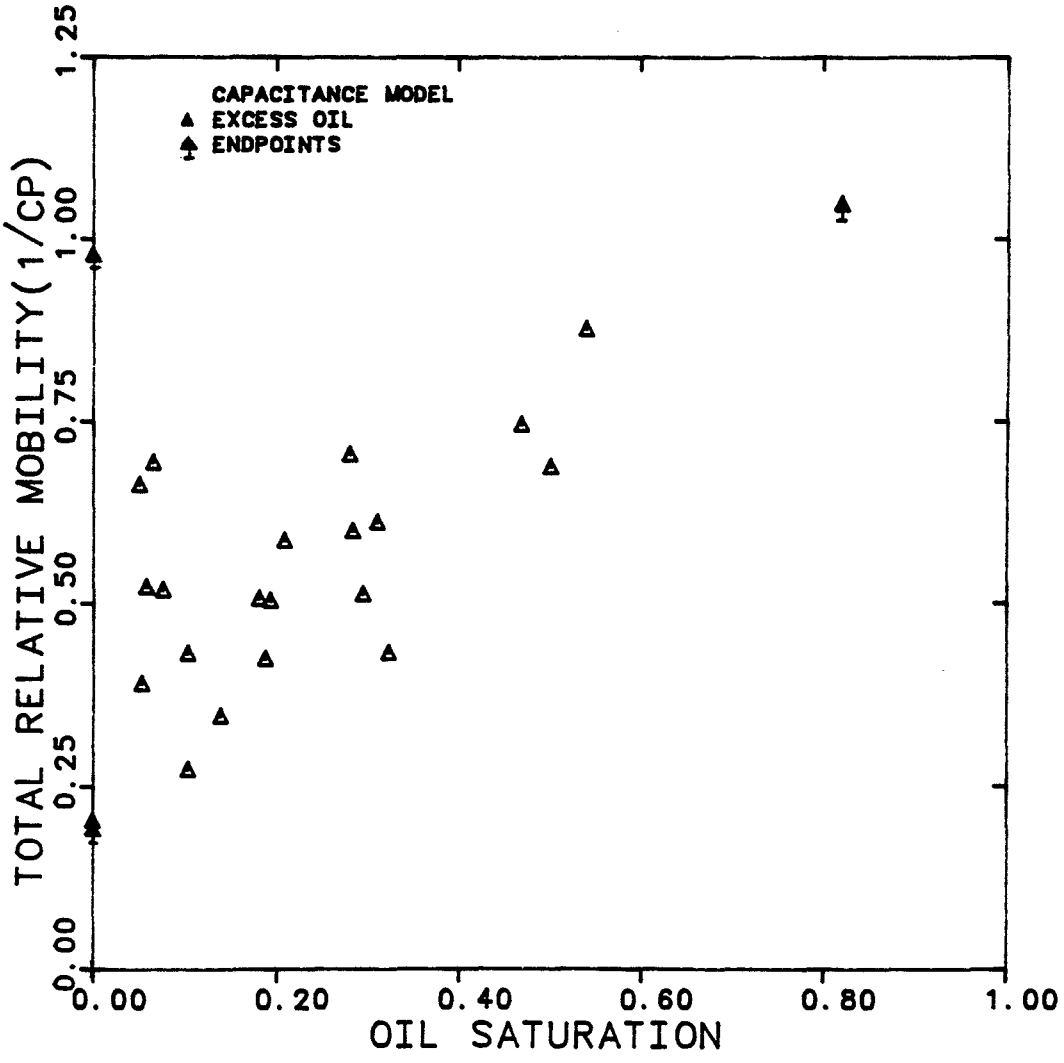

Figure 6.4.4.14 The Total Relative Mobility Versus Oil Saturation for Three-Phase Flow Experiments

EXPERIMENT NUMBER	BMO
REF. PERMEABILITY	0.936 D
CAPILLARY NUMBER	0.01
TEMPERATURE	30° C

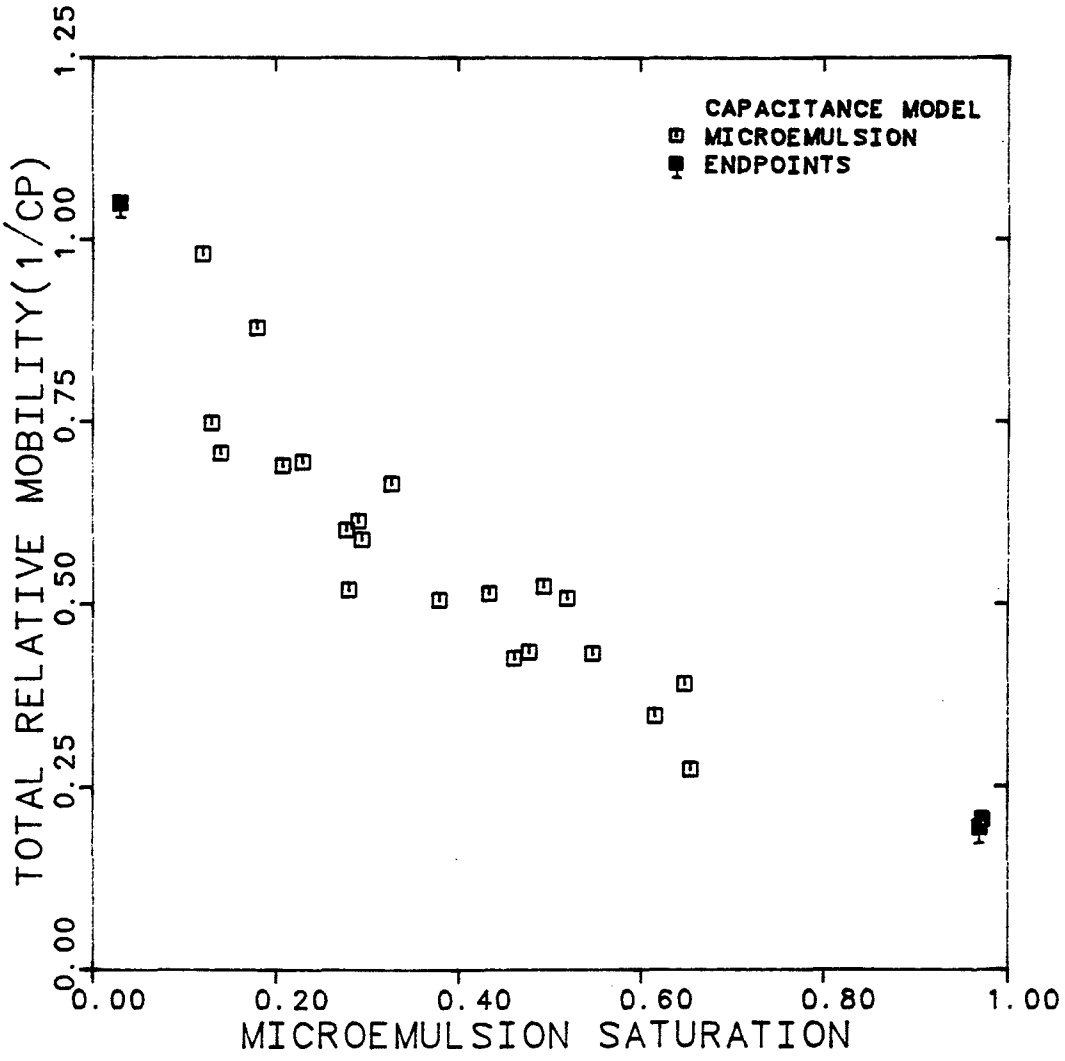

Figure 6.4.4.15 The Total Relative Mobility Versus M.E. Saturation for Three-Phase Flow Experiments

SATURATION TERNARY

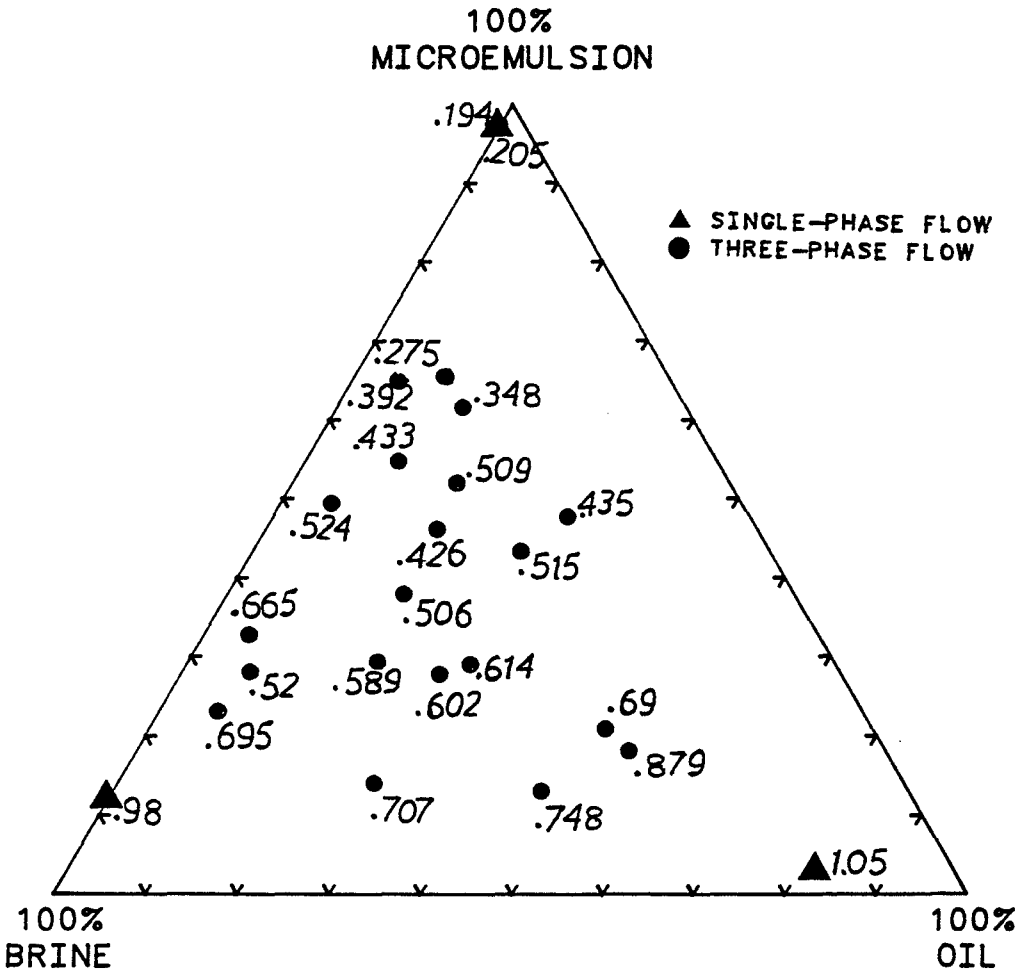

Figure 6.4.4.16 Total Relative Mobility on Saturation Ternary

EXPERIMENT NUMBER	BMO
REF. PERMEABILITY	0.936 D
CAPILLARY NUMBER	0.01
TEMPERATURE	30°C

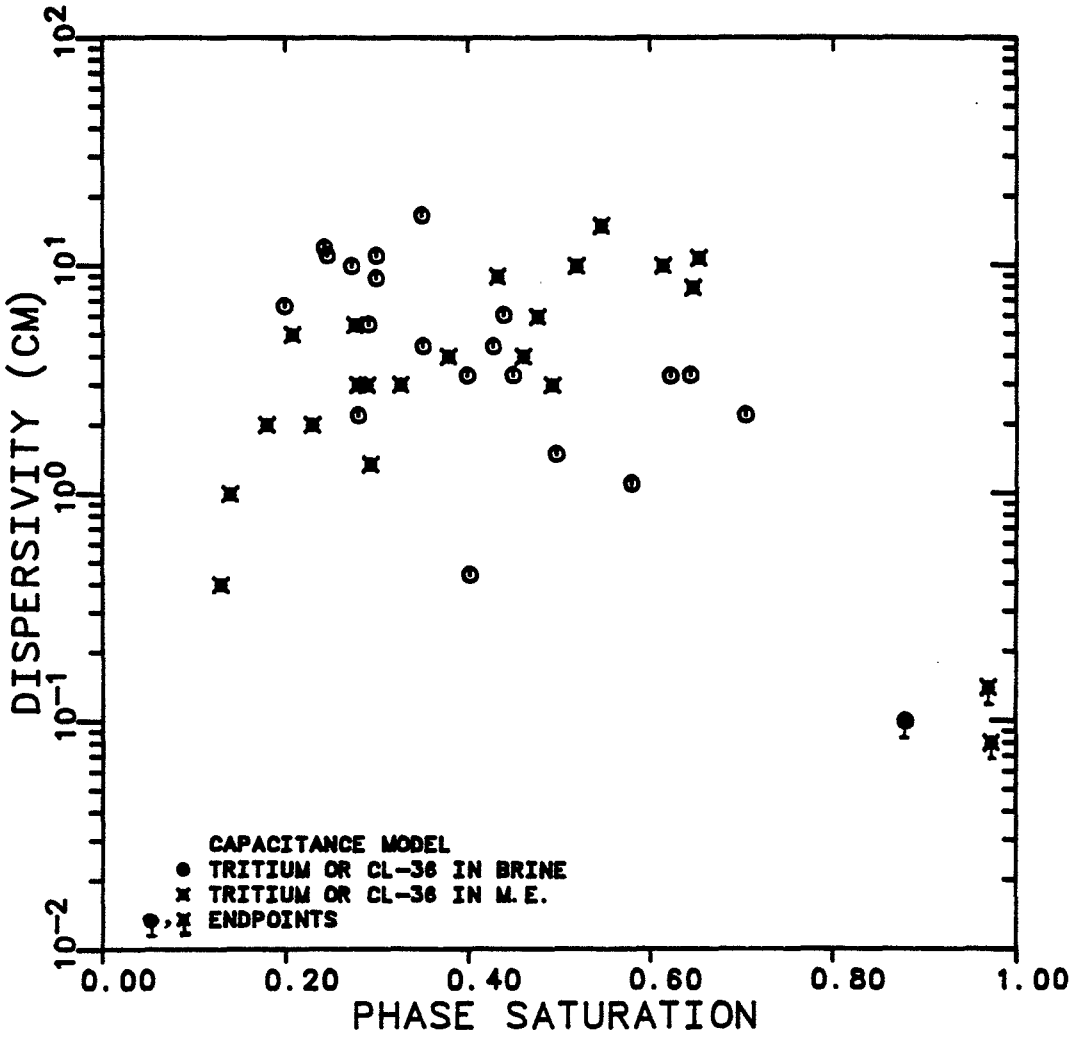

Figure 6.4.4.17 Dispersivity of Tritiated Water or Chloride-36 in Brine and M.E. as a Function of Phase Saturation for Three-Phase Flow Experiments

EXPERIMENT NUMBER	BMO
REF. PERMEABILITY	0.936 D
CAPILLARY NUMBER	0.01
TEMPERATURE	30° C

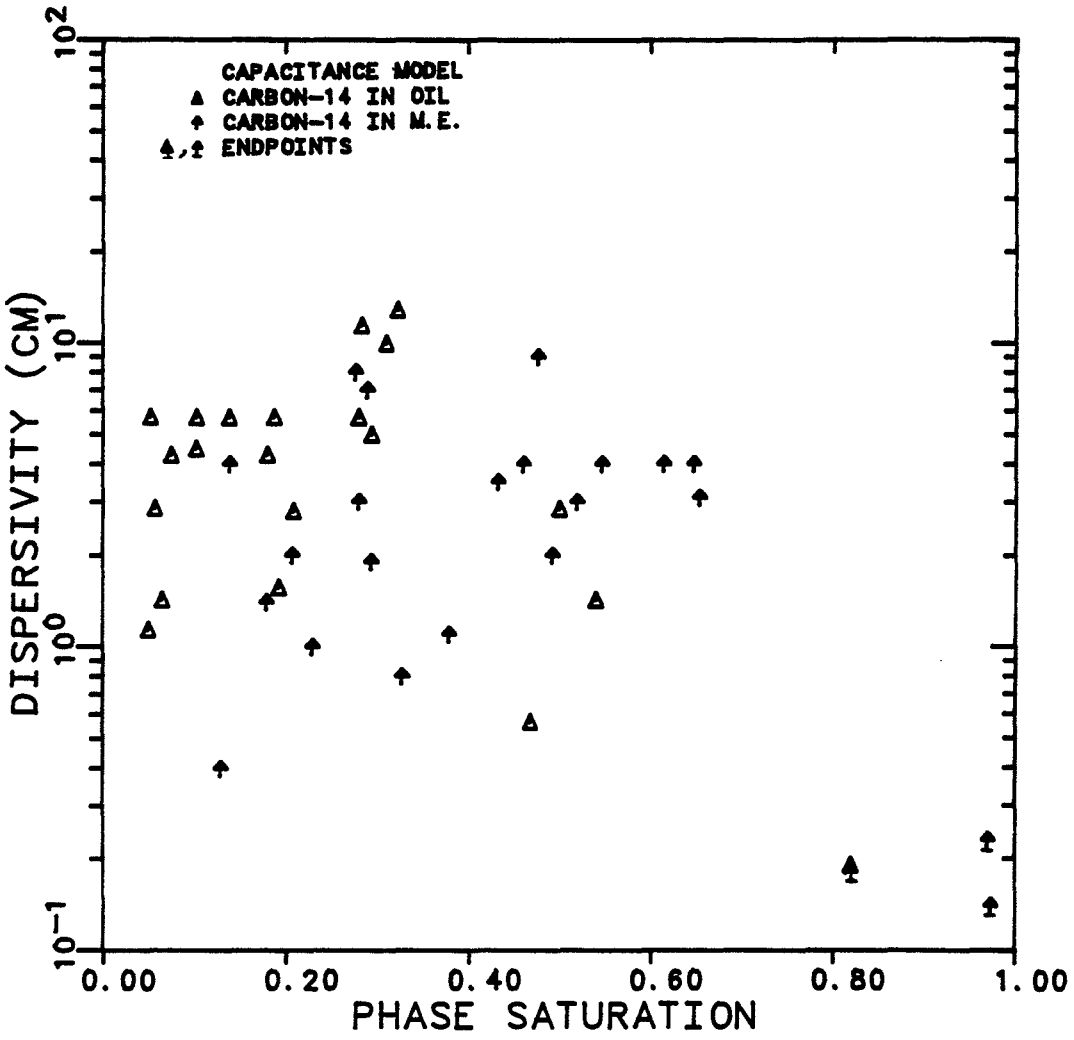

Figure 6.4.4.18 Dispersivity of Carbon-14 in Oil and M.E. as a Function of Phase Saturation for Three-Phase Flow Experiment

EXPERIMENT NUMBER	BMO
REF. PERMEABILITY	0.936 D
CAPILLARY NUMBER	0.01
TEMPERATURE	30 C

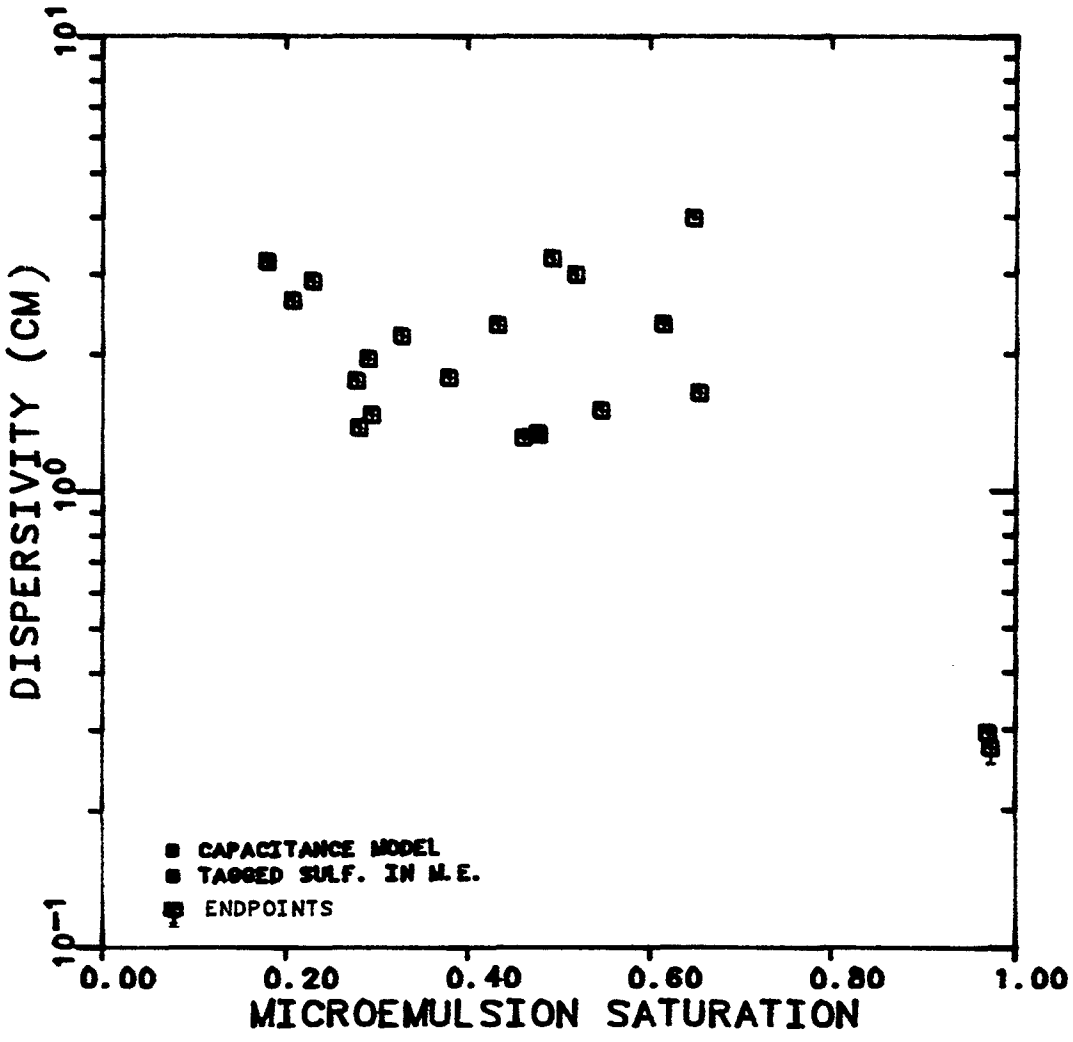

Figure 6.4.4.19 Dispersivity of Labelled Sulfonate in M.E. as a Function of M.E. Saturation for Three-Phase Flow Experiments

EXPERIMENT NUMBER	BMO
REF. PERMEABILITY	0.936 D
CAPILLARY NUMBER	0.01
TEMPERATURE	30°C

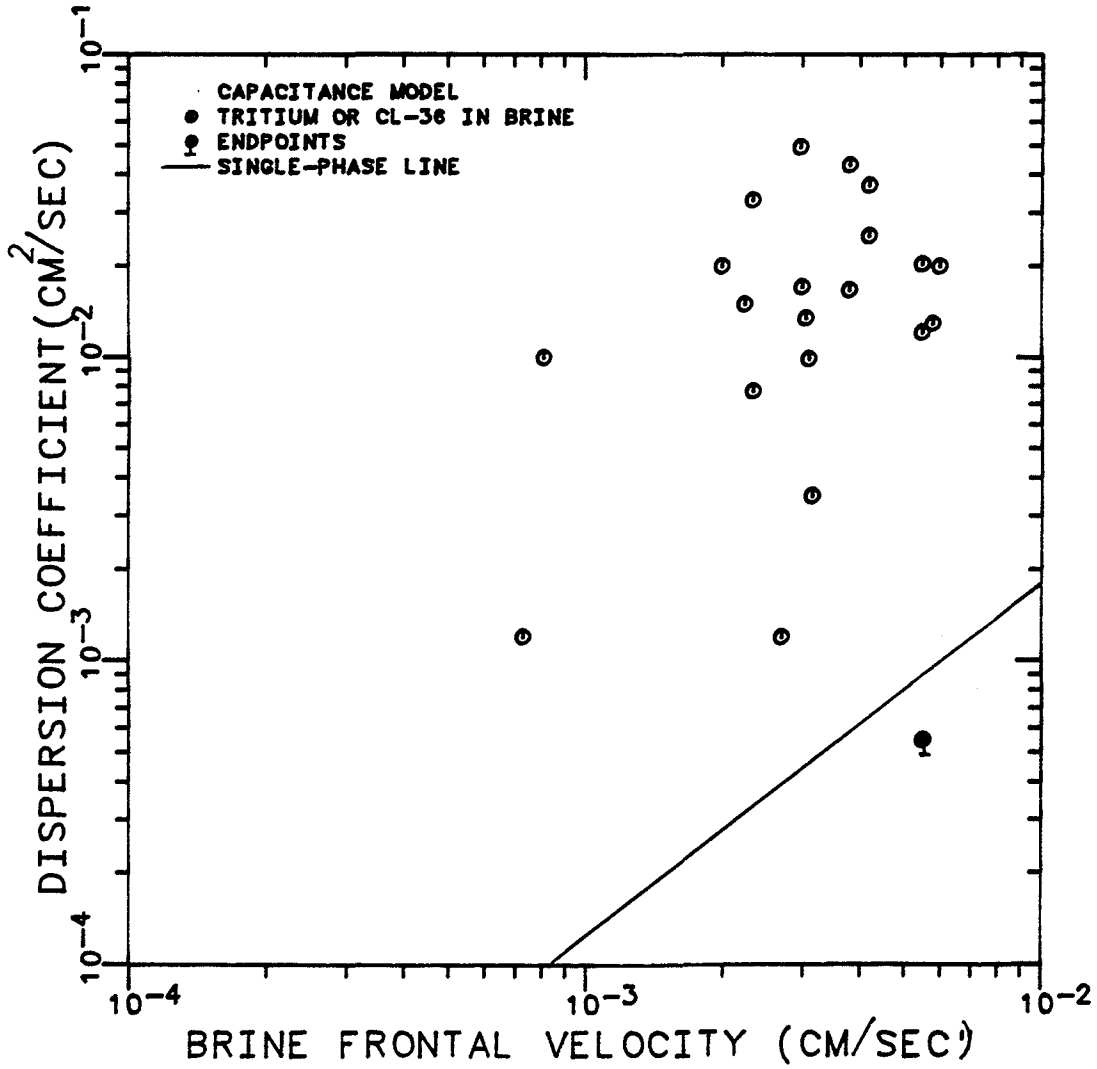

Figure 6.4.4.20 Dispersion Coefficient of Tracer in Brine as a Function of Brine Frontal Velocity for Three-Phase Flow Experiments

EXPERIMENT NUMBER	BMO
REF. PERMEABILITY	0.936 D
CAPILLARY NUMBER	0.01
TEMPERATURE	30° C

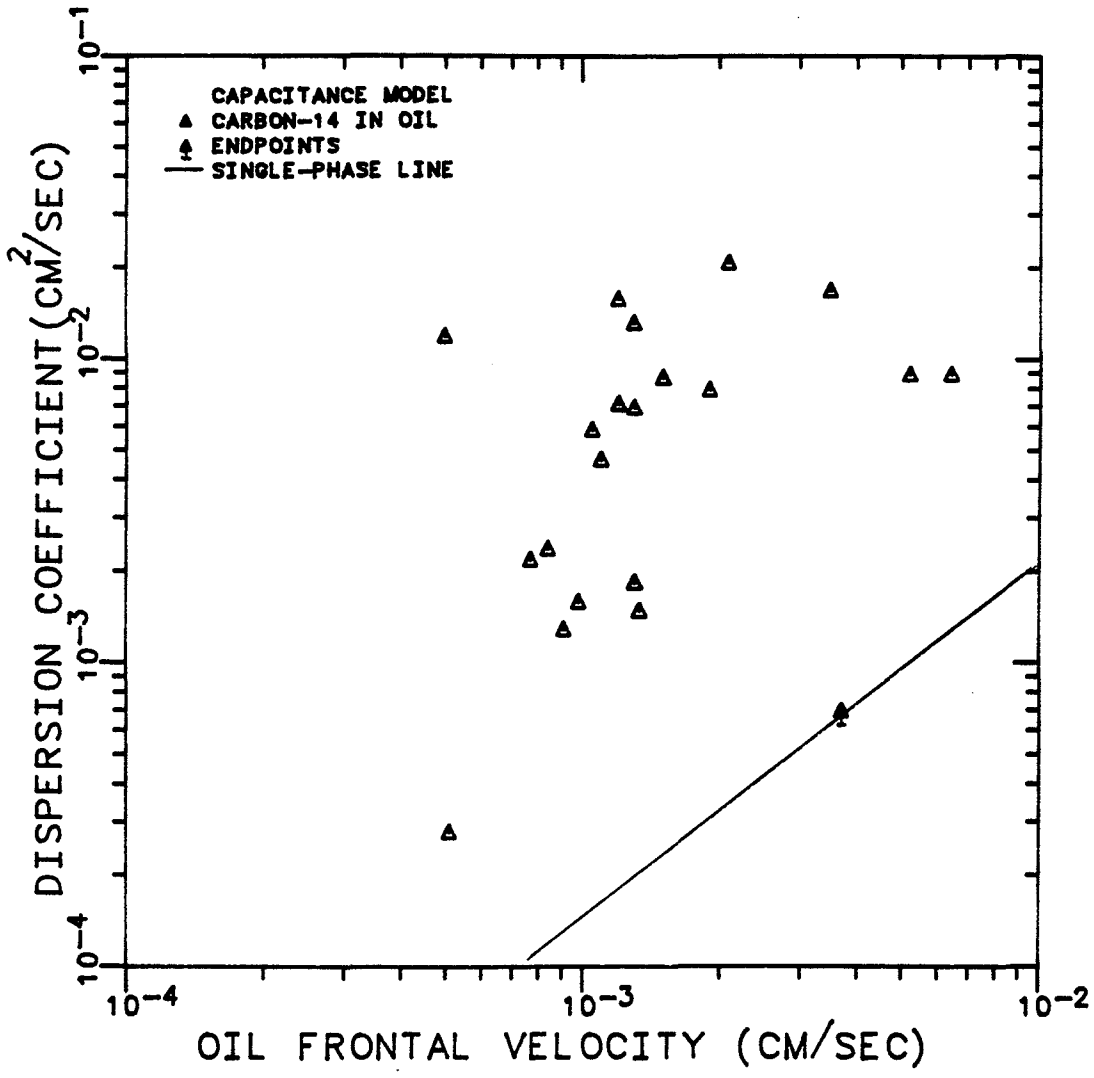

Figure 6.4.4.21 Dispersion of Carbon-14 in Oil as a Function of Oil Frontal Velocity for Three-Phase Flow Experiments

EXPERIMENT NUMBER	BMO
REF. PERMEABILITY	0.936 D
CAPILLARY NUMBER	0.01
TEMPERATURE	30° C

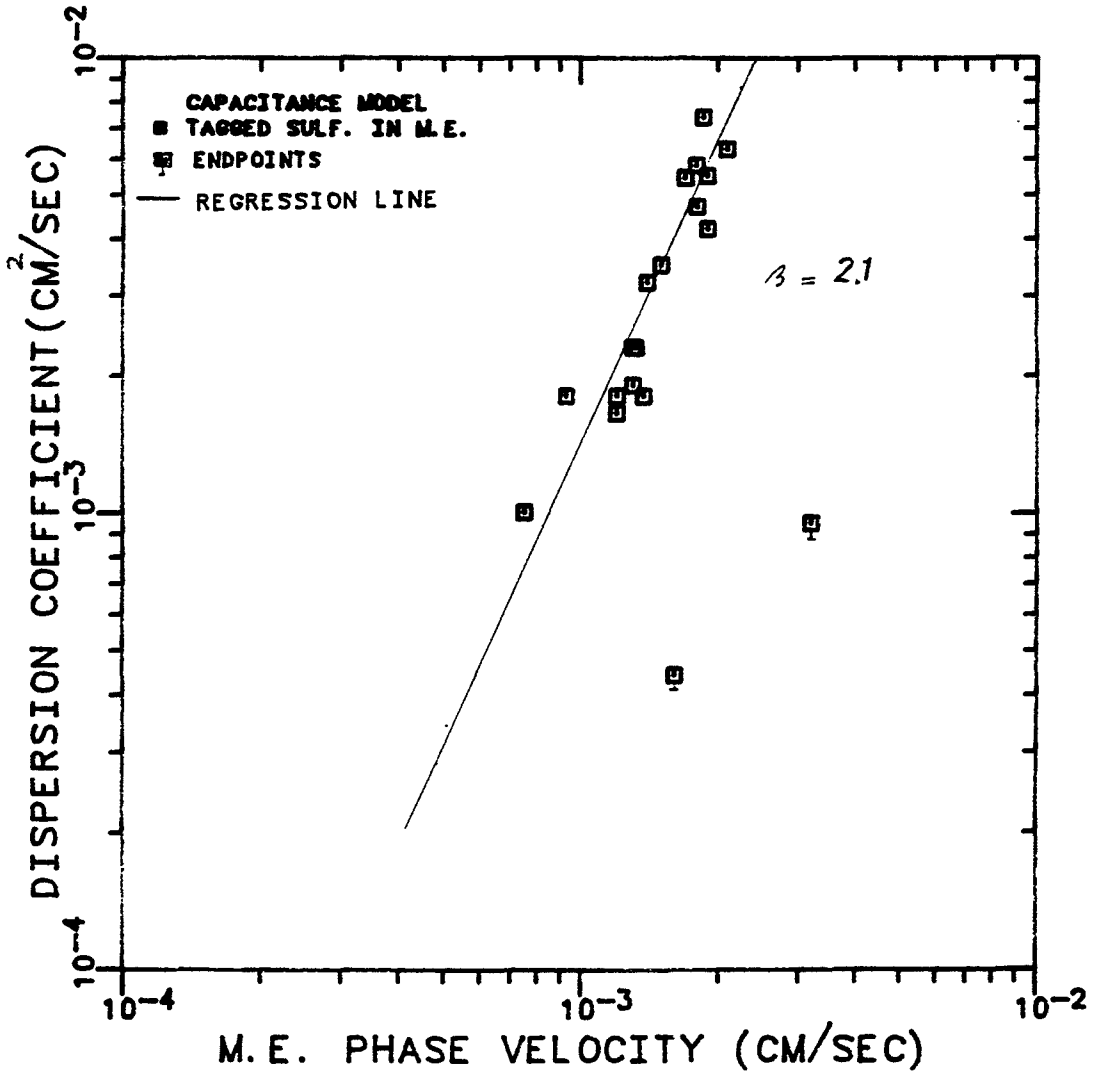

Figure 6.4.4.22 Dispersion Coefficient of Labelled Sulfonate in M.E. as a Function of M.E. Frontal Velocity for Three-Phase Flow Experiments

EXPERIMENT NUMBER	BMO
REF. PERMEABILITY	0.936 D
CAPILLARY NUMBER	0.01
TEMPERATURE	30° C

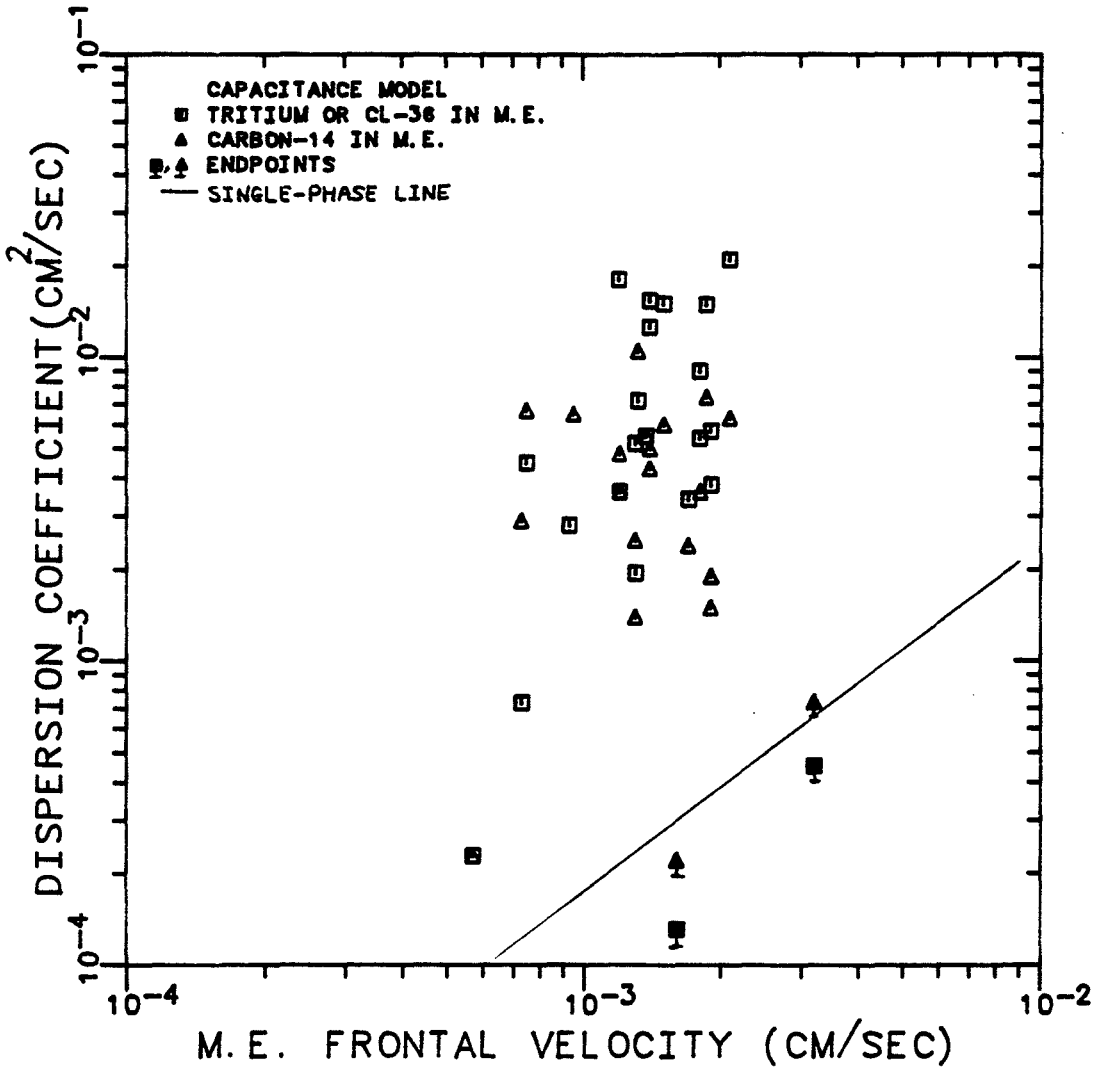

Figure 6.4.4.23 Dispersion Coefficient of Tracers in M.E. as a Function of M.E. Frontal Velocity for Three-Phase Flow Experiments

	DELSHAD	DELSHAD (REF. D6)
THREE PHASE	BMO	BMD
CAPILLARY NO.	0.01	0.01
REFERENCE PERM.	0.936 D	0.826 D

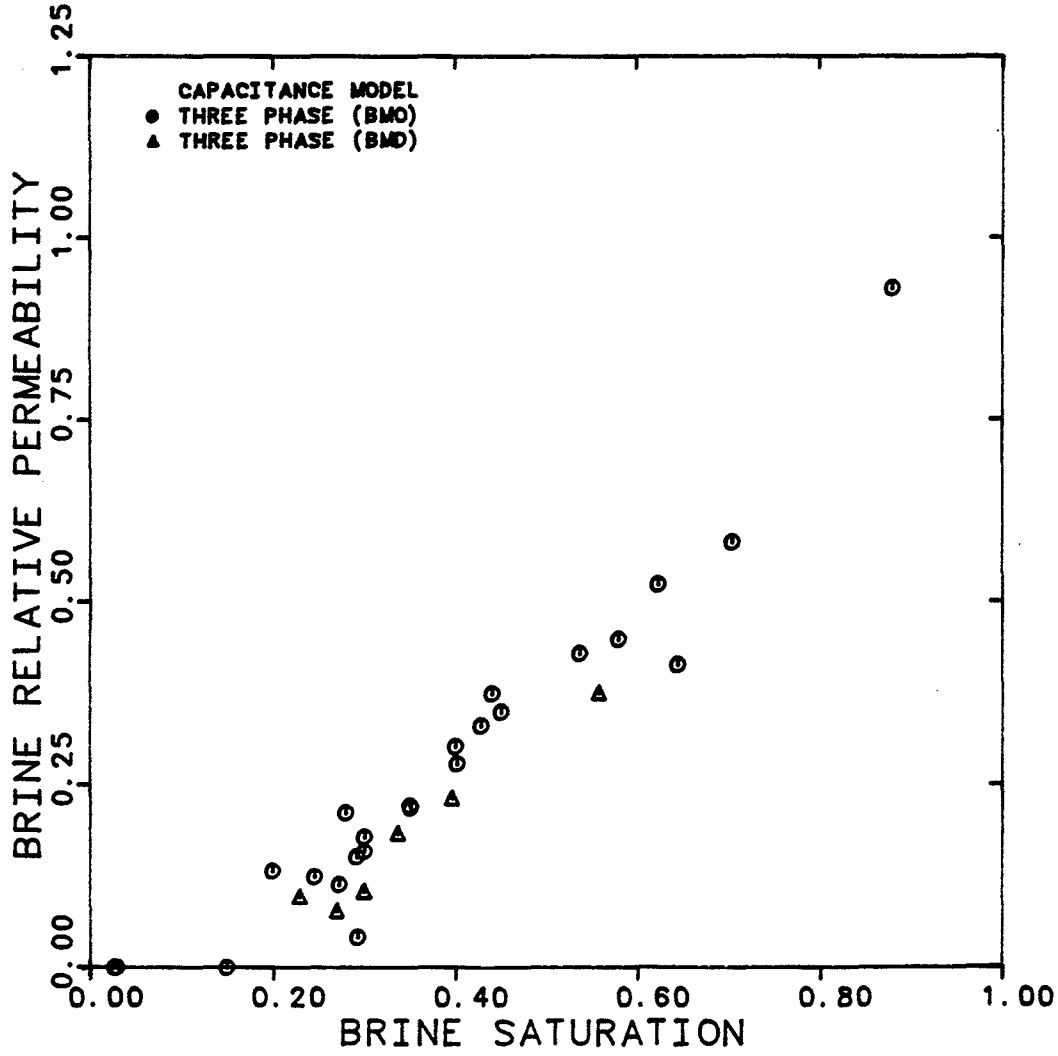

Figure 6.4.4.24 Comparison of Brine Relative Permeabilities for Three-Phase Flow Experiments

	DELSHAD	DELSHAD (REF. D.6)
THREE PHASE	BMO	BMD
CAPILLARY NO.	0.01	0.01
REFERENCE PERM.	0.936 D	0.826 D

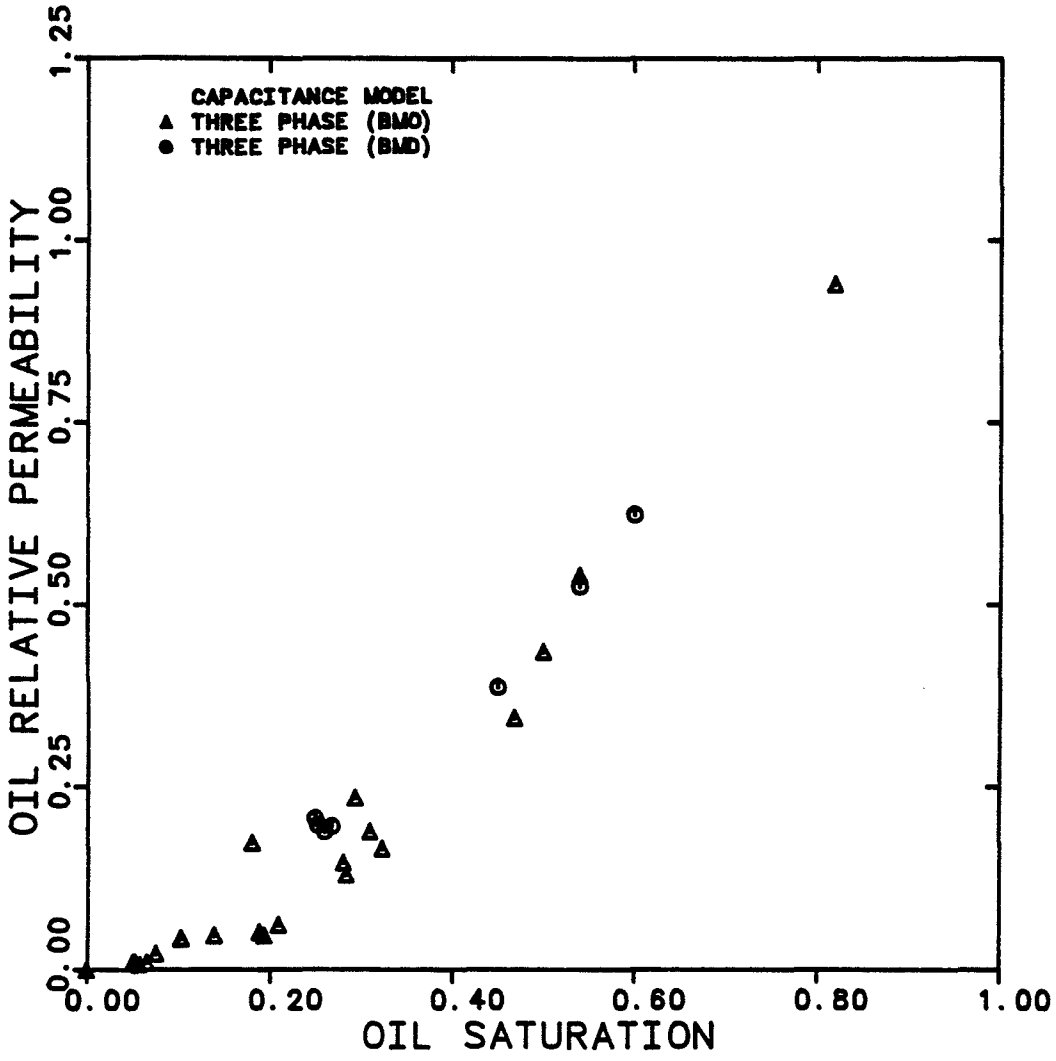

Figure 6.4.4.25 Comparison of Oil Relative Permeabilities for Three-Phase Flow Experiments

	DELSHAD	DELSHAD (REF. D.6)
THREE PHASE	BMO	BMD
CAPILLARY NO.	0.01	0.01
REFERENCE PERM.	0.936 D	0.826 D

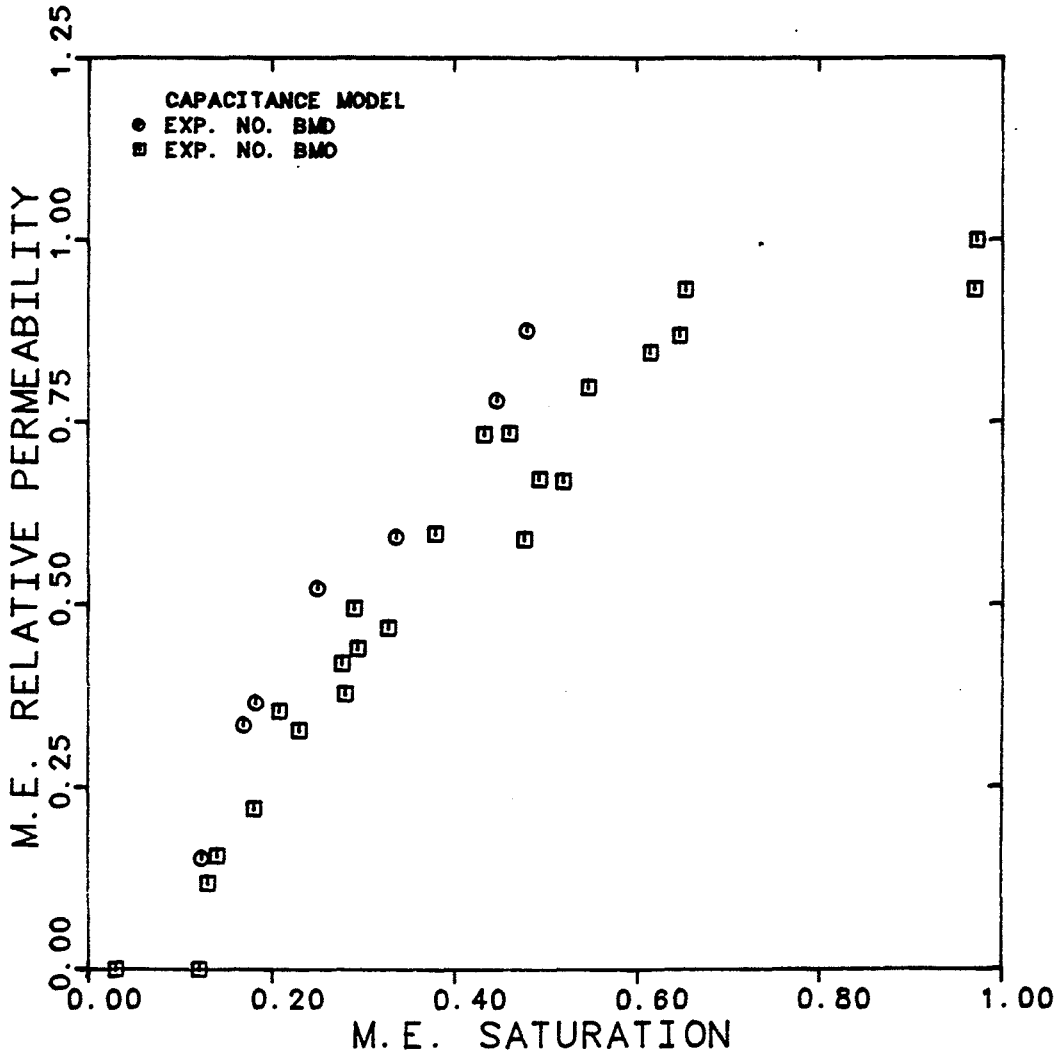

Figure 6.4.4.26 Comparison for M.E. Relative Permeabilities for Three-Phase Flow Experiments

	DELSHAD	DELSHAD (REF. D.6)
EXPERIMENT NO.	BMO	BMD
CAPILLARY NO.	0.01	0.01
REFERENCE PERM.	0.936 D	0.826 D

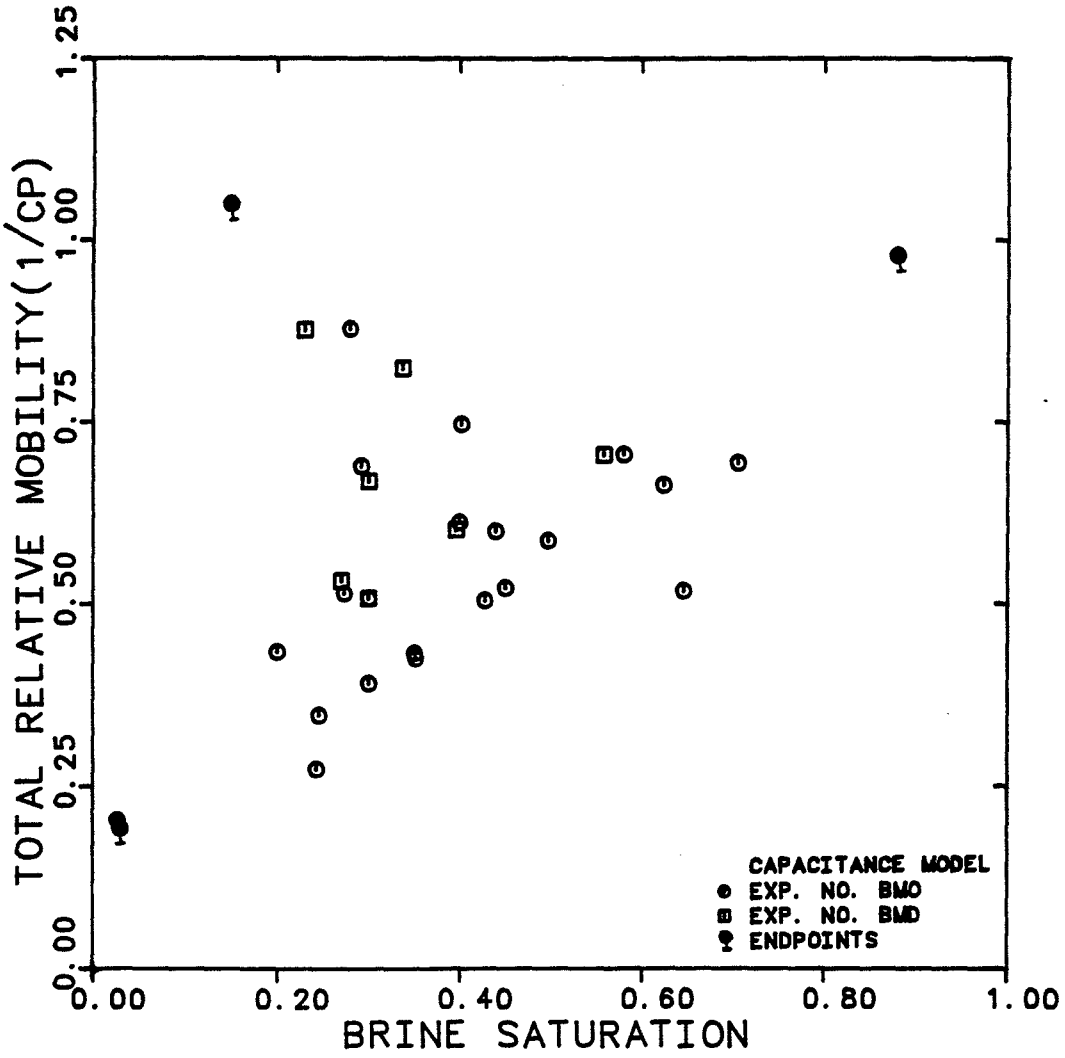

Figure 6.4.4.27 Comparison of Total Relative Mobilities Versus Brine Saturation for Three-Phase Flow Experiments

	DELSHAD	DELSHAD (REF. D.6)
EXPERIMENT NO.	BMO	BMD
CAPILLARY NO.	0.01	0.01
REFERENCE PERM.	0.936 D	0.826 D

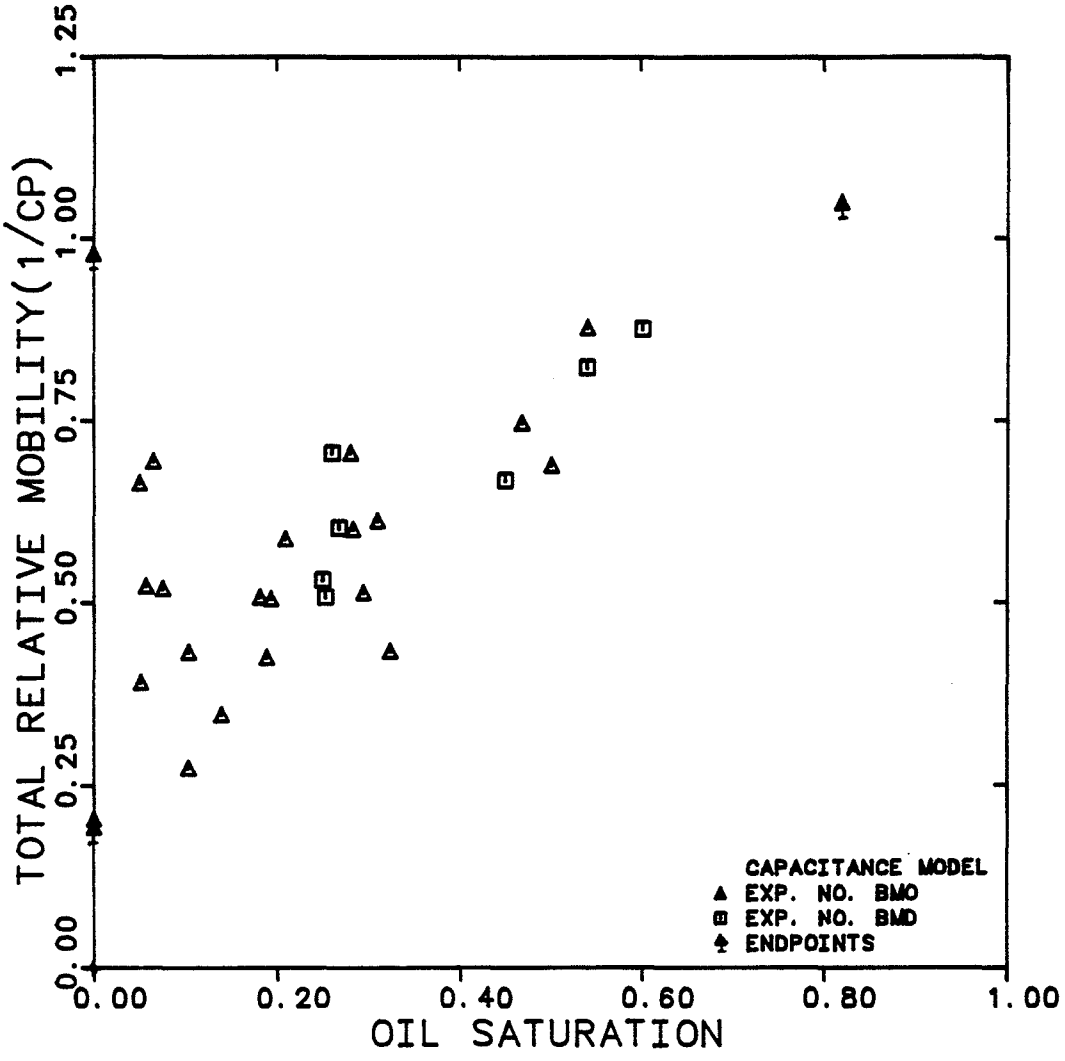

Figure 6.4.4.28 Comparison of Total Relative Mobilities Versus Oil Saturation for Three-Phase Flow Experiments

	DELSHAD	DELSHAD (REF. D.6)
EXPERIMENT NO.	BMO	BMD
CAPILLARY NO.	0.01	0.01
REFERENCE PERM.	0.936 D	0.826 D

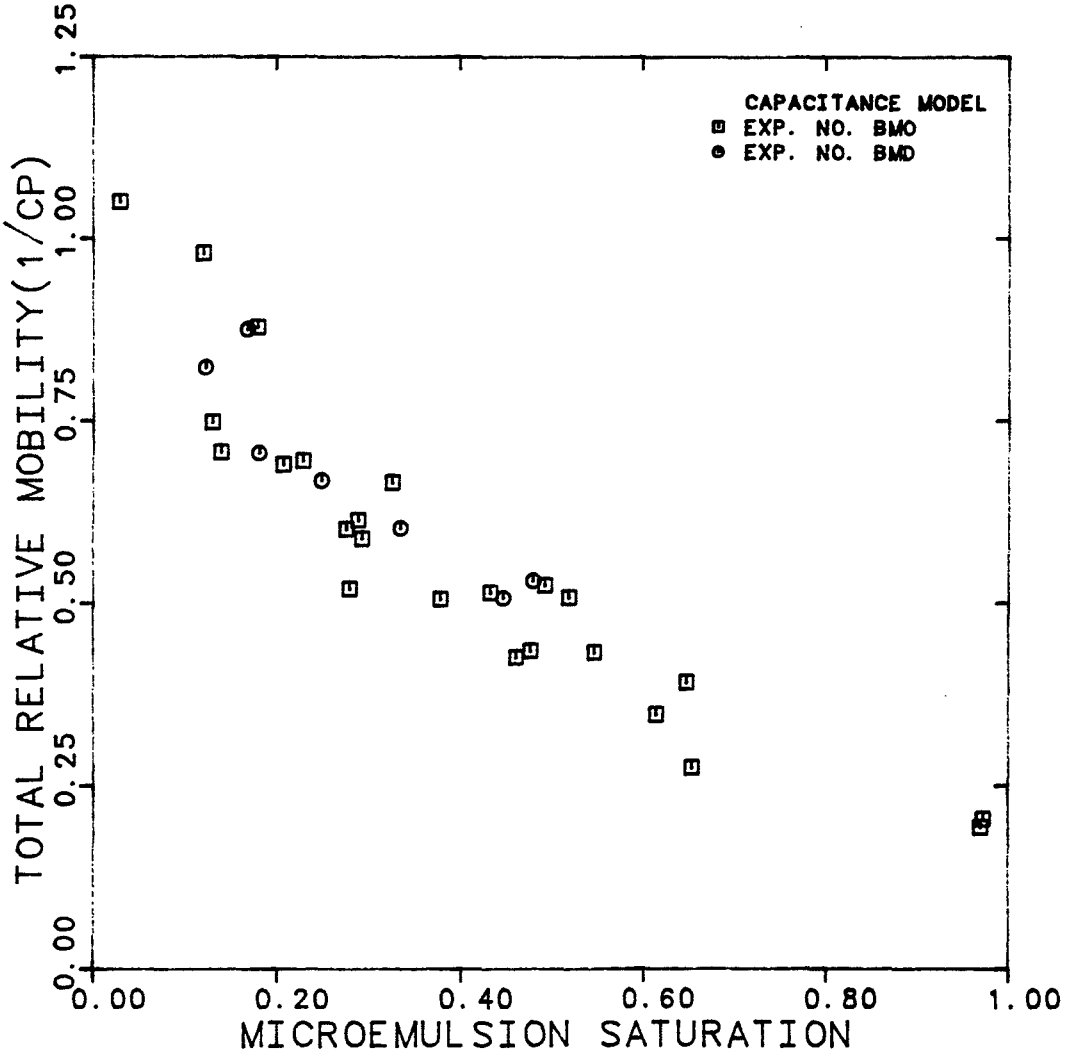

Figure 6.4.4.29 Comparison of Total Relative Mobilities Versus M.E. Saturation for Three-Phase Flow Experiments

6.4.5 Comparison of Two- and Three-Phase Data

Results of the two three-phase relative permeability experiments, BMO and BMD, are compared with those of the two-phase experiments (SMW, SMO, MB) discussed in section 6.3.3.

Figures 6.4.5.1 through 6.4.5.3 compare relative permeabilities versus saturation estimated from capacitance model for each phase. The phase relative permeabilities obtained in two- and three-phase flow are very close enforcing the conclusion that relative permeability of each phase is a function of its own saturation only.

	DELSHAD	DELSHAD (REF. D.6)
THREE PHASE	BMO	BMD
TWO PHASE (1&3)	SMW	MB
NC (3 , 2 PHASE)	0.01, 0.0066	0.01, 0.02

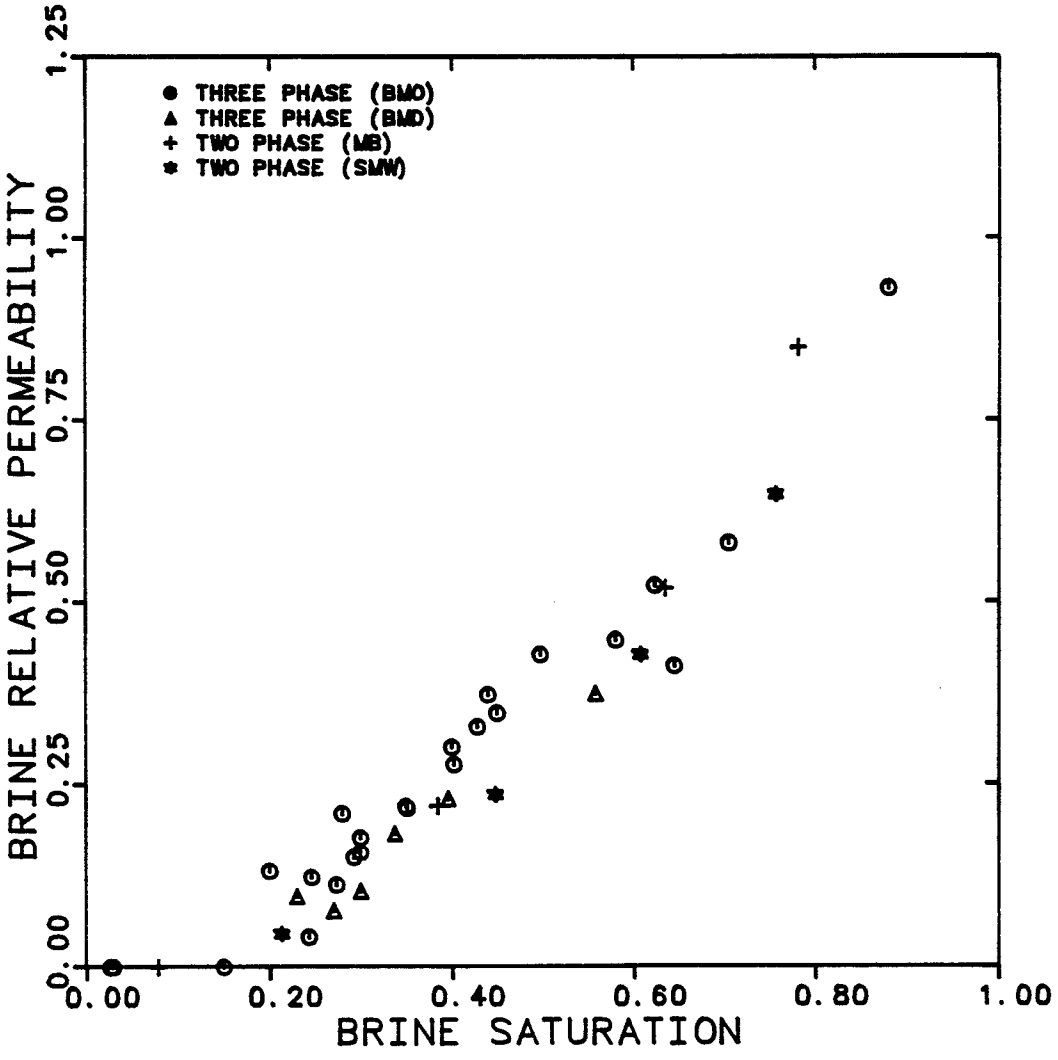

Figure 6.4.5.1 Comparison of Brine Relative Permeabilities for Two- and Three-Phase Flow Experiments

	DELSHAD	DELSHAD (REF. D.6)
THREE PHASE	BMO	BMD
TWO PHASE(2&3)	SMO	MO
NC (3 , 2 PHASE)	0.01, 0.01	0.01, 0.009–0.1

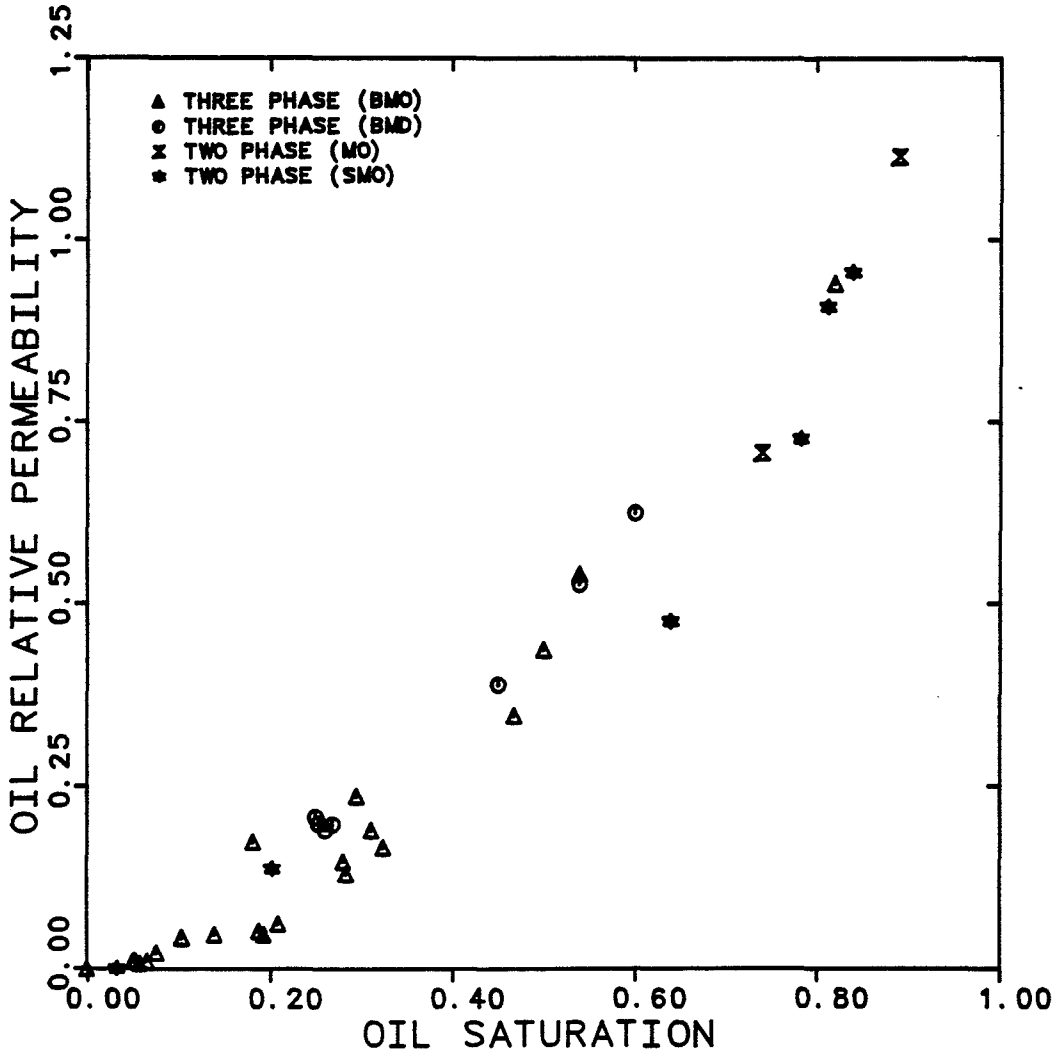

Figure 6.4.5.2 Comparison of Oil Relative Permeabilities for Two- and Three-Phase Flow Experiments

	DELSHAD	DELSHAD (REF. D.6)
THREE PHASE	BMO	BMD
TWO PHASE (1&3)	SMW	MB
TWO PHASE (2&3)	SMO	MO

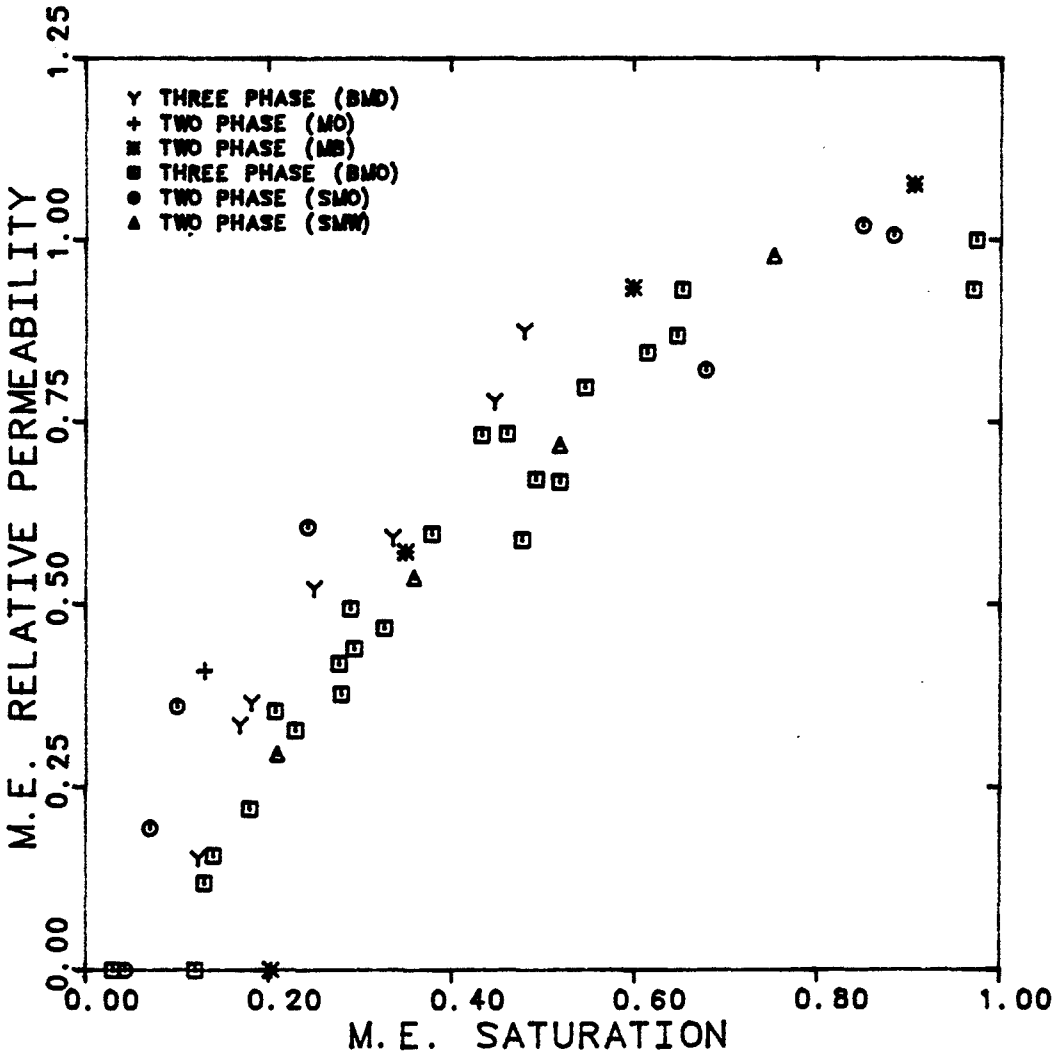

Figure 6.4.5.3 Comparison of M.E. Relative Permeabilities for Two- and Three-Phase Flow Experiments

CHAPTER 7

DEVELOPMENT OF A THREE-PHASE RELATIVE PERMEABILITY MODEL

For the performance prediction of multiphase oil recovery processes such as chemical flooding, there is an acute need for a reliable three-phase relative permeability model. To develop and test such a model, experimental data are needed as well. A review of the petroleum literature, however, reveals the apparent lack of these data, especially for systems containing low-tension additives. In chemical flood simulators [P.2,C.0], therefore, interpolation models such as those of Hirasaki et al. [H.4], Pope [P.2,C.0] or Lake [L.1], [C.0] are used for calculation of three-phase relative permeabilities at high capillary numbers.

This chapter presents a detailed description of the above-mentioned models. The predicted relative permeabilities using these models are also compared with

the available experimental data. Finally, a new three-phase relative permeability model is described and a comparison of computed and experimental values is given. This new model can be considered a generalization of the one implemented by Camilleri [C.0] in the University of Texas micellar/polymer simulator which was itself a generalization of the original version of Pope and Nelson [P.2].

7.1 Description of the Available Three Liquid Phase Relative Permeability Models

7.1.1 Hirasaki's Model

Hirasaki et al. [H.4] developed a model to calculate the residual saturation and relative permeability of each phase based on the basic assumption that for a preferentially water-wet reservoir, the excess brine phase is more wetting compared to the microemulsion phase and the latter wets preferentially compared to the excess oil phase. They also presented the following equations to describe the trapping of wetting and non-wetting phases.

- Trapping of non-wetting phases (excess oil and microemulsion) by the excess brine phase is described by the non-wetting phase capillary desaturation function, $f(\sigma)$ using the appropriate IFT value as follows:

$$S_{3r} + S_{2r} = f(\sigma_{mw}) \qquad (7.1)$$

- Trapping of wetting phases with excess oil phase is described by the wetting phase capillary desaturation function, $g(\sigma)$, using oil-microemulsion interfacial tension as follows:

$$S_{3r} + S_{1r} = g(\sigma_{om}) \qquad (7.2)$$

- Trapping of the excess oil and brine phases by the microemulsion are defined as

$$S_{2r} = f(\sigma_{om}) \qquad (7.3)$$

$$S_{1r} = g(\sigma_{wm}) \qquad (7.4)$$

After evaluating the above expressions, the residual phase saturations are expressed as follows:

$$S_{1r} = \max \begin{cases} g(\sigma_{wm}) \\ g(\sigma_{wm}) - S_3 \end{cases} \qquad (7.5)$$

$$S_{2r} = \max \begin{cases} f(\sigma_{om}) \\ f(\sigma_{wm}) - S_3 \end{cases} \qquad (7.6)$$

$$S_{3r} = \max \begin{cases} f(\sigma_{wm}) - S_2 \\ g(\sigma_{om}) - S_1 \end{cases} \qquad (7.7)$$

Hirasaki assumes an exponential functional form for the relative permeabilities as

$$k_{rj} = k^{\circ}_{rj}(\bar{S}_j)^{n_j} \qquad j=1,2,3 \qquad (7.8)$$

Where the normalized phase saturations are

$$\bar{S}_1 = \frac{S_1 - S_{1r}}{1-f(\sigma_{mw}) - S_{1r}} \qquad (7.9)$$

$$\bar{S}_2 = \frac{S_2 - S_{2r}}{1-g(\sigma_{om}) - S_{2r}} \qquad (7.10)$$

$$\bar{S}_3 = \frac{S_3 - S_{3r}}{1-S_{1r}-S_{2r}-S_{3r}} \qquad (7.11)$$

And the endpoint relative permeabilities are defined as

$$k^{\circ}_{r1} = k^{\circ}_{r1c} - (k^{\circ}_{r1c} - k^{\circ}_{r1w}) \frac{f(\sigma_{mw})}{S_{2rw}} \qquad (7.12)$$

$$k^{\circ}_{r2} = k^{\circ}_{r2c} - (k^{\circ}_{r2c} - k^{\circ}_{r2w}) \frac{g(\sigma_{om})}{S_{1rw}} \tag{7.13}$$

$$k^{\circ}_{r3} = \omega k^{\circ}_{r1} + (1 - \omega) k^{\circ}_{r2} \tag{7.14}$$

And the exponents which are empirical functions of the capillary number are given as below

$$n_1 = n_{1c} + (n_{1w} - n_{1c}) \frac{f(\sigma_{wm})}{S_{2rw}} \tag{7.15}$$

$$n_2 = n_{2c} + (n_{2w} - n_{2c}) \frac{g(\sigma_{om})}{S_{1rw}} \tag{7.16}$$

$$n_3 = \omega n_1 + (1 - \omega) n_2 \tag{7.17}$$

While the weighting function ω is expressed as

$$\omega = \frac{S_{2T}}{S_{1T} + S_{2T}} \tag{7.18}$$

where

$$S_{1T} = \min(S_{1r}, S_1) \tag{7.19}$$

$$S_{2T} = \min(S_{2r}, S_2) \qquad (7.20)$$

In the above equations, subscript w designates a water-oil (no chemical) quantity and subscript c the infinte capillary number value. Hirasaki assumed the value of one for exponents and endpoint relative permeabilities at infinite capillary number (n_{1c}, n_{2c}, k°_{r1c}, k°_{r2c}).

7.1.2 Lake's Model

The model introduced by Lake [L.1], [C.0] is based on a simple interpolating function which satisfies the idea that the intermeadiate wetting phase becomes the wetting phase when the original wetting phase is absent. He introduced the interpolating function g as follows

$$g = \frac{S_2(1 - S_1)}{S_1 + S_2} \qquad (7.21a)$$

This function approaches 1.0 or zero as the saturation of brine or oil approaches zero, respectively.

The g function proposed by Lake does not approach the limits of one or zero if there is a third trapped phase (oil or brine) present during the oil/microemulsion or brine/microemulsion two-phase flow.

Examples of this type of results are those of experiments SMO and SMW. Thus, a more general form of the interpolating function is as follows

$$g = \frac{(S_2-S_{2r})(1 - (S_1-S_{1r}))}{(S_1-S_{1r})+(S_2-S_{2r})} \qquad (7.21b)$$

In order to make the relative permeabilities approach the proper limits, linear interpolation of endpoint relative permeabilities of excess brine and oil phases are performed based on the change in the residual phase saturations [L.1,P.2] as follows:

$$k^{\circ}_{r1} = k^{\circ}_{r1w} + \frac{S_{2rw}-S_{2r}}{S_{2rw}} (k^{\circ}_{r1c}-k^{\circ}_{r1w}) \qquad (7.22a)$$

$$k^{\circ}_{r2} = k^{\circ}_{r2w} + \frac{S_{1rw}-S_{1r}}{S_{1rw}} (k^{\circ}_{r2c}-k^{\circ}_{r2w}) \qquad (7.23a)$$

Where subscript w designates a water-oil (high tension) quantity and subscript c the infinite capillary number value. The residual saturations (S_{1r} and S_{2r}) are estimated from the capillary desaturation curves (CDC). He also estimates the exponents (n_1, n_2) from the same

curves. The endpoint relative permeabilities at infinite capillary number (k°_{r1c}, k°_{r2c}) are assumed to be one.

A more general form for Equations 7.22a and 7.23a is the one that allows for a non-zero residual phase saturation (S_{2rc}, S_{1rc}) at the infinite capillary number. The latter feature is commonly seen in displacements of wetting phase by non-wetting phase where the non-wetting endpoint relative permeability reaches a value of one before a complete desaturation of the wetting phase occurs [A.2]. Therefore, Equations 7.22a and 7.23a are modified as follows;

$$k^{\circ}_{r1} = k^{\circ}_{r1w} + \frac{S_{2rw}-S_{2r}}{S_{2rw}-S_{2rc}} (k^{\circ}_{r1c} - k^{\circ}_{r1w}) \qquad (7.22b)$$

$$k^{\circ}_{r2} = k^{\circ}_{r2w} + \frac{S_{1rw}-S_{1r}}{S_{1rw}-S_{1rc}} (k^{\circ}_{r2c} - k^{\circ}_{r2w}) \qquad (7.23b)$$

The relative permeabilities for the excess brine, microemulsion, and excess oil phases during three-phase flow is then calculated as below

a- First the microemulsion phase quantities are calculated using the interpolating function and the two-phase oil and brine properties at the same capillary

number

$$k^{\circ}_{r3} = k^{\circ}_{r2} + g(k^{\circ}_{r1} - k^{\circ}_{r2}) \qquad (7.24)$$

$$n_3 = n_2 + g(n_1 - n_2) \qquad (7.25)$$

$$S_{3r} = S_{2r} + g(S_{1r} - S_{2r}) \qquad (7.26)$$

b- Then, the three-phase relative permeabilities are calculated as follows

$$k^{\circ}_{rj} = k^{\circ}_{rj}\left(\frac{S_j - S_{jr}}{1 - \sum_{j=1}^{3} S_{jr}}\right)^{n_j} \qquad j=1,2,3 \qquad (7.27)$$

where

$$S_{jr} = \min(S_j, S_{jr}) \qquad (7.28)$$

7.2 Test of Hirasaki and Lake Models Against Experimental Data

Two sets of three-phase relative permeability were used in checking the three-phase relative permeability models of Hirasaki and Lake. These data are the work of this study and Delshad [D.6]. Both sets of data were obtained at the same capillary number ($N_c = 10^{-2}$) using Berea sandstone cores with similar properties. Since the two-phase relative permeabilities of microemulsion/oil and microemulsion/brine were also available at the same capillary number, the exponents and endpoints (Table 7.2.1) found by matching Equation 6.5 to excess oil and brine relative permeabilities were used in Lake's model rather than using interpolation between high and low capillary number values for endpoints or estimating the exponents from the capillary desaturation curves. The endpoints and exponents found by matching the two-phase data were also used in Hirasaki's model rather than the value of one originally used in his model.

Figures 7.2.1 - 7.2.3 show the comparison between the computed relative permeabilities and experimental data for oil, brine, and microemulsion phases consecutively. The comparison shows that

- The prediction of brine relative permeabilities is rather poor by both models but a little better using Hirasaki et als.

- The prediction of oil relative permeabilities is reasonably good by Hirasaki but rather poor by Lake model.

- The prediction of microemulsion relative permeabilities is very poor by both models.

Table 7.2.1

Parameters for Two-Phase Relative Permeability Curves

Exp. No.	Phase Number (j)	Exponent (n_j)	End-Point (K°_{rj})	Residual Saturation (S_{jr})	Capillary Number (N_c)
Oil/brine (high tension)	1	1.50	0.062	0.40	0.000005
	2	1.41	0.80	0.352	
Microemulsion/ oil	1	-	-	0.117	0.01
	2	1.98	0.955	0.033	
	3	0.48	1.0	0.044	
Microemulsion/ brine	1	1.50	0.850	0.117	0.0066
	2	-	-	0.033	
	3	0.58	1.0	0.120	

COMPARISON OF CALCULATED THREE-PHASE
RELATIVE PERMEABILITY WITH THE
EXPERIMENTAL DATA

EXPERIMENT NUMBERS BMO . BMD
CAPILLARY NUMBER 0.01

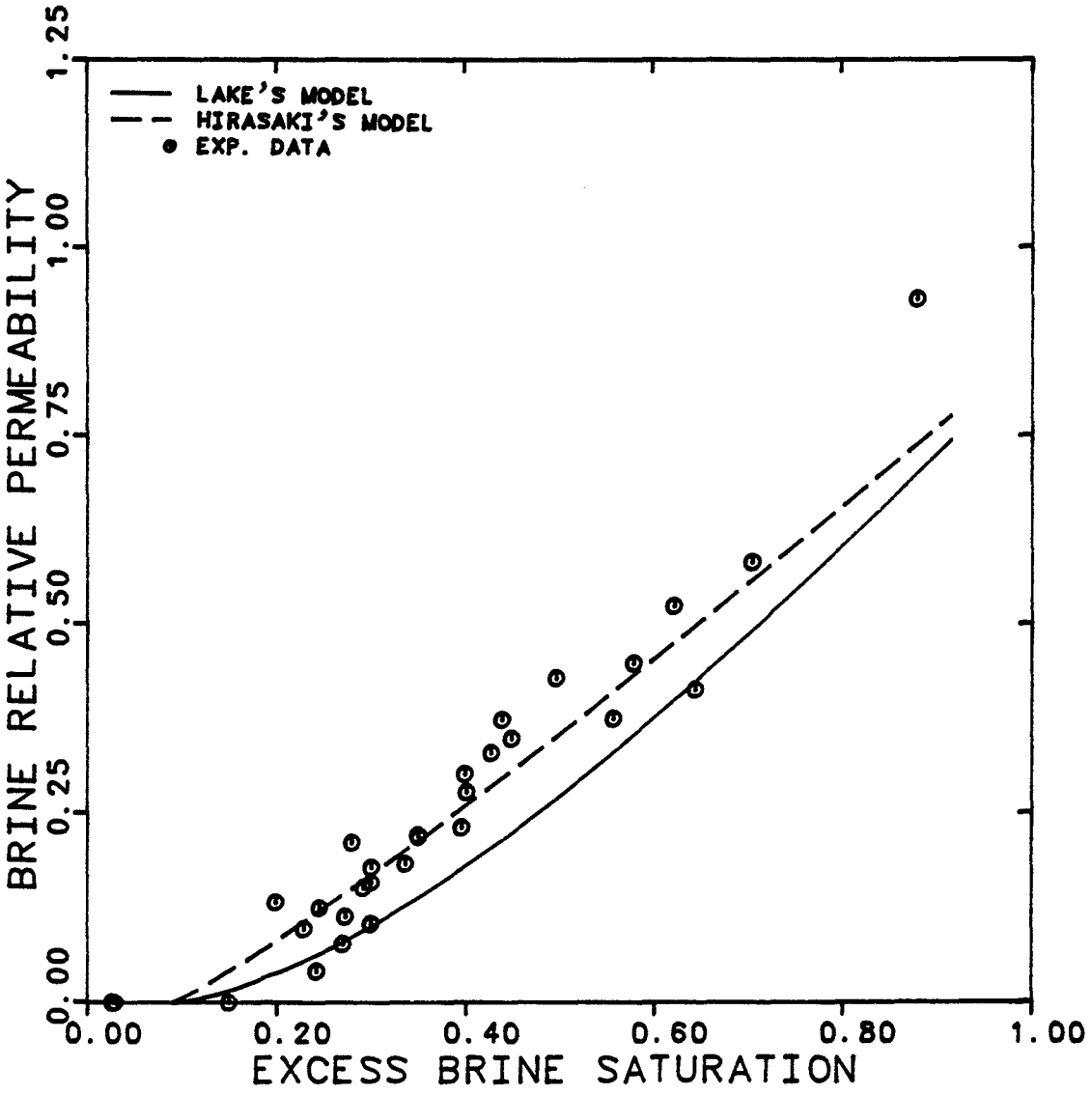

Figure 7.2.1 Comparison of Computed Brine Relative Permeabilities using Lake and Hirasaki Models with the Experimental Data

COMPARISON OF CALCULATED THREE-PHASE
RELATIVE PERMEABILITY WITH THE
EXPERIMENTAL DATA

EXPERIMENT NUMBERS BMO . BMD
CAPILLARY NUMBER 0.01

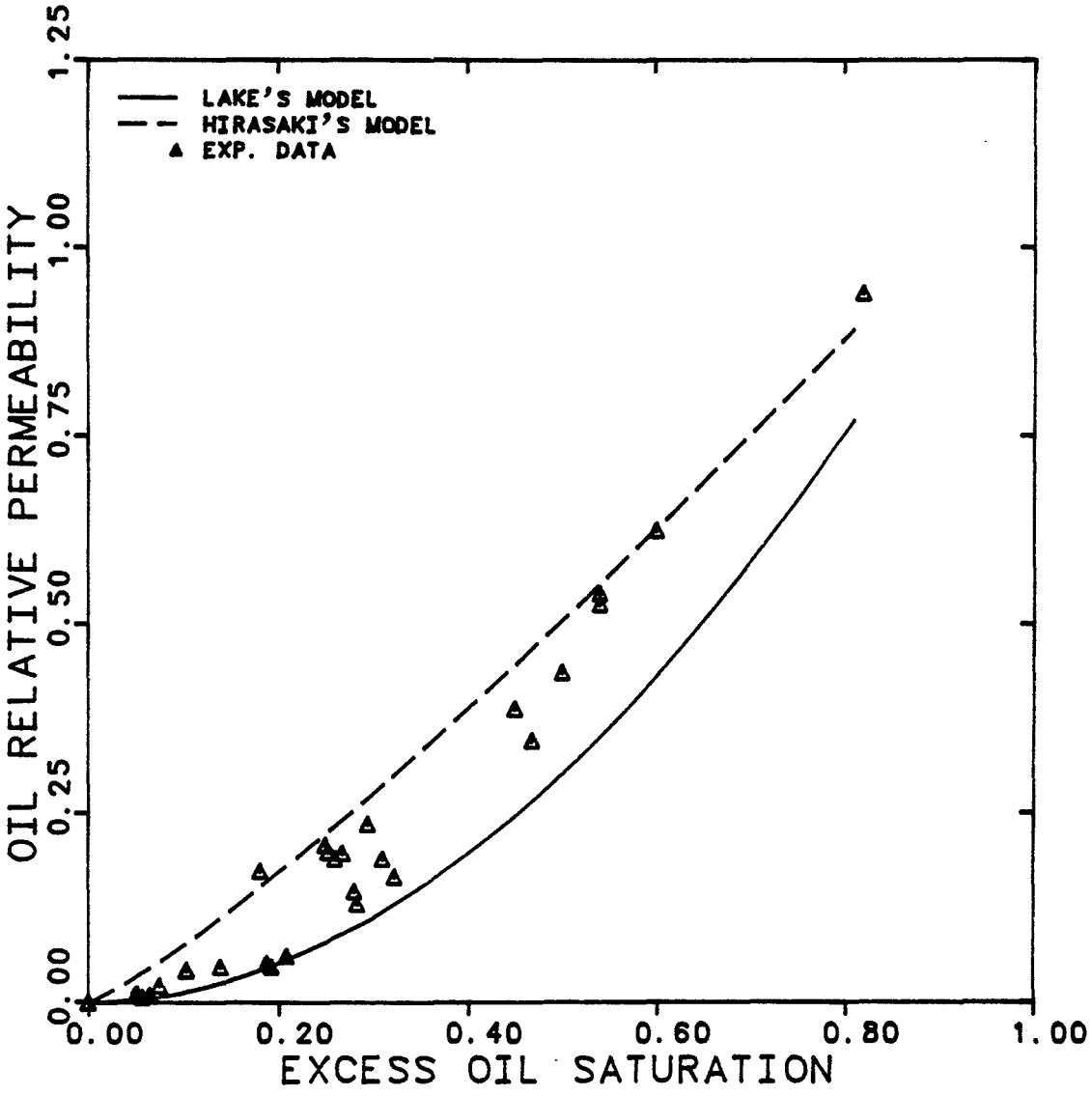

Figure 7.2.2 Comparison of Computed Oil Relative Permeabilities using Lake and Hirasaki Models with the Experimental Data

COMPARISON OF CALCULATED THREE-PHASE
RELATIVE PERMEABILITY WITH THE
EXPERIMENTAL DATA

EXPERIMENT NUMBERS	BMO . BMD
CAPILLARY NUMBER	0.01

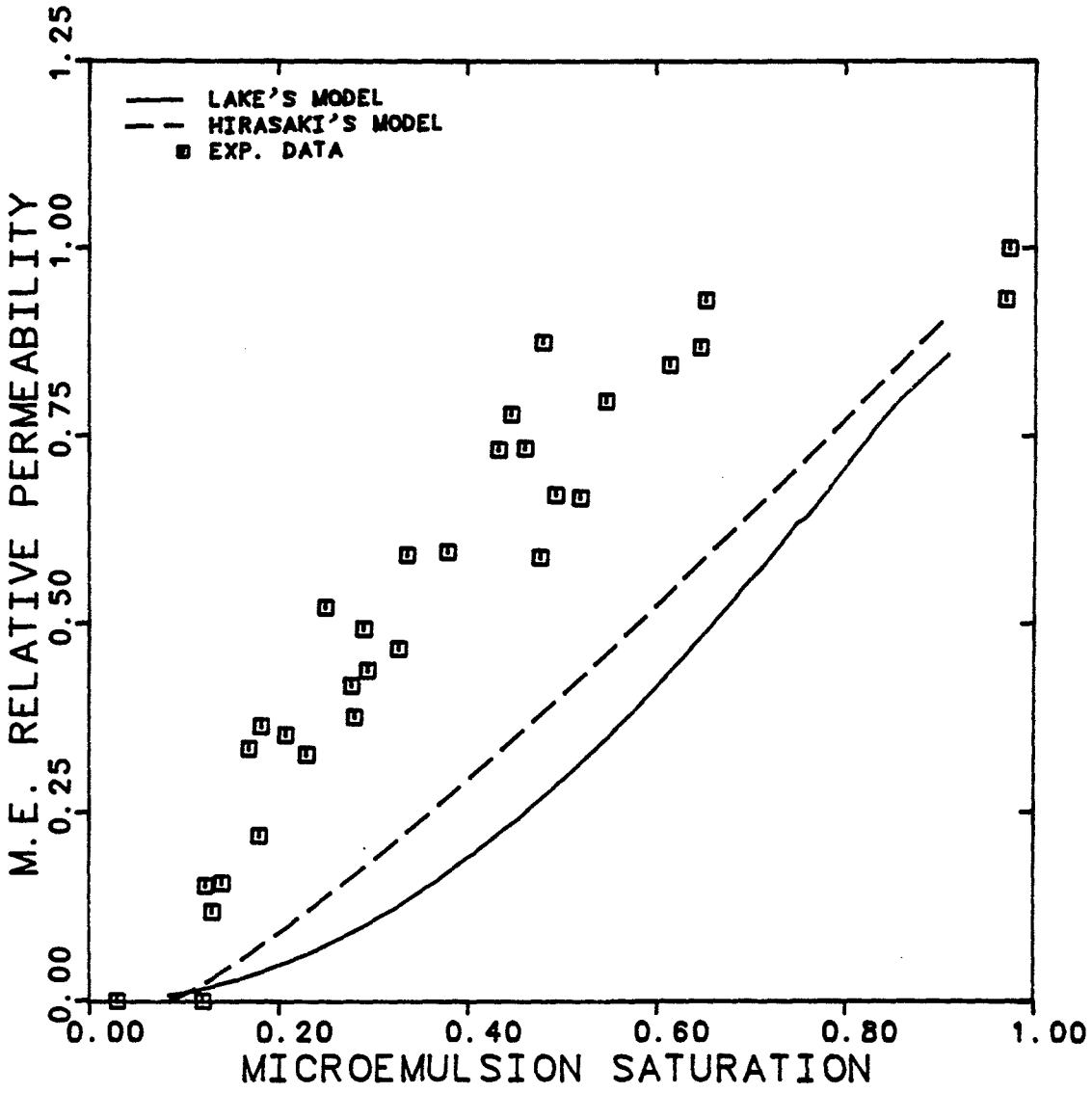

Figure 7.2.3 Comparison of Computed M.E. Relative Permeabilities using Lake and Hirasaki Models with the Experimental Data

7.3 Test of Modified Hirasaki and Lake Models Against Experimental Data

In order to improve the prediction of three-phase relative permeabilities, the following modification supported by the experimental observations in two- and three-phase system was done to both models. This modification was to change the wettability of microemulsion from intermediate wetting phase, which they assumed, to be the wetting phase. The same equations (7.1 - 7.28) were used for computing the relative permeabilities except that the indices of phase 1 and 3 were interchanged everywhere but in the high tension (water-oil) quantities.

Figures 7.3.1 through 7.3.4 show the comparison of computed and experimental brine, oil, and microemulsion relative permeabilities during three-phase flow. The comparison shows that

- The prediction of brine and oil relative permeabilities is acceptable using the modified Hirasaki's model but the prediction on the microemulsion permeabilities is still poor.

- The prediction of oil and microemulsion relative permeabilities are reasonably good using the modified Lake model. But, this model predicts a family of

relative permeabilty curves for the brine phase. These curves are plotted as a function of S_1/S_2 (Figure 7.3.2) which indicate that the brine relative permeability depends on the saturation of two phases, which is not supported by the experimental data.

Table 7.3.1

Parameter for Three-Phase Relative Permeability Curves

MODEL	Phase Number (j)	Exponent (n_j)	End-Point (k°_{rj})	Residual Saturation (S_{jr})	Capillary Number (N_c)
Hirasaki [H.4]	1	1.50	0.662	0.090	0.01
	2	1.732	0.888	0.0	
	3	1.732	0.888	0.084	
Lake [L.1]	1	1.50	0.85	0.090	0.01
	2	1.98	0.955	0.0	
	3	1.81	0.918	variable	
Modified Hirasaki	1	1.73	0.888	0.090	0.01
	2	1.73	0.888	0.0	
	3	0.741	0.760	0.084	
Modified Lake	1	variable	variable	variable	0.01
	2	1.98	0.955	0.0	
	3	0.48	1.0	0.084	
Delshad	1	1.50	0.850	0.090	0.01
	2	1.98	0.955	0.0	
	3	0.48	1.00	0.084	

COMPARISON OF CALCULATED THREE-PHASE
RELATIVE PERMEABILITY WITH THE
EXPERIMENTAL DATA

EXPERIMENT NUMBERS BMO , BMD
CAPILLARY NUMBER 0.01

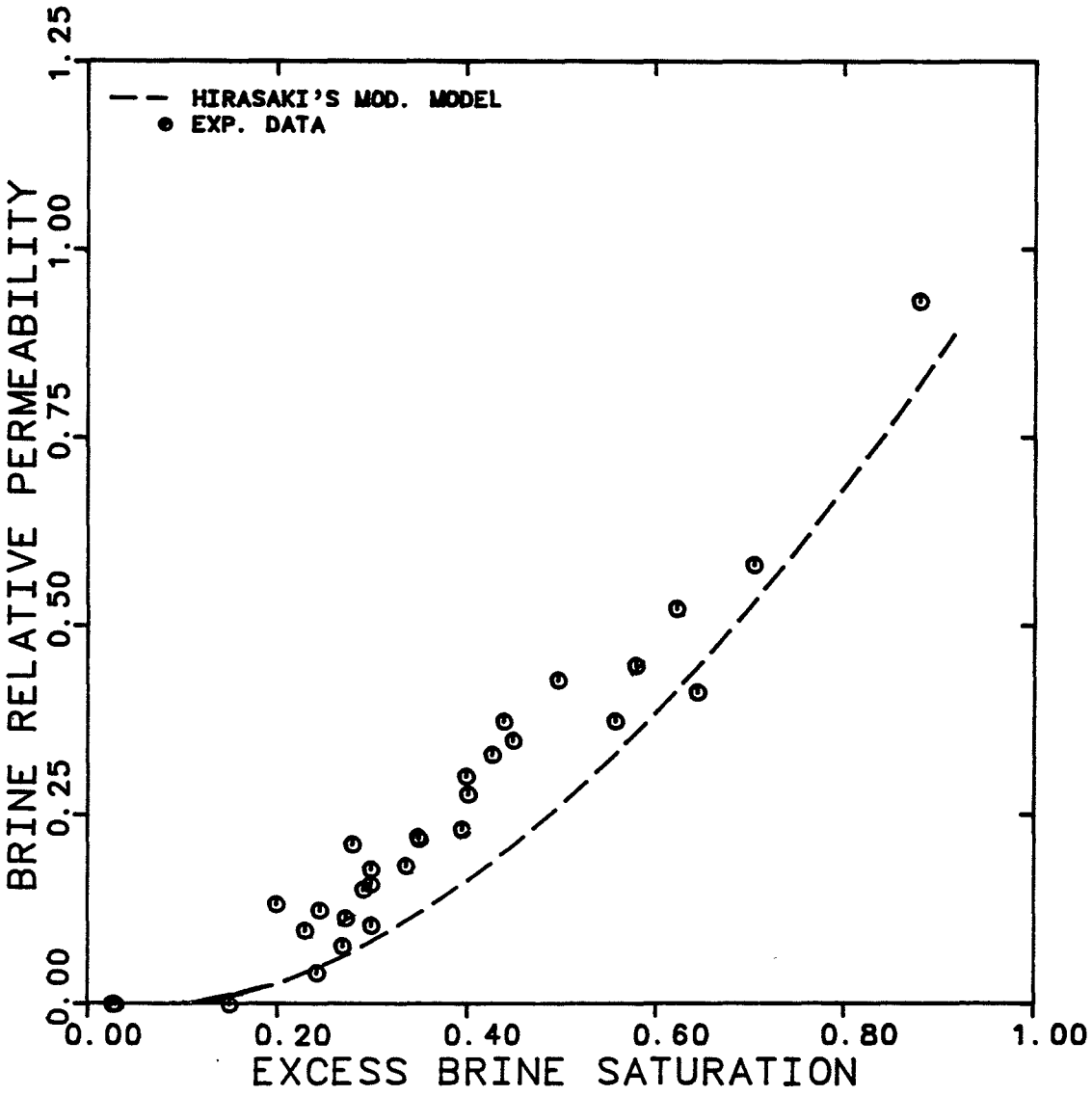

Figure 7.3.1 Comparison of Computed Brine Relative Permeabilities using Modified Hirasaki Models with the Experimental Data

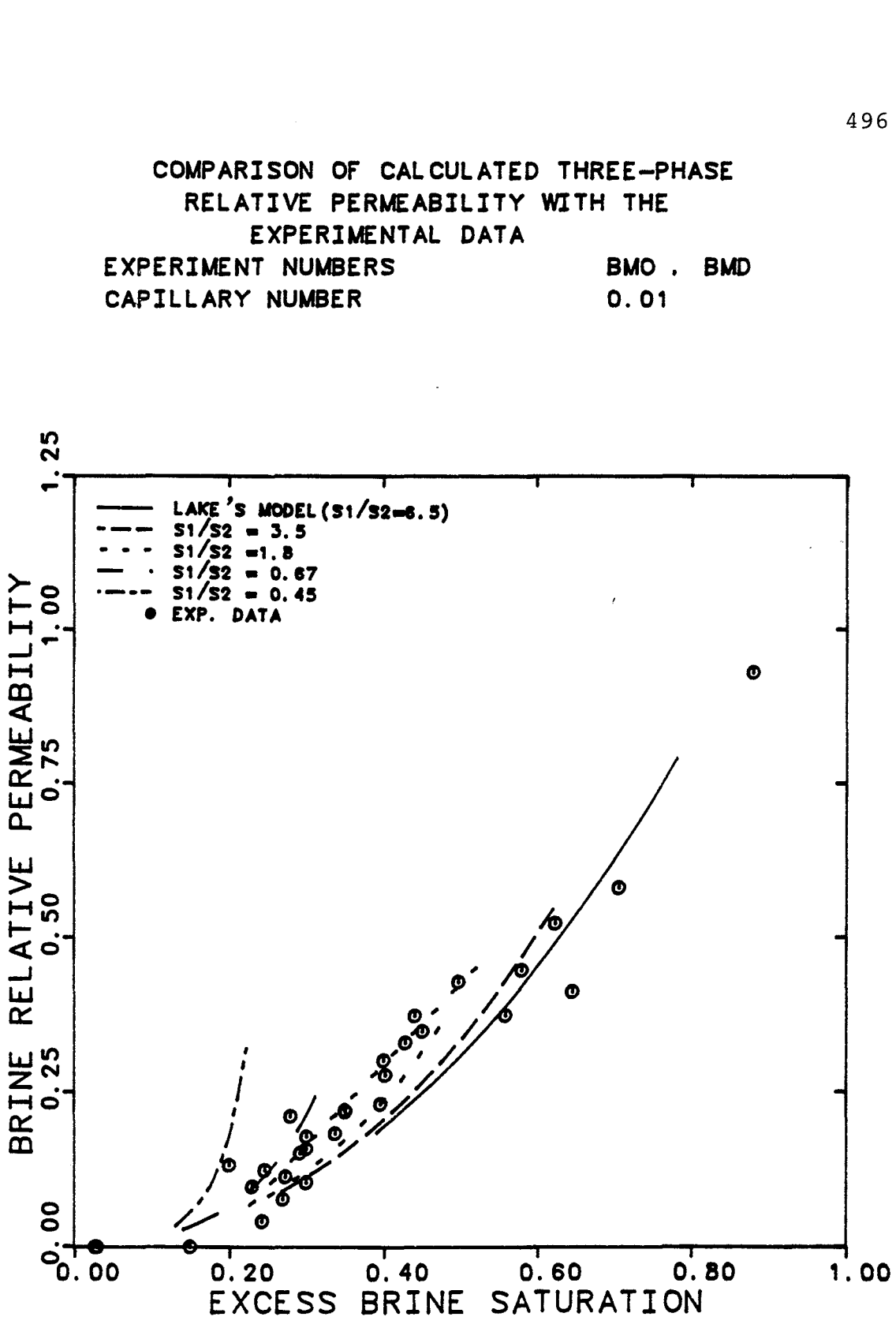

Figure 7.3.2 Comparison of Computed Brine Relative Permeabilities using Modified Lake Model with the Experimental Data

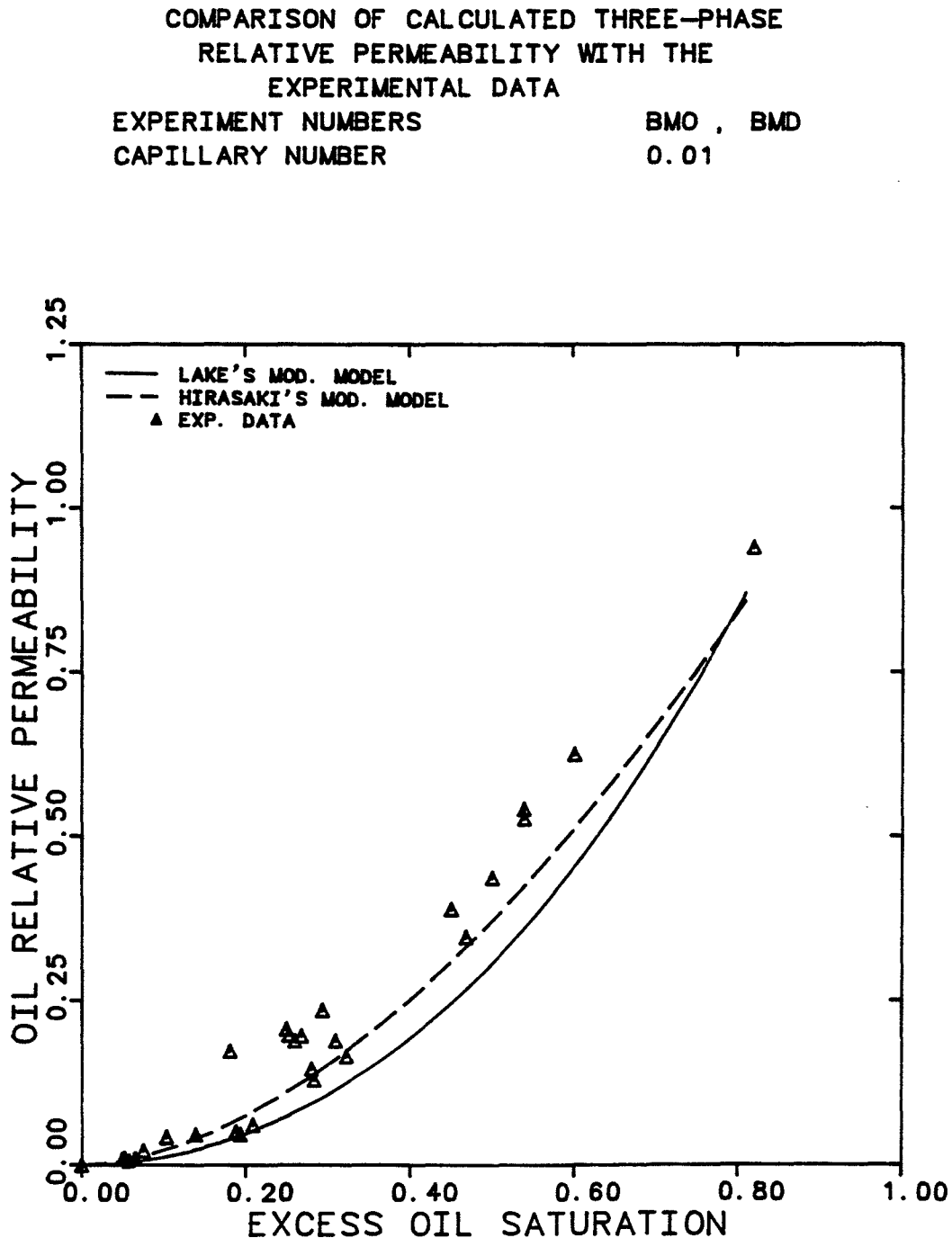

Figure 7.3.3 Comparison of Computed Oil Relative Permeabilities using Modified Lake and Hirasaki Models with the Experimental Data

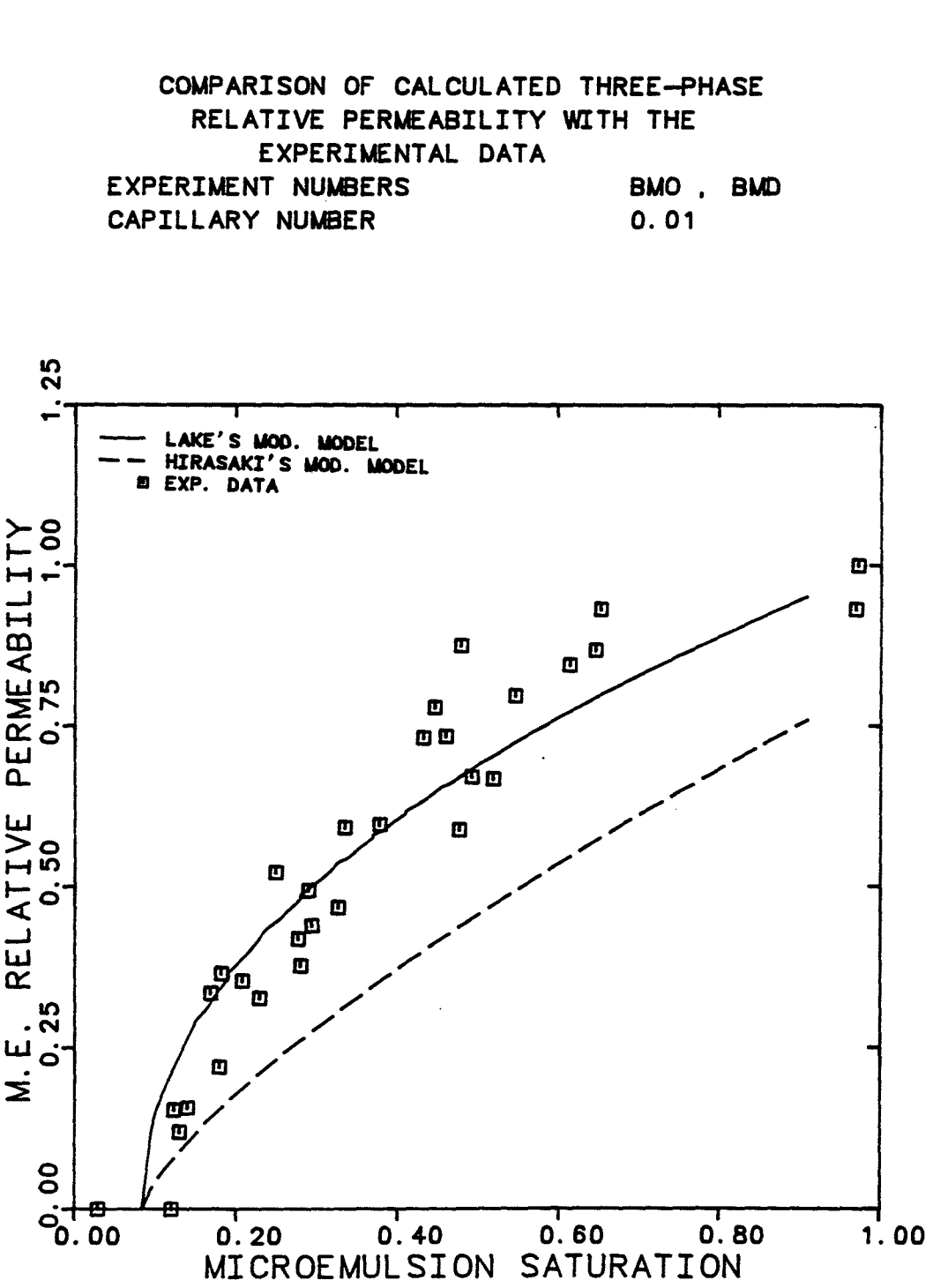

Figure 7.3.4 Comparison of Computed M.E. Relative Permeabilities using Modified Lake and Hirasaki Models with the Experimental Data

7.4 Three-Phase Relative Permeability Model

A new three-phase relative permeability model is proposed since neither of the two previously mentioned models appear capable of predicting the relative permeabilty curves for all three-phases that are reasonably close to the experimentally determined values. This model makes use of the experimental observations which indicate that oil, brine, and microemulsion relative permeabilities are the same functions in three-phase flow as in two-phase oil/microemulsion and brine/microemulsion flows.

The description of this model and a comparison of the computed relative permeabilities with the available three-phase data are given below.

7.4.1 Description

Handling of the three-phase relative permeability model is based partly on the experimental observations in two- and three-phase flow. The relative permeability of each phase is a function of the respective saturation only. This model also treats each phase independently and does not make assumptions regarding the wettability.

The proposed three-phase relative permeability model at a constant capillary number has the following

functional form,

$$k_{rj} = k^{\circ}_{rj}\left(\frac{S_j - S_{jr}}{1 - \sum_{j=1}^{3} S_{jr}}\right)^{nj} \qquad j=1,2,3 \tag{7.29}$$

Where endpoint relative permeabilities (k°_{rj}), exponents (n_j), and residual phase saturations (S_{jr}) are functions of the capillary number.

The experimentally obtained data for residual saturation, endpoint relative permeability, and exponent for the microemulsion, oil, and brine phases are shown as a function of capillary number in Figures 7.4.1 through 7.4.3.

Figure 7.4.1 shows the residual phase saturation as a function of capillary number for the three phases of a three-phase micellar solution. There are four distinguishable capillary desaturation curves as opposed to the two (wetting and non-wetting) assumed by others [H.4,L.1].

The endpoint relative permeability of the oil phase (Figure 7.4.2) shows a weak dependence on the capillary number since it starts at a high value ($k^{\circ}_{r2} = 0.918$) at the low capillary number of $N_c = 5\text{x}10^{-6}$.

On the other hand, the brine endpoint relative permeability appears to have a strong dependence on the capillary number and it approaches the plateau value at the capillary number of greater than 1.0. The dependence of the microemulsion endpoint relative permeability at low capillary numbers ($N_c < 10^{-3}$) is not well defined.

The exponents of oil and brine phases (Figure 7.4.3) appear to have a weak dependence on the capillary number. To evaluate the dependence of the exponent of the microemulsion phase, more data are required at capillary numbers less than 10^{-2}.

To compare the predicted relative permeabilities using this model with the experimental data, experimental values of all the parameters for the three phases were used. Table 7.3.1 shows the matching parameters which are endpoint relative permeabilities exponents, and residual saturations. The parameters used in Lake and Hirasaki's models are also listed in Table 7.3.1.

The endpoints and exponents of the relative permeabilities used in three-phase flow are the values found by matching the two-phase data of microemulsion/oil and microemulsion/brine against Equation 7.29. The residual phase saturations estimated for the three-phase

flow is based on the following,

- Find the best estimate of residual phase saturations at $N_c = 10^{-2}$ which are

Residual brine (S_{1r}) to microemulsion = 0.030

Residual brine (S_{1r}) to excess oil = 0.150

Residual microemulsion (S_{3r}) to brine = 0.120

Residual microemulsion (S_{3r}) to oil = 0.047

Residual oil (S_{2r}) to microemulsion = 0.0

- Use the average of the two values for each phase as the residual saturation during three-phase flow,

$$S_{1r} = 0.09$$

$$S_{2r} = 0.0$$

$$S_{3r} = 0.084$$

The relative permeability estimates obtained from Equation 7.29 are plotted as solid curves in Figures 7.4.4 through 7.4.6. As can be seen from these plots, Equation 7.29 with the parameters listed in Table 7.3.1 predicts behavior very similar to that observed from laboratory data.

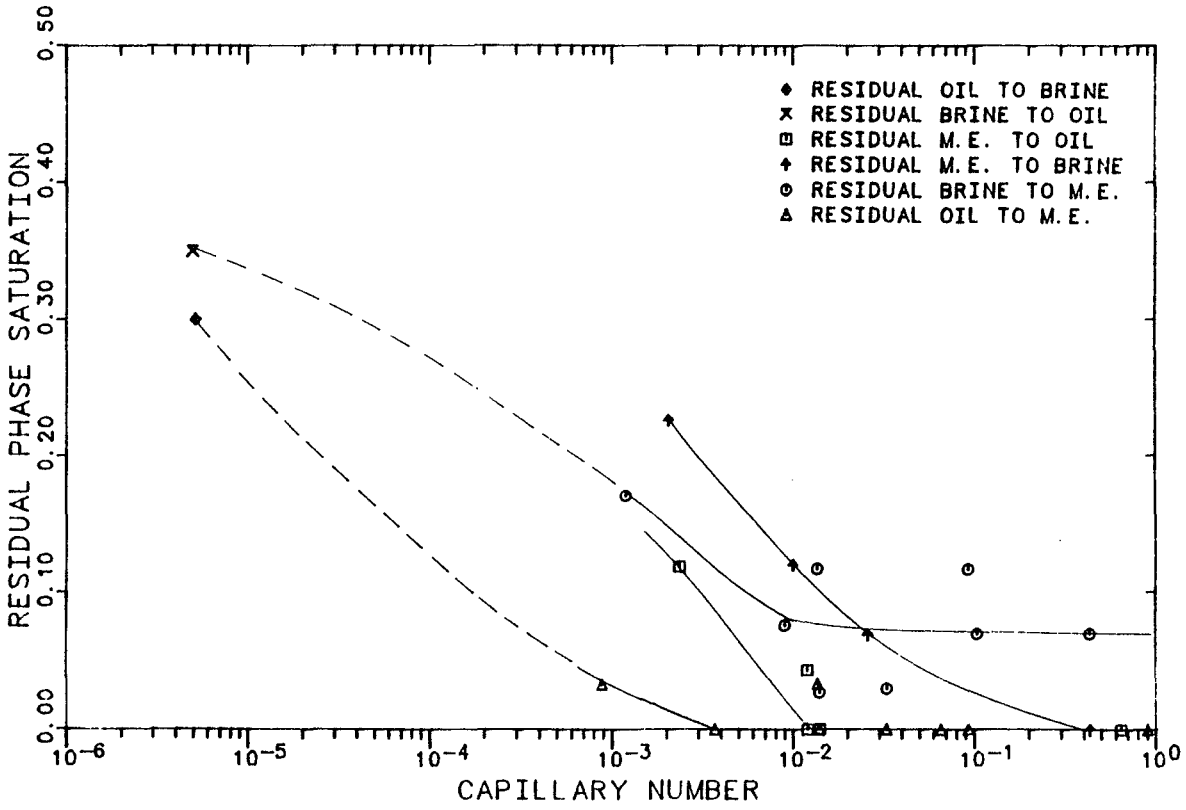

Figure 7.4.1 Capillary Desaturation Curves for Brine, Oil, and M.E. Phases

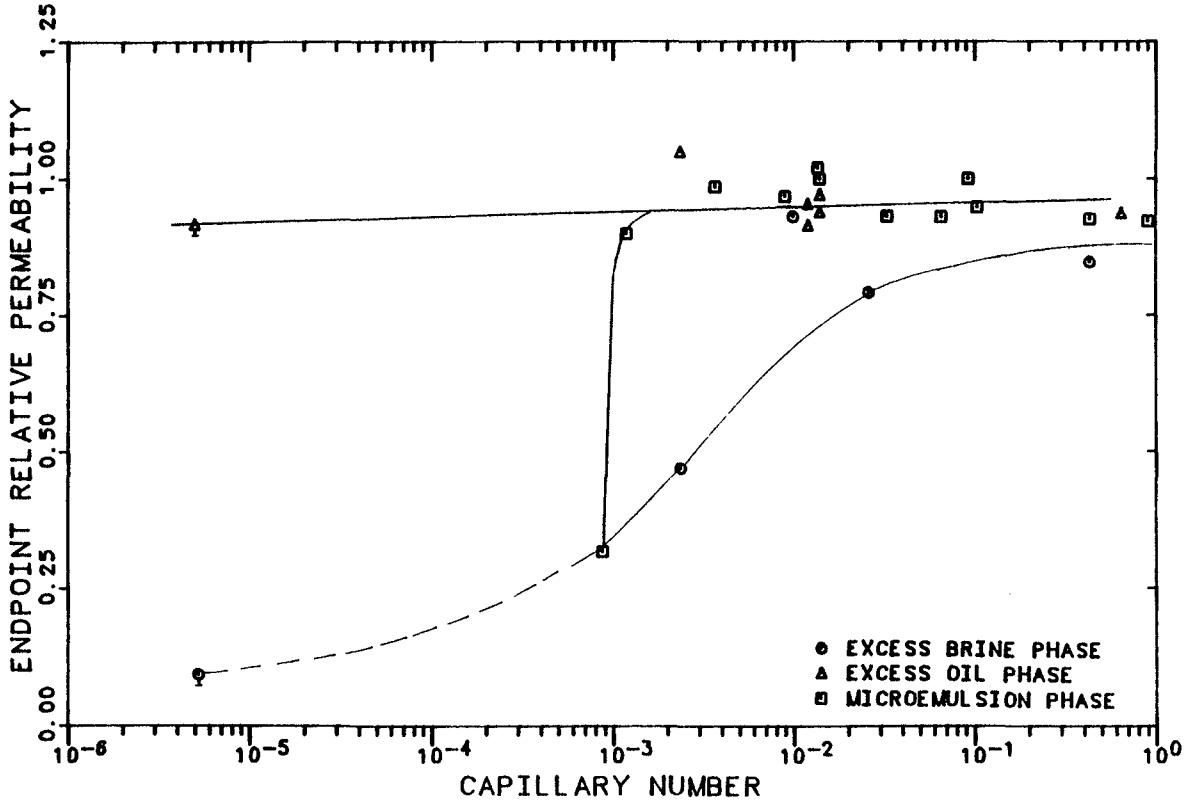

Figure 7.4.2 Endpoint Relative Permeability for Brine, Oil, and M.E. Phases as a Function of Capillary Number

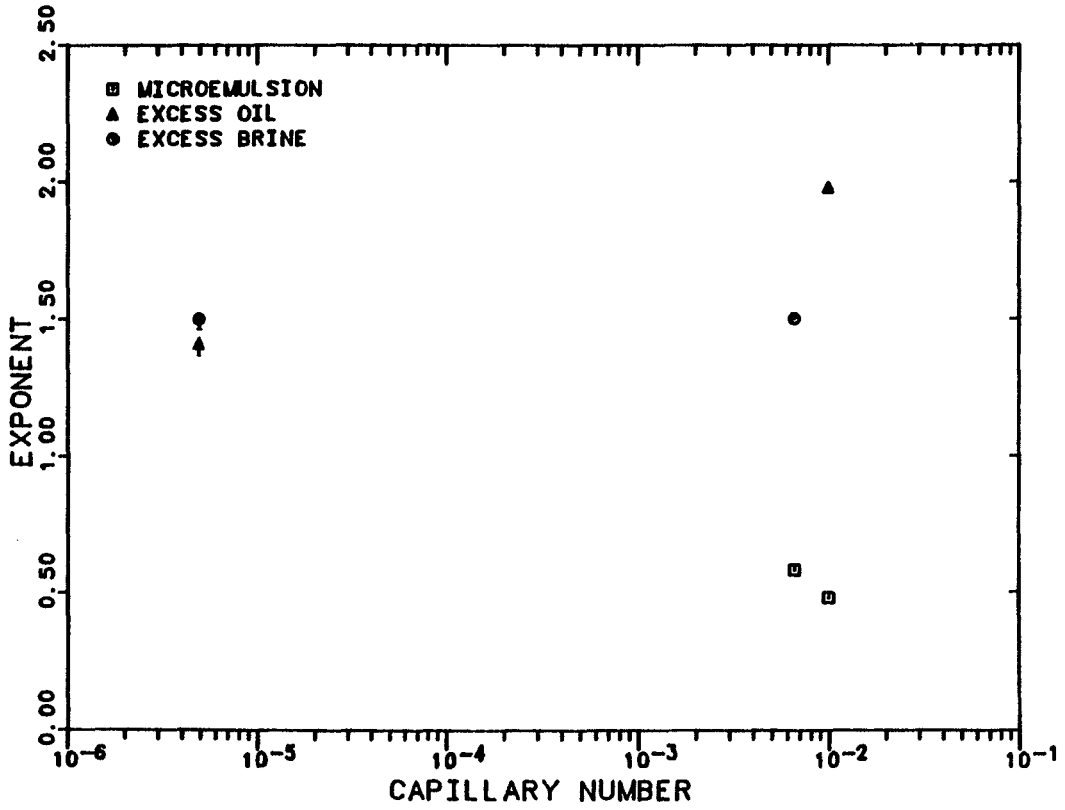

Figure 7.4.3 Exponent of Brine, Oil, and M.E. Relative Permeability Curves as a Function of Capillary Number

COMPARISON OF CALCULATED THREE-PHASE
RELATIVE PERMEABILITY WITH THE
EXPERIMENTAL DATA

EXPERIMENT NUMBERS BMO , BMD
CAPILLARY NUMBER 0.01

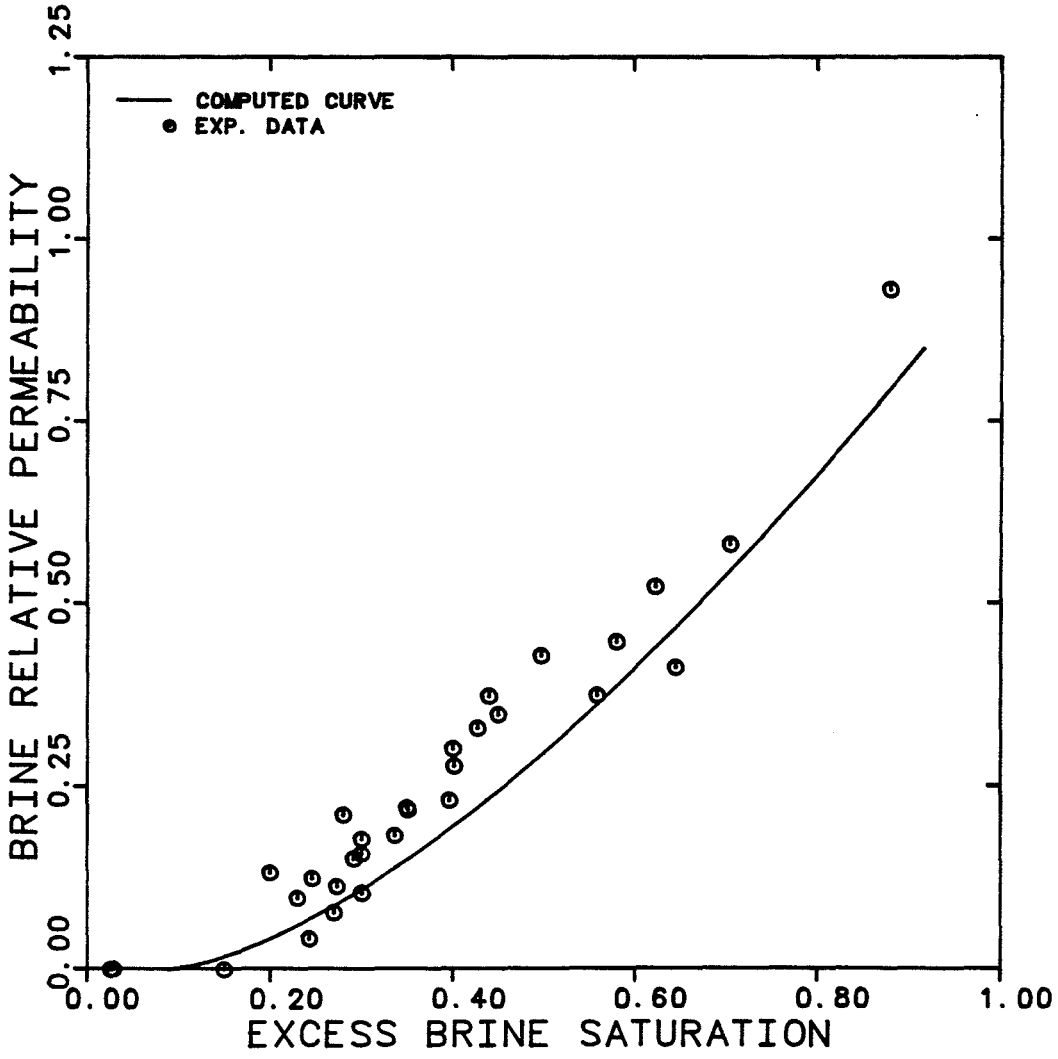

Figure 7.4.4 Computed and Experimental Brine Relative Permeability as a Function of Brine Saturation

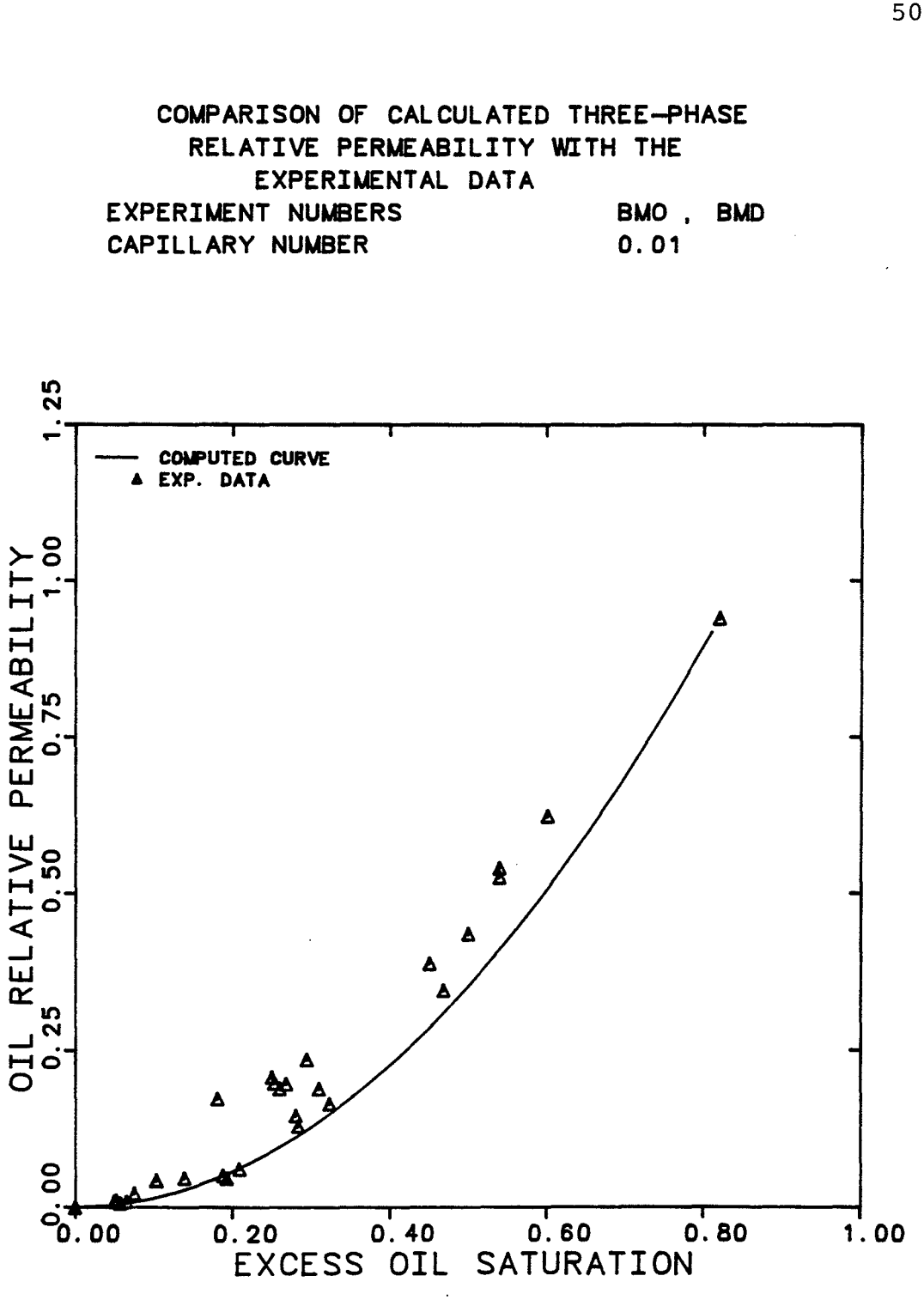

Figure 7.4.5 Computed and Experimental Oil Relative Permeability as a Function of Oil Saturation

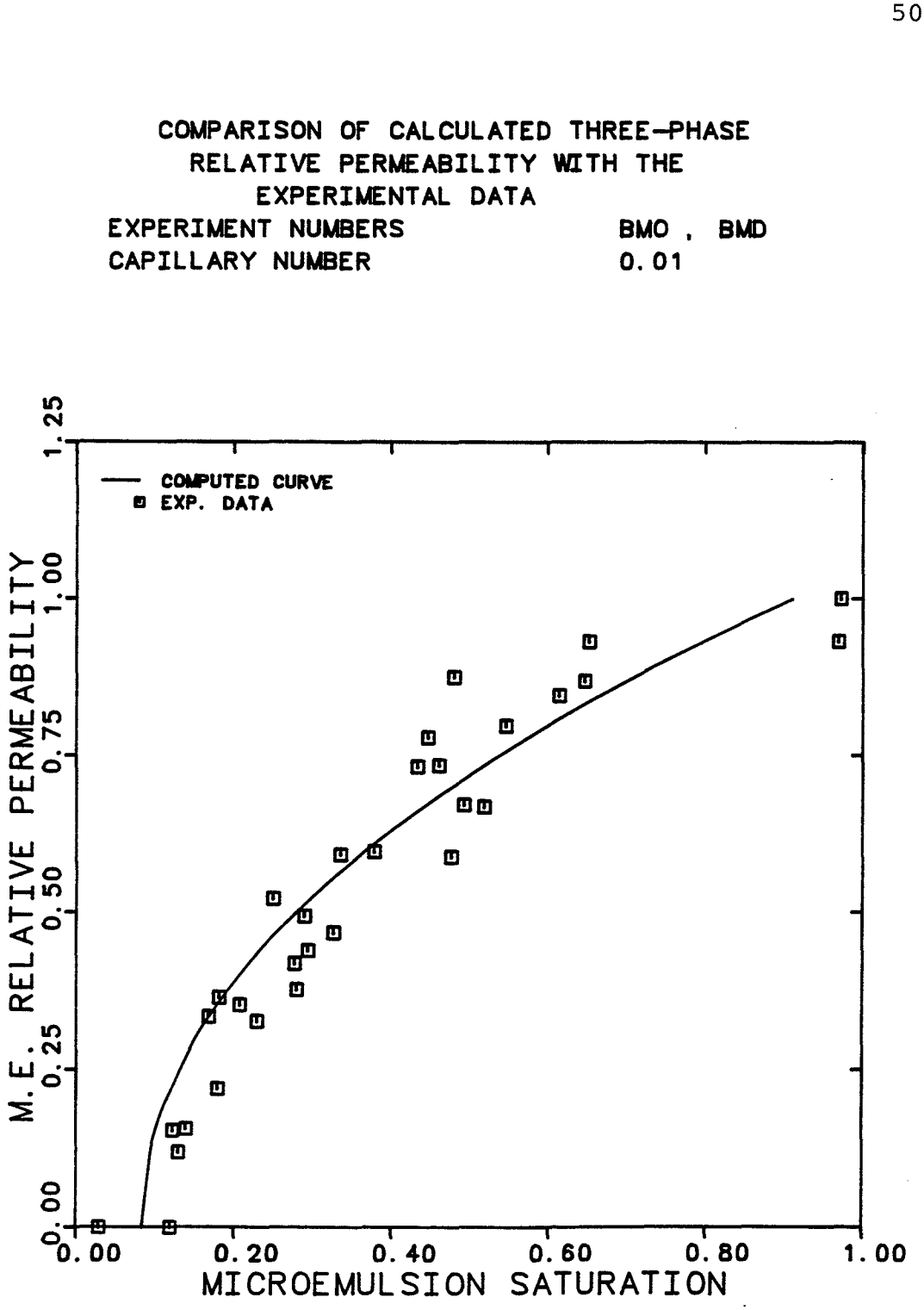

Figure 7.4.6 Computed and Experimental M.E. Relative Permeability as a Function of M.E. Saturation

7.4.2 Prediction of Endpoint Relative Permeability as a Function of Capillary Number

- Lake's Model

Lake [L.1] and Pope and Nelson [P.2] proposed a relationship to predict endpoint relative permeability as a function of capillary number (N_c). The endpoints are computed as linear interpolation between the water/oil endpoint values and the microemulsion/oil endpoint values. Lake and Pope and Nelson assumed a value of 1.0 (Eqs. 7.22a, 7.23a) for all endpoints (k°_{rjc}) with the assumption that the residuals were zero at that capillary number. As discussed in Section 7.1.2, Equations 7.22a and 7.23a were modified to account for a non-zero residual saturation at a capillary number at which the endpoint relative permeability is 1.0.

To test these relationships (Eqs. 7.22b and 7.23b), the residual saturations (S_{1r} and S_{2r}) obtained by Abrams, Amaefule et al., Bhuyan, and the results of Exp. CDC (Figures 6.2.44, 6.2.46) were used to predict the endpoint relative permeabilities of oil and aqueous phases as a function of capillary number. The predicted endpoint relative permeabilities were then compared with the experimental data reported by each investigator. The endpoints are computed as interpolation between the

water/oil endpoints and the residual saturation and endpoint relative permeability (S_{jrc}, k°_{rjc}) at the highest capillary number each investigator obtained (Table 7.4.1). Shown in Figures 7.4.7 through 7.4.9 are comparisons of predicted and experimental aqueous phase endpoint relative permeabilities. The excess brine endpoint relative permeabilities (k°_{r1}) of Exp. CDC are also compared with the computed values (Figure 7.4.10) substituting residual microemulsion (S_{3r}) to oil for residual oil in Equation 7.22b. The agreement between the predicted and experimental values is excellent considering the errors involved in both residual saturation and endpoint relative permeability measurements as well as in the capillary number.

Oil endpoint relative permeabilities were also calculated in the same manner using residual aqueous (or microemulsion for Exp. CDC) saturation in Equation 7.23b (Section 7.1.2). The predicted oil phase endpoint relative permeabilities are in fair agreement with the experimental data (Figures 7.4.11 - 7.4.13).

- Hirasaki's Model

A similar calculation was performed using the equations developed by Hirasaki et al. The trapping functions (Eqs. 7.1 - 7.4) reduce to the following for

two-phase flow displacements.

- Trapping of aqueous (or microemulsion) phase with oil phase is

$$S_{1r} = g(\sigma_{om})$$

- Trapping of oil by aqueous phase is

$$S_{2r} = f(\sigma_{om})$$

Equations 7.12 and 7.13 were then used to calculate the endpoint relative permeabilities using the experimentally obtained residual saturations. The endpoints were calculated for two cases as follows,

1- use a value of 1.0 for all k°_{rjc}

2- use the residual saturation and endpoint relative permeability at the highest capillary number that each investigator obtained.

The computed endpoint relative permeabilities for aqueous and oleic phases are in Figures 7.4.7 through 7.4.13.

The calculated endpoints using Hirasaki's model with $k^{\circ}_{rjc} = 1.0$ are close to values predicted from Lake's model. The use of non-unit high capillary endpoints in

Hirasaki's expression gives values that are too low compared to the experimental data.

7.4.3 Prediction of Exponent of Relative Permeability Curves as a Function of Capillary Number

Camilleri et al. [C.0] proposed relationship to calculate exponents of the relative permeability curves as a function of capillary number. Similar to the endpoint relative permeabilities in Lake's model, the exponents are computed as linear interpolation between the water/oil exponents and the microemulsion/oil exponents.

$$n_1 = n_{1w} + \frac{S_{2rw} - S_{2r}}{S_{2rw}} (n_{1c} - n_{1w}) \qquad (7.30a)$$

$$n_2 = n_{2w} + \frac{S_{1rw} - S_{1r}}{S_{1rw}} (n_{2c} - n_{2w}) \qquad (7.31a)$$

Here, n_{1c} and n_{2c} were assumed to be 1.0. Thus, n_1 and n_2 are equal to 1.0 when the residuals are zero for the trapped phase.

More general forms of the above equations which account for the case where exponents are 1.0 at non-zero trapped saturations (S_{jrc}) are as follows

$$n_{1c} = n_{1w} + \frac{S_{2rw} - S_{2r}}{S_{2rw} - S_{2rc}} (n_{1c} - n_{1w}) \qquad (7.30b)$$

$$n_{2c} = n_{2w} + \frac{S_{1rw} - S_{1r}}{S_{1rw} - S_{1rc}} (n_{2c} - n_{2w}) \qquad (7.31b)$$

To test the above relationships, the experimental data of Amaefule and Handy was used. The exponents at various capillary numbers were found by matching the relative permeability curves against the exponential function (Eq. 7.29). The exponents for oil and aqueous phases are in Table 7.4.2. The aqueous phase exponents show no significant change with the capillary number. Thus, the oil phase exponents were used to test both the Equation 7.31b and the relationship proposed by Hirasaki (Eq. 7.16). Figure 7.4.14 shows the comparison between the experimental data and the predicted oil exponents as a function of capillary number. The agreement between the values computed using Equation 7.31b and experimental data is remarkable. The calculated exponents using Hirasaki's expression for both $n_{2c} = 1.0$ and $n_{2c} \neq 1.0$ are consistently higher than the experimental values.

TABLE 7.4.1

Endpoint Relative Permeability and Residual Saturations
at Low and High Capillary Numbers

	Abrams [A.1]	Amaefule [A.2]	Bhuyan [B.2]	Delshad (Exp.CDC)
S_{1rw}	-	0.40	0.391	0.35
S_{2rw}	0.33	0.20	0.33	0.30
k°_{r1w}	0.078	0.130	0.116	0.0933
k°_{r2w}	-	0.76	0.53	0.918
S_{1rc} $[g(\sigma_{om})]$	-	0.28	0.074	-
S_{2rc} $[f(\sigma_{om})]$	0.138	0.02	0.003	-
S3r to oil and brine $[g(\sigma_{om}, g(\sigma_{mw})]$	-	-	-	0.0
k°_{r1c}	0.64	0.96	1.0	0.89
k°_{r2c}	-	1.0	0.89	0.941

TABLE 7.4.2

Exponent of Relative Permeability Curves of Amaefule at Various Capillary Numbers

N_c^{ave}	n_1	n_2	S_{1rc}
8.7×10^{-6}	2.09	2.59	-
7×10^{-4}	2.27	2.32	-
3×10^{-3}	2.39	1.67	-
0.012	2.05	$1.43(n_{2c})$	0.20

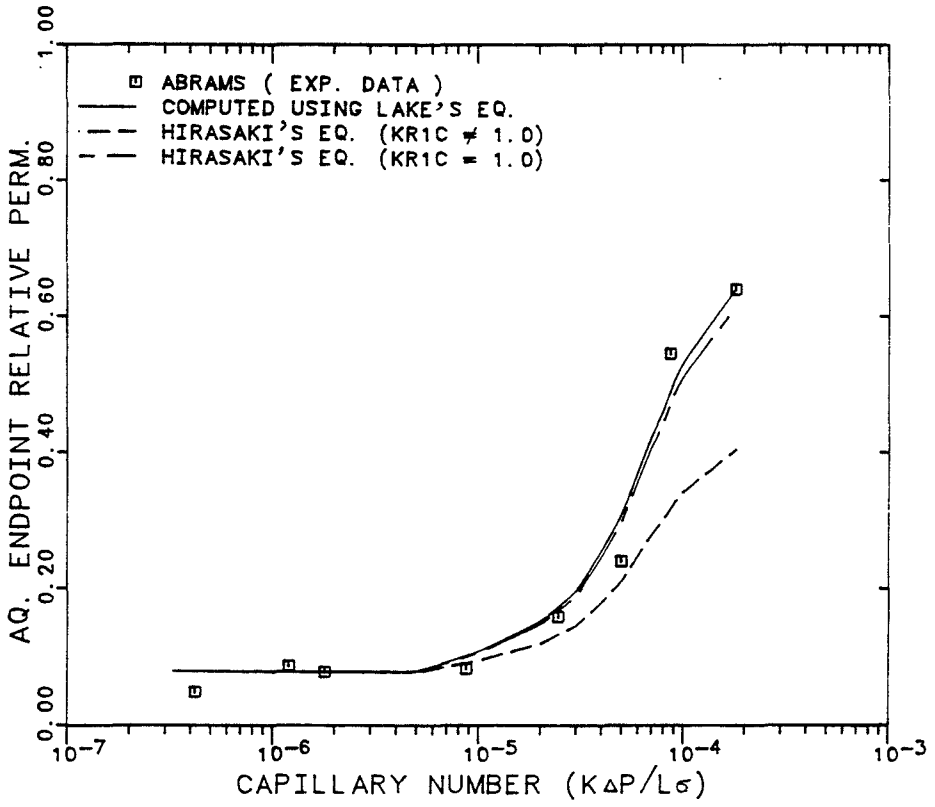

Figure 7.4.7 Comparison of Computed and Experimental Aqueous Phase Endpoint Relative Permeability (Abrams's Data)

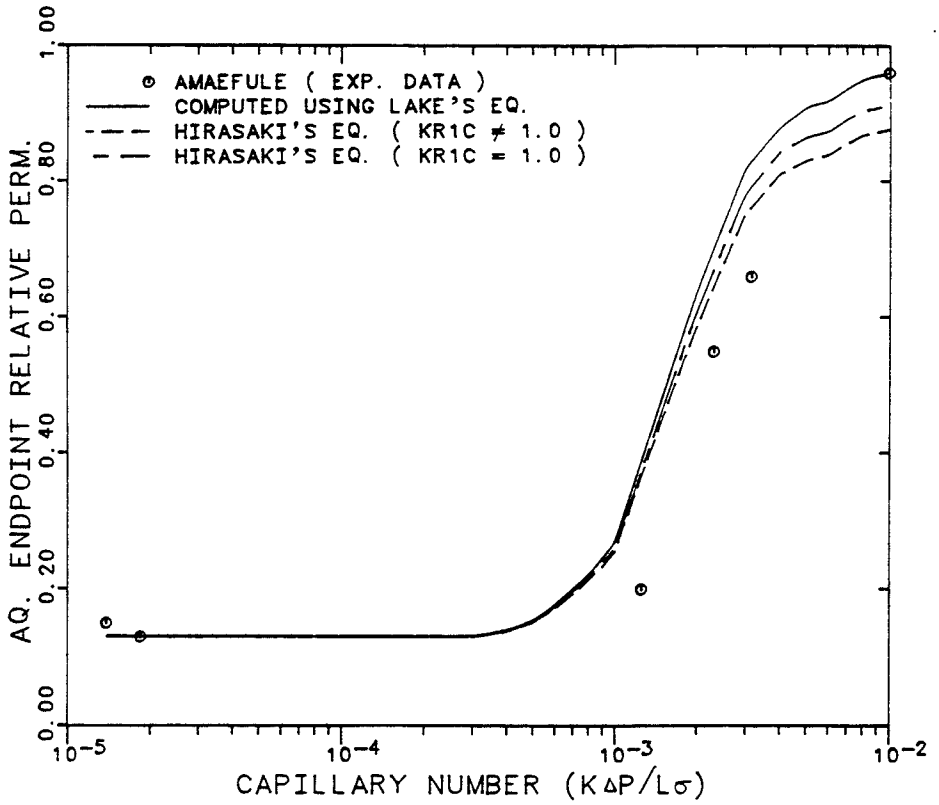

Figure 7.4.8 Comparison of Computed and Experimental Aqueous Phase Endpoint Relative Permeability (Amaefule's Data)

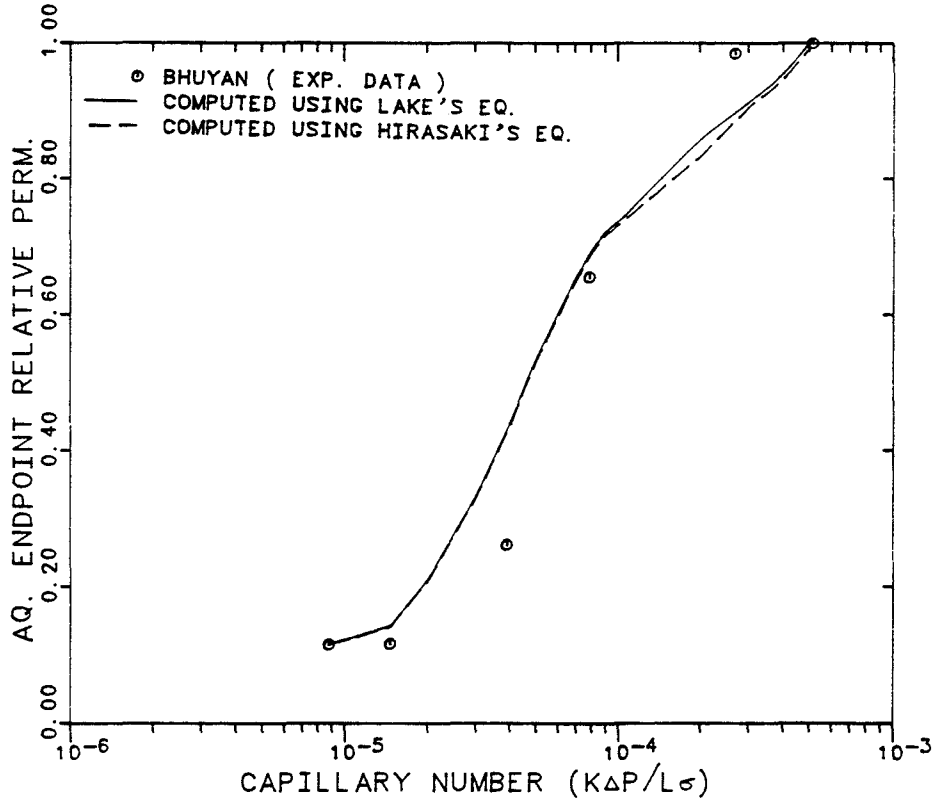

Figure 7.4.9 Comparison of Computed and Experimental Aqueous Phase Endpoint Relative Permeability (Bhuyan's Data)

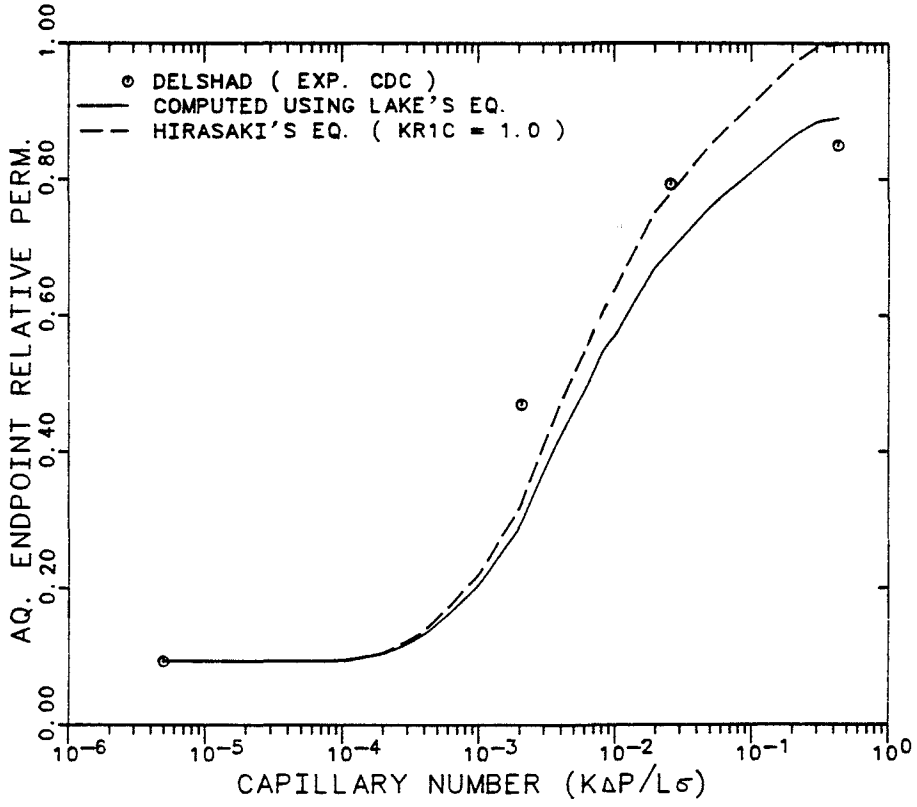

Figure 7.4.10 Comparison of Computed and Experimental Aqueous Phase Endpoint Relative Permeability (Exp. CDC)

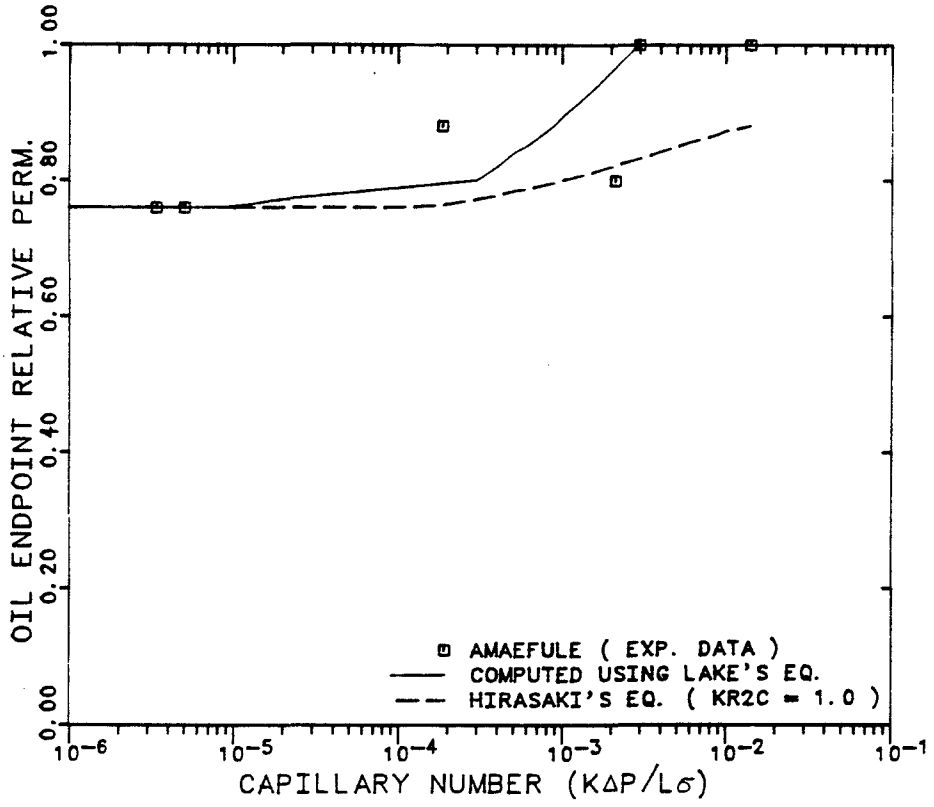

Figure 7.4.11 Comparison of Computed and Experimental Oleic Phase Endpoint Relative Permeability (Amaefule's Data)

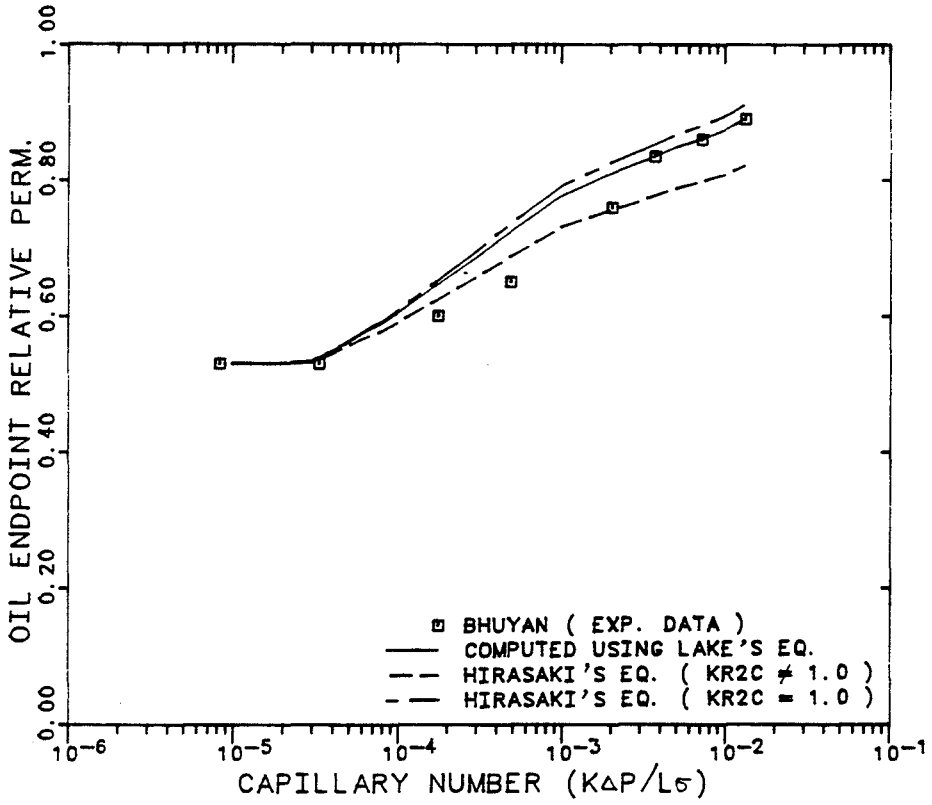

Figure 7.4.12 Comparison of Computed and Experimental Oleic Phase Endpoint Relative Permeability (Bhuyan's Data)

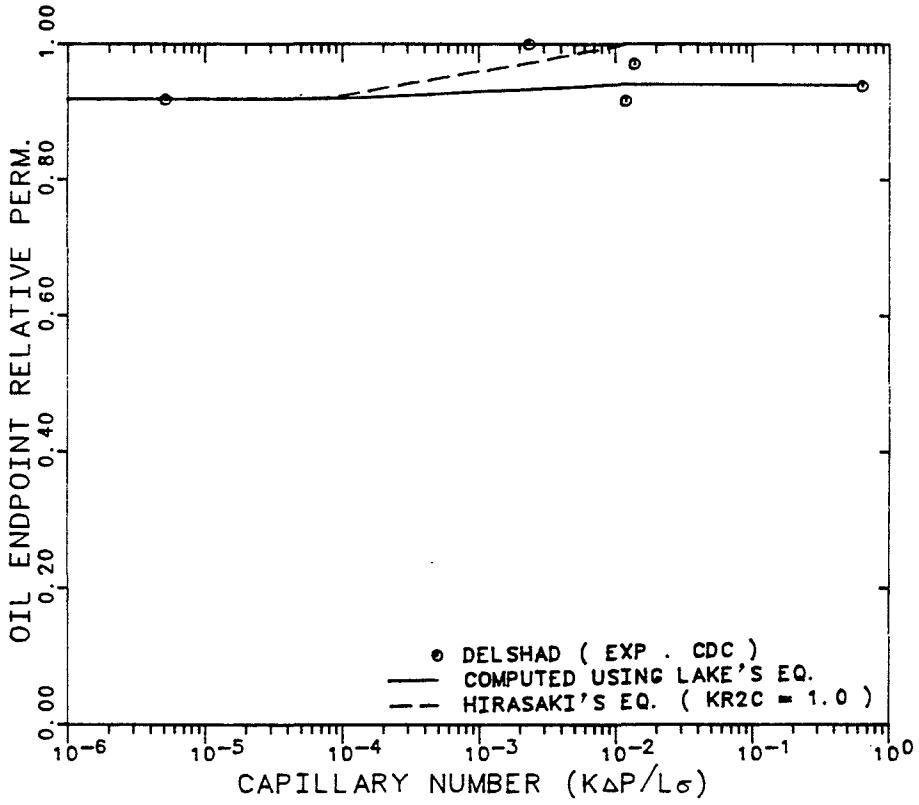

Figure 7.4.13 Comparison of Computed and Experimental Oleic Phase Endpoint Relative Permeability (Exp. CDC)

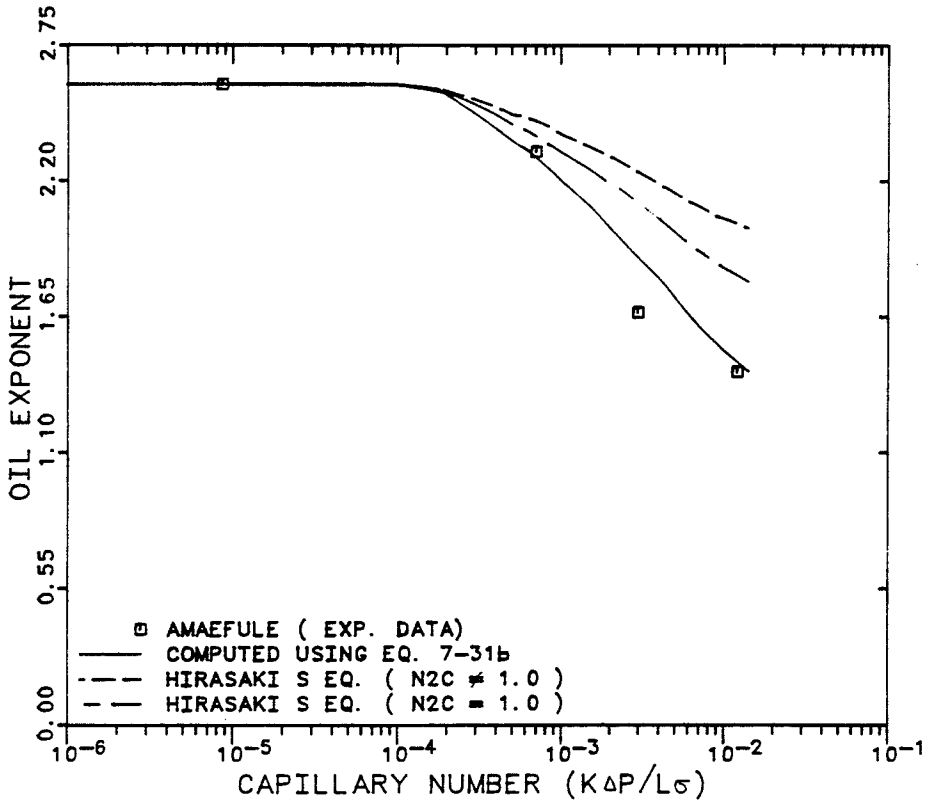

Figure 7.4.14 Comparison of Computed and Experimental Exponent of Oil Relative Permeability Curve (Amaefule's Data)

7.4.4 Summary

The new three-phase relative permeability model proposed here (Eq. 7.29) is a simple, exponential function capable of predicting phase relative permeability as a function of its own saturation at various capillary numbers (N_c). This model also treats each phase independently and does not make assumptions regarding the wettability of the phases. The dependence of the new model on capillary number is through the dependence of its parameters on capillary number. The necessary parameters of the model are endpoint relative permeability (k°_{rj}), exponent (n_j), and residual saturation (S_{jr}) of each phase.

When experimental values of the parameters are not available, the endpoint relative permeabilities and exponents can be calculated as a function of N_c using Equations 7.22b, 7.23b; 7.30b, and 7.31b, respectively. These equations were tested and compared with the available experimental data of oil and brine phases in Sections 7.4.2 and 7.4.3. But, due to the lack of experimental data, these relationships were not tested for the microemulsion phase.

The residual saturations used in this model are based on the experimental values obtained during single-

phase displacements. There are some uncertainties regarding the values of residual saturation during three-phase flow. The uncertainty arises due to the following

- The residual saturation may depend on whether or not a third phase is present.

- The residual saturation of a phase depends on the properties of the displacing phase.

For instance, the residual microemulsion (S_{3r}) to oil may be different from the residual microemulsion to brine at the same N_c due to differences in interfacial tension values ($\sigma_{mo} \neq \sigma_{mw}$ at non-optimal microemulsion formulation) and to differences in the degree of wettability of microemulsion compared to oil or brine. In the present work, the arithmetic average of the two values (S_{3r} to oil and S_{3r} to brine) were used as an approximation for residual microemulsion during three-phase flow. The same interpretation is also applied to the excess phases. There are some work that needs to be done to resolve the issue of residual saturation during three-phase flow.

CHAPTER 8

DISCUSSION OF PAPER BY RAIMONDI AND TORCASO

This chapter deals with equilibrium in miscible flow studied by Raimondi and Torcaso [R.1] in 1965. Equilibrium between phases is a very important subject in the single well chemical tracer test for measuring residual oil saturation [D.5,T.6] and other applications such as oil recovery by extraction [T.2] or chromatography [C.1].

The production of hydrocarbons by gas cycling, enriched gas drive and CO_2 or alcohol flooding involves relative motion between two phases and solutes which are mutually soluble. The solute is carried forward at a velocity lower than the average velocity. This retardation is caused by chromatographic absorption in the slower flowing phase and by the degree of departure from equilibrium.

Raimondi and Torcaso developed a method to predict the velocity of a solute slug and peak height and then compared these values with those of experimental results to determine when the assumption of equilibrium is valid.

A more thorough analysis of their results showed that equilibrium was not reached in some of their experiments even though they concluded the opposite.

8.1 A Brief Review of the Raimondi and Torcaso's Paper

Raimondi and Torcaso (R-T) used a variety of porous media with a mobile phase containing a small amount of solute and a stationary phase (either the oleic or the aqueous phase) to study the movement of the solute. They investigated the effect of parameters such as flow rate, type of porous media, partition coefficient and carrier phase on equilibrium in the absence of segregation and fingering. Their procedure was the following:

1- Saturate the core with a mobile and a stationary phase.

2- Inject a slug made of the same fluid as the mobile phase and a small concentration of a mutually soluble solute.

3- Measure the lag and the peak height of the slug

at arrival.

4- Combine the principle of chromatography with the convection-dispersion equation to predict the velocity of a solute slug compared to the bulk velocity and the peak height of a slug. The prediction is valid under equilibrium conditions only.

5- Compare the experimental and theoretical results to measure the departure from equilibrium.

They performed the experiments in three different Berea sandstone cores and one sandpack. Their properties are listed in Table 8.1.

R-T used ethyl benzene (EB) as the oleic phase, 2 percent NaCl brine as the aqueous phase, and the solutes were iso-propyl alcohol (IPA), tert-butyl alcohol (TBA), iso-butyl alcohol (IBA), and benzyl alcohol (BA). Table 8.2 gives the concentration and reported partition coefficient ($K = C_{sw}/C_{so}$) of solutions of these fluids.

Tables 8.3 through 8.5 show the calculated values of the arrival of the leading edge of the slug and peak height together with the observed values.

The R-T conclusions based on their experimental results were

- Mass transfer between phases takes place under equilibrium conditions since the volume at peak arrival

agrees well with the volume calculated from equilibrium data.

- Equilibrium conditions exist at relative velocities between phases as high as 100 ft/day for consolidated cores and up to 500 ft/day in unconsolidated media.

8.2 Analysis of the Raimondi and Torcaso Results using a Capacitance-Dispersion Model

To analyze the solute breakthrough curves, I took an approach different from that of the R-T. The basic differences are

- I analyzed the entire breakthrough curve while R-T considered only the peak height and the arrival time of the peak in their analysis.

- I estimated the saturations from matching the breakthrough curves against the capacitance-dispersion model. Their only estimate of saturation was from the material balance.

Shown in Figures 8.1 through 8.4 are the R-T results which I analyzed using the capacitance-dispersion model. This model was used since non-equilibrium or microscoping bypassing are evident in these experiments. The evidences that suggest non-equilibrium behavior (in Figures 8.2 through 8.4) are

- Asymmetry in the effluent concentration histories, and

- Effect of velocity on the breakthrough curves. This is indicated as the shift in the volume at peak concentration with a change in velocity. The velocity should have no effect on the solute breakthrough curve if

there exists equilibrium.

In summary, I analyzed the breakthrough curves using the capacitance-dispersion model to investigate the following:

1- the magnitude of non-equilibrium.

2- the error involved in estimating the saturations when the assumption of equilibrium is imposed.

TABLE 8.1 (after Raimondi and Torcaso[R.1])

PROPERTIES OF CORES

Core	Type of Porous Medium	Length (cm)	Diameter (cm)	Pore Volume (ml)	Permeability (Darcys)	Porosity (Per Cent)
A	Consolidated Berea	70	5.08	336	0.650	23.6
B	Consolidated Berea	183	5.08	755	0.181	20.4
C	Consolidated Berea	365	5.08	1525	u.315	20.6
D	30-35 Mesh Glass Beads	183	2.54	325	49.5	35.2

TABLE 8.2 (after Raimondi and Torcaso [R.1])

PARTITION COEFFICIENT K

	Starting Liquids			Equilibrated Liquids			
	Aqueous		Oleic	Aqueous	Oleic		
Liquid or Slug Designation	Solute (Per Cent)	Brine (Per Cent)	Ethyl Benzene (Per Cent)	Solute C_{sw} (Per Cent)	Solute C_{so} (Per Cent)	Partition Coefficient, K C_{sw}/C_{so}	
5-IPA-Na	4.76 IPA	95.24	100	4.55	0.50	9.1	9.1 avg.
5-TBA-Na	4.76 TBA	95.24		4.23	1.23	3.4	
2.5-TBA-Na	2.44 TBA	97.56		1.50	0.82	2.6	3.0 avg.
5-IBA-Na	4.76 IBA	95.24		3.1	3.86	0.80	
2.5-IBA-Na	2.44 IBA	97.56		1.72	1.66	1.03	0.91 avg.
5-BA- EB	4.76 BA	95.24		1.65	3.88	0.42	
2.5-BA-Na	2.44 BA	97.56		1.08	3.14	0.34	0.38 avg.
2.5-IBA-W	2.44 IBA	97.56		2.13	1.76	1.21	1.21 avg.
6-Brine							∞

TABLE 8.3 (after Raimondi and Torcaso [R.1])

BEHAVIOR OF AN AQUEOUS SLUG, EFFECT OF SOLUTE ON PEAK ARRIVAL AND ON C_{max}/C_o, CORE B, S_{or} 30 PER CENT, v = 32.7 FT/DAY, SLUG VOLUME 50 ML

Run No.	Type of Slug	K, Partition Coefficient	K , Solute Fraction in Aqueous Phase	V_{tw}, Volume Produced at Peak Arrival		C_{max}/C_o Peak Concentration	
				Calc. ml	Exp'l. ml	Calc. (Per Cent)	Exp'l. (Per Cent)
1	6-brine	∞	1	553	555	–	53
2	5-IPA-Na	9.1	0.95	585	570	52	48
3	5-TBA-Na	3.0	0.88	630	605	46	45
4	5-IBA-Na	0.91	0.68	820	770	32	28
5	2.5-BA-Na	0.38	0.47	1180	1140	19	18

TABLE 8.4 (after Raimondi and Torcaso [R.1])

BEHAVIOR OF AN AQUEOUS SLUG.
EFFECT OF RATE ON PEAK ARRIVAL AND ON C_{max}/C_o.

Run No.	Velocity (ft/day)	Type of Slug	a, Coefficient of Mixing (cm)	V_{tw}, Volume Produced at Peak Arrival		C_{max}/C_o Peak Concentration	
				Calc. (ml)	Exp'l. (ml)	Calc. (Per Cent)	Exp'l. (Per Cent)
		Core B, S_{or} 30%, Slug Volume 50 ml, Solute BA					
6	3.27	6-Brine	0.30	553	550	—	59
		2.5-BA-Na	–	1180	1190	22.5	21
5	32.7	6-Brine	0.39	553	560	–	53
		2.5-BA-Na	–	1180	1140	19	18
8	98.5	6-Brine	0.42	553	555	–	51
		2.5-BA-Na	–	1180	1170	17.5	17
		Core A, S_{or} 32%, Slug Volume 40 ml, Solute BA					
9	0.29	6-Brine	–	–	–	–	–
		2.5-BA-Na	–	515	540	–	31
10	2.94	6-Brine	0.25	250	250	–	78
		2.5-BA-Na	–	515	525	24.5	26
11	29.4	6-Brine	0.33	250	255	–	66
		2.5-BA-Na	–	515	490	21	23
		Core D, S_{or} 17%, Slug volume 20 ml, Solute IBA					
15	8.6	Brine	0.067	–	–	–	–
		2.5-IBA-W	–	328	321	71	61
16	41	Brine	0.035	268	268	–	–
		2.5-IBA-W	–	328	310	63	53
17	472	Brine	0.25	268	268	–	–
		2.5-IBA-W	–	328	307	41	37

TABLE 8.5 (after Raimondi and Torcaso [R.1])

BEHAVIOR OF AN OLEIC SLUG, CORE C, S_{wi} 36.5 PER CENT,
SLUG VOLUME 100 ML, SOLUTE BA, K' 0.824

Run No.	Velocity (ft/day)	Type of Slug	Coefficient of Mixing (cm)	V_{tw}, Volume Produced at Peak Arrival		C_{max}/C_o Peak Concentration	
				Calc. (ml)	Exp'l. (ml)	Calc. (Per Cent)	Exp'l. (Per Cent)
13	3.64	5-N-EB	.485	1020	1030	–	69
		5-BA-EB	–	1230	1200	55	50
14	36.4	5-N-EB	.776	1020	1020	–	57
		5-BA-EB	–	1230	1230	44	44

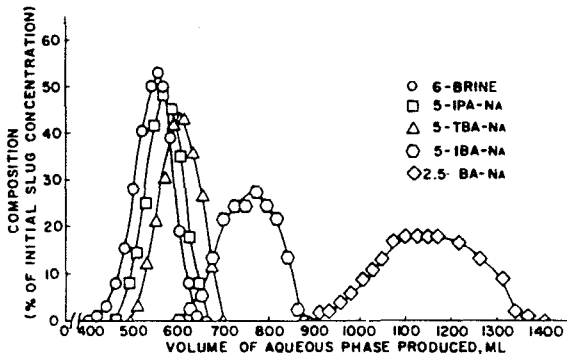

Figure 8.1 Behavior of Aqueous Slugs Composed of Different Solute Flowing Past a Stationary Oleic Phase Core B, S_{or} =30%, Slug Volume 50cc ,v=32.7 ft/day(after Raimondi and Torcaso [R.1])

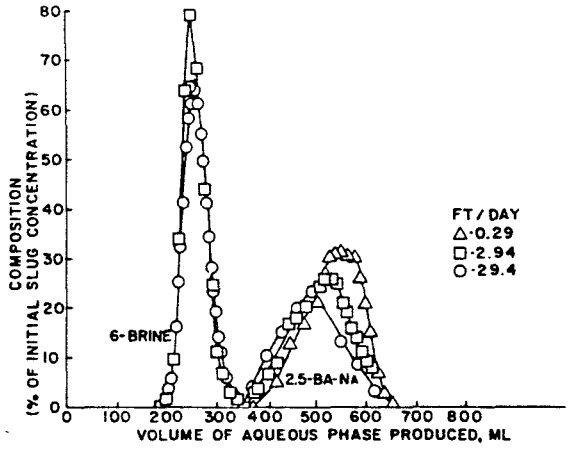

Figure 8.2 Effect of Velocity on the Movement of Aqueous Slug Flowing Past a Stationary Oleic Phase Core A, S_{or} =32%, Slug Type 2.5 -BA-NA, Slug Volume 40cc(after Raimondi and Torcaso[R.1])

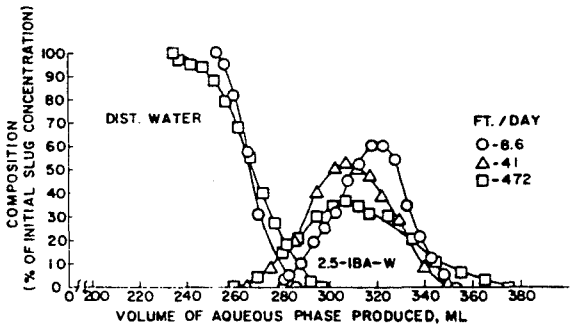

Figure 8.3 Effect of Velocity on the Movement of Aqueous Slug Flowing Past a Stationary Oleic Phase Core D, S_{or} =17%, Slug Type 2.5-IBA-W, Slug Volume 20cc (after Raimondi and Torcaso[R.1])

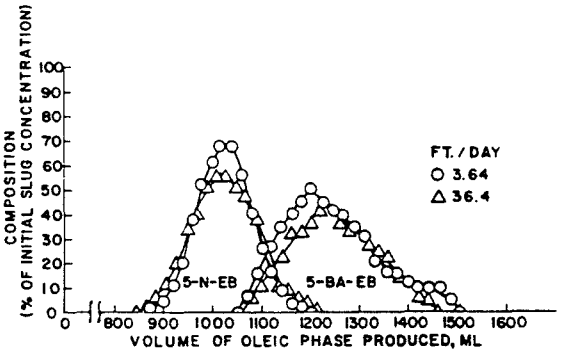

Figure 8.4 Effect of Velocity on the Movement of Oleic Slug Flowing Past a Stationary Aqueous Phase Core C, S_{wi} =36.5%, Slug Type 5-BA-EB, Slug Volume 100cc (after Raimondi and Torcaso[R.1])

8.2.1 Effect of Solute Type on Equilibrium

R-T performed several experiments using aqueous slugs composed of different solutes flowing past a residual oleic phase at a constant velocity. In order to determine the value of dispersivity, the displacement was first performed using an inert tracer (6 percent NaCl brine) which is soluble only in the mobile (brine) phase.

The breakthrough curve of the inert tracer in brine phase, Figure 8.5, was matched with the solution of the convection-dispersion (C-D) equation using their material balance saturations (brine saturation (S_1 = 0.70) and oil saturation (S_{2r} = 0.30) reported by R-T). The estimated dispersivity (α) was 0.40 cm as compared to the value of 0.39 cm in their paper.

The first partitioning tracer used was 5-IPA-Na (partition coefficient, C_{11}/C_{12} = 9.1) in a Berea core (L = 183 cm) at a velocity of 32.7 ft/day. The breakthrough curve was matched with the C-D equation (Figure 8.6). Since the solubility of the tracer is very low in the oleic phase, this tracer acts almost as an inert tracer.

Next, 5-TBA-Na with the partition coefficient 3.0 was used; its breakthrough curve is in Figure 8.7. I had to use the capacitance-dispersion model to match

these data. The best match was with the oil flowing fraction of F_2 = 0.80 which implies that only 80% of the residual oil was in the equilibrium with the flowing brine phase. The contribution of the remaining 20% was through diffusion with a mass transfer coefficient (M_{12}) of 10^{-6} sec^{-1}.

Similar data are shown for 5-IBA-Na and 2.5 BA-Na in Figures 8.8 and 8.9. The breakthrough curve of 5-IBA-Na was matched with the capacitance model with the oil flowing fraction of 0.85 and mass transfer coefficient of 10^{-6} sec^{-1} while the 2.5 BA-Na breakthrough curve was matched with the C-D equation. The high partition coefficient or solubility (C_{11}/C_{12} = 1.21) of 2.5 BA-Na caused a fast equilibration.

The conclusions based on these data are that equilibrium is achieved under these specific conditions when tracers with very high or very low partition coefficients are used, while a non-equilibrium model such as the capacitance-dispersion is required to explain the movement of tracers with a mid-range of partition coefficient.

EXPERIMENT NUMBER	FIG1
TRACER & PHASE	6-BRINE BR
FRACTIONAL FLOW	1 : 1.0
SLUG SIZE	0.066 P.V.
VELOCITY	32.7 FT/DAY

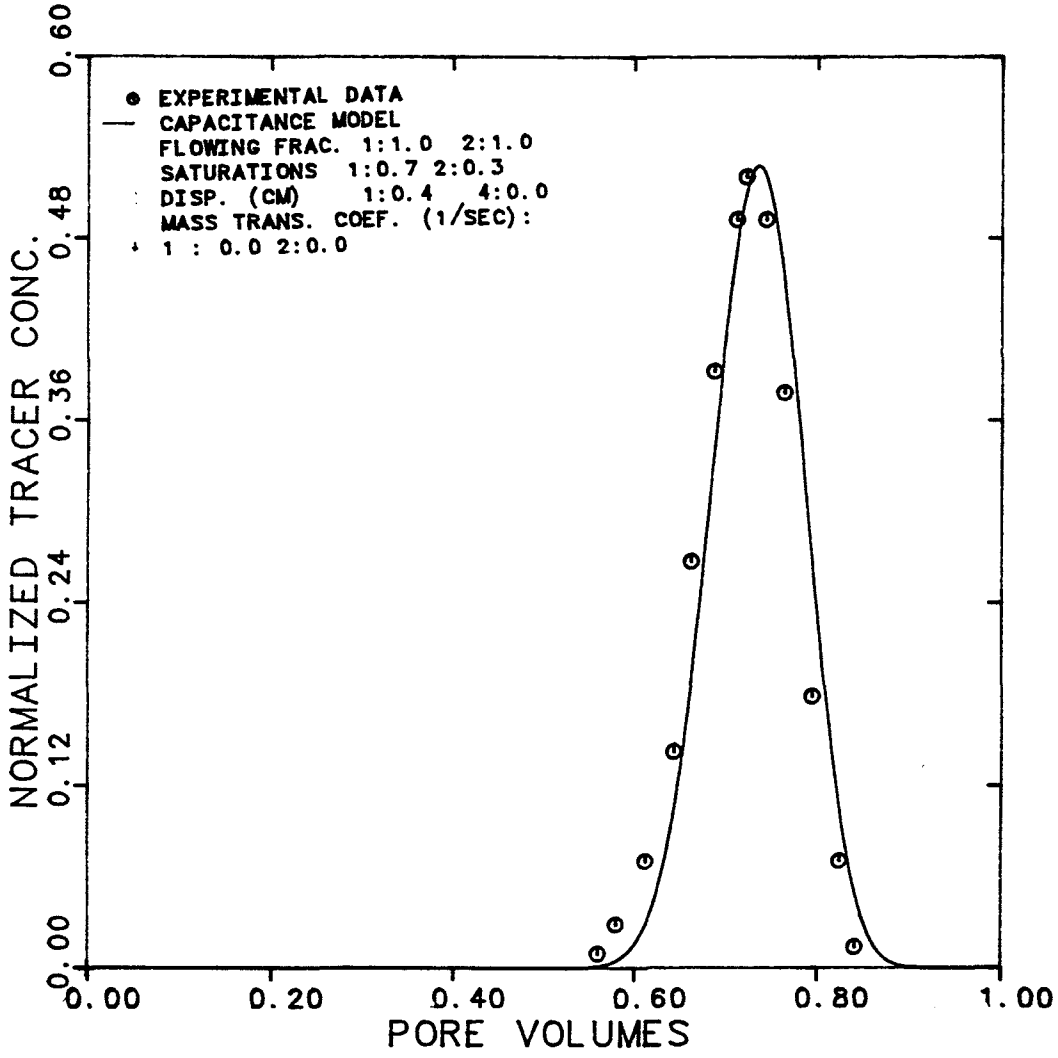

Figure 8.5 Effluent History for 6-Brine in Brine for Single-Phase Flow of Brine

EXPERIMENT NUMBER	FIG1
TRACER & PHASE	5-IPA-NA BR..
FRACTIONAL FLOW	1 : 1.0
SLUG SIZE	0.066 P.V.
VELOCITY	32.7 FT/DAY

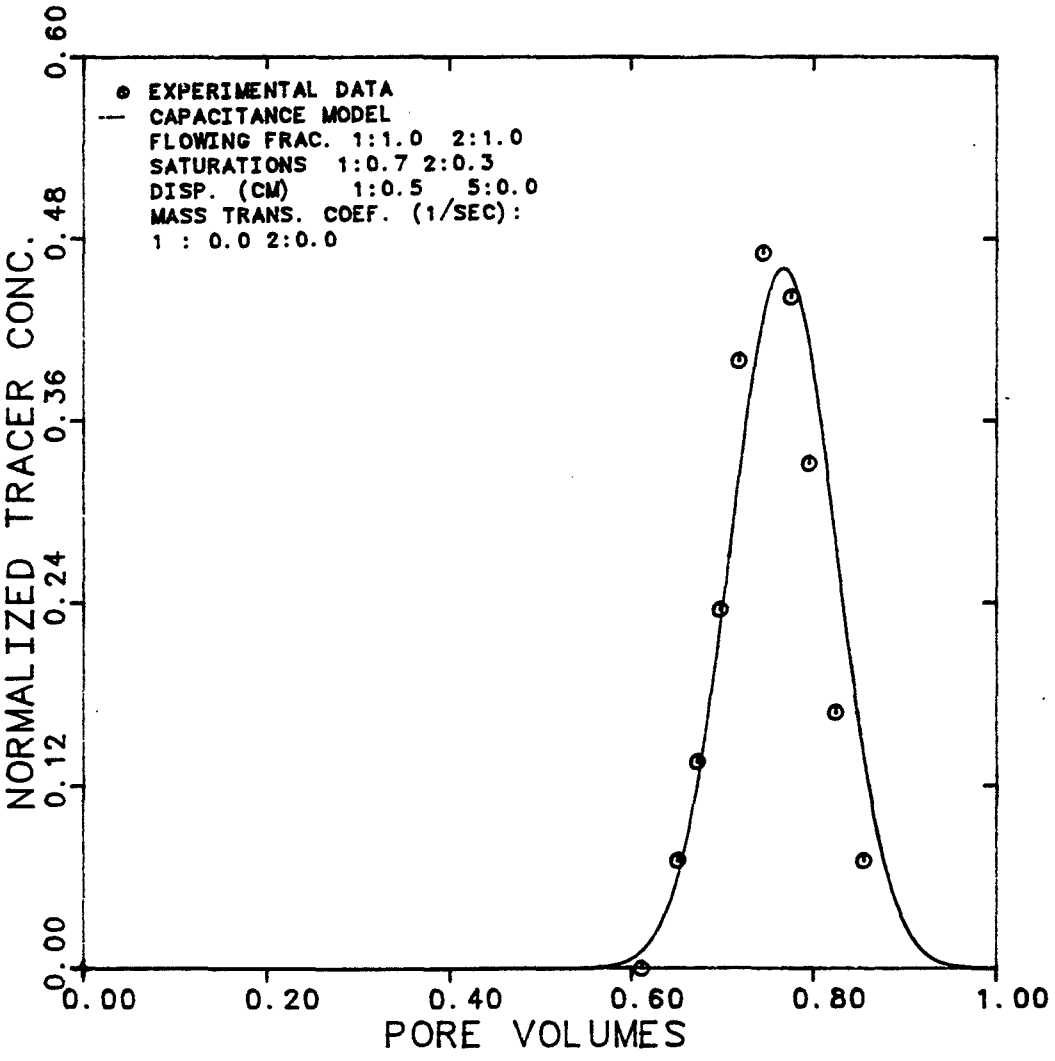

Figure 8.6 Effluent History for 5-IPA-NA in Brine for Single-Phase Flow of Brine

EXPERIMENT NUMBER	FIG 1
TRACER & PHASE	5-TBA-NA BRINE
FRACTIONAL FLOW	1: 1.0
SLUG SIZE	0.066 P.V.
VELOCITY	32.7 FT/DAY

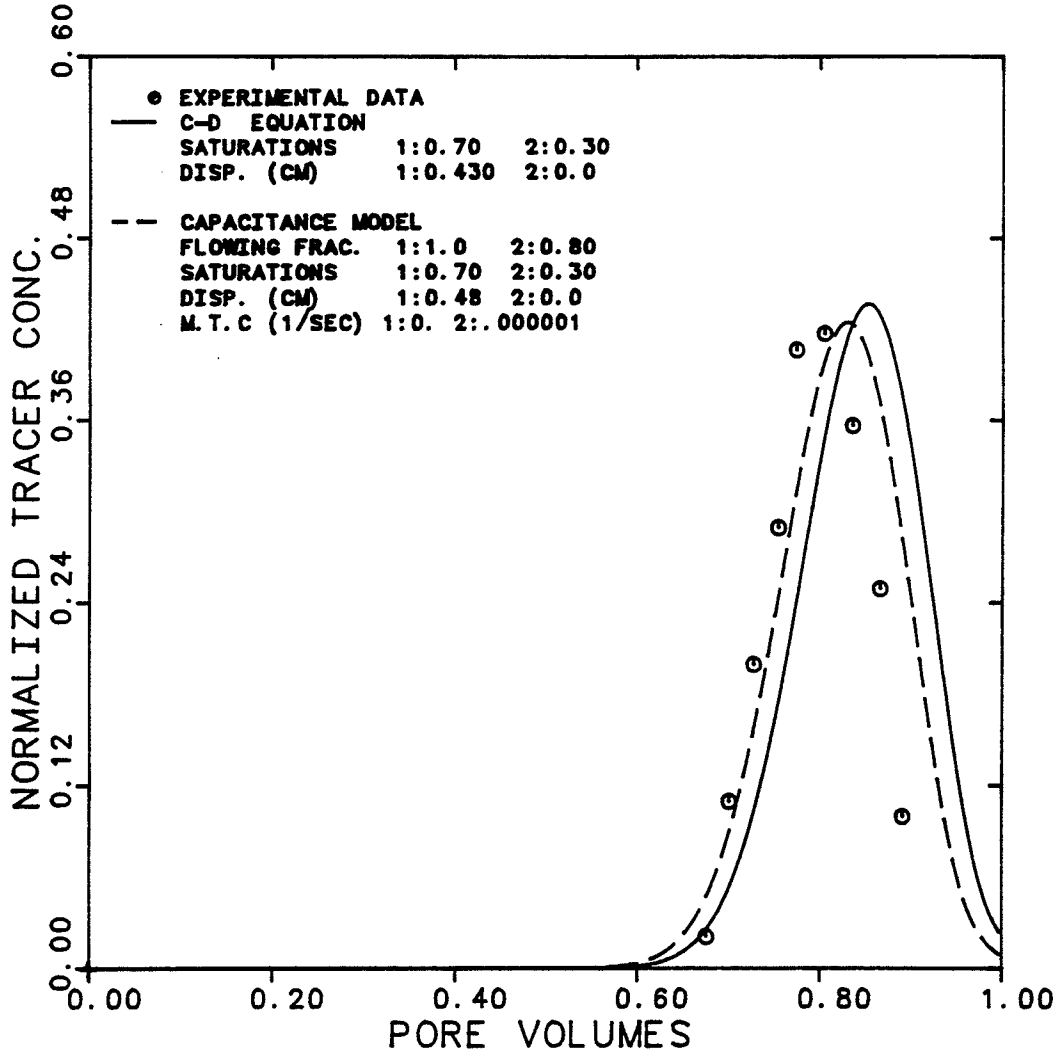

Figure 8.7 Effluent History for 5-TBA-NA in Brine for Single-Phase Flow of Brine

EXPERIMENT NUMBER	FIG 1
TRACER & PHASE	5-IBA-NA BRINE
FRACTIONAL FLOW	1: 1.0
SLUG SIZE	0.066 P.V.
VELOCITY	32.7 FT/DAY

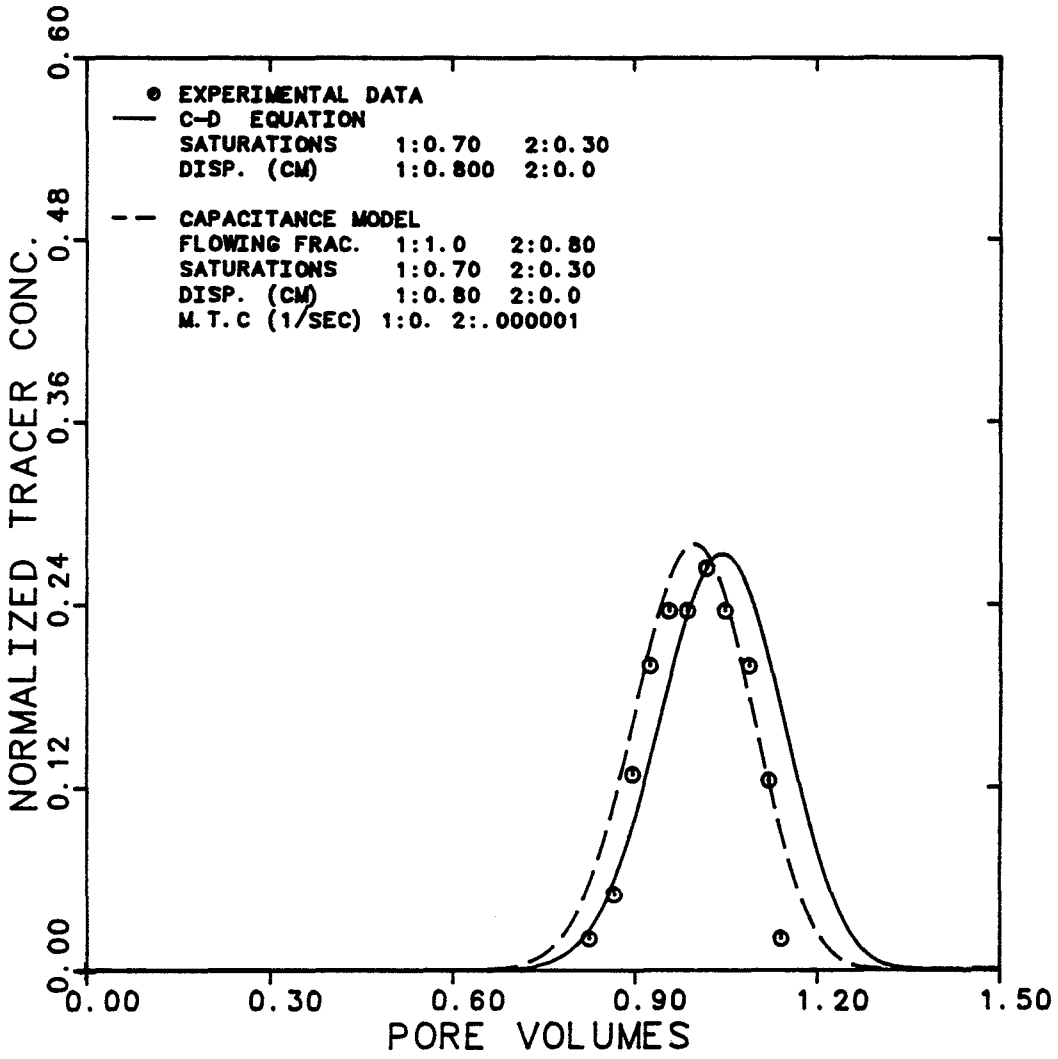

Figure 8.8 Effluent History for 5-IBA-NA in Brine for Single-Phase Flow of Brine

EXPERIMENT NUMBER	FIG1	
TRACER & PHASE	2.5-BA-NA	BR.
FRACTIONAL FLOW	1 : 1.0	
SLUG SIZE	0.066 P.V.	
VELOCITY	32.7	FT/DAY

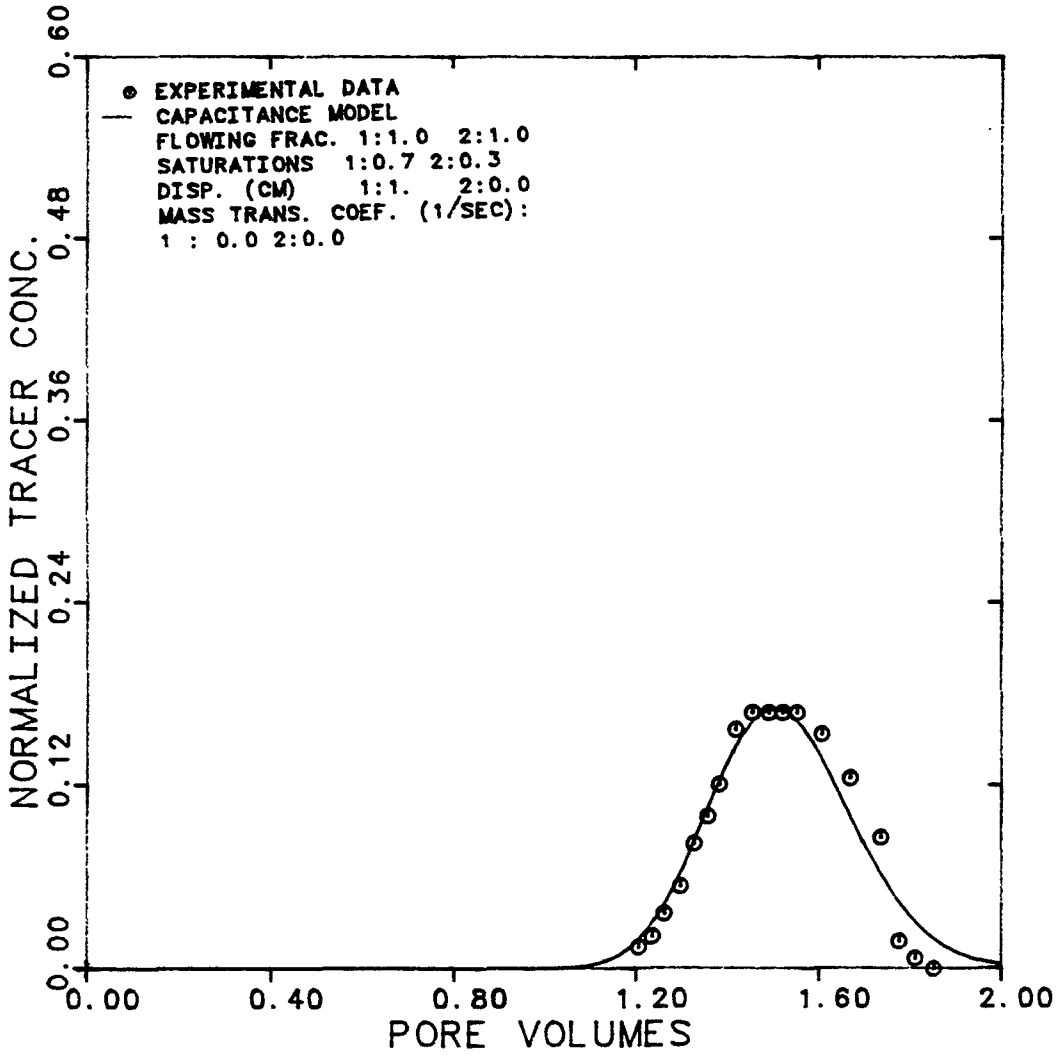

Figure 8.9 Effluent History for 2.5-BA-NA in Brine for Single-Phase Flow of Brine

8.2.2 Effect of Velocity on Equilibrium

The second set of experiments R-T performed was to investigate the effect of velocity on the breakthrough curves of an aqueous slug (2.5 BA-Na in brine) flowing past a residual oleic phase in a Berea core (L = 70 cm). Three different velocities were used: 0.29, 2.94, and 29.4 ft/day. Figures 8.10 through 8.12 show the breakthrough curves for these runs.

The theoretical curves of both the C-D equation and capacitance model were also generated using the material balance saturations of S_1 = 0.68 and S_{2r} = 0.32. These computed curves are also shown in Figures 8.10 through 8.12. The experimental data are matched better with the capacitance model and, as expected, the degree of non-equilibrium (indicated by the oil flowing fraction, F_2) is higher at higher velocities (0.95, 0.90 and 0.85).

The effect of velocity was also investigated for the aqueous slugs of 2.5-IBA-W flowing past a residual oil saturation in a 183 cm long glass bead pack. The velocities investigated were 8.6, 41 and 472 ft/day. Once again the capacitance model was used to match the breakthrough curves (Figures 8.13 through 8.15). Phase saturations used were the material balance data

(S_1 = 0.83, S_{2r} = 0.17) reported in their paper. The flowing fraction was 0.70 for the lowest velocity and 0.60 for the other two values.

R-T also performed an experiment to study the effect of velocity on the oleic slug flowing past an aqueous residual phase in a consolidated core with the length of 365 cm. Figures 8.16 through 8.18 show the effluent histories for the velocities of 3.64 and 36.4 ft/day. The breakthrough curve of the inert tracer (S-N-EB) in oil was matched well with the C-D equation using the material balance saturations reported in the paper and the dispersivity of 0.40 cm. The capacitance model was then used to match the data of partitioning tracer (5-BA-EB) in oil. The oil flowing fraction was 0.95 with the mass transfer coefficient of 10^{-7} sec^{-1} for both runs. This low degree of non-equilibrium of the non-wetting oil phase flowing past a wetting residual may be in part related to the long residence time of tracer due to the length of the core. Thus, there is more diffusion of tracer from the flowing to the dendritic portion of the oil phase.

EXPERIMENT NUMBER	FIG 3
TRACER & PHASE	2.5-BA-NA BRINE
FRACTIONAL FLOW	1: 1.0
SLUG SIZE	0.12 P.V.
VELOCITY	0.29 FT/DAY

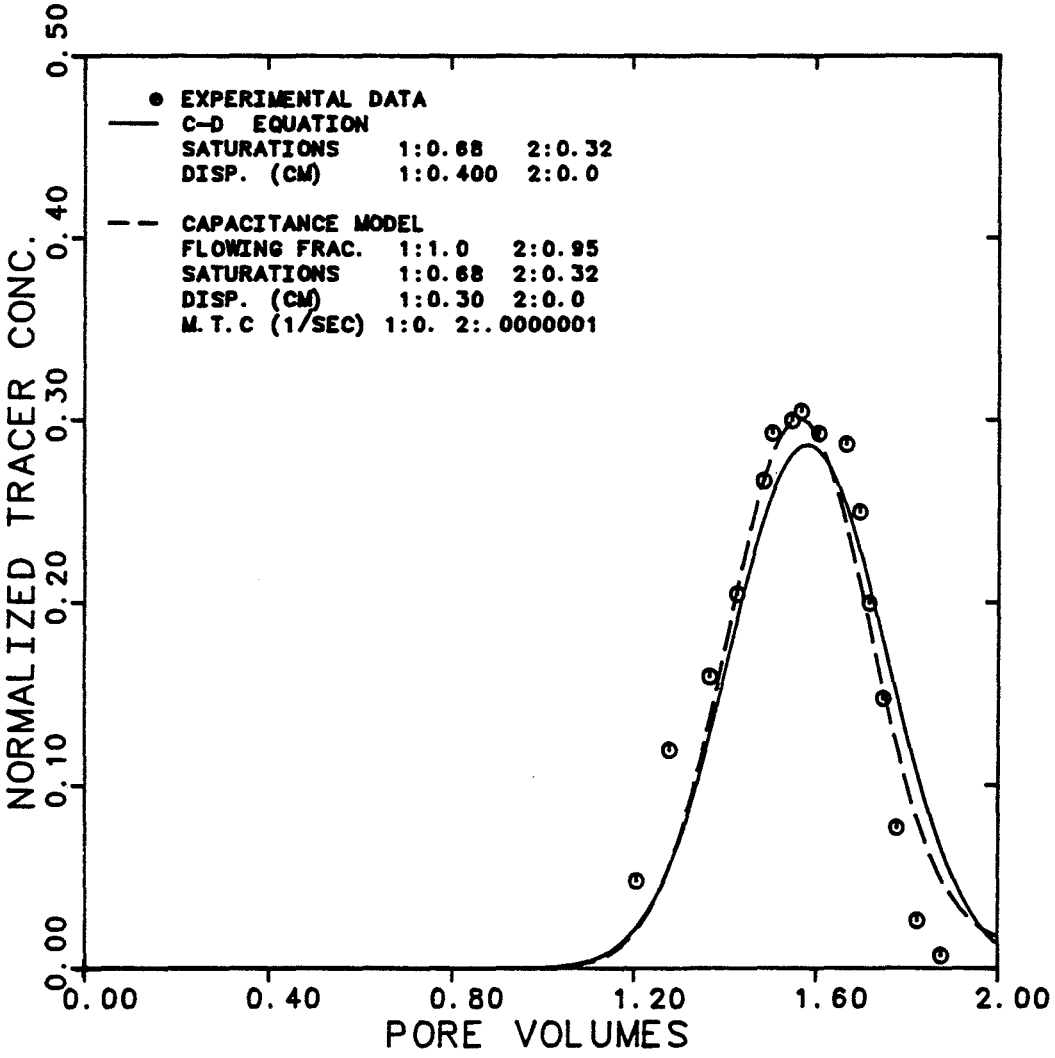

Figure 8.10 Effluent History for 2.5-BA-NA in Brine for Single-Phase Flow of Brine at 0.29 ft/day

EXPERIMENT NUMBER	FIG 3
TRACER & PHASE	2.5-BA-NA BRINE
FRACTIONAL FLOW	1: 1.0
SLUG SIZE	0.12 P.V.
VELOCITY	2.94 FT/DAY

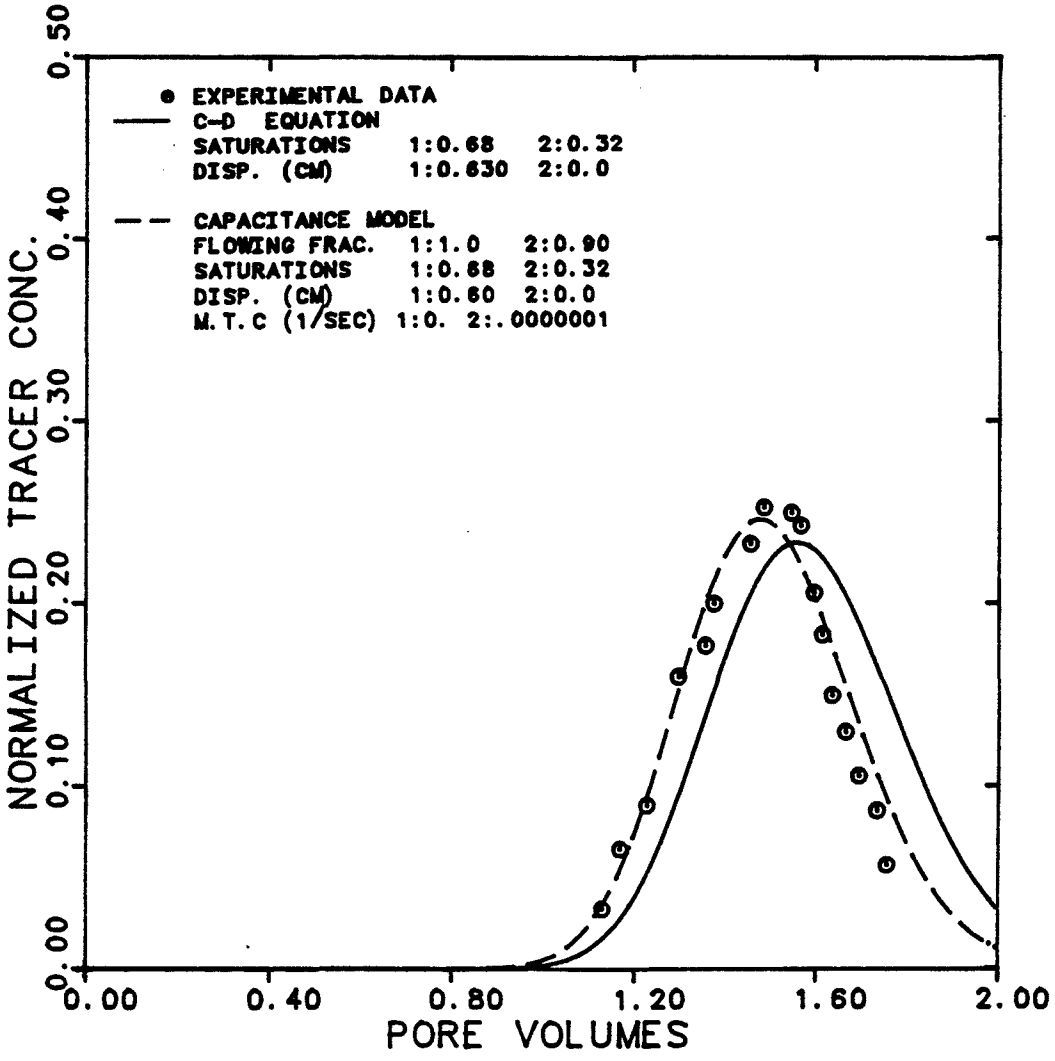

Figure 8.11 Effluent History for 2.5-BA-NA in Brine for Single-Phase Flow of Brine at 2.94 ft/day

EXPERIMENT NUMBER	FIG 3
TRACER & PHASE	2.5-BA-NA BRINE
FRACTIONAL FLOW	1: 1.0
SLUG SIZE	0.12 P.V.
VELOCITY	29.4 FT/DAY

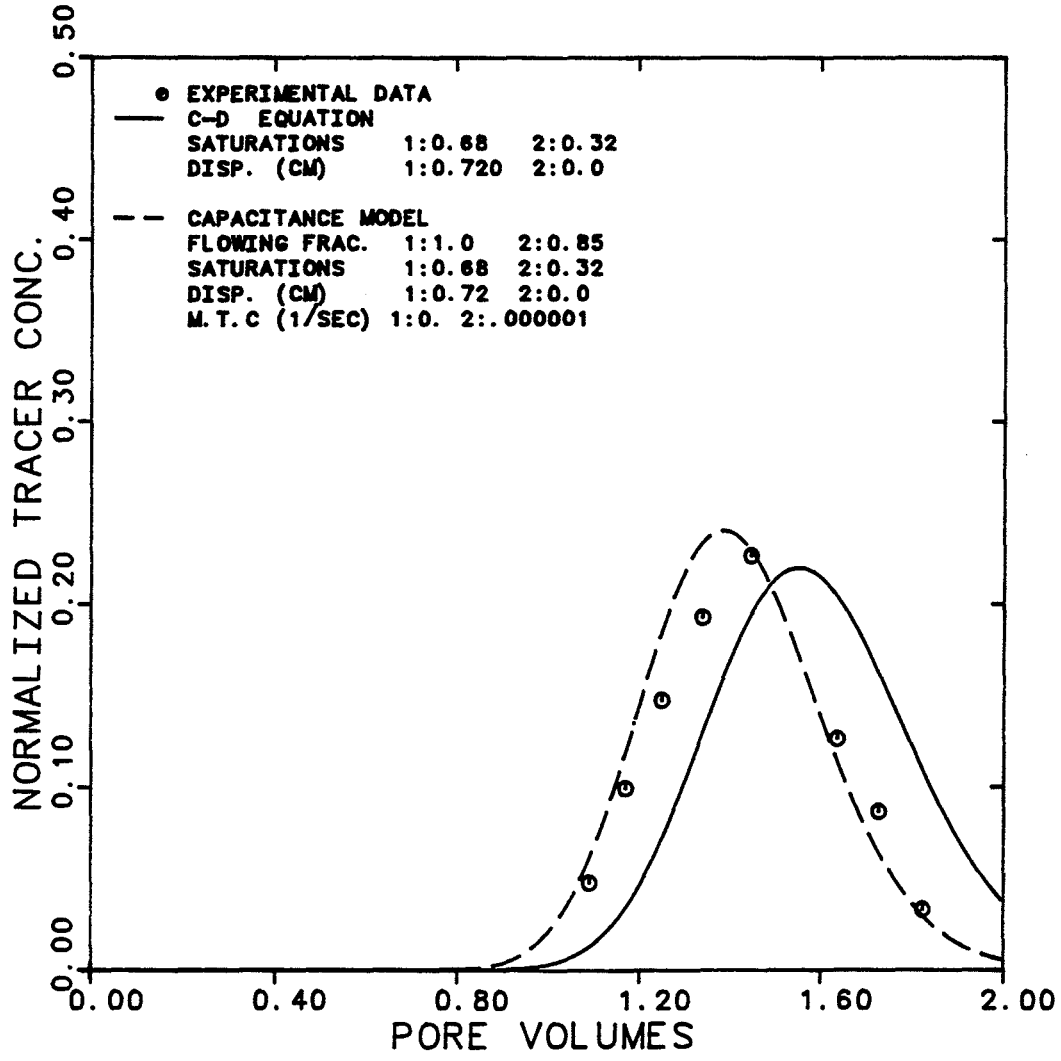

Figure 8.12 Effluent History for 2.5-BA-NA in Brine for Single-Phase Flow of Brine at 29.4 ft/day

EXPERIMENT NUMBER	FIG 4
TRACER & PHASE	2.5-IBA-W BRINE
FRACTIONAL FLOW	1: 1.0
SLUG SIZE	0.0615 P.V.
VELOCITY	8.6 FT/DAY

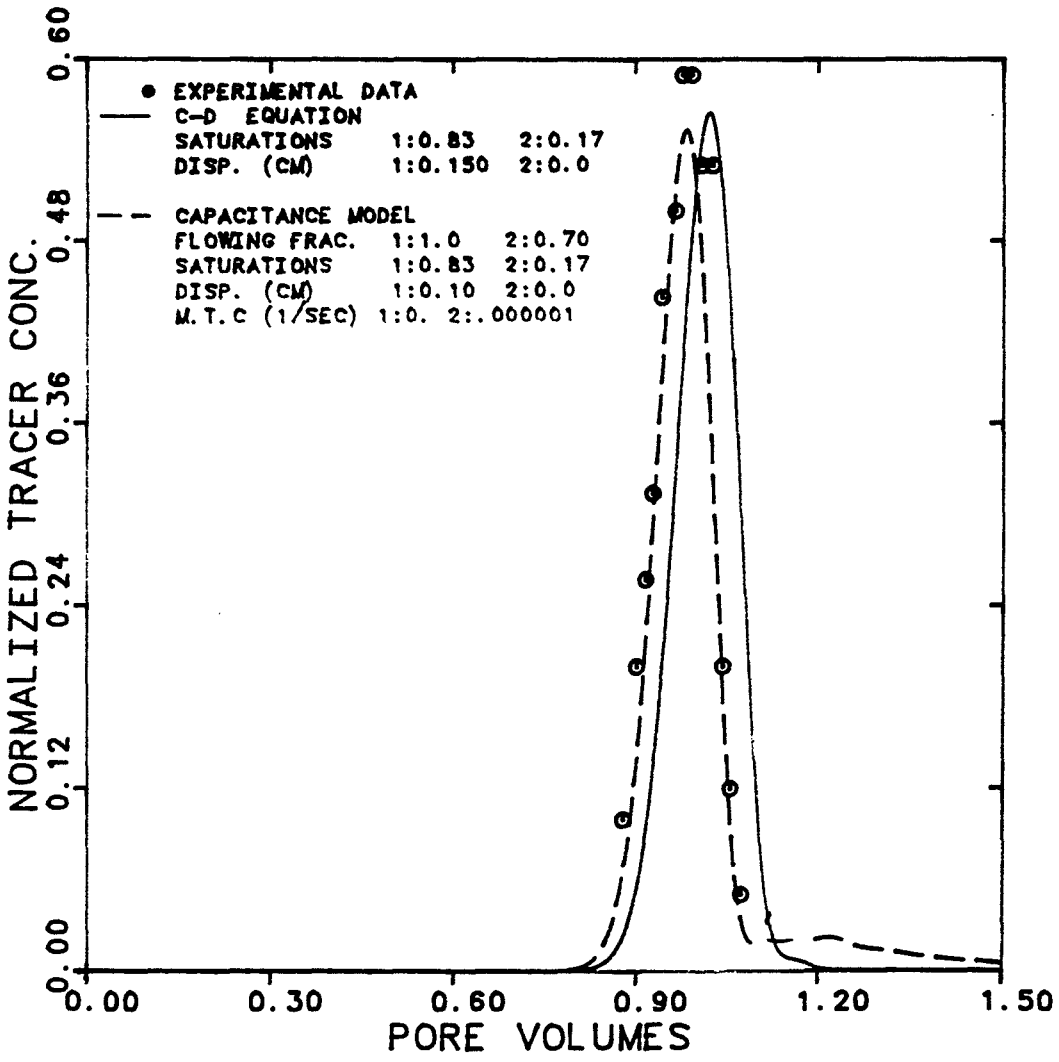

Figure 8.13 Effluent History for 2.5-IBA-W in Brine for Single-Phase Flow of Brine at 8.6 ft/day

EXPERIMENT NUMBER	FIG 4
TRACER & PHASE	2.5-IBA-W BRINE
FRACTIONAL FLOW	1: 1.0
SLUG SIZE	0.0615 P.V.
VELOCITY	41 FT/DAY

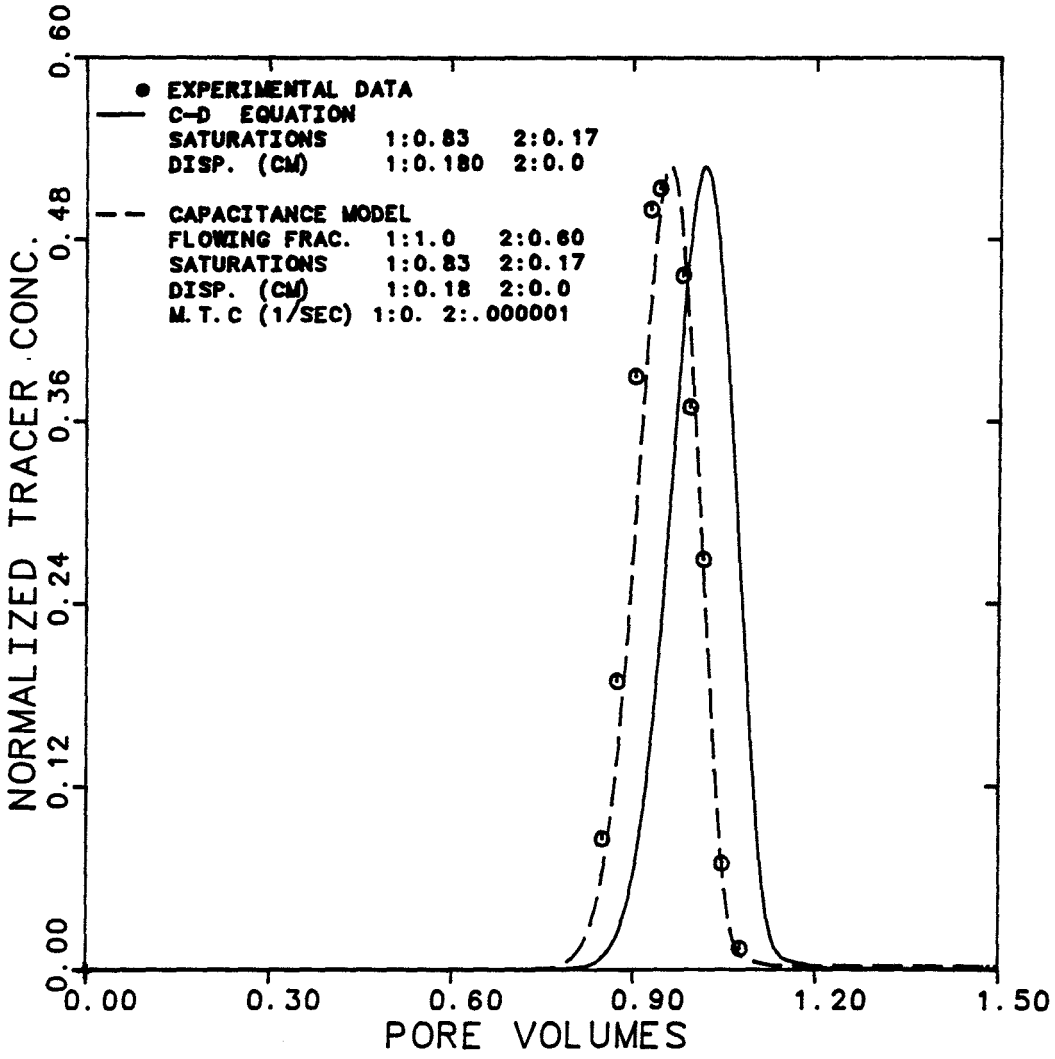

Figure 8.14 Effluent History for 2.5-IBA-W in Brine for Single-Phase Flow of Brine at 41 ft/day

EXPERIMENT NUMBER	FIG 4
TRACER & PHASE	2.5-IBA-W BRINE
FRACTIONAL FLOW	1: 1.0
SLUG SIZE	0.0615 P.V.
VELOCITY	472 FT/DAY

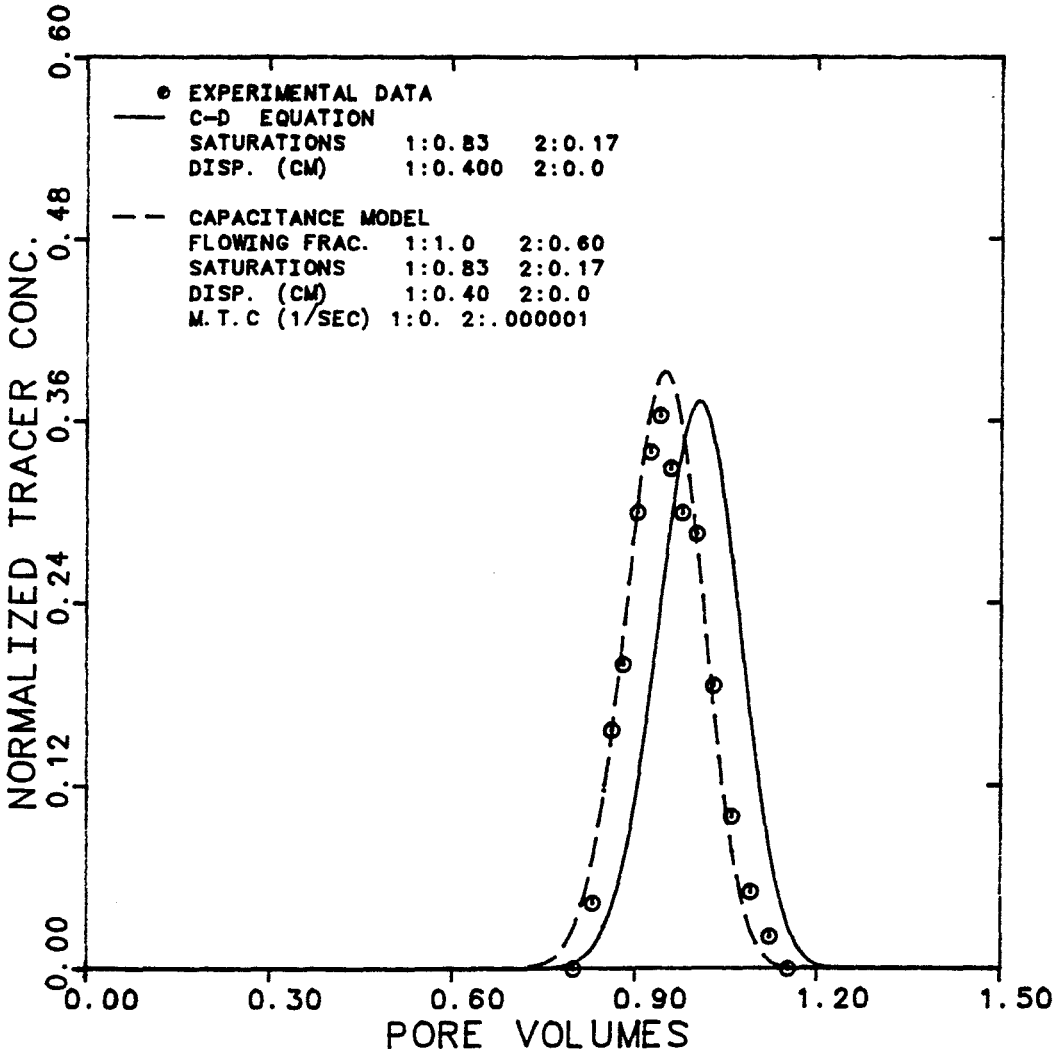

Figure 8.15 Effluent History for 2.5-IBA-W in Brine for Single-Phase Flow of Brine at 472 ft/day

EXPERIMENT NUMBER	FIG 5	
TRACER & PHASE	5-N-EB	OIL
FRACTIONAL FLOW	2: 1.0	
SLUG SIZE	0.0656	P.V.
VELOCITY	3.64	FT/DAY

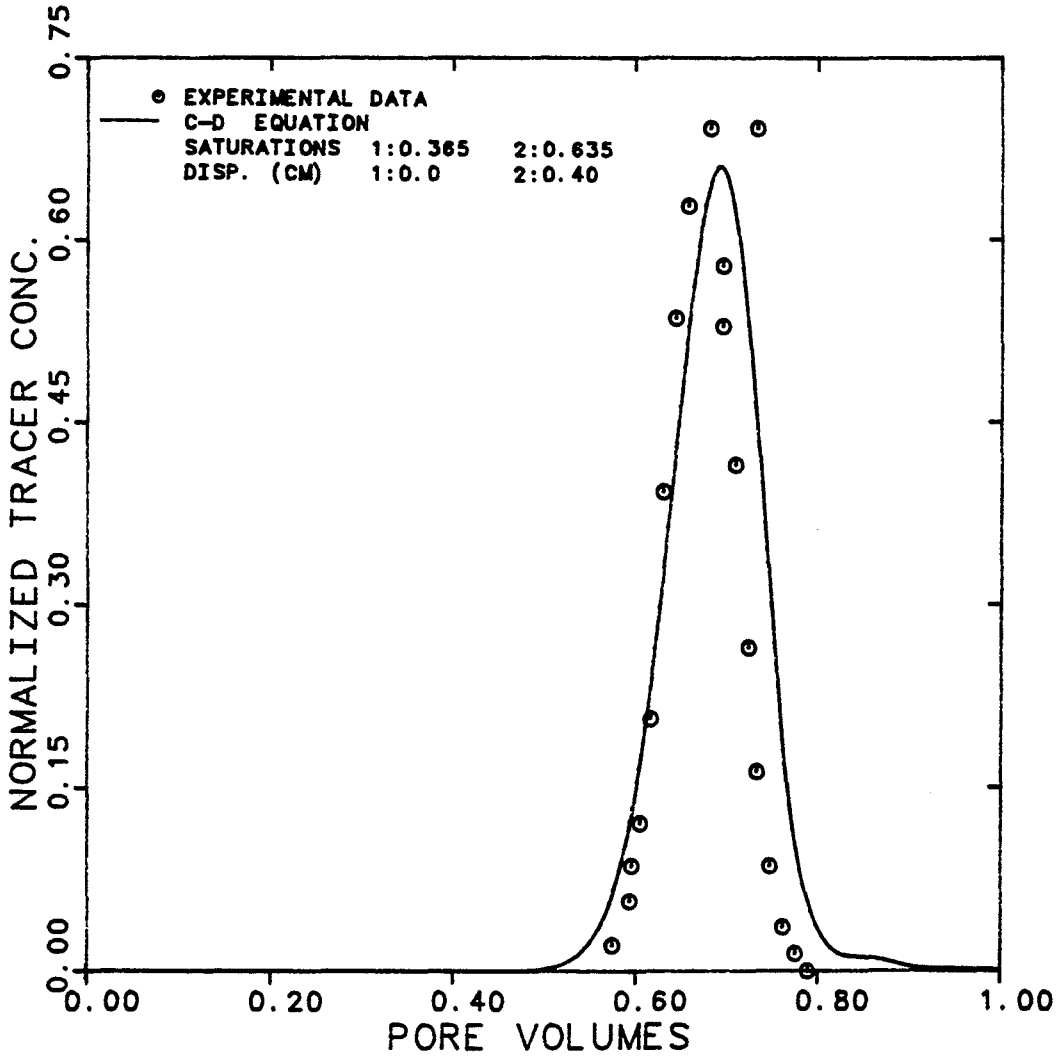

Figure 8.16 Effluent History for 5-N-EB in Oil for Single-Phase Flow of Oil at 3.64 ft/day

EXPERIMENT NUMBER	FIG 5
TRACER & PHASE	5-BA-EB OIL
FRACTIONAL FLOW	2: 1.0
SLUG SIZE	0.0656 P.V.
VELOCITY	3.64 FT/DAY

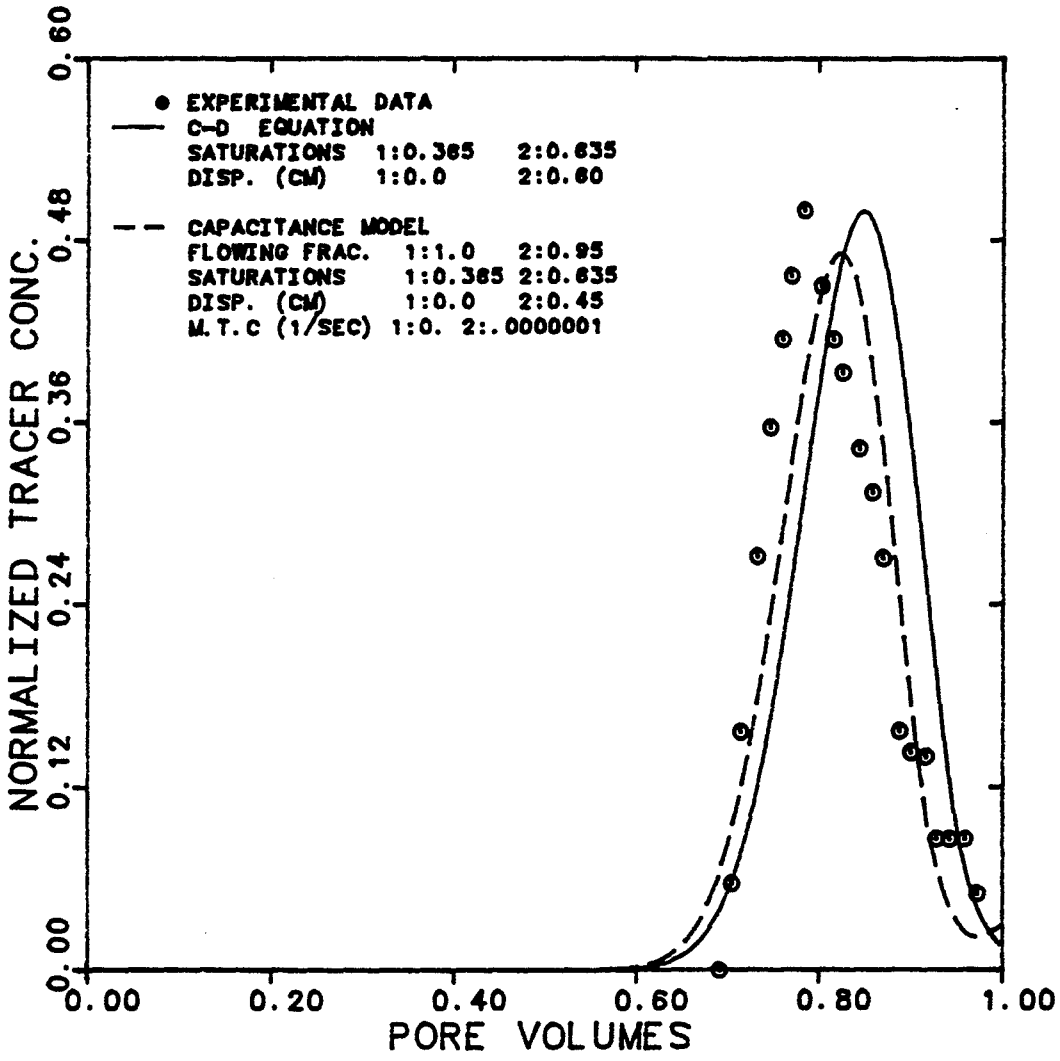

Figure 8.17 Effluent History for 5-BA-EB in Oil for Single-Phase Flow of Oil at 3.64 ft/day

EXPERIMENT NUMBER	FIG 5	
TRACER & PHASE	5-BA-EB	OIL
FRACTIONAL FLOW	2: 1.0	
SLUG SIZE	0.0656	P.V.
VELOCITY	36.4	FT/DAY

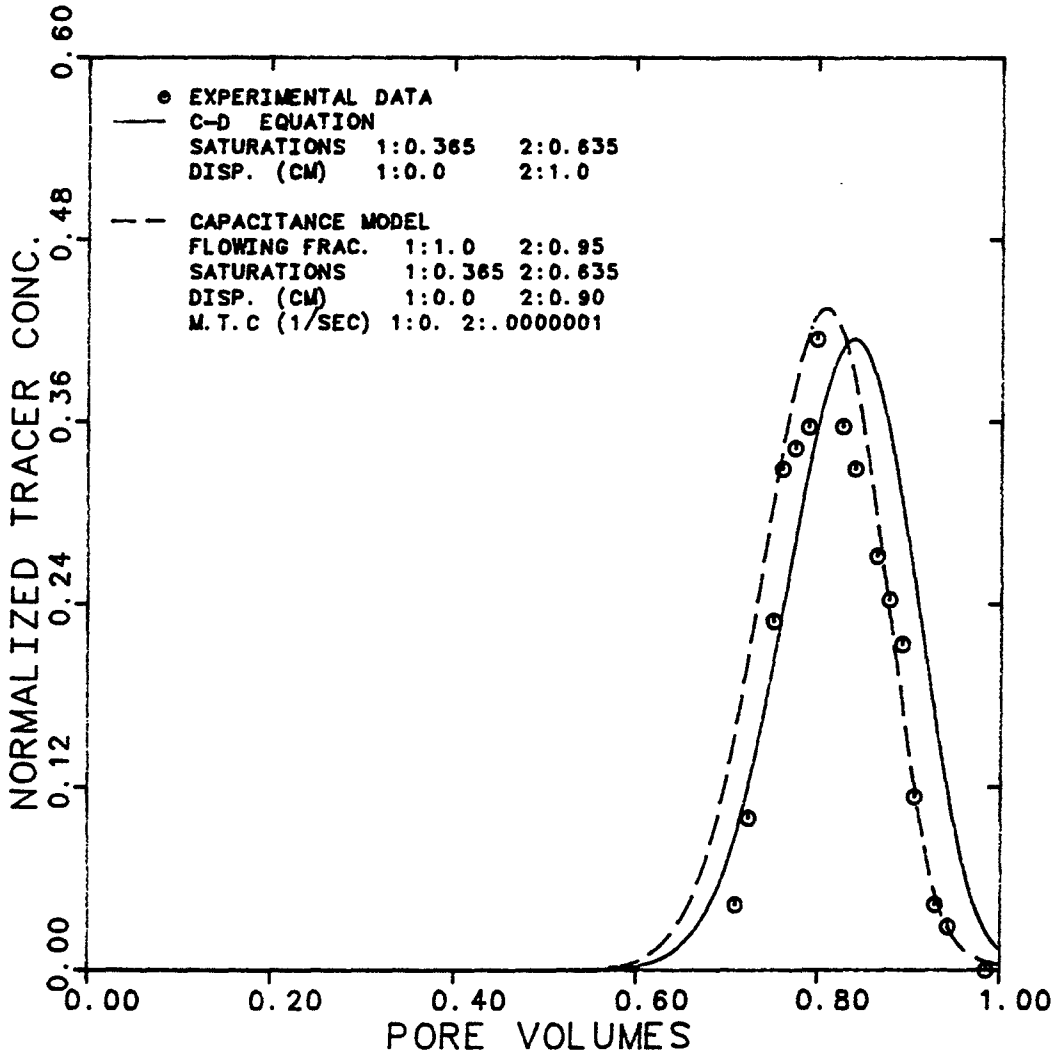

Figure 8.18 Effluent History for 5-BA-EB in Oil for Single-Phase Flow of Oil at 36.4 ft/day

8.3 Error Analysis on Saturations

There are three ways to estimate the phase saturation in the R-T experiments,

1- Material balance calculation

2- Dean's equation [D.4] (see below)

3- Capacitance-dispersion model

Residual oil saturations estimated in these three different ways are listed in Table 8.5.

The material balance values are the data reported by R-T. I also estimated the residual phase saturation using Dean's equation [D.4] as follows,

$$S_{jr} = \frac{V_B/V_A - 1}{K_{12}^{(i)} + (V_B/V_A - 1)} \qquad j = 1, 2$$

where V_B is the volume at peak breakthrough

V_A is the aqueous phase volume (or the volume at peak of the inert tracer)

$K_{12}^{(i)}$ is the partition coefficient of tracer between oil (2) and brine (1)

One of the assumptions implicit in this equation is that equilibrium exists, therefore S_{jr} is the phase saturation in equilibrium with the flowing phase.

The third means of estimating residual saturation was by matching the experimental breakthrough curve against the non-equilibrium capacitance-dispersion model. This analysis gives both the total saturation (S_j) and the dendritic or the non-equilibrium portion ($S_j(1-F_j)$) of that phase.

Table 8.5 also compares the dendritic saturation estimated by both methods (Dean's equation and capacitance model). The saturations estimated with the assumption of equilibrium are in error of up to 10%.

Table 8.6

Error Analysis on Saturation

Experiment Number	Residual Saturation (R-T) Material Balance	Residual Saturation Equilibrium Tracer Deans' Equation	Residual Saturation Capacitance Model	Dendritic Saturation from Capacitance ($S_j(1-F_j)$)	Dendritic Saturation from Deans eq. ($S_{M.B.}-S_{Dean's}$)
Fig. 1					
5-IPA-NA	0.30	0.197	0.30	0.0	0.103
5-TBA-NA	0.30	0.212	0.30	0.06	0.088
5-IBA-NA	0.30	0.260	0.30	0.06	0.040
2.5-BA-NA	0.30	0.286	0.30	0.0	0.014
Fig. 3					
0.29 ft/day	0.32	0.306	0.32	0.016	0.014
2.94 ft/day	0.32	0.295	0.32	0.032	0.005
29.4 ft/day	0.32	0.267	0.32	0.048	0.052
Fig. 4					
8.6 ft/day	0.17	0.193	0.17	0.051	-0.023
41 ft/day	0.17	0.160	0.17	0.068	0.01
472 ft/day	0.17	0.150	0.17	0.068	0.02
Fig. 5					
3.64 ft/day	0.365	0.282	0.365	0.03175	0.083
36.4 ft/day	0.365	0.329	0.365	0.03175	0.036

8.4 Conclusions and Remarks

The procedure used by Raimondi and Torcaso seems not only incapable of determining whether the assumption of equilibrium can be made but also leads to erroneous conclusions. The saturations obtained from the breakthrough data are underestimated when the assumption of equilibrium is imposed.

Questions remain about the impact of stagnant volumes (or non-equilibrium) on displacements at reservoir scale and field applications such as the single well tracer test. Coats and Smith [C.5] argued on dimensional grounds as follows

- In laboratory experiments, the flow velocity (v) may be larger and the length (L) definitely will be smaller than in the actual field. Thus, the mass transfer group ($M_D = \frac{ML}{v}$) is sufficiently small to result in a significant contribution to mixing by capacitance effects.

- In interwell field scale, however, with lengths typically hundreds of times longer, the mass transfer group may be so large as to preclude any contribution to mixing from capacitance effects.

Therefore, based on the Coats and Smith argument, the capacitance effect may have little

importance in causing asymmetry or mixing at field conditions but nevertheless may be very important in interpreting laboratory data. To confirm the latter, more investigation is required on how important the equilibrium behavior is in field studies.

CHAPTER 9

SUMMARY, CONCLUSIONS, AND RECOMMENDATIONS

Single, two- and three-phase flow experiments were conducted using a low interfacial tension (IFT) brine-oil-surfactant-alcohol mixture in a Berea sandstone core. The measurements were all performed using a two-foot long by two-inch square core at a temperature of 30°C. The microemulsion contained Witco TRS 10-410, n-decane, IBA, and 1.2 wt% NaCl and 13.7 ppm $CaCl_2$ brine. IFTs between both oil and microemulsion and brine and microemulsion were about 7×10^{-4} dyne/cm under the three-phase, optimal salinity conditions used. This IFT is lower than that for all previously reported relative permeability experiments. The primary quantities investigated were:

- Residual phase saturation and endpoint relative permeability as a function of capillary number ($N_c = \frac{k\Delta P}{L\sigma}$).

- Two- and three-phase relative permeabilities at a constant N_c.

- Tracer dispersivities in each phase at each steady-state fractional flow.

- Capacitance parameters for each phase.

There are six possible CDCs for three phases. Four of these were measured. The other two were not measured due to anticipated experimental difficulties. These CDCs have been measured by stepwise increases in flow rate of the displacing phase at a fixed IFT of 0.0007 dyne/cm. At steady-state, radioactive tracers were injected to estimate both phase saturations and dispersivities. The following conclusions are made for these single-phase flow experiments:

1- There are four distinct capillary desaturation curves for brine, oil, and microemulsion phases (Figure 6.2.37).

2- The microemulsion phase is the most strongly trapped phase which implies that the microemulsion is the wetting phase - even more wetting than the excess brine.

3- Single-phase tracer histories were all matched using the convection diffusion (C-D) equation.

4- The tracer dispersivities showed no dependence on phase saturation (Figure 6.2.42).

5- The dispersion coefficient for tracers in all three phases showed the well-known increase with phase frontal velocity ($v_j = \frac{q_j}{A\phi S_j}$). A straight line on a log-log scale was obtained for the data in each phase with slope of about 1.1 (Figures 6.2.39 - 6.2.41).

6- The endpoint relative permeabilities (Figure 6.2.38) showed the following:

a- The oil phase value did not change because it was already near one at low N_c.

b- Both the brine and microemulsion values showed a strong dependence on the capillary number.

The results of CDCs and endpoint relative permeabilities suggest an acute need for more data of residual oil to microemulsion for filling the gap on both the CDC and endpoint relative permeability curves at low capillary numbers ($N_c < 10^{-3}$). Experiments along this line are in progress by Mohammad Delshad [D.7].

Two- and three-phase relative permeabilities were measured at selected steady-state cuts which gave a constant nominal capillary number of 10^{-2}. During these experiments the core was vertical to prevent gravity segregation with fluid injection from the top. Continuous and slug displacements of both partitioning and non-partitioning radioactive tracers were run for

each steady-state cut. The steady-state low IFT relative permeability measurements suggest the following conclusions:

7- The relative permeability of each phase is a function only of its own saturation even during three-phase flow since the two-phase relative permeability curves for oil, microemulsion, and brine are in a very good agreement with three-phase curves (Figures 6.4.5.1 - 6.4.5.3).

8- The microemulsion phase is the most wetting based on the following evidence,

a- The irreducible saturation of the microemulsion is higher than the irreducible saturation of the excess brine at the same high capillary number ($10^{-4} < N_c < 3x10^{-2}$).

b- Breakthrough curves of the labelled sulfonate in the microemulsion phase are symmetric and show no capacitance. Both excess phases show capacitance.

c- Microemulsion phase saturation from tracer data are in fair agreement with material balance. The excess phases are not until capacitance is accounted for.

9- The relative permeabilities during two- and three-phase flow showed significant curvature despite the high N_c of 10^{-2}.

10- The microemulsion relative permeability curve during two- and three-phase flow has a concave curvature ($n_3 < 1.0$) while that of the excess phases are convex (n_1; $n_2 > 1.0$).

11- Relative permeability of the microemulsion phase is higher than that of the excess phases at the same saturation. This difference is less when compared on a flowing saturation basis (Figures 6.4.4.8 and 6.4.4.9).

The later may first seem contradictory to the conclusion number 8 because of the idea which says lower relative permeability is associated with the wetting phase in a water-wet medium. The basis for this idea is that in strongly water-wet media and under usual flow rate and viscosity conditions the capillary forces are larger than the viscous forces. Hence, the wetting phase (water) invades small pores, leaving oil in the large pore spaces. But, this concept may not apply to low interfacial flood when the capillary forces are very small. The microscopic distribution of the low IFT fluids is not yet well defined.

Some kind of visual test to find out how the fluids are distributed and flowing is necessary and may also resolve the mistery regarding the curvature of the microemulsion phase. Preliminary experiments were

performed using a microvisual cell and microscope, but no conclusions were possible. The use of Nuclear Magnetic Resonance (NMR) may give answers to some of these questions.

The two- and three-phase relative permeabilities were modelled using a simple exponential function as introduced in Chapter 7. This model is capable of predicting phase relative permeability as a function of its own saturation at various capillary numbers. The dependence of this model on capillary number is through the dependence of its input parameters (endpoint relative permeability, exponent, residual saturation) on capillary number. The exponent of oil and brine relative permeability curves show no significant dependence on N_c. The trend for microemulsion is not obvious since all the data for it are at a capillary number of 10^{-2}.

The endpoint relative permeabilities and exponents were also calculated as a function of capillary number using Equations 7.22b, 7.23b, 7.30b, and 7.31b. The predicted values using these equations showed an excellent agreement with the available experimental data.

To test the proposed relative permeability model at a capillary number different from 10^{-2}, there is

need for experimental data at that capillary number. There are experimental restrictions concerning capillary numbers greater or less than 10^{-2} using the present three-phase formulation. At low capillary number the pressure drop is too low to measure while at high capillary number the problem of non-equilibrium arises. Thus, Delshad [D.7] has plans to run such experiments using a two-phase type II(-) formulation and He (chinese visitor at the University of Texas) uses a two-phase type II(+) formulation. The interfacial tensions are at least an order of magnitude higher than that in the three-phase region. Therefore, the low capillary numbers can be obtained with normal pressure drop and flow rate conditions.

The conclusions drawn from the dispersion experiments during two- and three-phase flow are as follows:

12- A convection-diffusion equation adequately models the tritium labelled sulfonate breakthrough of microemulsion phase during multiphase flow.

13- The transport of tracers in the excess oil and brine phases is modelled by a capacitance-dispersion model. This model breaks each phase into flowing and dendritic fractions.

14- Dispersivities estimated from the capacitance-dispersion model are lower than those estimated from the C-D equation.

15- The following conclusions were made during two-phase flow of microemulsion and excess oil,

a- The dispersivities of carbon-14 labelled decane in oil and microemulsion and tritiated water in microemulsion show a strong decrease with phase saturation increase (Figure 6.3.1.18).

b- The oil flowing fraction varied between 0.8-0.95.

c- The carbon-14 mass transfer coefficient, a measure of the rate at which diffusion between the flowing and dendritic oil fraction occurs, was constant and equal to 10^{-6} sec^{-1}.

16- The following conclusions were made during the two-phase flow of microemulsion and excess brine,

a- The dispersivities of tritiated water in brine and microemulsion and carbon-14 labelled decane in microemulsion show no dependence on the phase saturation (Figure 6.3.2.14).

b- The brine flowing fraction was 0.9 for the continuous dispersion experiments and 0.5 and 0.7 for the finite slug ones. The finite slugs usually give lower

values for the flowing fraction. These results are also consistent with those observed by Mohammad Delshad [D.6].

c- The tritium mass transfer coefficient varies from 10^{-6} to $9x10^{-6}$ sec^{-1}. Another observation regarding the finite slugs was that they are more sensitive to the mass transfer coefficient than the continuous ones.

17- The dispersion results of three-phase flow lead to the following conclusions;

a- The dispersivities of chloride-36 in brine and microemulsion, carbon-14 labelled decane in oil and microemulsion and tritium labelled sulfonate in microemulsion show no specific trend with phase saturations. But, the dispersivities are higher than those observed during single-phase flow (Figures 6.4.4.17 - 6.4.4.19).

b- The dispersion coefficients of tritium labelled sulfonate in microemulsion as a function of microemulsion frontal velocity on a log-log scale lie on a straight line with the slope of about 2.10 (Figure 6.4.4.22).

c- The dispersion coefficients of carbon-14 labelled decane in oil, chloride-36 in brine as a function of phase velocity on a log-log scale do not lie on a straight line (Figures 6.4.4.20 and 6.4.4.21).

d- The flowing fraction for brine was 0.9 and constant during the three-phase flow cuts.

e- The flowing fraction for oil was 0.7 and constant during the three-phase flow cuts.

f- The mass transfer coefficients for carbon-14 and chloride-36 are 10^{-7} sec^{-1} with the exception of only two cuts. The dispersion runs were in decreasing direction of concentration in these two cuts.

Due to higher sensitivity of the finite slugs to capacitance parameters compared to the continuous ones, it is recommended that the tracer displacement to be performed only as finite slugs.

NOMENCLATURE

A: Area of cross-section, L^2

C_D: Normalized tracer concentration

C_{ij}: Flowing concentration of tracer i in phase j

$C^{\dagger}_{ij}$: Concentration of tracer i in dendritic fraction of phase j

C°_{ij}: Injected concentration of tracer i in phase j

D: Molecular diffusion coefficient, L^2/t

F: Formation resistivity factor

F_j: Flowing fraction of phase j

f_j: Fractional flow or cut of phase j

g: Gravity constant

h: Height of the core (vertical orientation), L

k: Permeability at 100% brine saturation, L^2

k_j: Effective permeability of phase j, L^2

k_{rj}: Relative permeability of phase j

k°_{rj}: End-point relative permeability of phase j

K_{ℓ}: Longitudinal dispersion coefficient, L^2/t

K_t: Transverse dispersion coefficient, L^2/t

K_{ij}: Longitudinal dispersion coefficient of tracer i in phase j, L^2/t

$K_{31}^{(1)}$: Partition coefficient of tracer 1 $(\frac{C_{13}}{C_{11}})$

$K_{32}^{(2)}$: Partition coefficient of tracer 2 $(\frac{C_{23}}{C_{22}})$

$K_{13}^{(3)}$: Partition coefficient of tracer 3 $(\frac{C_{31}}{C_{33}})$

L: Length of the core (horizontal), L

M_{ij}: Mass transfer coefficient of tracer in phase j, 1/t

M_{Dij}: Normalized mass transfer coefficient (Damkohler number) of tracer i in phase j

N_{cj}: Capillary number of phase j

N_{pe}: Peclet number

n_j: Exponent of relative permeability curve of phase j

ΔP_L: Pressure drop across length of L, F/L^2

ΔP_j: Pressure drop of phase j, F/L^2

ΔP_T: Pressure drop from pressure transducer, F/L^2

q: Total flow rate, L^3/t

R_{so}: Solubilization ratio of oil

R_{sw}: Solubilization ratio of water

S_j: Total saturation of phase j

S_j^f: Flowing saturation of phase j, $(S_j^f = S_j F_j)$

S_j^I: Initial saturation of phase j

S_j^{ss}: Steady-state saturation of phase j

S_{jr}: Residual saturation of phase j

t: Time, t

t_D: Dimensionless time or pore volumes

t_{DS}: Slug size in pore volume

$t_{DBT}^{0.5}$: Breakthrough time (in pore volume) at $C/C_o = 50\%$

u: Total volumetric flux, Darcy velocity (q/A), L/t

u_j: Flux of phase j, L/t

V: Volume, L^3

V_E: Deadend volume, L^3

V_p: Pore volume of core, L^3

v: Frontal velocity ($q/A\phi$), L/t

v_j: Velocity of phase j ($\frac{qf_j}{A\phi S_j}$), L/t

v_j^f: Flowing velocity of phase j ($\frac{qf_j}{A\phi S_j^f}$), L/t

x: Distance, L

x_D: Dimensionless distance

Greek Characters

σ: Interfacial tension, F/L^2

σ_{ave}: Average interfacial tension, F^2/L

μ_j: Viscosity of phase j, Ft/L^2

$\Delta\Phi_j$: Potential drop of phase j ($\Delta\Phi_j = \Delta P \pm \rho_j gh$), F/L^2

ϕ: Porosity

β_ℓ, β_t: Dispersion parameters

α_ℓ: Longitudinal dispersivity, L

α_t: Transverse dispersivity, L

α_{ij}: Longitudinal dispersivity of tracer i in phase j, L

ρ_j: Density of phase j, M/L^3

ρ_x: Density of fluid in pressure lines, M/L^3

λ_{rj}: Relative mobility of phase j $(\frac{k_{rj}}{\mu_j})$, L^2/Ft

λ_{rT}: Total relative mobility, L^2/Ft

Subscripts

j:	Phase number	1: excess brine 2: excess oil 3: microemulsion
i:	Tracer number	1: tritium (T_2O) or chloride-36 (^{36}Cl) 2: carbon-14 (^{14}C) 3: tritium labelled sulfonate (TS)
r:	Residual	
w:	Water	
o:	Oil	
me:	microemulsion	
s:	surfactant	
mw:	microemulsion-water	
mo:	microemulsion-oil	

Superscripts

F:	Flowing fraction	
i:	Tracer number	1: T_2O or ^{36}Cl 2: ^{14}C 3: TS
BT:	Breakthrough	
+:	Non-flowing fraction (dendritic)	

APPENDIX A

PERMEABILITY AND MOBILITY CALCULATIONS

The description of the equations used in the determination of permeability, capillary number, mobility and total relative mobility are introduced as follows.

A.1 Calculation of Permeability and Mobility

The calculations for reference, effective, and relative permeability; relative and total mobility are outlined in the following subsections.

A.1.1 Reference Permeability

The reference permeability is defined as the permeability of the rock when it is completely saturated with brine solution. Darcy's equation is

$$k = \frac{-q\mu_w L}{A(\Delta P_L + \rho_w g L)} \qquad (A.1)$$

since the force causing flow in the vertical displacement

is the vector sum of the pressure drop and gravity head.

A.1.2 Effective Permeability

The effective permeability is the ability of the porous medium to transmit one fluid phase when the medium is saturated with more than one fluid. Effective permeabilities can be calculated from

$$k_j = \frac{-qf_j\mu_j L}{A(\Delta P_L + \rho_j g L)} \qquad (A.2)$$

A.1.3 Relative Permeability

The relative permeability is the ratio of the effective permeability of a phase to a reference permeability (k). Different reference permeabilities can be used (1) the brine permeability, (2) the effective permeability to microemulsion at the residual brine saturation, (3) the effective permeability to oil at the residual brine saturation.

$$k_{rj} = \frac{k_j}{k} \qquad (A.3)$$

A.1.4 Mobility Calculation

The basic mechanics of any fluid displacement by another fluid can be understood by considering the

mobilities of the separate fluids. The relative mobility of any fluid phase is

$$\lambda_{rj} = \frac{k_{rj}}{\mu_j} \tag{A.4}$$

and the total relative mobility is

$$\lambda_{rT} = \sum_{j=1}^{3} \lambda_{rj} \tag{A.5}$$

A.2 Capillary Number Calculation

The capillary number is the ratio of capillary to viscous forces. The definition that is used in this study is

$$N_{cj} = \frac{k\Delta\Phi_j}{L\sigma_{ij}} \qquad i \neq j \tag{A.6}$$

In the case of horizontal flow, the change in pressure drop was used rather than $\Delta\Phi_j$, so

$$N_{cj} = \frac{k\Delta P}{L\sigma_{ij}} \qquad i \neq j \tag{A.7}$$

APPENDIX B

MATCHING PROCEDURE OF TRACER BREAKTHROUGH CURVES

Five sets of breakthrough curves are obtained for each cut of a three-phase flow experiment. These are carbon-14 labelled n-decane in the excess oil and microemulsion phases, chloride-36 in the excess brine and microemulsion phases, and tritium labelled sulfonate in the microemulsion phase. The procedure for matching these breakthrough curves against the convection-dispersion (C-D) or capacitance models is as follows:

1- Calculate the microemulsion saturation using the 50 percent breakthrough time (pore volume at $C/C_0 = 0.50$) of tritium labelled sulfonate as

$$t_{DBT} = \frac{S_3}{f_3}$$

$$S_3 = f_3 \, t_{DBT}^{0.50}$$

2- Compare the breakthrough curve of tritium labelled sulfonate in the microemulsion phase with the solution of the C-D equation using the microemulsion saturation obtained in step 1. This is a first approximation to determine the dispersivity of labelled sulfonate in the microemulsion (α_{33}) and microemulsion saturation (S_3).

3- Compare the breakthrough data of carbon-14 in both oil and microemulsion phases with the capacitance model computed curves using the microemulsion saturation obtained in step 2. The experimental breakthrough curves were visually compared with the computed curves to obtain the best estimates of the capacitance parameters which are:

Oil saturation (S_2), oil flowing fraction (F_2), mass transfer coefficient (M_{22}), and dispersivities of carbon-14 in oil and microemulsion phases (α_{22}, α_{23}).

The following assumption was made regarding the values of dispersivities since the breakthrough curves of carbon-14 in microemulsion and oil are almost identical,

$$\alpha_{22}F_2 = \alpha_{23}$$

4- Compare the breakthrough curves of chloride-36 in both brine and microemulsion phases with the computed curves of the capacitance model. The matching parameters are as follows:

Brine flowing fraction (F_1), mass transfer coefficient (M_{11}), and dispersivities of chloride-36 in brine and microemulsion (α_{11}, α_{13}) with the restriction of $\alpha_{11}F_1 = \alpha_{13}$. The saturation is not a parameter since $S_1 = 1 - S_2 - S_3$.

If a good match was not obtained by changing the above listed parameters, step 3 should be repeated for a new set of parameters. This trial and error procedure is repeated until satisfactory matches are obtained for both carbon-14 and chloride-36 breakthrough curves.

Satoh [S.8] generated capacitance type curves to match steady-state tracer experiments. Figures B.1 through B.4 show examples of these type curves. Figures B.1 and B.2 show the effect of changing flowing fraction when Peclet number (N_{pe}) and mass transfer coefficient ($M_D = \frac{ML}{u}$) are constant. The change in tracer histories by changing the mass transfer coefficient at constant flowing fraction and Peclet number are demonstrated in Figures B.3 and B.4.

- Procedure for Global Match of Tracer Histories

The mass transfer coefficient, flowing fraction, and dispersivities found by matching the tracer breakthrough curves against the capacitance model were plotted as a function of variables such as phase velocity ($v_j = \frac{qf_j}{A\phi S_j}$), and phase saturation.

The tracer histories of different cuts should then be re-matched with unique values of mass transfer coefficient, flowing fraction, and dispersivity for each phase if no specific trend shown with the phase velocity and phase saturation. In our analysis, we could match the breakthrough curves with a constant mass transfer coefficient and flowing fraction for each phase. We were not able to match these curves with a single dispersivity value for tracer in each phase. This may be because of the dependence of dispersivity on other parameters such as tortuosity and microscopic fluid distribution.

FIG. B.1

HISTORIES UP TO 2.00 PV. INJECTED

TOTAL CONCENTRATIONS VS. PV. INJECTED

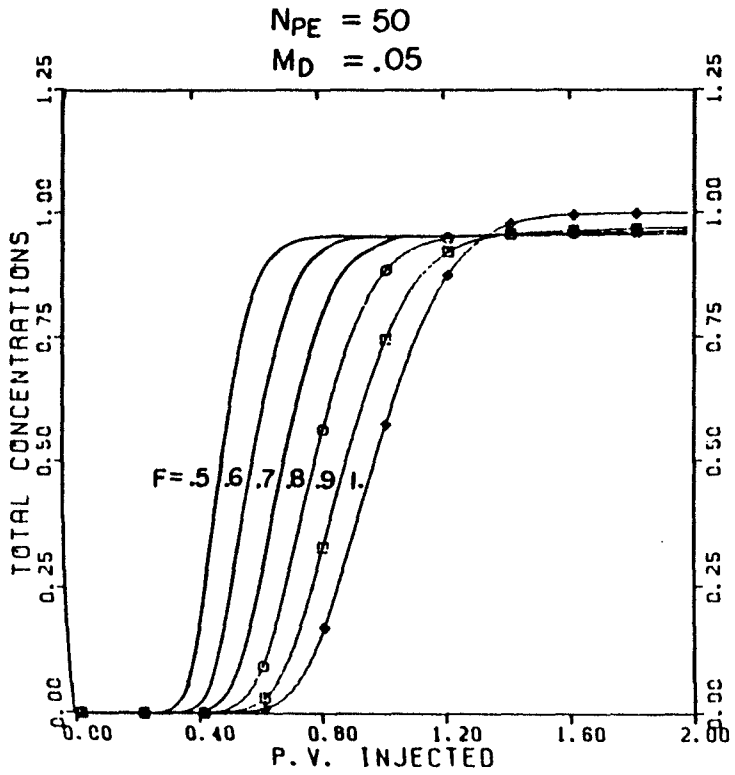

FIG. B.2

HISTORIES UP TO 2.00 PV. INJECTED

TOTAL CONCENTRATIONS VS. PV. INJECTED

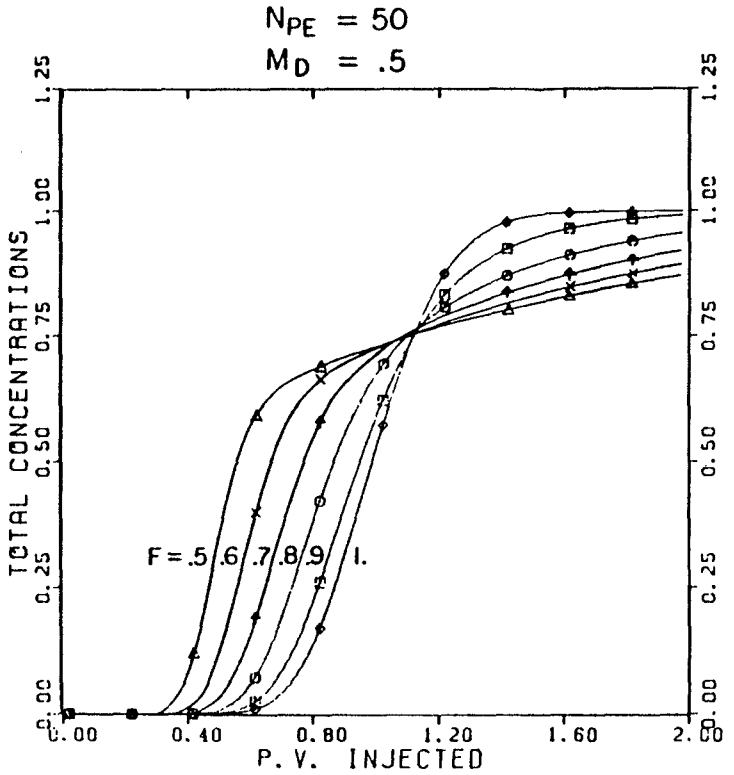

APPENDIX C

MIXING PROCEDURE FOR MICELLAR SOLUTION

The numerical examples given in this appendix demonstrate how the micellar solsution for both static and flow experiments were prepared.

- First, prepare the following stocks:

A - Micellar Stock

(1) Heat surfactant (in the original container), as is, in a 50°C air bath for 1-1/2 hours.

(2) Mix by hand until sample is homogeneous.

(3) Weigh out appropriate amount of surfactant (with the density of 1.0 g/cm^3) and using appropriate activity.

(4) Weigh out alcohol; and de-ionized water.

(5) Mix the above fluids with magnetic stirrer for at least 15 hours while the solution is sealed with stopper.

B - Brine Stocks

(1) Weigh out appropriate amount of anhydrous salts

(2) Weigh out de-ionized water

(3) Mix with magnetic stirrer until solution is clear.

C.1 Mixing Procedure for Phase Behavior Samples

Using the above stocks, prepare the samples at desired composition in 25 cm^3 screw cap glass vials as follows:

(1) pipette brine stock

(2) pipette micellar stock and mix

(3) pipette de-ionized water

(4) pipette oil and screw on cap tightly

(5) invert tube gently four times and set in temperature bath (30°C) to equilibrate.

EXAMPLE

(1) For desired stock A consisting of

30 vol% TRS 10-410

30 vol% isobutyl alcohol (IBA)

21.61 vol% de-ionized water

MIX

1935.5 g TRS 10-410

1200 cm^3 IBA

864.5 g de-ionized water

(2) For desired stock B1 consisting of 3.685 wt% NaCl brine

MIX

147.46 g NaCl

3852.54 g de-ionized water

(3) For desired stock B2 consisting of 150 ppm Ca^{++} brine

MIX

0.416 g $CaCl_2$

999.584 g de-ionized water

(4) For desired micellar composition consisting of

1.5 vol% TRS 10-410

1.5 vol% IBA

50 vol% $n\text{-}C_{10}$

47 vol% brine (1.1 wt% NaCl, 13.7 ppm Ca^{++})

MIX

1 cm^3 of stock A

2.75 cm^3 of stock B1

0.86 cm^3 of stock B2

5.39 cm^3 of de-ionized water

10 cm^3 n-decane

C.2 Mixing Procedure for 15 liter stock (for flow experiments)

EXAMPLE: Consider the stock with 1.2 wt% NaCl salinity

(1) For stock I consisting of

1.5 vol% active TRS 10-410

75.8 vol% de-ionized water

MIX

967.75 g TRS 10-410

3032.25 g de-ionized water

(2) For desired stock II consisting of 3.685 wt% NaCl brine

MIX

147.46 g NaCl

3852.54 g de-ionized water

(3) For stock III consisting of 150 ppm Ca^{++}

MIX

0.416 g $CaCl_2$

999.584 g de-ionized water

(4) For micellar solution with the overall composition as

1.5 vol% TRS 10-410

1.5 vol% IBA

50 vol% n-C_{10}

47 vol% brine (1.2 wt% NaCl, 13.7 ppm Ca^{++})

MIX

1500 g filtered stock I

2298.26 g filtered stock II

645 g filtered stock III

2882.53 g de-ionized water

181.8 g IBA

5475 g filtered n-decane

N-decane and stocks I, II, and III were filtered through 0.45 micron Millipore filter paper.

APPENDIX D

SAMPLE CALCULATION OF EXPERIMENTAL PLAN

The numerical examples given in this appendix demonstrate how the flow rates and fractional flows were initially estimated to design the two- and three-phase displacements for a given capillary number.

D.1 Example Calculation for Two-Phase Flow

To design a constant potential drop (or constant capillary number) two-phase flow displacement, the relative permeabilities for given saturations are necessary to calculate flow rates and fractional flows. The relative permeability data provided by Delshad [D.8] were used and curve-fitted with an exponential relative permeability function (Eq. 6.5) to obtain estimates of the exponents. These data (Figure D.1) were obtained at a constant flow rate rather than a constant capillary number, but the range of change in the capillary number (N_c) was fairly small (from 0.0048 to 0.0214).

The example calculation for the two-phase flow, for example microemulsion/oil, at a constant capillary number of 10^{-2} is as follows:

Core Properties	Fluid Properties	
	Density (g/cm^3):	water (ρ_1) = 1.0
		oil (ρ_2) = 0.729
k = 0.739 Darcy		m.e. (ρ_3) = 0.838
	Viscosity (CP):	water (μ_1) = 0.906
A = 25.5 cm^2		oil (μ_2) = 0.840
		m.e. (μ_3) = 4.55
L = 60.96 cm	IFT (dyne/cm):	$\sigma_{mo} = 3 \times 10^{-4}$
		$\sigma_{mw} = 8.6 \times 10^{-4}$

The endpoint relative permeabilities and residual saturations estimated from the capillary desaturation data (Figures 6.2.37 and 6.2.38) at $N_c = 10^{-2}$ are as follows:

$k^{\circ}_{r2} = 0.90$ $\quad$ $S_{1r} = 0.117$ (constant)

$k^{\circ}_{r3} = 1.0$ $\quad$ $S_{2r} = 0.0$

$S_{3r} = 0.04$

The exponents of the relative permeability curves obtained by matching the two-phase microemulsion/oil data to the exponential function are

$$n_2 = 1.25$$

$$n_3 = 0.77$$

For a given capillary number of 10^{-2}, the potential drop is calculated from the following

$$N_c = \frac{k^{(D)}{}_{\Delta\Phi_2}(psi)}{L^{(ft)}\,\sigma_{mo}(dyne/cm)} \times 2.23 \times 10^{-5} \qquad (D.1)$$

$$\Delta\Phi_2 = 0.364 \text{ psi/2 ft}$$

and the potential drop for the microemulsion phase is

$$\Delta\Phi_3 = \Delta\Phi_2 + (\rho_3 - \rho_2)gh$$

$$\Delta\Phi_3 = 0.364+(0.838-0.729) \times 0.433x2 = 0.458 \text{ psi/2 ft}$$

Now, for a given microemulsion saturation of 0.3, the relative permeability functions become,

$$k_{rj} = k^{\circ}_{rj}\left(\frac{S_j - S_{jr}}{1 - \sum_{j=1}^{3} S_{rj}}\right)^{n_j} \qquad j=2,3 \qquad (D.2)$$

$$k_{r3} = 1\left(\frac{0.3-0.04}{1-0.04-0.117}\right)^{0.77} = 0.404$$

$$k_{r2} = 0.90\left(\frac{0.583-0.0}{1-0.04-0.117}\right)^{1.25} = 0.567$$

The flow rates are then calculated using Darcy's equation,

$$q_j = \frac{kk_{rj} A \Delta\phi_j}{L\mu_j} \qquad (D.3)$$

$$q_2 = \frac{0.739(0.567)(25.5)(0.364/14.7)}{60.96 \times 0.84} = 0.0051 \text{ cm}^3/\text{sec}$$

$$q_3 = \frac{0.739(0.404)(25.5)(0.458/14.7)}{60.96 \times 4.55} = 0.00085 \text{ cm}^3/\text{sec}$$

And the fractional flows are

$$f_2 = \frac{q_2}{q_2 + q_3} = 0.857$$

$$f_3 = \frac{q_3}{q_2 + q_3} = 0.143$$

These values were then used as the nominal flow rates injected necessary to maintain a constant capillary number for the predicted saturations. The actual phase fractional flows were calculated from the effluent sample volume measurements at steady-state.

The phase saturations and thus the potential

drop may be different from the predicted values in the actual displacement of microemulsion and oil phases at the pre-selected nominal flow rates. The total flow rate can then be adjusted in the following manner to account for the above mentioned difference.

- Lets say that the potential drop measured at steady-state is $\Delta\Phi_2^* = 0.45$ psi/2ft rather than the desired value of $\Delta\Phi_2 = 0.364$ psi/2ft. The total flow rate is then changed with the ratio of $\frac{\Delta\Phi_2^*}{\Delta\Phi_2} = 1.23$ to obtain a new value for $\Delta\Phi_2$ which is closer to the pre-selected one.

A similar procedure can be applied when designing the microemulsion/brine experiment at a constant capillary number. The residual phase saturations and the endpoint relative permeabilities can be estimated from the capillary desaturation data. The values used for the exponent of the relative permeability curves are listed in Table 6.3.3.2.

D.2 Example Calculation for Three-Phase Flow

A modified version of Lake's three-phase relative permeability model was used to plan the three-phase flow experiments at a constant capillary number. The description of this model is given in Chapter 7.

Endpoint relative permeabilities and residual

saturations were estimated from the capillary desaturation curve at the selected capillary number. Exponents used in the model were the values found by matching the two-phase data of microemulsion/oil to the exponential function. The total flow rate and fractional flow rates for selected saturations were then calculated using the above information.

The numerical example given in this section is for the capillary number of 10^{-2} and the phase saturations are

$$S_1 = 0.40$$

$$S_2 = 0.30$$

$$S_3 = 0.30$$

and the core and fluid properties are given in the previous section. The exponent and endpoint for the excess brine phase is then calculated as follows,

- From two-phase data (Figure D.1),

$$n_2 = 1.25$$

$$n_3 = 0.770$$

- From the capillary desaturation data (Figures 6.2.37 - 6.2.38) at $N_c = 10^{-2}$,

$$S_{1r} = 0.07$$

$$S_{2r} = 0.0$$

$$S_{3r} \text{ to oil} = 0.04$$

$$S_{3r}^{ave} \text{ to brine} = 0.14 \implies S_{3r}^{arc} = 0.09$$

- The interpolating function (g) becomes

$$g = \frac{S_2(1 - S_3)}{S_3 + S_2}$$

$$g = \frac{0.30(1 - 0.30)}{0.30 + 0.30} = 0.35$$

- The endpoint relative permeability for the brine phase is

$$k_{r1}^{\circ} = k_{r2}^{\circ} + g(k_{r3}^{\circ} - k_{r2}^{\circ})$$

$$k_{r1}^{\circ} = 0.90 + 0.35(1 - 0.9) = 0.935$$

and the exponent is

$$n_1 = n_2 + g\,(n_3 - n_2)$$

$$n_1 = 1.25 + 0.35(0.77 - 1.25) = 1.08$$

The relative permeabilities are then calculated using Eq. C.2 as follows

$$k_{r1} = 0.935\left(\frac{0.40 - 0.07}{1-0.07-0.0-0.09}\right)^{1.08} = 0.340$$

$$k_{r2} = 0.9\left(\frac{0.30 - 0.0}{1-0.07-0.0-0.09}\right)^{1.25} = 0.248$$

$$k_{r3} = 1.0\left(\frac{0.30 - 0.09}{1-0.07-0.0-0.09}\right)^{0.77} = 0.344$$

The flow rates are estimated using Darcy's equation (Eq. D.3) knowing the potential drops from Equation D.1.

$$\Delta\bar{\phi}_2 = 0.364 \text{ psi/ft}$$

$$\Delta\bar{\phi}_3 = 0.458 \text{ psi/ft}$$

$$\Delta\bar{\phi}_1 = \Delta\bar{\phi}_2 + (\rho_1 - \rho_2)gh = 0.364 + (1-0.729)\times 0.433 \times 2$$
$$= 0.598 \text{ psi/2 ft}$$

$$q_1 = \frac{0.739 \times 0.34 \times 25.5 \times 0.598/14.7}{0.906 \times 60.96} = 0.0047 \text{ cm}^3/\text{sec}$$

$$q_2 = 0.0022 \text{ cm}^3/\text{sec}$$

$$q_3 = 0.0072 \text{ cm}^3/\text{sec}$$

And the fractional flows (cuts) are

$$f_1 = 0.616$$

$$f_2 = 0.288$$

$$f_3 = 0.096$$

FIG. D.1

COMPARISON OF CALCULATED TWO PHASE
RELATIVE PERMEABILITY AND
EXPERIMENTAL DATA
EXPERIMENT NUMBER II-MM/D
CAPILLARY NUMBER 0.0048-0.0214

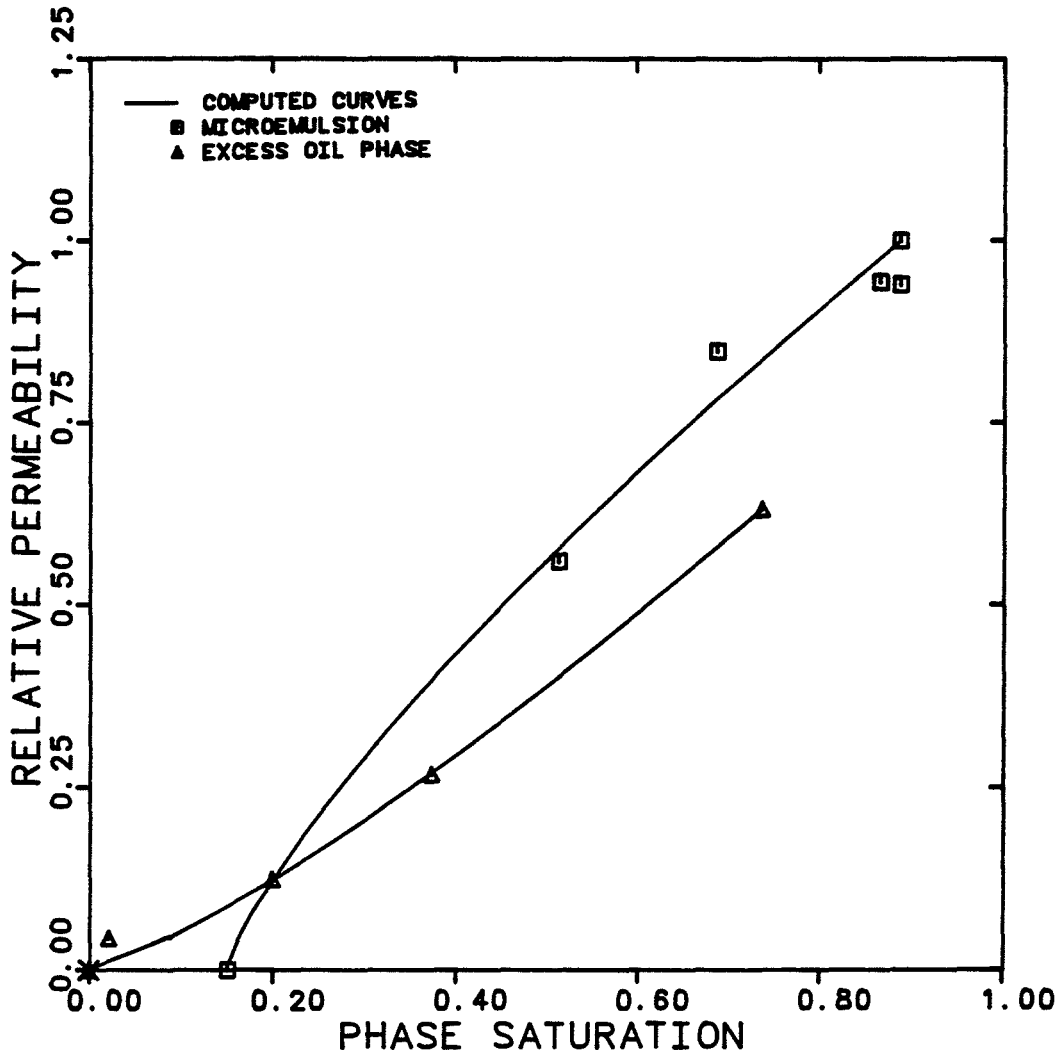

REFERENCES

[A.1] Abrams, A., "The Influence of Fluid Viscosity, Interfacial Tension and Flow Velocity on Residual Oil Saturation Left by Waterflood," SPE Journal (Oct. 1975), 437-447.

[A.2] Amaefule, J.O., and Handy, L.L., "The Effect of Interfacial Tension on Relative Oil and Water Permeabilities of Consolidated Porous Media," SPE Journal (June 1982), 371-381.

[A.3] Aronofsky, J.S., and Heller, J.P., "A Diffusion Model to Explain Mixing of Flowing Miscible Fluids in Porous Media," Trans. AIME, Vol.210 (1957), 347-351.

[B.1] Baker, L.E., "Effects of Dispersion and Dead-End Pore Volume in Miscible Flooding," SPE Journal (June 1977), 219-227.

[B.2] Bardon, C., and Longeron, D.C., "Influence of Very Low Interfacial Tensions on Relative Permeability," SPE Journal (Oct. 1980), 391-401.

[B.3] Batycky, J.P., Maini, B.B., and Fisher, D.B., "Simulation of Miscible Displacement in Full-Diameter Carbonate Cores," SPE Journal (Oct. 1982), 647-657.

[B.4] Batycky, J.P., and McCaffery F.G., "Low Interfacial Tension Displacement Studies," Paper No. 78-29-26 Presented at 29th Annual Technical Meeting of the Petroleum Society of CIM, (1978), Calgary.

[B.5] Bhuyan, D., "The Effect of Wettability on the Capillary Desaturation Curves," M.S. Thesis, The University of Texas at Austin, (1985).

[B.6] Blackwell, R.J., "Laboratory Studies of Microscopic Dispersion Phenomena," SPE Journal (March 1962).

[B.7] Brigham, W.E., "Mixing Equations in Short Laboratory Cores," SPE Journal (Feb. 1974), 91-99.

[B.8] Brigham, W.E., Reed, P.W., and Dew, J.N., "Experiments on Mixing During Miscible Displacement in Porous Media," SPE Journal (March 1961), 1-8.

[B.9] Brownell, L.E., and Katz, D.L., "Flow of Fluids Through Porous Media - Part II," Chemical Engineering Progress, 43 (Nov. 1947), 601-612.

[C.0] Camilleri, D., et al., "Description of an Improved Compositional Micellar/Polymer Simulator," To be Published in SPE Journal (1986).

[C.1] Cassidy, H.G., "Fundamentals of Chromatography" Interscience Publisher, Inc., New York (1957), 30.

[C.2] Caudle, B.H., Slobod, R.L., and Brownscomb, E.R., "Further Developments in the Laboratory Determination of Relative Permeability," Trans. AIME Vol.192 (1951), 145-150.

[C.3] Cayias, J.L., Schechter, R.S., and Wade, W.H., "The Measurement of Low Interfacial Tension Via the Spinning Drop Technique," Ed. K.L. Mittal ACS Symposium Series, Adsorption at Interfaces, 8 (1975), 234-248.

[C.4] Chatzis, I., and Morrow, N.R., "Correlation of Capillary Number Relationships for Sandstones," SPE 10114, Presented at the 56th Annual Technical Conference and Exhibition of the SPE, San Antonio, October 5-7, 1981.

[C.5] Coats, K.H., and Smith, B.D., "Dead-End Pore Volume and Dispersion in Porous Media," SPE Journal (March 1964), 73-84.

[C.6] Corey, A.T., Rathjens, C.H., Henderson, J.H., and Wyllie, M.R.J., "Three-Phase Relative Permeability," Trans. AIME, Vol.207 (1956), 349-351.

[D.1] Dai, K.K,, and Orr, F.M., "Prediction of CO_2 Flood Performance: Interaction of Phase Behavior with Microscopic Pore Structure Heterogeneity," SPE 13115 Presented at 59th Annual Meeting, Houston, Texas, Sept. 16-19, 1984.

[D.2] Dalton, R.I., Daumann, V.D., Kyle, J.R. - Private Communication to H.L. Stone.

[D.3] Deans, H.A., "A Mathematical Model for Dispersion in the Direction of Flow in Porous Media," SPE Journal (March 1963), 49-52.

[D.4] Deans, H.A., "Method for Determining the Relations Between Fractional Flow and Saturation in a Reservoir," U.S. Patent # 3,990,298 (Nov. 9, 1976).

[D.5] Deans, H.A., "Using Chemical Tracers to Measure Fractional Flow and Saturation in-Situ," SPE 7076 Presented at the Fifth Symposium on Improved Oil Recovery, Tulsa, Oklahoma, April 16-19, 1978.

[D.6] Delshad, Mohammad, "Relative Permeability and Dispersion Measurement for a Three-Phase Micellar/Polymer Mixture," M.S. Thesis, The University of Texas at Austin, (1984).

[D.7] Delshad, Mohammad, Ph.D. Dissertation, in Progress.

[D.8] Delshad, Mojdeh, "Measurement of Relative Permeability and Dispersion for Micellar Fluids in Berea Rock," M.S. Thesis, The University of Texas at Austin, (1981).

[D.9] Delshad, M., Delshad, M., Pope, G.A., and Lake, L., "An Investigation of Two- and Three-Phase Relative Permeabilities of Micellar Fluids," SPE 13581 Presented at SPE International Symposium on Oilfield and Geothermal Chemistry held in Phoenix, Arizona April 9-11, 1985.

[D.10] Delshad, M., MacAllister, D.J., Pope, G.A., and Rouse, B.A., "Multiphase Dispersion and Relative Permeability Experiments," SPE Journal (Aug. 1985).

[D.11] Dietrich, J.K., and Bondor, P.L., "Three Phase Oil Relative Permeability Models," SPE 6044 Presented in New Orleans Oct. 3-6, 1976.

[D.12] Dombroski, H.S., and Brownell, L.E., "Residual Equilibrium Saturation of Porous Media," Industrial and Engineering Chemistry, V.46, (June 1954), 1207-1218.

[D.13] Donaldson, E.C., and Dean, G.W., "Two- and Three-Phase Relative Permeability Studies," RI 6826, USBM (1966).

[D.14] Donaldson, E.C., and Kayser, M.B., "Three-Phase Fluid Flow in Porous Media," DOE/BTEC/IC-80/4, April 1981.

[E.1] Ehrlich, R., Hasiba, H.H., and Raimondi, P., "Alkaline Waterflooding for Wettability Alteration - Evaluating a Potential field Application," Journal of Pet. Tech. (Dec. 1974), 1335-1343.

[F.1] Fayers, F.J., and Mathews, J.D., "Evaluation of Normalized Stone's Methods for Estimating Three-Phase Relative Permeabilities," Submitted for Publication to SPE Journal.

[F.2] Foster, W.R., "A Low-Tension Waterflooding Process," Journal of Pet. Tech. (Feb. 1973), 205-210.

[F.3] Fulcher, R.A., "The Effect of the Capillary Number and Its Constituents on Two-Phase Relative Permeabilities," Ph.D. Dissertation, Pennsylvania State University, (1982).

[F.4] Fulcher, R.A., Eterkin, T., and Stahl, C.D., "The Effect of the Capillary Number and Its Constituents on Two-Phase Relative Permeability Curves," Journal of Pet. Tech. (Feb. 1985).

[G.1] Glinsmann, G.R., "Surfactart Flooding with Microemulsion Formed in-Situ Effect of Oil Characteristics," SPE 8326 Presented at the SPE-AIME 54th Annual Fall Technical Conference, Las Vegas (Sept. 1979).

[G.2] Graciaa, A., Schechter, R.S., Wade, W.H., and Yiu, S., "Criteria for Structing Surfactants to Maximize Solubilization of Oil and Water I: Commercial Non-Ionics," SPE/DOE 9815, Tulsa, Oklahoma (April 1981).

[G.3] Gupta, S.P., and Trushenski, S.P., "Micellar Flooding-Compositional Effects on Oil Displacement," SPE Journal (April 1979), 116-128.

[G.4] Gupta, S.P., "Dispersion and Adsorption in Porous Media," Ph.D. Dissertation, Purdue University (1972).

[H.1] Harbort, L.W., "Low Interfacial Tension Relative Permeability," SPE 12171 Presented at the 58th Annual Technical Conference held in San Francisco, CA., Oct. 5-8, 1983.

[H.2] Healy, R.N., Reed, R.L., and Stenmark, D.G., "Multiphase Microemulsion Systems," SPE Journal (June 1976), 147-160.

[H.3] Hedges, J.H., and Glinsmann, G.R., "Compositional Effects on Surfactant Flood Optimization," SPE 8324 Presented at 54th Annual Technical Conference held in Las Vegas, Sept. 1979.

[H.4] Hirasaki, G.J., van Domselaar, H.R., and Nelson, R.C., "Evaluation of the Salinity Gradient Concept in Surfactant Flooding," SPE Journal (June 1983), 486-500.

[H.5] Holmgren, C.R., and Morse, R.A., "Effect of Free Gas Saturation on Oil Recovery by Water Flooding," Trans. AIME Vol. 192 (1951), 135-140.

[J.1] Johnson, E.F., Bossler, D.P., and Neumann, V.O., "Calculation of Relative Permeability from Displacement Experiments," Journal of Pet. Tech. Vol.61 (Jan. 1959).

[J.2] Jones, K., "Rheology of Viscoelastic Fluids for Oil Recovery," M.S. Thesis, The University of Texas at Austin (1981).

[K.1] Klaus, E.E., "Enhanced Recovery of Pennsylvania Grade Crude Oil with Surfactant Solutions," Annual Report for October 1978 - September 1979, Contract No. DE-AS19-78BC20009.

[L.1] Lake, L.W., "High Capillary Number Relative Permeability Model," Private Notes (1980).

[L.2] Land, C.S., "Calculation of Imbibition Relative Permeability for Two- and Three-Phase Flow from Rock Properties," SPE Journal (June 1968), 149-156.

[L.3] Larson, R.G., "From Molecules to Reservoirs: Problems in Enhanced Oil Recovery," Ph.D. Dissertation, The University of Minnesota (1980).

[L.4] Lefebvre due Prey, E.J., "Factors Affecting Liquid-Liquid Relative Permeability of a Consolidated Porous Medium," SPE Journal (Feb. 1973), 39-47.

[L.5] Leverett, M.C., "Flow of Oil-Water Mixtures Through Unconsolidated Sands," Trans. AIME (1938), 132-149.

[L.6] Leverett, M.C., and Lewis, W.B., "Steady Flow of Gas-Oil-Water Mixtures through Unconsolidated Sands," Trans. AIME (1941), 107-116.

[M.1] MacAllister, D.J., "Measurement of Two- and Three-Phase Relative Permeability and Dispersion for Micellar Fluids in Uconsolidated Sand," M.S. Thesis, The University of Texas at Austin (1982).

[M.2] Mohanty, K.K., and Salter, S.J., "Multiphase flow in Porous Media: III. Oil Mobilization, Transverse Dispersion and Wettability," SPE 12127, Presented at the 58th Annual Technical Conference and Exhibition of SPE, San Francisco, October 5-8, 1983.

[M.3] Mcore, T.F., and Slobod, R.L., "The Effect of Viscosity and Capillarity on the Displacement of Oil by Water," Producers Monthly, Vol.20 (Aug. 1956), 20-30.

[N.1] Naiki, M., "Numerical Simulation of Polymer Flooding Including the Effects of Salinity," Ph.D. Dissertation, The University of Texas at Austin, 1979.

[O.1] Ojeda, E., Preston, F., and Calhoun, S.C., "Correlation of Oil Residuals Following Surfactant Floods," Producers Monthly (December 1953), 20-27.

[O.2] O'Meara, Jr., D.J., and Lease, W.O., "Multiphase Relative Permeability Measurements using an Automated Centrifuge," SPE 12128 Presented at the 58th Annual Technical Conference in San Francisco, CA., Oct. 5-8, 1983.

[P.1] Perkins, T.K., and Johnston, O.C., "A Review of Diffusion and Dispersion in Porous Media," SPE Journal (March 1963), 70-84.

[P.2] Pope, G.A., and Nelson, R.C., "A Chemical Flooding Compositional Simulator," SPE Journal (1978), 339-354.

[R.1] Raimondi, P., and Torcaso, M.A., "Mass Transfer Between Phases in a Porous Medium: A Study of Equilibrium," SPE Journal (March 1965), 51-59.

[R.2] Raimondi, P., Torcaso, M.A., and Henderson, J.H., "The Effect of Interstitial Water on the Mixing of Hydrocarbons during a Miscible Displacement Process," Mineral Industries Experiment Station Circular No.61, The Pennsylvania State University, Oct. 23-25, 1961.

[R.3] Ramakrishnan, T.S., Wassan, D.T., "The Relative Permeability Function for Two-Phase Flow in Porous Media: Effect of Capillary Number," SPE/DOE 12693 Presented at SPE/DOE Fourth Symposium on Enhanced Oil Recovery held in Tulsa, Oklahoma, April 15-18, 1984.

[R.4] Ramirez, W.F., Shuler, P.J., and Friedman, F., "Convection, Dispersion and Adsorption of Surfactants in Porous Media," SPE Journal (Dec. 1980), 430-438.

[R.5] Reed, R.L., and Healy, R.N., "Physicochemical Aspects of Microemulsion Flooding: A Review," Improved Oil Recovery by Surfactant and Polymer Flooding, D.O. Shah and R.S. Schechter, Edited, Academic Press (1977), 383-438.

[S.1] Salager, J.L., "Physico-Chemical Properties of Surfactant-Oil-Water Mixtures, Phase Behavior, Microemulsion Formation and Interfacial Tension, Ph.D. Dissertation, The University of Texas at Austin (1977).

[S.2] Salager, J.L., Morgan, J.C., Schechter, R.S., Wade, W.H., and Vasques, E., "Optimum Formulation of Surfactant-Water-Oil System for Minimum Interfacial Tension or Phase Behavior," SPE Journal (April 1979).

[S.3] Salter, S.J., and Mohanty, K.K., "Multiphase flow in Porous Media: I. Microscopic Observations and Modelling," SPE 11017 Presented at 57th Annual Fall Meeting of SPE of AIME, New Orleans, Sept. 26-29, 1982.

[S.4] Saraf, D.N., Batycky, J.P., Jakson, C.H., and Fisher, D.B., "An Experimental Investigation of Three-Phase Flow of Water-Oil-Gas Mixtures through Water-Wet Sandstones," SPE 10761 Presented at the California Regional Meeting of SPE, San Francisco, March 24-26, 1982.

[S.5] Saraf, D.N., and Fatt, I., "Three-Phase Relative Permeability Measurement Using a Nuclear Magnetic Resonance Technique for Estimating Fluid Saturation," Trans. AIME, Vol.240 (1967), 235-242.

[S.6] Saraf, D.N., and McCaffery, F.G., "Two- and Three-Phase Relative Permeabilities: A Review," PRI Research Report No. 81-8 (Sept. 1981).

[S.7] Sarem, A.M., "Three-Phase Relative Permeability Measurements by Unsteady-State Method," Trans. AIME, Vol.237 (1966), 199-205.

[S.8] Satoh, T., "Treatment of Phase Behavior and Associated Properties Used in a Micellar-Polymer Flood Simulator," M.S. Thesis, The University of Texas at Austin (1984).

[S.9] Schneider, F.N., and Owens, W.W., "Sandstone and Carbonate Two- and Three-Phase Relative Permeability Characteristics," Trans. AIME, Vol.249 (1970), 75-84.

[S.10] Shuler, P.J., "A Study of the Mechanisms Affecting the Enhanced Recovery of Oil by Surfactant Flooding," Ph.D. Dissertation, University of Colorado at Boulder (1978).

[S.11] Snell, R.W., "The Saturation History Dependence of Three-Phase Oil Relative Permeability," Journal of Inst. Petroleum Vol. 49 (1963), 81-84.

[S.12] Spence, A.P., and Watkins, R.W., "The Effect of Microscopic Core Heterogeneity on Miscible Flood Residual Oil Saturation," SPE 9229 Presented at the 55th Annual Meeting held in Dallas, Texas, Sept. 21-24, 1980.

[S.13] Stalkup, F.I., "Displacement of Oil by Solvent at High Saturation," Journal of Pet. Tech. Vol.10 (1970), 337-348.

[S.14] Stone, H.L., "Probability Model for Estimating Three-Phase Relative Permeability," Journal of Pet. Tech. (1970), 214-218.

[S.15] Stone, H.L., "Estimation of Three-Phase Relative Permeability and Residual Oil Data," Journal of Canadian Pet. Tech. (Oct.-Dec. 1973), 53-61.

[T.1] Taber, J.J., "Dynamics and Static Forces Required to Remove a Discontinuous Oil Phase from Porous Media Containing Both Oil and Water," SPE Journal (March 1969), 3-12.

[T.2] Taber, J.J., Kamath, I.S.K., and Reed, K.L., "Miscible Displacement in Multiphase System," SPE Journal (1963), 189-196.

[T.3] Talash, A.W., "Experimental and Calculated Relative Permeability Data for System Containing Tension Additives," SPE 5810 Presented at Improved Oil Recovery Symposium, Tulsa, Oklahoma, March 1976.

[T.4] Taylor, G.I., "Dispersion of Soluble Matter in Solvent Flowing Slowly through a Tube," Proc., Royal Soc. 219, London (1953), 186-203.

[T.5] Thomas, G.H., Countryman, G.R., and Fatt, I., "Miscible Displacement in Multiphase System," SPE Journal (1963), 189-196.

[T.6] Tormich, J.F., Dalton, R.L., Deans, H.A., and Shallerberger, L.K., "Single-Well Tracer Method to Measure Residual Oil Saturation," Journal of Pet. Tech. (Feb. 1973), 211-218.

[T.7] Torabzadeh, S.J., and Handy. L.L., "The Effect of Temperature and Intefacial Tension on Water/Oil Relative Permeabilities of Consolidated Sands," SPE 12689 Presented at the SPE/DOE Fourth Symposium on Enhanced Oil Recovery held in Tulsa, Oklahoma, April 15-18, 1984.

[V.1] Van Spronsen, E., "Three-Phase Relative Permeability Measurements using the Centrifuge Method," SPE Paper 10688 Presented at the SPE/DOE Third Joint Symposium on Enhanced Oil Recovery, Tulsa, Oklahoma (April 4-7, 1982).

[W.1] Welge, H.J., "A Simplified Method for Computing Oil Recovery by Gas or Water Drive," Trans. AIME, Vol.195 (1952).

[W.2] Wyllie, M.R.J., and Gardner, G.H.F., "The Generalized Kozeny-Carmen Equation," World Oil, Vol.146 (1958), 210-228.

[Y.1] Yuan, M.K., "A Rheological Study of Polymer and Microemulsion in Porous Media," M.S. Thesis, The University of Texas at Austin (1981).

VITA

Mojdeh Delshad was born in Tehran, Iran, on May 6, 1955, the daughter of Mahin and Hassan Delshad. After completing her work at Marjan High School, Tehran, Iran, in 1972, she entered Aryamehr University of Technology in Tehran, Iran. She received a Bachelor of Science degree in Chemical Engineering in May 1978. She entered the Graduate School at The University of Texas at Austin in September 1979. In December 1981, she was awarded a Master of Science degree in Petroleum Engineering. Since January 1982, she has been working on her doctoral degree in Petroleum Engineering at The University of Texas at Austin. During her graduate studies she was awarded a Texas Mining and Mineral Resources Fellowship and an Arco Fellowship.

Permanent Address: P.O. Box 7995
Austin, Texas 78713 - U.S.A.

This dissertation was typed by Silvia B. Craveiro de Sa